

ANALYTICA CHIMICA ACTA

International journal devoted to all branches of analytical chemistry

EDITORS

A. M. G. MACDONALD (Birmingham, Great Britain)

HARRY L. PARDUE (West Lafayette, IN, U.S.A.)

Editorial Advisers

- | | |
|---------------------------------|-----------------------------------|
| F. C. Adams, Antwerp | W. C. Purdy, Montreal |
| R. P. Buck, Chapel Hill, NC | J. P. Riley, Liverpool |
| G. den Boef, Amsterdam | J. Růžička, Copenhagen |
| G. Duyckaerts, Liège | D. E. Ryan, Halifax, N.S. |
| D. Dyrssen, Göteborg | J. Savory, Charlottesville, VA |
| W. Haerdi, Geneva | W. D. Shults, Oak Ridge, TN |
| G. M. Hieftje, Bloomington, IN | W. Simon, Zürich |
| J. Hoste, Ghent | W. I. Stephen, Birmingham |
| A. Hulanicki, Warsaw | G. Tölg, Schwäbisch Gmünd, B.R.D. |
| E. Jackwerth, Bochum | A. Townshend, Birmingham |
| G. Johansson, Lund | B. Trémillon, Paris |
| D. C. Johnson, Ames, IA | A. Walsh, Melbourne |
| J. H. Knox, Edinburgh | H. Weisz, Freiburg i. Br. |
| P. D. LaFleur, Washington, DC | P. W. West, Baton Rouge, LA |
| D. E. Leyden, Denver, CO | T. S. West, Aberdeen |
| F. E. Lytle, West Lafayette, IN | J. E. Willis, Melbourne |
| H. Malissa, Vienna | Yu. A. Zolotov, Moscow |
| A. Mizuike, Nagoya | P. Zuman, Potsdam, NY |
| E. Pungor, Budapest | |

ANALYTICA CHIMICA ACTA

International journal devoted to all branches of analytical chemistry
Revue internationale consacrée à tous les domaines de la chimie analytique
Internationale Zeitschrift für alle Gebiete der analytischen Chemie

PUBLICATION SCHEDULE FOR 1980 (incorporating the section on Computer Techniques and Optimization).

	J	F	M	A	M	J	J	A	S	O	N	D
Analytica Chimica Acta	113/1 113/2	114	115	116/1	116/2	117	118/1	118/2	119	120/1	120/2	121
Section on Computer Techniques and Optimization			122/1			122/2			122/3			122/4

Scope. *Analytica Chimica Acta* publishes original papers, short communications, and reviews dealing with every aspect of modern chemical analysis, both fundamental and applied. The section on *Computer Techniques and Optimization* is devoted to new developments in chemical analysis by the application of computer techniques and by interdisciplinary approaches, including statistics, systems theory and operation research. The section deals with the following topics: Computerized acquisition, processing and evaluation of data. Computerized methods for the interpretation of analytical data including chemometrics, cluster analysis, and pattern recognition. Storage and retrieval systems. Optimization procedures and their application. Automated analysis for industrial processes and quality control. Organizational problems.

Submission of Papers. Manuscripts (three copies) should be submitted as designated below for rapid and efficient handling:

Papers from the Americas to: Professor Harry L. Pardue, Department of Chemistry, Purdue University, West Lafayette, IN 47090, U.S.A.

Papers from all other countries to: Dr. A. M. G. Macdonald, Department of Chemistry, The University, P.O. Box 363, Birmingham B15 2TT, England.

For the section on *Computer Techniques and Optimization:* Dr. J. T. Clerc, Universität Bern, Pharmazeutisches Institut, Sahlistrasse 10, CH-3012 Bern, Switzerland.

American authors are recommended to send manuscripts and proofs by INTERNATIONAL AIRMAIL.

Information for Authors. Papers in English, French and German are published. There are no page charges. Manuscripts should conform in layout and style to the papers published in this Volume. Authors should consult Vol. 111, p. 343 for detailed information. Reprints of this information are available from the Editors or from: Elsevier Editorial Services Ltd., Mayfield House, 256 Banbury Road, Oxford OX2 7DE (Great Britain).

Reprints. Fifty reprints will be supplied free of charge. Additional reprints (minimum 100) can be ordered. An order form containing price quotations will be sent to the authors together with the proofs of their article.

Advertisements. Advertisement rates are available from the publisher.

Subscriptions. Subscriptions should be sent to: Elsevier Scientific Publishing Company, P.O. Box 211, 1000 AE Amsterdam, The Netherlands. The section on *Computer Techniques and Optimization* can be subscribed to separately.

Publication. *Analytica Chimica Acta* (including the section on *Computer Techniques and Optimization*) appears in 10 volumes in 1980. The subscription for 1980 (Vols. 113–122) is Dfl. 1390.00 plus Dfl. 160.00 (postage) (total approx. U.S. \$756.00). The subscription for the *Computer Techniques and Optimization* section only (Vol. 122) is Dfl. 139.00 plus Dfl. 16.00 (postage) (total approx. U.S. \$75.50). Journals are sent automatically by airmail to the U.S.A. and Canada at no extra cost and to Japan, Australia and New Zealand for a small additional postal charge. All earlier volumes (Vols. 1–112) except Vols. 23 and 28 are available at Dfl. 150.00 (U.S. \$73.00), plus Dfl. 10.00 (U.S. \$5.00) postage and handling, per volume.

Claims for issues not received should be made within three months of publication of the issue, otherwise they cannot be honoured free of charge.

Customers in the U.S.A. and Canada who wish to obtain additional bibliographic information on this and other Elsevier journals should contact Elsevier/North Holland Inc., Journal Information Center, 52 Vanderbilt Avenue, New York, NY 10017. Tel: (212) 867-9040.

Reagents

MERCK



Suprapur[®]

Ultrapure reagents

Suprapur reagents are chemicals of the highest degree of purity, painstakingly prepared and extra-carefully packaged. In some cases the foreign substance content is several powers of ten lower than for guaranteed pure reagents. Suprapur reagents are therefore eminently suited for trace analysis work, for biochemical research and for measurements in physical chemistry.

Please ask for our special brochure.

**E. Merck, Darmstadt,
Federal Republic of Germany**

The Handbook of Environmental Chemistry

edited by **Professor O. Hutzinger**,

Director of the Laboratory of Environmental and Toxicological Chemistry at the University of Amsterdam, in cooperation with about 50 Internationally known specialists.

Volume I: ISBN 3-540-09688-4

Volume II: ISBN 3-540-09689-2

Volume III: ISBN 3-540-09690-6

The first two of three scheduled volumes are planned to appear by the middle of 1980.

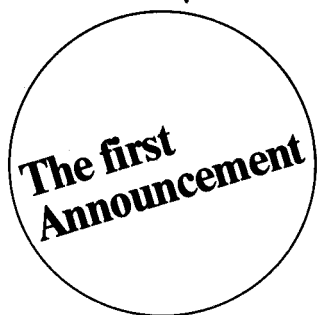
The work covers

1. natural environment: chemicals, processes, cycles
2. reactions and behaviour of chemicals in the environment: distribution, chemical, photochemical and microbial transformations.
3. chemistry and environmental behaviour of pollutant compounds, including a description of their toxicology and analysis.

The work is a comprehensive and critical presentation of current knowledge in these areas and will be of great interest to

- environmental scientists
- biologists
- chemists, biochemists and agricultural chemists
- analytical chemists
- medical scientists, occupational and environmental hygienists
- scientists in the earth sciences

in research, industry and administrative bodies.



If you want more information, send this coupon to:

Springer-Verlag KG
Wissenschaftliche Information
Dr. B. Volkmann
Postfach 105280
D-6900 Heidelberg 1

5637/5/1

Springer-Verlag Berlin Heidelberg New York

JOURNAL of ANALYTICAL and APPLIED PYROLYSIS

EDITORS

H.L.C. Meuzelaar, Salt Lake City, UT, U.S.A.
H.-R. Schulten, Bonn, G.F.R.

ASSOCIATE EDITOR

C.E.R. Jones, Redhill, Surrey, Great Britain

EDITORIAL BOARD

K.V. Alekseeva, Moscow, U.S.S.R.
J.M. Bracewell, Aberdeen, Great Britain
D.C. DeJongh, Cincinnati, OH, U.S.A.
K. Habfast, Bremen, G.F.R.
W.J. Irwin, Birmingham, Great Britain
P.G. Kistemaker, Amsterdam, The Netherlands
R.L. Levy, St. Louis, MO, U.S.A.
I. Lüderwald, Mainz, G.F.R.

F.W. McLafferty, Ithaca, NY, U.S.A.
N.M.M. Nibbering, Amsterdam, The Netherlands
E. Reiner, Atlanta, GA, U.S.A.
F. Shafizadeh, Missoula, MT, U.S.A.
T. Székely, Budapest, Hungary
S. Tsuge, Nagoya, Japan
P.C. Uden, Amherst, MA, U.S.A.
N.E. Vanderborgh, Los Alamos, NM, U.S.A.

VOL. 1, NO. 1

JOURNAL OF ANALYTICAL AND APPLIED PYROLYSIS

JUNE 1979

CONTENTS

Editorial	1
Analytical pyrolysis — An overview (Part 1)	
W.J. Irwin (Birmingham, Great Britain)	3
Determination of the temperature — time profile of the sample in pyrolysis — gas chromatography	
E.M. Andersson and I. Ericsson (Lund, Sweden)	27
The effects of sample preparation, pyrolysis and pyrolyzate transfer conditions on pyrolysis mass spectra	
W. Windig, P.G. Kistemaker and J. Haverkamp (Amsterdam, The Netherlands) and H.L.C. Meuzelaar (Salt Lake City, Utah, U.S.A.)	39
Data analysis of pyrolysis chromatograms by means of SIMCA pattern recognition	
G. Blomquist and E. Johansson (Umeå, Sweden), B. Söderström (Lund, Sweden) and S. Wold (Umeå, Sweden)	53
Use of principal components analysis for displaying variation between pyrograms of micro-organisms	
C.S. Gutteridge, H.J.H. MacFie and J.R. Norris (Bristol, Great Britain)	67
Pyrolysis—gas chromatography of methyl methacrylate—styrene and methyl methacrylate— α -methylstyrene copolymers	
T. Shimono, M. Tanaka and T. Shono (Osaka, Japan)	77
Information for authors	85

ELSEVIER SCIENTIFIC PUBLISHING COMPANY
AMSTERDAM

ELECTROPHORESIS

A SURVEY OF TECHNIQUES AND APPLICATIONS

Part A: Techniques

Z. DEYL, Czechoslovak Academy of Sciences, Prague (editor)
F. M. EVERAERTS, Z. PRUSÍK, and P. J. SVENDSEN (co-editors)

JOURNAL OF CHROMATOGRAPHY LIBRARY 18

This first volume in a two part set, deals with the principles, theory and instrumentation of modern electromigration methods. The second volume will be concerned with details of applications of electromigration methods to diverse categories of compounds, although a few applications are already discussed in Part A.

Some electromigration methods have become standard procedures because of their extensive use in analytical and preparative separations. These are discussed together with newer developments in the field. Hints are included to help the reader to overcome difficulties frequently arising from the lack of suitable equipment. Adequate theoretical background of the individual techniques is included. A theoretical approach to the deteriorative processes is presented in order to facilitate further development of a particular technique and its application to a special problem.

In each chapter practical realizations of different techniques are discussed and examples are presented to demonstrate the limits of each method. The mathematical and physicochemical background is arranged so as to make it coherent as possible for both non-professionals such as post-graduate students and experts using electromigration techniques.

CONTENTS: Preface. Foreword. Introduction. Chapters: 1. Theory of electromigration processes. 2. Classification of electromigration methods. 3. Evaluation of the results of electrophoretic separation. 4. Molecular size and shape in electrophoresis. 5. Zone electrophoresis (except type techniques and immunoelectrophoresis). 6. Gel-type techniques. 7. Quantitative immuno-electrophoresis. 8. Moving boundary electrophoresis in narrow-bore tubes. 9. Isoelectric focusing. 10. Analytical isotachopheresis. 11. Continuous flow-through electrophoresis. 12. Continuous flow-through electrophoresis. 13. Preparative electrophoresis in gel-media. 14. Preparative electrophoresis in columns. 15. Preparative isoelectric focusing. 16. Preparative isotachopheresis. 17. Preparative isotachopheresis on the micro scale. List of frequently occurring symbols. Subject index.

1979 xvi + 492 pages US \$83.00/Dfl. 170.00 ISBN: 0-444-41721-4



ELSEVIER

P.O. Box 211,
1000 AE Amsterdam
The Netherlands

52 Vanderbilt Ave
New York, N.Y. 10017

The Dutch guilder price is definitive. US \$ prices are subject to exchange rate fluctuations.

ANALYTICA CHIMICA ACTA

VOL. 114 (1980)

ANALYTICA CHIMICA ACTA

International journal devoted to all branches of analytical chemistry

EDITORS

A. M. G. MACDONALD (Birmingham, Great Britain)

HARRY L. PARDUE (West Lafayette, IN, U.S.A.)

Editorial Advisers

F. C. Adams, Antwerp
R. P. Buck, Chapel Hill, NC
G. den Boef, Amsterdam
G. Duyckaerts, Liège
D. Dyrssen, Göteborg
W. Haerdi, Geneva
G. M. Hieftje, Bloomington, IN
J. Hoste, Ghent
A. Hulanicki, Warsaw
E. Jackwerth, Bochum
G. Johansson, Lund
D. C. Johnson, Ames, IA
J. H. Knox, Edinburgh
P. D. LaFleur, Washington, DC
D. E. Leyden, Denver, CO
F. E. Lytle, West Lafayette, IN
H. Malissa, Vienna
A. Mizuike, Nagoya
E. Pungor, Budapest

W. C. Purdy, Montreal
J. P. Riley, Liverpool
J. Růžička, Copenhagen
D. E. Ryan, Halifax, N.S.
J. Savory, Charlottesville, VA
W. D. Shults, Oak Ridge, TN
W. Simon, Zürich
W. I. Stephen, Birmingham
G. Tölg, Schwäbisch Gmünd, B.R.D.
A. Townshend, Birmingham
B. Trémillon, Paris
A. Walsh, Melbourne
H. Weisz, Freiburg i. Br.
P. W. West, Baton Rouge, LA
T. S. West, Aberdeen
J. B. Willis, Melbourne
Yu. A. Zolotov, Moscow
P. Zuman, Potsdam, NY



ELSEVIER SCIENTIFIC PUBLISHING COMPANY

Anal. Chim. Acta, Vol. 114 (1980)

© Elsevier Scientific Publishing Company, 1980.

All rights reserved. No part of this publication may be reproduced, stored in a retrieval system or transmitted in any form or by any means, electronic, mechanical, photocopying, recording or otherwise, without the prior written permission of the publisher, Elsevier Scientific Publishing Company, P.O. Box 330, 1000 AH Amsterdam, The Netherlands.

Submission of an article for publication implies the transfer of the copyright from the author to the publisher and is also understood to imply that the article is not being considered for publication elsewhere.

Submission to this journal of a paper entails the author's irrevocable and exclusive authorization of the publisher to collect any sums or considerations for copying or reproduction payable by third parties (as mentioned in article 17 paragraph 2 of the Dutch Copyright Act of 1912 and in the Royal Decree of June 20, 1974 (S. 351) pursuant to article 16 b of the Dutch Copyright Act of 1912) and/or to act in or out of court in connection therewith.

Printed in The Netherlands.

SPECIAL ISSUE

FLOW ANALYSIS

Proceedings of a Conference held in Amsterdam, September 11–13, 1979

Foreword

About 20 years ago Skeggs introduced the concept of air-segmented continuous flow systems in chemical analysis. Its application has led not only to an increased sample throughput but also to an improvement in accuracy, reproducibility and reliability for routine work. Analyzers based on this principle are now conventional equipment in many analytical laboratories.

Even a cursory glance through recent issues of journals on analytical chemistry indicates a renewed interest in continuous flow analysis. This renewed interest has mainly been caused by the work started by Růžička and Hansen in Copenhagen, and Stewart and colleagues in Washington, D.C. about five years ago. They have shown that under certain flow conditions air segmentation is not a prerequisite to avoid carry-over of the successive samples in the system; it appeared to be possible to inject the samples directly in a carrier stream at a rate of over 200 samples per hour.

After an incubation period of about five years, the time seems ripe to assess the results of non-segmented continuous flow systems in comparison to air-segmented systems. Such an evaluation was the immediate motive for organizing the International Conference on Flow Analysis in Amsterdam in September 1979. The plenary lectures as well as most of the submitted research papers are compiled in this special issue of *Analytica Chimica Acta*.

The reactions of many participants proved that the conference fulfilled its objectives. It is hoped that this publication will stimulate many other analytical chemists as well.

The meeting was held under the auspices of the Royal Netherlands Chemical Society, Analytical Division.

G. den Boef	Laboratory for Analytical Chemistry,
W. E. van der Linden	University of Amsterdam,
	The Netherlands.

B. Griepink	Laboratory for Analytical Chemistry,
	State University Utrecht,
	The Netherlands.

CONTINUOUS-FLOW ANALYSIS: PRESENT AND FUTURE

L. R. SNYDER

Technicon Instruments Corporation, Tarrytown, NY 10591 (U.S.A.)

(Received 24th July 1979)

SUMMARY

The present and probable future performance of continuous-flow analysis is discussed in terms of design considerations and new analytical modules. Comparison of throughput rates and reagent/sample consumption with the competitive technique of flow-injection analysis shows that the latter is better suited for very simple processing schemes that require only a small dwell time (e.g., 5 s or less) within the flow system. For more complicated manipulation of sample and/or longer reaction times, continuous flow analysis generally has a substantial advantage with respect to analysis rate, reagent consumption and required sample size.

The general technique of continuous-flow analysis (c.f.a.) has been reviewed within the past few years [1, 2], but the field continues to advance at such a rate that another review at the present time is justified to keep the reader up to date. In addition, the related procedure of flow-injection analysis (f.i.a.) (see, e.g. [3, 4]) has shown rapid development since 1975 in terms of the volume of published work. This has naturally led to questions concerning the relative advantages and limitations of each technique for application to the area of high-speed automated chemical analysis. Fortunately, there now exists a body of theoretical and experimental data which allows comparisons to be made between c.f.a. and f.i.a. in terms of such practical questions as sample throughput rate, optimum experimental design, etc. Such a comparison makes it possible to determine which procedure will be preferable in specific applications; it also allows the potential future performance of these two methods to be examined.

In the present review, the theory which is basic to sample-throughput in both c.f.a. and f.i.a. is developed and applied to a comparison of the performance of each procedure. Recent developments in c.f.a. that extend the overall range of its application are also discussed, with emphasis on combining c.f.a. with high-performance liquid chromatography (h.p.l.c.).

C.F.A. VERSUS F.I.A.: SOME PRELIMINARY CONSIDERATIONS

Some familiarity with the general principles and experimental approach used for these two techniques (see, e.g. [1-4]) is assumed. Here it is useful to focus on the major differences. The simplest possible example of either technique is the addition of sample to a reagent stream, flow of the combined

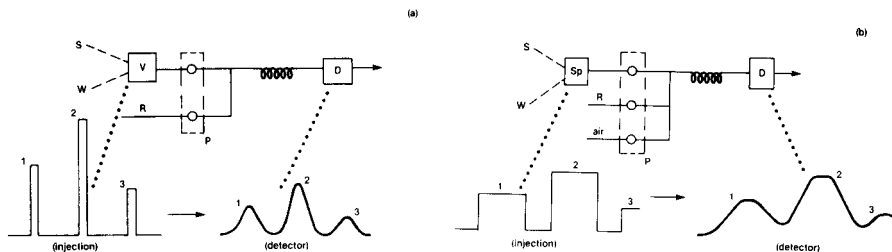


Fig. 1. Comparison of (a) flow-injection analysis with (b) continuous-flow analysis as normally practiced. Sample concentration—time profiles shown below each equipment diagram. S, sample solution; W, wash solution; V, sample valve; Sp, automatic sampler; P, pump; R, reagent solution; D, detector.

stream through an incubation coil for some time t (to complete reaction of sample and reagents, provide for mixing, etc.), followed by passage of the stream through some detector (often a simple photometer). In present f.i.a. systems, the sample is injected as a plug into the reagent stream, usually as a narrow "spike", as shown in Fig. 1(a). In present c.f.a. systems, the sample is usually added in alternation with wash solution to a reagent line, usually as a broad slug as shown in Fig. 1(b). In c.f.a. the combined stream after sample introduction is then segmented with air bubbles, and the segmented stream flows through the incubation coil and into the detector. Variations on the latter theme may involve addition of the air bubbles to the reagent stream before sample addition, debubbling of the combined stream before detection, etc. These latter features have little fundamental significance so far as the performance of c.f.a. is concerned.

The final output sensed by the detector is shown in Fig. 1(a) and (b). In the case of f.i.a., a series of more or less sharp bell-shaped "peaks" are obtained, with peak-height h being proportional to analyte concentration. In assays by c.f.a., each sample curve shows a plateau, and the height of this plateau ("flat") is similarly proportional to analyte concentration. The latter differences between c.f.a. and f.i.a. with respect to the shape of the final sample curve are actually not basic to either method. One can run either system so as to get bell-shaped or flat curves, simply by modifying the sample-introduction procedure. In fact, c.f.a. systems (so-called generation-I systems) were originally run to obtain bell-shaped curves. Whether one prefers bell-shaped or flat curves depends on the characteristics of these two approaches, as outlined in Table 1. Since c.f.a. systems have an inherently high throughput rate, the normal selection of flat curves allows increased emphasis on such aspects as reliability (function monitoring), precision, etc.

The apparent differences in equipment for f.i.a. and c.f.a. are also not of fundamental interest. Thus, a sample valve (V in Fig. 1a) is normally used in f.i.a., while an automated sampler (Sp in Fig. 1b) is customary in c.f.a. However, either sampling device can be used interchangeably. Only questions of cost, precision, convenience, etc., affect the choice of sampling means in a

TABLE 1

Characteristics of flat versus bell-shaped sample curves in flow analysis

<i>Advantages</i>	<i>Disadvantages</i>
1. Greater precision possible as a result of averaging data points across flat.	1. Sample throughput is cut by about half versus bell-shaped curves.
2. Greater reliability of final result, as a result of inspecting the curve "flat" (function monitoring).	2. Achieving the benefits of advantages 1, 2 above requires more complex data-processing.
3. Precision unaffected by small variations in sample size.	3. Sample and reagent consumption are increased about two-fold.
4. Less dilution of the sample, and resulting greater detection sensitivity.	

system of given design. In principle, sample valves provide greater precision when a flow analysis system is run with bell-shaped sample curves, as opposed to flats, and this advantage of sample valves increases with reduction in sample size.

The basic difference between f.i.a. and c.f.a. appears to be the use of bubbles for segmentation in the latter procedure. As will be seen, this provides for a major decrease in the dispersion or intermixing of adjacent samples in the flow system, and allows greater throughput rates, other factors being equal. Conversely, the insertion of air bubbles adds a further level of complexity to the system for c.f.a., in terms of equipment, operator interaction with the system, and hydraulic performance. Which approach should be selected — f.i.a. or c.f.a. — will depend on such questions as the throughput rate required, the degree of dispersion associated with a given assay, and the importance of system simplicity. Because c.f.a. has been practiced for about 20 years and is now the major technique for automated chemical analysis, its adherents have become accustomed to the complexity (such as it is) associated with the use of air segmentation.

BASIC THEORY OF SAMPLE DISPERSION IN C.F.A. AND F.I.A.

The spreading of sample bands as in Fig. 1 (detector) obviously limits the spacing of samples in the flow network and the resulting throughput rate. The shape of the resulting curves in each case (Fig. 1a or b) can be approximated by a Gaussian distribution, as illustrated in Fig. 2. In the first case (initial sample "spike", 2a), the resulting curve is a simple Gaussian curve; in the second case (initial sample slug, 2b), the wash-in and wash-out portions of the curve are integrated Gaussian curves [5]. In either case, the extent of sample dispersion is given by the quantity σ_t (Fig. 2) which is the standard deviation (in seconds) of the appropriate Gaussian curve.

The throughput rate for a f.i.a. or c.f.a. system depends on the spacing of sample bands in units of σ_t . A previous paper [6] has suggested a value of $8\sigma_t$ for sample curves with "flats" (Fig. 2b). Similarly, a spacing of $4\sigma_t$ seems

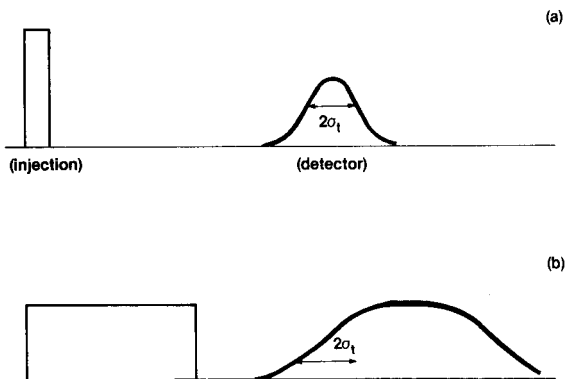


Fig. 2. Shape of sample curves for injection of a "spike" (a) or "slug" (b). Dispersion is measured in each case by the Gaussian standard deviation σ_t .

appropriate for final bell-shaped curves (Fig. 2a). The latter figure is suggested by the related problem in chromatography of the resolution between adjacent bands. A spacing of $4\sigma_t$ is equivalent to a resolution $R_s = 1$, which is better illustrated in an earlier paper [7]. In the latter case, carryover corrections will be small (or negligible) for most adjacent samples, and can be estimated [7]. However, it should be noted that previous applications of f.i.a. often involve poorer resolution of adjacent sample curves (i.e. sample spacing of about $3\sigma_t$).

Given the above spacing between adjacent samples in f.i.a. or c.f.a., it is possible to calculate sample analysis rates f (samples/h) as a function of σ_t (s):

$$\text{(no flats)} \quad f = 3600/4 \sigma_t = 900/\sigma_t \quad (1)$$

$$\text{(flats)} \quad f = 3600/8 \sigma_t = 450/\sigma_t \quad (1a)$$

Now the estimation of throughput rate f is seen to require only the value of σ_t for a given system to be specified. The evaluation of σ_t in c.f.a. or f.i.a. applications must next be considered.

Dispersion in c.f.a.

The evaluation of σ_t as a function of experimental conditions has been studied exhaustively, and on the basis of these data a semi-rigorous theory relating σ_t to all experimental variables has been proposed [5, 7, 8]. This relationship can be cast into the following form:

$$\sigma_t^2 = \left[\frac{538 d_t^{2/3} (F + 0.92 d_t^3 n)^{5/3} \eta^{7/3}}{\gamma^{2/3} F D_{w,25}} + 1/n \right] \left[\frac{2.35 (F + 0.92 d_t^3 n)^{5/3} \eta^{2/3} t}{\gamma^{2/3} F d_t^{4/3}} \right] \quad (2)$$

Here, the various quantities are defined as follows: d_t , internal diameter of the tubing comprising the flow network (in cm); F , the flow-rate of the total liquid within the network (ml s^{-1}); n , the frequency of segmentation (in

bubbles/s); η , the viscosity of the flowing solution (in Poise); γ , the surface tension of the flowing solution (dyne cm^{-1}); t , the time spent by a given segment between injection and detection (s); $D_{w,25}$, a mass transfer coefficient which varies between 2×10^{-5} and 12×10^{-5} for sample molecular weights of 400,000 to 27. $D_{w,25}$ is smaller for straight tubing than for coiled tubing.

While eqn. (2) may appear somewhat complex, it can be derived from fairly straightforward starting relationships that are well accepted in physical chemistry [7, 8]. More important, it has been tested over a wide range in values of the various parameters contained within eqn. (2), including conditions which are both typical of c.f.a. and those which are atypical. Figure 3 illustrates the correlation between calculated (eqn. 2) and experimental values of σ_t from one study [5, 7]. Generally, agreement within $\pm 10\%$ (1 SD) appears to be found.

Equation 2 does represent an oversimplification to the extent that the effect of bubbles on detection is not considered. In second-generation systems (e.g., SMA), debubbling of the flowing stream occurs before the detector. In third-generation systems (SMAC), bubbles pass through the detector. In either case, there is an effective increase in σ_t which results either from mixing in the debubbler, or the requirement that each liquid segment be large enough to more than fill the detector flowcell. The problem

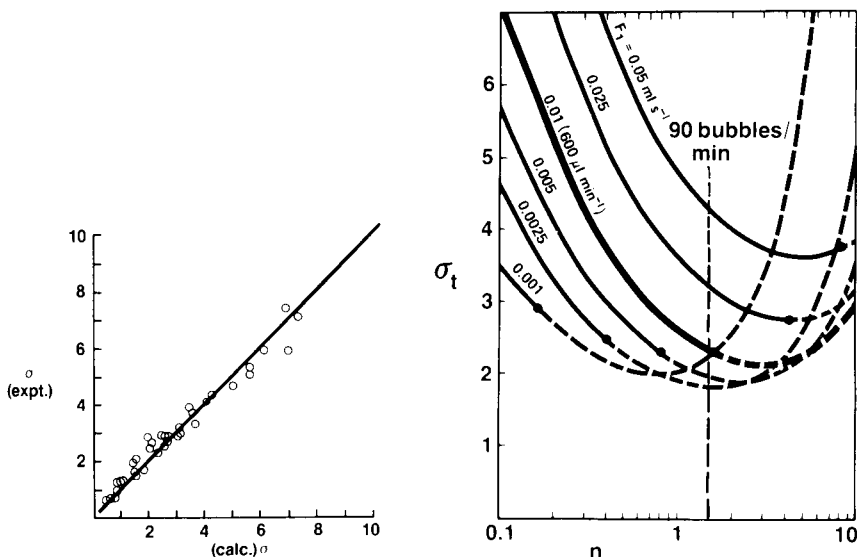


Fig. 3. Validation of eqn. 2. Comparison of sample dispersion (experimental values of σ_t) in c.f.a. with values calculated from eqn. 2. Data of [7].

Fig. 4. Calculated dispersion (values of σ_t) for the Technicon SMAC Analyzer as a function of flow-rate F and n (bubbles/s). Conditions assume dilute aqueous solution at 25°C ; 500-s incubation (dwell) time, and solute molecular weight of 167; internal diameter of open tube, 1.00 mm. Reprinted from [6].

is illustrated for SMAC in Fig. 4. Here, calculated values of σ_t are plotted versus segmentation frequency n , for different flow-rates ($F = 0.001\text{--}0.05$ ml s⁻¹); the dashed part of each curve represents "forbidden" values, because resulting liquid segments are too small for the flowcell. While in theory a minimum value of $\sigma_t = 1.8$ s should be possible for SMAC, in practice the flowcell-volume restriction places a lower limit on $\sigma_t = 2.3$, which means about a 25% decrease in maximum sample throughput.

The σ_t values for other c.f.a. systems can be similarly calculated; some resulting values are listed in Table 2. According to Table 2, it should be possible to run an SMA system at about 130 samples/h. In fact, such systems are typically run at half this rate: 60/h. The reason is the debubblers and other unsegmented mixing volumes (e.g., detector flowcell) present in an SMA system. The effect of the latter contributions to dispersion can be removed electronically in so-called curve-regeneration devices [9], and the analysis rate is thereby increased to 120/h [10]. The latter figure is seen to be in reasonable agreement with the value of 129/h shown in Table 2. Similarly, the calculated throughput rate for SMAC (196/h in Table 2) agrees reasonably well with the 150/h at which SMAC actually runs. Finally, Table 2 presents predicted sampling rates for a "generation-IV" c.f.a. system based on 0.5-mm i.d. tubing in the flow network. The latter approach, combined with a reduction in dwell time within the system (from present 10 min or so, to 100 s), would allow sampling rates of up to 590/h. However, such a system has not yet been demonstrated, although the prediction appears plausible on the basis of the above discussion.

Dispersion in f.i.a.

Although f.i.a. systems appear physically simpler than their analogous c.f.a. counterparts, the prediction of σ_t values is less well developed — at least in the case of the commonly used coiled-tube modules. Dispersion in flow-through straight tubing is given by the Taylor equation (see, e.g. [11]):

$$\sigma_t^2 = t d_t^2 / 96 D_m. \quad (3)$$

TABLE 2

Possible sampling rates f for various continuous-flow systems
(Calculations assume sample "flats" as in Fig. 1(b); data based on calculations of [6].)

System	Dwell time (s)	σ_t (s)	Sampling time (s)	Analysis rates (samples/h)
SMA 12/60	500	3.5	28	129
SMAC	500	2.3	18.4	196
Generation-IV	500	1.7	13.6	265
	100	0.76	6.1	590

Here, D_m is the diffusion coefficient ($\text{cm}^2 \text{s}^{-1}$) of the sample molecules in the surrounding solution. Equation (3) is readily derived from the commoner form of the Taylor equation: $H = d_t^2 u / 96 D_m$ where H is the height equivalent of a theoretical plate (equal to tube-length L divided by plate number N ; N is the theoretical plate number, equal to t^2 / σ_t^2 [11]), and u is the velocity of the liquid stream (cm s^{-1}).

Equation 3 predicts rather large values of σ_t , and therefore low sample analysis rates. For example, for a sample (analyte) molecular weight of 167 as in Fig. 4 for that c.f.a. system, the value of D_m is estimated from the Wilke—Chang equation (see, e.g. [12]) as 0.8×10^{-5} (in water at 25°C). Taking the same value of d_t (0.1 cm) and t (500 s), eqn. (3) for f.i.a. predicts a value of σ_t equal to 81 s, which is some 35-times greater than for SMAC in Table 1, and therefore yields a sample throughput 35-times less.

Of course, f.i.a. is not usually carried out in straight tubing. If coiled lengths of tubing are used instead, it is known that the resulting secondary flow (not turbulence [11, 13]) provides improved dispersion within the flow system (i.e., smaller values of σ_t). There is at present no rigorous equation to predict the decrease in σ_t versus eqn. (3) in coiled tubing, but Tijssen [13] has presented an experimental correlation of this reduction in σ_t with the dimensionless parameter De^2Sc (the product of the Dean Number squared times the Schmidt Number). The latter parameter can be expressed in terms of primary experimental variables:

$$De^2Sc = d_t^2 \rho u^2 / \eta d_c D_m \quad (4)$$

Here, ρ is the density of the flowing liquid, u is the velocity of the liquid stream (cm s^{-1}), d_c is the diameter of the coil or helix, and D_m is the solute (sample) diffusion coefficient. If H_0 refers to the value of H for straight tubing (eqn. 3), and H_c is the corresponding value for a coiled tube (with other variables held constant), then the improvement in sample dispersion as a result of coiling the tube can be expressed by the parameter ξ , where

$$\xi = (H_0/H_c) - 1 \quad (5)$$

If σ_t values are similarly defined for straight (σ_o) and coiled (σ_c) tubing, the advantage of coiling the tube (in terms of improved dispersion) can be expressed as

$$\sigma_o/\sigma_c = (\xi + 1)^{1/2} \quad (5a)$$

The improvement in sample throughput (f_c/f_o) for coiled versus straight tubing is seen to be equal to (σ_o/σ_c) from eqn. (5a). The latter quantity is replotted from Tijssen [13] as a function of De^2Sc in Fig. 5. The plot of Fig. 5 in conjunction with eqn. 3 ($\sigma_t = \sigma_o$) allows values of $\sigma_t = \sigma_c$ to be estimated in f.i.a. with coiled tubing.

Before proceeding with an analysis of dispersion and throughput in f.i.a. with coiled tubing, it is of interest to consider the accuracy of the above scheme [13] for this purpose. Data from the work of Hofmann and Halasz

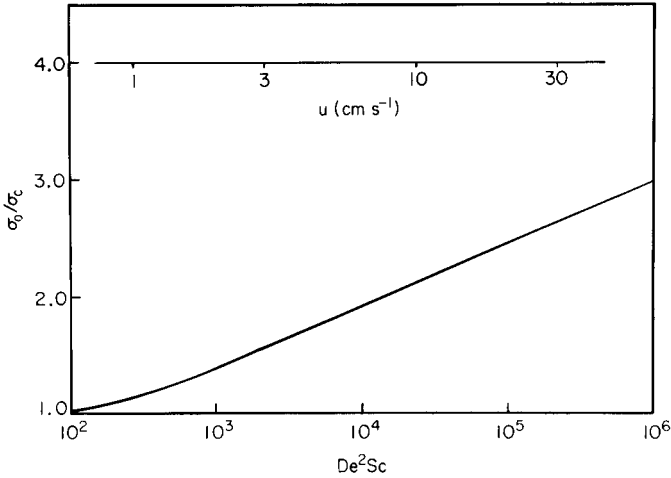


Fig. 5. Improved dispersion in f.i.a. with coiled tubing, as a function of experimental conditions (De^2Sc from eqn. 4). Values of u at top of figure are for $d_t = 0.025$ cm, water at 25°C , $d_c = 1.0$ cm, and $D_m = 7.4 \times 10^{-5}$ cm² s⁻¹.

[11] for relatively large coil diameters (d_c) show experimental σ_t values that are smaller than predicted from the data of Tijssen [13] by a factor of 2 to 3. The reason for this is that eqn. (4) probably overestimates the importance of d_c when d_c is large. Thus, small values of d_c (e.g. 1 cm vs. 2 cm) may be important in determining secondary flow, whereas the difference between coil diameters of 20 and 40 cm is probably less important. A similar independence of secondary flow on d_c when d_c is large (4–35 cm) has been noted for segmented flow [5].

Values of u are plotted across the top of Fig. 5, for water at 25°C , a tube of diameter 0.025 cm and coil diameter of 1.0 cm, and a solute molecular weight of 167. Typical values of u in f.i.a. are less than 30 cm s⁻¹, which leads to an improvement in throughput f (as a result of coiling) of 3-fold or less in the usual case.

Comparison of dispersion in c.f.a. versus f.i.a.

The preceding treatments allow values of σ_t to be calculated for either c.f.a. or f.i.a. systems as a function of experimental conditions. For either c.f.a. (eqn. 2) or f.i.a. (eqn. 3), σ_t is predicted to increase as $t^{1/2}$, assuming that other variables are held constant, and t refers to some required time for incubation. This means that very small values of σ_t are possible, as t approaches zero. For such applications requiring only a few seconds of incubation time, it will be seen that high throughput rates are possible with either c.f.a. or f.i.a. Therefore, so far as dispersion and throughput are concerned, the question of what happens at larger values of t is of greater interest, since it is for large values of t that dispersion and throughput become a practical problem.

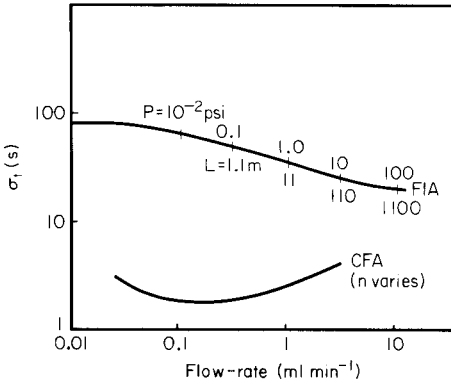


Fig. 6. Comparison of sample dispersion in f.i.a. and c.f.a. systems. Incubation time $t = 500$ s, $d_t = 0.1$ cm, $d_c = 1.3$ cm, other conditions as in Fig. 4.

The first comparison, in Fig. 6, is for an incubation or dwell time of 500 s, with a tubing diameter of 0.1 cm and a coil diameter of 1.3 cm. Here and elsewhere, the solute molecular weight is taken as 167, and the liquid within the flow network is water (plus surfactant) at 25°C. In Fig. 6 σ_t is plotted as a function of flow-rate F for both f.i.a. and c.f.a., by using the equations developed in the preceding sections. Values of the pressure drop P (psi) and tube length L (m) are marked on the f.i.a. plot, and these are seen to increase as F increases. The c.f.a. values are taken directly from Fig. 4, and are the "best" values (optimum n) for each value of F ; i.e., the curve of Fig. 6 for c.f.a. is the lower envelope of the curves of Fig. 4. This c.f.a. curve predicts smaller σ_t values than will be found in practice, because of the need to eliminate bubbles by either electronic or physical means. In the preceding analysis of Fig. 4, it was noted that for conditions as they exist on SMAC, the actual values of σ_t are about 25% higher than predicted in Fig. 6. This arises from the electronic debubbling used on SMAC, and the size of the detector flowcell. For physical debubbling, other calculations [8] suggest a smaller increase in σ_t relative to the values of Fig. 6. One experimental study [14] found a 10% increase in σ_t as a result of physical debubbling. In any case, it will be seen that this 10–25% increase in σ_t values in c.f.a. as a result of debubbling does not affect the comparison of c.f.a. and f.i.a. throughput rates. The c.f.a. curve of Fig. 6 also assumes that the length of the incubation coil will be adjusted to provide the required dwell time (500 s) at the specified flow-rate F , which is normal practice in c.f.a.

Figure 6 shows that σ_t for f.i.a. is generally much larger than the values for c.f.a. This reflects the marked ability of air-segmentation to break up laminar flow and decrease sample dispersion. There is an optimum flow-rate F for minimum dispersion in c.f.a., with the optimum F value being 0.1–0.2 ml min⁻¹ in the system shown; σ_t is then equal to 1.8 s. The pressure drop P

for this optimum value of σ_t for c.f.a. is a few psi. In the case of f.i.a., values of σ_t are quite large at low flow-rates ($\sigma_t = 82$ s). With increase in F , secondary flow becomes more important (as in Fig. 5), and the values of σ_t for f.i.a. decrease. However, the ultimate decrease in σ_t is limited by two considerations: increasing pressure P and increasing consumption of reagents. For the peristaltic pumps commonly used in f.i.a., a maximum value of P equal to 10 psi can be assumed. This corresponds to a value of $F = 3$ ml min⁻¹ in Fig. 6, and yields $\sigma_t = 26$ s. Thus in the example of Fig. 6, σ_t for c.f.a. is (26/1.8) or 14-fold smaller than for f.i.a., which means that throughput rates should be 14-fold greater in c.f.a. Reagent consumption would be over 400-fold greater per assay.

Dispersion in f.i.a. can be significantly reduced by using tubing of smaller diameter, and tubing diameters of 0.025 cm have been used. While a similar reduction in dispersion occurs for c.f.a. as d_t is decreased [8], this involves practical difficulties which have not yet been completely resolved (hydraulic effects, increased pressure drop, higher required segmentation rates). Therefore, for the moment, it is assumed that $d_t = 0.1$ cm is the lower practical limit for c.f.a. Figure 7 illustrates the dependence of σ_t on F for $d_t = 0.025$ cm in f.i.a., with other conditions the same as in Fig. 6 (same curve for c.f.a.). As expected, the value of σ_t at low values of F is decreased significantly (from 82 to 20.5 s). However, the pressure drop for smaller d_t is increased substantially for the same values of F . This means that the further decrease of f.i.a. σ_t values at higher values of F is more limited than in Fig. 6. For an

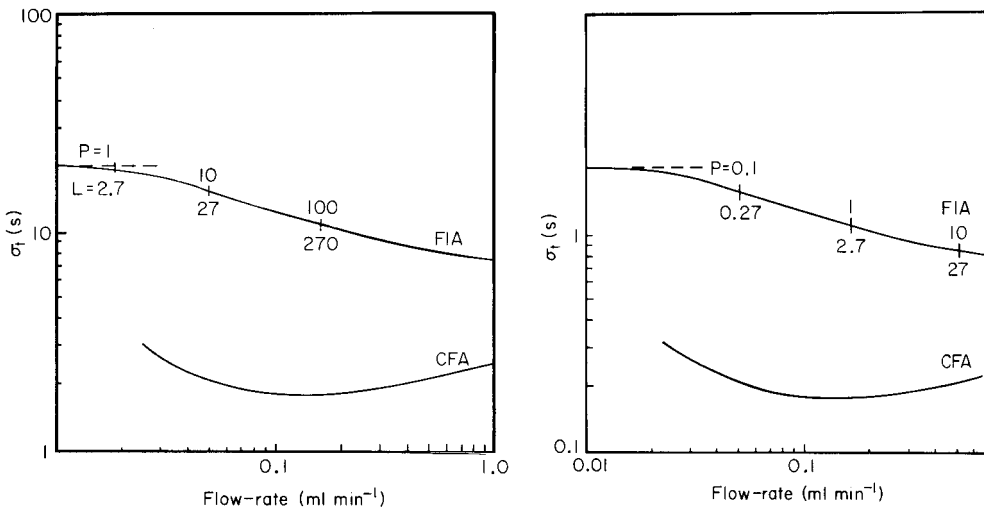


Fig. 7. Comparison of sample dispersion in f.i.a. and c.f.a. systems. Conditions as in Fig. 6, except d_t (f.i.a.) reduced to 0.025 cm.

Fig. 8. Comparison of sample dispersion in f.i.a. and c.f.a. systems. Conditions as in Fig. 7 ($d_t = 0.025$ cm for f.i.a., 0.1 cm for c.f.a.) except $t = 5$ s.

upper limit on $P = 10$ psi, σ_t is equal to 15.5 s for f.i.a. This now corresponds to a value 8-fold greater than the corresponding c.f.a. case. Thus even with a small tube diameter, f.i.a. is still slower in terms of throughput than is c.f.a.

The situation becomes more favorable for f.i.a. if the incubation time t is decreased, since this allows higher flow-rates and greater secondary-flow effects. This is illustrated in Fig. 8, for $t = 5$ s. While both curves are displaced downward by 10-fold ($100^{1/2}$) compared with Fig. 7, much higher flow-rates are possible with f.i.a. because of the shorter tube lengths now required; thus, for P equal 10 psi, a value of $\sigma_t = 0.85$ s is possible. The throughput advantage of c.f.a. is now reduced to 4.7-fold ($0.85/0.18$). However, even for short incubation times, c.f.a. retains an advantage over f.i.a., although debubbling effects are more important for smaller values of t , which can substantially reduce this advantage in practice.

If only very short incubation times are required, and high throughput rates are advantageous, f.i.a. becomes preferable to c.f.a. Tijssen [13] has shown that analysis rates of up to 900/h are practical with f.i.a. when 0.2-cm-diameter tightly-coiled (0.2-cm diameter) tubing is used. However, the incubation times under these conditions are of the order of 2 s, which limits this application to very fast reactions — if reaction of the sample is required for detection.

C.f.a. versus f.i.a.: overview

Apart from the considerations discussed above, f.i.a. has advantages over c.f.a. (as now practiced) for the rapid analysis of samples that require short incubation times (e.g., of the order of a few seconds). But this limits f.i.a. applications to very simple situations, and to dedicated as opposed to flexible or multi-channel analyzers. Many automated assays require longer incubation times, and c.f.a. then offers higher possible throughput rates. In addition, automated chemical analysis derives much of its appeal from its ability to mimic other laboratory manipulations: dialysis, evaporation-to-dryness, solvent extraction, etc. For these situations, the increased dwell time t within the system clearly gives the advantage to c.f.a. over f.i.a. It thus appears that there is a place for both f.i.a. and c.f.a. in automated chemical analysis. The choice of one technique over the other should be made on the basis of the various compromises involved.

RECENT DEVELOPMENTS IN CONTINUOUS-FLOW ANALYSIS

Apart from the possibilities of increased sample-throughput rate discussed in the preceding sections, c.f.a. can be further improved by increasing its versatility; that is, its practical utility can be broadened by adding new modules or cartridge modifications that provide new processing options. Since the earlier reviews [1, 2], several such developments have occurred. While some of these may prove applicable to f.i.a. systems as well, they are

for the most part better adapted for use in systems that allow fairly long dwell times. Several of these new c.f.a. options have been developed specifically for systems that incorporate high-pressure liquid chromatography (h.p.l.c.) into the system.

Evaporation-to-dryness (EDM) module

Automated sample pretreatment prior to h.p.l.c. separation and analysis is becoming increasingly necessary [15, 16]. Thus in many h.p.l.c. applications it is undesirable to inject the raw sample into the column, and often in such cases it is preferable to automate the sample pretreatment scheme. Many such sample-pretreatment schemes require the evaporation of some solvent A from the sample, followed by redissolution of sample into a different solvent B (e.g., the h.p.l.c. mobile phase). At the same time, the concentration of sample in the final solution can be increased (if desired) by decreasing the ratio of final to initial solvent volumes.

The Technicon EDM module, shown schematically in Fig. 9, was designed to provide just this capability. The sample in solvent A is allowed to flow onto the moving teflon wire at position 1. Under the influence of the vacuum (at point 2), the sample stream is pulled into the tube which surrounds the wire, and coats the wire. Sample flow-rates of $0.5\text{--}1.0\text{ ml/min}^{-1}$ can be accommodated without any loss of sample (by dripping off the moving wire). During passage of the wire through the tube, the temperature within the tube can be elevated by heating the air entering the tube (at point 2). This serves to evaporate solvent A, so that sample arriving at the end of the tube is free of solvent A. At this point, the moving wire enters a crosspiece (3), where solvent B is pumped into a right-angle port of the cross and flows across the wire during its transit through the cross, dissolving the sample from the wire in the process. Solvent B is then pumped out of the cross at a slightly higher flow-rate than is used to deliver B to the cross. This serves to draw air bubbles into the cross (through the ports holding the wire), resulting in segmentation of solvent B leaving the cross. This allows for exchange of solvent A by B, as well as for increasing the concentration of sample in B

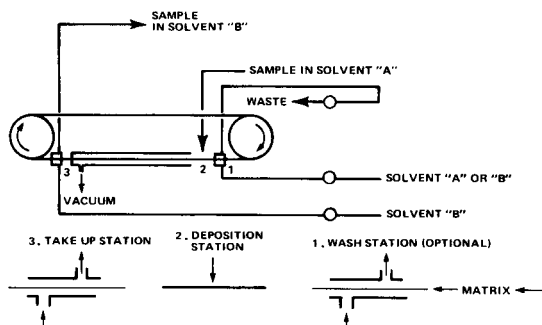


Fig. 9. Schematic diagram of Technicon evaporation-to-dryness (EDM) module. See text for explanation.

versus A (by reducing the flow of B into the cross, relative to flow of A onto the wire).

The utility of the EDM module for automated sample pretreatment in h.p.l.c. has been demonstrated in several applications (see e.g., [17]). This same capability should also be useful in other types of automated analyses, wherever solvent exchange or sample concentration is required.

Coated-tube separations

Simple separation steps are often involved in manual assay procedures. Sample dialysis was one of the first of these to be adapted to the Auto-Analyzer. Other operations for which automation is desirable include sample filtration and low-pressure chromatography. While the latter operations have already been adapted to c.f.a., these procedures have so far proven more or less cumbersome and unreliable. A new approach to this general class of separations is the use of coated tubes: so-called segmented-flow capillary liquid chromatography [18, 19].

The principle of operation of coated-tube separations in c.f.a. systems is illustrated in Fig. 10. A length of narrow-diameter tubing is coated internally with a thin layer of retentive material (stationary phase). The solvent (mobile phase) flowing through the coated tube is segmented with air bubbles, and samples are periodically introduced into the tube. Within the tube, any of the usual chromatographic processes can be carried out, depending on the choice of solvent and stationary phase. In this way, it is possible to automate chromatographic separation in c.f.a. without the need for intermediate debubbling and rebubbling, and with minimum pressure drop across the separation module. Furthermore, these coated tubes accommodate particulate-containing samples with no problem, and can also be used to filter such samples during the separation.

The application of these coated-tube separations in c.f.a. systems has so far been confined to the use of agarose-coated tubes for gel-permeation separations. In this mode, rapid filtration of particulates (or proteins) from the sample is possible, with complete recovery of desired sample constituents, and with no need for renewable filter elements (filter paper, membranes, etc.). Figure 11 shows a flow diagram for one such application of coated tubes in c.f.a., the h.p.l.c. of therapeutic drugs in serum. In manual sample pretreatment for this assay by h.p.l.c., the usual procedure is to precipitate the sample protein, spin down the sample, filter the supernatant liquid through a

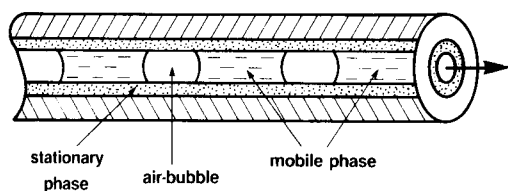


Fig. 10. Separation by means of segmented flow through coated tubes.

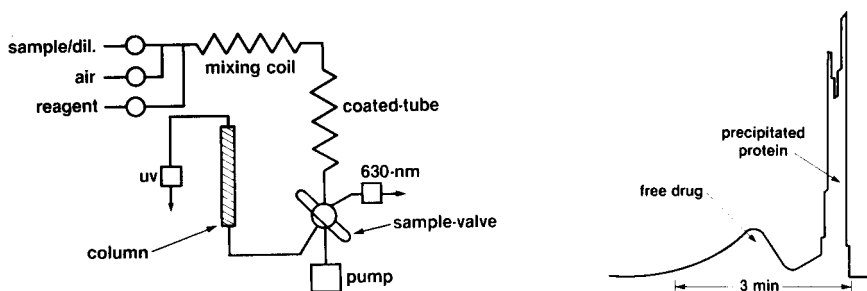


Fig. 11. Flow diagram for automated h.p.l.c. of therapeutic drugs in serum with segmented flow.

Fig. 12. Coated-tube separation of free drug from precipitated protein in a 200×0.1 cm tube.

0.5- μ m filter, and then inject the sample. In the coated-tube approach (Fig. 11), the sample is combined with a precipitating reagent, passed through an incubation coil to allow completion of precipitation, and then enters a tube coated with agarose. During passage through this tube, the drug(s) of interest is separated from precipitated protein, leaving the tube as shown in Fig. 12. The combined protein/drug fractions are passed through the sample loop of the automatic injection-valve of Fig. 11, and the passage of particulates (precipitated protein) from the valve loop is monitored by the 630-nm detector. When the protein band has cleared the sample loop, the valve injects the sample onto the h.p.l.c. column, and the analysis is completed in a conventional manner. It can be seen in Fig. 12 that assay rates of 20/h are possible, as far as the coated-tube separation is concerned; at present, faster analysis rates are precluded by the speed of the h.p.l.c. separation. However, improvements in the design of the coated tubes should allow considerably faster throughput rates in such separations [18].

These c.f.a. coated-tube separations can be extended to other applications as well. Thus the use of solid reagents would allow reaction with the sample, after which the excess of reagent could be separated as in Fig. 11. Other applications will be suggested by different separation problems.

Long-term incubation

When a segmented stream is at rest, there is essentially no dispersion of sample bands during this "storage" period. This suggests various valving schemes, in which a series of sample/reagent mixtures can be fed into storage coils, and then allowed to stay (at rest) in the coils for an extended incubation time. This overcomes the normal tendency for sample dispersion to increase with incubation time (eqn. 2), and in principle would allow long reaction times plus high throughput rates of analysis.

One application of this principle has been discussed for c.f.a. reaction-detectors for h.p.l.c. [20], but the same approach could be used for other applications, e.g., the multi-hour incubations required in radioimmunoassay, when sample concentrations are extremely small.

Fully automated sample-pretreatment for liquid chromatography (FAST-LC)

The combination of various AutoAnalyzer modules including the Solid-Prep sampler and other units described above allows the complete automation of virtually any operation now carried out for the purpose of sample pretreatment prior to h.p.l.c. analysis. These FAST-LC systems are being used for a variety of purposes, including the determination of vitamins in tablets, therapeutic drugs in serum, etc. While the advent of these systems is relatively recent, and therefore published examples are still rather few in number, the potential area of application is extremely broad. The use of such FAST-LC systems should see a very rapid growth during the next few years.

Magnetic-particle reagents

In many situations it is desirable to be able to separate sample from reagent(s) upon completion of some assay reaction. A common example is provided by radioimmunoassay (r.i.a.), where an antibody reagent, labeled antigen and sample are incubated together, and then separated into antibody and non-antibody fractions. Counting of the separate fractions then allows the determination of the fraction of labeled antigen which is bound to the antibody. From this measurement the concentration of antigen (analyte) in the original sample can be determined.

The Technicon STAR system provides for fully automated r.i.a. determinations of various analytes of interest [21]. In the STAR system, the separation of antibody reagent from the remainder of the sample is achieved as follows.

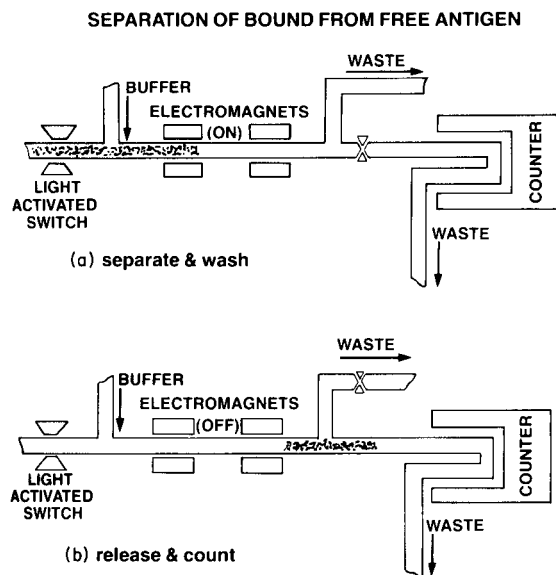


Fig. 13. Separation of solid-phase (antibody) reagent from sample in the STAR r.i.a. system. (a) Separate and wash: magnet ON, particles about to be collected. (b) Release and count: magnet OFF, particles just released.

The antibody is bonded to particles which have metallic iron incorporated into the particle matrix, thereby rendering the particles susceptible to magnetic attraction. The antibody particles react with labelled antigen and sample within the STAR system, followed by incubation for completion of the antibody-antigen reaction. The resulting mixture of particles and unreacted antigen-plus-sample is then directed to an electromagnet which surrounds part of the flow network (Fig. 13a). At this stage of the analysis, the magnet is switched on and the magnetic particles collect on the walls of the tube near the magnet. Once the remainder of the sample and unbound reagents are swept past the magnet, the latter is switched off, releasing the magnetic particles (Fig. 13b). In this fashion, the solid-phase antibody reagent (plus bound antigen) is separated cleanly from the soluble reagents plus sample. The particle fraction is then directed to an on-line radiocounter, to measure the radioactivity of the bound-antigen fraction.

It is apparent that the general principle of the STAR magnetic reagents can be extended to other applications. In fact, this approach is similar to the gel permeation coated-tube procedure described above, and certain problems that can be solved by application of the coated-tube technique can also be handled with magnetic particles.

REFERENCES

- 1 W. B. Furman, *Continuous-Flow Analysis. Theory and Practice*. M. Dekker, New York, 1976.
- 2 L. R. Snyder, J. Levine, R. Stoy and A. Conetta, *Anal. Chem.*, 48 (1976) 942A.
- 3 J. Růžička and E. H. Hansen, *Anal. Chim. Acta*, 78 (1975) 145.
- 4 J. Růžička and H. Hansen, *Anal. Chim. Acta*, 99 (1978) 37.
- 5 L. R. Snyder and H. J. Adler, *Anal. Chem.*, 48 (1976) 1017.
- 6 L. R. Snyder, in *Advances in Automated Analysis, 1976*, Technicon International Congress, Mediad Press, Tarrytown, NY, 1977, p. 76.
- 7 L. R. Snyder and H. J. Adler, *Anal. Chem.*, 48 (1976) 1022.
- 8 L. R. Snyder, *J. Chromatogr.*, 125 (1976) 287.
- 9 W. H. C. Walker, J. C. Hephherdson and G. K. McGowan, *Clin. Chim. Acta*, 35 (1971) 455.
- 10 W. H. C. Walker, private communication.
- 11 K. Hofmann and I. Halasz, *J. Chromatogr.*, 173 (1979) 211.
- 12 B. L. Karger, L. R. Snyder and C. Horvath, *An Introduction to Separation Science*, Wiley-Interscience, New York, 1973, p. 78.
- 13 R. Tijssen, *Axial Dispersion in Helically Coiled Tubes for Chromatography*, Thesis, University of Delft, 1979.
- 14 R. S. Deelder, M. G. F. Kroll, A. J. B. Beeren and J. H. M. van den Berg, *J. Chromatogr.*, 149 (1978) 669.
- 15 L. R. Snyder and J. J. Kirkland, *Introduction to Modern Liquid Chromatography*, 2nd edn., Wiley-Interscience, New York, 1979, Chap. 17.
- 16 D. A. Burns, Research/Department, April 1977, p. 21.
- 17 J. W. Dolan, J. R. Gant, R. W. Giese and B. L. Karger, *Advances in Automated Analysis, 1976 Technicon International Congress*, Vol. 2, p. 332.
- 18 L. R. Snyder and J. W. Dolan, *J. Chromatogr.*, 185 (1979) 43.
- 19 J. W. Dolan and L. R. Snyder, *J. Chromatogr.*, 185 (1979) 57.
- 20 L. R. Snyder, *J. Chromatogr.*, 149 (1978) 653.
- 21 E. Cohen and M. Stern, in *Advances in Automated Analysis, 1976 Technicon International Congress*, Mediad Press, Tarrytown, NY, 1977, p. 232.

FLOW INJECTION ANALYSIS. PRINCIPLES, APPLICATIONS AND TRENDS

J. RŮŽIČKA* and ELO H. HANSEN

Chemistry Department A, The Technical University of Denmark, DK-2800 Lyngby (Denmark)

(Received 5th July 1979)

SUMMARY

The basic principles of Flow Injection Analysis are outlined. The parameters governing the dispersion of the injected sample zone in the system are discussed, and it is demonstrated how these parameters can be manipulated in order to suit the requirements of an individual analytical procedure. A number of examples illustrating the practical application of f.i.a. are described, comprising the use of automated, stopped-flow, merging-zones, extraction techniques as well as f.i.a. scanning and methods based on intermittent pumping. Updated lists on f.i.a. procedures published and species that can be determined by f.i.a. are included.

There are many examples of how progress of science or technical development has been hindered by a well established concept or technology. Thus, it took ten years for A. G. Bell to convince the telecommunication experts of his era that it is at least as useful to transmit the human voice by wire as it is to transmit the Morse code (without the aid of the Brazilian Emperor Pedro the 2nd, who took a fancy to the telephone, it would certainly have taken even longer). It is hard to believe now that World War II was fought almost entirely with piston engine propelled aircraft although Whittle designed the jet engine in 1930 and made the first test run in 1937. Yet, the established British aircraft engine manufacturers were not interested in this crackpot idea because they "knew" from experience that it would not work. Thus it comes as no surprise that the areas of lesser technical importance, such as automation of chemical analysis, are also not immune to this kind of technological and scientific orthodoxy. The initial scepticism towards Flow Injection Analysis (f.i.a.) [1—79], which is based on the use of non-segmented streams, emanated from the fact that the new method ostensibly contradicted the basic principles of continuous flow analysis. It was Skeggs' concept of continuous, air-segmented flow [80] which, being truly ingenious, had resulted in the widespread use of continuous flow systems for performing discrete chemical analyses. Thus, it became generally assumed that air segmentation and the attainment of the "steady-state" signal were essential prerequisites for performing continuous flow analysis. Yet, although the

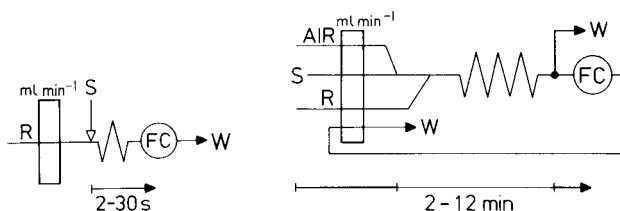


Fig. 1. Comparison of two continuous flow systems with colorimetric flow-through cell (FC) designed for a simple method based on the colour formation between the sample (S) and the reagent (R) solutions. The residence time of the sample in the f.i.a. system (left) is much shorter than in the air-segmented system (right), where the stream has also to be split prior to measurement between two different waste lines (W) to remove the air segments from the monitored stream.

presence of air decreases the carryover, this air also prevents miniaturization of the system and limits its usefulness: because of the inherent compressibility of air which causes the stream to pulsate; because the air has to be added to the stream and then removed prior to measurement (Fig. 1); and because the air segmentation unselectively hinders dispersion of the sample zone with the sole aim of decreasing the carryover.

While the f.i.a. system might at first seem to offer only some kind of technical improvement, such as a high sampling rate or a nearly instant availability of the analytical readout, its concept of controlled dispersion is in fact entirely new in analytical chemistry and it may very well be the most important aspect of this new technique.

THE PRINCIPLES OF FLOW INJECTION ANALYSIS

The key to understanding how and why flow injection analysis works lies in the knowledge of how a sample zone disperses when injected into a continuously moving, unobstructed carrier stream of reagent and how this dispersion can be manipulated so that its degree exactly suits the requirements of an individual analytical procedure. Leaving chemistry aside, one can simply measure the dispersion in a simple f.i.a. system, such as that shown in Fig. 1 (left), by pumping a colourless carrier stream and by injecting an exact volume of a coloured dye and by recording the peak as detected by means of a flow-through spectrophotometer. Such an experiment will reveal that, if the solution flows through a thin tube of uniform diameter (say 0.5 mm) in a laminar flow fashion, then the height, width and shape of the recorded peak will be affected by three interrelated factors, i.e., sample volume, tube length and pumping rate. At constant pumping rate the influence of sample volume and tube length is shown in Fig. 2 which depicts the relation between the peak height and the length of the measuring cycle in relation to the sample volume (Fig. 2A) and the tube length (Fig. 2B). It follows that any point of the rising part of the peak is as good a measure of the analyte concentration as the "steady-state" value eventually reached and it is there-

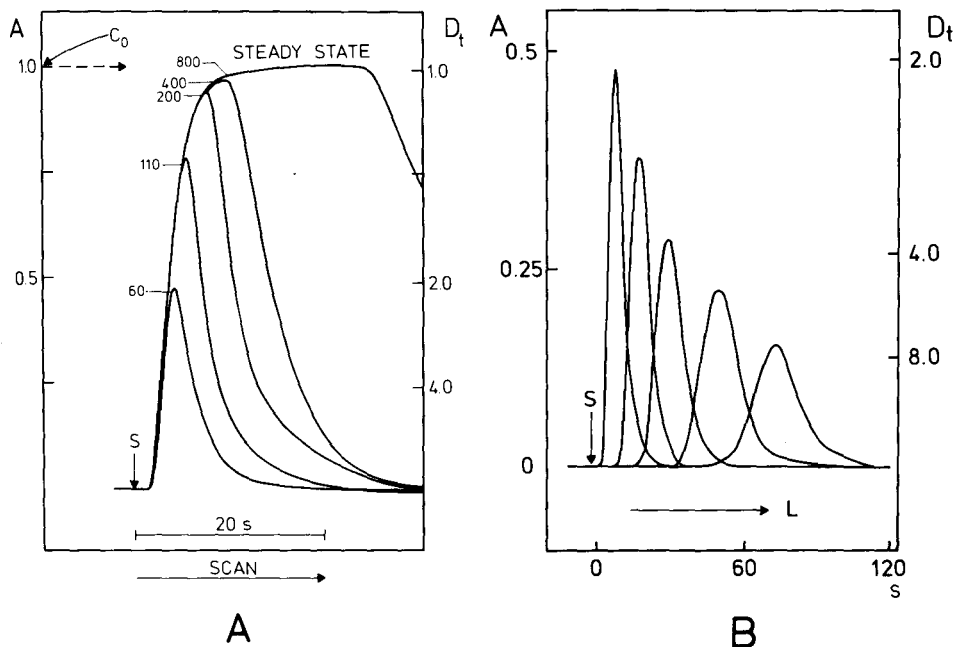


Fig. 2. (A) F.i.a. response curves as a function of injected sample volume. The peak height increases with the volume of the sample injected until the "steady-state" signal is reached. All curves recorded from the same starting point S with sample volumes of 60, 110, 200, 400 and 800 μl . Note that $D_t = 1$ for the "steady state", and that the peak width increases dramatically with increasing sampling volume. (B) Dispersion of an injected sample zone as a function of tube length travelled.

fore a waste of sample and reagent solutions and of time to try to reach the plateau of the response curve. In order to obtain reproducible results, however, the carrier stream must not pulsate and the injection has to be performed so that always exactly the same volume of the sample solution is introduced into the carrier stream in a reproducible way. This is best achieved by a rotary valve furnished with a bypass (Fig. 3).

When a sample zone moves through an open tube in a laminar flow fashion, the original square-wave concentration profile, which the zone had when residing in the injection valve, disperses and the degree of dispersion increases with the length of the tube through which the sample zone has travelled (Fig. 2B). Thus one can manipulate the dispersion of the sample zone by choosing the injected volume and the length of tube through which the sample zone will travel. In order to obtain maximum sampling frequency it is necessary to prevent peak spreading as otherwise the sample solution would occupy an undue length of the carrier stream and would intermix with the next oncoming sample zone. An excessively small dispersed sample zone, on the other hand, would not be sufficiently mixed with the carrier stream of reagent and thus the chemical reactions would not take place.

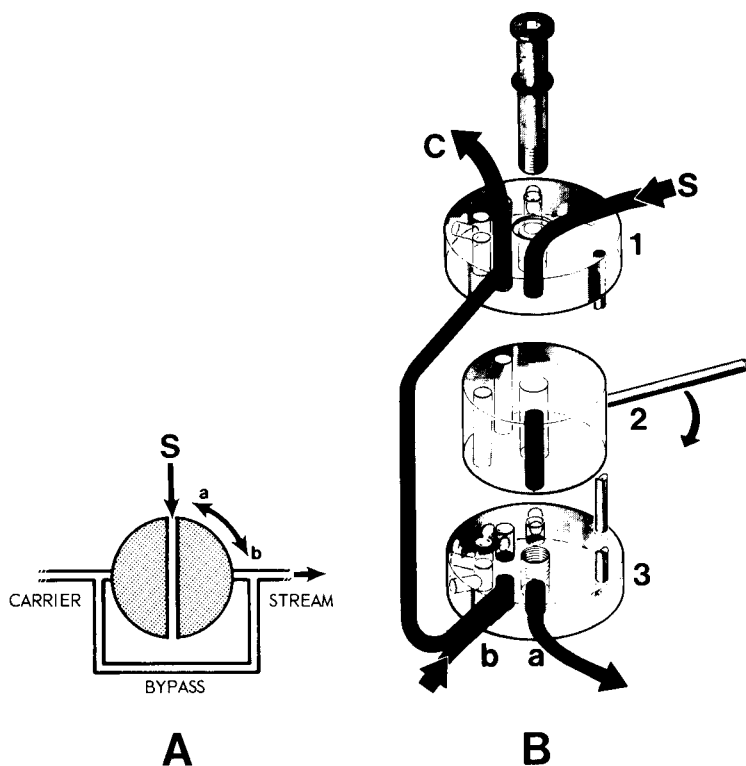


Fig. 3. (A) The principle of a simple rotary valve, the bore of which determines the injected volume. The valve is furnished with a bypass of higher hydrodynamic flow resistance than the volumetric bore so that the carrier stream can flow continuously through the manifold lines when the valve is turned from the inject (b) to the sampling (a) position. (B) Multi-injection valve consisting of a rotor (2) sandwiched between two stators (1 and 3), the whole system being clamped together by a bolt when assembled. The rotor (20 mm high) has three volumetric bores of which one is shown filled by sample solution S, the excess of which is drained through the bottom stator at (a). In the rotor position shown, the carrier stream C bypasses the rotor through a shunt, entering the valve through the bottom stator at (b). Thus, after turning the rotor (as indicated by the arrow), the precisely measured sample zone is swept by the carrier stream into the system, because the bypass conduit has a higher hydrodynamic flow resistance.

As the analytical readout in f.i.a. is obtained from the peak height, the dispersion D_t has been defined [20] (Fig. 4) as the ratio of the original analyte concentration C_0 to the concentration of the analyte in that element of fluid which corresponds to the maximum of the peak C^{\max} : $D_t = C_0/C^{\max}$. This means, that for $D_t = 2$, for example, the sample solution has been diluted 1:1 by the reagent carrier stream. For convenience, dispersion has been classified as limited, medium and large, and the flow injection systems designed accordingly have been used to accommodate various analytical methods (Tables 1–3).

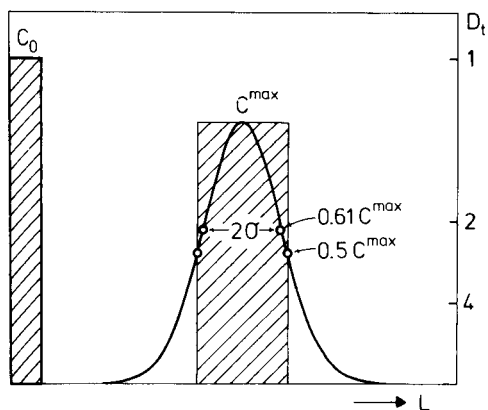


Fig. 4. Dispersion in the f.i.a. system. At the point of injection the sample solution is undiluted with a concentration C_0 through all its length, i.e. the injection has a square form. Dispersion causes the concentration to decrease to C^{\max} , as a function of the length travelled (L).

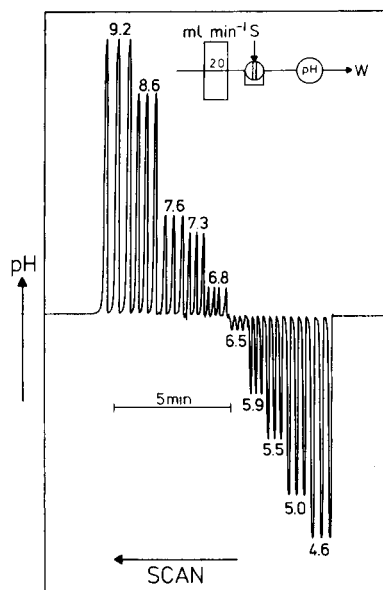


Fig. 5. F.i.a. system with limited dispersion used for rapid pH measurement, comprising a flow-through capillary glass electrode and a conventional calomel reference electrode [43]. The carrier stream is 2×10^{-4} M phosphate buffer in 0.14 M NaCl (pH 6.64), each sample ($30 \mu\text{l}$) being injected in triplicate (tube: 10 cm long, 0.5 mm i.d.).

An example of a design of a system with limited dispersion, in which the original composition of an undiluted sample solution is to be assayed, is the measurement of pH which can be performed at a rate of over 240 samples per hour with a reproducibility of 0.01 pH unit using a simple experimental setup (Fig. 5). As there is always only one sample in the system at a time, the measuring cycle, including the washout period, lasts only 15 s and the actual analytical readout is available less than 5 s after sample injection. The injected sample volume is $30 \mu\text{l}$ (or less) and the consumption of carrier stream (0.14 M NaCl— 1×10^{-4} M NaH_2PO_4 — 1×10^{-4} M Na_2HPO_4) per measurement is $500 \mu\text{l}$. The well defined flow geometry of the system, the reproducible sample injection and the exact timing allow simple measurements of peak heights instead of the time-consuming approach of measuring the “steady-state” signals.

Limited dispersion has also been used for the potentiometric determination of the calcium activity in serum or the so-called ionized fraction of calcium [21]. The calcium electrode was placed in a specially designed flow-

TABLE 1

Instrumental analytical methods and techniques used with f.i.a.

Method/technique	Reference
Amperometry	65, 74
Atomic absorption spectrophotometry	40
Chemiluminescence	79
Conductivity	77
Fluorimetry	28, 44, 75
Immunoassay	78
Potentiometry	1, 3, 16
pH and ion-selective electrode	8, 12, 13, 20, 21, 35, 47, 53, 55
Potential difference	26, 68
Titration	10, 41
Spectrophotometry	1, 2, 3, 4, 5, 13, 14, 15, 17, 18, 20, 21, 22, 24, 25, 27, 31, 48, 49, 50, 52, 54, 55, 57, 59, 61, 63, 66, 67, 68, 71
Colour-indicator (pH)	52, 63
Dialysis	6, 9, 52
Enzymatic analysis	9, 20, 60, 63
Extraction	19, 20, 22, 28, 38, 51, 56, 69, 70
Isothermal distillation	47
Differential kinetic	36, 42, 46, 62
Merging zones	23, 39, 40, 43, 45, 47, 58, 60, 61, 63
Multielement analysis	29, 76
pH-Gradient formation	29, 76
Refractive index	25, 77
Stopped-flow (kinetic)	20, 43, 59, 60
Titration	10, 57, 67
Turbidimetry/nephelometry	11, 18, 34, 72, 76
Viscosity	7, 77
Voltammetry (anodic stripping)	20, 37
F.i.a. with microprocessor	29, 63, 64, 67, 76, 77
F.i.a. theory	1, 20, 73

through cell, which also accommodated the reference electrode, and by incorporating a pH glass capillary flow-through electrode into the system it was possible to measure simultaneously the pH and pCa of the injected sample at a rate of ca. 100 samples per hour with high reproducibility.

Systems with medium dispersion are the most interesting from an analytical viewpoint as they encompass a large number of procedures, in which one or several reagents are mixed with the sample solution in order to form a coloured, fluorescent, electroactive or other product which then can be sensed by a flow-through detector (Tables 1–3). In this type of determination not only sufficient mixing must take place, but also sufficient time should elapse before the sample zone reaches the detector to ensure that the chemical reactions involved are allowed enough time to produce an adequate amount of coloured or other detectable product. Again, because of the high

TABLE 2

Flow injection references listed according to area of application

Area of chemical analysis	Reference
Agricultural	2, 3, 5, 8, 11, 12, 13, 16, 17, 22, 23, 35, 40, 44, 45, 47, 49, 50, 51, 55, 59, 60, 71
Pharmaceutical	7, 19, 26, 28, 34, 36, 37, 38, 44, 60, 62, 65, 66, 68, 69, 70, 74, 77, 78, 79
Clinical	6, 8, 9, 21, 39, 42, 43, 44, 46, 52, 53, 54, 60, 63, 78
Environmental	4, 8, 11, 12, 15, 18, 21, 24, 25, 27, 29, 31, 41, 48, 49, 50, 55, 56, 57, 71, 72, 76
Review articles	20, 30, 32, 33, 58, 60

reproducibility of the mixing and timing in the unsegmented stream, there is no need to reach chemical equilibrium in order to obtain valid analytical results. Here, however, lies the true limitation of the flow injection method, because if one chooses, say, 30 s as the maximum acceptable residence time of a sample in the system, then the chemical reactions may reach less than ca. 25% of their equilibrium signal within the residence time chosen, and this may not provide sufficient sensitivity for the particular analytical purpose. Surprisingly, very few spectrophotometric methods have so far been encountered where an insufficient change of absorbance, caused by a low reaction rate, has proved to be an obstacle. This has very probably happened because most analytical methods used in practice are based on fast reactions, and perhaps also because the samples in many manual methods often have become very diluted prior to actual measurement as it is more convenient in classical techniques to pipet and handle large volumes of liquids. In f.i.a. one can, if necessary, choose precisely a combination of minimum dispersion and maximum residence time that will exactly suit a particular chemistry.

Many simple colorimetric procedures can be automated by injecting a sample directly into a carrier stream of reagent (Table 1). An example of this approach is the determination of nitrite based on reaction with sulphanilamide forming a diazo compound which is subsequently coupled to *N*-(1-naphthyl)ethylenediamine yielding a strongly coloured dye, the absorbance of which is measured at 520 nm. The automated manifold for this purpose (Fig. 6A) has an injection valve (Fig. 3) which is integrated into one unit with the sample changer so that the aspiration tube is only 10 cm long. A bypass is used so that the system consists of two independent circuits, one for sampling and the other for performing the chemistry and measurement, both circuits being served by the same pump. A series of nitrite standards and various samples were analyzed by using two different pumping rates in the reagent line ($x = 4.0 \text{ ml min}^{-1}$ or $x = 1.4 \text{ ml min}^{-1}$) and by sampling either at 110 samples/h or 240 samples/h. The sampling line was operated by the same rate in all cases, though obviously lower pumping rate could have been used for lower sampling rate. The remarkable absence of carryover in three

TABLE 3

Species determined by f.i.a.

Species	Reference	Species	Reference
Acids, strong	10, 41, 57	Lead	20, 29, 34, 56
Albumin	39, 44	Magnesium	36, 40, 42, 46, 54, 62
Aliphatic amines	79	Manganese	50, 79
Aluminum	24, 45	Molybdenum	22, 51
Ammonia/ammonium	1, 3, 5, 13, 35, 47, 49, 55	Nitrate	8, 12, 13, 31, 35, 48, 55, 71
Ascorbic acid	20, 26, 37, 65	Nitrite	15, 18, 48, 55, 71
Cadmium	20, 34, 56	Nitrogen, total (inorg. and org.)	3, 5, 47, 55
Calcium	10, 21, 36, 40, 46, 54, 62	pH	20, 21, 53, 58
Carbon dioxide	52	Phosphate	1, 2, 5, 6, 13, 14, 23, 35, 57, 58
Chloride	4, 6, 14, 18, 57	Potassium	8, 13, 28, 40
Chromium	27	Proteins	3, 17
Cobalt	25	Silver	20
Copper	20, 25, 34	Sodium	8
Codeine	38	Strontium	36, 42, 62
Caffeine	19	Sulfate	11, 18, 72, 76
Corticosteroids	66	Sulfite/sulfur dioxide	16, 59
Gallium	75	Thiamine (Vitamin B ₁)	69
Glycerol	7	Urea	53, 58, 60, 63
Glycine	44	Vanadium	29
Glucose	9, 20, 43, 60	Water, in org. solvents	68
Iron	26, 74	Zinc	34

of the four presented runs (Fig. 6B) is a typical feature of a well designed flow injection system.

The previous examples have dealt with simple procedures where sample solution was injected directly into one carrier stream thus yielding a signal to be measured. Often, however, several chemistries have to be done sequentially as the reagent or the reaction products are incompatible. Initially, it was doubted that f.i.a. would be capable to accommodate such procedures requiring addition of further reagents downstream, because it was thought that the mixing at the confluence points would be either insufficient, or possibly excessive; in the latter case the carryover would become unacceptable. Since then, however, various sequential systems have been designed, such as the method for the determination of urea, which is based on enzymatic formation of ammonia, its oxidation to chloramine, coupling with phenol and subsequent measurement of indophenol blue; all of this is manageable in a relatively simple setup (Fig. 7) from which the analytical readout is available 20 s after sample injection.

The large dispersion may serve two different purposes, either to obtain a

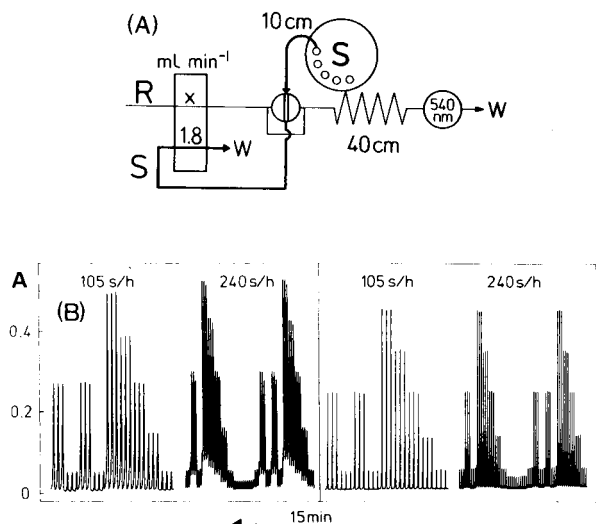


Fig. 6. (A) Automated f.i.a. manifold used for the determination of nitrite. The sample ($30 \mu\text{l}$) is aspirated from the sample changer (S) into the injection valve (Fig. 3B), the surplus going to waste (W). After injection the sample is mixed with the reagent stream (10.0 g of sulphanimide, 0.5 g of *N*-(1-naphthyl)ethylenediamine and 100 ml of phosphoric acid (85%) diluted to 1 l with water) in the coil (40 cm long) and then led to a flow-through optical cell and finally to waste (W). X denotes pumping rate (see B). Tubes in sampling and carrier stream lines were 0.5 mm i.d. (B) Calibration curves for nitrite obtained in the system shown at two different pumping rates of the carrier stream (X). Standard nitrite solutions containing 0.25 , 0.50 , 1.00 , 1.50 and 2.00 ppm N-NO_2 , are followed by a number of samples (all solutions injected in triplicate). Each run, lasting exactly 15 min , shows from left to right sampling rates of 105 and 240 samples/h at $X = 1.4 \text{ ml min}^{-1}$, followed by 105 and 240 samples/h at $X = 4.0 \text{ ml min}^{-1}$ ($S = 1.8 \text{ ml min}^{-1}$ in all cases). Note that the first and last runs use the appropriate pumping rate X, while the two runs shown in the centre have either too high carryover (left) or too high reagent consumption per analysis (right).

suitable sample dilution, or to produce a concentration gradient which extends over a well defined period of time. If the sample material is too concentrated to be directly assayed, rapid dilution can be effected simply by injecting a very small volume (1 to $5 \mu\text{l}$) into a system designed to yield for instance $D_t = 20$. As such a small injected sample zone is very short, it will, even when dispersed twenty times, pass through the flow cell in less than 5 s at a pumping rate of 1 ml min^{-1} , and therefore, the sampling frequency would be as high for this system with large dispersion as for the above-mentioned systems with limited and medium dispersion.

In other applications, however, it may be desirable to stretch the length of the sample zone so that the concentration gradients formed at the interface between the carrier stream and the sample zone might take 30 s or even more to pass through the flow cell. Examples of such an approach are the Flow Injection Titrations, where not the peak height, but the peak width is

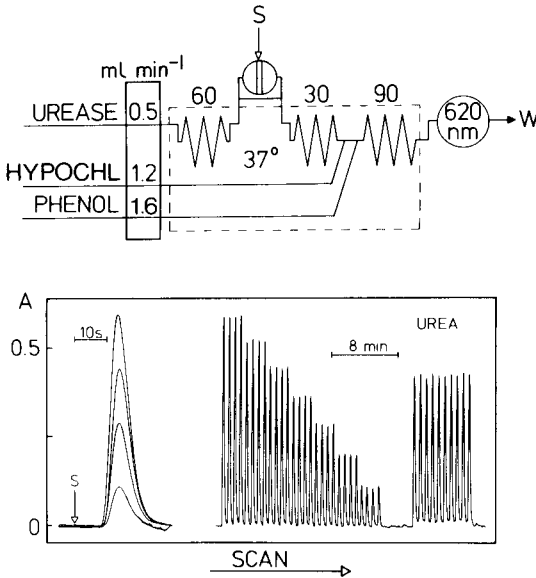


Fig. 7. F.i.a. manifold for determination of urea in serum where ammonia from the enzymatic conversion of urea is oxidized to chloramine and coupled with phenol, and the resulting indophenol blue is measured at 620 nm. The sample ($30 \mu\text{l}$) is injected at point S; all tubes are of 0.5 mm i.d.; tube lengths are stated in cm. The output on the left side is a series of peaks recorded from the same starting point (S) which confirms that regardless of the concentration of urea the whole measuring cycle is complete within 20 s after sample injection. The output on the right-hand side is from triplicate injections of a series of standards in the range 2–20 mM urea and ten injections of a serum sample containing a normal urea level.

measured (in time units); this width corresponds to the amount of titrant equivalent to the amount of analyte injected into the system [10, 57]. Thus, the f.i.a. system used for titration is built around a mixing chamber (Fig. 8) which provides not only the large dispersion of the sample, but also a strictly exponential concentration gradient because the chamber volume dominates the total volume of the system. For instance, when a sample of acid is injected into a carrier stream consisting of strong base and an indicator (e.g., bromothymol blue), the photometer will record a change from the basic (blue) to the acid (yellow) form of the indicator twice during each titration cycle (Fig. 8): first when the front of the sample zone passes through the detector, and second when the equivalence point, located on the falling "tail" of the peak, leaves the flow cell. The time interval between the two colour changes t_{eq} , therefore increases with the concentration of the acid in the injected sample (C_{acid}) and it can be shown that:

$$t_{\text{eq}} = (V/v) \ln 10 \log C_{\text{acid}} - (V/v) \ln 10 \log C_{\text{base}}$$

where V is the volume of the mixing chamber, v is the pumping rate, and

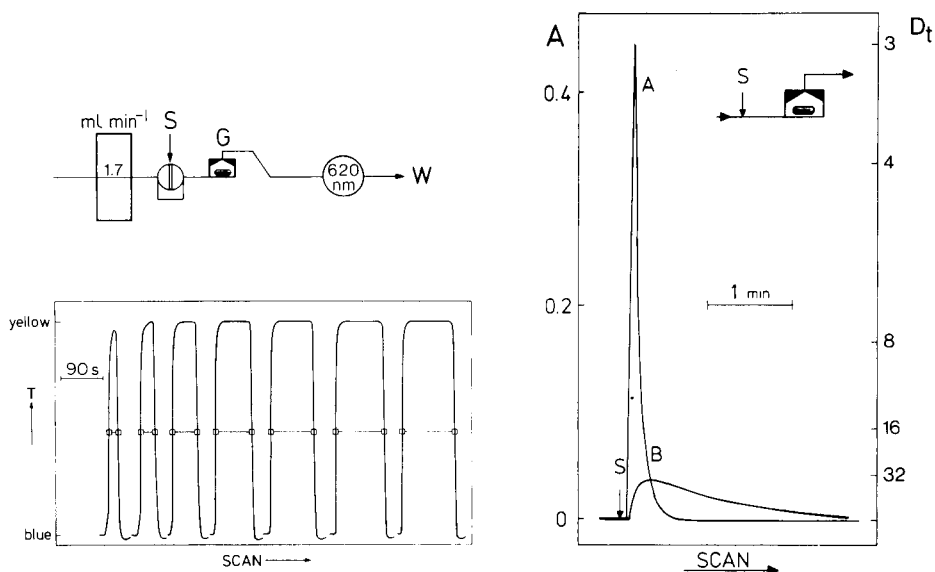


Fig. 8. F.i.a. titration of acid with base. The manifold (top) comprises a mixing chamber having a volume of 1 ml (G), where a well defined concentration gradient is formed of the injected acid sample zone within the alkaline carrier solution containing the indicator. The change of the indicator colour from blue to yellow is monitored as shown in the record below. The time interval (t_{eq}) between the two square points on the ascending and descending parts of each curve is the measure of the concentration of the injected sample (for details see text).

Fig. 9. The influence of a mixing chamber on the dispersion of a 50- μ l sample of a dye injected into a f.i.a. system consisting of 50 cm of 0.5 mm i.d. tubing without (curve A), and with (curve B) a mixing chamber having a volume of 1.9 ml; pump rate 1.5 ml min⁻¹ in both cases. (S is the point of injection, D_t is the total dispersion of the sample in the system.)

C_{base} is the concentration of the base (in the carrier stream) which reacts with the injected acid in a 1:1 stoichiometric ratio.

Exploitation of such concentration gradients seems to be one of the most interesting aspects of f.i.a., as in principle it becomes possible to extract several items of information from one injected sample zone. Based on this concept a mixture of metal ions was analysed by measuring the extent of colour formation with the PAR reagent along an elongated pH gradient [30].

Unless, however, that there is a need to create a concentration gradient, which is stretched in time, i.e., in cases where it is not the peak height but the peak width which is to give the analytical information, the use of a mixing chamber should be strongly discouraged as its presence not only greatly diminishes the sampling frequency but also dramatically decreases the recorded peak height. Thus, a simple dispersion experiment, performed on a zone of injected dye in a system without (Fig. 9, curve A) and with a very small mixing chamber (Fig. 9, curve B), shows the substantial decrease

in the peak height and in the sampling frequency caused by increased dispersion. In this context it should be emphasized that it is not only the mixing chamber *per se* which should be avoided but also dead volumes of any kind in the system caused by, e.g., a poorly designed injection port, bad connections between coils, and the use of a flow-through cell with excessive capacity.

CHEMICAL SEPARATIONS

The f.i.a. systems described above were designed to handle one-phase systems consisting of one or several aqueous carrier streams. It was therefore a significant advance when Karlberg [19] and Bergamin et al. [22] independently designed a f.i.a. system for solvent extraction capable of mixing and separating two immiscible liquids. This technique proved to be very efficient and has become successfully adapted in pharmaceutical control [38, 69, 70].

As an example, the aqueous sample is injected into an aqueous carrier stream (Fig. 10) to which at (a) the organic phase is continuously added, and after passing through the extraction coil (b), the phases are separated at point (c) and further carried through the flow cell for continuous measurement. The key to successful performance of this method, which has a standard deviation of less than 1%, is the extreme regularity with which small droplets of organic phase are dispersed within the carrier stream and collected for spectrophotometric measurement free of any trace of aqueous phase. The truly ingenious design of the dispersing and separating devices can be found in the original work of Karlberg et al. [19].

Though solvent extraction so far has been employed in connection with spectrophotometry and fluorimetry (Table 1) (interestingly, in the latter

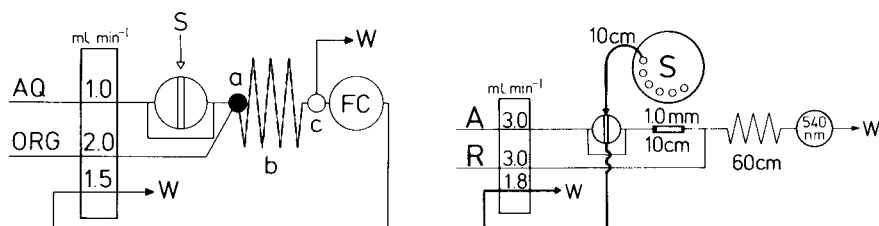


Fig. 10. F.i.a. manifold for the determination of trace metals by solvent extraction with dithizone in CCl_4 . The aqueous sample (S) is injected into the aqueous carrier stream (AQ) to which at (a) the organic phase (ORG) is continuously added and after passing through the extraction coil (b), made of teflon tubing, the organic phase is again separated at point (c) and further carried through the flow cell for spectrophotometric measurement.

Fig. 11. Automated f.i.a. manifold used for the determination of nitrate by reduction to nitrite with spectrophotometric detection (Fig. 6). The sample ($30 \mu\text{l}$), aspirated from the sample changer (S), is injected into a 0.25 M acetate solution of pH 6.0 (A) and then carried to the reduction column filled with small zinc chips. The nitrite produced is then mixed with the colour-forming reagent solution (R) (see Fig. 6). All tubing 0.5 mm i.d.

case the organic phase was not separated from the aqueous phase prior to measurement [28], it should be very rewarding to use solvent-extraction f.i.a. systems in connection with atomic absorption.

Gas diffusion from a donor stream into an acceptor stream, where two streams run in parallel separated from each other by a suitable membrane, is a well known, highly selective technique, frequently used in air-segmented continuous flow systems. In unsegmented streams the diffusion unit can be much miniaturized and the flow rate considerably reduced. For ammonia measurements, microporous teflon membranes are the most suitable, while nonporous silicone rubber or cellophane membranes have been used for measurements of carbon dioxide [52]. The absorbed gas changes the pH of the acceptor stream and this can be most conveniently measured spectrophotometrically via an acid-base indicator, the change in absorbance being proportional to the logarithm of the concentration of analyte. However, by adding a mixture of appropriately selected indicators to the acceptor stream and ensuring that its buffering capacity is maintained at a constant level, the change of absorbance will be a linear function of the concentration of analyte, thus greatly enhancing the precision of measurement [63]. Most recently an ingenious isothermal distillation system was designed for f.i.a. [47] in which the diffusion membrane is replaced by an air gap.

SYSTEMS WITH A COLUMN

As the f.i.a. apparatus is, in contradistinction to chromatographic setups, a low-pressure system operated by a simple peristaltic pump, the use of solid particles in the form of columns is restricted to very short units. Furthermore, whereas the purpose of the column in chromatography is to separate each individual sample into several separate components, the column in the f.i.a. system is designed to perform the same chemistry on each individual sample with the aim of producing a detectable species. The column material might thus contain an insoluble enzyme, an oxidant or a reductant. As an example of such an approach may serve the determination of nitrate which is done colorimetrically after reducing nitrate to nitrite on a column filled with particles of a reducing metal [48, 71]. An automated f.i.a. system equipped with a column filled with small zinc chips (Fig. 11) is capable of operating at a sampling rate of 180 samples per hour, with the analytical readout available within 15 s of sample injection (Fig. 12). There are two interesting features of this approach: first, it is possible to design the column in such a way that the dispersion of the sample zone is kept at a minimum, permitting a complete washout of the system within 20 s after sample injection. Despite the short residence time, the efficiency of the reduction of nitrate to nitrite is 5% for the sampling rate of 180 samples/h and 45% when the system was operated at correspondingly lower pumping rates ($A = R = 1.2$ ml min⁻¹), at 90 samples/h; thus by decreasing the sampling frequency by

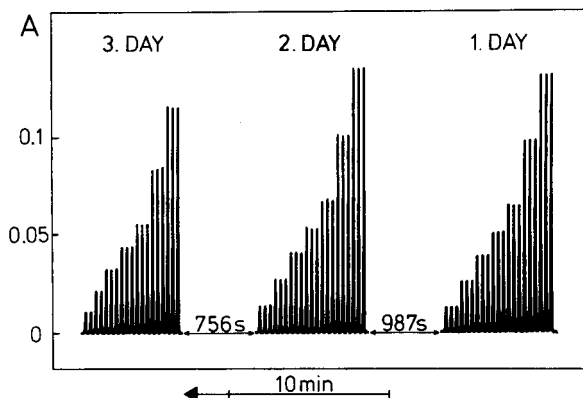


Fig. 12. Long-term stability test of the nitrate reduction column used in the system shown in Fig. 11. A series of 7 samples (1.0, 2.0, 3.0, 4.0, 5.0, 7.5 and 10.0 ppm N-NO₂), each in triplicate, were placed in the sample changer and the system was then operated continuously for 6 h every day over a period of 3 days (sampling rate 180 samples/h). Only during the 3rd day did the column show signs of gradually reduced efficiency.

a factor of 2 the sensitivity of measurement is increased almost 10 times. The other interesting aspect is that the life-time of the column in terms of days, and in terms of numbers of analyses performed (Fig. 12), is prolonged compared to conventional "steady-state" operation because the exposure time to the sample solution is shorter and the wash periods are longer.

STOPPED FLOW AND F.I.A. SYSTEMS WITH INTERMITTENT PUMPING

One of the most important findings of f.i.a. theory [20] has been that in order to increase the residence time one should decrease the velocity of the carrier stream rather than increase the length of the reaction coil, because the latter technique leads to increased dispersion (cf. Fig. 2) whereas lower pumping rates result in less dispersion. Should the carrier stream cease to move, then dispersion of the sample zone will cease (except for a negligible contribution from molecular diffusion) and D_t will become independent of time. Thus by applying intermittent pumping, reaction time can be gained during the stop interval when the carrier stream does not move.

If the sample zone is stopped within the flow cell itself, it is possible to record the change of, say, absorbance, caused by the reaction between the sample component and the reagent constituting the carrier stream. The obvious prerequisite for success of such a reaction rate measurement is that movement of the carrier stream can be exactly controlled from the operational pumping rate used to complete standstill, and that always the same section of the sample zone can be reproducibly held within the flow cell for measurement. In practice this is best achieved by using an electronic timer (T, Fig. 13) which is activated by a microswitch connected to the

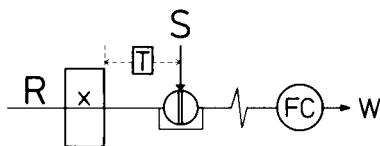


Fig. 13. Simple stop-flow f.i.a. manifold. When the sample (S) is injected, the electronic timer (T) is activated by a microswitch positioned on the injection valve. The time from injection to stopping of the pumping (delay time) and the length of the stop time can both be preset on the timer.

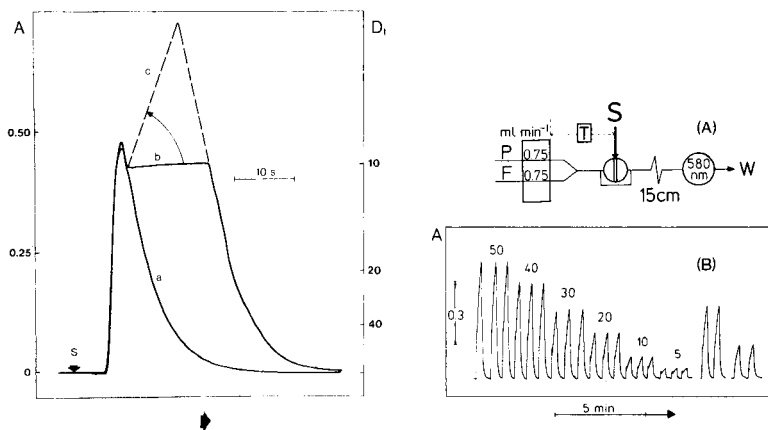


Fig. 14. The principles of the stop-flow f.i.a. method demonstrated by injecting a dye sample into a colourless carrier stream and recording the absorbance in a flow-through cell. All curves recorded from the same point (S) by injecting $26 \mu\text{l}$ of the same dye: (a) continuous pumping; (b) 9 s pumping, 14 s stop and continuous pumping again; (c) hypothetical line corresponding to any chemical reaction during the 14-s stop interval.

Fig. 15. (A) F.i.a. manifold for stop-flow determination of SO_2 in wine. The sample ($10 \mu\text{l}$) is injected into a carrier solution of pararosaniline (0.08% in 0.3 M H_2SO_4) to which is added a solution of formaldehyde (0.5% in 0.3 M H_2SO_4) which catalyzes the reaction. After mixing in the 15-cm (0.5 mm i.d.) coil, the sample zone is stopped in the flow-through cell for measurements. (B) Calibration record for sulphur dioxide with the system in (A). The concentrations are given in ppm SO_2 . The delay time was slightly longer than the residence time, i.e., the samples were stopped shortly after the peak maxima had been passed. As the stop time was identical in all cases (15 s), the analytical result corresponds to the peak increase during the stop interval. To the right are shown recordings for determination of the free sulphur dioxide contents in two white wines (Touraine Blanc, 29 ppm; and Gumpoldskirschner, 1977, 18 ppm).

injection valve. Thus any delay time as well as any length of stop time can be chosen so that it suits the chemical reaction rate involved. The performance of an f.i.a. system made for this purpose was tested by injecting a solution of a dye and by measuring the absorbance when pumping continuously (Fig. 14a) and then during a stop-flow cycle (Fig. 14b). The horizontal portion of the curve recorded during the stop period confirms

the feasibility of this type of measurement; the dotted line (c) indicates the record that would have been obtained if a chemical reaction had taken place. Rate measurements are often used in clinical chemistry and therefore the enzymatic assay of glucose based on the use of glucose dehydrogenase coupled to the spectrophotometric measurement of the coenzyme NADH became the first chemistry incorporated into a stopped-flow f.i.a. system [43].

Another interesting example is the determination of sulphur dioxide in wine, based on the well known West—Gaeke [81] method in which the pink compound formed by the reaction between pararosaniline and sulphur dioxide, and catalyzed by formaldehyde, is measured at 580 nm. While sulphur dioxide (which is always present in wine as a preservative) can be determined in samples of white wine by simple direct measurements, the colour of red wines interferes, especially because different wines provide variable blanks. This, however, can be corrected for each individual sample by measuring the increase of absorbance caused by the sulphur dioxide—pararosaniline reaction while the sample zone is stopped within the flow-through cell (cf. Fig. 14). As the premixed reagent is not stable in time, the simplest stop—flow system (Fig. 13) had to be slightly modified (Fig. 15A) to accommodate two reagent lines. This arrangement allowed the sulphur dioxide to be determined in wines at a rate of 105 samples/h with the analytical readout available 23 s after sample injection (Fig. 15B).

It is interesting that the stop—flow technique can utilize any section of the dispersed sample zone, i.e., by monitoring not only the peak maximum, but any segment on the tailing portion (Fig. 16, curves a—e). At the top of the peak the sample/reagent ratio corresponds to D_t , but this ratio will gradually change along the tail and so will the rate of the reaction, consequently causing different slopes of the rate curves. Hence, the dispersion along the length of the peak zone can be exploited in order to discover the section of the sample zone in which the sample/reagent or sample/enzyme ratio is most suitable for the particular assay, without the need to change any other feature of the f.i.a. system. Thus, in contrast to conventional stopped flow systems in which sample and reagent solutions are completely mixed by force in a special chamber, the stop—flow injection method readily allows adjustment to obtain optimum measurement conditions. Also, mixing takes place in the simple tubing without any special auxiliaries, so that the apparatus is simple to construct, and the stop—flow method is obviously less demanding on reagent consumption than the continuous flow approach. It should, however, be pointed out that if the rate of the sample zone dispersion is slower than the rate of the chemical reaction involved, the result will be distorted, and therefore f.i.a. is unsuitable for extremely fast reaction rate measurement.

Another aspect of operating a flow injection system with intermittent pumping becomes apparent when two pumps are used in such a way that they operate at different time intervals in a prefixed time sequence. The simplest use of such a system is to increase the sampling frequency by

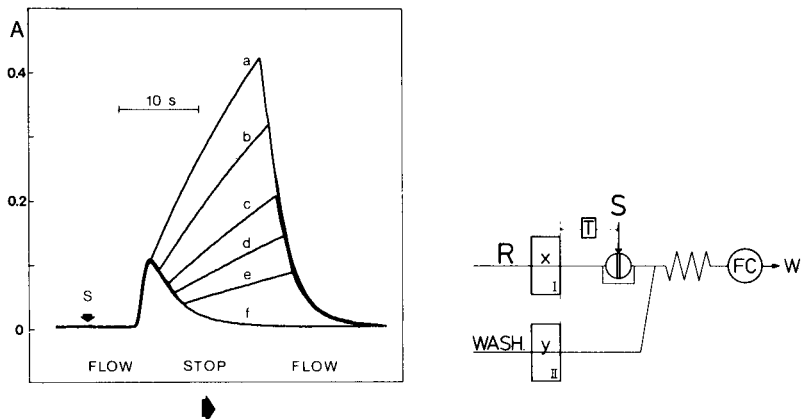


Fig. 16. Stop—flow analysis for glucose [43] showing the influence of increasing stop delay time on the slope of the reaction curve. The stop period of 15 s started after sample injection (S) within: (a) 7.8 s; (b) 8.8 s; (c) 9.8 s; (d) 10.8 s; and (e) 11.8 s (curve f corresponds to continuous pumping). The sample volume was 26 μ l; glucose concentration 10 mM; manifold Fig. 22.

Fig. 17. F.i.a. system operated with intermittent pumping. The sample (S) is injected into the reagent stream (R) propelled by pump I. After the peak maximum has been recorded by the detector, pump I is stopped and pump II is activated to wash the sample out of the system (pumping rate $y > x$, c.f. Fig. 18). After a preset time, pump I is restarted and pump II stopped, thus permitting a new sample injection. All lines are 0.5 mm i.d.; the line length from the point of injection to the T-joint is 25 cm, and from there to the flow cell 75 cm.

increasing the wash-out speed of a coil and a flow cell by stopping the first pump and starting the second one immediately after the top of the peak has been measured. This is simply achieved by using a f.i.a. system such as that depicted in Fig. 17 where the first pump of slower pumping rate delivers the reagent stream while the second pump, having a higher pumping rate, delivers only wash solution (water). Thus, immediately after the peak maximum has passed the detector, the first pump is stopped and the second one is operated until the next sample is injected into the system. This approach allows an increase of the sampling frequency (Fig. 18) and greatly economizes on reagent solution.

THE MERGING ZONES PRINCIPLE

High reagent consumption is a main disadvantage of all continuous flow systems which, in contrast to batch analyzers, use the reagent continuously even when no sample is present in the apparatus — notably during the start-up and shut-down procedures, as well as through coffee breaks. This problem is less serious in f.i.a. where the volume of the sample path is seldom larger than a few hundred microlitres, and is therefore easy to fill and wash in less than 1 min with small amounts of reagent or wash solutions. If, however, an

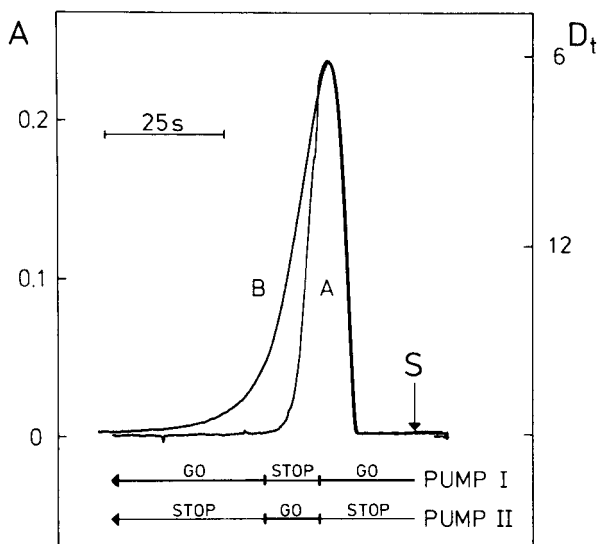


Fig. 18. Curve (A) was obtained with the intermittent pumping system in Fig. 17 by injecting $20 \mu\text{l}$ of a coloured dye solution. Pumping rates: $x = 0.9 \text{ ml min}^{-1}$; $y = 4.0 \text{ ml min}^{-1}$. As the residence time of the sample in the system was 18 s , pump I was operated for a preset time of 19.9 s while pump II was stopped; then pump I was stopped and pump II operated for a preset period of 12 s to flush out the sample, whereupon pump I was reactivated and pump II stopped. This allows the sampling rate to be approximately doubled compared to continuous pumping of pump I alone (curve B).

expensive reagent or an enzyme is used, it is wasteful to pump these solutions continuously, because the reagent occupies the entire flow system.

The merging zone principle avoids this uneconomical approach by injecting the sample and introducing the reagent solutions in such a way that the sample zone meets the selected section of the reagent stream in a controlled manner, while the rest of the system is filled with wash solution or only pure water. This can be achieved in two different ways (Fig. 19A and B), by intermittent pumping [61] or by the use of a multiple injection valve [23, 39, 43].

The merging zones system based on intermittent pumping is shown in Fig. 20 where two pumps are operated in such a way that when pump I is in go position, pump II is in stop and vice versa. Thus the sample zone can be first brought from the injection port by means of a pump I, then at a chosen distance from the merging point pump II can be started which still brings the carrier stream forward while the reagent is being added (cf. Fig. 19A); after the sample zone has passed the merging point, pump I can be reactivated while pump II is stopped again. This approach allows the length of the reagent zone to be regulated simply by choosing different go and stop periods on the timer, and makes it possible to create different concentration gradients on the interface between the sample zone, reagent solution and carrier stream (Fig. 21).

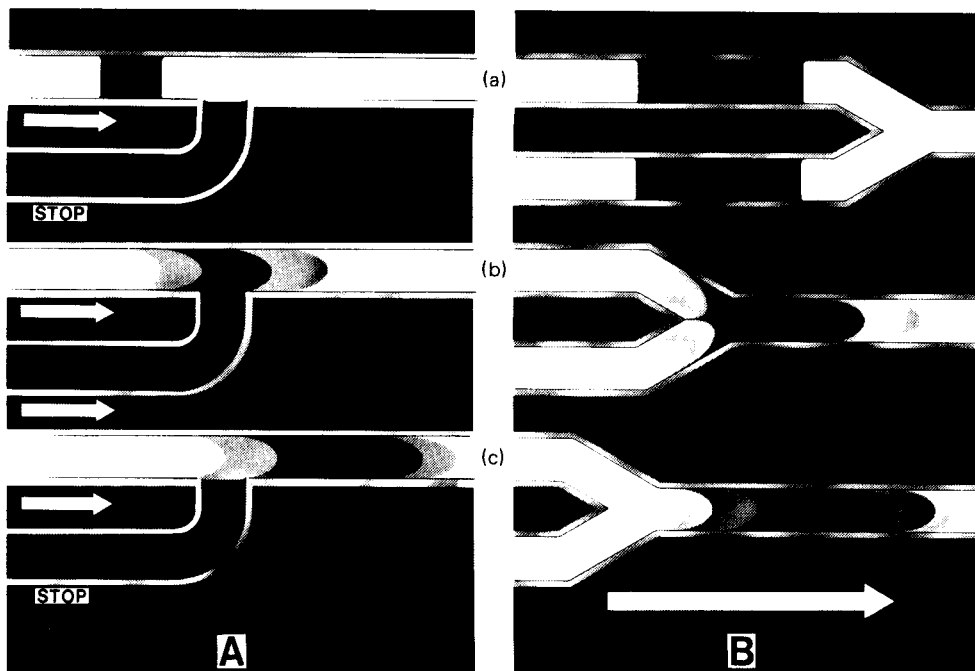


Fig. 19. (A) Merging zone system with intermittent pumping: (from top) (a) the sample zone is injected into line I and propelled forward (by pump I) by an inert carrier solution, while pump II controlling the reagent solution, is stopped. When the sample zone has reached the merging point (b), pump II is activated, delivering reagent, and pump I is stopped. After addition of reagent, pump I is reactivated and pump II stopped. (B) Synchronous merging of two zones in a symmetrical system with continuous pumping: (from top) (a) equal sample and reagent volumes are injected, (b) merge with identical velocities after passing through equal lengths of tubing, and (c) continue downstream while being mixed and dispersed into the carrier stream.

Bergamin et al. [23] and Mindegaard [39] independently suggested the use of a multi-injection valve and demonstrated that the f.i.a. merging zone approach is feasible. The purpose of using a valve, such as that shown in Fig. 3B, is to inject sample and reagent zones into two separate carrier streams pumped at the same speed (Fig. 19B and Fig. 22) which then meet in a controlled manner. As distilled water (or diluted buffer-detergent mixture) might be used as carrier in both streams, the reagent volume consumed per determination may be as little as $30 \mu\text{l}$ [43]. The carrier streams can be pumped continuously — for single point measurements — or intermittently, for stop-flow rate measurements. In fact, the above-mentioned stop-flow glucose measurements [43] were done by using the merging zone system depicted in Fig. 22. The enzyme consumption, about half an enzyme unit per sample, was about twenty times lower than that of the corresponding AutoAnalyzer method, and the analytical result was available 30 s after injection of $10 \mu\text{l}$ aqueous standard or serum sample solutions [43].

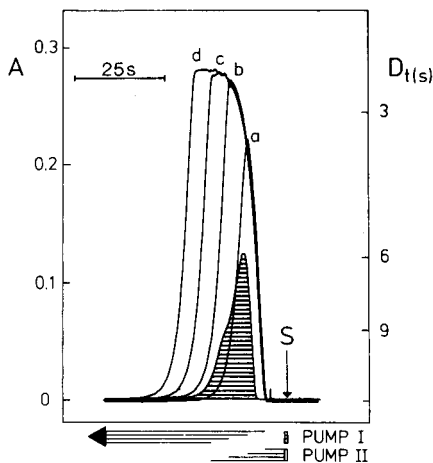
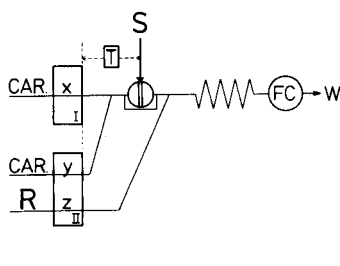


Fig. 20. F.i.a. manifold for merging zones system based on intermittent pumping (cf. Fig. 19A), operated so that when pump I is in the GO position, pump II is on STOP, and vice versa. After sample injection ($20 \mu\text{l}$) and a preset delay, the timer (T) stops pump I and activates pump II. Reagent is added at $z \text{ ml min}^{-1}$, while the sample zone is carried forward at $y \text{ ml min}^{-1}$ by pump II. After a preset time, pump II is stopped and pump I is reactivated. All lines 0.5 mm i.d. ; tube length from injection point to T-joint 25 cm ; from there to the flow cell (including the coil) 75 cm .

Fig. 21. Trace obtained with the f.i.a. system in Fig. 20 demonstrating the merging zones principle with intermittent pumping. Pumping rates: $x = 2.0 \text{ ml min}^{-1}$, $y = z = 1.0 \text{ ml min}^{-1}$. The shaded peak was recorded by injecting $20 \mu\text{l}$ of bromothymol blue solution ($1.0\% \text{ w/v}$) into a colourless carrier stream, pumped by all three lines x , y and z . Next, colourless solution was injected as well as pumped by lines x and y , while a bromothymol blue solution ($0.5\% \text{ w/v}$) was pumped through line z . A delay time of 0.3 s was used in all experiments, but pump II was activated for increasingly longer periods: (a) 5 s , (b) 10 s , (c) 15 s , (d) 20 s . The reagent zone broadens over the sample zone, until a "reagent steady-state" (where $D_R = 1$) is reached. Obviously pumping for 10 s (curve b), corresponding to $166 \mu\text{l}$ of reagent per sample, is more than sufficient to cover the shaded sample zone.

The merging zone concept might, if applied to a wider range of enzymatic assays, reverse the present trend towards the use of insolubilized enzymes, not only because of the high sampling rate and instant response of the f.i.a. system, but also because rate measurements and blanking are not so readily accomplished in systems where enzymes are fixed in the form of columns or tubes.

The drawback of the merging zones approach is that a variable baseline signal will affect the measurement unfavourably if the injected reagent zone alone is sensed by the flow-through detector. Thus in spectrophotometry the reagent should be colourless or at least should not absorb significantly at the wavelength at which the reaction product is being monitored. The most interesting aspect of the merging zones approach is its great versatility when accomplished by intermittent pumping (Figs. 18, 19A and 21). By

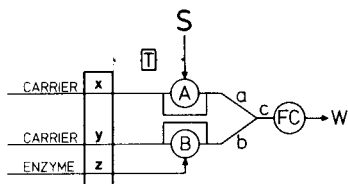


Fig. 22. F.i.a. manifold for the synchronous merging of two zones in a symmetrical system as used for determination of glucose [43] where the carrier stream is pumped at equal rates in lines x and y (1 ml min^{-1}) through tubes of equal length ($a = b = 10 \text{ cm}$, i.d. 0.5 mm). The merged zones are then transported through line c (30 cm long, 0.75 mm i.d.) to the flow cell (FC). The sample is injected at S through port A, while the reagent (enzyme) is injected through port B to which the reagent (enzyme solution) is transported through the line z . The volume of injected reagent (enzyme) was $26 \mu\text{l}$, while the sample volume was 26 or $10 \mu\text{l}$ depending on the required sensitivity. T denotes the electronic timer.

choosing different lengths of reagent zone, it is possible to obtain individual blanks for the reagent alone, sample alone as well as the rate of formation of the reaction product.

DEVELOPMENT OF F.I.A. PROCEDURES

It is an interesting experience as well as a challenge to adapt an existing analytical method to a f.i.a. system. When searching for a suitable chemistry for a given determination, a great deal of inspiration is to be found in the older as well as the more recent literature on colorimetry and spectrophotometry and in newer works on fluorimetry and luminescence. Naturally, fast chemical reactions, which can be accommodated in the simplest f.i.a. system, ought to be tried first, and no efforts should be spared in trying to increase the reaction rate by changing the reaction medium, by applying heat or by using catalysis. As a rule of thumb, any colour-forming reaction which yields an observable change in colour in a test tube within a minute of mixing the sample and reagent solutions should be adaptable for f.i.a.; in contrast to manual procedures, it is not essential that the reactions used in a f.i.a. system attain chemical equilibrium and the reaction product does not have to be stable for more than, say, 1 min. For the same reason, the conditions of manual procedures, such as pH, which may have been chosen to ensure the stability of the reaction product rather than to increase the initial reaction rate, may often serve merely as guides rather than represent optimal conditions for an f.i.a. procedure. Therefore, following an initial "test tube" test, a simple manifold must be constructed in which the influence of the coil length, pumping rates, and reagent concentrations as well as the sample volume should be further investigated.

The influence of pH is best investigated by the f.i.a. scanning method, the principle of which is shown in Fig. 23 for a study of solvent extraction of metal dithizonates [56], where the pH of the carrier stream is continuously altered by means of potentiostatic control. Thus, by injecting a number of

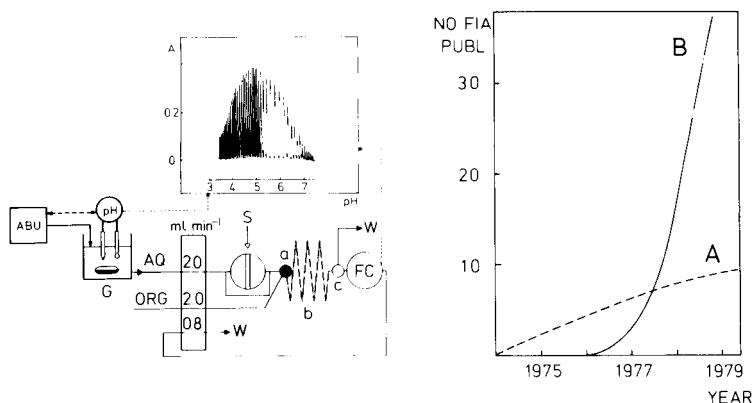


Fig. 23. The f.i.a. scanning method, illustrated by the solvent extraction of lead by 1×10^{-4} M dithizone solution in carbon tetrachloride. The pH in the gradient vessel G, originally containing 1×10^{-3} M HNO_3 , is gradually changed via a potentiostatically-controlled pH electrode by adding 0.1 M NaOH from an autoburette (ABU). Thus an aqueous carrier stream (AQ) of gradually changing pH is pumped to the sampling valve (S) where $30\text{-}\mu\text{l}$ aliquots of 1×10^{-4} M $\text{Pb}(\text{NO}_3)_2$ solution are injected at regular intervals. After extraction with organic phase (ORG) and phase separation (point c), the absorbance (A) of the extracted lead dithizonate is continuously measured at 520 nm in the flow cell (FC). The pH and the absorbance are simultaneously fed to an x-y recorder, the output of which is shown atop the figure. Less than 25 min is needed for this complete investigation.

Fig. 24. Number of f.i.a. papers published per year since 1974 — when the technique was first introduced — by the research group of this Department (line A) and by others (line B). The latter line is not fully drawn at the end as it includes only the references listed at the end of this paper.

samples of identical analyte content (10^{-4} M $\text{Pb}(\text{NO}_3)_2$ in the example shown), and by recording the absorbance of the extracted species on the vertical axis and simultaneously recording the pH on the horizontal axis of an x-y recorder, it is possible to obtain, in less than 30 min, the pH profile of the extraction procedure, which would require at least ten times more chemicals and time to investigate by manual methods. The catalytic activity of enzymes, the influence of pH on ion-selective electrode measurements and numerous other investigations can be done even faster in a similar way, as they do not involve mixing and separation of two immiscible phases. Admittedly, in this type of flow injection scanning, the true equilibrium conditions are not measured, because the sample residence time in the system is too short, but the measurements reflect correctly the conditions in that dynamic situation valid for that particular f.i.a. manifold, and therefore yield the optimum conditions for automated determinations.

In this context, it is appropriate to mention the advantages of using micro-computers in connection with the development of chemistries for f.i.a. systems and in processing the read-out signals from the f.i.a. systems. An example of

choosing the optimum buffer composition for an indicator—buffer system with a linear pH response is the work on enzymatic analysis [63], recently completed in this laboratory, in which programmes for automatic measurement of buffering capacity and digital readout at peak maximum are described. With regard to controlling the functions of the f.i.a. system and the timers which control the pumps for intermittent pumping, conventional electronic circuits have hitherto been employed. Yet, for this purpose also, the use of a hobby-type microcomputer, such as the Commodore PET, offers advantages in providing greater flexibility, primarily because of the easy reprogramming of the system.

FUTURE DEVELOPMENTS

The versatility and simplicity of the f.i.a. systems will possibly lead to a significant change of attitude towards automation in the analytical laboratory where the use of an automated system is still viewed as justifiable only when large numbers of samples of the same type have to be analyzed daily. Yet, it is worthwhile to analyse even small numbers of samples with a simple system which can be started and closed down in a few minutes, and which can be easily reprogrammed from one type of analysis to another.

It might be objected that such a change of attitude should have happened 20 years ago, when segmented continuous flow analysis was introduced. Yet, the use of air-segmented systems remained confined to the routine assay of many samples, either because of the slowness of response, bulkiness, or cost of the instrumentation, or because the philosophy of ready-made automated procedures did not appeal to pedagogic and research-oriented university chemists. The enthusiasm with which f.i.a. experiments have been greeted by undergraduate and graduate students in this Department [57], the recent increase in publications dealing with new f.i.a. methods (Fig. 24), as well as the present symposium indicate that such a change of attitude is now taking place.

How soon this change will reach the routine laboratory depends entirely on when a well designed, fully automated f.i.a. instrument becomes commercially available, because, as experience has shown in the past, no instrumental method has become widely used until, say, a reliable polarograph or atomic absorption spectrophotometer could be purchased. It is, however, very important that the f.i.a. instrument should fulfil certain minimum requirements as to the degree of dispersion, residence time, sample and reagent consumption, and maximum size (it certainly should not be larger than a typewriter); otherwise it would not reach the sampling frequency and yield the almost instantaneous response which are the main features of a well designed f.i.a. system.

Even more has to be done on the theoretical side, where the dispersion of the sample zone must be investigated in much greater detail. Very little is known about the microstructure of the concentration profiles when the sample zones merge, pass sharp bends and change velocity or direction. The

theory of dispersion, although very useful, is far from exact and complete. Its further pursuit will allow better understanding of the concept of controlled dispersion, which is entirely new in analytical chemistry, where complete mixing of sample and reagent solutions was thought to be a necessary prerequisite for performing a chemical assay. Only deeper theoretical studies will lead to design of even more advanced continuous flow techniques, which, together with the numerous different techniques discussed in this paper, will allow chemical analyses to be performed in new ways.

The authors express their appreciation to Inge Marie Johansen and Flemming Mikkelsen for conscientious technical assistance; to Anders Ramsing for stimulating discussions; to Susanne Helmark, Ove Broo Sørensen and Eva Thale for help in preparing the figures; and to the Danish Council for Scientific and Industrial Research, the Danish Natural Science Research Council and the International Atomic Energy Agency, Austria, for financial support.

REFERENCES

- 1 J. Růžička and E. H. Hansen, *Anal. Chim. Acta*, 78 (1975) 145 (Danish Patent Application No. 4846/74, Sept. 1974; U.S. Patent No. 4,022,575).
- 2 J. Růžička and J. W. B. Stewart, *Anal. Chim. Acta*, 79 (1975) 79.
- 3 J. W. B. Stewart, J. Růžička, H. Bergamin Filho and E. A. Zagatto, *Anal. Chim. Acta*, 81 (1976) 371.
- 4 J. Růžička, J. W. B. Stewart and E. A. Zagatto, *Anal. Chim. Acta*, 81 (1976) 387.
- 5 J. W. B. Stewart and J. Růžička, *Anal. Chim. Acta*, 82 (1976) 137.
- 6 J. Růžička and E. H. Hansen, *Anal. Chim. Acta*, 87 (1976) 353.
- 7 D. Betteridge and J. Růžička, *Talanta*, 23 (1976) 409.
- 8 J. Růžička, E.H. Hansen and E. A. Zagatto, *Anal. Chim. Acta*, 88 (1977) 1.
- 9 E. H. Hansen, J. Růžička and B. Rietz, *Anal. Chim. Acta*, 89 (1977) 241.
- 10 J. Růžička, E. H. Hansen and H. Mosbaek, *Anal. Chim. Acta*, 92 (1977) 235.
- 11 F. J. Krug, H. Bergamin Filho, E. A. G. Zagatto and S. S. Jørgensen, *Analyst*, 102 (1977) 503.
- 12 E. H. Hansen, A. K. Ghose and J. Růžička, *Analyst*, 102 (1977) 705.
- 13 E. H. Hansen, F. J. Krug, A. K. Ghose and J. Růžička, *Analyst*, 102 (1977) 714.
- 14 J. Růžička, E. H. Hansen and H. Mosbaek, *Anal. Chem.*, 49 (1977) 1858.
- 15 S. Storgaard-Jørgensen, H. Bergamin Filho, E. A. Zagatto, F. J. Krug and S. R. B. Bringel, *Boletim Cientifico No. 047 (1977)*, CENA/ESALQ/USP, Brazil.
- 16 H. Bergamin Filho, F. J. Krug, E. A. G. Zagatto, H. Fonseca, M. Graner, J. N. Nogueira and A. V. R. O. Annicchino, *Boletim Cientifico No. 049 (1977)*, CENA/ESALQ/USP, Brazil.
- 17 L. Sodek, J. Růžička and J. W. B. Stewart, *Anal. Chim. Acta*, 97 (1978) 327.
- 18 H. Bergamin Filho, B. F. Reis and E. A. G. Zagatto, *Anal. Chim. Acta*, 97 (1978) 427.
- 19 B. Karlberg and S. Thelander, *Anal. Chim. Acta*, 98 (1978) 1.
- 20 J. Růžička and E. H. Hansen, *Anal. Chim. Acta*, 99 (1978) 37.
- 21 E. H. Hansen, J. Růžička and A. K. Ghose, *Anal. Chim. Acta*, 100 (1978) 151.
- 22 H. Bergamin Filho, J. X. Medeiros, B. F. Reis and E. A. G. Zagatto, *Anal. Chim. Acta*, 101 (1978) 9.
- 23 H. Bergamin Filho, E. A. G. Zagatto, F. J. Krug and B. F. Reis, *Anal. Chim. Acta*, 101 (1978) 17.
- 24 B. F. Reis, M.Sc. Thesis, CENA/ESALQ/USP, Brazil, 1978.

- 25 D. Betteridge, E. L. Dagless, B. Fields and N. F. Graves, *Analyst*, 103 (1978) 897.
26 B. Karlberg and S. Thelander, *Analyst*, 103 (1978) 1154.
27 S. S. Jorgensen and M. A. B. Regitano, *Analyst*, 105 (1980) 000.
28 K. Kina, K. Shiraiishi and N. Ishibashi, *Talanta*, 25 (1978) 295.
29 D. Betteridge and B. Fields, *Anal. Chem.*, 50 (1978) 654.
30 D. Betteridge, *Anal. Chem.*, 50 (1978) 832.
31 J. Slanina, F. Bakker, A. G. Bruijre-Hess and J. J. Möls, *Fresenius Z. Anal. Chem.*, 289 (1978) 38.
32 B. Karlberg, *Svensk Kem. Tidskr.*, 90(12) (1978) 26.
33 K. Kina and N. Ishibashi, *Dojin*, 10 (1978) 1.
34 E. Bylund, R. Andersson and J.-A. Carlsson, *Pharmacia AB, Uppsala, Sweden*.
35 M. Koshino, *Bunseki*, 11 (1978) 803.
36 J. H. Dahl, Ph.D. Thesis, Royal Dan. School Pharm., Denmark, 1978.
37 A. Ramsing, M.Sc. Thesis, Tech. Univ. Denm., Denmark, 1978.
38 B. Karlberg, P. A. Johansson and S. Thelander, *Anal. Chim. Acta*, 104 (1979) 21.
39 J. Mindegaard, *Anal. Chim. Acta*, 104 (1979) 185.
40 E. A. G. Zagatto, F. J. Krug, H. Bergamin Filho, S. S. Jørgensen and B. F. Reis, *Anal. Chim. Acta*, 104 (1979) 279.
41 O. Aström, *Anal. Chim. Acta*, 105 (1979) 67.
42 J. H. Dahl, D. Espersen and A. Jensen, *Anal. Chim. Acta*, 105 (1979) 327.
43 J. Růžička and E. H. Hansen, *Anal. Chim. Acta*, 106 (1979) 207.
44 J. L. Braithwaite and J. N. Miller, *Anal. Chim. Acta*, 106 (1979) 395.
45 B. F. Reis, H. Bergamin Filho, E. A. G. Zagatto and F. J. Krug, *Anal. Chim. Acta*, 107 (1979) 309.
46 D. Espersen and A. Jensen, *Anal. Chim. Acta*, 108 (1979) 241.
47 E. A. G. Zagatto, B. F. Reis, H. Bergamin Filho and F. J. Krug, *Anal. Chim. Acta*, 109 (1979) 45.
48 L. Andersson, *Anal. Chim. Acta*, 110 (1979) 123.
49 F. J. Krug, J. Růžička and E. H. Hansen, *Analyst*, 104 (1979) 47.
50 M. F. Gine, E. A. G. Zagatto and H. Bergamin Filho, *Analyst*, 104 (1979) 371.
51 J. X. Medeiros, M.Sc. Thesis, CENA/ESALQ/UPS, Brazil, 1979.
52 H. Baadenhuijsen and H. E. H. Seuren-Jacobs, *Clin. Chem.*, 25 (1979) 443.
53 J. Růžička, E. H. Hansen, A. K. Ghose and H. A. Mottola, *Anal. Chem.*, 51 (1979) 199.
54 D. Espersen, Ph.D. Thesis, Royal Dan. School Pharm., Denmark, 1979.
55 E. H. Hansen, J. Růžička and A. K. Ghose, *STI/PUB/OO, IAEA, Vienna, 1979, in press*.
56 O. Klinghoffer, J. Růžička and E. H. Hansen, *Talanta*, in press.
57 E. H. Hansen and J. Růžička, *J. Chem. Educ.*, 56 (1979) 677.
58 J. Růžička and E. H. Hansen, *Chem. Technol.*, Dec. (1979).
59 E. H. Hansen and J. Růžička, *Anal. Chim. Acta*, in prep.
60 J. Růžička and E. H. Hansen, *NBS Spec. Publ.*, 519 (1979) 501.
61 J. Růžička, E. H. Hansen and A. Ramsing, *Anal. Chim. Acta*, in prep.
62 H. Kagenow and A. Jensen, *Anal. Chim. Acta*, 114 (1980) 227.
63 A. Ramsing, J. Růžička and E. H. Hansen, *Anal. Chim. Acta*, 114 (1980) 165.
64 C. B. Ranger, FA-Meeting, 1979 (not printed in this special issue).
65 K. Brunt, C. H. P. Bruins, B. Oosterhuis and D. A. Doornbos, *Anal. Chim. Acta*, 114 (1980) 257.
66 J. B. Landis, *Anal. Chim. Acta*, 114 (1980) 155.
67 K. K. Stewart, J. F. Brown and B. M. Golden, *Anal. Chim. Acta*, 114 (1980) 119.
68 I. Kågevall, O. Åström and A. Cedergren, *Anal. Chim. Acta*, 114 (1980) 199.
69 B. Karlberg and S. Thelander, *Anal. Chim. Acta*, 114 (1980) 129.
70 P.-A. Johansson, B. Karlberg and S. Thelander, *Anal. Chim. Acta*, 114 (1980) 215.
71 M. F. Giné, H. Bergamin Filho, E. A. G. Zagatto and B. F. Reis, *Anal. Chim. Acta*, 114 (1980) 191.

- 72 H. F. R. Reijnders, J. S. van Standen, J. H. B. Eelderink and B. Griepink, *Anal. Chim. Acta*, 114 (1980) 235.
- 73 J. M. Reijn, W. E. van der Linden and H. Poppe, *Anal. Chim. Acta*, 114 (1980) 105.
- 74 J. W. Dieker and W. E. van der Linden, *Anal. Chim. Acta*, 114 (1980) 267.
- 75 N. Ishibashi, K. Kina and Y. Goto, *Anal. Chim. Acta*, 114 (1980) 325.
- 76 S. Baban, D. Beetlestone, D. Betteridge and P. Sweet, *Anal. Chim. Acta*, 114 (1980) 319.
- 77 K. Cheng, E. L. Dagless, P. David and T. Goad, FA-Meeting, 1979 (not printed in this special issue).
- 78 C. S. Lim, J. N. Miller and J. W. Bridges, *Anal. Chim. Acta*, 114 (1980) 183.
- 79 J. L. Burguera, A. Townshend and S. Greenfield, *Anal. Chim. Acta*, 114 (1980) 209.
- 80 T. Skeggs, *Am. J. Clin. Pathol.*, 28 (1957) 311.
- 81 P. W. West and G. C. Gaeke, *Anal. Chem.*, 28 (1956) 1816.

THE APPLICATION OF ELECTROANALYTICAL DETECTORS IN CONTINUOUS FLOW ANALYSIS

KLÁRA TÓTH*, GÉZA NAGY, ZSÓFIA FEHÉR, GYÖRGY HORVAI and ERNŐ PUNGOR

Institute for General and Analytical Chemistry, Technical University of Budapest, 1502 - Budapest XI (Hungary)

(Received 10th September 1979)

SUMMARY

A survey is given of the different fields of application of flow-through techniques employing electroanalytical detectors. Emphasis is placed on recently developed titration techniques.

Analyses in flowing systems produced their first remarkable results in the field of the elucidation of reaction mechanisms and determination of reaction kinetic relationships in the 1940's. Despite these initial successes, flow-through techniques were introduced into general analytical practice only about twenty years ago. There are two main reasons for the present widespread use of these methods. On one hand, the analytical problem itself may require that the analysis be carried out in streaming solution, when for example continuous information is demanded on the composition of a streaming solution (biological fluid, industrial effluent, eluent, etc.). On the other hand, the special advantages offered by flow-through analytical techniques can justify their use for other routine purposes. In general, the main fields of application of flow-through techniques are: laboratory analysis, i.e. automatic serial analysis, analysis under flow-through conditions, e.g. study of dissolution processes, and industrial and environmental monitoring.

The flow-through analytical channel is the essential part of the technique; its construction and size may differ widely depending on the nature of the analytical problem. The design of flow-through analysis systems is increasingly based on theoretical considerations borrowed from chemical engineering, for example, in gradient titrations [1, 2], injection techniques [3, 4] and continuous calibration of ion-selective electrodes [5]. The dispersion of dissolved material in segmented [6, 7] and unsegmented [8] flowing streams has also been described by using the concepts of chemical engineering. Surprisingly, the description of phenomena in unsegmented streams seems to be more complicated than in segmented ones.

The common feature of such systems is that a flow-through detector cell

is always situated at the end of the analytical channel. Although most instrumental methods may be employed for following the concentration profile prevailing in the detector cell, optical detectors are most widely used. Consequently, most of the knowledge concerning flow-through methods and apparatus is related to the application of optical detectors. The parallel improvement of flow-through techniques and the development of new types of electroanalytical detectors have introduced more theoretical and technical problems, and have also led to the accumulation of a new range of knowledge. The present paper provides a survey of recent results and problems connected with the application of flow-through techniques employing electroanalytical detectors, with special emphasis on laboratory methods and equipment.

Ion-selective and voltammetric electrodes are the main electroanalytical detectors used for carrying out analyses in flowing solutions; conductimetric detection is mainly used for process streams. Such detection generally has a number of advantages in flowing systems compared with stationary systems [4], e.g., higher sensitivity, shorter response time and elimination of manipulation effects caused by displacement of the sensors. The requirements for electroanalytical sensors under flow-through conditions are increased in several respects: (a) response time; (b) long-term stability, which involves reproducible renewal of the working electrode surface area; (c) the constancy of the potential of the reference electrode, etc. The detailed requirements depend on the measuring technique employed.

The development of flow-through analysis systems and of the detectors used are interdependent. For a certain type of flow system, the detector must be capable of extracting the sought information at the output of the analysis channel. If, for example, fast concentration changes must be followed, an enzyme sensor or gas-sensing probe is unsuitable because of its slow response [4]. An important feature of some electrochemical detectors is that their signal is determined by the concentration or activity of the measured species in the vicinity of the electrode surface; such detectors measure local rather than volume average concentrations. Therefore it is very important that there be an unambiguous relation between the average concentration in the cross-section of the analysis channel and the concentration at or near the electrode surface. (Naturally, there are detectors such as dielectrometric and conductimetric detectors, the response from which is characteristic of the average concentration of the solution between the electrodes.) Other requirements for detector cells incorporating electroanalytical sensors are generally the same as those for other types of flow-through detectors (e.g., small dead volume and thus small cell volume, long-term stability, simple construction, in some cases high sensitivity). In addition, low electrical resistance and, in most cases, well defined hydrodynamic conditions in the detector cell are especially important. Detector cells of different construction have been described. In flow-through voltammetry, tubular cells [4, 9], possibly containing tubular working electrodes, [10], and thin-layer cells [11, 12] are most commonly used. For potentiometric measurements, tubular cells [13, 14],

microcapillary indicator electrodes [4] and flow-through caps [15] have been employed.

If the choice of detector and detector cell has already been made, the analysis system usually has to be adapted accordingly. This adaptation may consist of choosing the appropriate flow rate, mixing a conditioning solution for the electrode with the effluent of the analysis system, changing the pH of the effluent, etc. In some cases, fundamental changes in the analysis channel are necessary to match the features of the detector, e.g. for the measurement of the total nitrogen content of foodstuffs with an ammonia probe [16].

Flow-through analyzers designed originally with optical detection can be equipped with electroanalytical sensors. However, numerous new techniques have been developed recently which are more suitable for use with electroanalytical detection and flow-through conditions.

An arbitrary classification of flow-through techniques can be as follows.

Methods based on direct evaluation of detector signals. These are methods in which a component of the sample is determined from a single signal which is unambiguously related to the concentration of that component. They have received widest acceptance both in analytical practice and in the solution of research problems.

Titration techniques. Here, the measurement of reagent consumption in the titration of the sample is used for evaluation.

Reaction rate methods. This group includes those methods in which the concentration of a component is determined from the change in the rate of a chemical reaction caused by the particular component.

This classification is based on one of the most important characteristics of flow-through techniques, although other classifications can be based on other characteristics. The direct detector signal used for estimating concentrations may be a steady-state signal or a dynamic signal. The analysis can be carried out with or without the addition of one or more reagents. The solution stream in the analysis channel may be continuous (non-segmented) or segmented. The results can be evaluated by calibration or standard addition or subtraction.

The conditions of measurement in the analysis channel can be chosen so that the time spent by the sample solution (often after the addition of reagent or auxiliary solutions) in contact with the sensor in the detector cell is long enough for establishment of a steady-state signal corresponding to the concentration of the sample (or reaction product). Such conditions are ensured mainly in the Technicon-type analyzers with segmented flow. In the injection technique, which is receiving increasing attention nowadays, small volumes of sample are introduced into a continuously flowing solution, the conditions of flow having been adjusted so as to produce a concentration profile, which is measured by the appropriate detector. The profile, however, is determined by the concentration of the sample and the hydrodynamic parameters. Accordingly, a dynamic signal serves as the basis of the concentration determination.

In cases where a sensor is available to detect a given component, the deter-

mination can often be carried out, selectively and with sufficient precision and accuracy, directly without a chemical reaction, that is without reagent addition. In such applications ion- and molecule-selective sensors and voltammetric electrodes are of great practical importance. In many systems, however, the species to be determined undergoes a chemical reaction in the flowing solution and is transformed, partly or totally, into product(s). This might be considered as indirect detection. There may be various reasons for carrying out the reaction, for example, no suitable detector may be available for the analyte but the reaction product, in an equivalent amount, is easily monitored (e.g. spectrophotometric detection after a chromogenic reaction or voltammetric detection of a reaction product). Similarly, a detector may be available only for sensing a reaction partner, the excess of which is measured after the reaction. Chemical reactions may also be used to increase the precision and accuracy of the analysis. Examples involve various subtraction and titration methods. These are generally based on the stoichiometric reaction of the sample with a near-equivalent amount of reagent and measurement of the small excess of either reagent or sample. The amount of this small excess need not be measured very accurately, i.e. the detector need not be very accurate, but it has to be sufficiently sensitive because only a small fraction of the original sample or reagent concentration is measured.

Analyses in flowing systems usually require preliminary calibration. The frequency of calibration is defined by the properties of the detector and by the analytical problem involved. Data handling, evaluation of results and control of calibration frequency are often done with a desk-top computer or microprocessors.

METHODS BASED ON DIRECT EVALUATION OF DETECTOR SIGNALS

Electroanalytical detectors are being increasingly employed in flow-through analytical methods based on direct signal measurement. Several publications have appeared on the use of ion-selective electrodes in Technicon-type analyzers [7, 17–21], and analyzers with ion-selective electrode detection have become commercially available [22, 23]. Mainly pH, sodium, potassium, calcium, fluoride and chloride ion-selective electrodes have been used, especially for the analysis of biological and environmental samples. Essentially the same is true of applications of ion-selective electrode detection with the injection technique [13, 24, 25]. However, for successful use of the injection technique, it is important to note that the stability of the system is greater if the analyte is present in the continuously streaming background electrolyte at a relatively low concentration [13, 15]. This constant addition gives a more stable base line, which may also serve as a calibration point, although it may reduce the sensitivity of the injection measurement to a certain extent [4].

Various voltammetric sensors have been constructed. For example, lead and zinc [27] and calcium and magnesium [28] have been determined using a polarographic flow-through cell. Cinci and Silvestri [29] and Lund and

Opheim [30, 31] described systems for use in pharmaceutical analysis. In the construction of these systems, considerable effort was devoted to solving the problems of continuous deaeration of the sample solution, but unfortunately this aspect still has not been solved satisfactorily. A differential pulse polarographic system has been described by Alexander and Shah [32] for automatic continuous measurement of serum proteins in a Technicon-type analyzer system, which ensures a high analysis rate.

The injection technique based on voltammetric detection as first described by Pungor et al. [3] is particularly suited to analysis with voltammetric electrodes of constant surface area. The possibility of reproducible conditioning offered by flow-through techniques has special advantages for the application of such electrodes. Fehér [33] pointed out that the injection technique with voltammetric detection is suitable for fast serial determination of the active ingredient in various pharmaceutical preparations, or for the discontinuous periodical control of the dissolution of the active ingredients in pharmaceutical products and for dissolution rate measurements [9]. Commercial production of such voltammetric analyzers is envisaged [26].

In serial analyzers high sensitivity is not usually a general requirement, yet voltammetry carried out under hydrodynamic conditions (hydrodynamic voltammetry or amperometry) can be considered as one of the most sensitive voltammetric techniques. The voltammetric signal measured under flow-through conditions may reach a value many times greater than the signal measured under stationary conditions, because of convective diffusion mass transport. At the same time, current measurement at a constant working electrode potential, which is used almost exclusively in flow-through techniques, is characterized by a very low residual current which, as is well known, determines the sensitivity of voltammetric measurements. Thus the components of the condenser current, which decreases exponentially with time, make a smaller contribution to the signal, and the background current measured when the background electrolyte flows through the system can be compensated electronically or by physical or chemical methods, e.g. by difference measurement.

Nowadays the rate of analytical measurement by automatic analyzers has increased to such an extent that the duration of the overall analysis is often determined by the time needed for sample pretreatment. It is an old-established concept to carry out the pretreatment procedure in the analyzer itself, e.g. Kjeldahl digestion or acid digestion. Recently, efforts have been made to combine continuous sample pretreatment with the injection technique [34, 35].

Combinations of special sample pretreatment and electrochemical detectors

In certain cases, the concentration measurement is, by its nature, closely connected with the sample treatment procedure, for example in chromatography with electroanalytical detection and in stripping analysis under flow-through conditions. Chromatography is certainly one of the oldest areas

where detection is done in flowing systems, and Kemula [36] was the first to combine chromatographic separation with electroanalytical (polarographic) detection (so-called chromato-polarography). Usually photometric detectors are used in liquid chromatographs but the use of electroanalytical detectors is increasing. Kissinger and his co-workers [37] have made remarkable contributions to the development of electroanalytical detectors for chromatography. Initially, the dropping mercury electrode was used as a detector in chromatopolarography. Its unsatisfactory sensitivity, because of noise and the relatively large dead volume, has directed attention to solid electrodes, primarily various types of graphite. Carbon paste and glassy carbon electrodes have been successfully used for determining biogenic amines, therapeutic compounds and their metabolites in biological fluids, and pharmaceutical and food products [11, 36–41]. Detector cells incorporating graphite electrodes are now commercially available. In view of the limited negative potential range of these solid electrodes, continuous efforts are still being made to enable mercury electrodes to be used in flowing systems. Attempts have been made to use special cell constructions (with horizontal or tilted capillaries) or solid (mainly platinum) electrodes covered with a mercury film [42–44]. The present authors have no experience with the PAR flow-through cell incorporating a dropping mercury electrode [45], but it seems to be a good solution of the problem.

There are several directions for research and development work connected with the adaptation of electrochemical detectors to chromatographic systems. Here only work aimed at increasing the sensitivity and selectivity will be discussed. One way of increasing the sensitivity is to construct the cell so that the rate of mass transport to the electrode surface is greatly increased. Thus, remarkable results can be obtained, for example, with wall-jet electrodes at high flow rates [46–48]. The signal and thus also the sensitivity can be enhanced by enlarging the surface area of the working electrode relative to cell volume, which involves a complete or nearly complete transformation of the electroactive component at the electrode. By ensuring 100% conversion, coulometric evaluation becomes possible [12, 49–51]. In this case, however, the residual current can be greater than in general voltammetry, therefore in some cases no actual gain in sensitivity is achieved. Highly sensitive voltammetric methods, primarily differential pulse polarography, should be considered when greater sensitivity is needed. However, as shown below, their use is of greater importance for solving selectivity problems. It should be noted that, under flow-through conditions for voltammetry or amperometry, the simple d.c. method can provide as high a sensitivity as the a.c. methods.

The use of electroanalytical detectors in liquid chromatography is very often justified more by the attainable sensitivity and measuring conditions than by the need to identify the species. However, the application of such detectors is restricted: only components reduced or oxidized within the available potential range of the measuring system can be determined. At the same time, electroanalytical detection sets limitations on the separation tech-

nique and composition of the mobile phase. Thus, very often it is necessary to solve the problems of selective detection, in addition to the chromatographic separation. Voltammetric (amperometric) detection can be made more selective by an appropriate choice of the potential of the working electrode. In practice, the current is usually measured at a potential within the range of the convective diffusion limiting current. In some cases greater selectivity is attained by choosing a lower potential, but at the cost of reduced sensitivity [52]. A cell incorporating a working electrode connected to two electrical circuits has been constructed by Blank [53]; by applying different voltages, components with very similar half-wave potentials could be determined simultaneously. Methods more selective than classical d.c. voltammetry have been used; differential pulse voltammetry [52, 54, 55] and differential double pulse voltammetry [55] have been examined successfully.

In addition to the more widely used voltammetric detectors, detector cells measuring conductivity or permittivity and others incorporating ion-selective electrodes have been described [56]. However, ion-selective electrodes can only be applied for detecting inorganic ions, after separation by ion-exchange chromatography. Organic substances can be determined in the effluent (gas or liquid) from the chromatographic column only after some conversion process (oxidation, hydrogenation, etc.) and absorption of the product in a suitable liquid. Detectors incorporating ion-selective electrodes have been used to measure compounds containing fluorine, chlorine, sulphur or nitrogen [56]. Among recent studies, Kojima et al. [57] used chloride- and bromide-selective electrodes for simultaneous detection or identification of chlorine and bromine compounds. Such applications are justified only in special cases.

Another technique combined with special sample pretreatment, with the aim of increasing sensitivity, is flow-through stripping. This technique, applicable to trace metal analysis, is basically a hydrodynamic method, since the metal to be determined has to be deposited on a working electrode under well defined hydrodynamic conditions. In earlier experiments, electrolysis was done in solutions stirred at a constant rate, but later a rotating disc electrode was used [58, 59]. Deposition (mainly of metals) from a flowing solution is advantageous because of the simplicity of ensuring well-defined hydrodynamic conditions, the possibility of automation and the reduction in analysis time. Deposition and stripping have both been done in flowing solution by some authors [60, 61], whereas stripping in a stationary solution has been found advantageous by others [62]. Tubular electrodes are often used as working electrodes [60, 61] but the use of a fixed [62] or rotating disc electrode [58, 59] has also been described. The main problems connected with stripping analysis under flow-through conditions are the construction of the working electrode (generally platinum or graphite electrodes covered with a mercury film), de-aeration of the sample and auxiliary solutions, but remarkable efforts have been made to solve them.

FLOW-THROUGH TITRATION TECHNIQUE

Titration techniques are superior to methods based on direct signal measurement with respect to both accuracy and reliability, and it is in this area that electroanalytical detection is used almost exclusively. This superiority arises because the concentration determination is made on the basis of the chemical equivalence, thus the results of the analysis are not, or only slightly, influenced by changes in the properties of the sensor used; and, in contrast to direct methods, these techniques do not require individual standard materials, the purity of which is often questionable.

There are numerous possibilities for carrying out titrations in flow-through circumstances, a number of which have already been realized. The titration procedure may be conducted on a batch basis, followed by a fast washing procedure, or it can be done under continuous flow conditions. In the latter case, the streaming sample is mixed with the streaming reagent, the mass flow rate of one of these usually being controlled by some means. The detector is placed downstream from the mixing device. The mass flow rate of the reagent may be controlled so as to keep the reaction always at the equivalence point. In this case the output parameter of the system is the mass flow rate of the reagent. Optimal ways of controlling the mass flow rate of the reagent have been worked out by van Osch and Griepink [63].

In another version of titration in flowing solutions, the mass flow of the titrant is controlled by a predetermined program, preferably linearly. The detector senses the resulting transient which is used to calculate the sample concentration. There are different ways of programming the titrant mass flow rate, e.g. by using dilution flasks [1, 2, 64] or, more simply, by coulometric generation of the reagent [65]. Recently it was pointed out [66] that a continuous titration can be carried out with constant mass flow rates of reagent and sample, at least if there are no broad variations in sample concentrations. Suitable reagent mixtures can be used to titrate sample concentrations in a broader range [67].

In a very interesting version of such a titration, a rotating ring-disc electrode is used [68–70]. Although it cannot be considered as a real flow-through technique, it operates under hydrodynamic conditions. The titrant (e.g. bromine) is generated at the disc and reacts with the surrounding sample. If the rate of reagent generation is high enough, a fraction of the excess of reagent will arrive at the ring where it is detected. The ring current vs. disc current graphs can be used to evaluate the sample concentration or the reaction rate.

Triangle-programmed titrations

A method based on triangle-programmed reagent addition has been developed [65] for titrations in flowing systems. A flow-through analytical channel was designed (Fig. 1), in which the sample of concentration c_s is streamed at a constant flow rate v_s . The channel is constructed so as to enable reagent

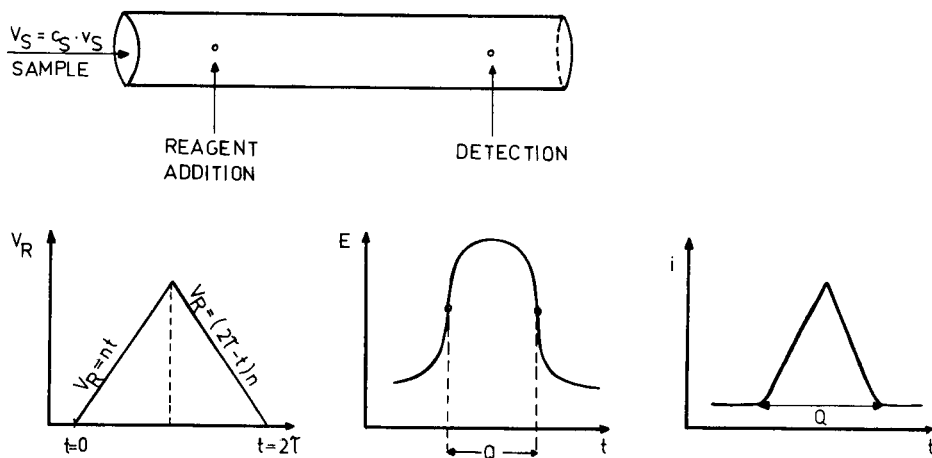
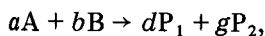


Fig. 1. Outline of the basic principles of the triangle titration technique.

introduction to the sample stream at a programmed mass flow rate (V_R). The combined homogeneous stream flows to the detector during which time a chemical reaction takes place. The mass flow of the reagent is changed by means of an isosceles triangle program. For time $t \leq \tau$, $V_R = nt$, while during $t > \tau$, $V_R = (2\tau - t)n$, where n and τ are constants (see below). The reagent addition program is chosen so that the maximum reagent mass flow, V_{RT} , should exceed the sample mass flow ($V_S = c_S v_S$).

Because of the programmed reagent addition, the ratio of the sample to reagent and also the degree of titration become different in the subsequent infinitesimal solution segments arriving at the detector. By following the composition of these segments over a period of time, with an appropriate detector, a complete titration curve can be obtained. As a result of the triangle-programmed reagent addition, two titration curves connected to each other are recorded.

There is a well defined relationship between the time elapsed between the appearance of the two equivalence points and the sample mass flow, which can be derived from the mass balance [71]. If the instantaneous titration reaction is:



the time elapsed (Q) between the two equivalence points can be given as

$$Q = t_{E_2} - t_{E_1} = 2\tau - 2ac_S v_S / bn,$$

where 2τ is the total length of the reagent addition program (s), a and b are stoichiometric constants, v_S is the volume flow rate of the sample solution ($\text{dm}^3 \text{s}^{-1}$), c_S is the concentration of the sample solution [mol dm^{-3}] and n is the slope of the reagent addition program [mol s^{-2}]. If the equivalence points can be detected, the concentration of the sample solution can be

calculated from Q on the basis of the known parameters of the titration. It should be emphasized that the slope of the Q vs. c_s function, i.e. the sensitivity of concentration measurement, depends on the values of 2τ , n and v_s .

Such triangle-programmed titrations can be classified in different ways, for example, based on volumetric or coulometric reagent addition, or according to the nature of the reagent (acid-base titrations, titrations with silver(I) [72], mercury(II) or bromate solutions [73] or iodimetric titrations), or according to the detector used (potentiometric, amperometric, photometric, conductimetric). The shape of the titration curve depends on the signal vs. concentration relationship valid for the detector employed. Automatic data processing was used in the determination of the equivalence point of amperometric titration curves by least-squares curve fitting [74]. The automatic evaluation of potentiometric titration curves has also been reported [75].

In the theory and practice of triangle-programmed titrations, it is of major importance to know whether the determinations are feasible when two or more species capable of reacting with the titrant are present in the sample. This problem arises when halides, acids or complexes are to be determined. In such cases the feasibility of the selective determination is affected by the ratio of the solubility products of the precipitates, dissociation constants of the acids, stability constants of the complexes, as well as the concentrations of the components.

Very many organic compounds react with bromine, so theoretically they can all be determined by titration with bromine. However, classical direct titrations are feasible only if the reaction with bromine is fast and stoichiometric. For slow reactions end-points are difficult to detect and there may be other sources of uncertainty. In such cases, time-consuming back-titrations must be used. The special importance of triangle-programmed titrations with bromine carried out in flow-through systems is that they enable compounds to be determined even when classical titration of discrete samples is not feasible (i.e. when there is no definite end-point, because the reaction is slow or because after the first bromine-consuming reaction step the product slowly reacts further with bromine or analyte). In triangle-programmed titrations the reaction conditions are well defined and the reaction time is controlled by the flow rate and the geometry of the analytical channel. The reaction products rapidly leave the detector cell, so that no undesirable effects are caused by their accumulation in the cell.

A great variety of organic compounds can be determined by the technique, including prostaglandin-type preparations [76]. By an appropriate choice of time and reaction conditions, compounds reacting with bromine at different rates can be determined without preliminary separation. The great accuracy of coulometric reagent generation combined with the high sensitivity of amperometric detection renders possible the determination of low concentrations of many organic compounds.

REACTION-RATE METHODS

Reaction-rate methods can be divided into two groups according to how they are carried out. In one case, the chemical reaction on which the determination is based is followed continuously by a detector with a relatively fast response, and evaluation is made on the basis of the detector signal vs. time function or another function derived from time. In the other case, evaluation is based on a change in concentration or detector signal within a constant reaction time. In analyses in flowing systems, the use of the latter method is obviously more practicable, as uniform handling of samples and constant reaction times can easily be ensured.

A remarkable proportion of the methods described during the past few years as flow-through analytical methods can be considered as reaction-rate methods, in which electroanalytical detectors have been increasingly applied. Among them, methods based on the specific catalytic effect of dissolved enzymes or those used for enzyme activity measurements [77-81] are worth mentioning. In other cases a column containing an immobilized enzyme [82-87], a tube reactor [88] or enzyme electrode [91] is used for the measurements. Enzyme inhibitors can also be determined in flow-through systems, by using a dissolved [90] or immobilized enzyme [91]. Much of the apparatus used has been assembled from modules of commercially available segmented-flow analyzers, e.g. [79-81], whereas in other cases apparatus was designed for the special purposes of the analysis [77, 89, 92]. The evaluation can be done on steady-state [79-81] and transient signals [89, 93, 94].

A flow-through technique, when used for analyses based on reactions involving a single detector signal corresponding to a fixed reaction time, is not always particularly reliable. Usually, no background signal correction can be carried out under the conditions applied. Batch type or centrifugal analyzers are usually preferred to flow-type apparatus, so that the course of the reaction can be followed.

Several attempts have been made to eliminate the above sources of uncertainty. Among these the stopped-flow technique should be mentioned. Recently a few papers have been published on the combination of injection and the stopped-flow technique for the special purposes of kinetic analysis [95]. The system in which the flow of the reaction mixture is stopped for a certain period of time offers a number of obvious advantages, although it is more complicated than the usual flow-through analyzers. Additionally, in this case, only a few electroanalytical detectors can be used.

In several cases [77, 90, 93], two detectors have been used to eliminate the errors arising from differences in the background signal, and evaluation is based on the difference of the signals of the two detectors. Usually one detector is inserted at a point before the reaction has started, and the other at a point after the reaction zone. Enzyme electrodes present a special opportunity to observe the differential signal produced by the enzyme elec-

trode and a sensor identical with the fundamental electrode of the enzyme electrode. The system developed by Thevenot et al. [96] for measuring glucose is a good example of this measuring principle. Many interesting developments are clearly probable in this field.

The authors thank Dr. A. Hrabéczy-Páll for her contribution to this work.

REFERENCES

- 1 D. L. Eichler, Technicon Symposium, 1969, Vol. 1, Mediad, New York, 1970, p. 51.
- 2 B. Fleet and A. Y. W. Ho, *Anal. Chem.*, 46 (1974) 9.
- 3 G. Nagy, Zs. Fehér and E. Pungor, *Anal. Chim. Acta*, 52 (1970) 47.
- 4 E. Pungor, Zs. Fehér, G. Nagy, K. Tóth, G. Horvai and M. Gratzl, *Anal. Chim. Acta*, 109 (1979) 1.
- 5 G. Horvai, K. Tóth and E. Pungor, *Anal. Chim. Acta*, 82 (1976) 45.
- 6 L. R. Snyder and H. J. Adler, *Anal. Chem.*, 48 (1976) 1022.
- 7 L. Snyder, J. Levine, R. Stoy and A. Conetta, *Anal. Chem.*, 48 (1976) 942A.
- 8 J. Růžička and E. H. Hansen, *Anal. Chim. Acta*, 99 (1978) 37.
- 9 E. Pungor, Zs. Fehér and G. Nagy, *Pure Appl. Chem.*, 44 (1975) 595.
- 10 W. J. Blaedel and S. L. Boyer, *Anal. Chem.*, 43 (1971) 1538.
- 11 P. T. Kissinger, C. Refshauge, R. Dreiling and R. N. Adams, *Anal. Lett.*, 6 (1973) 465.
- 12 J. Lankelma and H. Poppe, *J. Chromatogr.*, 125 (1976) 375.
- 13 Zs. Fehér, G. Nagy, K. Tóth and E. Pungor, *Anal. Chim. Acta*, 98 (1978) 193.
- 14 H. F. Osswald, R. Asper and W. Simon, *Clin. Chem.*, 25 (1979) 39.
- 15 W. E. Van der Linden and R. Oostervink, *Anal. Chim. Acta*, 101 (1978) 419.
- 16 G. K. Buckee, *J. Inst. Brewing*, 80 (1974) 291.
- 17 P. L. Bailey and M. Riley, *Analyst*, 100 (1975) 145.
- 18 P. W. Alexander and G. A. Rechnitz, *Anal. Chem.*, 46 (1974) 860.
- 19 B. Fleet and Y. W. Ho, *Talanta*, 20 (1973) 793.
- 20 J. Sekerka and J. F. Lechner, *Anal. Lett.*, 7 (1974) 463.
- 21 J. Mertens, P. Van der Winkel and D. L. Massart, *Anal. Chem.*, 48 (1976) 272.
- 22 Stat/Ion-Technicon Product Information Leaflet, Technicon Instrument Corporation, Ardsley, New York, 10502, U.S.A.
- 23 W. J. Scott, On-line Analysis in Clinical Chemistry using ISE-s, paper presented on Symposium Electroanalysis in Hygiene, Environmental Clinical and Pharmaceutical Chemistry, Chelsea College, London, 1979.
- 24 J. Růžička and E. H. Hansen, *Anal. Chim. Acta*, 78 (1975) 145.
- 25 E. H. Hansen, A. K. Ghose and J. Růžička, *Analyst*, 102 (1977) 705.
- 26 Zs. Fehér, G. Nagy, L. Bezur, J. Szovik, K. Tóth and E. Pungor, *Hung. Sci. Instrum.*, 45 (1979) 1.
- 27 H. G. Lento, Automation in Anal. Chem. Technicon Symposium 1966, Vol. 1, Mediad, White Plains, New York, 1967, p. 598.
- 28 M. D. Booth, B. Fleet, S. Win and T. S. West, *Anal. Chim. Acta*, 48 (1969) 329.
- 29 A. Cinci and S. Silvestri, *Farmaco, Ed. Prat.*, 27 (1972) 28.
- 30 W. Lund and L.-N. Opheim, *Anal. Chim. Acta*, 79 (1975) 35.
- 31 W. Lund and L.-N. Opheim, *Anal. Chim. Acta*, 82 (1976) 245; 88 (1977) 275.
- 32 P. W. Alexander and N. H. Shah, *Talanta*, 26 (1979) 97.
- 33 Zs. Fehér, Voltammetric Measurements in Flow-through System, Candidates thesis, Budapest, 1975.
- 34 B. Karlberg and S. Thelander, *Anal. Chim. Acta*, 98 (1978) 1.
- 35 B. Karlberg, P. Johansson and S. Thelander, *Anal. Chim. Acta*, 109 (1979) 21.
- 36 W. Kemula, *Rocz. Chem.*, 26 (1952) 281.

- 37 P. T. Kissinger, *Anal. Chem.*, 49 (1977) 477A.
- 38 P. T. Kissinger, L. J. Felice, R. M. Riggan, L. A. Pachla and D. C. Wenke, *Clin. Chem.*, 20 (1974) 992.
- 39 L. A. Pachla and P. T. Kissinger, *Anal. Chem.*, 48 (1976) 237.
- 40 L. A. Pachla and P. T. Kissinger, *Anal. Chim. Acta*, 88 (1977) 385.
- 41 U. R. Tjaden, J. Lankelma, H. Poppe and G. Muusze, *J. Chromatogr.*, 125 (1976) 275.
- 42 R. Stillman and T. S. Ma, *Mikrochimica Acta*, (1973) 491.
- 43 L. Michel and A. Zátka, *Anal. Chim. Acta*, 105 (1979) 109.
- 44 R. C. Buchta and L. J. Papa, *J. Chromatogr. Sci.*, 14 (1976) 213.
- 45 Princeton Applied Research Co., *Product Information Leaflet*, 1979.
- 46 H. Matsuda and J. Yamada, *J. Electroanal. Chem.*, 44 (1973) 189.
- 47 M. Váradi, Zs. Fehér and E. Pungor, *J. Chromatogr.*, 20 (1974) 259.
- 48 B. Fleet and C. J. Little, *J. Chromatogr. Sci.*, 12 (1974) 747.
- 49 G. Johansson, *Talanta*, 12 (1965) 163.
- 50 D. C. Johnson and J. Larochelle, *Talanta*, 20 (1973) 959.
- 51 Y. Takata and G. Muto, *Anal. Chem.*, 45 (1973) 1864.
- 52 W. A. MacCrehan and R. A. Durst, *Anal. Chem.*, 50 (1978) 2108.
- 53 C. L. Blank, *J. Chromatogr.*, 117 (1976) 35.
- 54 D. G. Swartzfager, *Anal. Chem.*, 48 (1976) 2189.
- 55 R. F. Lane and A. T. Hubbard, *Anal. Chem.*, 48 (1976) 1287.
- 56 E. Pungor, K. Tóth, Zs. Fehér, G. Nagy and M. Váradi, *Anal. Lett.*, 8 (1975) 9.
- 57 T. Kojima, M. Ichise and Y. Seo, *Anal. Chim. Acta*, 101 (1978) 273.
- 58 H. Monien and P. Jacob, *Fresenius Z. Anal. Chem.*, 255 (1971) 33.
- 59 M. Kapanica and V. Stara, *J. Electroanal. Chem.*, 77 (1977) 57.
- 60 S. H. Lieberman and A. Zirino, *Anal. Chem.*, 46 (1974) 20.
- 61 W. R. Seitz, R. Jones, L. N. Klatt and W. D. Mason, *Anal. Chem.*, 45 (1973) 840.
- 62 J. Wang and M. Ariel, *J. Electroanal. Chem.*, 83 (1977) 217.
- 63 G. W. S. van Osch and B. Griepink, *Fresenius Z. Anal. Chem.*, 284 (1977) 267.
- 64 J. Růžička, E. H. Hansen and H. Mosbaek, *Anal. Chim. Acta*, 92 (1977) 219.
- 65 G. Nagy, K. Tóth and E. Pungor, *Anal. Chem.*, 47 (1975) 1460.
- 66 G. Horvai, K. Tóth and E. Pungor, *Anal. Chim. Acta*, 107 (1979) 101.
- 67 O. Aström, *Anal. Chim. Acta*, 105 (1979) 67.
- 68 W. J. Albery, S. Bruckenstein and D. C. Johnson, *Trans. Faraday Soc.*, 62 (1966) 1938.
- 69 S. Bruckenstein and D. C. Johnson, *Anal. Chem.*, 36 (1964) 2186.
- 70 F. Rauwel and D. Thevenot, *J. Appl. Electrochem.*, 6 (1976) 119.
- 71 G. Nagy, Zs. Fehér, K. Tóth and E. Pungor, *Anal. Chim. Acta*, 91 (1977) 87.
- 72 G. Nagy, Zs. Fehér, K. Tóth and E. Pungor, *Anal. Chim. Acta*, 91 (1977) 97.
- 73 G. Nagy, Zs. Fehér, K. Tóth and E. Pungor, *Anal. Chim. Acta*, 100 (1978) 181.
- 74 G. Nagy, Z. Lengyel, Zs. Fehér, K. Tóth and E. Pungor, *Anal. Chim. Acta*, 101 (1978) 261.
- 75 G. Nagy, A. Ivaska, Zs. Fehér, K. Tóth and E. Pungor, *Talanta*, in press.
- 76 Zs. Fehér, G. Nagy, K. Tóth, E. Pungor and A. Tóth, *Analyst*, 104 (1979) 560.
- 77 W. Hussain, L. H. von Storp and G. G. Guilbault, *Anal. Chim. Acta*, 51 (1972) 89.
- 78 G. G. Guilbault and L. H. von Storp, *Anal. Chim. Acta*, 62 (1972) 425.
- 79 R. A. Llenado and G. A. Rechnitz, *Anal. Chem.*, 45 (1973) 826.
- 80 R. A. Llenado and G. A. Rechnitz, *Anal. Chem.*, 46 (1974) 1109.
- 81 D. S. Papastathopoulos and G. A. Rechnitz, *Anal. Chem.*, 47 (1975) 1792.
- 82 B. Watson and M. H. Keyer, *Anal. Lett.*, 9 (1976) 713.
- 83 B. Watson, D. N. Stifel and F. E. Semersky, *Anal. Chim. Acta*, 106 (1979) 233.
- 84 T. Karube, K. Hara, I. Satoh and S. Suzuki, *Anal. Chim. Acta*, 106 (1979) 243.
- 85 I. Satoh, L. Karube, S. Suzuki and K. Aikawa, *Anal. Chim. Acta*, 106 (1979) 369.
- 86 G. Johansson and L. Ögren, *Anal. Chim. Acta*, 84 (1976) 23.
- 87 G. Johansson, K. Edström and L. Ögren, *Anal. Chim. Acta*, 85 (1976) 55.
- 88 L. P. Leon, S. Narayanan, R. Dellenbach and Cs. Horváth, *Clin. Chem.*, 22 (1976) 1017.

- 89 E. Pungor, G. Nagy and Zs. Fehér, *J. Electroanal. Chem.*, 75 (1977) 241.
90 L. H. von Storp and G. G. Guilbault, *Anal. Chim. Acta*, 62 (1972) 421.
91 G. Johansson, L. Ögren and L. Gorton, in *Ion-Selective Electrodes*, E. Pungor (Ed.), Akadémiai Kiadó, 1977.
92 G. Nagy, L. H. von Storp and G. G. Guilbault, *Anal. Chim. Acta*, 66 (1973) 443.
93 Ch. M. Wolff and H. A. Mottola, *Anal. Chem.*, 50 (1978) 94.
94 D. P. Nikolelis and H. A. Mottola, *Anal. Chem.*, 50 (1978) 1665.
95 J. Růžička and E. H. Hansen, *Anal. Chim. Acta*, 106 (1979) 207.
96 D. R. Thevenot, R. Sternberg, P. R. Coulet, J. Laurent and D. C. Gautheron, *Anal. Chem.*, 51 (1979) 96.

CHARACTERIZATION AND DESIGN OF LIQUID PHASE FLOW-THROUGH DETECTOR SYSTEMS

H. POPPE

Laboratory for Analytical Chemistry, University of Amsterdam, Nieuwe Achtergracht 166, Amsterdam (The Netherlands)

(Received 23rd July 1979)

SUMMARY

Characterization of liquid phase flow-through detection systems as used in column liquid chromatography and flow injection analysis is discussed. Linear range, selectivity, peak broadening and detection limit are the most important characteristics. Peak broadening is treated with the aid of the concepts of systems analysis. The total peak broadening effect is given as the sum of contributions from connecting tubes or reactors, measuring volume and time constants in electronics and transducers. The influence of noise and signal frequency content on the precision of analytical results is treated qualitatively. The detection limit of a flow-through detection system is defined, taking these effects into account qualitatively. These characteristics are related to the performance of the whole analytical system with regard to concentration detection limit, absolute detection limit and maximum sample frequency.

There is some ambiguity about the definition of a detection system in analytical chemistry. It may be clear in flow injection analysis (f.i.a.) that the detector is some physical or chemical transducer, but for other specialists the detector may be quite differently defined. In chromatography the detection device is defined as consisting of all parts which serve the purpose of detecting rather than of separating. Thus, detection devices can be as simple as an electrode in a tube, or a refractometer or u.v. absorbance meter, but they may also consist of complete reaction detectors comprising flow-through reactors, reagent pumps, cooling tubes, flow extractors and one or more u.v., fluorescence, electrochemical or other physical devices. In fact, the detection device may be a whole flow injection system in itself with the only difference that analytes are not injected into it directly from sample containers, but are delivered by the chromatographic separation unit, as a time sequence that is determined by the dynamics of the chromatographic process (Fig. 1).

The proper characterization of flow-through detection devices, and their optimal design, accepting certain physical, practical, or financial boundary conditions, is important not only for chromatography and flow injection analysis, but also for applications such as process control. The general topic requires knowledge from various fields, such as chemistry, materials science,

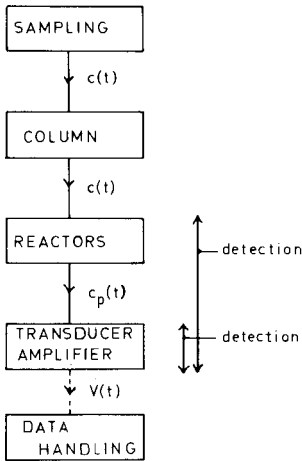


Fig. 1. Building blocks or sub-systems constituting a liquid chromatographic or flow injection system, showing the ambiguity in the concept of detection: $c(t)$ concentration time function of analyte; $c_p(t)$ concentration time function of reaction products; $V(t)$ signal time function.

physics and electronics, to mention but a few. The fact that these devices are operated in a flow-through mode, necessitates also the incorporation of knowledge about transport phenomena and systems analysis which have been particularly developed in chemical engineering. Great advantage has been taken of this source in the development of gas and liquid chromatography. Nowadays f.i.a. tends to use chemical engineering concepts. However, it should be emphasized strongly that these new studies of transport phenomena, etc., should incorporate ideas, methods and techniques from chromatography as well as from chemical engineering. There are two reasons for this. First, the single discipline of analytical chemistry would be much stronger if all specialists used the same technical terminology. Secondly, f.i.a. development would be speeded up considerably if knowledge and experience from liquid and gas chromatography were properly utilized. The pitfalls in the application of transport equations and correlations are manifold, and the confusing mistakes made earlier in liquid chromatography should not be repeated in f.i.a. development.

In the study of flow-through detection systems, two stages can be distinguished; description and then design or improvement. In the first stage, the measuring system can be considered as a black box, having one input, into which the liquid stream is fed, and one output, i.e. the electrical output delivering the signal to the recorder or other data handling equipment. No attention is given to the fact that the actual device has many other connections with the surroundings, e.g. it mostly needs an electrical power supply reacting to changes in supply voltage, etc. As a first approach, entirely as in treatments by systems analysis, these external factors are ignored and

only input-output relations are considered. In particular, the relation between concentration in the input stream and the output signal must be studied and the following characteristics must be established by proper experimentation [1].

(a) *Calibration curve.* The functional relationship between input and output must be known. Preferably it should be linear over a large range.

(b) *Dynamic behaviour.* The dynamic behaviour of the system must be well understood. A change in the input will bring about a certain time function as the output behaviour; or more generally, the relation between the output time function and the input time function must be studied.

(c) *Selectivity.* The dependence of the calibration curve on the type of compound must be known. A universal detector will respond to a wide range of compounds to about the same extent, whereas a selective detector will respond much more sensitively to certain ions or compounds or groups of compounds than to others.

(d) *Noise and detection limit.* Finally, uncertainties connected with the value of the output parameter must be investigated. This determines the smallest concentration (change) that can be determined with a specified precision (i.e. the determination limit) and the smallest concentration change that can be observed with a specified uncertainty (i.e. the detection limit).

Calibration curves and selectivity will not be discussed here, as these two characteristics play a role in every analytical method. Attention will be concentrated on the problems associated with dynamic behaviour and noise, because these are the vital features which arise from the very nature of the measurement process in f.i.a., i.e. the continuous measurement made possible by the continuous flow in the system.

PEAK-BROADENING EFFECTS OF DYNAMIC BEHAVIOUR

The dynamic behaviour of detection systems should be more carefully measured and described than is usually done in analytical chemistry. The reason is that peak broadening in the detection system ultimately limits the speed with which the total analytical system can generate new independent information. In chromatography, the sequence of peaks delivered to the detection device should be monitored without distortion [2]; thus the maximum frequency with which the peaks may elute from the column depends on the detection system. Analogously, in flow injection analysis, the dynamic behaviour of the detection system sets an upper limit to the frequency with which samples can be injected. If this limit is exceeded, peak width will be larger than the time spacing between peaks, and the measurement at a peak maximum will be influenced by the intensity of the preceding peak; this is known analytically as a carry-over effect.

For a general discussion of peak broadening, it is first assumed that the calibration curve is linear from the region where signal changes are indistinguishable from noise, up to a certain concentration of the analyte. Next

it is assumed that the detector is time-invariant, i.e. the input—output relation of the detector itself is not a function of time. This condition is fulfilled for instance in the u.v. absorption detector, but not in a polarographic detector where the signal for a constant input fluctuates with drop frequency. Linear time-invariant systems can be studied most easily.

The output signal function can be described as the convolution of the concentration input function with the impulse response function of the system [2] (Fig. 2):

$$V(t) = c(t) * h_d(t) = \int_0^{\infty} c(t - \tau)h_d(\tau)d\tau \quad (1)$$

where $V(t)$ is the signal value at moment t , $c(t)$ is the concentration at moment t , τ is a dummy time variable, and $h_d(\tau)$ is the impulse response function of the detection system.

The signal value therefore depends not only on the momentary value of the concentration $c(t)$ but on its value during the time preceding the moment t ; in principle the integral should be extended to minus infinity. The integral (eqn. 1) is the mathematical formulation of a phenomenon which, depending on circumstances and physical causes, can be described more or less accurately as memory effect, carry-over, (extra) peak broadening, dispersion, or amplifier time constant. The function $h_d(\tau)$ can be observed if the $\delta(t)$ function can be approached experimentally as a concentration input profile, by means of a very fast injection device.

The function $h_d(\tau)$ is related to the static sensitivity S , which is defined as the ratio between signal change and concentration change. If $c(t)$ in eqn. (1) is maintained constant, then it can immediately be derived that

$$S = \int_0^{\infty} h(\tau)d\tau \quad (2)$$

Manipulation with the full $h(\tau)$ function is rather awkward in practice, hence it is indeed useful to express the intensity of the $h(\tau)$ function in this one value,

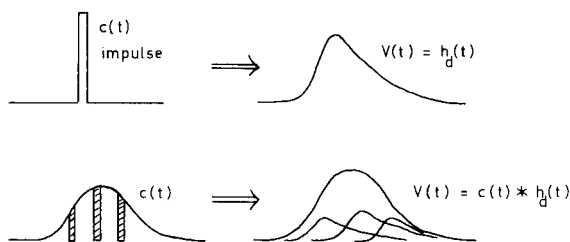


Fig. 2. Illustration of the convolution integral in the response of a detection system to the input concentration profile. Upper drawings refer to the case where an impulse input is applied to the concentration input of the detection device and the impulse response is obtained at the output. Lower drawings refer to the case where a concentration profile of significant width is input to the detector. If the input is regarded as an infinite sum of impulses, the linear time-invariant detector will have a response which is the sum of the responses to each of these impulses.

S , which can quite easily be obtained experimentally. Such reduction, which neglects the width of the $h(\tau)$ function, is however rather crude, and so at least one additional feature is needed to indicate the width of this function. This can be done in numerous ways; concepts like "full width at half maximum", "standard deviation", "time constant" are in use to indicate widths of peaks. Shapes of response curves for various detectors differ widely, and even for one detector the shape depends on the conditions. It is then obviously impossible to describe the $h(\tau)$ function by one or even two features or numbers; it is important to realize that whatever measure of broadening is adopted, some approximation is intrinsic in the use of one number for this effect.

Chromatographers express peak width as a standard deviation σ_t . Irrespective of the method of measuring the width, the standard deviation in a gaussian curve necessary to give this measured result is calculated; for example, drawing tangents would give $4\sigma_t$ for the base-line intersection distance in a gaussian curve, and σ_t is therefore calculated as one fourth of the intersection distance observed. Such methods have a number of advantages: they are simple, the influence of noise is small, and the data handling equipment can be as simple as a strip-chart recorder.

Mathematical elegance is obtained at the price of numerical complexity, if the peak width is measured by the real standard deviation of the response curve, the root of the centralized and normalized second moment of this curve. The elegance lies in the fact that if a number of systems k are placed in series, e.g. an injection device, reactor and detecting device, then additivity of the variances is obtained in the final result [1-3]:

$$\sigma_{t,\text{tot}}^2 = \sum_k \sigma_{t,k}^2 \quad (3)$$

Fortunately, this relation is also a very realistic approximation when the standard deviation is determined in simpler ways, which do not require numerical integration to obtain the second moment. For gaussian response curves, all the simple estimates coincide with the real standard deviation. Equation (3) indicates that the weakest link in the chain of systems is largely responsible for determining the final width of the peak.

For some purposes it is more convenient to express the peak width or standard deviation in volume units rather than in time units by using the equation: $\sigma_{v,d} = w\sigma_{t,d}$, in which $\sigma_{v,d}$ is the volume standard deviation, $\sigma_{t,d}$ is the time standard deviation of the detector and w is the flow rate. The standard deviation should be measured by injecting in such a way that a $\delta(t)$ input is approached as closely as possible. A septum injection device [1] (one of the experimental assets adaptable from chromatographic experience) connected with as narrow and short tubes as possible, would serve the purpose. Once the $\sigma_{t,d}$ or $\sigma_{v,d}$ value has been obtained as a function of the flow rate, on which it depends, its relative contribution to the peak broadening in the whole system can be judged. In particular, it becomes possible to draw conclusions for two situations. First, if the detector is used for measuring the

peak broadening characteristic of another element k in the system, it is essential to ensure that the results reflect this element and not some deficiency of the detection system. Thus, for an accuracy criterion of 5%: $\sigma_{t,d} < 0.3 \sigma_{t,k}$. Secondly, for optimized performance of f.i.a. in terms of sample throughput per hour, it can be stated that a sample peak should not come earlier than $k_1 \sigma_{t,tot}$ after the previous peak, in order to avoid carry-over. Thus $f_{max} < 1/k_1 \sigma_{t,tot}$, in which f_{max} is the maximum sample frequency and k_1^{-1} is a factor depending on the acceptable amount of carry-over (peak overlap), i.e. the accuracy of the analysis, and also on the data handling method (peak height/area). k_1 should usually lie between 4 and 6 and corresponds to the chromatographic resolution R .

This f_{max} relationship enables the maximum sampling frequency to be inferred directly from the detector characteristic $\sigma_{t,d}$ when all other subsystems are "perfect", i.e. they contribute nothing to $\sigma_{t,tot}$.

These considerations may seem trivial, but experience in gas and liquid chromatography has shown that quite often much effort is devoted to improving the better-performing components of the systems in series, which according to eqn. (2) is useless.

Causes of peak broadening

Once the black box concept has served its purpose, the system itself must be examined in order to establish the features actually responsible for the peak broadening. Essentially there are three causes of peak broadening: (1) dispersion in tubes; (2) finite effective measuring volume; (3) dynamic behaviour of transducer, and signal amplifying and handling equipment.

Dispersion in tubes. The dispersion in connecting tubes has been the subject of a number of studies [4–6]. For straight and sufficiently narrow and long tubes of radius R_t and length L_t , the volume standard deviation $\sigma_{V,t}$ is given [7] by

$$\sigma_{V,t}^2 = \pi R_t^4 L_t w / 24D \quad (4)$$

and the time standard deviation by

$$\sigma_{t,t}^2 = t_{Rt} R^2 / 24D \quad (5)$$

where t_{Rt} is the residence time and D is the diffusion coefficient.

The application of these reactions, known as the Taylor equation, requires some care in f.i.a. as well as in liquid chromatography. The equation was derived (and in fact can only be derived) under the condition that the length of the tube, its radius and the mean residence time satisfy the criterion $Dt_R > R_t^2$. With tubes of 0.5–2 mm inner diameter and residence times of a few seconds, this condition is not met at all. The equations in that case predict a standard deviation much larger than that actually found. Moreover, coiling of the tube diminishes the dispersion.

Nevertheless, eqns. (4) and (5) are useful in that they predict the qualitative influence of the various parameters properly, and become more and more

accurate when longer lengths or residence times and smaller diameters (the critical cases) are used. Finally, they constitute a reference point from which the effect of coiling can be discussed [10].

When tubes are used simply for connections, length L_t and radius R_t are determined by practical considerations. If a tube is to be used as a flow-through chemical reactor, the residence time t_{Rt} in the tube is fixed by the time requirement of the chemical reaction, and in that case the second formula is more instructive. Expression (5) shows that the volume standard deviation increases with flow rate, and increases for lower diffusion coefficients D . Also, a dramatic increase is to be expected from an increase of the tube diameter; in order not to impair the performance of detectors, tubes preferably should be 0.5 or even 0.25 mm in diameter.

When tubes are used as reactors (delay elements), the choice of the diameter becomes critical as soon as the required reaction time exceeds 20 s. A compromise between pressure drop and peak broadening has then to be made. This has been discussed in several papers [8, 9]. The peak broadening is significantly smaller if the tube is coiled, because of the effect known as secondary flow [8–11]. When the required reaction time is even larger, other types of reactors should be used; a packed-bed reactor gives a more favourable compromise than an open tube [8, 9] at least at practical values of the flow rate. Reaction times in excess of 10 min generally should not be attempted in a homogeneous flow-through reactor; the air-segmentation principle [12–14] then shows superior performance.

Finite effective measuring volume. The peak broadening effect caused by the finite effective measuring volume is rather difficult to predict, because the exact flow profile is usually unknown, and the effective measuring volume is often also unknown. For some extreme situations, however, estimates are possible. If the effective measuring volume equals the cell volume V_c and plug flow prevails, a molecule will contribute to the signal during a time V_c/w . An impulse input will yield a rectangular block output, with a base V_c/w and a (volume) standard deviation (second moment) $V_c/12^{1/2}$. If, however, the cell behaves as an ideal mixer, an exponential with time constant V_c/w will be the response, corresponding to a volume standard deviation equal to V_c . Most practical cases will lie in between these two extremes, so that generally the volume standard deviation can be expressed as $\sigma_{V,c} = \alpha V_c$, in which α is a numerical factor between 1 and 0.3.

For some measuring techniques, such as u.v.-visible absorption and radioactivity counting, the detection limit in concentration diminishes with increasing cell volume [15, 16]. In such cases, the choice of V_c constitutes a compromise between peak broadening and detection limit.

Dynamic behaviour of transducer and electronics. Finally, peak broadening is caused by the transducer and electronics. In many cases, these effects can be measured directly by some artificial excitation of this last subchain, e.g. in light absorption by modulating the intensity of the source with an impulse and monitoring the output response curve. These effects are, of course, con-

stant when expressed in time units: $\sigma_{t,e} = C_e$ and $\sigma_{v,e} = wC_e$. Also, they are often predictable from amplifier time constants; every time constant T_k in the amplifier chain contributes T_k^2 to the time variance C_e^2 .

The whole detection system then will have a volume standard deviation determined according to eqn. (3) by adding quadratically the various contributions. Focusing on the dependence on flow rate we get:

$$\sigma_{v,d}^2 = \sigma_{v,t}^2 + \sigma_{v,c}^2 + \sigma_{v,e}^2 = \pi R_t^4 L_t / 24D w + \alpha^2 V_c^2 + C_e^2 w^2 \quad (6)$$

In many cases these three terms are all important, and one or other may predominate depending on the flow rate (Fig. 3).

NOISE AND DETECTION LIMIT

Once the peak broadening effects have been established, the noise in flow-through detectors can be considered. Proper characterization of noise in continuous systems has been widely studied, but the results of these studies have rarely been incorporated [17, 18] in analytical chemistry. Noise is defined as all the changes in the output voltage which do not carry information about the input (concentration). This definition thus includes "drift", "wander", etc.

Under certain conditions [18], noise can be characterized by its power spectrum, or its autocorrelation function; the resulting mean squared error in the measuring result, peak area or height, can then be calculated ab initio. For practical characterization of systems this is too elaborate, but a simpler procedure should at least take into account some qualitative facts emerging from the full description. First, noise in a frequency range considerably lower than $1/\sigma_t$ is observed as a drifting baseline and hardly impairs the precision

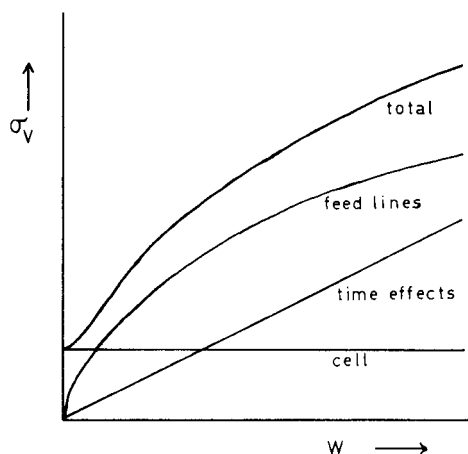


Fig. 3. The three main contributions to the peak broadening and the total peak broadening in a flow-through detector plotted as a function of the flow rate w .

of the results, as readings are made relative to the baseline in the neighbourhood of the peak. Secondly, noise in a frequency range considerably higher than $1/\sigma_t$ can be removed by filtering when peak heights are measured. (When areas are determined, high-frequency noise is without effect anyhow [18].) The filtering constitutes a compromise between peak broadening and detection limit, and the optimal filtering constant depends on the peak width σ_t . Mostly $\tau_{\text{filter}} \approx 0.3 \sigma_t$ is a sensible choice. When these results are taken into account, it becomes possible to determine s_v , the standard deviation* of the noise in the output voltage V . When the signal is low, its influence on s_v can be neglected, and s_v characterizes the baseline noise. The concentration detection limit c_d of the detection system is then $c_d = k_2 s_v / S$, where k_2 is a numerical factor which depends on the statistical confidence level required ($k_2 = 2-4$). It follows from the above that s_v and c_d are in principle dependent on the peak width, but in the following paragraphs this effect, which is usually not strong, will be neglected.

RELATION BETWEEN DETECTOR CHARACTERISTICS AND PERFORMANCE OF THE WHOLE SYSTEM

Speed and dilution

Once the detection system has been characterized by the two performance parameters $\sigma_{v,d}$ and c_d the influence of this performance on the performance of a whole analytical set-up which includes the detection system can be considered.

For the maximum sample frequency:

$$f_{\text{max}} = 1/k_1 \sigma_{t,\text{tot}} = w/k_1 \sigma_{v,\text{tot}} \quad (7)$$

in which the subscript tot refers to the whole set-up. Combination with eqn. (3), taking into account peak broadening from injection (i) and detection, gives

$$f_{\text{max}} = w/k_1 (\beta^2 V_i^2 + \sigma_{v,d}^2 + \dots)^{1/2} \quad (8)$$

in which it is assumed [19-21] that the standard deviation of the injection $\sigma_{v,i}$ is proportional to the injected volume V_i ; β is the proportionality factor. Given a certain detection system and a fixed flow rate w , the ultimate speed is obtained when the injected volume is small compared to $\sigma_{v,d}$. However, this is also the situation where appreciable dilution of the analyte occurs. For gaussian peak shapes,

$$c = M/(2\pi)^{1/2} \sigma_{v,\text{tot}} = V_i c_0 / (2\pi)^{1/2} (\beta^2 V_i^2 + \sigma_{v,d}^2)^{1/2} \quad (9)$$

(where M and c_0 are the amount and concentration on injection)

and in this extreme case of maximum speed there is a dilution factor

$$c_0/c = (2\pi)^{1/2} \sigma_{v,d} / V_i \quad (10)$$

* σ and s are used here consistently for peak broadening and noise statistics standard deviations, respectively; confusion with nomenclature where σ = population s.d. and s = estimate of s.d. should be avoided.

and the concentration detection limit of the system is worse than that of the detector by this factor. The dilution factor occurring in one stage is not a characteristic of this stage, but depends on the preceding stages. The variances (or standard deviations) are characteristics, and are additive; from the result the dilution can be estimated, as in eqns. (9) and (10).

If dilution is to be avoided, in order to keep the detection limit of the analysis as low as possible, $\beta^2 V_i^2$ should be large compared to $\sigma_{V,d}^2$. A loss in maximum speed is then unavoidable, because the maximum sampling frequency approaches $f_{\max} = w/\beta V_i$. This shows, incidentally, the importance of the injection performance parameter β , as discussed elsewhere [20, 21].

When both speed and detection limit are critical, a compromise is necessary. As shown by Huber et al. [19] and Karger et al. [20], when V_i is of the order of $\sigma_{V,d}$, the losses both in speed (chromatographic resolution in their case) and detection limit can be kept acceptable, a result which can easily be derived from the above expressions.

It should be noted that this compromise is significantly more unfavourable if a third peak-broadening element is present in the system which broadens the peak more than the detection system does. In that case the ultimate speed is determined by this third element, even when considerable dilution is acceptable. Dispersion may be used deliberately as a third element for dilution of samples in those cases where high concentrations in the original samples would lead to interference and measuring problems. The inherent loss in speed can be avoided in two ways: first, the required dilution can be obtained simply by decreasing the injected volume V_i ; secondly, if the necessary values of V_i become impractically small, dilution can be achieved by admixing of the solvent at a T-piece.

Longitudinal dispersion is widely used in f.i.a. to bring about proper mixing of reagent(s) and analyte [22]. Appreciable dilution of the sample is then inevitable. If the reagent is to penetrate by dispersion into the sample zone so effectively that, e.g., the reagent concentration is at 90% of its original value in the centre of the zone, the same dispersion process will dilute the sample to 10% of its original concentration. Unless the injected volume is small compared to the peak broadening of the detection device $\sigma_{V,d}$, by the same reasoning, it can be shown that a loss in speed will result. These drawbacks again can be mitigated by admixing in a T-piece. The design of the T-piece should aim at efficient transversal mixing of reagent and sample, while avoiding longitudinal mixing (dispersion). This approach, commonly used in post-column reaction detection in liquid chromatography [23], also introduces an additional degree of freedom in the design of the whole system, as the reagent concentration and the pumping speed of the reagent solution can be varied independently while their product is kept constant.

It should be noted that some delay elements used as reactors, e.g. capillaries and packed-bed columns, do not effectively mix reagent and sample transversally. Introduction of a mixture which is not homogeneous over the cross-section in such reactors may lead to very erratic results. Suitable mixing devices in front of these reactors are essential.

Absolute detection limit

The above considerations are relevant if the concentration in the sample is low but the sample size can still be adjusted to the required optimal compromise without problems. However, in certain analytical problems, the sample size may also be limited, e.g. in forensic and clinical work. For such cases it is better to derive from eqns. (9) and (10)

$$\underline{M} = k_2 c_d (2\pi)^{1/2} \sigma_{V,\text{tot}} = \underline{c}_d \cdot (\beta V_i^2 + \sigma_{V,d}^2 + \dots)^{1/2} \quad (11)$$

which, for $V_i \rightarrow 0$, gives $\underline{M} = k_2 c_d \cdot \sigma_{V,d}$ as the ultimate detection limit (in mass) which can be realized (when peak broadening contributions from other elements are negligible) with the detector available.

CONCLUSION

Detection systems and detectors constitute building blocks for analytical systems. The proper design of an analytical system is greatly facilitated if separate building blocks, such as sampling devices, reactors, detectors, etc., can be characterized by parameters which describe their effect on the performance of the whole analytical system, but do not depend on the particular set-up in which the building block is used.

For liquid phase flow-through detection systems, the volume standard deviation $\sigma_{V,d}$ and the concentration detection limit \underline{c}_d constitute the two parameters which are most relevant if the total analytical system is to be evaluated in terms of speed of analysis (throughput) and detection limit, either in concentration or in mass. By simple deductions, which take into account the additivity of variances and the dilution factors from reagent addition, etc., the influence of the detection device in determining maximum speed and detection limit of the whole system can be quantitatively discussed. Such an approach facilitates the search for optimal combinations and diminishes the risk of unjustified experimental efforts.

REFERENCES

- 1 J. F. K. Huber, *J. Chromatogr. Sci.*, 7 (1969) 172.
- 2 J. C. Sternberg, *Advances in Chromatography*, Vol. 2, M. Dekker, New York, 1966.
- 3 J. Kirkland, *J. Chromatogr. Sci.*, 15 (1977) 303.
- 4 I. Halász and P. Walking, *Ber. Bunsenges. Phys. Chem.*, 74 (1970) 66.
- 5 R. P. W. Scott and P. Kucera, *J. Chromatogr. Sci.*, 9 (1971) 641.
- 6 J. F. K. Huber, R. van der Linden, E. Ecker and M. Oreans, *J. Chromatogr.*, 82 (1973) 267.
- 7 R. Aris, *Proc. Roy. Soc. London, Ser. A*, 235 (1956) 67.
- 8 R. S. Deelder, M. G. F. Kroll, A. J. B. Beeren and J. H. M. van den Berg, *J. Chromatogr.*, 149 (1978) 669.
- 9 J. F. K. Huber, K. M. Jonker and H. Poppe, *Anal. Chem.*, in press (Dec. 1979).
- 10 R. Tijssen, *Sep. Sci.*, 13 (1978) 681.
- 11 K. Hofmann and I. Halász, *J. Chromatogr.*, 173 (1979) 211.
- 12 L. R. Snyder, *J. Chromatogr.*, 125 (1976) 287.

- 13 L. R. Snyder and H. J. Adler, *Anal. Chem.*, 48 (1976) 1017.
- 14 L. R. Snyder and H. J. Adler, *Anal. Chem.* 48 (1976) 1022.
- 15 W. Baumann, *Fresenius Z. Anal. Chem.*, 284 (1977) 31.
- 16 G. B. Sieswerda, H. Poppe and J. F. K. Huber, *Anal. Chim. Acta*, 78 (1975) 343.
- 17 P. C. Kelly and W. E. Harris, *Anal. Chem.*, 43 (1971) 1170.
- 18 H. C. Smit and H. L. Walg, *Chromatographia*, 8 (1975) 311.
- 19 J. F. K. Huber, J. A. R. J. Hulsman and C. A. M. Meijers, *J. Chromatogr.*, 62 (1971) 79.
- 20 B. L. Karger, M. Martin and G. Guiochon, *Anal. Chem.*, 46 (1974) 1640.
- 21 J. M. Reijn, W. E. van der Linden and H. Poppe, *Anal. Chim. Acta*, 114 (1980) 105.
- 22 J. Růžička and E. H. Hansen, *Anal. Chim. Acta*, 99 (1978) 37.
- 23 R. W. Frei, L. Michel and W. Santi, *J. Chromatogr.*, 126 (1976) 665.

AXIAL DISPERSION AND FLOW PHENOMENA IN HELICALLY COILED TUBULAR REACTORS FOR FLOW ANALYSIS AND CHROMATOGRAPHY

R. TIJSSEN

Koninklijke/Shell Laboratorium (Shell Research B.V.), Amsterdam (The Netherlands)

(Received 12th September 1979)

SUMMARY

Open tubular reactors for flow analysis and post-column reactors for chromatography are commonly designed as rather tightly coiled helices. It is shown experimentally that the dynamics of flow and axial dispersion in such coiled tubes can differ substantially from behaviour in straight tubes. The differences are almost quantitatively accounted for by the existence of secondary flow phenomena in coiled tubes. On the basis of these coiling effects, practical parameters such as sampling rate, reagent consumption, tube dimensions, pressure drop, etc. are estimated, optimized and compared with those in other systems (segmented-flow and packed-bed reactors).

Peak or zone broadening in flow-through open tubes is a classical problem encountered in analytical separation techniques as well as in physical and chemical technology (where it is called residence time distribution or axial dispersion). In flow injection analysis (f.i.a.), an analytical technique introduced by Růžička and Hansen [1] and Stewart et al. [2], the transport phenomena in the flowing medium are analogous to those in the mobile phase flowing through chromatographic separation columns. However, instead of chromatographic partitioning, commonly a chemical reaction occurs in flow analysis. The f.i.a. column may thus be regarded as a (chromatographic) tubular reactor and for a study of axial dispersion the vast amount of data published in the chromatographic and technological literature should be consulted. On the basis of this information, Růžička and Hansen [3] decided to use descriptive models, such as the tank-in-series model, for representing their experimental results on axial dispersion and concentration profiles in f.i.a. systems. Although they certainly succeeded in formulating practically useful rules with the aid of such a plate model, more sophisticated models, which account for the underlying physical (and chemical) mechanisms, are necessary for making predictions for future optimization work. Růžička and co-workers [3–5] were aware of at least one of the physically more realistic models, which they used in a qualitative sense only, namely Taylor's concept of axial dispersion in flow-through (straight) open tubes [6]. Taylor's concept also played a decisive role in the development of

capillary chromatography. His analysis is valid only for times t longer than $(R/3.8)^2/D_M$ [6]. (For explanation see list of symbols, Table 1.) In contrast to a statement by Betteridge [5], this condition is nearly always met in f.i.a. practice. Hence, at least in straight tubing, Taylor's model should apply and nearly symmetric peaks of a Gaussian shape may be expected. However, in f.i.a., peaks mostly show a tailing character, even in the absence of T-piece mixers and chemical reactions [1, 3–5]. This behaviour is just the opposite of the only slightly asymmetric peaks which are predicted by Taylor's model and are indeed observed in numerous experiments in capillary chromatography. Chromatographic experience also reveals that asymmetries like those observed in f.i.a. can be easily generated by extra-column effects such as nonideal connections between column, injector and detector, poor T-piece connections, abrupt changes in internal diameter, slowness of injection, detection and recording, etc. [7]. In chromatography these non-idealities have been quite successfully overcome by a judicious design of all parts of the system. This of course increases the cost of instrumentation, which runs counter to the popular philosophy behind f.i.a., i.e. to keep designs as simple as possible so as to arrive at inexpensive (though inefficient) apparatus. Undoubtedly, for optimal f.i.a. work future designs will have to be changed so as to match those of present-day chromatography. By way of example, in Fig. 1 a comparison is made between the peak shape obtained by Růžička

TABLE 1

List of symbols used

d	internal tube diameter, $d = 2R$ (cm)	R_h	helix radius (cm)
d_p	particle diameter (μm or cm)	Re	Reynolds number, $2uR/\nu$
D	plate height H at $u = 1$ cm/s (eqn. 14) (cm)	Re_c	critical Reynolds number
De	Dean number, $Re \lambda^{1/2}$	S	sampling rate (min^{-1})
D_M	molecular diffusion coefficient ($\text{cm}^2 \text{s}^{-1}$)	Sc	Schmidt number, ν/D_M
D_r	radial dispersion coefficient (total) ($\text{cm}^2 \text{s}^{-1}$)	t	time (s)
D_s	radial dispersion coefficient from secondary flow ($\text{cm}^2 \text{s}^{-1}$)	u	linear flow velocity (cm s^{-1})
f	friction factor	α	defined in eqn. (2)
F	volumetric flow rate; flow limit in Figs. ($\text{cm}^3 \text{s}^{-1}$)	γ	surface tension (dynes cm^{-1})
h	peak height in Fig. 1 (arb. units)	η	dynamic viscosity (P)
H	plate height (cm)	κ	velocity profile factor
L	length (cm)	λ	aspect ratio, R/R_h
n	segmentation rate (eqn. 12) or power (eqn. 14)	ν	kinematic viscosity, η/ρ ($\text{cm}^2 \text{s}^{-1}$)
Δp	pressure drop (dynes cm^{-2})	ρ	density (g cm^{-3})
P	pressure limit in Figs.	σ_t	standard deviation in time units (s)
Q	reagent consumption per peak (cm^3)	ϕ	angle
R	internal radius of tube (cm)	<i>Indices</i>	
		cf	centrifugal
		o	straight tube
		s	secondary flow

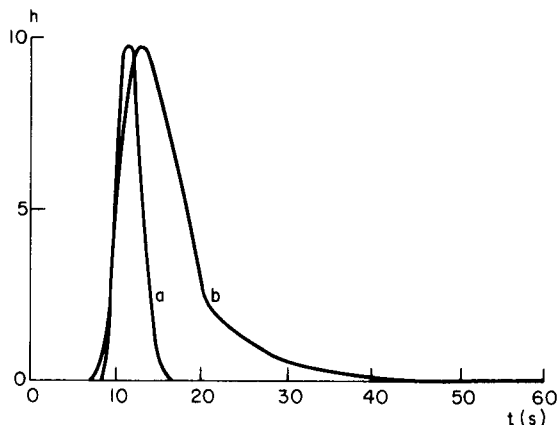


Fig. 1. Comparison of peak shapes of response curves obtained here (a) and by Růžička and Hansen (b) [3] under comparable conditions. (a) Toluene injected into iso-octane pumped at a rate of 7.06 ml min^{-1} . Tube: $R = 0.0383 \text{ cm}$; $L = 300 \text{ cm}$; $\lambda = 0.08$. (b) Dye solution injected into water pumped at a rate of 1.5 ml min^{-1} . Tube: $R = 0.025 \text{ cm}$; $L = 125 \text{ cm}$ [3].

and Hansen [3] and that recorded by using the apparatus to be described in the Experimental section. The two peaks were generated under comparable conditions (nearly the same residence times; similar tube dimensions). The peak of case (b) is typical of published f.i.a. work; its pronounced asymmetry should be ascribed to large extra-column effects. Even with strongly reduced tube diameters and with incorporation of a mixing T-piece, no peak asymmetry was observed in our apparatus, which is a critical test for extra-column broadening in view of the reduced column volume. In fact, with the experimental set-up used here no significant deviation from Taylor behaviour was found for nearly straight tubes, which opens up the possibility of optimizing f.i.a. on the basis of the principle that peak dispersion is determined by the dynamics of flow and diffusion within the column itself. Complications which have to be considered and dealt with in future work stem from sample size and chemical reaction, both of which are well known sources of peak asymmetry [3, 7, 8].

EXPERIMENTAL

A detailed description of the apparatus and the manner of data interpretation used in this work has been given elsewhere [9, 10]. The essentially chromatographic apparatus had been designed in such a way that dead volumes, abrupt changes in internal diameters and the occurrence of large time constants in detectors, recorders and accompanying electronic circuitry were reduced to a minimum.

Liquid samples were injected into a liquid mobile phase by means of a Waters U6K injector. A convenient injection technique, which largely obviates

the occurrence of asymmetrical tailing peaks, consists in filling the sample loop of the injector completely with the sample solution and rapidly switching the handle into the injection mode and immediately back into the standby mode. The peak trains recorded for flow analysis in this background study were generated by manual operation of the injector (which explains the differences in peak height in Fig. 2, A and B). In a final version for flow analysis application this operation should of course be automated, e.g. by pneumatic means.

The main detector used in this work was a Waters Model 440 u.v. absorbance detector (254 nm) with a flow cell of 12.5- μ l dead volume. The total dead volume of the detector system including a short connecting line amounted to 25 μ l. This relatively large volume in combination with the

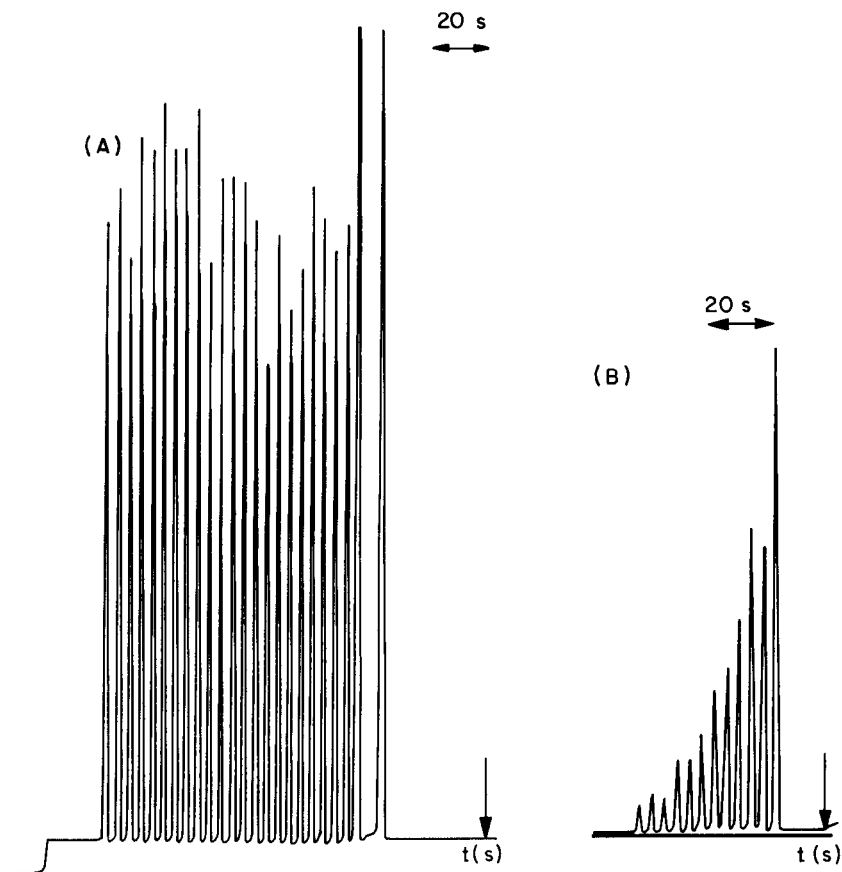


Fig. 2(A). F.i.a. in a microcapillary tube ($R = 14 \mu\text{m}$, $L = 325 \text{ cm}$) for toluene in iso-octane; residence time per peak, 42 s. (B) F.i.a. in a coiled tube ($R = 0.01 \text{ cm}$, $L = 920 \text{ cm}$, $\lambda = 0.02$) for toluene in iso-octane; residence time per peak, 13.8 s; sample rate, 15 peaks/min; expected rate, 18; sample rate in straight tube under same conditions, 5 peaks/min.

type of electronic circuitry used in the detector resulted in a time constant of several tenths of a second. Hence, only peaks with a total width corresponding to more than say 0.5 s could be handled without distortion (tailing), while a minimum flow rate of 0.5–1 ml min⁻¹ had to be maintained in order to avoid additional peak broadening and tailing. This meant that particularly with microcapillaries, where flow rates can be as low as 1–100 μ l min⁻¹, the addition of extra mobile phase via a T-piece construction at the column outlet was sometimes necessary. A similar T-piece was used as a splitter at the column inlet in order to avoid peak broadening and tailing caused by the abrupt change in diameter on going from the sample loop to the column. Both T-pieces had been constructed with great care in order to minimize additional peak broadening in this model study. Again, in a final version for practical flow analysis application, both T-pieces should be avoided by using effectively miniaturized detectors and injectors instead.

All the columns with internal diameters in excess of 100 μ m employed in this study consisted of commercially available metal tubing (stainless steel, silver). Small-diameter tubing was drawn from soft-glass (AR-type) pipes by using an adapted Shimadzu (Model GDM-1) glass-drawing machine. Tight coiling of these columns (minimum coil diameter 8 mm) was accomplished with home-made apparatus. Glass–metal connections were made by glueing techniques.

THEORETICAL

For reasons of practical convenience, the tubing in f.i.a. (as well as in chromatography) is coiled into a helical configuration. In view of the centrifugal forces active in any curved flow channel, another flow, perpendicular to the main flow, is generated. As this secondary flow phenomenon stimulates transfer processes in a radial sense, coiled tubes have been in use for a long time, e.g. as effective mixing tubes for liquids and as effective heat exchangers. From earlier work [9–13], it can be concluded that peak dispersion can be far less pronounced in tightly coiled open tubes for chromatography than in straight tubes, as a consequence of the coiling effects induced by the secondary flow phenomenon.

The use of tightly coiled tubes for f.i.a. (and post-column reactors for chromatography) is recommended here as a means of arriving at a higher sampling rate and a lower reagent consumption than can be obtained with any other system, including segmented-flow and packed-bed reactors.

Flow phenomena in coiled tubes

As a result of the curved nature of the flow channel in a coiled tube, centrifugal forces produce a secondary flow in the radial direction; this phenomenon is well documented in the literature [9, 10, 14, 15].

At low velocities the centrifugal forces are still weak and the secondary flow hardly requires any additional pressure compared with straight-tube

flow; nor does the axial velocity profile differ much from the well-known parabolic profile after Poiseuille. Secondary flow manifests itself in the formation of two radial circulation patterns, which tend to divide the original tube into two parallel and equal halves (cf. Fig. 3).

At higher velocities the centrifugal forces increase sharply; particularly the faster moving central fluid elements are forced against the outer column wall. This results in a more or less linear velocity profile and a high boundary-layer flow along the inner column wall (Fig. 3, lower parts). At very high velocities the boundary layer thickness decreases and the velocity profile tends to plug flow while turbulence sets in. It is well known, however, that coiling tends to stabilize laminarity, i.e. the critical Reynolds number, Re_c , at which turbulence occurs, is much higher in coiled tube flow than in straight tubes, where $(Re_c)_0 \approx 2300$. In our experience a good estimate can be obtained from [15]:

$$Re_c/(Re_c)_0 = 1 + 12 \lambda^{1/2} \tag{1}$$

where λ represents the ratio between column radius R and coil radius R_h . This so-called aspect ratio is a significant parameter in characterizing flow-through coiled tubes; the Dean number, $De = Re \lambda^{1/2}$, rather than Re is commonly used as the (dimensionless) velocity parameter. From eqn. (1) it

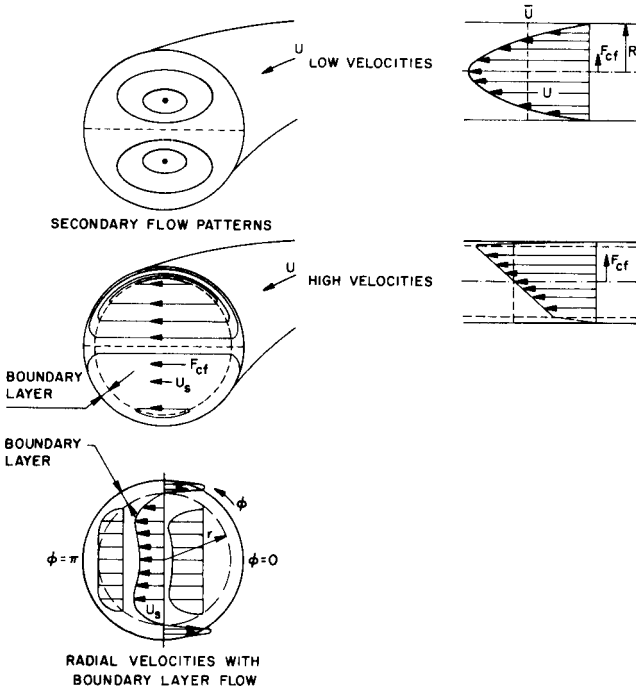


Fig. 3. Secondary flow patterns and velocity profiles in coiled tube flow at low and high velocities.

is seen that with $\lambda = 0.1$ turbulence sets in at about $Re \approx 11500$, which unambiguously explains why turbulence never has been of any importance in f.i.a., in contrast to what has been assumed in earlier work on f.i.a. [5].

Although laminar in nature, it remains to be seen how much additional pressure the secondary flow requires compared with straight tube flow. In view of this, friction factors ($f = (\Delta p/L)R/\rho u^2$) in coiled tubes were measured and compared with $f_0 = 16/Re$ for straight tubes under the same flow conditions, nitrogen being used as the mobile phase. The results are shown in Fig. 4 for a wide range of column radii, aspect ratios and velocities. The average line through the data points can be described by the function

$$f/f_0 = 1 + \alpha(De) ; \alpha(De) = 0.107 De^{1/2} / \{1 + (12/De^{1/2}) + (700/De^{3/2})\} \\ 1/1500 < \lambda < 1/12 ; 0.0125 < R < 0.1 ; 1 < De < 10^4 \quad (2)$$

As shown in Fig. 4 the present experiments agree well with theoretical predictions at high and low De numbers and also with experiments on liquid flow [10, 14–16, 20]. In normal practice De numbers hardly exceed values of about 100 and so it is concluded that commonly $f/f_0 \leq 1.3$; in other words, the pressure drop in coiled tube flow nearly equals that in straight tube flow at the same flow rate. Except for extremely high velocities, where $De > 100$, the Poiseuille relation

$$\Delta p/L = 8u\eta/R^2 \quad (3)$$

for estimating pressure drops will therefore be used in the following discussion.

Dispersion in coiled tube flow

In complete analogy with the Aris—Taylor—Golay [6, 21, 22] treatment of axial dispersion in open tubular columns it is possible, under certain simplifying conditions [9, 10, 12], to arrive at the general van Deemter-type relationship between plate height H and linear velocity u

$$H = (2D_M/u) + (2\kappa R^2 u/D_r) \quad (4)$$

in the absence of chromatographic retention effects. The first term on the right-hand side of eqn. (4) represents axial molecular diffusion, which can be often neglected in practice in view of the low values of D_M in liquids (10^{-5} – 10^{-6} $\text{cm}^2 \text{ s}^{-1}$) and the relatively high velocities u applied (say 1–100 cm s^{-1}). The second term represents the combined action of convective spreading by the velocity differences present in any velocity profile and the counteracting averaging action of radial mass exchange. Here κ is a function of the shape of the velocity profile and may be called the velocity profile factor. D_r is the radial dispersion coefficient which contains contributions from molecular diffusion (D_M) and secondary flow (D_s). Both κ and D_r are thus functions of velocity, as discussed in full detail elsewhere [9, 10]. Equation (4) is equally valid for straight tubes, where $\kappa = \kappa_0 = 1/48$ and $D_r = D_M$ are both constant. Thus

$$H_0 \cong R^2 u / 24 D_M \quad (5)$$

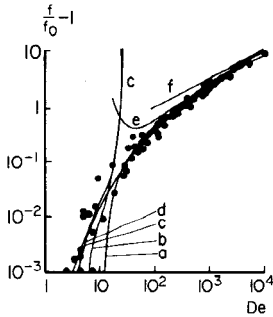


Fig. 4. Relative friction factors in coiled tubes compared with those for straight tubes under equal flow conditions. (a) Experimental correlation after White [16] for liquids; (b and c) theoretical after Topakoglu [17] for $\lambda = 1/175$ and $1/10$, respectively; (d) best fit to the present experiments (eqn. 2) with gases; (e) theoretical after Mori and Nakayama [18]; (f) asymptotic theoretical relation after Adler [19].

which equals the Taylor dispersion equation. Theory predicts [9, 10, 14] that in liquid flow-through coiled tubes both κ and D_r are mainly dependent on the velocity parameter De^2Sc . Thus it is expected that plotting H vs. De^2Sc will yield a single curve for all possible values of R , λ , and D_M . Figure 5 shows this to be approximately true for a large number of new experimental data and recalculated literature data. Part of the spread observed can be attributed to the fact that in the literature most data were obtained by straightforward determination of peak position and peak width instead of the much more correct moments [7, 8]. The remaining deviations from the average line

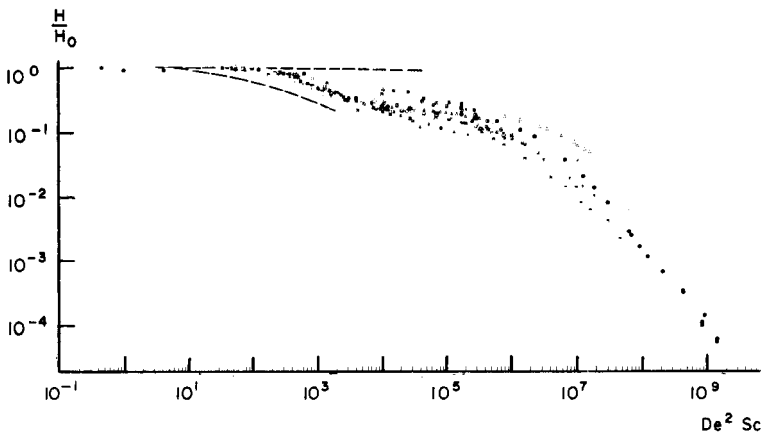


Fig. 5. Relative axial dispersion in liquid flow through coiled and straight tubes. This work: (\bullet) solute KI, $Sc = 525$; (\circ) solute dobanol, $Sc = 2450$; stainless steel column, $R = 0.040$ cm, $L = 10$ m, $\lambda = 1/20$; mobile phase H_2O for KI and dobanol; (\ominus) solute toluene, mobile phase iso-octane; $Sc = 266$; glass column, $R = 0.038$ cm, $L = 9$ m, $\lambda = 1/103$. Literature data recalculated: cf. ref. [10].

through the data in Fig. 5 can be explained by extra-column broadening effects and by the theoretically predicted small influences of changes in λ and D_M [9, 10]. The general tendency of lowering of the plate height (and hence peak width) with increasing velocity forms the basis of a further discussion, which considers the conditions under which coiled tubes can compete with existing f.i.a. systems.

The dependence of plate height on velocity observed in Fig. 5 is well explained by theory [9, 10] and has, for a restricted range of velocities, also been found by other authors [23, 24]. At very low velocities ($De^2Sc < 10$) H equals H_0 , i.e. the coiled tube behaves like a straight tube, as the centrifugal forces are too small to affect the flow patterns. At $De^2Sc > 10$, secondary flow develops gradually and is well established at $De^2Sc > 10^4$, where H reaches a kind of plateau value equal to ca. $H_0/4$. This corresponds to the reduction of the diffusion distances by a factor of about 1/2, accompanying the formation of the two equal parallel column halves (Fig. 3). The more or less linear drop of H/H_0 at still higher velocities is a consequence of the boundary layer flow and the change of velocity profile from parabolic to almost linear. (H/H_0) values of 10^{-4} are seen to be reached at $De^2Sc = 10^9$, which implies a substantial improvement in peak width by a factor of ca. 10^{-2} as compared with straight tubes, under still laminar flow conditions.

CONSEQUENCES FOR FLOW INJECTION ANALYSIS

Recently [4, 25] there has been some debate concerning the question whether or not segmented flow systems are to be preferred over non-segmented flows, based on a comparison of practical parameters such as sampling rate and reagent consumption. The discussion was centred on straight column behaviour; from the foregoing, coiled tubes may be expected to behave much more favourably.

Straight tubes

The sampling rate S equals the number of peaks of width $6\sigma_t$ that can be placed within a specified time, say 1 min. The factor 6 used in the peakwidth $6\sigma_t$ has deliberately been made rather large so as to obtain a pessimistic estimate of the parameters to be calculated. The peak variance σ_t^2 then follows, with $H = L(\sigma_t/t)^2$, from Taylor's equation (eqn. (5)), as:

$$(\sigma_t)_0^2 = R^2 t / 24 D_M \quad (6)$$

which is valid provided that $t > R^2 / (3.8)^2 D_M$ [6], i.e. with eqn. (6) $t \geq 1.5 (\sigma_t)_0$. Roughly speaking, this implies that the residence time t should be at least of the same order of magnitude as the peak width, which is always the case in practice. However, an upper limit in t for the validity of eqn. (6) can be formulated from the fact that eqn. (6) can be obtained from eqn. (4) only for negligible axial molecular diffusion and $\kappa = \kappa_0 = 1/48$. Hence, from eqn. (4) it follows that: $u > (D_r / \kappa R^2)^{1/2} \approx 7 D_M / R$ or $t = L/u < RL / 7 D_M$, which, in practice, is of the order of 10^3 s or more.

The sampling rate S_0 for straight tubes then equals $60/6(\sigma_t)_0 = 10/(\sigma_t)_0$ and so with eqn. (6):

$$S_0 = 10 (24D_M/R^2t)^{1/2} = (49/R) (D_M/t)^{1/2} (\text{min}^{-1}) \quad (7)$$

S_0 is seen to depend only on D_M , R and t and is thus independent of tube length L , flow F , pressure drop Δp , etc. L , F and Δp are important variables, however, with practical upper limits, which in turn determine limiting values for R and t , as will be seen shortly. Equation (7) suggests that small column diameters and short reaction (or residence) times favour high sampling rates, in accordance with earlier conclusions reached by several authors. Small column diameters are of course also favourable for reagent consumption (flow F) or reagent consumption per peak $Q = F.6\sigma_t$. From eqn. (3) with $u = L/t$ and from $F = u\pi R^2$, then

$$L^2/t = \Delta p R^2 / 8\eta \quad (8)$$

and so:

$$Q_0 = 6\pi R^3 L / (24D_M t)^{1/2} = (3\pi/4) R^4 (\Delta p / \eta D_M)^{1/2} (\text{cm}^3) \quad (9)$$

which reveals a very strong dependence on column radius indeed. Hence, this supports Ružička's arguments for miniaturization [4]. For example, the currently used common tubing of 0.5 mm internal diameter (i.d.) operated at say 4 bar requires (with $\eta D_M \approx 10^{-7}$) $Q_0 = 5.82$ ml/peak, whereas miniaturized tubing of say 50 μm i.d. would require a lower Q_0 value by a factor of 10^4 . As stated before, small column radii also favour high sampling rates (eqn. 7), and as $Re = R^2 \rho (\Delta p / 2\eta^3 t)^{1/2}$ this is equivalent to Ružička's statement [4] that low Reynolds numbers should be used. In a more recent publication by Ružička and Hansen [3] this statement has, however, been somewhat weakened: "Rule 7: To obtain maximum sampling frequency the linear flow velocity in the flow cell should be kept high". It is advisable to replace these kinds of rule of thumb by more absolute estimates such as those used in the present discussion. Margoshes [25] reached the opposite conclusion: ". . . . the maximum sampling rate falls off with decreasing Re ". In our opinion, this is not a justified conclusion as it is used on quite dissimilar experiments, with different tube dimensions (R and L), and on a strong belief in the necessity of vague notions like "incipient turbulence" probably active at higher velocities only. Margoshes is right, of course, in pointing out that certain pressure limitations should be kept in mind. The large work load often claimed in flow analysis work certainly justifies the use of (rather expensive) chromatographic solvent delivery pumps instead of the now commonly employed peristaltic pumps. The use of chromatographic pumps allows operation at a maximum pressure of say 400 bar. Another practical limitation can be found in the flow which, for most of these pumps, is limited to approximately 30 ml min^{-1} . Both limits are conveniently expressed in terms of the corresponding time limits, t_p and t_F respectively, associated with 400 bar and 30 ml min^{-1} : $t_p = 8\eta L^2 / 4 \times 10^8 R^2$ from eqn. (8), and $t_F = 2\pi R^2 L$ from $F = u\pi R^2$

$= (L/t) \pi R^2$. These limits are indicated in all following Figures by the symbols P and F , respectively.

Figure 6 shows how the sampling rate S_0 depends on the residence time, in accordance with eqn. (7), for a wide range of column radii. It is seen that hardly any limitation in flow occurs for $t > 10$ s (a kind of minimum reaction time in practice), $R < 0.4$ mm and tube lengths up to 10 m. In fact there seems to be no practical limitation in pressure, either, for $t > 10$ s, $R > 5 \mu\text{m}$ and $L < 1.5$ m. Hence, it can be concluded that miniaturization of flow analysis systems is a desirable future goal as it allows sampling rates up to 10^2 peaks/min with 10- or 20- μm i.d. columns and short reaction times ($t < 20$ s). Longer times require wider columns. Figure 6 also contains data points obtained with an actual miniaturized tube (28- μm i.d.) in the apparatus described in the Experimental section. It is seen that with careful avoidance of extra-column broadening effects, miniaturization indeed offers a means of attaining high sampling rates. The microcapillary under discussion behaves like a 30- μm i.d. tube, being only slightly less efficient than expected.

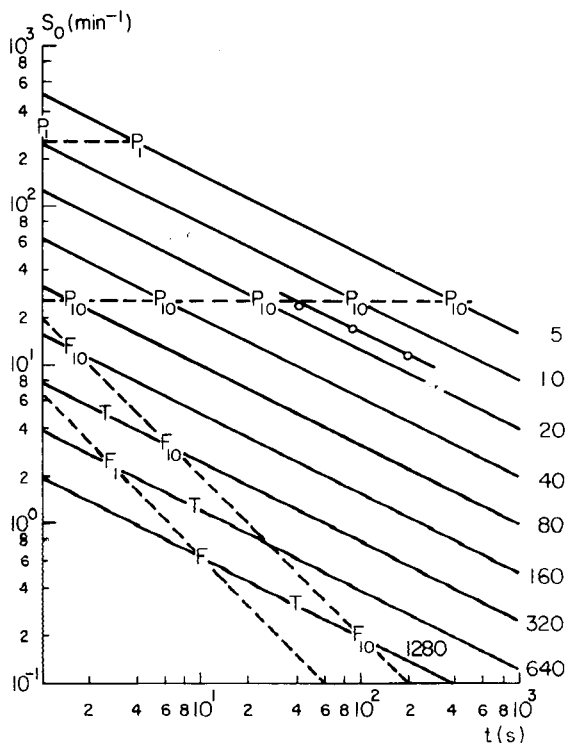


Fig. 6. Sampling rate in straight tubings with different radii. Flow limitation (F) and pressure limitation (P) are indicated for $L = 1$ and 10 m, respectively (broken lines). T is the time corresponding to the Taylor condition. Points (\circ) indicate actual experiments in miniaturized tubing ($R = 14 \mu\text{m}$; $L = 325$ cm) for toluene injected into iso-octane ($D_M = 2.66 \times 10^{-5} \text{ cm}^2 \text{ s}^{-1}$). The numbers on the lines correspond to the radii given in μm .

Figure 2(A) gives an example of a peak train generated with this microcapillary. Of course, sampling rates of the order of 100 peaks/min are seldom necessary in practice but they may eventually become of interest for process control purposes. Sampling rates of this magnitude imply peak widths of say 0.5 s, which is also a limit for currently available detectors such as the chromatographic u.v. liquid detectors which have typical time constants of say 0.25 s. Smaller peak widths can possibly be handled by rapid detection systems such as the diode array spectrometers recently described in the literature [see, e.g. 26].

To conclude this paragraph on straight tubes, it should be noted that the same arguments can be used to support the present-day tendency towards miniaturization in liquid chromatography.

Coiled tubes

In view of the fact that, as shown in Fig. 5, the axial dispersion behaviour in coiled tubes is equal to or better than that in straight tubes, both the sampling rate and the reagent consumption per peak may — qualitatively speaking — be expected to be the same or even better in coiled tubes. Only at very low velocities, corresponding to $De^2Sc < 10$, i.e. for relatively long times, do coiled tubes behave like straight tubes. At higher velocities a decrease in relative peak widths should lead to an increase in sampling rate and a decrease in reagent consumption. Secondary flow phenomena form a much better explanation for the influence of velocity than vague notions like “incipient turbulence” [5, 25]. More quantitatively, from eqns. (4) and (5):

$$(\sigma_t/(\sigma_t)_0)^2 = H/H_0 \quad (10)$$

This means that the gain in peak width can be found from Fig. 5 as a factor $(H/H_0)^{1/2}$ which may reach values of about 1/100 at $De^2Sc = 10^9$. In other words, coiled tubes may be said to behave like straight tubes with an effective radius that is reduced by a factor of $(H/H_0)^{1/2}$ when they are operated at the same velocity (or time) at nearly the same pressure. This may serve as a compromise in the striving after ever smaller tube diameters, which most certainly will give rise to practical problems (like blockage by particles in the sample). A drawback of coiling effects, of course, is that they become appreciable only at higher velocities, i.e. relatively short times. Figure 7 shows how this works out in practice for columns with lengths of 1 and 10 m, respectively. In long coils, the gain with respect to straight tubes is more easily reached than in short coils (compare Fig. 7, A and B) for all times $t < 10^3$ s and all column radii $R > 5 \mu\text{m}$. Columns with a radius smaller than $20 \mu\text{m}$ are seen to be impractical in view of the pressure limit of 400 bar; columns with a radius larger than $320 \mu\text{m}$ may give rise to flow problems (Fig. 7B). In wide tubing, say with $R > 80 \mu\text{m}$, coiling effects remain active even for $t > 10^3$ s and hardly any problems arise concerning pressure. The time variable t in the graphs is related to the velocity parameter De^2Sc via

$$De^2Sc = 4L^2R^2\lambda/\nu D_M t^2 = \Delta p R^4\lambda/2\nu^2\rho D_M t \quad (11)$$

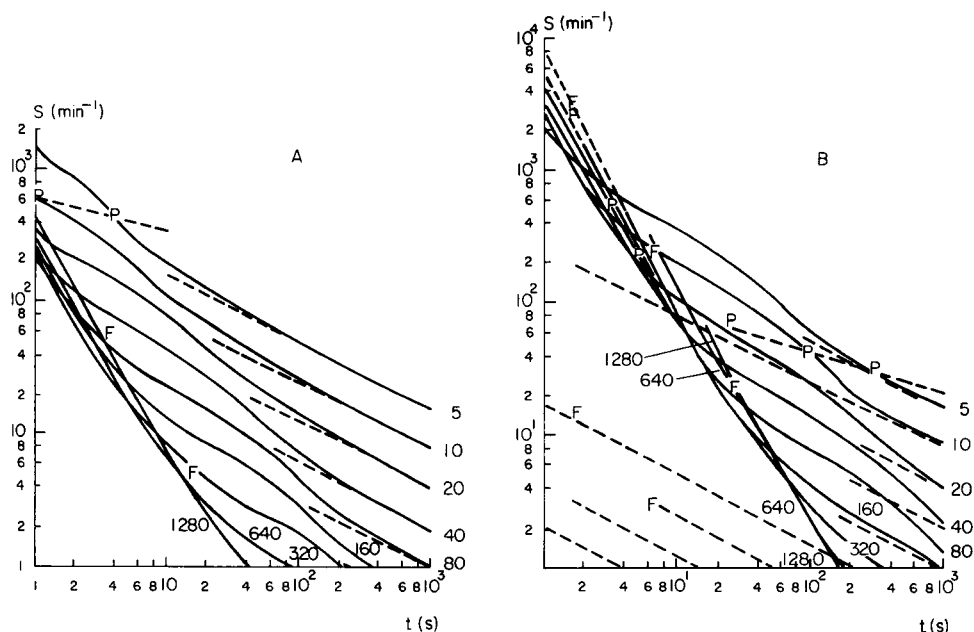


Fig. 7. Sampling rates in coiled tubings with different radii (R) and lengths. (A) 1 m; (B) 10 m; the numbers on the lines correspond to the radii given in μm . Other conditions: $D_M = 2.66 \times 10^{-5} \text{ cm}^2 \text{ s}^{-1}$, $\eta = 5.10^{-3} \text{ P}$; $\lambda = 0.1$. Broken lines: limiting cases for straight tubing ($\lambda = 0$).

Figure 8 compares the reagent consumption per peak for coils (Q) with that for straight tubing (Q_0) with a length of 1 m. Again, just as for the sampling rate S , coils are more advantageous by a factor of $(H_0/H)^{1/2}$. Thus $S/S_0 = Q_0/Q = (H_0/H)^{1/2}$.

It is obvious from the foregoing that f.i.a. analysis in tight coils is more efficient than in wide coils (i.e., nearly straight tubes) but that rather high velocities are necessary (say $De^2Sc > 10^4$) in order to obtain appreciable gain factors (say $(H_0/H)^{1/2} > 2$). In view of the pressure and flow limitations mentioned, one might ask what the maximum obtainable (= optimum) De^2Sc value is in tubings differing in length and radius. Figure 9 (a-c) shows how De^2Sc depends on t (after eqn. 11) for $L = 1, 10$ and 100 m, respectively, with column radius R as the parameter. It is clearly seen that only a limited working area (hatched in Fig. 9) is available and that the maximum obtainable values for De^2Sc are of the order of 10^8 (for $t \geq 10$ s). The optimum situation is one in which the maximum flow line and the maximum pressure line cross at the desired time of reaction. By way of example: for $\Delta p = 400$ bar, $F = 0.5 \text{ cm}^3 \text{ s}^{-1}$ and $t = 10$ s, the optimum values for L and R follow from $t = t_F = t_P$ (see above) as $R_{\text{opt}} = 192 \mu\text{m}$ and $L_{\text{opt}} = 43.2$ m (calculated with $\eta = 10^{-2} \text{ P}$). The corresponding De^2Sc amounts to 1.96×10^8 , while the gain factor $(H_0/H)^{1/2} = 40$, $S = 125$ peaks/min and $Q = 0.247 \text{ cm}^3/\text{peak}$. If longer residence

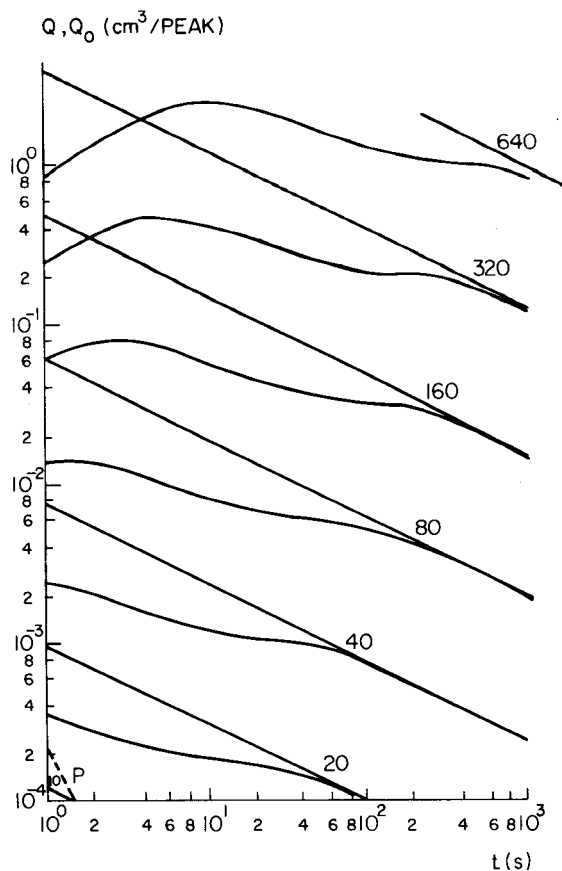


Fig. 8. Comparison of reagent consumption per peak in straight tubes (Q_0 , straight lines) and coiled tubes (Q , curved lines) for a length of 1 m and different radii (in μm).

times are required, say $t = 100$ s, still wider ($R_{\text{opt}} = 282 \mu\text{m}$) and longer ($L_{\text{opt}} = 200$ m) tubes are necessary [$De^2Sc = 9.07 \times 10^7$, $H/H_0 = 25.8$, $Q = 1.78 \text{ cm}^3/\text{peak}$, $S = 17.3$ peaks/min]. If, for practical convenience, flow and pressure limits are lowered to say $6 \text{ cm}^3 \text{ min}^{-1}$ ($= 0.1 \text{ cm}^3 \text{ s}^{-1}$) and 80 bar, t_F becomes $10\pi R^2 L$, $t_p = 10^{-7} \eta L^2/R^2$ and so for $t = 10$: $R_{\text{opt}} = 147 \mu\text{m}$, $L_{\text{opt}} = 14.7$ m [$De^2Sc = 1.33 \times 10^7$, $(H/H_0)^{1/2} = 8.2$, $S = 33.3$ peaks/min, $Q = 0.186 \text{ cm}^3/\text{peak}$].

Although the gain factor is less than under maximum flow and pressure, S is still appreciable and the value of Q is more attractive than that given above. Thus, it may be concluded that coiling effects are put to the best possible use in rather wide tubes ($R \approx 150 \mu\text{m}$) of great length ($L = 10\text{--}15$ m) at moderate flow rates and pressure drop; Fig. 2(B) shows an example of a peak train obtained from such a column. Of course, it is possible to achieve the same sampling rate in the same time with a straight column, but this

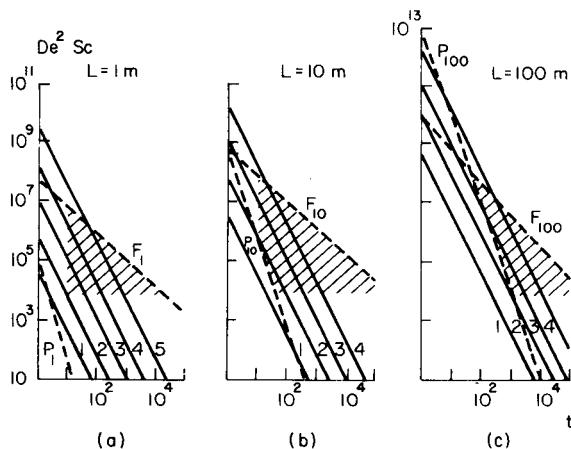


Fig. 9. Optimum working areas for coiled tubes of different lengths and radii with pressure limit at 400 bar and flow limit at 0.5 ml s^{-1} . (a) $L = 1 \text{ m}$; (b) $L = 10 \text{ m}$; (c) $L = 100 \text{ m}$. Numbers on the lines correspond to different tube radii (in μm): (1) 10; (2) 40; (3) 160; (4) 640; (5) 2560.

would require a column radius as small as $20 \mu\text{m}$ (see Fig. 7B). Although this can be realized (cf. Figs. 2 and 6), this kind of miniaturization is quite drastic and will be useful only if a very low reagent consumption is required (as $Q_0 \approx R^4$ after eqn. 9) and splitless sample introduction methods are available. The reduction by a factor of 8 in radius saves a factor of $8^4 (= 4096)$ in Q , whereas only a factor of 8 is lost in going from Q to Q_0 ; so in terms of reagent consumption the straight tube of such narrow bore is better by a factor of $8^3 = 512$ with $Q_0 = 3 \times 10^{-3} \text{ cm}^3/\text{peak}$. It is evident that for a very low reagent consumption coiling is of some use but that the main benefit comes from miniaturization (Fig. 8).

In summary, the conclusions are as follows: (1) coiling is useful with respect to sampling rate, particularly with short residence times and relatively wide tube diameters; (2) a coiled tube behaves like a straight tube with a greatly reduced internal diameter but requires much more reagent; (3) tightly coiled tubing is invariably more effective than straight (or widely coiled) tubing of the same dimensions; (4) the best way of obtaining high sampling rates together with a low reagent consumption is via miniaturization, but for the time being the use of coiled tubes of rather wide radii may serve as the most convenient practical compromise.

Comparison with other types of reactor

Two other types of reactor, employed not only for flow analysis but also for chromatographic post-column reactions, should be considered, namely the segmented-flow systems of the AutoAnalyzer type [25, 27–29] and packed-bed columns [23].

For segmented-flow systems, Snyder et al. [28] estimate a maximum sampling rate of 600/h (i.e. $S = 10$), which is seen to be easily surpassed by that for the unsegmented straight- or coiled-tube systems discussed above. As becomes clear from the arguments of Ružička et al. [4], segmented-flow systems have a reagent consumption that cannot compete with small-sized unsegmented-flow systems. On the whole there seems to be more scope for future developments with unsegmented- than with segmented-flow systems.

The thorough study of Deelder et al. [23] indicates that debubbling systems contribute very significantly to total zone broadening. These systems behave like ideal mixers ($\sigma_t = V/F$) with a quite substantial dead volume V . In the case of Deelder's apparatus, V is ca. 3 cm^3 and it is to be expected that a dead volume of less than $100 \mu\text{l}$ is necessary for the apparatus to be useful (see later). Peak broadening in the segmented-flow reactor itself can be found from Snyder's semi-empirical formula [29], which for negligible air flow can be written as:

$$\sigma_t^2 = 2 (L\eta/\gamma)^{2/3} t^{1/3} [(1/n) + 5 \times 10^3 d^2 (L\eta/\gamma t)^{2/3}] \quad (12)$$

where n is the important segmentation frequency and γ the surface tension at the air-liquid interface. Under normal conditions ($t > 10 \text{ s}$), the term $1/n$ between the square brackets dominates, since $\eta/\gamma \approx 10^{-2}/25 = 4 \times 10^{-4}$. Hence, approximately:

$$\sigma_t \approx (L\eta/\gamma)^{1/3} t^{1/6} \quad (13)$$

Here $n = 2$ is used as a practically useful segmentation rate [23], although optimum values for n may amount to 10 or even higher, depending on tube size [29]. It should be noted that the time dependence of σ_t according to eqns. (12) and (13) differs appreciably from that proposed by Snyder [29] and Schwedt [30], in both cases given as $\sigma_t \approx t^{1/2}$. This difference stems from the fact that we took L as a constant, whereas Snyder assumed F to be a constant. Snyder's assumption is somewhat impractical as $F = \pi R^2 L/t$, so for a constant flow, L must be changed in proportion to t . A good segmented-flow system (with $L = 10 \text{ m}$, $2R = 0.05 \text{ cm}$) is compared with the straight and coiled unsegmented-flow systems described earlier, in terms of σ_t vs. t (see Fig. 10). It is seen that for all times $t < 10^3 \text{ s}$ homogeneous flow yields a better result in both straight and coiled tubes than in the segmented system, particularly when broadening by the debubbling system is taken into account. For Fig. 10 this was done by using quite an optimistic value of $188 \mu\text{l}$ for the dead volume. Preferably, however, the debubbler volume should be say $50 \mu\text{l}$ or less if the rather horizontal (i.e. time-independent) dispersion characteristic of the segmented flow system is to be applicable up to longer times. Maybe electronic "debubbling" will be the ultimate solution to this problem [23].

The other type of reactor that should be considered is a packed column of the kind used for post-column reactions in modern liquid chromatography. Deelder et al. concluded [23] that "... even for fast reactions, i.e. $t = 30 \text{ s}$,

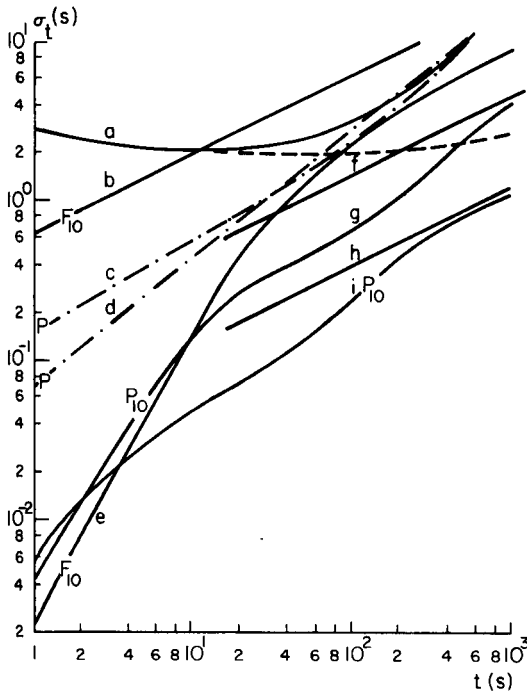


Fig. 10. Peak width (expressed as standard deviation) as a function of residence time in several flow systems. (a) Segmented flow after eqn. (12) ($n = 2$; $L = 10$ m; $R = 0.025$ cm) with (solid curve) and without (broken curve) debubbler; (b) homogeneous flow in straight tubes ($L = 10$ m) after eqn. (6); (c and d) packed columns ($L = 10$ cm; $d_p = 20$ μ m) after Done and Knox [31] and Snyder and Kirkland [32]; (e) homogenous flow in coiled tubes ($L = 10$ m, $\lambda = 0.1$) after eqn. (10); (f) same as (b) except $R = 40$ μ m; (g) same as (e) except $R = 40$ μ m; (h) same as (b) except $R = 10$ μ m; (i) same as (e) except $R = 10$ μ m.

the additional band broadening σ_t (of coiled tubes) will be about 1 s and packed reactors should be preferred". In their comparison these authors made use of the empirical Hiby correlation for axial dispersion in packed beds; this is probably too optimistic, especially for the currently used small particle sizes of 20 μ m and less. With such small particles packing structures are known to be less effective than is suggested by extrapolation from experiences with larger particles, on which Hiby's correlation is based. Preferably, use should be made of correlations based on measurements actually performed with such small particles; pertinent data are available from the chromatographic literature. For instance, the relation of Snyder and Kirkland [32]

$$H = D u^n \quad (\text{for } n = 0.4; D = 10^{-3} d_p^{1.4}) \quad (14)$$

with the given values of n and D (d_p in μ m) meets the requirements and is in good accordance with the relation of Done and Knox [31]

$$H/d_p = (ud_p/D_M)^{1/3} + 0.1 ud_p/D_M \quad (15)$$

which in turn is supported by theoretical considerations as discussed by Horvath and Lin [33]. Both equations (14) and (15), recalculated as σ_t vs t for a 10-cm column packed with 20- μm particles, are plotted in Fig. 10. It is seen that packed reactors are indeed better than, or equal to, segmented flow systems but that homogeneous flow in miniaturized straight tubes ($R \cong 40 \mu\text{m}$) or in normal coiled tubing ($R = 160 \mu\text{m}$ or less) is to be preferred. This conclusion is in contrast with that of Deelder et al. [23], who preferred packed reactors. In particular, small-diameter coiled tubing of, say, $R = 40 \mu\text{m}$ or less is unrivalled in dispersion properties over the whole range of reaction times.

CONCLUSION

The present study has shown the possibilities and limitations of homogeneous flow injection systems (straight and coiled) in comparison with segmented-flow systems and packed-bed reactors. It has been demonstrated experimentally that in homogeneous flow systems peak broadening is less pronounced for all residence times shorter than say 20 min — and hence, sampling rate and reagent consumption are far better — than in either segmented-flow or in packed-bed reactors. High sampling rates are obtained particularly in coiled tube flow, while a very low reagent consumption is characteristic of miniaturized tubing. Pressure and flow limitations should be virtually absent if the same apparatus is used as in chromatographic work.

The author wishes to thank J. P. A. Bleumer and N. van den Hoed for carrying out many of the experiments.

REFERENCES

- 1 J. Růžička and E. H. Hansen, *Anal. Chim. Acta*, 78 (1975) 145.
- 2 K. K. Stewart, G. R. Beecher and P. E. Hare, *Fed. Proc.*, 33 (1974) 1439; *Anal. Biochem.*, 70 (1976) 167.
- 3 J. Růžička and E. H. Hansen, *Anal. Chim. Acta*, 99 (1978) 37.
- 4 J. Růžička, E. H. Hansen, H. Mosbaek and F. J. Krug, *Anal. Chem.*, 49 (1977) 1858.
- 5 D. Betteridge, *Anal. Chem.*, 50 (1978) 832A.
- 6 G. I. Taylor, *Proc. Roy. Soc. London, Ser. A*, 219 (1953) 186; 223 (1954) 446.
- 7 J. C. Sternberg, *Adv. Chromatogr.*, 2 (1966) 205.
- 8 J. Villermaux, in E. sz. Kováts (Ed.), *Chromatographie sur Colonne*, Lausanne, 1969, p. 66.
- 9 R. Tijssen, *Sep. Sci. Technol.*, 13 (1978) 681.
- 10 R. Tijssen, Ph.D. Thesis, Delft, 1979.
- 11 R. Tijssen, *Chromatographia*, 3 (1970) 525.
- 12 R. Tijssen and R. T. Wittebrood, *Chromatographia*, 5 (1972) 286.
- 13 R. Tijssen, *Can. J. Chem. Eng.*, 55 (1977) 225.
- 14 L. A. M. Janssen, Ph.D. Thesis, Delft, 1976; *Chem. Eng. Sci.*, 31 (1976) 215.
- 15 P. S. Srinivasan, S. S. Nandapurkar and T. A. Holland, *Trans. Inst. Chem. Engrs., Chem. Eng.*, 46 (1968) 113.

- 16 C. M. White, *Proc. Roy. Soc. London, Ser. A*, 123 (1929) 645.
- 17 H. C. Topakoglu, *J. Math. Mech.*, 16 (1967) 1321.
- 18 Y. Mori and W. Nakayama, *Int. J. Heat Mass Transfer*, 8 (1965) 67; 10 (1967) 37 and 681.
- 19 M. Adler, *Z. Angew. Math. Mech.*, 14 (1934) 257.
- 20 W. M. Collins and S. C. R. Dennis, *Q. J. Mech. Appl. Math.*, 2, 28 (1975) 133.
- 21 R. Aris, *Proc. Roy. Soc. London, Ser. A*, 235 (1956) 67; 252 (1959) 538.
- 22 M. J. E. Golay, in D. H. Desty (Ed.), *Gas Chromatography 1958*, Butterworths, London, 1958, p. 36.
- 23 R. S. Deelder, M. G. F. Kroll, A. J. B. Beeren and J. H. M. van den Berg, *J. Chromatogr.*, 149 (1978) 669.
- 24 K. Hofmann and I. Halász, *J. Chromatogr.*, 173 (1979) 211.
- 25 M. Margoshes, *Anal. Chem.*, 49 (1977) 17, 1861.
- 26 L. N. Klatt, *J. Chromatogr. Sci.*, 17 (1979) 225.
- 27 L. R. Snyder and H. J. Adler, *Anal. Chem.*, 48 (1976) 1017, 1022.
- 28 L. R. Snyder, J. Levine, R. Stoy and A. Conetta, *Anal. Chem.*, 48 (1976) 942A.
- 29 L. R. Snyder, *J. Chromatogr.*, 125 (1976) 287.
- 30 G. Schwedt, *Angew. Chem.*, 91 (1979) 192.
- 31 J. N. Done and J. H. Knox, *J. Chromatogr. Sci.*, 10 (1972) 606.
- 32 L. R. Snyder and J. J. Kirkland, *Introduction to Modern Liquid Chromatography*, Wiley, New York, 1974.
- 33 Cs. Horvath and H.-J. Lin, *J. Chromatogr.*, 126 (1976) 401.

DISPERSION PHENOMENA IN REACTORS FOR FLOW ANALYSIS

J. H. M. VAN DEN BERG*, R. S. DEELDER and H. G. M. EGBERINK

DSM Research, Geleen (The Netherlands)

(Received 6th August 1979)

SUMMARY

Both coiled open tubular reactors and packed-bed reactors can be used in flow analysis. Band broadening and pressure drop in these reactors are discussed. Theoretical analysis shows that packed-bed reactors are to be preferred. It is shown that for a given residence time and equal band-broadening values the pressure drop over a packed-bed reactor is lower than over a coiled open tubular reactor. Rules for optimal design are given for coiled tubular reactors and packed-bed reactors. The application of both reactors is shown for the spectrophotometric determination of phosphate with a vanadomolybdate reagent yielding a yellow colour.

The introduction of flow analysis [1] marked an important breakthrough in automatic chemical analysis. In this technique the sample is injected into a carrier stream. The carrier stream is mixed with reagent and the resulting stream passes through a reactor and is fed to a suitable detection system which indicates the presence of the reaction product.

When a sample band passes through the flow system, axial dispersion takes place. This dispersion should be kept as low as possible, because it adversely affects the sample integrity and the throughput. Axial dispersion also causes sample dilution and thus decreases the sensitivity of the method. Axial dispersion can be reduced considerably by using gas-segmented liquid flow. The technique of gas segmentation has been applied in the AutoAnalyzer System, the first widely applied equipment for automatic chemical analysis. A elaborate theoretical model which describes sample dispersion in gas-segmented liquid flow has been given by Snyder and Adler [2–4].

Flow analysis without gas segmentation has lately been receiving attention [5–7]. In previous work [8–11] the use of post-column reaction systems in liquid chromatography was described. In these systems, the effluent of a chromatographic column is continuously mixed with a colour reagent that is specific for the group of compounds to be determined and the absorbance of the resulting reaction mixture is continuously measured. In the present paper, the theoretical description of dispersion phenomena in post-column reactors is applied to flow analysis. Two types of reactors are considered: a tubular reactor consisting of a narrow stainless-steel coiled tube and a packed-bed reactor, i.e. a tube packed with inert impervious particles such as glass beads.

The performance and characteristics of these reactor systems are described and compared, and rules for optimal design are given. This is illustrated by the application of both an open tubular reactor and a packed-bed reactor for the determination of phosphate in phosphate rocks by the vanadomolybdate method [12, 13].

THEORY

When a fluid flows through an open tubular reactor or a reactor packed with inert impervious particles the combination of convective mixing and molecular diffusion brings about a residence time distribution. This distribution can be measured by injection of a sharp concentrated pulse of an inert, non-reacting tracer material at time $t = 0$ and measuring its concentration at the reactor outlet as a function of time, $c(t)$.

The residence time distribution can be described by its statistical moments. For practical purposes, the most important characteristics are the mean residence time, t_v , or the first moment, given by:

$$t_v = \frac{\int_0^{\infty} t c(t) dt}{\int_0^{\infty} c(t) dt} \quad (1)$$

and the variance, σ_t^2 , or second moment about the mean

$$\sigma_t^2 = \frac{\int_0^{\infty} (t - t_v)^2 c(t) dt}{\int_0^{\infty} c(t) dt} \quad (2)$$

The simplest mathematical model used to characterize dispersion in flow reactors is axially dispersed plug flow. For this model:

$$t_v = L/u \text{ and } \sigma_t^2 = 2D_L L/u^3$$

where L is the length of the reactor tube, u the average linear flow velocity and D_L the axial dispersion coefficient. Both equations hold for $uL/D_L > 100$. It can also be shown that the $c(t)$ curve approaches a symmetrical Gaussian distribution curve around $t = t_v$, for sufficiently high values of uL/D_L [14–16].

A flow reactor can, however, be considered as a series of N ideal mixers. If the number of mixing stages, N , is sufficiently high, the resulting $c(t)$ curve has a Gaussian shape and its variance is given by $\sigma_t^2 = t_v^2/N$. For open tubular reactors as well as for packed bed reactors the axial dispersion coefficient, D_L , can be estimated from fluid properties and reactor characteristics, e.g. fluid velocity, molecular diffusivity of the tracer compound, tube diameter, etc., which in turn permits calculation of residence time distributions. This approach is applied in chemical engineering [14–16].

In flow analysis both sample throughput and sample dilution are directly related to dispersion. Sample throughput rate is limited to a maximum value, T , beyond which a reliable estimation of peak heights is no longer possible because of excessive carry-over between samples. For this maximum value, $T = 1/4 \sigma_t$ is considered. At this sampling rate the distance in time units between two successive sample peaks is $4\sigma_t$, and it can be seen from Fig. 1

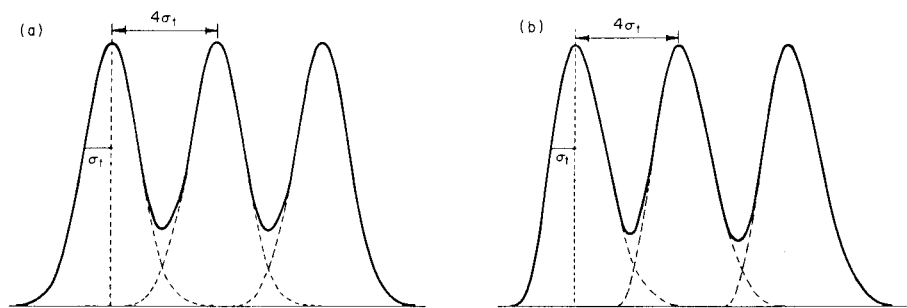


Fig. 1. Typical signals for flow analysis. (a) Gaussian peaks separated by a distance of $4\sigma_t$. (b) Tailing peaks separated by a distance of $4\sigma_t$.

that for symmetrical as well as for skewed peaks the peak height is not affected by leading or tailing edges from neighbours. For Gaussian peaks $T = N^{1/2}/4t_v$. Sample dilution is expressed as the quotient of the maximum concentration of the tracer at the reactor outlet, c_{\max} , and the uniform concentration of the sample at injection, c_0 . If the injected volume of the sample is V_0 , then

$$(2\pi)^{1/2}\sigma_t(\Phi_c + \Phi_r) c_{\max} = V_0 c_0 \quad (3)$$

where Φ_c and Φ_r are the volumetric flow rates of the carrier and the reagent, respectively. Combination of eqn. (3) with $\sigma_t^2 = t_v^2/N$ gives

$$c_{\max}/c_0 = V_0(N)^{1/2}/(2\pi)^{1/2} t_v(\Phi_c + \Phi_r) \quad (4)$$

These equations show the importance of using reactors with high plate numbers (N) for flow analysis.

Tubular reactors

In their simplest form, flow reactors consist of narrow tubing. In straight open tubes with laminar flow a residence time distribution originates from the combination of the parabolic velocity profile and molecular diffusion [17]. For the dispersion coefficient D_L , the following expression can be derived:

$$D_L = D_m + (d_t^2 u^2 / 192 D_m) \quad (5)$$

where D_m is the molecular diffusion coefficient of the tracer compound, d_t the internal diameter of the tube and u the average linear flow velocity. If this value is substituted into the equation $\sigma_t^2 = 2 D_L L / u^3$, then

$$\sigma_t^2 = (2 D_m t_v^3 / L^2) + (d_t^2 t_v / 96 D_m) \quad (6)$$

Except for extremely low and impractical flow velocities the first term on the right-hand side of eqn. (6) can be neglected, giving

$$\sigma_t^2 / t_v = d_t^2 / 96 D_m \quad (7)$$

Equations (5–7) can be used only if $\sigma_t \ll t_v$, $Ld_t/(t_v D_m) > 100$ and $t_v D_m/d_t^2 > 0.2$ [18].

For a non-parabolic flow profile, eqn. (7) can be modified to

$$\sigma_t^2/t_v = \kappa d_t^2/96 D_m \quad (8)$$

where κ depends on the particular flow profile [19].

When a fluid moves through a helically coiled tube, a secondary flow perpendicular to the main direction of flow sets in (Fig. 2). This secondary flow is due to centrifugal forces acting on the moving liquid. The axial velocity is greatest near the centre of the tube, and here centrifugal forces will act most strongly. The fluid near the centre is thrown outwards and is continuously replaced with fluid recirculating along the tube wall. The first theoretical study of flow in curved tubes was made by Dean [20], who obtained an approximate expression for the liquid velocity profile by solving analytically the equations of motion. He proposed the use of a dimensionless parameter known as the Dean number, $Dn = Re(d_t/d_c)^{1/2}$ for characterizing flow in curved tubes, where the Reynolds number $Re = 4\rho\Phi/\pi d_t \eta$, ρ is the density of the solvent, η is the viscosity, Φ the volumetric flow rate, d_t the tube diameter and d_c the coil diameter. Owing to simplifications made in the mathematical procedure, Dean's solutions are valid only for a very limited range of flow conditions.

More recently, numerical methods have been presented [21, 22] for solving the equations of motion over a wide range of Reynolds numbers and curvature ratios, $\lambda = d_c/d_t$. The calculated axial flow velocity profiles were found to deviate strongly from their parabolic straight-tube counterparts; the differences between the mean axial velocity and the velocity of the various axial flow lines are greatly reduced when coiled tubes are used. These results were confirmed experimentally [22]. Secondary flow in coiled tubes causes an increase in radial mass transfer and therefore reduces axial dispersion in comparison with flow through a straight tube.

From the point of view of fluid mechanics, the problem of dispersion in laminar flow of an incompressible fluid in curved channels consists essentially in solving the mass-transfer equation, accounting for both molecular and convective diffusion in a given flow field. Because of the complexity of the

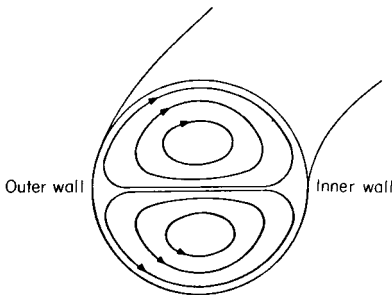


Fig. 2. Secondary flow pattern in the cross-section of a coiled tube.

equations involved, no satisfactory solution for this problem has so far been found.

Recently, Trivedi and Vasudeva [23] described experimental results for dispersion in coiled tubes over a wide range of Dean numbers; they plotted the experimental κ values against Dn and obtained a series of curves according to the Schmidt number, Sc , where $Sc = \eta\rho/D_m$. However, as the κ values were derived at least in part from asymmetrical step response curves, the reliability of these results is doubtful. A recent theoretical study [24] showed that κ can be calculated as a function of Dn^2Sc for $d_c/d_t > 20$ and $Dn < 15$, but no experimental verification was presented.

The κ values measured for three solute—solvent pairs in tubes of length 10–20 m (i.d. 0.5–1.0 mm) for various curvature ratios, λ [10], are plotted against $DnSc^{1/2}$ in Fig. 3. The measurements are represented by a single curve, as predicted by Janssen [24], which can approximately be described by the equations:

$$\kappa = 5.6 (DnSc^{0.5})^{-0.67} \text{ for } 12.5 < DnSc^{0.5} < 200; \kappa = 1 \text{ for } DnSc^{0.5} \leq 12.5$$

The full lines in Fig. 3 correspond to these equations. By using these correlations it is possible to predict band broadening, σ_t , in coiled tubular reactors for flow analysis. Figure 4 show plots of σ_t vs. the internal diameter, d_t , of the reactor tube and curvature ratios, λ , of 200 and 10, respectively. It can be seen from Fig. 4 that little band broadening and, therefore, a high sample throughput rate can be obtained for coiled tubes of narrow bore. Tight coiling (low λ values) favourably influences band broadening. It should be noted, however, that practical problems impede the maximum gain from the possibilities of open tubular reactors. For instance, although attractive from the theoretical point of view, the combination of narrow bore tubing and tight coiling will be troublesome. Tight coiling, e.g. a curvature ratio of 10, may be readily obtained for wide-bore tubing (e.g. 1 mm i.d.), but for 0.2 mm i.d. tubing, $\lambda = 10$ means a coil diameter of 2 mm, which would be difficult to realize.

Furthermore, at a given reaction time, t_v , the minimum internal diameter of the reactor tube, d_t , will be limited by pressure drop and tube length. The pressure drop for laminar flow through straight tubes is calculated from the Poiseuille equation

$$\Delta p/t_v = 512 \eta \Phi^2 / \pi^2 d_t^6 \quad (9)$$

Secondary flow in coiled tubes causes an increase in the axial pressure gradient. Considerable experimental data on pressure drop in coiled tubes are available [25, 26] and a good theoretical background for the empirical pressure drop relationship has been given [22]. It turns out that for $Dn < 25$ the increase in pressure drop is no more than 10% with respect to straight-tube flow. As in practice these conditions will always be fulfilled for flow analysis reactors, eqn. (9) can be used as a good approximation for calculating the pressure drop in these reactors.

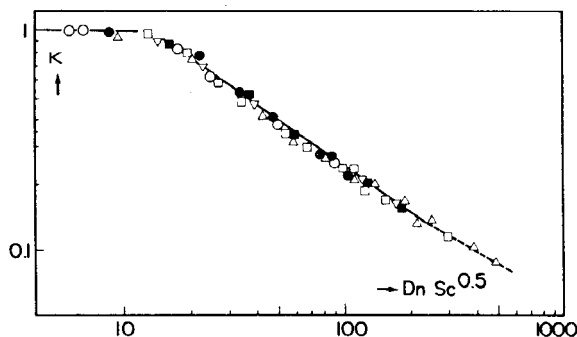


Fig. 3. Reduction of axial dispersion by secondary flow in coiled tubes; κ values were calculated from experimental data by using eqn. (6) [10]. Open symbols refer to nitrobenzene-iso-octane for different curvature ratios: (○) 1024; (▽) 305; (□) 155; (△) 55. (■) Benzene-chloroform for $\lambda = 305$; (●) benzene-hexane for $\lambda = 1024$.

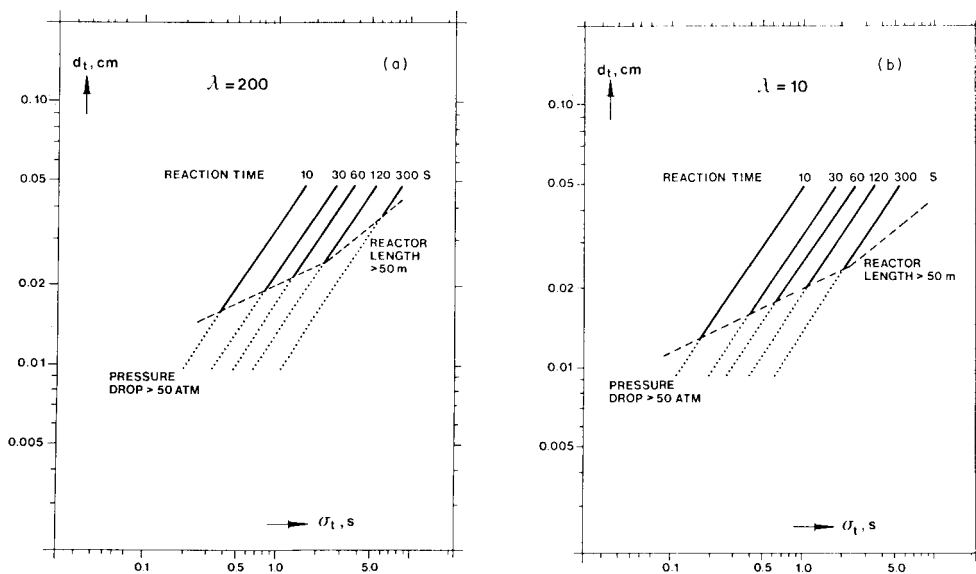


Fig. 4. Dispersion in a tubular reactor calculated for two coiling ratios λ : (a) $\lambda = 200$; (b) $\lambda = 10$. Band broadening, σ_t , is plotted versus tube diameter, d_t , for various reaction times, t_v , assuming a constant total volumetric flow rate ($\Phi = 1 \text{ cm}^3 \text{ min}^{-1}$) and a constant coiling ratio ($\lambda = 200$ or 10); $D_m = 2 \times 10^{-5} \text{ cm}^2 \text{ s}^{-1}$; $\eta = 0.5 \text{ mN s m}^{-2}$; $\rho = 0.7 \text{ g cm}^{-3}$.

A pressure limit of 50 atm was chosen and, for the conditions used in Fig. 4, the corresponding minimal values of the tube diameter, d_t , were calculated from eqn. (9). The broken lines in the left-hand bottom corners of Fig. 4 (a, b) correspond to this pressure limit. In contrast, a limiting value for d_t was calculated for a maximal tube length of 50 m from

$$d_t = (4\Phi t_v / \pi L)^{1/2} \quad (10)$$

This limit is indicated by the broken lines on the right-hand sides of Fig. 4 (a, b). The dotted lines in Fig. 4 correspond to combinations of σ_t and t_v for which the pressure limit and/or the maximal reactor length is exceeded. The pressure limit of 50 atm may appear somewhat conservative, since current pumping systems for high-performance liquid chromatography allow operations at pressures up to 500 atm. However, it can be seen from eqn. (9) that a ten-fold increase in pressure drop will result in a decrease of the minimal values of the tube diameter by a factor of $10^{1/6}$, i.e. only 1.47. Therefore the benefit of sophisticated pumps for liquid chromatography in flow analysis with open tubular reactors seems questionable.

Packed-bed reactors

Experience with packed reactors for post-column derivatization in liquid chromatography indicates that this reactor type is an attractive alternative to the open tubular reactors currently used in flow analysis [8–10]. Band broadening in reactors packed with inert, impervious particles such as glass beads, is due to a combination of axial molecular diffusion and convective mixing and can be expressed by the following empirical relationship according to Hiby [27]:

$$D_L = \gamma D_m + \{\lambda_1 d_p u / 2 [1 + \lambda_2 (D_m / u d_p)^{1/2}]\} \quad (11)$$

Combination with the equations $t_v = L/u$ and $\sigma_t^2 = 2 D_L L / u^3$ gives:

$$L \sigma_t^2 / t_v^2 = [2\gamma D_m / u] + \{\lambda_1 d_p / [1 + \lambda_2 (D_m / u d_p)^{1/2}]\} \quad (12)$$

where γ is the tortuosity factor, u the interstitial fluid velocity, d_p the mean particle size of the packing material and λ_1 and λ_2 are constants characterizing the geometry of the packed bed. The contribution of convective mixing, expressed in the second term on the right-hand side of eqn. (12), can be reduced considerably by using appropriate column packing techniques. The validity of these equations was verified for glass-bead packings with d_p ranging from 15 to 40 μm [10]. In a recent study, Horvath and Lin [28] proposed a different equation, which is based on an elaborate theoretical model. The same study, however, shows that the empirical Hiby relation, eqn. (11), matches the experimental dispersion data equally well.

When columns packed with glass beads are to be used as reactors for flow analysis, a suitable choice should be made for the reactor length, L , and the mean particle diameter of the glass beads, d_p , for a given combination of reaction time, t_v , and band broadening, σ_t . In practice, limits are set for the pressure drop over the reactor, Δp , and L . The pressure drop is calculated from the Darcy equation:

$$\Delta p = u \eta L / k_0 d_p^2 \quad (13)$$

where k_0 is the permeability of the reactor.

When σ_t and t_v are fixed, Δp can be calculated from eqns. (12) and (13) for any value of L [8]. The corresponding value of d_p is then calculated from

eqn. (13). These calculations were carried out for the values listed in the legend to Fig. 5. The values of the Hiby constants λ_1 and λ_2 and the permeability constant k_0 were determined in separate experiments with glass-bead columns [10]; the values of the diffusion coefficient and the viscosity correspond to those used in the preceding section. In Fig. 5 Δp and L are plotted against d_p for a constant value of σ_t (1 s). In this figure the reaction time t_v is varied between reasonable limits (60–180 s). Favourable conditions are found near the minimum of the Δp vs. d_p curves, corresponding to short reactors and low pressure drops.

The smallest peak broadening obtainable in practice is 0.5 s, because of the unavailability of glass beads smaller than 10 μm and because the use of very small beads leads to excessively high pressure drops.

In order to facilitate comparison of reactor types, Fig. 6 shows d_p plotted against σ_t for various reaction times, t_v , and for a reactor length of 25 cm. In practice, limits are set on the pressure drop, Δp , over the reactor and the broken lines interconnect points of equal pressure. For a given length of the reactor, the internal diameter, d_t , of the reactor should be chosen so as to fit in with the residence time and the volumetric flow rate Φ through the reactor:

$$d_t = [4t_v\Phi/\pi\epsilon_T L]^{1/2} \quad (14)$$

where ϵ_T is the void fraction of the reactor ($\epsilon_T = 0.4$ for non-porous particles).

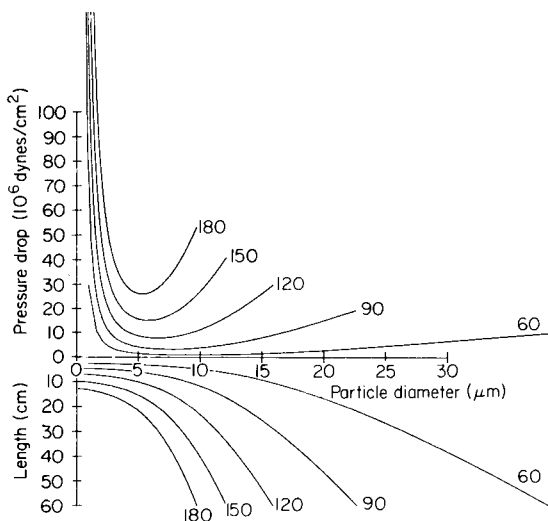


Fig. 5. Dispersion in a packed reactor. Reactor length, L , and reactor pressure drop, Δp , as a function of the particle diameter, d_p , for various reaction times, t_v , at a constant residence time distribution in the reactor, σ_t , of 1.0 s. Numbers plotted near the curves correspond to t_v in s. Conditions: $\gamma = 0.7$; $\lambda_1 = 10$; $\lambda_2 = 18$; $k_0 = 0.002$; $\eta = 0.5 \text{ mN s m}^{-2}$; $D_m = 2 \times 10^{-5} \text{ cm}^2 \text{ s}^{-1}$.

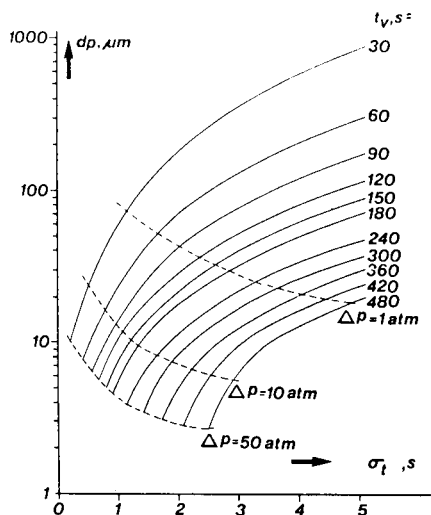


Fig. 6. The particle diameter, d_p , as a function of the band broadening, σ_t , for various reaction times, t_v , assuming a constant reactor length $L = 25$ cm. The broken lines interconnect points of equal pressure drop.

Selection of reactor type

Where practical applications of reactor systems are concerned, the chemistry of the reaction involved is of the utmost importance for the choice of the reactor type. For fast reactions this choice is straightforward. As demonstrated in the preceding section, the lowest additional band broadening is obtained for packed reactors, i.e. $\sigma_t \leq 1$ s for reaction times up to 5 min.

Helically coiled tubes are attractive as reactors, because of their simple construction and easily predictable dispersion. However, in spite of the "coiling effect", the dispersion in these reactors is relatively important: even for fast reactions ($t_v = 30$ s), the band broadening, σ_t , will be about 1 s (see Fig. 4) and packed reactors are to be preferred, when maximal sample throughput is required.

For slow reactions (reaction times above 5 min), neither glass-bead columns nor helically coiled reactors can be used without accepting large values for the band broadening, σ_t . Then gas-segmented liquid flow is a useful alternative [4, 9]. It should be noted, however, that many reputedly slow reactions can be considerably accelerated as the closed pressurized reactor allows the reaction mixture to be heated to temperatures that exceed the boiling point of the solvent [29]. For some applications, however, this approach is unsuitable, e.g., when aggressive reagents such as concentrated acids are used.

EXPERIMENTAL

Phosphate determination

At these laboratories, the phosphate content of raw phosphate is currently

determined by the vanadomolybdate method [12, 13]. An acidic solution of ammonium vanadate and ammonium molybdate is mixed with the acidified sample solution. The absorbance of the yellow reaction mixture is measured at 420 nm. This method was readily made automatic by using a flow system.

Chemicals

All chemicals were of analytical grade (Merck) and distilled water was used throughout. The reagent solution was prepared by dissolving 0.75 g of ammonium vanadate (NH_4VO_3) and 13 g of ammonium molybdate ($(\text{NH}_4)_6\text{Mo}_7\text{O}_{24} \cdot 4\text{H}_2\text{O}$) in about 900 ml of warm distilled water (90°C). After cooling, the solution was diluted to 1 l. Before use the reagent solution was filtered through a $0.2\text{-}\mu\text{m}$ filter (Sartorius, SM 11307). In addition, a 1 N nitric acid solution was prepared.

Instrumentation

Figure 7 gives the scheme of the reaction system for the photometric determination of phosphate. Two cheap reciprocating pumps (Nikkiso, type Inic 75-25-3 CAK) delivered the reagent and the carrier stream to the reactor. The volumetric flow rates were both $0.55\text{ cm}^3\text{ min}^{-1}$. Flow pulses were suppressed by a dampening system (Orlita, type MSDO) combined with a capillary restriction (length 10 m, 0.25 mm i.d. 316 SS tubing). The sample was injected into the nitric acid carrier stream by means of an injection valve (Rheodyne, type 7010) equipped with a $30\text{-}\mu\text{l}$ sample loop. Both streams were mixed in a T-piece and fed into the reactor. All connections were made of 316 SS tubing (0.25 mm i.d.). The reactor was thermostatted by a circulating water bath (Lauda, type U3-S15/12) at $30 \pm 0.1^\circ\text{C}$.

The absorbance of the reaction mixture was measured at 420 nm in a spectrophotometer (Zeiss, type PM2DLC) equipped with a $8\text{-}\mu\text{l}$ flowcell. The detector signal was recorded on a potentiometric recorder (Kipp & Zonen, type BD 8); peak areas were measured with an integrator (Minigrator, Spectra Physics).

Both an open tubular and a packed reactor were tested. The open tubular reactor was constructed of 316 SS tubing (10 m \times 0.25 mm i.d.) wound into a 2.5-cm diameter coil ($\lambda = 100$). The packed reactor was made of 4.6 mm i.d. 316 SS tubing (LiChroma) and had a length of 7 cm. The reactor was packed by means of a balanced density slurry technique [30]. A porous SS disc for supporting the packed bed and the column and fittings were supplied by Chrompak. Glass beads were obtained from Sovitec; narrow sieve fractions

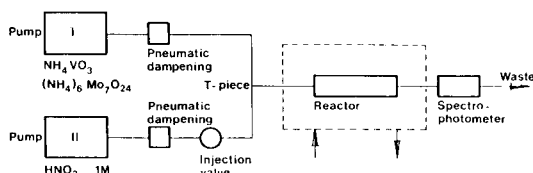


Fig. 7. Schematic diagram of the flow system for the determination of phosphate.

of these beads were prepared by means of an Alpine air classifier. A fraction with $d_p = 40 \mu\text{m}$ was used in this study.

RESULTS AND DISCUSSION

The dimensions of both reactors were chosen so as to give a mean residence time, t_v , of ca. 35 s. The reaction was found to be almost complete after this time. For the packed reactor, $\sigma_t = 1.8$ s was found at a pressure drop $\Delta p = 0.4$ atm. For the tubular reactor these values were 4.1 s and 4 atm, respectively. The value for σ_t was determined from the peak obtained on injection of $30 \mu\text{l}$ of a sample solution containing phosphate (20 mg l^{-1}). In Table 1 these values are compared with the theoretical values estimated from the equations for κ (Fig. 3) and eqn. (12) and for $D_m = 10^{-5} \text{ cm}^2 \text{ s}^{-1}$. As stated in the theoretical part, this estimation will be correct only if tracer substance, compound to be determined and reaction product all have the same value for D_m . There is a satisfactory agreement between the observed band broadening and the theoretically predicted values.

The smaller band broadening in the packed reactor leads to a maximal sample throughput rate of $T = 0.14 \text{ s}^{-1}$, corresponding to 500 samples per hour, while for the tubular reactor $T = 0.06 \text{ s}^{-1}$, or 220 samples per hour. The packed reactor has the higher number of mixing stages. Therefore, the dilution in this reactor is less than half that in the tubular reactor. Figure 8 shows the peak trains obtained for phosphate test solutions with the packed and tubular reactors. A typical calibration graph for the reactor system currently used was linear over the phosphate range $0.05\text{--}0.5 \text{ mg cm}^{-3}$ (corresponding to 1 000–12 000 integrator counts). Linear regression confirmed that a straight line with zero intercept could be fitted through the data points; the coefficient of regression was 0.999993. Table 2 gives relative standard errors for the determination of phosphate in standard solutions. The high reproducibility is mainly due to the excellent flow stability of the pumping system. The reliability of the analytical method is illustrated by the data in Table 3, which were obtained by analyzing periodically three standard phosphate rock samples. A long-term reproducibility of 0.5% (relative) was found and the differences between "known" and "found" phosphate contents were statistically insignificant.

TABLE 1

Comparison of estimated and measured characteristics of a packed and tubular reactor

	Estimated	Measured
<i>Packed reactor.</i> σ_t (s)	1.5	1.8
Δp (atm)	4	4
<i>Tubular reactor.</i> σ_t (s)	4.2	4.1
Δp (atm)	0.4	0.4

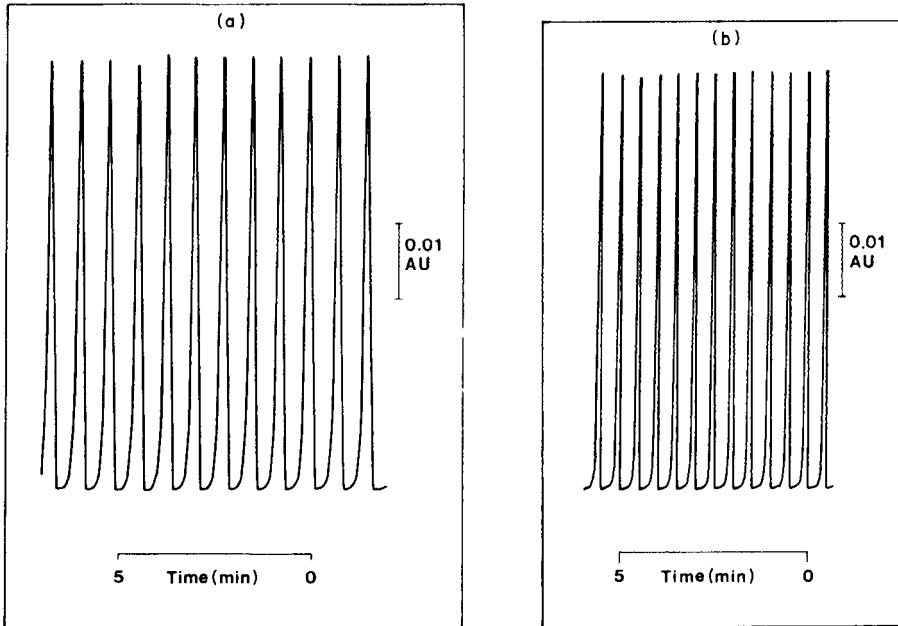


Fig. 8. Flow analysis for phosphate in phosphate rock samples with (a) a coiled tubular reactor and (b) a packed-bed reactor.

TABLE 2

Relative standard deviations for determination of phosphate in aqueous test solutions

Phosphate content (mg cm ⁻³)	0.050	0.100	0.375	0.500
No. of detns.	12	11	17	11
R.s.d. (%)	0.08	0.08	0.07	0.07

TABLE 3

Long-term reproducibility of phosphate determination in phosphate rock samples

Sample number	Phosphate content, weight (%) ^a	No. of observations	R.s.d. (%)
1	44.4	10	0.5
2	44.8	17	0.4
3	44.4	13	0.5

^aDetermined by gravimetry.

NOTE ADDED IN PROOF

During the conference, we became aware of efforts [31, 32] to describe dispersion phenomena in reactors for flow analysis that are similar to that outlined above. It may be time-consuming for readers interested in this subject to correlate the different conclusions reached from basically similar experimental and theoretical work, thus some clarification seems in order.

In the present work, limits were set to the pressure drop over the reactor tube as well as to the length and internal diameter of the tube. The aim was to keep the dimensions of the reactor used within the practical range of working conditions. Similar considerations applied to the design of packed-bed reactors. From this point of view our conclusion that a packed-bed reactor is a good alternative to a tubular reactor is still valid, especially for short reaction times. Because Tijssen [32] goes down to 10- μ m i.d. tubing in his calculations, he can conclude that these capillary tubes are to be preferred over packed-bed reactors.

On the other hand, in the comparison of gas-segmented reactors and coiled tubular reactors in Fig. 11 [32], the latter are favoured because in the calculations the length of the reactor is kept constant and the residence time is varied. In dealing with gas-segmented flow reactors the residence time is normally kept constant, while the reactor length and the segmentation frequency are varied, as is done by Snyder [31]. In that case the gas-segmented flow reactor is favoured.

It should be noted, however, that in applying a gas-segmented liquid flow reactor a considerable amount of dispersion is contributed by mixing tees and debubbler [33].

REFERENCES

- 1 L. T. Skeggs, *Am. J. Clin. Pathol.*, 28 (1957) 311.
- 2 L. R. Snyder and H. J. Adler, *Anal. Chem.*, 48 (1976) 1017.
- 3 L. R. Snyder and H. J. Adler, *Anal. Chem.*, 48 (1976) 1022.
- 4 L. R. Snyder, *J. Chromatogr.*, 125 (1976) 287.
- 5 J. Růžička and E. H. Hansen, *Anal. Chim. Acta*, 78 (1975) 145.
- 6 J. Růžička and E. H. Hansen, *Anal. Chim. Acta*, 99 (1978) 37.
- 7 K. K. Stewart, G. R. Beecher and P. E. Hare, *Anal. Biochem.*, 70 (1976) 167.
- 8 R. S. Deelder, M. G. F. Kroll and J. H. M. van den Berg, *J. Chromatogr.*, 125 (1976) 307.
- 9 R. S. Deelder, M. G. F. Kroll, A. J. B. Beeren and J. H. M. van den Berg, *J. Chromatogr.*, 149 (1978) 669.
- 10 J. H. M. van den Berg, Thesis, Eindhoven University of Technology, 1978.
- 11 J. H. M. van den Berg and R. S. Deelder, *Chem. Eng. Sci.*, 34 (1979) 1345.
- 12 R. E. Kitson and M. G. Mellon, *Ind. Chem. Eng., Anal. Ed.*, 16 (1944) 379.
- 13 I. M. Kolthoff, P. J. Elving and E. B. Sandell, *Treatise on Analytical Chemistry, Part II*, Vol. 5, Interscience, New York, 1961, p. 351.
- 14 H. Kramers and K. R. Westerterp, *Elements of Chemical Reactor Design and Operation*, Netherlands University Press, Amsterdam, 1963.
- 15 O. Levenspiel, *Chemical Reaction Engineering*, Wiley, New York, 1962.

- 16 P. V. Danckwerts, *Chem. Eng. Sci.*, 2 (1953) 1.
- 17 R. A. Aris, *Proc. Roy. Soc. London, Ser. A*, 235 (1956) 67.
- 18 V. Ananthakrishnan, W. N. Gill and A. J. Barduhn, *AIChE J.*, 11 (1965) 1063.
- 19 K. B. Bischoff and O. Levenspiel, *Chem. Eng. Sci.*, 17 (1962) 245; 17 (1962) 257.
- 20 W. R. Dean, *Philos. Mag.*, 4 (1927) 208; 5 (1928) 673.
- 21 L. C. Truesdell, Jr. and R. J. Adler, *AIChE J.*, 16 (1970) 1010.
- 22 L. R. Austin and J. D. Seader, *AIChE J.*, 19 (1973) 85.
- 23 R. N. Trivedi and K. Vasudeva, *Chem. Eng. Sci.*, 29 (1974) 2291; 30 (1975) 317.
- 24 L. A. M. Janssen, *Chem. Eng. Sci.*, 31 (1976) 215; Thesis, Delft University of Technology, 1977.
- 25 C. M. White, *Proc. Roy. Soc. London, Ser. A*, 123 (1929) 645.
- 26 L. Larrain and C. F. Bonilla, *Trans. Soc. Rheol.*, 14 (1970) 135.
- 27 J. W. Hiby, in P. A. Rottenburg (Ed.), *Proceedings of Symposium on Interaction between fluids and particles*, Institution of Chemical Engineers, London, 1962, p. 312.
- 28 C. Horvath and H. J. Lin, *J. Chromatogr.*, 126 (1976) 401.
- 29 K. M. Jonker, H. Poppe and J. F. K. Huber, *Chromatographia*, 11 (1978) 123.
- 30 R. E. Majors, *Anal. Chem.*, 44 (1972) 1722.
- 31 L. R. Snyder, *Anal. Chim. Acta*, 114 (1980) 3.
- 32 R. Tijssen, *Anal. Chim. Acta*, 114 (1980) 71.
- 33 R. S. Deelder and P. J. H. Hendricks, *J. Chromatogr.*, 83 (1973) 343.

SOME THEORETICAL ASPECTS OF FLOW INJECTION ANALYSIS

J. M. REIJN, W. E. VAN DER LINDEN* and H. POPPE

Laboratory for Analytical Chemistry, University of Amsterdam, Nieuwe Achtergracht 166, 1018 WV Amsterdam (The Netherlands)

(Received 23rd July 1979)

SUMMARY

The injection and detection methods in flow injection analysis (f.i.a.) are theoretically described. Theory is developed for a simple flow model based on laminar flow without diffusion. The results lead to the conclusion that exact specifications for injection and detection devices in experimental f.i.a. are necessary. The influence of the sample volume is described in more detail with a systems analysis model of f.i.a. in which the tanks-in-series model is used for transport of the fluid. The theoretical and experimental results are in good agreement, thus the theory developed for sample injection in f.i.a. appears to be valid.

THEORY

Influence of injection and detection methods on f.i.a. response curves

One of the most important parameters of experimental f.i.a. curves is the peak variance which has a direct influence on sample throughput. It is well realized that the peak variance can be built up from three contributions:

$$\sigma_{\text{peak}}^2 = \sigma_{\text{injection}}^2 + \sigma_{\text{transport}}^2 + \sigma_{\text{detection}}^2 \quad (1)$$

Just as in chromatography, the contribution of the detection to the overall variance can be neglected when the standard deviation caused by the detector is at least five times smaller than the standard deviation caused by the transport. This condition is nearly always met in f.i.a. In that case eqn. (1) can be simplified to

$$\sigma_{\text{peak}}^2 = \sigma_{\text{injection}}^2 + \sigma_{\text{transport}}^2 \quad (2)$$

The theoretical discussion of peak variances by Ružička and Hansen [1] is based on the concept of residence time distribution (r.t.d.) functions. In their models these authors assume delta functions for the injection and thus predict values for $\sigma_{\text{transport}}^2$ only. The goal of the present work was to account for the contribution of the injection to the overall variance as well. Levenspiel et al. [2, 3] have pointed out that the manner of injection and detection has an influence on the measured r.t.d., and their notation has been adopted for the description of this influence in the following discussion of f.i.a. The

theory of Levenspiel et al. was developed for delta input functions. As these functions are never realized in practice, a more general injection model will be introduced here. The curves calculated with this model will contain the contribution of the injection, so that σ_{peak}^2 is immediately available. (The symbols used in the subsequent argument are listed in Table 1.)

Although injection of a given amount of sample Q_0 in a flow system with volume flow rate f_v may appear to lead to an unambiguously defined injection process, this is not true. Two different cases will be considered here.

(A) *Time injection.* Here the sample is introduced during a finite time ΔT . The amount of sample introduced into each stream line is proportional to the velocity in that stream line (e.g. an ideal syringe). For this injection model, use will be made of a dimensionless parameter $\beta (= \Delta T/\tau)$, where τ is the mean residence time of the flow system.

(B) *Slug injection.* Here a slice with length ΔL of the flowing fluid is instantaneously replaced by the sample fluid (e.g. an ideal sample loop). This injection model is characterized by the dimensionless parameter $\alpha (= \Delta L/L)$, where L is the line length of the system. In some cases it will be convenient to define α based on volumes. Figure 1 shows schematically the two ways of injecting the sample. It is assumed that in the case of the time injection the concentration C_0 of the sample is constant during the injection time ΔT and that in the case of the slug-injection the sample loop with volume $\Delta L\pi R^2$ has been homogeneously filled with the sample of concentration C_0 .

For the detection two possibilities will also be considered.

(A') *Cup-mixing value detector.* In this kind of detector a weighted mean is determined

$$C_{\text{cup}} = \int_0^R [C(r)v(r)2\pi r dr / \langle v \rangle \pi R^2] \quad (3)$$

in which R is the radius of the detector, r is the radial coordinate, $\langle v \rangle$ is the mean velocity of the fluid and $v(r)$ is the velocity of the flow stream at a distance r from the middle of the detector. Examples of this kind of detection are given by all mass flow-sensitive devices, such as continuous titrators and coulometric sensors, and also by the method of collecting fractions and determining the mean concentration in these fractions.

(B') *Mean value detector.* This detector "looks" through a plane perpendicular to the direction of the flow. The mean concentration is defined by

$$C_m = \int_0^R C(r)2\pi r dr / \pi R^2 \quad (4)$$

This type of detector is approximated by an optical detector. The example of laminar flow neglecting diffusion will be used to illustrate the influence of the injection and detection methods on the r.t.d. function. In the case of a time-delta injection with a cup-mixing detection this r.t.d. function is given [4] by

$$\theta < \frac{1}{2} \quad E = 0; \theta \geq \frac{1}{2} \quad E = 1/(2\theta^3) \quad (5)$$

TABLE 1

List of symbols

C	concentration	t	time
C_{\max}	concentration at peak maximum	ΔT	injection time
C_0	concentration of sample without dilution	$v(r)$	velocity at radial position r
E	E function; exit-age distribution function	$\langle v \rangle$	mean velocity
f_v	volume flow rate	x	axial coordinate
L	line length	α	$\Delta L/L$
ΔL	length of the slug; sample loop length	β	$\Delta T/\tau$
n	number of imaginary tanks	θ	reduced time: $\theta = t/\tau$
Q	amount of sample	$\mu'_1 = m$	mean of a distribution
Q_0	total amount of sample injected	μ'_k	k -th moment about the origin
r	radial coordinate	σ^2	variance of a distribution
R	tube radius	τ	residence time
s	complex variable		

Mathematical symbols

$\bar{C}(s)$	Laplace transform
$\mathcal{L}, \mathcal{L}^{-1}$	Laplace transformation, back-transformation
$P(\chi^2 \nu)$	Chi-squared distribution with ν degrees of freedom
O notation	$f(\theta) = O(g(\theta))$ for $\theta \rightarrow \infty$; there exist positive δ and M such that $ f(\theta) \leq M g(\theta) $ for all $\theta > \delta$

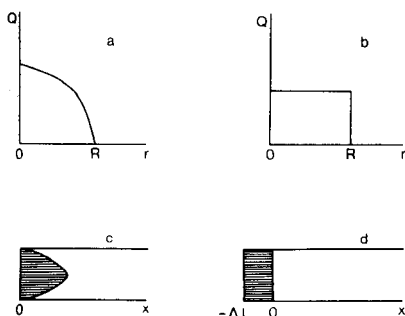


Fig. 1. Initial conditions resulting from type A and B injections. The model of laminar flow without diffusion is used. (a, b) Distribution of the injected amount Q over the radius; (c) initial distribution of the sample in type A; (d) initial distribution of the sample in type B.

where θ is the reduced time defined by $\theta = t/\tau$. The E function is the exit-age distribution function, i.e. the fraction of the sample fluid in the exit stream between θ and $\theta + d\theta$ (or t and $t + dt$) is given by $E(\theta)d\theta$ (or $E(t)dt$), thus

$$\int_0^{\infty} E(\theta)d\theta = 1 \text{ or } \int_0^{\infty} E(t)dt = 1 \text{ since } E(\theta) = \tau E(t) \quad (6)$$

The relation between the E function and the output concentrations is given by

$$E(t) = C(t) / \int_0^{\infty} C(t)dt = f_v C(t) / Q_0 \text{ or } E(\theta) = \tau f_v C(t) / Q_0 = C(\theta) \quad (7)$$

TABLE 2

Initial conditions	Time injection	Slug injection	
Initial conditions	Injection during time ΔT ; $\beta = \Delta T/\tau$	Slug length ΔL ; $\alpha = \Delta L/L$	(9)
Time injection	Initial conditions	Initial conditions	
$x \in IR$	$C = 0$	$-\Delta L \leq x \leq 0$	$C = C_0$
$t = 0$	$C = 0$	$x \leq -\Delta L$	$C = 0$
$t = \Delta T$	inside paraboloid with top at $x = 2 \psi \Delta T$ and bottom plane at $x = 0$ with radius R	$C = 0$	
$0 \leq x \leq 2 \psi \Delta T$	$C = C_0$		
All other points	$C = 0$		
First elution of sample (front-elution)	First elution of sample (front-elution)	First elution of sample (front elution)	(11)
$\frac{1}{2} \leq \theta \leq \frac{1}{2} + \beta$	(at $x = L$)	$\frac{1}{2} \leq \theta \leq (1 + \alpha)/2$	(at $x = L$)
$0 \leq r \leq a_1$	$C = C_0$	$0 \leq r \leq a_1$	$C = C_0$
$a_1 \leq r \leq R$	$C = 0$	$a_1 \leq r \leq R$	$C = 0$
Elution of front and tail	Elution of front and tail	Elution of front and tail	
$\theta \leq \frac{1}{2} + \beta$	(at $x = L$)	$\theta \geq (1 + \alpha)/2$	(at $x = L$)
$0 \leq r \leq a_2$	$C = 0$	$0 \leq r \leq a_2$	$C = 0$
$a_2 \leq r < a_1$	$C = C_0$	$a_2 \leq r \leq a_1$	$C = C_0$
$a_1 \leq r \leq R$	$C = 0$	$a_1 \leq r \leq R$	$C = 0$

TABLE 3

Detection		Mean value detection	Cup-mixing value detection
		$C_m = \int_0^R [C(r)2\pi r dr / \pi R^2]$	$C_{cup} = \int_0^R [C(r)v(r)2\pi r dr / \langle v \rangle \pi R^2]$
		(4)	(3)
		For laminar flow $v(r)/\langle v \rangle = 2(1 - r^2/R^2)$	For laminar flow $v(r)/\langle v \rangle = 2(1 - r^2/R^2)$
		(14)	(14)
		Case (a) front elution $0 \leq r \leq a_1$ $C = C_0$	Case (a) front elution $0 \leq r \leq a_1$ $C = C_0$
		$a_1 \leq r \leq R$ $C = 0$	$a_1 \leq r \leq R$ $C = 0$
		$C_m = \int_0^{a_1} [C_0 2\pi r dr / \pi R^2]$	$C_{cup} = \int_0^{a_1} [C_0 \langle v \rangle 2(1 - r^2/R^2) 2\pi r dr / \langle v \rangle \pi R^2]$
		(15)	(16)
		$C_m/C_0 = a_1^2/R^2$	$C_{cup}/C_0 = 1 - (1 - a_1^2/R^2)^2$
		(17)	(18)
		Case (b) front and tail elution $0 \leq r \leq a_2$ $C = 0$	Case (b) front and tail elution $0 \leq r \leq a_2$ $C = 0$
		$a_2 \leq r \leq a_1$ $C = C_0$	$a_2 \leq r \leq a_1$ $C = C_0$
		$a_1 \leq r \leq R$ $C = 0$	$a_1 \leq r \leq R$ $C = 0$
		$C_m = \int_0^{a_2} [C_0 2\pi r dr / \pi R^2] = C_0(a_1^2/R^2 - a_2^2/R^2)$	$C_{cup} = \int_0^{a_2} [C_0 2\langle v \rangle (1 - r^2/R^2) 2\pi r dr / \langle v \rangle \pi R^2]$
		(19)	(20)
		$C_m/C_0 = (1 - a_2^2/R^2) - (1 - a_1^2/R^2)$	$C_{cup}/C_0 = (1 - a_2^2/R^2)^2 - (1 - a_1^2/R^2)^2$
		(21)	(22)

TABLE 4

Elution conditions

Time injection	Slug injection
Case (a) front elution	Case (a) front elution
$\frac{1}{2} \leq \theta \leq \frac{1}{2} + \beta$	$\frac{1}{2} \leq \theta \leq (1 + \alpha)/2$ (11)
$v/\langle w \rangle = 2(1 - \alpha_1^2/R^2) = L/\langle w \rangle t = 1/\theta$	$v/\langle w \rangle = 2(1 - \alpha_1^2/R^2) = L/\langle w \rangle t = 1/\theta$ (23)
$(1 - \alpha_1^2/R^2) = 1/2\theta$	$(1 - \alpha_1^2/R^2) = 1/2\theta$ (24)
$\alpha_1^2/R^2 = (2\theta - 1)/2\theta$	$\alpha_1^2/R^2 = (2\theta - 1)/2\theta$ (25)
Case (b) front and tail elution	Case (b) front and tail elution
$\theta \geq 1/2 + \beta$	$\theta \geq (1 + \alpha)/2$ (13)
α_1 is given by	α_1 is given by
$v/\langle w \rangle = 2(1 - \alpha_1^2/R^2) = (L + v\Delta T)/\langle w \rangle t$	$v/\langle w \rangle = 2(1 - \alpha_1^2/R^2) = (L + \Delta L)/\langle w \rangle t = (1 + \alpha)/\theta$ (27)
$(1 - \alpha_1^2/R^2) = 1/2(\theta - \beta)$	$(1 - \alpha_1^2/R^2) = (1 + \alpha)/2\theta$ (29)

TABLE 5

Concentration functions

Time injection	Slug injection
Case (a) $\frac{1}{2} \leq \theta \leq 1/2 + \beta$	(a) $1/2 \leq \theta \leq (1 + \alpha)/2$ (11)
$C_m/C_o = (2\theta - 1)/2\theta$	$C_m/C_o = (2\theta - 1)/2\theta$ (30)
$C_{cup}/C_o = 1 - (1/2\theta)^2$	$C_{cup}/C_o = 1 - (1/2\theta)^2$ (31)
(b) $\theta \leq 1/2 + \beta$	(b) $\theta \geq (1 + \alpha)/2$ (13)
$C_m/C_o = 1/2(\theta - \beta) - 1/2\theta = \beta/2\theta(\theta - \beta)$	$C_m/C_o = (1 + \alpha)/(2\theta - 1)/2\theta = \alpha/2\theta$ (33)
$C_{cup}/C_o = \{1/2(\theta - \beta)\}^2 - \{1/2\theta - \beta\}/4\theta^2(\theta - \beta)^2$	$C_{cup}/C_o = [(1 + \alpha)/2\theta]^2 - (1/2\theta)^2 = (\alpha^2 + 2\alpha)/4\theta^2$ (35)
The maximum value of both C_m and C_{cup} is reached for $\theta = 1/2 + \beta$	The maximum value of both C_m and C_{cup} is reached for $\theta = (1 + \alpha)/2$
$C_m/C_o, \max = 2\beta/(1 + 2\beta)$	$C_m/C_o, \max = \alpha/(1 + \alpha)$ (37)

The function that is sought is $C(r, x, \theta)$ evaluated at $x = L$, i.e., $C(r, L, \theta)$. When this function is known, $C_{\text{cup}}(\theta)$ and $C_m(\theta)$ can be calculated via eqns. (3) and (4). The derivations are tabulated for clarity. In Table 2, initial conditions are given. Figure 2 gives a graphical presentation. In Table 3, C and C_{cup} are calculated (a) for the front of the peak, and (b) for the tail of the peak. In Table 4 the elution conditions are established. Finally Table 5 presents the results for $C_m(\theta)$ and $C_{\text{cup}}(\theta)$. These functions are not real r.t.d. functions because they are not yet normalized (zeroth moment is not equal to 1). However, this normalization only introduces a constant factor depending on α or β , so that the shape of the functions is not affected.

Table 6 summarizes the shape of the peak tails for various combinations. The results compare well with those of Levenspiel et al. [3]. Their results, however, are valid only for delta injections and thus take the simpler form

$$C_{A-A'} = C_{A-B'}/\theta = C_{B-A'}/\theta = C_{B-B'}/\theta^2 \quad (40)$$

The relation between the maximum peak height and α (or 2β) is shown in Fig. 3. It can be seen that the cup-mixing readings are always higher than the mean value readings. For small values of α (small loop volumes) the relative difference between the two readings becomes larger. For the case of a sample loop injection with cup-mixing detection, the reduced time θ needed for the tail of the concentration function to decrease to 2% of its peak value has been calculated. In this way an impression of the peak broadening is obtained. Calculation of the peak variance is impossible in this case because the second moment for this concentration function is infinite. Figure 4 gives a graph of the results. It should be noted that the contribution of the injection is included in this calculation.

In order to compare the results of Table 5 for the time- and slug-injections,

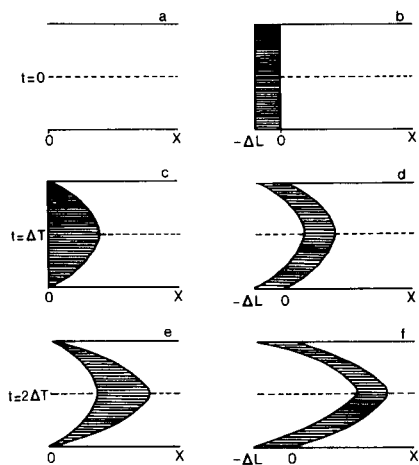
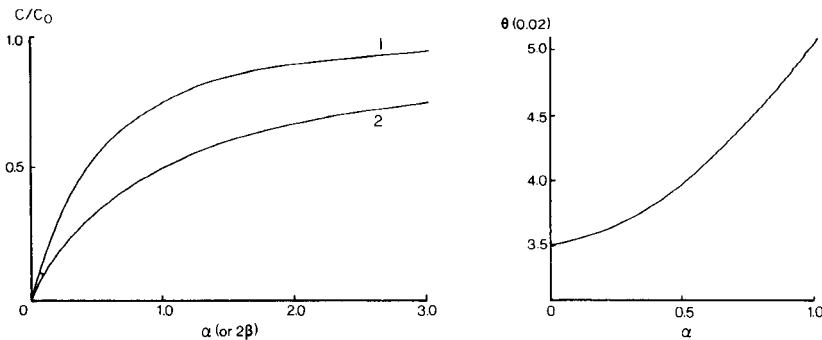


Fig. 2. Distribution of the sample in the laminar flow model without diffusion for time and slug injections at times $t = 0, \Delta T$ and $2\Delta T$.

TABLE 6

Tail shapes of peaks

Method	Shape of tail ^a
A-A'	$O(\theta^{-3}) \theta \rightarrow \infty$
B-A'	$O(\theta^{-2}) \theta \rightarrow \infty$
A-B'	$O(\theta^{-2}) \theta \rightarrow \infty$
B-B'	$O(\theta^{-1}) \theta \rightarrow \infty$

^aFor the O notation, see list of symbols.Fig. 3. Peak maximum as a function of α for cup-mixing (curve 1) and mean-value (curve 2) detection. Transport model is laminar flow without diffusion.Fig. 4. Peak broadening in the laminar flow model. θ (0.02) is the reduced time at which the concentration has decreased to 2% of its peak value.

it is necessary to calculate the relation between α and β . For reasons of equivalence it is assumed that equal amounts of sample are injected. For the slug case,

$$Q_0 = \pi R^2 \alpha L C_0 \quad (41)$$

For the time case the volume I of the paraboloid with a top at $x = 2\langle v \rangle \Delta T$ and bottom-plane at $x = 0$ with radius R has to be calculated by integration:

$$I = \pi R^2 \beta L \quad (42)$$

$$\text{and } Q_0 = \pi R^2 \beta L C_0 \quad (43)$$

Comparison of eqns. (41) and (43) shows that the injections are equivalent when $\alpha = \beta$.

The conclusion from the foregoing results is that care must be taken in the interpretation of f.i.a. experiments both in the calculation of the residence time from experimental data and in the calculation of the peak variance. Although it will in practice be difficult to decide which model for injection and detection is applicable, an exact specification of the injection and detection devices is certainly necessary.

The present authors are well aware of the very simplifying assumptions in the given model. The theory can perhaps be extended to the Aris—Taylor model, but this model is hardly applicable in f.i.a. (mainly because the line lengths used are often too small). A more realistic theory would involve very complicated mathematics. The advantage of the given model is that it clearly shows the influence of the different methods of injection and detection.

Influence of the sample loop volume in the tanks-in-series model

In this section, the influence of the sample volume is treated in a different way. Instead of a model based on physically meaningful parameters, use will be made of the tanks-in-series model, which is a descriptive model.

In Fig. 5a is shown a typical f.i.a. response curve. For convenience, the time axis can be transformed to reduced time θ and the concentrations normalized (Fig. 5b). The experimental parameters which describe the curve adequately are: C_{\max} , the maximum concentration reading; $\theta_{C_{\max}}$, the time when the maximum appears; m , the mean of the concentration distribution; and σ^2 , the variance of the concentration distribution.

When Fig. 5c, in which the response curve to a delta input function is shown, is compared to Fig. 5b, it can be seen that all these parameters are influenced. For a quantitative analysis, the systems analysis model for f.i.a. presented in Fig. 6 will be used. A good introduction to the application of

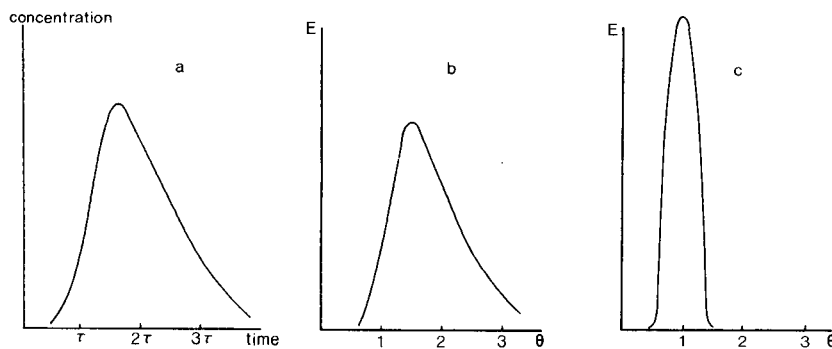


Fig. 5. (a) Typical f.i.a. curve; (b) normalized curve; (c) f.i.a. response curve with delta input function.

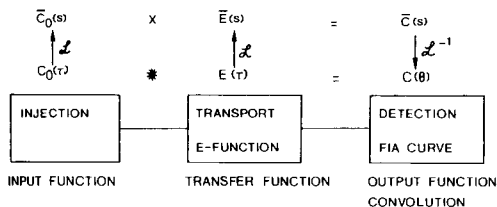


Fig. 6. Systems analysis model for f.i.a. \mathcal{L} is a Laplace transform, \mathcal{L}^{-1} is the back-transform, (\times) is multiplication and ($*$) is convolution.

systems analysis to chemical engineering in flowing systems has been given by Himmelblau and Bischoff [5]. For the flow model in this section, the tanks-in-series model is used. For this model, the E function can be calculated as

$$E(\theta) = n^n \theta^{n-1} \exp[-n\theta]/(n-1)! \quad (44)$$

where n is the number of (imaginary) tanks. The Laplace transform of this function is given [6] by

$$E(s) = n^n / (s + n)^n \quad (45)$$

For the injection model a sample loop with length $\alpha = \Delta L/L$ will be used. In this case the sample loop injection can be considered as a time injection; thus for the input function:

$$0 \leq \theta \leq \alpha \quad C_0(\theta) = 1/\alpha \quad \text{and} \quad \theta > \alpha \quad C_0(\theta) = 0 \quad (46)$$

This input function is normalized with respect to its area. The corresponding Laplace transform is

$$\bar{C}_0(s) = (1 - \exp[-\alpha s])/\alpha s \quad (47)$$

Referring to Fig. 6, the following relations hold:

$$C(\theta)_{\text{output}} = \int_0^{\infty} C_0(\tau) E(\theta - \tau) d\tau = C_0(\tau) * E(\tau) \quad (48)$$

where τ is a dummy time-variable. The convolution integral (48) in the Laplace domain is replaced by a multiplication:

$$\bar{C}(s)_{\text{output}} = \bar{C}_0(s)_{\text{input}} \times \bar{E}(s) \quad (49)$$

By means of a back-transformation of $\bar{C}(s)$ it is possible to find $C(\theta)_{\text{output}}$ [7]. Van der Laan [8] and Aris [9] have pointed out that from the Laplace transform of the output function, its moments (if they exist) can be calculated directly, thus avoiding the back-transformation according to the formula:

$$\mu'_k = \int_0^{\infty} \theta^k E(\theta) d\theta = (-1)^k \lim_{s \rightarrow 0} [\partial^k \bar{C}(s) / \partial s^k] \quad (50)$$

Thus for the mean: $m = \mu'_1 = -\lim_{s \rightarrow 0} [\partial \bar{C}(s) / \partial s]$, and for the variance: $\mu'_2 = \sigma^2 + \mu_1'^2 = \lim_{s \rightarrow 0} [\partial^2 \bar{C}(s) / \partial s^2]$. Hence, $\sigma^2 = \lim_{s \rightarrow 0} [\partial^2 \bar{C}(s) / \partial s^2] - \mu_1'^2$. Some algebra yields for the present system: $m = 1 + (\alpha/2)$ and $\sigma^2 = (1/n + \alpha^2/12)$. This has to be compared with the results for a delta input function, for which $m = 1$ and $\sigma^2 = n^{-1}$.

For calculation of the peak maximum it is necessary to perform the back-transformation. The back-transformation of $\bar{E}(s)$ for the present system gives

$$E(\theta) = \{P(2n\theta|2n) - P(2n(\theta - \alpha)|2n)\} \alpha^{-1} \quad (51)$$

which can be written as:

$$C(\theta)/C_0 = \{P(2n\theta|2n) - P(2n(\theta - \alpha)|2n)\} \quad (52)$$

$P(\chi^2|\nu)$ is the chi-squared distribution with ν degrees of freedom which is tabulated in [6].

The peak maximum is plotted as a function of α in Fig. 7 for $n = 5$ and $n = 10$. The time of the maximum can be found by differentiating eqn. (51) with respect to θ , putting the result equal to zero and solving for θ :

$$\theta_{C_{\max}} = -\alpha \exp\left(\frac{n\alpha}{n-1}\right) / \left[1 - \exp\left(\frac{n\alpha}{n-1}\right)\right]^{-1} \quad (53)$$

which has to be compared with the result for a delta input function:

$$\theta_{C_{\max}} = 1 - 1/n \quad (54)$$

From eqn. (53) it can be seen that there is a significant difference between the residence time ($\theta = 1$) and the time at which the maximum appears. Equation (54) shows that this is also true for a delta input and a moderate number of tanks.

Similar calculations were performed for a linear ramp input and an input model with one tank. The results for the mean and the variance are analogous to those for the sample loop input, i.e.

$$m = 1 + k_1\alpha \quad (55)$$

$$\sigma^2 = 1/n + k_2\alpha^2 \quad (56)$$

where for the ramp input $k_1 = 2/3$ and $k_2 = 2/9$ and for the input tank $k_1 = k_2 = 1$.

The conclusions from the above results lead to a rule of thumb similar to that given by Ružička and Hansen [1]: minimal variance in f.i.a. is achieved by minimizing the sample volume. As the peak height decreases with the smaller sample volumes, concentrated samples can be injected directly.

EXPERIMENTAL

All experiments were carried out in a manifold consisting of an injection valve with a sample loop, a straight length of tube and a home-made conductivity detector (Fig. 8). This detector was used in conjunction with a Philips PR 9501 conductivity meter. The carrier stream consisted of deionized water and the sample solution was 0.01 M potassium chloride. The flow was kept at 1.5 ml min^{-1} ($25 \mu\text{l s}^{-1}$) by a Gilson Minipuls II pump. The tube diameter was 0.54 mm, corresponding to a tube volume of $2.3 \mu\text{l cm}^{-1}$.

The influence of the injection method was investigated as follows. The normal sample loop injection in which the loop is completely emptied by the carrier stream was compared with an injection in which after a certain time the loop was switched back. In this way a time injection is approximated. Figure 9 gives the experimental curves obtained.

The influence of the sample volume was determined in two series of experiments. In the first series the detector was connected to the injection valve by a very short connecting tube (0.1 m); in the second series of experi-

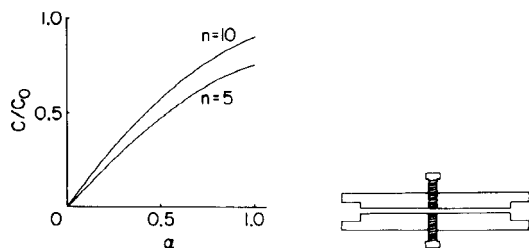


Fig. 7. Peak maximum as a function of α in the tanks-in-series model with sample loop injection.

Fig. 8. Home-made conductivity detector. The two screws are used as detector electrodes and can be adjusted for normalized response.

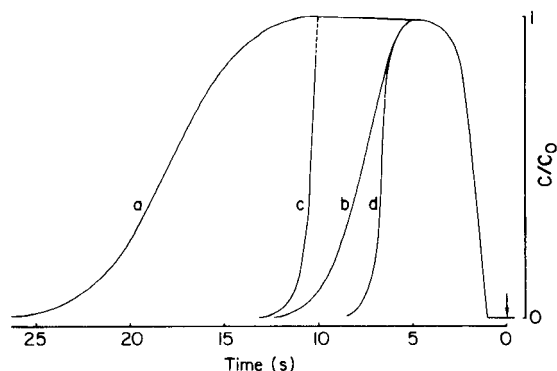


Fig. 9. Results of two different types of injection. Connecting tube, 0.1 m. (a) Injection with sample loop volume $340 \mu\text{l}$; (b) as (a) with $140\text{-}\mu\text{l}$ sample; (c) injection with back-switch after 10 s; (d), as (c) after 6 s. The arrow denotes the start of injection.

ments the connecting tube was 2.0 m. In both series of experiments the loop length (volume) was varied. Figure 10 shows the experimental curves, and Table 7 summarizes the calculated experimental parameters.

RESULTS AND DISCUSSION

The results in Fig. 9 give qualitative support for the calculations summarized in Table 6. Indeed, in the time case, the tails of the concentration functions fall more steeply than in the slug case. Also the peak variance is smaller in the time case.

Linear regression on the data of Table 7 gave the following results:

for the 0.1-m connecting tube: $\text{area} = 0.070 + 72\alpha$ ($r = 0.9991$); $m = 1 + 0.58\alpha$ ($r = 0.9997$); $\sigma^2 = 0.857 + 0.105\alpha^2$ ($r = 0.998$).

for the 2.0-m connecting tube: $\text{area} = -89 + 3517\alpha$ ($r = 0.9998$); $m = 1 + 0.58\alpha$ ($r = 0.9999$); $\sigma^2 = 0.041 + 0.133\alpha^2$ ($r = 0.996$).

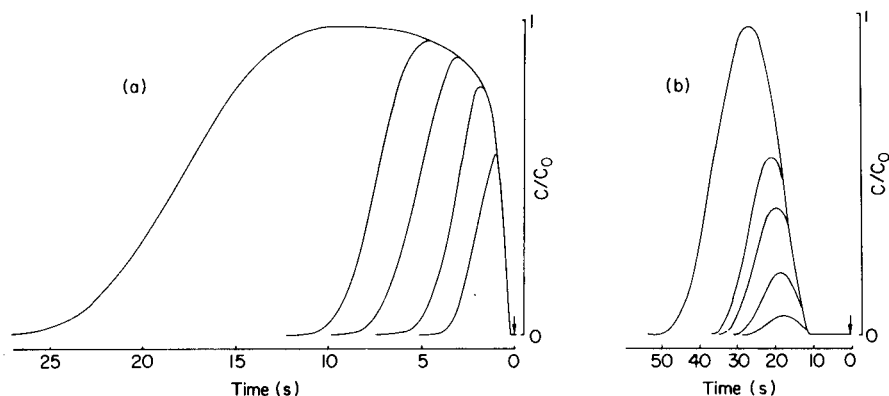


Fig. 10. Results of detection after passage through (a) 0.1 m of connecting tube and (b) 2.0 m of connecting tube. Sample loop lengths were 0.1, 0.25, 0.50, 0.70 and 1.85 m corresponding to sample volumes of ca. 20, 50, 100, 140 and 370 μl .

TABLE 7

Detection after connecting tubes of 0.1 m and 2.0 m

Loop length (m)	0.1 m tube					2.0 m tube				
	α	$\frac{C_{\max}}{C_0}$	Area ^a	μ_t (s)	σ_t^2 (s ²)	α	$\frac{C_{\max}}{C_0}$	Area ^a	μ_t (s)	σ_t^2 (s ²)
0.10	1.0	0.58	167	1.48	0.52	0.05	0.06	107	18.76	11.78
0.25	2.5	0.79	361	2.16	1.15	0.13	0.20	345	19.62	14.79
0.50	5.0	0.89	655	3.30	2.60	0.25	0.40	768	20.84	17.51
0.70	7.0	0.93	1055	4.38	4.90	0.35	0.56	1169	22.00	20.24
1.85	18.5	0.98	2670	10.31	28.13	0.92	0.96	3145	27.97	51.12

^aThe area is measured in arbitrary units.

From the good correlations for the area it can be seen that the detector is linear in the concentration range used. The correlations for μ are in excellent agreement for both experiments. The value of 0.58 for the coefficient of α is not equal to the value 0.50 predicted by $m = 1 + (\alpha/2)$, but it is less than the 0.66 predicted for the linear ramp input, so it can be concluded that the injection profile is more or less rectangular. The correlation for σ^2 is in fair agreement with the value predicted by eqn. (56). Again the value 1/12 for a rectangular injection profile is not reached, but the value found is less than the 0.222 predicted for a linear ramp input.

There are two possible explanations for the experimental scatter in the correlations. The first is that timing is very critical and preferably the switching of the sample valve should be automated by means of a pneumatic actuator. The second is that the numeric handling of the data gives an increasing error in going from the zeroth moment (the area) towards higher moments.

The conclusion from the present experiments is that the influence of sample volume is satisfactorily described by the systems analysis model leading to eqns. (55) and (56). Furthermore, in view of the good agreement between theory and experiment, it seems very probable that the tanks-in-series model provides a more adequate description of the transport under normal f.i.a. conditions in a straight tube than is given by the laminar flow model without diffusion.

REFERENCES

- 1 J. Růžička and E. H. Hansen, *Anal. Chim. Acta*, 99 (1978) 37.
- 2 O. Levenspiel and J. C. R. Turner, *Chem. Eng. Sci.*, 25 (1970) 1605.
- 3 O. Levenspiel, B. W. Lai and C. H. Chatlynne, *Chem. Eng. Sci.*, 25 (1970) 1611.
- 4 W. J. Beek and K. M. K. Mutzall, *Transport Phenomena*, Wiley, London, 1975.
- 5 D. M. Himmelblau and K. B. Bischoff, *Process Analysis and Simulation Deterministic Systems*, Wiley, New York, 1968.
- 6 M. Abramowitz and I. A. Stegun, *Handbook of Mathematical Functions*, Dover, New York, 1963.
- 7 M. R. Spiegel, *Laplace Transforms*, McGraw-Hill, New York, 1965.
- 8 E. T. van der Laan, *Chem. Eng. Sci.*, 7 (1955) 187.
- 9 R. Aris, *Proc. Roy. Soc. London, Ser. A*, 245 (1958) 268.

A MICROPROCESSOR CONTROL SYSTEM FOR AUTOMATED MULTIPLE FLOW INJECTION ANALYSIS

K. K. STEWART*, J. F. BROWN and B. M. GOLDEN**

Nutrient Composition Laboratory, Nutrition Institute, Human Nutrition Center, United States Department of Agriculture, Beltsville, Maryland 20705 (U.S.A.)

(Received 24th July 1979)

SUMMARY

A microprocessor control system is reported for automated multiple flow injection analysis. The control system consists of an IMSAI-8048 microprocessor, some associated electronic interfacing and a control computer command language. The system can be programmed to control any of three versions of automated multiple flow injection analysers. This control system is relatively inexpensive and is suitable for use by inexperienced personnel.

The recent independent development of unsegmented continuous flow analysis in the United States [1–3] and in Denmark [4] provides a unique alternative to the more classical segmented continuous flow systems first developed by Skeggs [5]. The two versions of unsegmented continuous flow process are basically the same. The European version has a low-pressure reaction system, uses peristaltic pumps and manual or semiautomated sample insertion system, and is commonly known as flow injection analysis (f.i.a.). The American version has a low-to-high pressure reaction system, depulsed positive displacement pumps, an automated sample insertion system and is commonly known as automated multiple flow injection analysis (a.m.f.i.a.) [6]. Both systems have successfully operated at sampling rates of over 100 samples per hour with a variety of detectors. Recently, Růžička et al. [7] demonstrated a means of performing titrations with f.i.a. Subsequently, the a.m.f.i.a. system was modified to do automated titrations [8]. Betteridge [9] has recently reviewed the field of unsegmented continuous flow analysis.

The a.m.f.i.a. system requires precise control of the operation of the sample tray, the sample probe, and the sample insertion valve if good precision is to be attained. Three versions of the system are shown in Fig. 1. The standard system and the dilution system use the configuration for limited or medium sample dispersion and the titration system uses the configuration for large sample dispersion. Růžička and Hansen [10] have described the three types of sample dispersion. The three a.m.f.i.a. systems have common

**Present address: Betz Laboratory, Treviso, PA 19047, U.S.A.

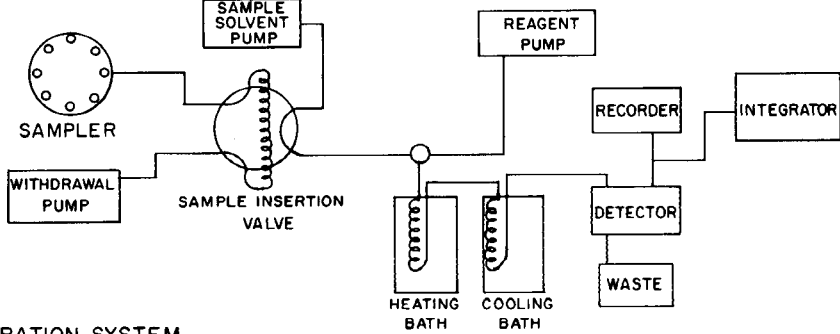
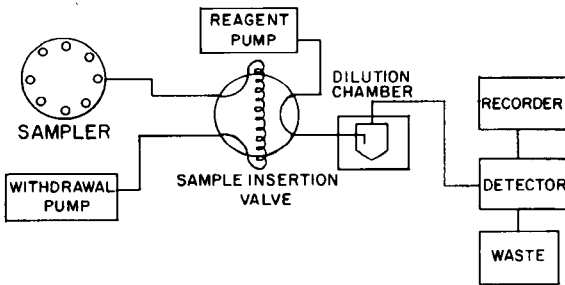
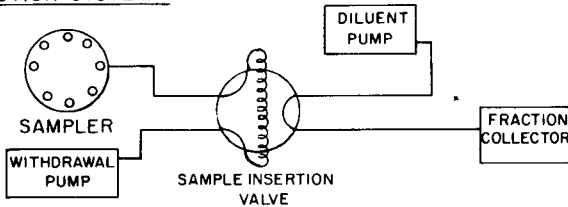
STANDARD SYSTEMTITRATION SYSTEMDILUTION SYSTEM

Fig. 1. A.m.f.i.a. configurations. The standard system with low or medium dispersion is used for colorimetric, fluorimetric and other standard continuous flow assay systems. The titration system with large dispersion is used for automated titrations. The dilution system with low sample dispersion is used for routine dilution of fixed volumes of multiple samples.

requirements for the control of the sampler probe, the sample tray and the sample insertion valve. The dilution system also requires fraction collector control. Data handling is needed for the standard system and the titration system, but not for the dilution system. In this paper, a simple inexpensive microprocessor control system is described which fulfills all the control requirements for the a.m.f.i.a. system as well as simple data collection for the titration configuration of the system.

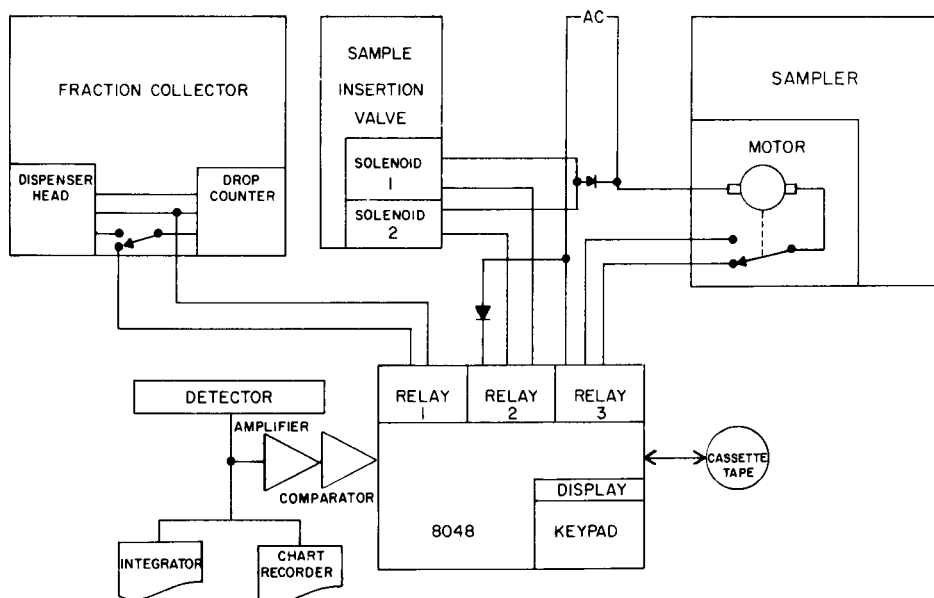


Fig. 2. A block diagram of the a.m.f.i.a. control and data system.

HARDWARE

The detailed a.m.f.i.a. system has been described elsewhere [3]. A block diagram of the microprocessor-controlled system is shown in Fig. 2. The control system is based on an IMSAI-8048 control computer with 2K random access memory, 27 I/O lines including interrupts, 90 control-optimized instructions, an internal timer/event counter, RS232 interface, and three 440-W three-way relays. A 1K system monitor provides an easy examination or modification of program memory, loading or dumping of information to (or from) external devices, or step-mode execution of user programs. An inexpensive cassette tape recorder was used for program storage.

The IMSAI-8048 was interfaced with a Technicon sampler, a pair of solenoid gas valves, a fraction collector and the appropriate detector. The Technicon sampler has two states, rinse and sample, which are activated by a continuous voltage (110 a.c.) at either of two locations on a microswitch which is mechanically linked to the motor output. Sample tray advance is automatic with each load-to-rinse transition. The pair of solenoid valves are activated individually to switch the sample insertion valve between its load and inject positions. Since the sampler and the valve each have only two states, interfacing is easily accomplished by direct connection to the on-board 3-way relays. The valve control circuit uses a full wave bridge, as direct current solenoid valves are used. The drop-counting feature of the fraction

collector is used as the control point for the microcomputer. In normal operation, sample drops increment a counting circuit as they pass between a light emitting diode and a phototransistor. The fraction-collector counter can be preset to advance the sample tray after 1—990 drops. As illustrated in Fig. 2, a three-way manual switch transfers the counter input to one of the microprocessor on-board relays, which can simulate the effect of sample drops by breaking closure at the phototransistor. A low-pass filter in the control line prevents erroneous triggering by electrical surges.

The critical measurement in a.m.f.i.a. titrations is the width of the sample peak at a fixed point above the base line. This peak width is usually measured in units of time. To make this measurement automatic, an electronic interface is inserted between the detector and the IMSAI-8048. This interface provides a signal to the IMSAI-8048 for the period of time that the detector output is above a preset level. The data collection system counts and stores the time that that signal is enabled. The interface first amplifies the detector signal and then compares it to a reference voltage. A 25-mV detector signal was found to be above line noise, and this voltage was selected to enable the signal to the microprocessor. A downward hysteresis of 15 mV was provided in the circuit to prevent a false retreat from the enabling state. Hence, detector transitions above 25 mV set the enabling state and cause an interrupt to occur in the IMSAI-8048. When the detector signal falls below 10 mV at the end of a titration, the IMSAI-8048 discontinues its timing operation and returns from interrupt.

Occasional malfunctioning of the computer has occurred; this is thought to be caused by electro-magnetic interference from the solenoid valves and from line voltage spikes. Substitution of shielded cable between system components, use of a regulated line transformer, enclosure of the IMSAI-8048 in a metal cabinet and humidity control are being evaluated in an attempt to increase the reliability of the system. Detailed electronic diagrams are available on request.

SOFTWARE

The control computer command language (CCCL) is an interpreter program which simplifies programming of the IMSAI-8048 computer. It gives the user a relatively easy means of controlling relays and I/O lines and some capacity to acquire and store data. Although the CCCL can control 16 I/O lines, only 3 of the output lines are used in the a.m.f.i.a. control. In addition, CCCL can acquire data from 12 input lines directly, and indirectly from a thirteenth input line, in a software interrupt mode. CCCL can be programmed to wait for a specified period of time and to perform branches within the user program which may or may not depend on input data.

Durations of an input state may be timed and stored in a 16-bit word, or integrations of a series of 12-bit input states may be stored in a 32-bit word. The CCCL software clock is programmable to 25 kHz or between 1×10^{-2} and 2.55 s per count.

Instructions are entered into the IMSAI-8048 in the form of hexadecimal (base 16) codes. Each instruction is 2 bytes long and must reside between hexadecimal C00 and CFF of the control computer memory. Each byte is represented by 2 hexadecimal (hex) digits. Therefore, each instruction implemented in CCCL is 4 hex digits long. The first digit represents the operation code which defines the type of instruction. The meanings of the second, third, and fourth digits depend on the instruction. Version II of CCCL has a total of 16 instructions at the disposal of the user. Programs may be up to 128 instructions long.

The instruction set for version II is listed in Table 1. A brief functional description of these commands is given below. The 16 output lines are controlled by the OUT P, RR command. RR represents a 2 hexadecimal digit code and P specifies port 1 or 2. The first hexadecimal digit of port 2 and both hexadecimal digits of port 1 control 12 uncommitted lines. The second hexadecimal digit of port 2 controls the 4 on-board relays and 4 additional lines. The GOTO LL command is used to cause an unconditional program branch, forcing the program to execute next the instruction at line LL. LL must be an even number because each instruction must start on an even number byte of the control computer memory. If LL is odd it will be decreased to the next lowest even number.

The WAIT N, CC command is used to program a delay. CC and N are hexadecimal digits, and their product determines the length of the delay or continuation of an OUT P, RR instruction. A delay of up to 255 (hexadecimal FF) times 15 (hexadecimal F) counts is possible with this command.

It is possible to activate an externally controlled interrupt in CCCL by a

TABLE 1

Instruction set of version II of the control computer command language

Hex code	Mnemonic instr.	Description
IPRR	OUT P, RR	Set output lines according to hex digits RR on port P
2XLL	GOTO LL	Branch to program line LL
3NCC	WAIT N, CC	Wait $N \times CC$ counts
4XVV	EN INT VV	Enable interrupt, set vector line to VV
5ILL	IF I GOTO LL	If inputs = I, then go to line LL
0XXX	DIS INT	Disable interrupt provision of CCCL
6IBB	GOTO BB, I	Go to line $(BB + 2 * \text{input value})$
7CNN	CTRC = NN	Initialize counter C to NN counts
8CLL	DGNZ C, LL	Decrement counter C, go to line LL if counter is non-zero
9TMM	TAB T, MM	Execute table T, MM times
APLL	CLR P, LL	Clear location LL on page P
BXLL	INCD LL	Increment 2-byte word at LL
CNLL	ADD N, LL	Add N to line LL
DILL	INT I, LL	Integrate input of I lines in 4-byte words starting at LL
EXTT	MOD TT	Modify count rate to $TT/100$ s/count
FPLL	ASM P, LL	Go to assembly program at line LL page P

change in voltage on a special input line. If the change of voltage occurs, and the interrupt provision of CCCL has been enabled, the program will immediately suspend execution of the regular user program and branch to another previously defined program line. The interrupt provision is enabled by the EN INT VV instruction. VV is a 2 hexadecimal digit that represents the line number where the program will branch should an interrupt occur. The interrupt provision can be disabled by the DIS INT instruction. If an interrupt occurs after this instruction has been executed, all voltage transitions on the interrupt input line will be ignored.

A conditional branch instruction is implemented with the IF I GOTO LL command. In this case, I represents one hexadecimal digit, or 4 bits of information. When this command is executed, 4 input lines are interrogated and compared to I. If I matches the inputs exactly, a GOTO command is issued, where LL again represents a program line number (in hexadecimal). If I does not equal the input, the normal sequence of program execution is followed.

Another type of branch is implemented with the GOTO BB, I command. This command interrogates the inputs, then multiplies the hexadecimal input value by 2 and adds this number to BB, a 2 digit hexadecimal number known as the base. This calculated value is used as a line number in a GOTO instruction. For example, if the instruction GOTO 20, I is executed; where the inputs have a value of hex 2, the program would calculate a line number of 24 then branch to line 24.

There are two complementary instructions which can be used to set up program loops. The CTR C = NN instruction sets the internal counter C to the hexadecimal value NN. C can equal 0 to F hexadecimal, thus there are 16 counters or 16 levels of nesting possible. The DGNZ C LL instruction decrements counter C and line LL is executed if counter C is not zero. If the counter equals zero, program execution proceeds to the next sequential instruction.

The TAB T, NN is an instruction that combines the elements of several of the preceding instructions. Often it is necessary to execute a fixed sequence of OUT instructions followed by WAITs. The TAB T, NN instruction allows the user to execute a sequence of events of this sort that have been placed in 'tables'. A table is a list of output states and delay times. For example, it may be desired to have relays 1 and 2 open for 10 s followed by closing relay 2 and opening relay 3 and then have the system remain in this state for another 5 s. Each of 16 available tables has the capability of defining 8 output states with 8 associated delays. The command TAB T, MM means execute table T MM times. T is a one hexadecimal digit value and MM is a 2 digit hexadecimal value.

The memory locations A00-AFF (page A, data memory) and C00-CFF (page C, user program memory) may be selectively cleared by the CLR P, LL instruction. P specifies the page memory, and LL is the line number to be cleared. The duration of an input state is measured and stored with the

INCD LL command. These values are limited to between 0 and 65535 counts. Each time this instruction is encountered, the value of a 16-bit word starting on page A at LL is incremented by one. The ADD N, LL command increases the value of line LL on page C by N. This command is used to change, by either CLR P, LL or CNT LL instructions, data storage locations or to alter the arguments of any CCCL instruction.

Integration of a sequence of input values is accomplished with the INT I, LL statement. The hexadecimal digit I specifies the number of input lines up to twelve to be integrated, and LL is the location on page A of the most significant byte of the sum. This statement uses four bytes of data memory per integration (0–4 billion).

MOD TT changes the count rate to TT (hexadecimal)/100 s per count. For example, if TT = C8, then the clock operates at 208/100 (C8 hexadecimal = 208 decimal) seconds per count. A value of zero in the MOD TT command sets the clock rate at 25 kHz.

Additional assembly language subroutines may be developed and executed in vacant regions of microprocessor memory by using the ASM P, LL instruction. Many useful monitor subroutines are also accessible. Page and line are specified respectively by P and LL.

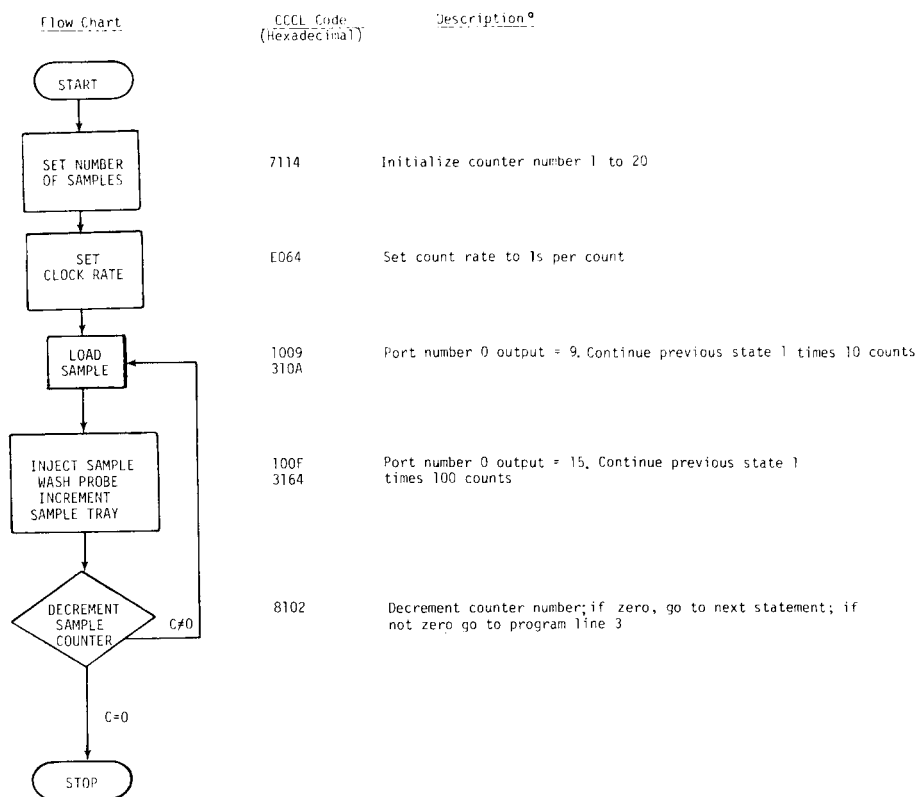
All CCCL user programs are limited to 128 total instructions. The user program must start at location C00 of the control computer memory space. All instructions must start at even numbered bytes. Tables use two separate areas of memory. Delay or state times begin at location D00 and output states start at location E00. Copies of the complete language are available on request.

Control of the solenoid valves which operate the pneumatic sample insertion valve is described below to illustrate the use of this control system. Since the IMSAI uses 3-way relays and both solenoids are activated alternately, only one control bit is needed for the operation. If control line 1 performs the task, and all other lines are to remain inactive, then the output from the CPU to Port 1 with lines 1–8 will be either (00) or (01) in hexadecimal, or (00000000) and (00000001) in binary.

DISCUSSION

Operation of this system is straightforward and can be easily taught to persons with little experience in microprocessors or programming. Most programs are short and straightforward. The flow chart for a standard program and the associated commands for the standard a.m.f.i.a. operation are shown in Fig. 3. Canned programs for routine analyses are easily developed and stored on magnetic tape cassettes. Thus, for a given analysis the operator need only turn on the system, load the cassette, enter the number of samples, start the run, and let the control system take over.

The usefulness of any continuous flow system is increased with automated system control and data acquisition. Precise control of the the timing is of



^oAll numbers in decimal

Fig. 3. A typical CCCL — a.m.f.i.a. program. This program is designed to control the analysis of twenty samples with the standard a.m.f.i.a. configuration.

particular concern in the f.i.a. and a.m.f.i.a. systems where the reaction times are usually less than 60 s and are often about 10 s. The newly introduced programmable control microprocessors are well suited for this type of control operation. They provide excellent control, are easy to use, inexpensive, small and can be built into the system. Inclusion of the cassette tape recorder in the system increases the utility of the system. The parameters for each assay can be developed and then stored on tape. Thus, the control system itself becomes modular, an important step to making the entire system modular. The development of such modular systems is an important step to the eventual acceptance of these techniques.

Data acquisition and calculation are important parts of automatic chemistry. To date, chromatographic integrators have been used here to measure peak areas in colorimetric and fluorescence assays. This approach has been successful, but it proved inadequate for the automation of the f.i.a. titration system [8]. The hardware—software system to measure and store the peak

width with the IMSAI-8048, the CCCL, and the hardware interface described above has worked well. Alternative approaches for data handling are being evaluated.

The CCCL—IMSAI-8048 combination provides a powerful tool for the control of the a.m.f.i.a. system. The IMSAI-8048 can provide all the control functions needed and the CCCL provides a convenient tool for the control of the IMSAI-8048 system by noncomputer-oriented personnel. Although such workers may find the commands cryptic, they easily master their use with a little practice. Operators now routinely program the control systems for various assay systems with ease using the 16 commands of CCCL. This system should be useful as a general programmable control system for many other laboratory operations.

REFERENCES

- 1 J. D. Frantz and P. E. Hare, *Annual Report of the Director, Geophysical Laboratory, Carnegie Institution*, 1972—1973, p. 704.
- 2 K. K. Stewart, G. R. Beecher and P. E. Hare, *Fed. Proc.*, 33 (1974) 1434.
- 3 K. K. Stewart, G. R. Beecher and P. E. Hare, *Anal. Biochem.*, 70 (1976) 167; U.S. Patent 4013413 (1977).
- 4 J. Růžička and E. H. Hansen, *Anal. Chim. Acta*, 78 (1975) 145; Danish Patent Application No. 4846/84 (Sept. 1974); U.S. Patent 4022575 (1977).
- 5 L. T. Skeggs, *Am. J. Clin. Pathol.*, 28 (1957) 311.
- 6 K. K. Stewart and G. R. Beecher, 176th National Meeting, American Chemical Society, Analytical Division, paper No. 87, Miami, FL, 1978.
- 7 J. Růžička, E. H. Hansen and H. Mosbaek, *Anal. Chim. Acta*, 92 (1977) 235.
- 8 K. K. Stewart and A. G. Rosenfeld, 1979 Pittsburgh Conference on Analytical Chemistry and Applied Spectroscopy, paper number 653.
- 9 D. Betteridge, *Anal. Chem.*, 50 (1978) 832A.
- 10 J. Růžička and E. H. Hansen, *Anal. Chim. Acta*, 99 (1978) 37.

EXTRACTION BASED ON THE FLOW-INJECTION PRINCIPLE Part 3. Fluorimetric Determination of Vitamin B₁ (Thiamine) by the Thiochrome Method

BO KARLBERG*^a and SIDSEL THELANDER

Astra Pharmaceuticals AB, Analytical Control, S-151 85 Södertälje (Sweden)

(Received 29th August 1979)

SUMMARY

The thiochrome method for determination of vitamin B₁ in pharmaceutical preparations has been adapted to a continuous flow system based on the flow-injection principle. The sample volume required for an analysis is about 150 μ l. For routine purposes a concentration range of 3×10^{-4} – 6×10^{-4} mg ml⁻¹ is used. Results obtained with the system agree well with results obtained manually. The consumption of organic phase is 2–3 ml/sample and the sampling rate is 30/h. A sampling rate of 70/h is easily attained if necessary. The relative standard deviation is about 1%.

The classical thiochrome method for determination of vitamin B₁ involves the reaction between the vitamin and hexacyanoferrate(III) in alkaline solution and the extraction of thiochrome from the aqueous phase to an organic phase [1]. Thiochrome is a fluorescent oxidation product of vitamin B₁ and the amount formed in the alkaline solution has been shown to be dependent on, for instance, the pH, the hexacyanoferrate(III) concentration, and the reaction time [2]. While constant pH, concentrations, and volumes of the different reagents can easily be established (even though non-optimum conditions apply) the problem of exact timing for each step in the analytical scheme still has to be coped with. Even experienced analysts very often fail to obtain reproducible results manually. The adaptation of such a method to a continuous flow system seems therefore justified, since both the reaction time and the extraction time then can be kept perfectly constant. Consequently, AutoAnalyzer methods have been proposed [2–4] and have gained acceptance in some laboratories.

Extraction based on the flow-injection principle [5–8] combines a low reagent consumption and small sample volumes with a high sample throughput and should therefore be an attractive alternative for routine purposes. The sample is introduced after the pump and not through the pump as in most AutoAnalyzer methods. The aqueous phase is segmented by the organic phase by the aid of a specially constructed segmentor [5]. The aqueous segments acquire an ellipsoid shape in the teflon extraction coil. The wall drag causes turbulence within the segments and this explains the

*Present address: Bifok AB, S-194 05 Upplands-Väsby, Sweden.

fast extraction process. The residence time of the sample in the system is short, typically 20–60 s.

This work shows how a relatively complex analytical method such as the thiochrome method containing both a reaction and an extraction step can be adapted to f.i.a.

EXPERIMENTAL

Reagents

Thiamine hydrochloride (aneurine hydrochloride) and polyvidone (polyvinylpyrrolidone) were of pharmacopeial quality; all other chemicals were of analytical-grade quality. Standard solutions of vitamin B₁ were prepared in the range 3×10^{-4} – 6×10^{-4} mg ml⁻¹ which corresponds to 8.4×10^{-7} – 1.7×10^{-6} M. Double-distilled water was used both for standard and sample solutions; deionized water was found to contain impurities causing degradation of the thiamine. Chloroform was used without any particular pretreatment. All aqueous solutions were degassed before they were pumped through the system.

Apparatus

The system comprised the following components: an eight-channel peristaltic pump (Bifok, Upplands-Väsby, Sweden), an injection valve (Rheodyne, Berkley, U.S.A.) with a volume of 103 μ l, a filter fluorimeter (Aminco, Silver Spring, U.S.A.) with a flow cell of 70 μ l, segmentor and separator constructed as previously described [5]. For experiments requiring independent variation of the flow rates an additional peristaltic pump was connected to the system (Ismatec, Zürich, Switzerland).

According to Khoury and Cali [2], the excitation maximum for thiochrome appears at 370 nm and the emission maximum at 465 nm. Thus, a primary filter, 370 nm, was used together with a secondary Wratten gelatin filter designed for wavelengths above 420 nm.

The analytical manifold is shown in Fig. 1. The aqueous sample is mixed with hexacyanoferrate(III) by means of dispersion so that oxidation takes place in the reaction coil (0.6 m). The segmentor is adjusted so that organic segments of a length of about 5 mm are formed in the extraction coil. The oxidation and extraction processes can now occur simultaneously in the extraction coil up to the separation site. Part of the organic phase is taken to the flow cell of the filter fluorimeter. All tubes are of teflon except the tube connecting the valve and the segmentor which is of polypropylene. The restricting coil (1.3 m, i.d. = 0.5 mm) prevents evaporation of the organic phase, making use of an ice bath prior to the segmentor unnecessary. The Acidflex pump tubings were found to be of varying quality; the lifetime varied from a couple of hours up to several days. The adjustment of the pressure on the tubing is especially important for the Acidflex tubings in order to achieve optimal stability of the flow. The starting-up and

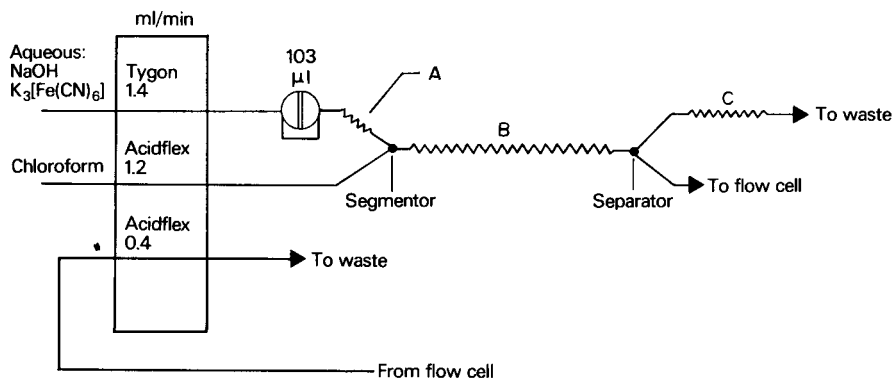


Fig. 1. Flow diagram for determination of vitamin B₁ in pharmaceutical preparations. Coil A, 0.6 m long, 0.7 mm i.d.; coil B, 2 m long, 0.8 mm i.d.; coil C, 1.3 m long, 0.5 mm i.d. Line from separator to flow cell, 0.3 m long, 0.5 mm i.d.

closing-down procedures were the same as described earlier [6]. All experiments were performed at $22 \pm 1^\circ\text{C}$.

RESULTS AND DISCUSSION

Routine analysis

A set of standard solutions was injected in duplicate to test the linearity of the calibration curve; the results are shown in Fig. 2. Conditions for the

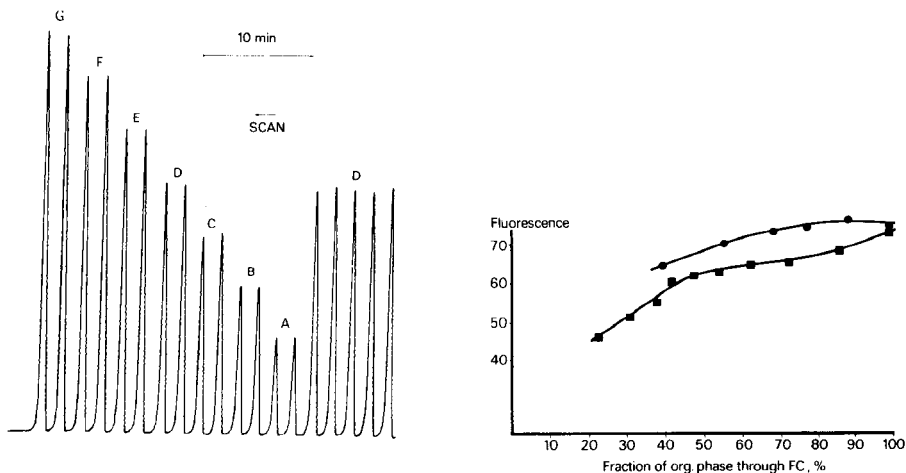


Fig. 2. Results of duplicate injections of vitamin B₁. Standard solutions: (A) $2 \times 10^{-4} \text{ mg ml}^{-1}$; (B) $3 \times 10^{-4} \text{ mg ml}^{-1}$; (G) $8 \times 10^{-4} \text{ mg ml}^{-1}$.

Fig. 3. Peak height plotted vs. fraction of the organic phase led through the flow cell. Injected standard solution, $5 \times 10^{-4} \text{ mg ml}^{-1}$. Flow rate (■) 1.62 ml min^{-1} ; (●) 0.69 ml min^{-1} .

test are given in Fig. 1. The normal range used routinely, 3×10^{-4} – 6×10^{-4} mg ml⁻¹, is covered by this set of standards. The sampling rate is about 30/h with this system design. For the specific needs of vitamin B₁ analyses at this laboratory such a sampling rate is quite sufficient. However, the number of analyses per time unit can easily be increased by increasing the flow rates. The repeatability of the method is good; a standard solution, 5×10^{-4} mg ml⁻¹, was injected 10 times (7 injections are included in Fig. 2, solution D) and a relative standard deviation of about 1% was found.

Table 1 contains results from routine analysis of several different vitamin preparations. The agreement between the f.i.a. method and the manual method is good. None of the preparations contain polyvidone; problems arising when this constituent is present are discussed in detail later.

During several hours of continuous operation of the system, the flow rates of the organic streams change because of mechanical deterioration of the Acidflex tubings. For this reason three standard solutions were introduced after each set of not more than six sample solutions. There is no doubt that the most welcome improvement of the system would be a pump able to deliver a constant flow of the organic solvent. Though very ingenious, the displacement bottle technique was found to be too laborious to apply in this connection. However, work is in progress with a new type of pump and the results so far are promising.

Reaction coil length

The reaction coil connects the valve and the segmentor (see Fig. 1). A large number of experiments were done in which this coil length was varied. Table 2 contains some condensed results. The interpretation of these results is complex because at least three different aspects should be considered from a theoretical point of view. First, the dispersion should increase with increasing coil length, and this would lead to a decrease in peak height because the peak area will be distributed over a longer distance. As a consequence the sample throughput should go down. (Dispersion in single-phase f.i.a. systems is

TABLE 1

Comparison between the manual and the f.i.a. thiochrome methods for determination of vitamin B₁ in some pharmaceutical preparations

Preparation	Label (thiamine hydrochloride) (mg ml ⁻¹)	Label (thiamine mononitrate) (mg/tablet)	Manual method	F.i.a. method
Vitamin solution 1	0.132	—	0.124	0.125
Vitamin solution 2	0.80	—	0.72	0.73
Tablet 1	—	2.75	2.66	2.70
Tablet 2	—	2.75	2.44	2.53
Tablet 3	—	5.50	4.95	5.14
Tablet 4	—	6.25	5.70	6.10

TABLE 2

Peak height and sample throughput as a function of reaction coil length (injected standard solution, 3×10^{-4} mg ml $^{-1}$.)

Coil length (cm) (i.d. 0.7 mm)	Peak height (cm)	Samples/h
50	6.2	40
65	6.2	38
95	6.1	35
135	5.8	31
185	5.1	28

defined as the ratio between the peak height of the original sample and the peak height of the dispersed sample [9]. Dispersion in two-phase systems can be defined analogously [6].) Secondly, a prolonged residence time of the sample within the reaction coil should give rise to an increased amount of oxidation products in the aqueous phase and should consequently be reflected in an increase in the total amount of extracted substance. This latter aspect favours increased sensitivity. Thirdly, one might argue that a longer residence time is disadvantageous with regard to the extraction yield because some degradation of the oxidation products may occur before extraction takes place. This, once again, should lead to lower peaks and lower sensitivity.

As can be seen in Table 2 the peak height decreases when the coil length is increased which means that the influence of the larger dispersion predominates. The possibility of formation of a larger amount of oxidation products when the residence time is prolonged cannot compensate for the effect of the increased dispersion.

The total flow rate

The peristaltic pump permits convenient variation of the total flow because the speed of the rollers can be changed in a stepless mode. Table 3 summarizes the results of such a variation over a ten-fold flow range. The same standard solution (6×10^{-4} mg ml $^{-1}$) was injected in quadruplicate for each pump speed and all individual flows were measured by direct reading on graduated flasks from which or into which all solvents were pumped.

The same pump tubings were utilized and the pressure on the tubings was not adjusted during the course of this study, hence the fraction of the organic phase going through the cuvette should be constant. However, because of the previously mentioned problem with the Acidflex tubings, some variation was obtained. Thus, for a flow rate of 2.17 ml min $^{-1}$ a slightly larger fraction of the organic phase was involuntarily pumped through the flow cell, but this explains only to some extent the increase in peak height. By comparing the results for almost identical fraction values for flows larger than 2.17 ml min $^{-1}$, e.g. 2.61 vs. 3.04, and 3.43 vs. 3.90 ml min $^{-1}$,

TABLE 3

Peak height and sample throughput as a function of the total flow (Injected standard solution, 6×10^{-4} mg ml $^{-1}$.)

Total flow (ml min $^{-1}$)	Percentage organic phase		Peak height (cm)	Samples/h
	Totally	Through f.c.		
0.43	48.8	25.6	12.8	12
0.81	48.1	27.2	14.0	20
1.23	47.2	27.6	14.9	30
1.69	47.3	28.4	15.6	37
2.17	47.0	29.5	15.6	40
2.61	47.1	28.4	15.1	45
3.04	47.0	28.6	14.1	50
3.43	47.5	27.1	13.5	55
3.90	47.4	26.9	12.7	60
4.40	47.3	25.0	12.5	70

the conclusion is quite obvious: the larger the flow, the shorter the reaction and extraction times, and the lower the peaks. The major cause of the lower peaks in this flow range is certainly the fact that the total dispersion increases when the flow rate increases [9].

It is difficult to make any prediction of the dispersion in the separator itself. However, visual inspection of the separation process inside this unit indicates an optimum mode of operation within the total flow range of 1.2–3.0 ml min $^{-1}$. Above this range the conditions within the separator seem to be "stressed", and below this range the separator intuitively acts as a mixing chamber whereby the dispersion should increase significantly. This latter assumption seems to be justified, for a decrease in peak height really was observed, cf. the values for the flow rates 1.23 and 0.81 ml min $^{-1}$.

It is interesting to note that the sample throughput may be raised up to at least 70/h without any apparent loss in precision and with only a minor loss in sensitivity.

Fraction of organic phase through the flow cell

By using a separate pump to suck organic phase through the flow cell, this particular flow rate could be varied keeping all other flow rates constant (cf. Fig. 1). The combined outflow of the aqueous plus the remaining part of the organic phase to waste will of course vary correspondingly. Figure 3 shows how the peak height changes when the fraction of organic phase through the flow cell varies. The same standard solution, (5×10^{-4} mg ml $^{-1}$) was injected for each fraction value. Different total flow rates of the organic phase were selected for this study. In both cases the organic phase amounted to about 50% of the total volume in the extraction coil resulting in the aqueous and organic flow rates being almost equal.

As expected, the peak heights increase when a larger part of the organic phase is taken to the flow cell even though a maximum seems to be attained

for the lower of the two flow rates (see Fig. 3). For analytical purposes the results obtained for the flow rate of 1.62 ml min^{-1} are especially important. In the region 25–50% the curve is rather steep which means that a small variation of the flow through the fluorimeter will influence the peak height significantly while in the region 50–80% this effect should be less pronounced. Hence, a larger standard deviation of the peak heights is to be expected in the region 25–50%. Fractions larger than 95% should be avoided because the risk of contaminating the flow cell with aqueous phase then becomes apparent.

Influence of polyvidone (polyvinylpyrrolidone)

Polyvidone is frequently used as a constituent in pharmaceutical preparations, especially tablet preparations. It is added as a binding agent to facilitate tablet compression. The solubility properties of drugs are very often changed in the presence of polyvidone [10] so it is reasonable to assume that the conditions for the extraction and the reaction in the thiochrome method may also be changed. Thiamine samples containing polyvidone were consequently found to give up to 9–10% lower values in assays when solutions not containing polyvidone were used for calibration. Since different vitamin preparations contain different amounts of polyvidone, several sets of calibration solutions would then be required to obtain valid analytical results. A more convenient means of cancelling out the effect of polyvidone is to add this compound to the aqueous reagent phase. When so added in an amount of $7.6 \times 10^{-3} \text{ mg ml}^{-1}$, a loss in sensitivity of about 20% was observed for samples containing no polyvidone at all. For samples containing polyvidone, the loss in sensitivity was self-evidently much smaller.

With polyvidone present in the aqueous phase, adjustment of the segmentation pattern in the extraction coil becomes trickier. Furthermore, the size of the segments becomes more irregular. The most reliable results were obtained with rather large segments (10–15 mm).

Yet another approach to eliminating the undesirable effect of polyvidone has also been tested. Non-fluorescent compounds with a simpler but analogous chemical structure to thiochrome are added to the aqueous reagent phase to bind polyvidone and thus suppress the interaction between thiochrome and polyvidone. A considerable reduction of the influence of polyvidone is then observed for some of the compounds tested so far. This investigation is still at an early stage but the approach seems to be promising.

REFERENCES

- 1 B. C. P. Jansen, *Rec. Trav. Chim. Pays-Bas*, 55 (1936) 1046.
- 2 A. J. Khoury and L. J. Cali, *Automation in Analytical Chemistry*, Technicon Symposia 1965, Mediad, White Plains, N.Y., 1966, p. 22.
- 3 A. J. Khoury, *Automation in Analytical Chemistry*, Technicon Symposia 1966, Mediad, White Plains, N.Y., 1967, p. 286.
- 4 T. Tsuda, T. Yamamoto and S. Yarimizu, *Ann. Sankyo Res. Lab.*, 16 (1964) 109.

- 5 B. Karlberg and S. Thelander, *Anal. Chim. Acta*, 98 (1978) 1.
- 6 B. Karlberg, P.-A. Johansson and S. Thelander, *Anal. Chim. Acta*, 104 (1979) 21.
- 7 H. Bergamin F^o, J. X. Medeiros, B. F. Reis and E. A. G. Zagatto, *Anal. Chim. Acta*, 101 (1978) 9.
- 8 K. Kina, K. Shiraishi and N. Ishibashi, *Talanta*, 25 (1978) 295.
- 9 J. Růžicka and E. H. Hansen, *Anal. Chim. Acta*, 99 (1978) 37.
- 10 T. Higuchi and R. Kuramoto, *J. Am. Pharmaceut. Assoc., Sci. Ed.*, 43 (1954) 393, 398.

PHOTOCHEMICAL REACTION DETECTORS IN CONTINUOUS-FLOW SYSTEMS — APPLICATIONS TO PHARMACEUTICALS

A. H. M. T. SCHOLTEN, U. A. TH. BRINKMAN and R. W. FREI*

Department of Analytical Chemistry, Free University, de Boelelaan 1083, 1081 HV Amsterdam (The Netherlands)

(Received 13th July 1979)

SUMMARY

Several basic parameters of a photochemical reactor coupled to a high-performance liquid chromatographic system are discussed. The non-fluorescent clobazam and desmethyloclobazam and three phenothiazines, which exhibit native fluorescence, are used as model compounds. On irradiation with ultra-violet light, the reaction products formed display fluorescence (clobazam, desmethyloclobazam) or improved fluorescence characteristics (phenothiazines). The effects of carrier stream (mobile-phase) composition, time of irradiation and band broadening in the reactor on the fluorescence signal are described. The polarity of the organic solvents used (methanol, ethanol, acetonitrile) appears to have an important effect on the fluorescence intensity. For clobazam and desmethyloclobazam, detection limits of 70 and 120 pg, respectively, were calculated after an irradiation time of 28 s with methanol–0.01 M (pH 5) acetate buffer (1 : 1) as mobile phase. The method is applied to the determination of both compounds in serum and urine samples.

The principle of adapting photochemical processes to detection in dynamic flow systems, particularly in on-line connection with liquid chromatography, has recently been gaining attention [1]. Photochemical reactions share the advantage that the resulting products often have improved detection properties because of an enhancement in fluorophore [2] or chromophore [3] activity and/or a shift in absorption or emission maximum. A photochemical reactor can be used to induce reactions with or without reagent addition, as was recently shown by Twitchett et al. [2] for the photochemical conversion of cannabinol to a fluorescent product. Inducing hydrolysis or oxidation reactions through a photochemical process is another possibility. An example of a photochemically catalysed hydrolysis is the conversion of nitrosamines to nitrite ions [3], while the use of an oxidative process is reported in the present paper. The potential of the (selective) decrease of fluorescence signals on u.v. irradiation has been demonstrated for LSD [2] and ergot alkaloids [4]. In the latter case, it has been suggested that the lowering of the signals after irradiation is due to hydrolysis or cleavage of the indole ring system.

In the present study, five model compounds were tested, namely clobazam, *N*-desmethyloclobazam and three phenothiazines. Clobazam, a 1,5-benzodiazepine, is a new tranquilizer [5, 6]; desmethyloclobazam is its

major plasma metabolite [7], which possesses psychosedative and anti-convulsant activity itself. The phenothiazines used were thioridazine, mesoridazine and sulphoridazine, a group of well-known psychopharmaceuticals [8, 9]. It was the aim of this investigation to study some basic parameters of a photochemical reaction detector coupled on-line to a high-performance liquid chromatographic (h.p.l.c.) system and to demonstrate the potential of photochemical detection by developing a sensitive and selective analytical method for the determination of some of these compounds.

EXPERIMENTAL

Materials

The structures and main characteristics of the model compounds are presented in Table 1. Clobazam was obtained from Hoechst-Roussel Pharmaceuticals Inc. (Somerville, N.J.); desmethylclobazam was a gift from Dr. I. L. Honigberg (University of Georgia, Athens, Ga., U.S.A.); the phenothiazines were gifts from Sandoz Ltd. (Basle, Switzerland). All the other chemicals were of analytical grade (Merck).

The stock solutions of clobazam and *N*-desmethylclobazam ($20 \mu\text{g ml}^{-1}$ in methanol) and the phenothiazines ($10 \mu\text{g ml}^{-1}$ in methanol—0.01 M pH 5 acetate buffer, 1:1 v/v) were stored in the dark. Throughout this paper, the compositions of the mobile phases are given as volume ratios.

All solvents were degassed before use in an ultrasonic bath.

Apparatus

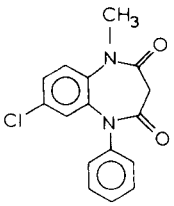
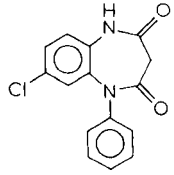
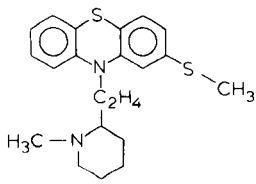
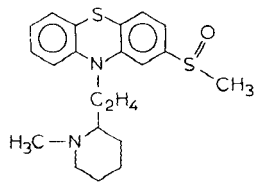
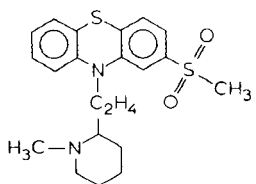
The chromatographic system consisted of an Altex-100 pump (Altex, Berkeley, Calif.), a Valco injection valve (Valco, Houston, Texas) with a 20- μl sample loop, a 10 cm \times 4.6 cm i.d. stainless steel column, home-packed with 10- μm LiChrosorb RP-18, a photochemical reactor (see below) with a LPS 251 (Schoeffel; Nema Electronics, Amsterdam) power supply and a vacuum cleaner as a cooling device. A Perkin-Elmer Model 204A fluorescence spectrophotometer was used as detector; the signal was recorded on a Kipp BD-8 recorder (Kipp, Delft). Several series of experiments were carried out without inserting the analytical column, plug injection being used to study the influence of the various parameters.

Photochemical reactor. The design of the reactor (Fig. 1) was slightly different from that used earlier [4]. The main improvements were the use of a 200-W Xe/Hg lamp as the light source, a vacuum cleaner which sucks air through the reactor and thus effects better and more reproducible cooling, and an aluminium reflector shield which encloses the lamp and capillary.

TABLE 1

Structure and fluorescence characteristics of clobazam, desmethyloclobazam and the phenothiazines

(Measurement conditions: methanol-0.01 M acetate buffer, pH 5 (1 : 1 v/v) for phenothiazines; methanol-water (1 : 1 v/v) for other compounds. All wavelengths in nm.)

	Name	Before irradiation		After irradiation	
		λ_{ex} (nm)	λ_{em} (nm)	λ_{ex} (nm)	λ_{em} (nm)
(A)	 Clobazam	—	—	356	395
(B)	 Desmethyloclobazam	—	—	356	395
(C)	 Thioridazine	325	455	340	378
(D)	 Mesoridazine	325	495	345	385
(E)	 Sulphoridazine	340	505	355	405

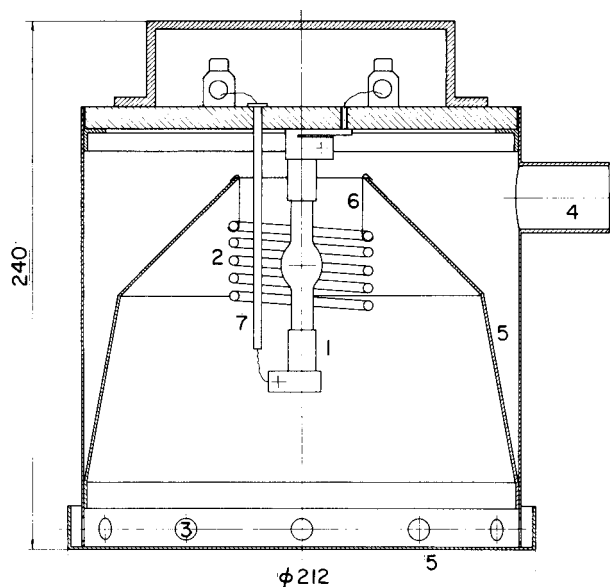


Fig. 1. Photochemical reactor. (1) Hanovia 200-W Xe/Hg high-pressure lamp; (2) quartz capillary, 0.5 mm i.d.; (3) inlet for air cooling; (4) outlet for air cooling; (5) aluminium reflector shield; (6) clip; (7) glass insulator (dimensions in mm).

RESULTS AND DISCUSSION

Fluorescence characteristics

Ultraviolet irradiation of clobazam and desmethyloclobazam resulted in the formation of highly fluorescent compounds within minutes (for excitation and emission maxima, see Table 1). This has been used by Stewart et al. [10] to develop a batch technique for the determination of clobazam. Clobazam and desmethyloclobazam themselves did not exhibit fluorescence, as was checked in h.p.l.c. experiments. Fluorescence signals observed in batch experiments, both by others [10] and by the present authors, were probably due to contamination or the presence of by-products.

The phenothiazines studied exhibit native fluorescence. Irradiation caused a photochemical oxidation process, which resulted [11, 12] in a shift of the emission maxima to shorter wavelengths (Table 1) and an increase of the fluorescence yield (Table 2). Table 2 also shows that the native fluorescence intensity increases from thioridazine to sulphoridazine, i.e. with increasing oxidation state. As is to be expected, irradiation produced the largest gain in fluorescence in the case of thioridazine; however, even with sulphoridazine a distinctly higher signal was obtained, which suggests that the sulphur atom in the ring system can be oxidized relatively easily.

Influence of mobile-phase composition

The influence of the carrier stream on the fluorescence signal was studied

TABLE 2

Comparison of fluorescence intensity of phenothiazines before and after u.v. irradiation (Conditions: mobile phase, methanol-0.01 M pH 5 acetate buffer (1 : 1, v/v); flow rate, 0.5 ml min⁻¹; reaction time, 50 s; solute conc., 10 µg ml⁻¹; plug-injection volume, 20 µl; detection at optimal wavelengths.)

Compound	Fluorescence intensity		Gain factor
	Non-irradiated	Irradiated	
Thioridazine	17.5	204	11.5
Mesoridazine	70	160	2.3
Sulphoridazine	102	327	3.2

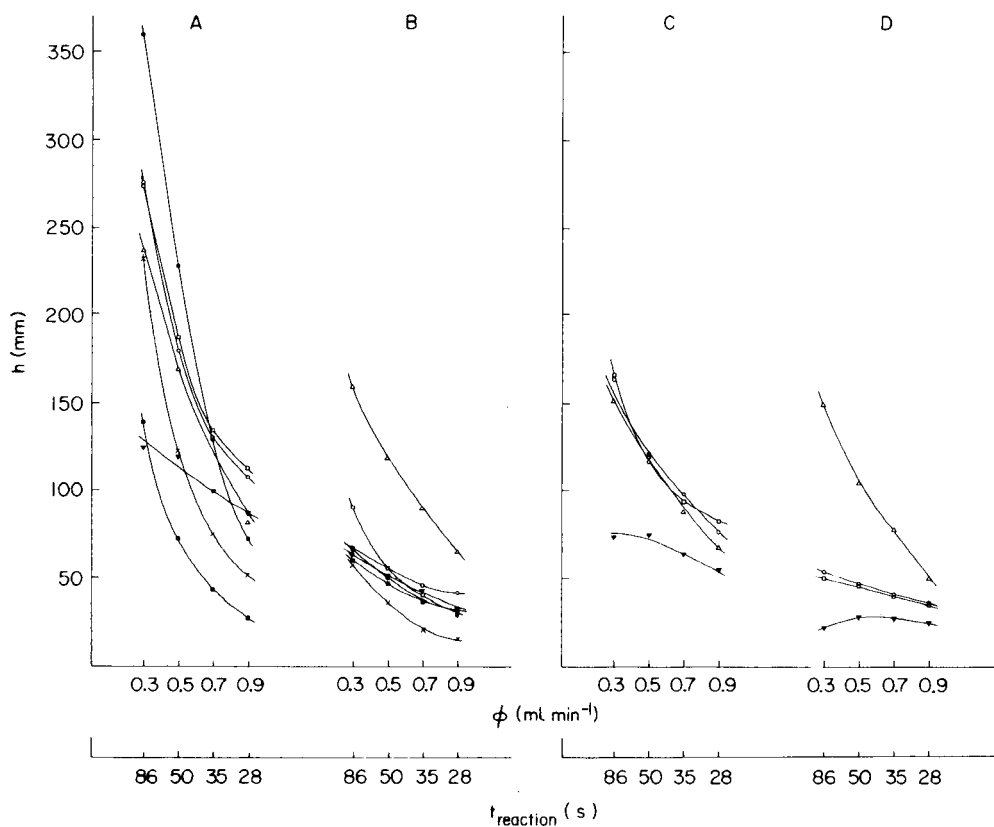


Fig. 2. Influence of mobile phase and reaction time on the fluorescence signal of clobazam (A, C) and desmethyloclobazam (B, D). A, B at 20 µg ml⁻¹; C, D at 0.4 µg ml⁻¹. (●) Methanol; (X) ethanol; (■) acetonitrile; (▼) water; (○) 1 : 1 ethanol-water; (□) 1 : 1 methanol-water; (△) 1 : 1 acetonitrile-water.

with a view to establishing preferred mobile-phase systems for h.p.l.c.; three organic solvents, namely methanol, ethanol and acetonitrile, and their mixtures with water, were tested. Clobazam and desmethylclobazam served as model compounds in this investigation.

The results for two drug concentrations and for flow rates of 0.3–0.9 ml min^{-1} , which correspond to residence, i.e. irradiation, times of 86–28 s, are shown in Fig. 2. The general trend observed for clobazam is an increase in fluorescence yield from acetonitrile to methanol, i.e., with increasing polarity of the solvent; as is to be expected, the effect is less pronounced at lower concentrations because of the lower absorbance of the irradiated solution. On the basis of these observations, it would be expected that even higher signals will occur with water as mobile phase. However, as can be seen in Fig. 2, the experimental data do not agree with this hypothesis: especially at low flow rates, the fluorescence signals measured for pure water lag distinctly behind. Admittedly, at low flow rates, the peaks recorded with water as carrier stream were 20–30% broader than were those recorded with any of the other solvents or solvent mixtures tested, and therefore plotting peak areas instead of peak heights resulted in a steeper slope of the pertinent curves. However, the expected solvent sequence still was not observed.

Desmethylclobazam shows a behaviour opposite to that of clobazam, as far as polarity is concerned. Moreover, changing the organic solvent or the flow rate of the carrier stream (see below) results in much smaller changes in fluorescence yield than with clobazam.

In order to study the influence of water in a h.p.l.c. system, the above experiments were repeated after the photochemical detector had been coupled to the outlet of the chromatographic column. Since the carrier stream now also acts as mobile phase, suitable mixtures of water and an organic solvent had to be selected in order to achieve appropriate retention behaviour of clobazam and desmethylclobazam. The results are shown in Fig. 3; the concentrations in the peak maximum have been corrected for the different degree of dilution in the column caused by differences in retention times observed with the different solvent mixtures, and for differences in plate number [4]. Obviously, over the range of mobile-phase compositions studied, varying the water content has only a relatively minor effect; small water contents are preferable on account of the slightly higher fluorescence signals. For the rest, the trend observed with regard to changes in organic solvent and the effect of carrier flow rate is the same as shown in Fig. 2.

Summarizing the above results it can be stated that with the present photochemical reactions, solvent polarity has an effect. A similar conclusion had earlier been reached in studies on benzophenone derivatives [13] and nitrogen-containing aromatics [14]. The contrasting behaviour of clobazam and desmethylclobazam cannot be explained as yet, since information is lacking on the photochemical reaction mechanism(s). Preliminary results of batch experiments suggest that, with clobazam, product formation is via an excited $n-\pi^*$ singlet state, which may be expected to show higher

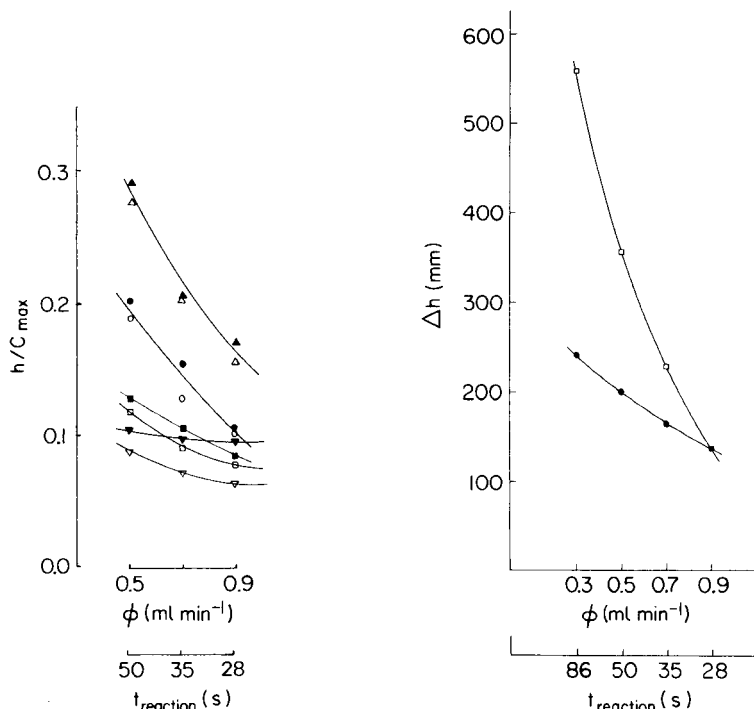


Fig. 3. Influence of water content in the mobile phase. For clobazam: (Δ) 1:1 methanol–0.01 M sodium acetate (NaAc); (\blacktriangle) 6:4 methanol–0.01 M NaAc; (\circ) 4:6 acetonitrile–0.01 M NaAc; (\bullet) 1:1 acetonitrile–0.01 M NaAc. For desmethylclobazam: (∇) 1:1 methanol–0.01 M NaAc; (\blacktriangledown) 6:4 methanol–0.01 M NaAc; (\square) 4:6 acetonitrile–0.01 M NaAc; (\blacksquare) 1:1 acetonitrile–0.01 M NaAc. Conditions: gain 3, sensitivity range 10, recorder 2 mV, concentration 70 ng ml⁻¹, 20- μ l injections.

Fig. 4. Influence of reaction time on thioridazine (\bullet) and sulphoridazine (\square). Mobile phase, methanol–0.01 M acetate buffer pH 5 (1:1). Δh difference in peak height before and after irradiation.

stability with increasing solvent polarity. The different nature of water compared to the organic solvents used with respect to viscosity (diffusion coefficients), heat capacity and/or temperature gradients in the flowing stream, should be considered in more detail when trying to explain the divergent behaviour of water (Fig. 2). This problem is currently being investigated.

Influence of the irradiation time

The time of irradiation was varied by varying the flow rate of the carrier stream (Fig. 2) or mobile phase (Fig. 3). For clobazam, increasing the residence time from 28 to 86 s resulted in a 2–3-fold increase in peak height. For desmethylclobazam, the effect was much smaller; this suggests a distinctly slower reaction rate for the fluorophore formation with the

metabolite. It should be added that with both clobazam and desmethyl-clobazam an irradiation time of 86 s was not nearly sufficient to reach plateau conditions, so that the use of longer residence times could well be beneficial.

For two phenothiazines, the dependence of fluorescence intensity on residence time is shown in Fig. 4. The general trend is similar to that observed for clobazam and its metabolite. It is noteworthy that results of batch experiments suggest that a more rapid oxidation can be obtained by adding an oxidizing agent such as ammonium peroxodisulphate to the carrier stream. The influence of dissolved oxygen is being investigated, but preliminary data suggest that it has only a minor effect.

Band broadening in the reactor

The dependence of band broadening in the photochemical reactor on residence time was studied with the phenothiazines as model compounds, since these exhibit native fluorescence and therefore can easily be detected without prior irradiation. Experiments were carried out with and without the photochemical reactor inserted in the line. In the former case, one series of data was collected under normal operating conditions, i.e. with irradiation, while a second series was obtained with the reactor shut off. The results are summarized in Table 3; typical peak shapes are shown in Fig. 5. From these results the band broadening caused by the reactor, $\sigma_{t,r}$, was calculated to be 10.4 s (at $\phi = 0.5 \text{ ml min}^{-1}$). Furthermore, the data indicate that the peak shape for the irradiated solutes is more symmetrical and narrower than the shape recorded with the reactor shut off. This is largely due to the higher diffusion rates prevailing under irradiation (high-temperature) conditions, as was demonstrated in a final series of experiments carried out at high temperature, but with the reactor shut off; these brought about a similar decrease in peak width and asymmetry.

TABLE 3

Dependence of band broadening on reactor conditions

(Conditions for h.p.l.c.: mobile phase, methanol–0.01 M pH 5 acetate buffer (1 : 1); flow rate, 0.5 ml min^{-1} ; reaction time, 50 s; model compounds, sulphoridazine and mesoridazine.)

Conditions	Band broadening (s)		Asymmetry factor ^c
	σ_t^a	$w_{t,10\%}^b$	
Without reactor	6	29	2.2
With reactor: non-irradiated	12	68	2.5
non-irradiated, 60°C	11.5	55	1.5
irradiated	12.5	57	1.5

^aMeasured at front of peak. ^bWidth measured at 10% peak height. ^cSee Fig. 5; asymmetry factor = b/a .

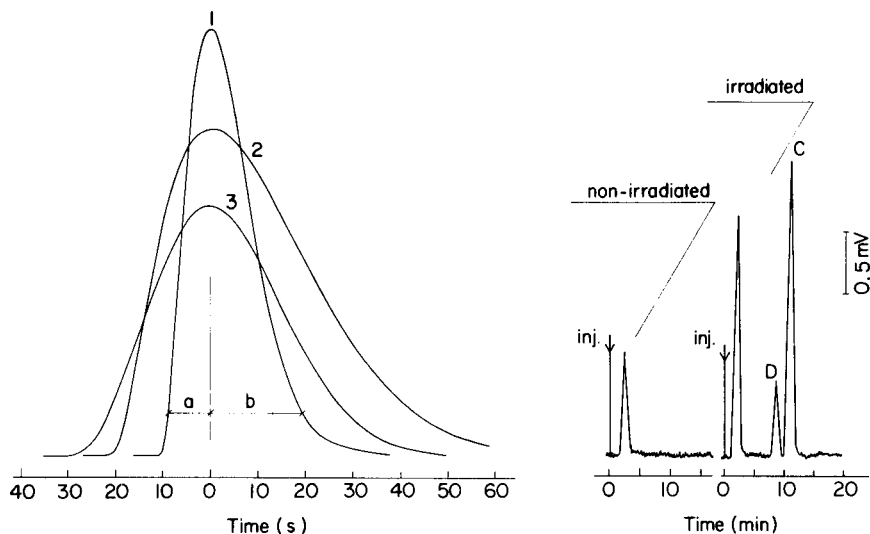


Fig. 5. Influence of reactor conditions on peak shape. (1) Without reactor; (2) with reactor, not irradiated; (3) with reactor, irradiated. b/a = asymmetry factor; cf. Table 3.

Fig. 6. Chromatogram of human serum sample spiked with 0.7 ppm of clobazam and desmethylclobazam, before and after irradiation. Conditions for h.p.l.c. mobile phase, methanol–0.01 M sodium acetate solution (1 : 1); flow rate, 0.9 ml min^{-1} . Detector conditions: gain, 3; sensitivity range, 10; slit widths, 10 nm; response, slow; recorder at 5 mV. C = clobazam and D = desmethylclobazam.

H.p.l.c. analysis

The photochemical reactor was coupled to a reversed-phase h.p.l.c. system and tested with clobazam and its major metabolite as model compounds. Some of the mobile phases which permitted a satisfactory separation of this pair on a LiChrosorb RP-18 column, are given in the legend to Fig. 3. A 1 : 1 mixture of methanol and aqueous 0.01 M sodium acetate solution proved to offer the best compromise between resolution and fluorescence yield. Under these conditions, the detection limits for clobazam and desmethylclobazam, calculated for a 2 : 1 signal peak-to-peak noise ratio, were 70 and 120 pg, respectively, after an irradiation time of 28 s (ϕ , 0.9 ml min^{-1}). For a residence time of 50 s (ϕ , 0.5 ml min^{-1}) and with methanol–aqueous 0.01 M acetate (6 : 4) as mobile phase, lower detection limits of 30–50 pg were calculated. With both compounds, linear calibration curves were obtained (r , 0.9988 and 0.9993) in the 0.01 – $4 \mu\text{g ml}^{-1}$ range. The relative standard deviation was better than 1.0% ($n = 8$).

As an application, 1 ml of human serum was spiked with 50 μl of methanol containing 0.7 μg each of clobazam and desmethylclobazam. After the addition of 1 ml of methanol and shaking, the sample was centrifuged for 3 min at 7 G, and 20- μl aliquots were injected onto the top of the analyt-

ical h.p.l.c. column. The chromatogram obtained is shown in Fig. 6. The recovery for clobazam was 95% and for desmethylclobazam 70%.

Analysis of spiked samples of human urine also was successful. Here, it is interesting to note that Sticht and Kaefenstein [15] have reported that clobazam is poorly excreted in urine. These authors, however, calculated a detection limit for (hydrolyzed) clobazam of 50 ng, i.e. some three orders of magnitude greater than that found in the present study.

CONCLUSION

The potential of the photochemical reactor, which can be constructed at moderate cost, for the sensitive and selective detection of suitable groups of compounds in continuous-flow systems has successfully been demonstrated. In contrast with many other detection techniques, post-column addition of reagent generally is not necessary. This implies that the design of the reaction detector can be rather simple and that no additional band broadening is introduced by reagent addition.

The relatively fast kinetics of reactions such as those studied so far have permitted the use of reasonably short irradiation times. This in its turn has enabled work to be carried out with non-segmented flow without undue band broadening. Thus, in practice a high throughput of samples will be obtainable when no separation is necessary. Still, although this mode of detection can be valuable in automatic analysis systems, one of the more interesting aspects is the coupling of the photochemical reaction detector to h.p.l.c. systems. In the present paper, this has been demonstrated by means of the trace determination of clobazam and its major metabolite in serum and urine samples.

In the future, work will be carried out to study the reaction mechanisms of these model systems. This should permit the design and use of the photochemical reaction detector to be optimized. Moreover, screening tests will be carried out with various other groups of compounds in order to define more closely the scope and limitations of the present technique.

REFERENCES

- 1 R. W. Frei and A. H. M. T. Scholten, *J. Chromatogr. Sci.*, 17 (1979) 152.
- 2 P. J. Twitchett, P. L. Williams and A. C. Moffat, *J. Chromatogr.*, 149 (1978) 683.
- 3 W. Iwaoka and S. R. Tannenbaum, *IARC Sci. Publ.*, 14 (1976) 51.
- 4 A. H. M. T. Scholten and R. W. Frei, *J. Chromatogr.*, 176 (1979) 349.
- 5 Clinical Investigator Literature, Hoechst-Roussel Pharmaceuticals Inc., Somerville, N.J., May 1973.
- 6 R. G. Borland and A. N. Nicholson, *Brit. J. Clin. Pharmacol.*, 2 (1975) 215.
- 7 S. Fielding and I. Hoffman, *Brit. J. Clin. Pharmacol.*, in press.
- 8 F. W. Kerner, FDA Bylines no. 1, (1973) 15.
- 9 P. Hadju and D. Damm, *Arzneim. Forsch.*, 26 (1976) 2141.
- 10 J. T. Stewart, I. L. Honigberg, A. Y. Tsai and P. Haydn, in preparation.
- 11 J. B. Ragland and V. J. Kinross-Wright, *Anal. Chem.*, 36 (1964) 1356.
- 12 V. R. White, Ch. S. Frings, J. E. Villafranca and J. M. Fitzgerald, *Anal. Chem.*, 48 (1976) 1314.
- 13 G. Porter and P. Suppan, *Trans. Faraday Soc.*, 61 (1965) 1664.
- 14 R. L. Letsinger and R. R. Hautata, *Tetrahedron Lett.*, 48 (1969) 4205.
- 15 G. Sticht and H. Kaefenstein, *Z. Rechtsmed.*, 82 (1978) 105.

THE USE OF SOLVENT SEGMENTATION IN CONTINUOUS-FLOW SYSTEMS, AND FLUORESCENCE LABELLING BY DERIVATIZATION

C. E. WERKHOVEN-GOEWIE, U. A. Th. BRINKMAN and R. W. FREI*

Department of Analytical Chemistry, Free University, de Boelelaan 1083, 1081 HV Amsterdam (The Netherlands)

(Received 15th July 1979)

SUMMARY

Solvent segmentation is valuable for reactions with up to 23-min residence times. Dansylation of pharmaceutically important secondary and primary amines is used as a model system. Plugs of organic solvent minimize band broadening, and act as reagent carrier as well as product carrier. Continuous-flow dansylation provides a sensitive fluorimetric detection system suitable for AutoAnalyzer systems and h.p.l.c.

The use of dynamic micro-extraction principles has long been known in AutoAnalyzer technology; three-phase systems (air bubble, segmented solvent stream, and immiscible solvent plug) have usually been applied. Continuous extraction without air segmentation has recently been introduced by Karlberg and Thelander [1] for the micro-extraction of caffeine in a continuous-flow system. Minimizing band broadening of sample zones is desirable in such flow-injection systems in order to improve sample throughput and to reduce dilution [2]. Also when micro-extraction principles are applied to design post-column reaction detectors [3] for column liquid chromatography (h.p.l.c.), usually to isolate a reaction product from an excess of interfering reagent, the band-broadening aspect becomes very critical. The first applications of the extraction detector principle to h.p.l.c. were developed by Gfeller et al. [4] and Frei et al. [5] for the detection of tertiary amines of pharmaceutical and agricultural importance by using on-line fluorescent ion-pair formation. The fluorescent ion partner was dimethoxyanthracene sulphonate (DAS) proposed by Westerlund and Borg [6] and used in AutoAnalyzer systems for the control of drugs in pharmaceutical formulations [7]. Initially, a three-phase system was used. Later, the air bubble was eliminated and the plug of the immiscible solvent was used to reduce band broadening [8]. Considering the flow phenomena in such a segmented system the term "solvent segmentation" was introduced [8]. The band-broadening and mixing phenomena are probably closer to those characteristic of air-segmentation systems such as described by Snyder and Adler [9] and by Lawrence et al. [10] than to the flow-injection characteristics [2].

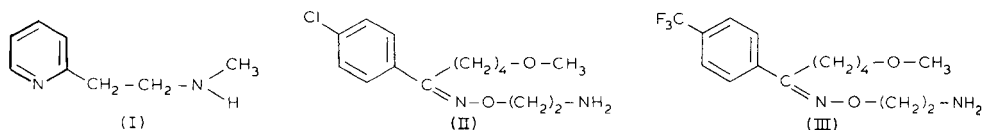
In an effort to assess the usefulness of these micro-extraction detectors for actual chemical reactions and long residence times, the fluorescence labelling

of amines with dansyl chloride (Dans-Cl) [11] was chosen as a model system. The reagent, dissolved in a water-immiscible solvent plug, was added to an aqueous stream containing the sample zones; the reaction then took place, probably at the organic solvent–water interface, and the less polar reaction product was extracted into the organic plug.

EXPERIMENTAL

Materials

The compounds tested are listed in Table 1. The structures of β -histine (I), clovoxamine (II; clovax) and fluvoxamine (III; fluvox), are depicted below:



Stock solutions of the model compounds were prepared in distilled demineralized water and stored at 4°C. Dansyl chloride (98% purity; Merck) was dissolved in dichloroethane and stored at 4°C. Dichloroethane and acetonitrile were of analytical-grade quality (Baker).

Methods

Figure 1 shows the Technicon (Tarrytown, N. Y.) AutoAnalyzer system as set up for solvent segmentation. Dichloroethane was invariably used as the organic solvent. An Aminco (Silver Springs, Md.) fluoromonitor was employed to detect the dansylated amines (excitation filter, 365 nm; emission cut-off filter, >450 nm). The T-piece was a Technicon part (No. 116B034-01A10); the all-glass phase separator was home-made and had a PTFE insert [10]. A Perkin-Elmer (Norwalk, Conn.) Series 2 liquid chromatograph was employed to pump the carrier stream, which consisted of an aqueous 0.05–0.1 M sodium hydrogencarbonate solution, containing

TABLE 1

Detection limit of amines (as their dansylamides) in a two-phase flow system

Compound	Reaction time (min)	Reaction temperature (°C)	Detection limit (ng)
β -Histine	5	ambient	1
Fluvoxamine	16	56	3
Clovoxamine	16	55	0.5
Ergotamine	6.5	54	8
Cephaeline	16	56	30
Emetine	16	56	30
Ephedrine	16	56	60
Histamine	6.5	54	600
Di-n-butylamine	10.5	54	18

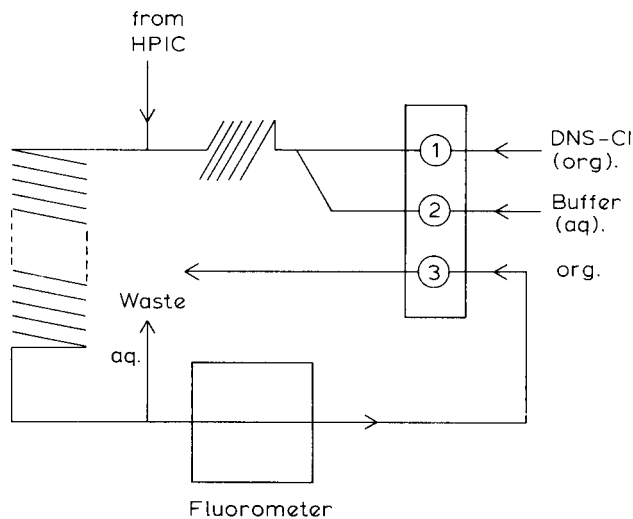
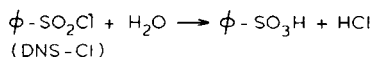
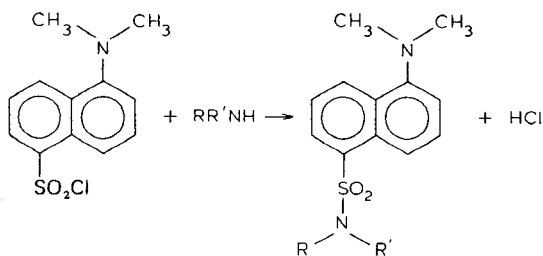


Fig. 1. AutoAnalyzer arrangement for post-column dansylation/extraction system. (1) 0.1 M sodium hydrogencarbonate solution (0.32 ml min^{-1} ; black); (2) dansyl chloride dissolved in dichloroethane (1.20 ml min^{-1} ; yellow); (3) organic solvent through fluorescence detector (0.80 ml min^{-1} ; red). The colours indicate the coding for the tubing.

0–30% (v/v) of acetonitrile; the flow-rate was $0.8\text{--}1.0 \text{ ml min}^{-1}$. A Rheodyne injection valve with $175\text{-}\mu\text{l}$ loop was used for plug injections. In band-broadening studies a variable-wavelength u.v.-detector (LC 55, Perkin-Elmer) was inserted between the injection valve and the reactor.

RESULTS AND DISCUSSION

The dansylation reaction has been widely used in batch experiments to form fluorescent derivatives of primary and secondary amines of phenolic compounds prior to their liquid-chromatographic separation [11, 12]. The feasibility of using dansyl chloride in a two-phase system has also been demonstrated [13]. During the dansylation, two competing reactions occur. One is the actual labelling reaction, the other is the hydrolysis of the reagent to form the unreactive but highly fluorescent sulphonic acid (Dans-OH):



The dansylated amines have their excitation and emission maxima in dichloroethane at 348 and 500 nm, respectively.

In a two-phase system, with the reagent in the organic phase, formation of the dansylamides will proceed much faster than does the hydrolysis. Hence background fluorescence arising from extraction of Dans-OH (which will be co-extracted by acetonitrile or another such solvent in the mobile phase used for h.p.l.c.) will remain low; accordingly, in principle, such a two-phase medium seems well suited for a dynamic derivatization system.

For the solvent-segmented system, the experiments described below were carried out with plug injection. Di-n-butylamine was selected as a model compound. The parameters investigated were reagent concentration, temperature and time of reaction and carrier-stream composition.

In experiments on reagent-concentration effects the reactor was maintained at room temperature, while the time of reaction was invariably 8 min. The amount of amine injected was kept constant at 200 ng. It was found that the fluorescence produced increased substantially as the Dans-Cl concentration increased from 0 to 350 $\mu\text{g ml}^{-1}$, but relatively little thereafter. A concentration of 350 $\mu\text{g ml}^{-1}$ was thus chosen for all further work. Varying the temperature of the reaction had a considerable effect on the height of the fluorescence signal. As expected, the dansylation reaction proceeds faster at higher temperatures: the relative fluorescence intensities generated at 20°C, 30°C and 60°C were 1.0, 1.25 and 1.85, respectively. However, there are two limiting factors, viz. the boiling point of the organic solvent (dichloroethane) and the fact [11, 12] that the dansylated amines decompose above ca. 60°C. Hence, 55°C was selected as the optimal reaction temperature.

Increasing the acetonitrile content of the carrier stream from 0 to 30% (v/v) did not noticeably affect the peak heights; it did, however, result in distinctly increased noise levels which, at 30% acetonitrile, were about twice as high as with a purely aqueous solution. Varying the pH over the range 8.5–11.5 did not significantly change either the peak height of the dansylamide or the fluorescence background.

Under the optimal conditions (i.e., 55°C, a reagent stream containing 350 $\mu\text{g Dans-Cl ml}^{-1}$ of dichloroethane and 0.1 M sodium hydrogencarbonate as carrier stream) the dependence of peak height on time of reaction was studied. The pertinent curves are shown in Fig. 2. After a 23-min reaction time plateau conditions were reached only for β -histine and di-n-butylamine. The rate of reaction in the two-phase system, where the reaction probably proceeds at the organic–aqueous interface, is evidently much slower than that observed in homogeneous systems where dansylation was complete within 2 min for β -histine and in less than 1 h (at room temperature) for the three alkaloids. This agrees with earlier data [14], which showed that at ca. 50°C, maximal reaction times of 10 min were needed for quantitative derivatization of cephaline, emetine and ephedrine. Fortunately, one of the advantages of post-column derivatization is that there is

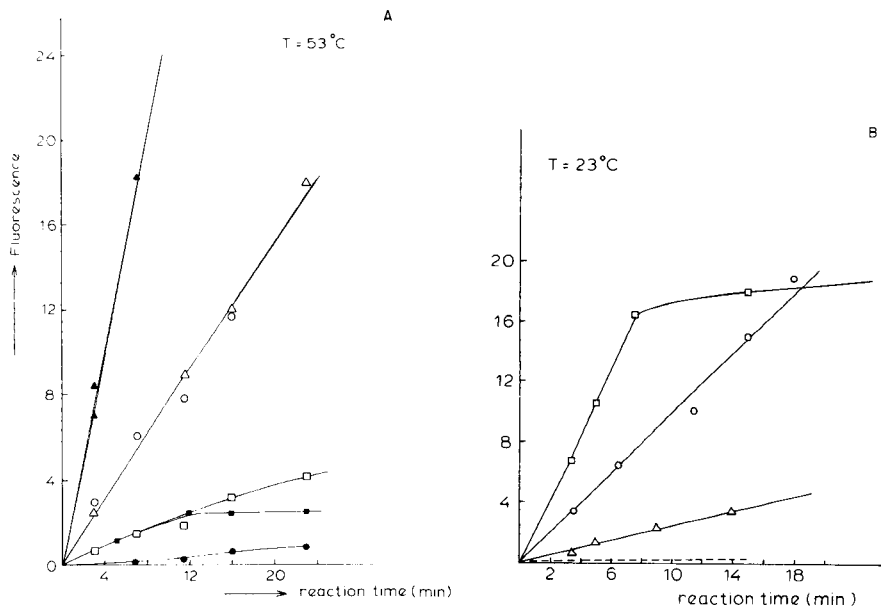


Fig. 2. Dependence of peak height of fluorescence signal on reaction time, at (A) 53°C and (B) 23°C. Equimolar amounts of the various amines were used. The peak heights are in arbitrary units, which are different for the two sets of plots. For A: (▲) fluvoxamine; (○) cephaline; (△) emetine; (□) ephedrine; (■) di-n-butylamine; (●) histamine. For B: (□) β-histidine; (○) clovoxamine; (△) fluvoxamine; (---) emetine.

no need to reach plateau conditions in order to make the technique analytically useful, provided that it is reproducible [15]. The widely diverging slopes of the curves shown in Fig. 2 probably reflect the important role played by structural and other related effects. The differences are not due to highly different extractabilities of the various dansylated amines: in batch experiments, with a solution of Dans-Cl in dichloroethane as extractant, the percentage extraction of all the dansylated compounds tested was between 76 and 99%.

Band-broadening aspects

The ultimate goal of this work is to couple the reaction detector to a h.p.l.c. system. Knowledge of the contribution of the various parts of the post-column system to band broadening is therefore of special interest. Previous work [5, 8, 10] had proved that post-column band broadening is chiefly due to the phase separator and, possibly, the mixing T-tubes. Even with the residence times below 1 min (i.e., where essentially no reaction coils are needed) band broadening, calculated as the standard deviation, (σ_t) was 4–7 s. In the present study, similar results were obtained. It was also observed that relatively minor changes in T-piece and phase-separator design or in the connecting parts caused substantial differences in dead volume and, consequently, band broadening. For example, on decreasing the inner volume of a glass phase

separator by inserting PTFE tubing, thereby effecting a smoother phase separation [10], the total band broadening of the system decreased from 11.1 to 9.4 s; that is the additional broadening arising from the unmodified glass phase separator was 6 s. In another experiment, replacing the glass T-piece by a PTFE version which had a reagent inlet with a somewhat wider internal diameter, caused a reduction of σ_t from 11.6 to 9.3 s; this corresponds to an additional contribution of the PTFE T-piece of about 7 s.

The dependence of band broadening on reaction-coil design (i.e. the length, diameter and construction material of the coils) was studied for relatively long reaction times, such as are required for the dansylation reaction. The results are presented in Table 2. The main conclusion to be drawn from these data is that varying the residence time from 2 to ca. 20 min does not noticeably increase the band broadening, nor does increasing the internal diameter of the capillary tubing from 1 to 2 mm. Further, the results are similar for glass, stainless-steel and PTFE coils. However, the use of PTFE as the construction material is not recommended: a large number of the experiments carried out with PTFE coils failed, probably because of wetting phenomena [10]. In such cases phase separation was rather poor; this had the fatal result that part of the aqueous phase was drawn through the flow-cell of the fluorimeter.

TABLE 2

Dependence of total band broadening on reaction-coil design for the dansylation of fluvoxamine

Coil material	Internal diameter (mm)	Coil diameter (cm)	Residence time (min)	σ_t , total ^a (s)
Glass	2.0	2	2.5	9
			10.5	9
			12	9
			15	9
Stainless steel	1.1	25	2	9
			7	9
			16	9
			23	9
			5	10
PTFE	0.9	0.7	4	13
		12.5	4	9
		12.5	9	9
	1.1	6	4	9
		6	5	9

^aRelative standard deviation was $\pm 5\%$; the flow-rate was 0.8 ml min^{-1} through the detector cell.

Lastly, it is noteworthy that working with tightly wound PTFE coils having a small internal diameter led to an increase in band broadening (cf. Table 2). This is due to secondary mixing effects which cause partial merging of successive organic segments, as could be observed visually.

Analytical aspects. The detection limits for the compounds examined were calculated for a signal to peak-to-peak noise ratio of 3 : 1; the results are shown in Table 1. Calibration graphs were linear over concentration ranges up to 3 orders of magnitude. Regression coefficients for clovoxamine and β -histine were 0.9957 and 0.9997, respectively. The relative standard deviation was $<2\%$ ($n = 6$).

Conclusions

The present study demonstrates the feasibility of the solvent-segmentation approach for chemical reactions with relatively slow kinetics. The solvent segments, besides acting as the reagent carrier and extractant, also effectively suppress band broadening, hence rendering the approach suitable for detection in h.p.l.c. The principle should also be of interest in AutoAnalyzer work where relatively long reactions are involved, since dilution is suppressed and sensitivity will thus be high; also, sample throughput can be increased when no separation is necessary. The large contribution of mixing T-tubes and phase separators to band broadening will necessitate improvement and possible miniaturization of their design. Electronic desegmentation principles might be feasible. The post-column dansylation reaction offers an interesting alternative to pre-column techniques, the major advantage being the absence of artefact formation [16, 17].

Continuous-flow dansylation appears to have a high potential in trace analysis for β -histine, clovoxamine and fluvoxamine.

Thanks are due to Philips-Duphar (Weesp, The Netherlands) for gifts of β -histine, fluvoxamine and clovoxamine.

REFERENCES

- 1 B. Karlberg and S. Thelander, *Anal. Chim. Acta*, 98 (1978) 1.
- 2 J. Růžicka and E. H. Hansen, *Anal. Chim. Acta*, 99 (1978) 37.
- 3 R. W. Frei and A. H. M. T. Scholten, *J. Chromatogr. Sci.*, 17 (1979) 152.
- 4 J. C. Gfeller, G. Frey, J. M. Huen and J. P. Thevenin, *J. High Res. Chromatogr.*, 1 (1978) 213.
- 5 R. W. Frei, J. F. Lawrence, U. A. Th. Brinkman and I. L. Honigberg, *J. High Res. Chromatogr.*, 2 (1979) 11.
- 6 D. Westerlund and K. O. Borg, *Anal. Chim. Acta*, 67 (1973) 89.
- 7 J. C. Gfeller and G. Frey, *Fresenius Z. Anal. Chem.*, 291 (1978) 332.
- 8 J. F. Lawrence, U. A. Th. Brinkman and R. W. Frei, *J. Chromatogr.*, 171 (1979) 73.
- 9 L. R. Snyder and H. J. Adler, *Anal. Chem.*, 48 (1976) 1017, 1022.
- 10 J. F. Lawrence, U. A. Th. Brinkman and R. W. Frei, *J. Chromatogr.*, in press.
- 11 N. Seiler and L. Demisch, in K. Blau and G. Kind (Eds.), *Handbook of Derivatives in Chromatography*, Heyden, London, 1978, p. 349.

- 12 J. F. Lawrence and R. W. Frei, *Chemical Derivatization Techniques in Liquid Chromatography*, Elsevier, Amsterdam, 1976.
- 13 J. F. Lawrence, C. Renault and R. W. Frei, *J. Chromatogr.*, 121 (1976) 343.
- 14 F. Nachtman, H. Spitzzi and R. W. Frei, *Anal. Chim. Acta*, 76 (1975) 57.
- 15 R. W. Frei, L. Michel and W. Santi, *J. Chromatogr.*, 142 (1977) 261.
- 16 R. W. Frei, M. Thomas and I. Frei, *J. Liq. Chromatogr.*, 1 (1978) 443.
- 17 R. W. Frei, *J. Chromatogr.*, 165 (1979) 75.

RAPID DETERMINATION OF CORTICOSTEROIDS IN PHARMACEUTICALS BY FLOW INJECTION ANALYSIS

JOHN B. LANDIS

The Upjohn Company, Kalamazoo, Michigan 49001 (U.S.A.)

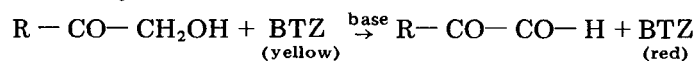
(Received 5th July 1979)

SUMMARY

The proposed method is based on the reduction of blue tetrazolium by the steroid in an alkaline medium to form a highly colored formazan. The effects of reagent concentration, temperature, flow rate, and manifold design on the reaction are discussed for a typical steroid, methylprednisolone acetate. Analytical readout is obtained within 30 s after sample introduction and up to 100 samples/h can be processed with baseline resolution between peaks. Typical relative standard deviations of 0.5% are obtained with 10- μ l injection volumes. Results obtained by flow injection analysis are similar to those obtained with the AutoAnalyzer technique.

Corticosteroids are an important class of compounds widely used therapeutically for their anti-inflammatory action. They are administered as suspensions, creams, ointments, tablets, solutions, and suppositories. Numerous methods have been described for their determination in pharmaceutical preparations, including ultraviolet [1], colorimetric [2], fluorimetric [3], h.p.l.c. [4], and polarography [5]. Colorimetric methods are widely used by the pharmaceutical industry for the determination of the content uniformity of corticosteroid products because they are rapid and can be readily automated by AutoAnalyzer technology. The most widely used colorimetric reaction is the blue tetrazolium (BTZ) reaction. The USP XIX [6] and NF XIV [7] contain slight modifications of the original procedure of Mader and Buck [8] and almost all major pharmacopoeias contain some version of this method.

Blue tetrazolium [3,3'-(3,3'-dimethoxy-4,4'-biphenylene)bis(2,5-diphenyl-2H-tetrazolium chloride)] quantitatively oxidizes the α -keto moiety of the C-17 side-chain of corticosteroids in strongly alkaline solution to form a 20-hydroxy-21-aldehyde carboxylic acid derivative of the steroid and a highly colored formazan whose concentration is measured spectrophotometrically at 525 nm



where R is the steroid backbone. The reaction has been studied extensively, both kinetically and mechanistically [9–14]. The reaction is not specific for the corticosteroid side-chain. Numerous non-steroidal reducing agents as

well as Δ^4 -3-ketones also give the reaction, which is therefore suitable only for applications where the matrix is well controlled and when reducing agents other than the steroid of interest are absent.

Recently, numerous papers have described the application of flow injection analysis (f.i.a.) for the automation of wet chemistry procedures [15–17]. The reported f.i.a. features which make it attractive for pharmaceutical analysis are the short start-up time, simplicity of instrumentation, the high sample throughput, and rapid manifold changeover, making it well suited to batch-type analysis where a few to hundreds of samples are to be analysed. The purpose of this investigation was to explore the feasibility of applying the f.i.a. technique to the determination of corticosteroids in pharmaceutical preparations. The effect of reagent concentration, temperature, flow rate, and manifold design was studied for a typical corticosteroid, methylprednisolone acetate. The procedure was also extended to 12 additional steroids.

EXPERIMENTAL

Reagents and samples

All chemicals and solvents were of analytical-reagent grade when available.

Blue tetrazolium reagent (BTZ). A stock solution (10 g l^{-1}) of blue tetrazolium (Dajac Laboratories) was prepared by dissolving the compound in 95% ethanol. Working solutions were prepared by suitable dilution. The stock solution is stable for at least 6 months.

Tetramethylammonium hydroxide reagent (TMAH). A stock solution containing 5% (w/v) TMAH was prepared by diluting an aqueous 10% (w/v) stock (MCB) with 95% ethanol. Working solutions were prepared by suitable dilution. The solution was stable for at least 6 months.

Steroid standards and samples

The steroids used were: methylprednisolone acetate, methylprednisolone, hydrocortisone acetate, hydrocortisone, prednisolone acetate, prednisolone, cortisone acetate, cortisone, prednisone acetate, prednisone, 9- α -fluorocortisone acetate, isofluoropredone acetate, and desoxycorticosterone acetate (Upjohn, Kalamazoo, Michigan). Stock solutions of steroid (1 mg ml^{-1}) were prepared by dissolving the compound in 95% ethanol. Working standards were prepared weekly by suitable dilution.

Steroid suspension samples. These samples were prepared by shaking the sample to obtain a uniform suspension, sampling, diluting with 95% ethanol to obtain a final concentration of 0.2 mg ml^{-1} or 0.32 mg ml^{-1} , and shaking to dissolve.

Apparatus

A diagram of the flow injection system is shown in Fig. 1. It consisted of an eight-channel peristaltic pump (Gilson, Minipuls II), a Valco six-port rotary injection valve fitted with a $10\text{-}\mu\text{l}$ or $25\text{-}\mu\text{l}$ sample loop (Valco

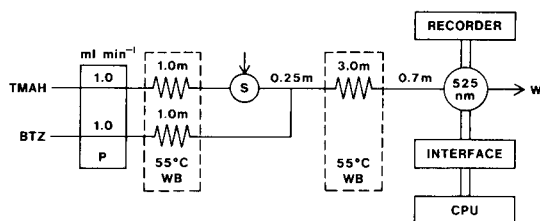


Fig. 1. Manifold for the determination of corticosteroids with blue tetrazolium: (P) eight-channel peristaltic pump; (WB) water bath; (S) sample injection valve; (W) waste. All manifold tubing was 1.5/0.5 o.d./i.d. teflon tubing.

Instrument Company, Model 9080), a Schoeffel variable-wavelength h.p.l.c. detector with a 10-mm pathlength 8- μ l volume cell (Model SF-770), a Sargent-Welch recorder, and a Lauda water bath (Model K-2/R).

All manifolds were made from thick-walled teflon tubing (1.5 mm o.d./0.5 mm i.d.; Durrum Flarefit). Pump manifold tubing was Auto-Analyzer Solvaflex (0.030 in. i.d.; Technicon 116-0533P07). Teflon tubing connections were made with polypropylene gland nuts and couplings (Durrum).

Peak heights were manually collected from the strip-chart recorder or collected and processed automatically with a PDP 11/40 computer and a series of programs developed in-house for collecting and processing h.p.l.c. data [18].

In all experiments, samples and standards were injected in duplicate or triplicate.

For some experiments, a commercial f.i.a. unit was used (Bifok, FIA-05). The instrument consists of a two-channel rotary valve with a high-resistance bypass so that flow is never interrupted during the filling and injection cycles [19], a water bath, and perspex blocks for constructing manifolds.

RESULTS AND DISCUSSION

Manifold design

Except where otherwise specified, the parameters used in the experiments described below were as follows: [TMAH] 1% (w/v), [BTZ] 1 g l⁻¹, flow rate (TMAH, BTZ) 1.0 ml min⁻¹, temperature 55°C, reaction coil tube length 3.75 m, pump speed 600. These were the parameters finally selected for use with the f.i.a. manifold shown in Fig. 1.

Several manifolds were tested before the configuration shown in Fig. 1 was achieved. In one design, the TMAH and BTZ streams were mixed prior to sample introduction. The sample was injected into this stream and then entered the reaction coil. In the second design, the manifold was identical to Fig. 1 except that the sample was injected into the BTZ stream. These two designs resulted in small negative peaks preceding the analytical peak. This phenomenon is caused by a refractive index change resulting from injecting

the sample into a colored stream (BTZ) which absorbs significantly at the wavelength being monitored [20]. These negative peaks were eliminated when the sample was injected into the colorless TMAH stream and then mixed with the BTZ stream. The temperature equilibration coils for the reagent were added to bring the reagents to the reaction temperature and to act as pulse dampeners to reduce fluctuations in the baseline caused by pumping.

Reaction coil length. The dependence of the peak absorbance on the reaction coil length for three concentrations of methylprednisolone acetate is given in Fig. 2. The reaction coil is defined as the total length of tubing from the point of sample introduction to the detector. In all cases, only a portion of the coil was placed in the water bath. The remainder of the tubing was required to make connections. The reaction coil length was varied between 1.5 to 4.75 m with 0.95 m used for connections and the remainder placed in the water bath in a coil of approximately 2-cm diameter. Examination of Fig. 2 shows that the peak absorbance increased with reaction coil length up to an optimum at 3.75 m and then decreased. The rise in absorbance is due to the increased extent of reaction caused by a longer residence time of the sample in the reaction coil and by the increased residence time of the sample in the temperature bath which increases the reaction rate. At the shorter reaction coil lengths, increased sample throughput resulted but small negative peaks occurred because of incomplete mixing of the sample and reagent streams. At lengths greater than 2.0 m this was

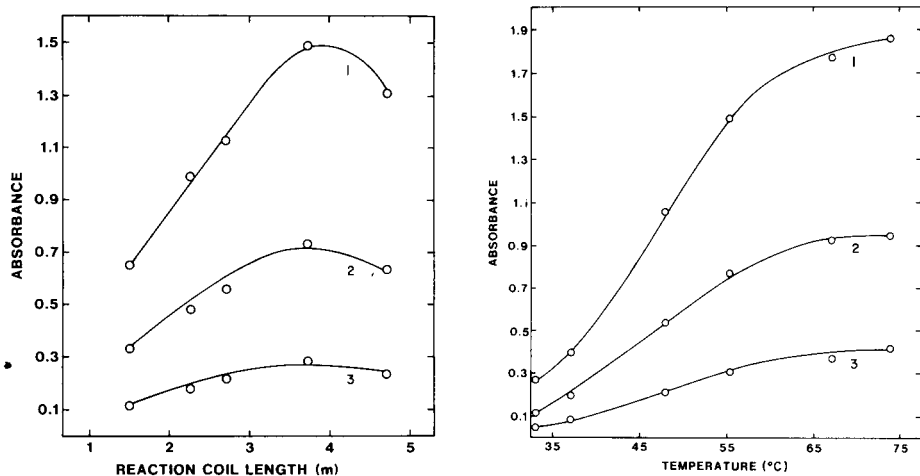


Fig. 2. Influence of the reaction coil length for three concentrations of methylprednisolone acetate on the peak absorbance. Steroid concentration: (1) 0.365 mg ml^{-1} ; (2) 0.183 mg ml^{-1} ; (3) 0.073 mg ml^{-1} .

Fig. 3. Influence of temperature for three concentrations of methylprednisolone acetate on the peak absorbance. Curves 1–3 relate to the concentrations given in Fig. 2.

no longer observed. The decrease in sensitivity at lengths greater than 3.75 m is caused by the increased dispersion of the sample in the reaction coil which dilutes the sample. Therefore, an optimum reaction coil length is reached when reaction-rate considerations are balanced against dispersion of the sample in the carrier.

BTZ concentration. The influence of the blue tetrazolium concentration on the peak absorbance was studied for the three concentrations of methylprednisilone acetate previously mentioned. Increasing the BTZ concentration from 1 to 3 mg ml⁻¹ resulted in a slight increase in sensitivity, but further increases up to 8 mg ml⁻¹ did not improve the sensitivity. However, as the BTZ concentration increased, the background absorbance of the carrier stream increased at 525 nm and slight negative peaks preceded the analytical peak at the higher BTZ concentration because of the refractive index effect discussed earlier. At the highest BTZ concentration tested, baseline noise increased, owing to the generation of schlieren patterns.

TMAH concentration. The dependence of the absorbance on the TMAH concentration in the range 0.1–3% (w/v) was then examined for the same three concentrations of methylprednisilone acetate. Increasing the TMAH concentration from 0.1% to 1.0% resulted in a dramatic increase in sensitivity which began to level off at TMAH concentrations greater than 1%. The marked dependence of the reaction on the alkali concentration is due to two factors. First, increasing the TMAH concentration increases the rate of ester hydrolysis to give the free alcohol. Secondly, as the alkali concentration increases, the 20-hydroxy group ionizes to give the highly reactive enolate species.

Temperature. The influence of temperature in the range 25–75°C on the peak absorbances is shown in Fig. 3. It was not possible to extend measurements above 75°C since the boiling point of the carrier was being approached and bubbles rapidly evolved. As can be seen, the sensitivity rapidly increased between 25 and 70°C and then leveled off. Clearly, the reaction is far from equilibrium below 75°C, but this is not critical, as long as the carrier flow is maintained constant. Micro-bubble evolution caused noisy baselines at temperatures above 65°C.

Flow rates. The effect of the flow rates of the BTZ and TMAH streams on the peak absorbance is shown in Fig. 4. As the flow rate increased, there was a slight decrease in the peak absorbance, which was caused by the corresponding decrease in the residence time of the sample in the reaction coil so that equilibrium was not achieved. At the lower pump speeds the baseline noise increased owing to pulsations in the stream. At higher pump speeds the pulsations tend to average out, giving a smoother baseline. Therefore, within certain limits, it is easier to vary residence time, i.e. the extent of reaction, not by changing the reaction coil length but by simply varying the flow rate.

Parameter selection. Consideration of all these features led to the choice of parameters listed at the start of this section. The BTZ and TMAH concentrations were chosen to optimize sensitivity and to minimize baseline noise.

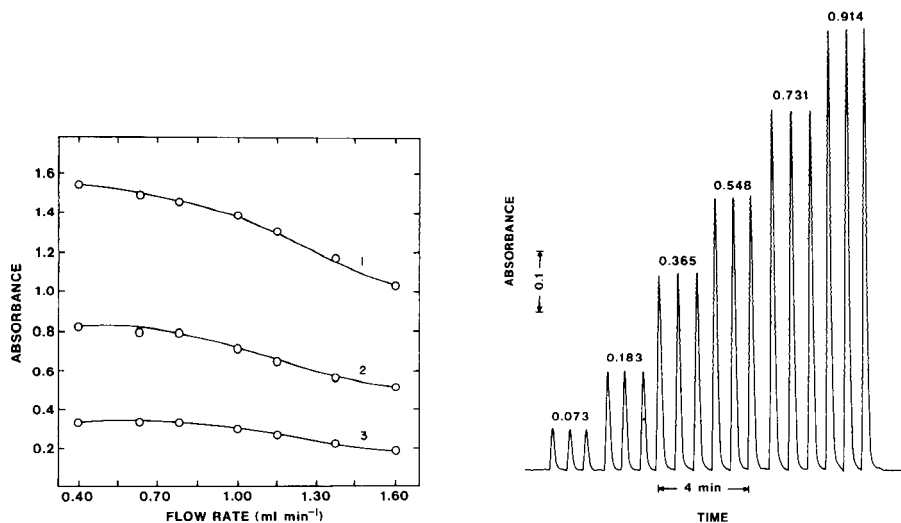


Fig. 4. Influence of flow rate for three concentrations of methylprednisolone acetate on the peak absorbance. Curves 1–3 relate to the concentrations given in Fig. 2.

Fig. 5. Recorder tracing for a series of standard methylprednisolone acetate solution run in triplicate (0.073–0.914 mg ml⁻¹).

The flow rate and the pump speed were chosen to give a sampling rate of 90 samples/h with baseline resolution between samples. The reaction coil length was chosen to optimize sensitivity and reduce baseline noise. The reaction temperature was selected to minimize baseline noise and give absorbances between 0.2 and 0.6 for the suspension samples. Under these conditions, it was possible to assay the steroid suspensions after one dilution and obtain absorbance values which minimized photometric error. The final concentration of steroids assayed in this manner was approximately 0.2 mg ml⁻¹. If greater sensitivity is needed, a higher reaction temperature should be used. If a higher sample throughput is desired, the flow rate speed can be increased to 1.4 ml min⁻¹ resulting in sampling rate of 120/h.

Applications

Figure 5 shows the recorder tracing for a series of methylprednisolone acetate standards run in triplicate at 90 samples/h. The corresponding Beer's law plot was linear over this range with an insignificant intercept and a 0.9992 correlation coefficient. The peak shape was gaussian with a total residence time of 32 s; peak width at 60% peak height was 9 s, which is a measure of the total sample dispersion in the system [22]. The peak width at baseline was 35 s which defines the maximum sampling rate if <0.1% carryover is expected. In this case, the maximum sampling rate was 100 samples/h.

Figure 6 shows a typical recorder tracing for a series of methylprednisolone acetate suspensions (40 mg ml⁻¹). All standards and samples were run in duplicate. Two standards were run after every five samples.

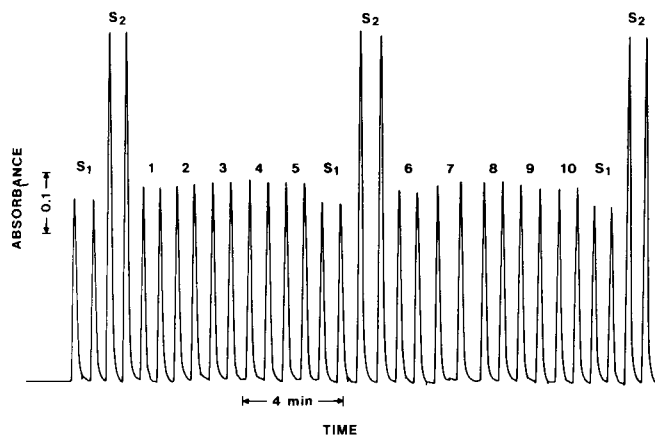


Fig. 6. Typical f.i.a. results of methylprednisolone acetate suspension sample run in duplicate. Standard solutions: S1, 0.183 mg ml^{-1} ; S2, 0.365 mg ml^{-1} . Sample rate is approximately 90 samples/h.

The relative standard deviation for the standards after several hours of running was usually less than 0.5%. Results of the f.i.a. procedure were compared with the AutoAnalyzer procedure [23] for 20, 40, and 80 mg ml^{-1} suspensions of methylprednisolone acetate. One hundred samples were assayed in duplicate by both procedures. The same sample preparation was used for both methods, with the exception of one more dilution required for the AutoAnalyzer procedure, to minimize errors from sample preparation. Table 1 lists the results for 15 randomly selected samples. The overall means of the two procedures differed by 0.5% which was within the RSD of the assay. There was excellent agreement between the procedures and no evidence of positive or negative bias.

Other steroids

This procedure can be applied to a variety of other steroids with no change in the manifold or parameters. Table 2 gives a list of steroids assayed by f.i.a. All absorbances were recorded for 0.2 mg ml^{-1} solutions of the steroid and all are relative to methylprednisolone acetate. In all cases, the sensitivity was greater for the parent steroid than for the ester. This indicates the rate of ester hydrolysis is significant with respect to the rate of blue tetrazolium reduction in the f.i.a. system so that optimization of the system must take this into account.

Conclusions

Corticosteroids can be successfully assayed by the BTZ reaction with f.i.a. The most important characteristics of f.i.a. for this study were the instrumental simplicity and the rapid instrument "start-up" time. This made it ideally suitable for running a few or hundreds of samples in a batch

TABLE 1

Comparison of procedures for the determination of methylprednisolone acetate in a suspension formulation
(All values are given in mg ml⁻¹.)

Sample No.	Flow injection method	AutoAnalyzer method	Theory	Sample No.	Flow injection method	AutoAnalyzer method	Theory
1	20.0	19.9	20	9	40.9	40.6	40
2	19.6	20.2	20	10	40.2	40.3	40
3	19.9	20.3	20	11	80.9	80.7	80
4	20.2	20.7	20	12	80.1	80.7	80
5	19.5	19.9	20	13	80.0	81.1	80
6	39.9	41.0	40	14	81.0	80.6	80
7	40.1	40.7	40	15	80.0	80.6	80
8	40.9	40.7	40				

TABLE 2

Relative absorbance values for some corticosteroids (0.2 mg ml⁻¹) reacted with blue tetrazolium

Steroid	Absorbance ^a	Relative absorbance ^a	Steroid	Absorbance ^a	Relative absorbance ^a
Methylprednisolone acetate	0.345	1.00	Cortisone acetate	0.436	126 ^b
Methylprednisolone	0.431	1.25	Cortisone	0.510	1.36
Hydrocortisone acetate	0.370	1.07	Prednisone acetate	0.447	1.20
Hydrocortisone	0.382	1.11	Prednisone	0.512	1.49
Prednisolone acetate	0.392	1.14	9- α -Fluorocortisone acetate	0.389	1.04
Prednisolone	0.450	1.33	Isofluroropredone acetate	0.393	1.14
			Desoxycorticosterone acetate	0.448	1.20

^aAll values are relative to methylprednisolone acetate.

mode. The instrument was ready for analyses 5–10 min after it had been switched on. This warm-up time was necessary to establish a constant flow which is essential in all f.i.a. applications. Baseline integrity is maintained between samples and existing software developed for h.p.l.c. can be used with minor modification to collect and process the data.

Of secondary importance was the high sampling rate. The data obtained by f.i.a. at a sampling rate twice that with the AutoAnalyzer were similar to those obtained with the AutoAnalyzer.

The author expresses his gratitude to Dr. Bo Karlberg (Astra Pharmaceuticals, Södertälje, Sweden) for performing the initial experiments and advice in setting up an f.i.a. system, and to Rune Lundin (Bifok, Sollentuna, Sweden) for providing the commercial instrument used for some experiments.

REFERENCES

- 1 R. E. Graham, P. A. Williams and C. T. Kenner, *J. Pharm. Sci.*, 59 (1970) 1152.
- 2 R. E. Graham, P. A. Williams and C. T. Kenner, *J. Pharm. Sci.*, 59 (1970) 1472.
- 3 C. E. White and A. Weissler, *Anal. Chem.*, 44 (1972) 182R.
- 4 N. W. Tymes, *J. Chromatogr. Sci.*, 16 (1977) 151.
- 5 H. S. DeBoer, J. Hartigh, H. H. Ploegmakers and W. J. VanOort, *Anal. Chim. Acta*, 102 (1978) 141.
- 6 The United States Pharmacopoeia, 19th edn., Mack Publishing, Easton, PA, 1975, 622.
- 7 The National Formulary, 14th edn., Mack Publishing, Easton, PA, 1975, 976 pp.
- 8 W. J. Mader and R. R. Buck, *Anal. Chem.*, 24 (1952) 666.
- 9 S. Görög and P. Horvath, *Analyst*, 103 (1978) 346.
- 10 R. Oteiza, R. Wooten, C. Kenner, R. Graham and E. Biehl, *J. Pharm. Sci.*, 66 (1977) 1385.
- 11 R. Graham, E. Biehl and C. Kenner, *J. Pharm. Sci.*, 67 (1978) 792.
- 12 R. Graham, E. Biehl, C. Kenner, G. Luttrell and D. Middleton, *J. Pharm. Sci.*, 64 (1975) 226.
- 13 S. Görög and P. Horvath, *Analyst*, 103 (1978) 346.
- 14 R. Graham, E. Biehl and T. Kenner, *J. Pharm. Sci.*, 65 (1976) 1048.
- 15 D. Betteridge, *Anal. Chem.*, 50 (1978) 832A.
- 16 F. J. Krug, J. Růžicka and E. Hansen, *Anal. Chim. Acta*, 104 (1979) 47.
- 17 H. Baadenhuijsen and H. E. H. Seuren-Jacobs, *Clin. Chem.*, 25 (1979) 443.
- 18 L. E. Fox, R. A. Johnson and N. D. Young, *Ind. R/D*, (Aug. 1978).
- 19 H. Bergamin F^o, E. A. G. Zagatto, F. J. Krug and B. F. Reis, *Anal. Chim. Acta*, 101 (1978) 17.
- 20 H. Bergamin F^o, B. F. Reis and E. A. G. Zagatto, *Anal. Chim. Acta*, 97 (1978) 427.
- 21 D. E. Guttman, *J. Pharm. Sci.*, 55 (1966) 919.
- 22 J. Růžicka and E. H. Hansen, *Anal. Chim. Acta*, 99 (1978) 37.
- 23 W. F. Beyer, *Automation in Analytical Chemistry*, Technicon Symposium (1965) 7.

A NEW APPROACH TO ENZYMATIC ASSAY BASED ON FLOW-INJECTION SPECTROPHOTOMETRY WITH ACID–BASE INDICATORS

A. RAMSING, J. RŮŽIČKA* and E. H. HANSEN

Chemistry Department A, Technical University of Denmark, Building 207, DK-2800 Lyngby (Denmark)

(Received 18th July 1979)

SUMMARY

The design of a mixed indicator–buffer system which yields a linear change of absorbance versus pH over a wide pH range is described. Its use for enzymatic analysis in continuous and stopped flow f.i.a. systems is demonstrated for the determination of urea via degradation by urease. A microcomputer (PET) was connected to the f.i.a. systems, and the programs used for retrieving peak-height values and computing buffering capacities are described.

The glass electrode is often viewed as a well-nigh universal detector [1–3] because there are so many analytical reactions which, as a result of proton exchange, cause a pH change in the reaction medium. The most notable examples of this approach are the gas-sensing electrodes for CO₂, NH₃ and SO₂ measurements in which a glass electrode senses the pH change in a thin layer of an electrolyte, separated from the sample solution by a gas-permeable membrane. Equally elegant, but less practical, are enzyme electrodes [4] where the glass electrode is used to sense a pH change in a thin layer of an electrolyte gel containing an enzyme capable of catalyzing a reaction which involves proton exchange. Many other reactions involving proton exchange are available such as the now historical way of utilizing compleximetric titrations [5], before metallochromic indicators were introduced. Yet, the common denominator of the above-mentioned systems, i.e., selectivity based on gas diffusion or enzyme catalysis, must be kept in mind as otherwise any measurement based on proton exchange would be prone to many interferences.

Enzymatic reactions are very selective and frequently involve direct proton exchange

SUBSTRATE $\xrightarrow{\text{enzyme}}$ PRODUCT + PROTON

and this is why pH measurement with a glass electrode has been so frequently used for their monitoring [1–3, 6]. This potentiometric pH measurement has, however, a number of distinctive drawbacks. The glass electrode, having a dynamic response range well over 10 decades of proton activities, yields,

according to the Nernst law, a 59-mV change of potential per decade or an 18-mV change when the analyte concentration is doubled. Because of this logarithmic response, the range of clinically significant substrate concentrations, as converted enzymatically and measured via one proton exchange reaction, would maximally be reflected by a change of up to 40 mV, and a reproducibility of ± 1 mV would correspond to an error of $\pm 4\%$.

To avoid the difficulties connected with the logarithmic response of the glass electrode, the concept of constant buffering capacity has been applied either by (a) keeping the pH constant and measuring the amount of acid (or base) used in the course of a measurement [7] or (b) keeping the buffering capacity (β) constant and measuring the pH change which thus becomes a linear function of the amount of protons consumed or released [3, 6]. The first approach is awkward and time-consuming, whereas the second method relies on a high reproducibility of the electrode measurements in a rather narrow potential range.

Last, but not least, a significant drawback of electrode measurements arises from the fact that the ion to be sensed has to reach the ion-sensitive surface of the electrode and therefore the speed of the electrode response depends on the intensity of mixing of the measured solution. In contrast to this, spectrophotometric measurements yield instant response to the changes within the bulk of the solution through which the light beam passes, while the diffusion layers situated at the walls of the vessel (where the change of composition occurs last) yield a negligible contribution to the overall signal.

The above reasons, of which the last was the decisive one because the slowness of response actually hinders a fast enzymatic rate measurement, led to the concept of using acid-base indicators for monitoring of proton-exchange reactions in f.i.a. systems. There are two ways in which an enzymatic f.i.a. analysis can be performed: by continuous flow or by stopped flow measurement (Fig. 1). The continuous flow measurement is simpler as it is based on injecting a sample into a continuously moving carrier stream of reagent (enzyme + buffer + indicator), which, after passing through a suitable length of a coil (a), is measured spectrophotometrically and recorded in the form of a peak, the height of which (h or A) is proportional to the sample concentration. The residence time of the sample zone (T) in the f.i.a. system depends on the pumping rate and coil length (a) and is chosen to yield an easily measurable peak height. The drawback of this approach is that the determination is affected by a variable blank which will arise if varying amounts of an interfering buffer are present in samples and standards (unless two separate injections are made of each sample, one in the presence and one in the absence of enzyme [3]).

The stopped flow approach avoids this interference by measuring the increase of absorbance (Δh or ΔA) caused by the enzymatic reaction during the interval Δt that the sample zone is retained within the cell for monitoring. Thus any colour present (or formed) prior to entering the flow cell can be disregarded. (Obviously, to keep h small in relation to Δh , and T in relation to Δt , coil a must be kept as short as possible.)

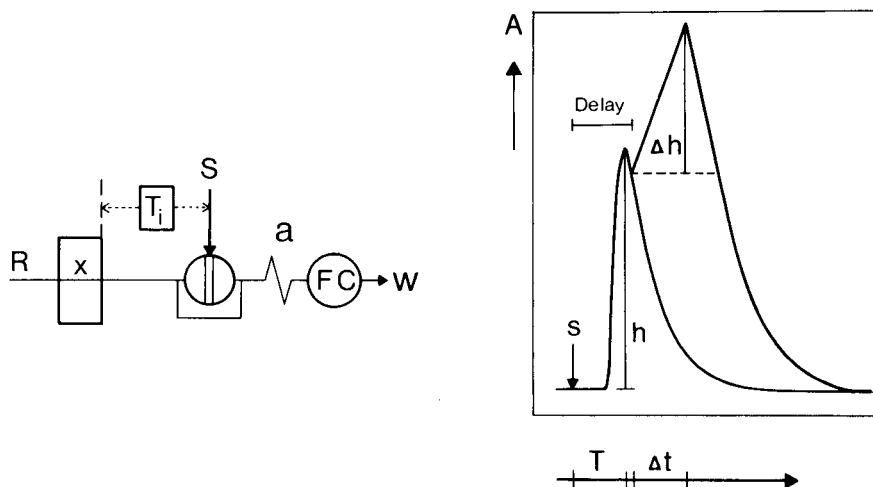


Fig. 1. Simple f.i.a. system for spectrophotometric continuous and stopped flow analysis and corresponding response curves, shown as absorbance (A) vs. time. In the continuous flow mode, the timer (T_i) is not active and the colour formed within the injected sample zone, after passage through coil a , is measured in a flow-through cell (FC) and recorded as a peak (of height h). In the stopped flow mode the timer, after a delay time (T), stops the zone in the flow cell from which, after a stop period Δt , the zone is flushed into waste (W).

THEORY

As mentioned above, a linear response can be obtained by keeping the buffering capacity β of the system constant: $\beta = dC_B/dpH$. The observed pH change will then become a linear function of the amount of protons consumed or produced by the monitored reaction: $dpH = dC_B/\beta$.

By using an acid–base indicator HIn for which

$$pH = pK_{In} + \log [In^-]/[HIn] \quad (1)$$

the linear change of pH can be converted to a linear change of absorbance A , provided that dpH lies within a range ± 0.5 pH of pK_{In} . In such a case, $dpH = k_1[In^-]$, and if the indicator and its concentration are properly chosen so that the Lambert–Beer law applies, then $dpH = k_1 k_2 A$, i.e.

$$A = dC_B/k \beta, \quad (2)$$

where k comprises the “indicator constants” k_1 and k_2 and β is the buffering capacity of the predominant buffer(s) in the system.

For an enzymatic reaction the Michaelis–Menten equation applies:

$$dP/dt = V_m S/(K_m + S) \quad (3)$$

where P is the product concentration, t is the reaction time, K_m is the Michaelis constant and S is the substrate concentration, while V_m is the maximum

velocity of the catalyzed reaction. When an excess of enzyme is used ($K_m \gg S$) and dP is related to dC_B ($dP = (1/q)dC_B$), eqns. (2) and (3) yield

$$A = (S \, dt \, V_m / \beta K_m) (q/k) \quad (4)$$

where dt is the residence time T of the sample plug in a continuous flow system (or Δt in a stopped flow system), while q and k involve indicator and stoichiometric constants.

Equation (4) predicts a linear relationship between absorbance and substrate concentration(s) provided that the constancy of β and k is maintained. Theoretically, k and β could involve properties of one and the same compound if an acid-base indicator of sufficiently high buffering capacity were available. In practice, however, the buffering capacity of an indicator has to be supplemented by a colourless buffer with a pK value as close as possible to pK_{In} . Furthermore, if linearity over a wider range than about one pH unit is required, a mixture of several buffers and indicators must be prepared. Yet another reason why several buffer and indicator systems should be studied is that this knowledge would make it possible to choose a suitable indicator-buffer pair, the pK/pK_{In} value of which would be situated at that pH value where the enzyme used has its maximum catalytic activity and where the influence of any interfering buffer system(s) (see below) is minimal. Equally important is the flexibility with which the buffering capacity can be adjusted. While low values of the carrier stream buffer allow higher sensitivity of measurement (see eqn. 4), higher values assist in suppressing the influence of interfering buffers.

EXPERIMENTAL

Apparatus

The flow-injection systems used were essentially the same as those described previously [3, 8]. Reagents and buffers were pumped by a four-channel peristaltic pump, Ismatec Model Mini-S-840. The spectrophotometer, Corning Model 256, was furnished with a Hellma flow cell (type OS 178.12, 10-mm optical path, 18- μ l volume). The coils and the injection valve (30 μ l) were assembled from the modular block system described previously [9]. Coils as well as flow cell were thermostated by means of a Heto circulation bath (type 01 T 623 K). The recorder used in this work was an $xy-yt$ recorder (Brüel & Kjær type 2308).

The pH measurements were done with a digital pH meter (Radiometer, PHM 64 Research pH meter), a saturated calomel reference electrode (Radiometer K 401), a pH glass electrode (Radiometer G 202 B) and a magnetic stirrer (Cenco, No. 34532). To establish the wavelengths of maximum absorbance of the indicators in the blue region, spectra were recorded with a Beckman DB-GT spectrophotometer.

Determination of pK values of the indicators

For the determination of the pK values of the indicators, a pH meter was used in connection with an autoburette (Radiometer, ABU 12) and a scanning titrator (home-made), which generated a linear pH gradient as a function of time (5 min/pH) in the gradient vessel (G) by adding 0.1 M HCl (NaOH) from the autoburette (Fig. 2). The gradient vessel was filled initially with 2.5 ml of indicator stock solution and 250 ml of 0.14 M NaCl, whereupon the pH in the mixture was adjusted to approximately 2 pH units higher (lower) than the expected pK value. From the gradient vessel the solution was pumped at 10.7 ml min^{-1} through the flow cell in the spectrophotometer (where the colour of the indicator was measured at the wavelength of maximum absorbance) and then returned to the gradient vessel, so that the volume of circulating liquid was kept constant. As the pH gradient changed linearly with time, it was easy to correct for the pH difference between the vessel and the flow cell caused by the time delay between these two containers. The pH measured by the glass electrode and the absorbance measured by the spectrophotometer were simultaneously fed to the x - y recorder as shown in Fig. 2.

Determination of the buffering capacity (β) and the pK values for the buffers

The arrangement shown in Fig. 3 was used for simultaneous determination of the pK values and the buffering capacity of the buffers. The acidity of each buffer was adjusted to approximately 2 pH units higher than the expected pK value and then titrated with 0.5 M HCl in vessel G by constant addition of titrant (i.e., dC_B constant). The pH change was monitored on the y - t recorder as a function of time (and therefore as a function of dC_B). Simultaneously, the signal from the pH meter was fed into a microcomputer (Commodore PET 2001 series — 16 N Professional Computer) through an interface (Hewlett-

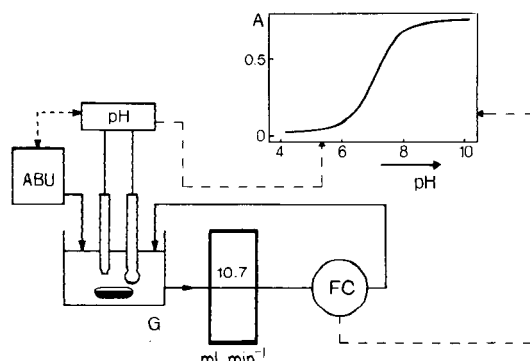


Fig. 2. Automated system for measuring the transition regions of acid-base indicators. A spectrophotometric flow cell (FC, volume $18 \mu\text{l}$) monitors absorbance in a closed loop through which a stream is pumped at a rate of 10.7 ml min^{-1} . The pH in the gradient vessel (G) is changed at a fixed rate by means of an autoburette (ABU) controlled by a pH-stat. The change in colour of the indicator in the circulating solution is recorded by an x - y recorder.

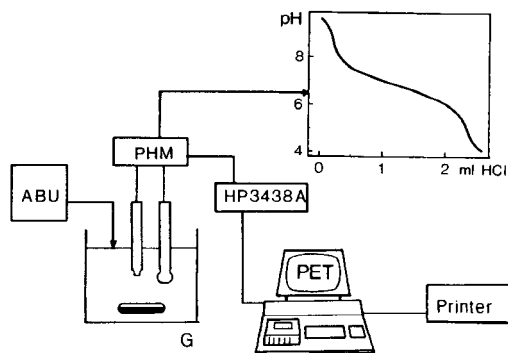


Fig. 3. Automated system for measuring pK values and buffering capacities where the test compounds are titrated by means of an autoburette (ABU) run at constant speed. The resulting change of pH is recorded, and also fed into a computer (PET) via an interface (HP 3438 A), for computing of buffering capacities (Table 1).

Packard digital multimeter HP 3438 A, $3\frac{1}{2}$ digit), at regular time intervals, so that dpH was monitored. As dC_B was kept constant with time and dpH was measured at a fixed frequency, β values could be calculated with the algorithm shown in Table 1. After the measurement cycle was completed, the data and the calculated β values as a function of pH were printed out (Commodore Tractor Printer 3022 series).

Reagents

Carrier buffer solution. This contained 1×10^{-3} M TRIS (tris-(hydroxymethyl)aminomethane) and 10^{-3} M phosphate buffer in 0.14 M NaCl and was adjusted to pH 6.8–7.0 at 32°C in experiments where no sodium hydrogencarbonate was present in the samples (carrier buffer A). When sodium hydrogencarbonate was present in the standards (20 mmol l^{-1}), the solution contained 1×10^{-3} M TRIS and 5×10^{-4} M phosphate buffer in 0.14 M NaCl and the pH was again adjusted to 6.8–7.0 at 32°C (carrier buffer B).

Mixed indicator solution. This contained 0.02% cresol red, 0.04% bromothymol blue and 0.08% bromocresol purple (all w/v) in 0.14 M NaCl. The indicators were dissolved in 7 ml of 0.1 M NaOH and the solution was diluted to a final volume of 250 ml which was 0.14 M in NaCl; 2-ml portions of this solution were added to 98 ml of carrier buffer solutions A and B, respectively.

Urea standards. Reagent-grade urea (Merck) was dissolved in 0.14 M NaCl to obtain a 100 mmol l^{-1} stock solution. This was diluted to obtain standards in the range 1 – 10 mmol l^{-1} . With special reference to the possible analysis of serum samples, a series of urea standard solutions containing sodium hydrogencarbonate (20 mmol l^{-1}) was also prepared.

Prior to injection, the standards were diluted 1 + 1 (continuous flow) and 1 + 3 (stopped flow) with carrier solution. To the 2% indicator-containing carrier solution used for dilution of the standards was also added 2% (for the

continuous flow method) or 0.66% (for the stopped flow method) of the mixed indicator solution. This was done to compensate for the decrease in the absorbance which would otherwise arise when the colourless standards were mixed with the coloured carrier solution.

Urease. Urease (114 units mg^{-1} ; Worthington Biochemical Corporation, New Jersey) was dissolved in the carrier solution in an amount of 30 mg per 100 ml (continuous flow) or 80 mg per 100 ml (stopped flow).

All solutions were made in 0.14 M NaCl to keep the ionic strength constant and distilled water was used throughout. All chemicals were of analytical-reagent grade.

Microcomputer

The computer used (Commodore PET 2001 Model 16 N) is an all-purpose cheap hobby computer with moderately priced accessories: a printer (Commodore Tractor Printer Model 3022) and a floppy disk (Commodore CBM Model 2040 Dual Drive Floppy Disk). As it uses BASIC, it is easy to program. One of the reasons for using this instrument, rather than other possibilities (e.g. Apple) was that it can be attached, by means of a standard connector via a low-priced HP analog/digital interface, directly to the analog output of a spectrophotometer or a pH meter.

The programs are self-explanatory (with a little knowledge of BASIC). Another program, based on the algorithm given in Table 2, is used to capture the data and display peak heights. It is interesting to note that the standard deviations of the digital peak-height values as read out by the PET are smaller than the standard deviations of the peak-height values recorded by the x - y recorder. This happens because the microcomputer is measuring point by point while the recorder may also register occasional high-frequency noise.

INDICATOR AND BUFFER SYSTEMS

Indicator systems

Though a single indicator can well be used, a mixture of several indicators gives a choice of measurement conditions. In order to obtain an indicator mixture with a linear response of A vs. pH (constancy of k , eqn. 2) the following two conditions must be fulfilled: (a) there should be maximally 1 pH unit difference between the $\text{p}K_{\text{in}}$ values of the individual indicators; and (b) their protolytic forms, preferably the basic ones, should have molar absorptivities as close as possible at approximately the same wavelength. In addition, the indicators should be water-soluble and should preferably have a blue basic form so as to make them easily distinguishable from the yellow or red background of biological fluids.

Following the guidelines of tabulated data [10], a number of indicators was considered, yet the final choice was made from pH-absorbance scans by the procedure (Fig. 2) described above. The mixed indicator solution finally selected, containing 0.02% cresol red, 0.04% bromothymol blue and 0.08%

TABLE 2

The peak height algorithm used when the PET is interfaced via the multimeter to the analog output (recorder output) of the measuring instrument. By comparing (lines 600—1200) the point-by-point measured data (lines 8000—8200), the algorithm stores (lines 1300—1400) the maximum value for each peak (for possible statistical treatment). When the peak height has decreased to a given percentage of the recorder full scale (lines 50, 51, 2100—2200), the next sample can be injected. The algorithm has a peak detection limit to avoid baseline noise being detected as peaks; this limit is chosen as a percentage of the recorder full scale (lines 30, 40)

```

1 PRINT"" PRINT"" PRINT""
2 PRINT" *** PEAK HEIGHT IN FIR ***"
3 PRINT""
6 PRINT""
10 PRINT"BASELINE VALUE (IN VOLTS)"
20 INPUT B
21 PRINT"FULL SCALE OF THE RECORDER (IN VOLTS)"
22 INPUT R
30 PRINT"PEAK DETECTION LIMIT (% OF RECORDER FULL SCALE)"
40 INPUT L
41 LET G=L*R
50 PRINT"LIMIT FOR THE NEXT INJECTION (% OF RECORDER FULL SCALE)"
51 INPUT I
60 PRINT"SIGN OF THE SIGNAL (1 IF POSITIVE AND -1 IF NEGATIVE)"
62 INPUT A
100 OPEN 5,5
110 REM ADDRESS 5 IS THE ADDRESS FOR THE MULTIMETER INTERFACE
120 C#=CHR$(29)
130 F#="AAAAAAAAAAAAAAAAAAAAAAAAAAAA 9999 AAAAAAAAA 9999,9"
150 DIM P(100): REM SPACE IN MEMORY FOR 100 PEAKS
200 OPEN 4,4,1: REM OPEN LOGICAL FILE 4, DEVICE 4 (THE PRINTER) AND THE
210 REM SECONDARY ADDRESS 1 (DATA IN FORMAT AS DEFINED IN LINE 320)
220 P#="THE PEAK HEIGHT FOR PEAK NO. "
230 I#="IS ....."
300 OPEN 6,4,2: REM OPEN LOGICAL FILE 6, DEVICE 4 (THE PRINTER) AND
301 REM SECONDARY ADDRESS 2 (F# AS FORMAT FOR THE DATA OUTPUT)
310 OPEN 4,4,4
315 PRINT#3, REM PRINTS DIAGNOSIS OF POSSIBLE ERRORS
320 PRINT#6,F#
330 CLOSE 6
500 GOSUB 8000
550 IF X<(B*100) THEN 500
600 LET P1=X
700 GOSUB 8000
800 IF P1<X THEN 600
900 LET P2=X
1000 GOSUB 8000
1100 IF P2<X AND P1<X THEN 600
1110 LET P2=X
1200 IF P2<.75*P1 THEN 1000
1300 J=J+1
1400 LET P1(J)=P1
1550 PRINT#4,P#C#,J,I#C#,P1(J)*1000
2000 GOSUB 8000
2100 IF X<(I*P#I)/100 THEN 2000
2200 PRINT "INJECT NEXT SAMPLE !!"
2300 GOSUB 8000
2400 IF X<(I*8.9*(G/100)) THEN 2300
2500 GOTO 500
3000 INPUT#5,D#
3100 LET X=(VAL(D#))*R
3200 RETURN
READY.

```

bromocresol purple, consists of indicators which fulfil all the above conditions (Fig. 4). The mixture thus yields a linear response vs. pH over more than 2 pH units (Fig. 5). In order to compensate for differences in the molar absorptivities and in the shapes of the individual spectra different concentrations of these indicators are used in the final mixture.

Buffer systems

Though mixtures of buffers with constant buffering capacity have been used for many years, and the pK values of many buffering substances are

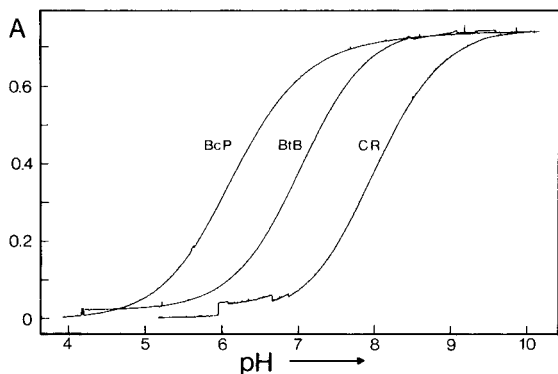


Fig. 4. Transition regions of bromocresol purple (BcP), bromothymol blue (BtB) and cresol red (CR) measured by the system shown in Fig. 2.

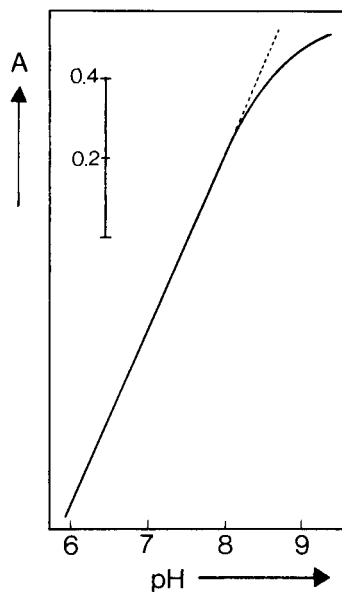


Fig. 5. Response curve (absorbance vs. pH) of the mixed indicator solution, measured at 580 nm.

amply tabulated, it was nevertheless found necessary to titrate the buffer systems to be used as carrier stream, not only to control their correct composition, but also because the ionic strength and temperature of the carrier stream would influence the β value. Typically, the position of the maximum β value vs. pH for a TRIS buffer is strongly temperature-dependent (Fig. 6), while that of phosphate buffer is not ($pK = 6.76 \pm 0.02$ in the range 20–45°C). Consequently, by increasing the temperature the pK values of these two buffer systems will become sufficiently close that their mixture at 30°C will yield a carrier stream having a wide range of constant buffering capacity (Fig. 7).

Interfering buffers and optimum pH range

In continuous flow analysis the samples and standards should ideally have the same matrix composition. Thus, in the present case their buffering capacities should be as close as possible. Moreover, if the samples do not contain any buffering substance, standards may be prepared in distilled water, as the same degree of mixing in the f.i.a. system will provide the same reaction medium. However, in the presence of a weak buffer, the samples and standards have to be prediluted with carrier stream (e.g., in the ratio 1 + 1) in order to make the differences in the buffering capacities between the samples and standards negligible. The obvious limitation of the present system is that the

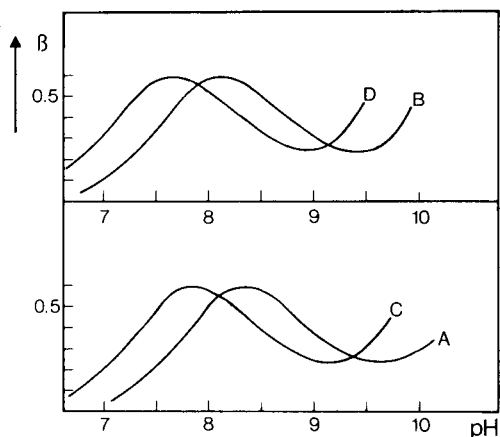


Fig. 6. The buffering capacity of TRIS buffer vs. pH and its dependence on temperature: (A) 20°C; (B) 30°C; (C) 40°C; (D) 50°C. All curves measured and computed by means of the system shown in Fig. 3.

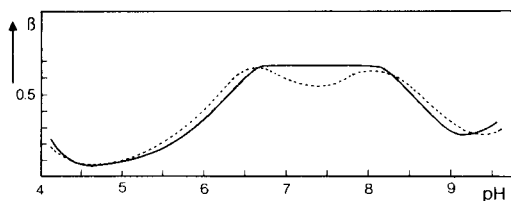


Fig. 7. The buffering capacity of an equimolar mixture of TRIS and phosphate buffers vs. pH at two different temperatures, as measured and computed by means of the system shown in Fig. 3. (—) 30°C; (---) 21°C.

β value of the carrier stream buffer must be at least ten times higher than that of the interfering buffer to even out the differences between individual samples. At the same time, however, the overall β value should be as low as possible, otherwise the pH change caused by the enzymatic reaction would be "buffered out" (cf. eqn. 4).

As a means of eliminating the influence of an interfering buffer one can either (a) measure in a pH range where its influence is minimal, or (b) if the interfering buffer is present in all samples at a relatively constant level, as is the case for most biological fluids, simply use this buffer to maintain the constancy of the overall β value. Thus, as a typical serum sample contains 20 mmol l^{-1} of hydrogencarbonate, this system will always constitute the principal interfering buffer in clinical analysis. Therefore, at pH 6.3 and 10.3, the buffering capacity of this system will be $0.576 \times 20 \text{ mmol}$, (Fig. 8), which is obviously too high to be tolerated; the ten-fold buffering capacity of the carrier stream needed to eliminate the influence of the interfering buffer at these pH values would obliterate the pH change caused by any enzymatic

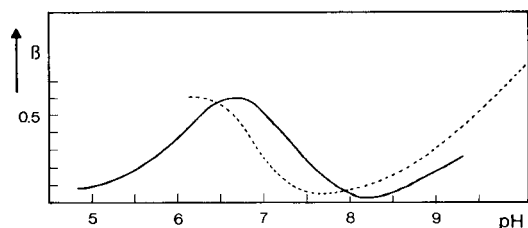


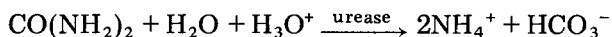
Fig. 8. The buffering capacities of phosphate (—) and hydrogencarbonate (----) buffers, measured at 25°C and computed using the system shown in Fig. 3. The buffering capacity—pH curve for hydrogencarbonate shows a maximum at pH 6.3 and a minimum at pH 7.8. (The “abnormal” increase of β at high pH values is due to the contribution from water; the concentrations of the buffers were 10^{-3} mol l^{-1} .)

reaction. Yet, at pH 7.8, approximately half way between the two pK values of hydrogencarbonate (Fig. 8), the β value of hydrogencarbonate would be ten times lower than β_{max} , and if a TRIS buffer is used in the carrier stream at 40°C (Fig. 6, curve C) its buffering capacity would be maximal. Thus by diluting the serum samples with 4 mmol l^{-1} TRIS buffer in the ratio 1:5, the buffering capacity of the carrier stream buffer at pH 7.8 would be ten times higher than that of interfering hydrogencarbonate. As pointed out earlier [3], in order to obtain the widest possible range of linear response, the pH of the carrier stream buffer should be adjusted to be 0.2 pH unit from the TRIS pK value in the direction opposite to the expected pH change. In this way, the buffering capacity will be 94.8% of β_{max} at the baseline, around 100% β_{max} for a medium range sample, and would decrease only to 94.8% of β_{max} if the pH change from the baseline for the highest sample were 0.4 pH unit. By using a mixture of buffers and the mixed indicator solution, the linearity can be extended over a wide range of concentrations of substrate or pH (Figs. 5 and 7).

As mentioned above, there is, however, another way of suppressing the influence of an interfering buffer, provided that it is present at a relatively constant level, i.e., to exploit its presence to adjust the overall β value. In order to illustrate this procedure, the determination of urea was chosen as a model system. One inherent advantage of the method is that because of the large range of constant β values (see Fig. 7) the pH of the carrier solution can be lowered to 6.8, where the enzyme (urease) has higher activity than at the pH value (7.8) used previously [3].

DETERMINATION OF UREA

The enzymatic determination of urea



was examined in manifolds designed for continuous flow and for stopped

flow. Carrier solution A was used in the analysis of urea standards without any interfering buffer (NaHCO_3), while carrier solution B was employed for the NaHCO_3 -spiked standards. These were all made to contain NaHCO_3 at the level 20 mmol l^{-1} (to simulate biological samples). As the total dilution of the samples (predilution and dispersion) in the f.i.a. system is ca. 18, the contribution of the hydrogencarbonate system to β will be approximately equivalent to 5×10^{-4} phosphate buffer, i.e., the phosphate buffer content in carrier B is half that of carrier solution A.

For continuous flow measurements, the manifold shown in Fig. 9 was used with the above-mentioned carrier streams, containing 35 units of urease per ml. The injected sample volume was $30 \mu\text{l}$ and the sampling frequency was 90–100 samples/hour. A recording obtained by injecting a series of standards is shown in Fig. 10; this gave a linear calibration curve over the whole range

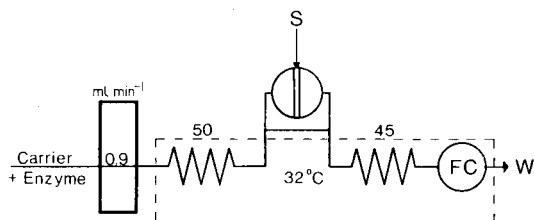


Fig. 9. Manifold for continuous flow analysis of urea. The sample ($30 \mu\text{l}$) is injected (S) into a carrier stream (carrier buffer A in absence of hydrogencarbonate, or carrier buffer B in its presence) containing 30 units urease/ml and 2% of mixed indicator solution (pH adjusted to 6.8 at 30°C). All tubes 0.5 mm i.d.; total dispersion $D_t = 8.6$.

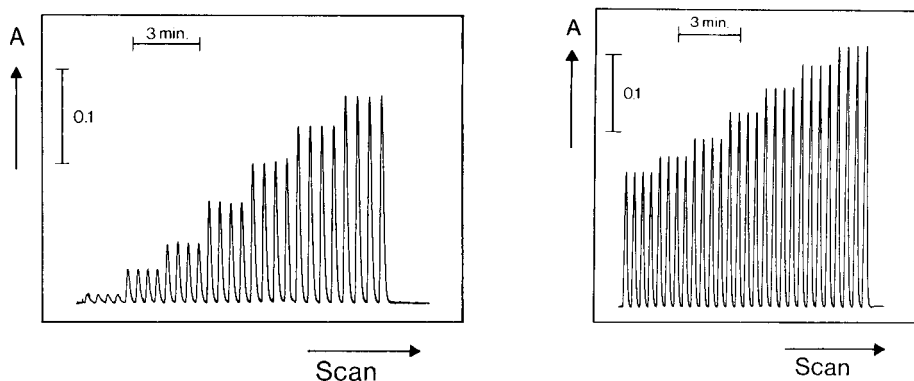


Fig. 10. Calibration run for urea in absence of hydrogencarbonate, at a rate of 90 samples/hour in the manifold depicted in Fig. 9. The urea samples contained 0, 1, 2, 4, 6, 8 and 10 mmol l^{-1} . Absorbance (A) recorded at 580 nm. Residence time T , 20 s; total dispersion D_t , 8.6.

Fig. 11. Calibration run for urea in presence of hydrogencarbonate (20 mmol l^{-1}) at a rate of 100 samples/hour in the manifold depicted in Fig. 9. Samples and conditions were otherwise exactly as for Fig. 10.

of urea samples ($0\text{--}10\text{ mmol l}^{-1}$) with a regression coefficient of 0.995; the blank was equivalent to 0.4 mmol urea/l . In the presence of 20 mmol of hydrogencarbonate (Fig. 11), the blank increased to 7.5 mmol urea/l and the slope of the calibration curve decreased, but the linearity of response was still preserved. The reproducibility of the determinations was satisfactory in both cases. This can be judged from Figs. 10 and 11, where all samples were injected in quadruplicate, or from Table 3 where peak-height values obtained with the aid of the algorithm listed in Table 2 are listed together with their standard deviations.

Stopped flow measurements were used when hydrogencarbonate was present in order to eliminate the blank values. The manifold, shown in Fig. 12 is in principle the same as that outlined in Fig. 1, but contains two pumping lines, one of which delivers carrier solution alone, while the second pumps a carrier stream to which urease has been added at a concentration of 90 units ml^{-1} . The reason was that when moderate pumping rates were used, the residence time T of the sample zone in a single-line system was so long that a

TABLE 3

Summarized data from the peak-height algorithm for the determination of urea in the absence of hydrogencarbonate. The input data for the PET were baseline (in V) 0.00 recorder f.s.d. (in V) 0.040; peak detection limit (in %) 10; limit for next injection (in %) 10; sign of the signal 1. An example of the actual data output for each peak is as follows THE PEAK HEIGHT FOR PEAK NO. 1 IS 10.9

Urea standard (mmol l^{-1})	2	4	6	8
Mean peak height (mV) ^a	10.95	21.13	30.85	39.40
R.s.d. (%)	0.5	0.5	0.6	0.4

^aFour injections for each concentration.

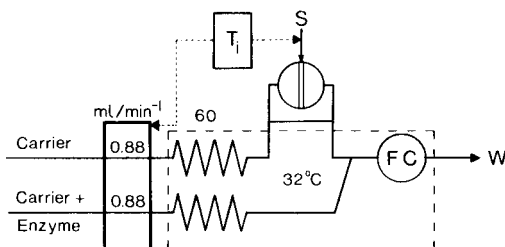


Fig. 12. Manifold for the stopped flow determination of urea. Samples ($30\text{ }\mu\text{l}$) are injected (S) into a carrier stream containing 0.001 M TRIS buffer and $5 \times 10^{-4}\text{ M}$ phosphate buffer in 0.14 M NaCl containing 2% mixed indicator solution. The second channel delivers the same solution to which $90\text{ units urease/ml}$ has been added. Both carrier streams are adjusted to pH 7.00 at 32°C . All tubes 0.5 mm i.d. The length between the point of injection (S) and the confluence point is 8 cm ; that between the confluence point and flow cell (FC) is 10 cm . Total dispersion D_t , 5.2. Residence time, 6.7 s. Contact time between sample and enzyme before measurement, 3.5 s. Absorbance measured at 580 nm .

large proportion of the urea was converted to the reaction products before the sample zone reached the flow cell. Consequently, h (or A) was unfavourably large compared to Δh (or ΔA), and this ratio was even worse in the presence of a hydrogencarbonate blank. Therefore it was decided to inject urea into a carrier stream without enzyme and to add the enzyme close to the flow cell so that T became shorter (and h or A lower).

An interesting feature of the stopped flow f.i.a. system is that various sections of the sample zone can be stopped and held within the optical path for recording of reaction rate. Because of the formation of concentration gradients at the interface between the carrier and sample solutions, various mixing ratios are observed in various sections of the sample zone and this allows a continuous choice of reaction conditions to be made. Thus, while the total dispersion can be manipulated by an appropriate choice of tube length and sample volume, a fine adjustment can be achieved by choosing an appropriate delay time from the moment of injection until the sample zone is stopped in the flow cell. This flexibility is demonstrated in Fig. 13, where urea samples (10 mmol l^{-1}) were injected into the stopped flow system (Fig. 12); the delay time was increased from 6.5 s to 17.5 s while the stop time (during which the increase in absorbance was recorded) was kept constant at 15 s. As the delay time increases, the sample solution along the zone length becomes more dispersed (diluted) and therefore the slope of the reaction rate line decreases. Simultaneously, there is an increase in the ratio between the enzyme

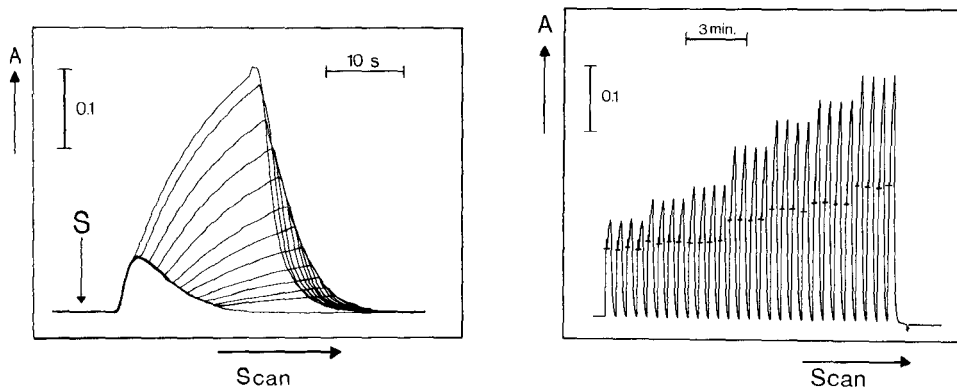


Fig. 13. Repeated injections of urea standard (10 mmol l^{-1}) into the stopped flow f.i.a. system (Fig. 12) recorded from the same point of injection (S) at fast paper speed (5 mm s^{-1}). Stop period Δt constant at 15 s; delay period increased from 6.5 to 17.5 s in steps of 1 s (the last curve was run continuously). For details see text.

Fig. 14. Calibration run for stopped flow determination of urea in the presence of hydrogencarbonate. Samples containing $20 \text{ mmol HCO}_3^- \text{ l}^{-1}$ and 0, 1, 2, 4, 6, 8 and 10 mmol urea/l were injected in quadruplicate. Delay time 7.6 s, stop time (Δt) 15 s. Total measuring cycle (including wash period) 36 s. Sampling rate 100 samples/h. The start of the stop period can be readily observed on the original recording, but is emphasized by the horizontal lines in this photographic reproduction.

dissolved in the carrier stream and the substrate contained in the sample, and so the reaction rate lines become progressively more linear with increase in the delay time. In actual serum analyses, the choice of delay time can also be used to optimize the sample dispersion in order to eliminate any differences in viscosities between serum and aqueous standards.

Because not only the delay time, but also the stop time Δt is exactly fixed by an electronic timer, measurements of the slope of the rate curve are equivalent to measurements of Δh which are simpler to evaluate. Such a calibration run (obtained at a much slower paper speed than that in Fig. 13) is shown in Fig. 14, where samples encompassing the range 0–10 mmol urea/l were injected. When the Δh values obtained were plotted versus the urea content in the individual samples, a straight line was obtained (regression coefficient 0.996) with a blank value corresponding to 2.1 mmol urea/l.

CONCLUSION

Compared with the previously developed method for determination of urea in serum, which used a glass electrode as a pH sensor [3], the present method allows twice as high a sampling rate, including the blanking of individual samples. Another advantage of the present approach is that it uses a spectrophotometric detector which is more robust and easier to operate than a capillary glass electrode. The enzyme consumption is moderate: for the continuous flow method 14 units of urease was used per determination, and for the stopped flow method 30 units of urease per determination. Work is in progress to reduce the enzyme consumption even further, by applying the merging-zones approach [8, 11]. While the decomposition of urea by urease leads to an increase of pH of the monitored carrier stream, the determination of glucose based on the use of glucose dehydrogenase [11] would cause a decrease in the pH of the reaction medium. Preliminary experiments with an f.i.a. system using the mixed indicator—carrier buffer solution, based on the same principles as described above, confirm that also glucose can be determined in this way.

Besides enzymatic analyses, the buffer indicator mixture is suitable for assays of gases which would, after diffusion or isothermal distillation from a donor stream [12], change the pH of an acceptor stream. As the acceptor stream would not contain any interfering buffers, the mixed indicator alone, or together with a very dilute mixture of several buffers, would be suitable for fast, selective and sensitive measurement of small amounts of gases.

The authors express their appreciation to the Danish Natural Science Research Council and to the Danish Council for Scientific and Industrial Research for partial financial support.

REFERENCES

- 1 H. Nilsson, A. Ch. Akerlund and K. Mosbach, *Biochim. Biophys. Acta*, 320 (1973) 529.
- 2 H. Nilsson, K. Mosbach, S. O. Enfors and N. Molin, *Biotechnol. Bioeng.*, 20 (1978) 529.
- 3 J. Růžička, E. H. Hansen, A. K. Ghose and H. A. Mottola, *Anal. Chem.*, 51 (1979) 199.
- 4 G. G. Guilbault, *Handbook of Enzymatic Methods of Analysis*, M. Dekker, New York, 1976.
- 5 G. Schwarzenbach, E. Kampitsch and R. Steiner, *Helv. Chim. Acta*, 28 (1945) 828.
- 6 J. F. Rusling, G. H. Luttrell, L. F. Cullen and G. J. Papareillo, *Anal. Chem.*, 48 (1976) 1211.
- 7 R. E. Adams and P. W. Carr, *Anal. Chem.*, 50 (1978) 944.
- 8 J. Růžička and E. H. Hansen, *Anal. Chim. Acta*, 114 (1980) 19.
- 9 J. Růžička and E. H. Hansen, *Anal. Chim. Acta*, 99 (1978) 37.
- 10 E. Bishop, *Indicators*, Pergamon, Oxford, 1972.
- 11 J. Růžička and E. H. Hansen, *Anal. Chim. Acta*, 106 (1979) 207.
- 12 E. A. G. Zagatto, B. F. Reis, H. Bergamin F^o and F. J. Krug, *Anal. Chim. Acta*, 109 (1979) 45.

AUTOMATION OF AN ENERGY-TRANSFER IMMUNOASSAY BY USING STOPPED-FLOW INJECTION ANALYSIS WITH MERGING ZONES

C. S. LIM and J. N. MILLER*

Department of Chemistry, Loughborough University, Loughborough, Leicestershire (Gt. Britain)

J. W. BRIDGES

Institute of Industrial and Environmental Health and Safety, University of Surrey, Guildford, Surrey (Gt. Britain)

(Received 16th August 1979)

SUMMARY

A homogeneous fluorescence energy-transfer immunoassay for serum albumin has been automated by using flow-injection analysis. Application of the merging-zone and stopped-flow principles permits low consumption of labelled reagents and samples, and sub-micromolar concentrations of albumin can be rapidly and precisely determined. Studies on individual serum samples show good agreement with other techniques, including a fluorimetric dye-binding assay that has also been automated by using merging-zone flow-injection analysis.

Since its introduction by Ružička and Hansen [1] and by Stewart et al. [2], flow-injection analysis has been applied to the automation of a number of determinations [3]. These analyses have mostly been done by injecting precisely measured sample zones into a reagent-containing carrier stream; by varying the design of the flow system, a wide range of interfacial gradients can be exploited. This approach is less well suited to analyses in which the reagent is a biological macromolecule such as an antibody or enzyme, because such reagents may be costly and are often available only in small quantities: published applications include the use of readily-available enzymes in analyses for glucose [4] and urea [5] in serum. Two additional principles recently applied to flow-injection analysis have, however, opened up new potential applications of the technique. It has been shown [6] that stopped-flow analyses are feasible, i.e. that the dispersion of a sample zone in the carrier stream will remain constant if the flow rate of the stream is reduced to zero. This principle is of great value in kinetic assays [6, 7] and in analyses where an incubation period is required before the sample zone reaches the detector. In addition, economies of sample and of reagent can be achieved by using the merging-zone approach, in which small volumes of sample and reagent are injected into inert carrier streams and merge before reacting and being carried to the detector. The merging-zone principle has

been applied to a number of analyses [8, 9] including, in conjunction with the stopped-flow principle, the enzymatic assay of serum glucose [7].

The present paper describes for the first time the application of flow-injection analysis in the field of immunoassay. The stopped-flow and merging-zone principles are applied to the homogeneous energy-transfer immunoassay method originally described by Ullman et al. [10]. In this type of assay, the antigen (serum albumin in the present work) and the appropriate antibody are labelled with different fluorescent groups. The labels are chosen so that the emission spectrum of one (the donor, normally attached to the antigen) overlaps the excitation spectrum of the other (the acceptor, normally attached to the antibody). Only when the labels are very close to each other, i.e. when labelled antigen and labelled antibody specifically combine, can energy transfer from the donor to the acceptor occur, resulting in quenching of the donor fluorescence and (possibly) enhancement of the acceptor fluorescence. In the presence of unlabelled (i.e. sample), antigen these effects are reversed and the consequent enhancement of the donor label fluorescence, for example, can be used to determine the antigen. Since the analysis depends on a change in label properties on antigen-antibody binding, it is homogeneous (i.e. no separation step is required) and very suitable for automation. The present study follows Ullman et al. [10] in using fluorescein and rhodamine as donor and acceptor fluorescent labels, respectively, though these groups are far from ideal [11] and other donor-acceptor pairs are under development. Previous studies have shown that a fluorimetric detector can be combined successfully with flow-injection analysis in the determination of albumin by a dye-binding procedure with anilidonaphthalene [12]. The present paper also describes a modification of that assay by using the merging-zone principle.

EXPERIMENTAL

Equipment

Flow-injection analysis was done with the arrangement shown in Fig. 1.

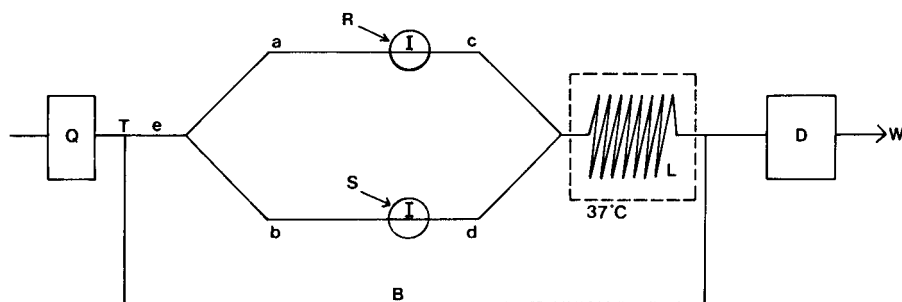


Fig. 1. Flow-injection analysis arrangement. (B) Bypass; (D) fluorimetric detector; (I) injection valve; (L) reaction coil; (Q) pump; (R) reagent; (S) sample; (T) 3-way valve; (W) waste.

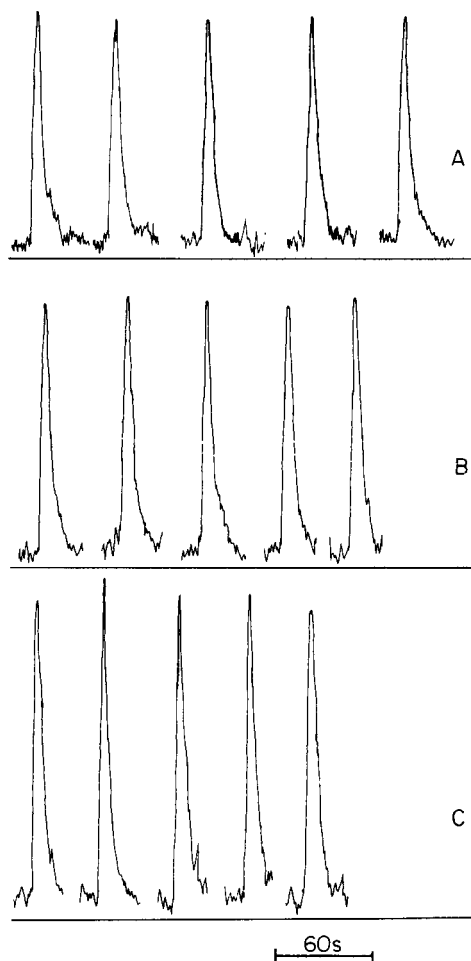
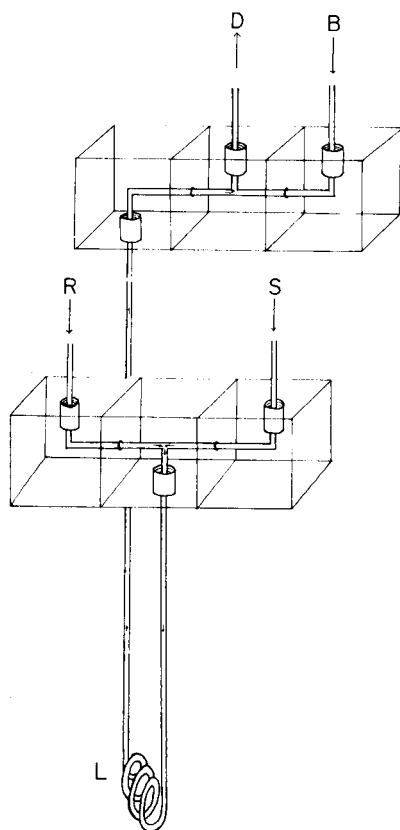


Fig. 2. Manifold arrangement; lettering as in Fig. 1.

Fig. 3. Examples of recorder responses obtained during the energy-transfer immunoassay of serum albumin in diluted standard serum. The albumin concentrations were: (A) 1.1×10^{-6} M; (B) 5.5×10^{-6} M; (C) 1.1×10^{-5} M.

A Gilson Minipuls HP-4 8-channel pump and a double-injection valve [7] (Bifok, Sweden) were used. Polyethylene tubing was used throughout and was connected by using the manifold system shown in Fig. 2. The lengths and diameters of the tubing used were as follows: $a = b = 250$ mm long, 0.5 mm i.d.; $c = d = 150$ mm long, 0.5 mm i.d.; $e = 100$ mm long, 0.7 mm i.d.; bypass (B) = 320 mm long, 0.7 mm i.d. The reaction coil, L, was made of 0.7-mm i.d. tubing and was 650 mm long for the dye-binding assay and 950 mm long for the immunoassay. The detector was a Perkin-Elmer model 1000 M filter fluorimeter, with a flow cell specially adapted with silica

tubing (1 mm i.d.). The illuminated volume of the cell was ca. 16 μl . Excitation and emission wavelengths were 364 and 470 nm, respectively, for the dye-binding assay, and 470 and 541 nm, respectively, for the immunoassay. The fluorimeter was connected to an Omniscrite 10-mV recorder (Houston Instruments).

Reagents

The carrier stream was a phosphate buffer (0.067 M, pH 7.0 for the dye-binding assay; 0.01 M, pH 7.2, containing 0.145 M NaCl for the immunoassay). The 8-anilino-1-naphthalene sulphonic acid (ANS; Sigma) was used at a concentration of 15 mg l^{-1} . Pure serum albumin and standard human serum were obtained from Hoechst (London, U.K.), and purified rabbit anti-albumin antibodies from Dakopatts (Mercia Brocades Ltd., West Byfleet, Surrey). Albumin and antibodies were labelled with fluorescein isothiocyanate and rhodamine isothiocyanate, respectively, by standard methods [11]. Electroimmunoassay was done on Cellogel cellulose acetate membranes [13]. Individual serum samples were obtained from healthy laboratory workers.

RESULTS

ANS binding procedure

This assay, previously done by conventional flow-injection procedures [12], was successfully adapted to the merging-zone approach. A flow rate of 1.03 ml min^{-1} was used. The volumes of sample and reagent injected (determined by injecting an air bubble into the carrier stream) were 10.4 μl . This represents a substantial saving in reagent compared with the previous method. The merging time, sampling time, and residual time (without stopped flow) were 9.8 s, 3 s and 23.6 s, respectively. A linear relationship was obtained between the fluorimeter response (fluorescence of protein-bound ANS) and albumin concentration in the range 0–200 mg dl^{-1} . When diluted standard serum was used, the coefficients of variation were 2.3% at 18 mg dl^{-1} and 2.1% at 180 mg dl^{-1} . The coefficients of variation for diluted test sera were somewhat higher, averaging 4.5%. The albumin concentrations of four test sera were determined with the results given in Table 1.

Energy-transfer immunoassay

Initial attempts to automate this assay by using conventional flow-injection procedures gave unsatisfactory results. Not only was the consumption of labelled albumin and labelled antibody unacceptably high, but the high background fluorescence of the carrier stream (a mixture of the labelled species) severely restricted the precision and sensitivity of the assay. These objections were overcome by using the stopped-flow, merging-zone method. The injected reagent was a solution containing 2.4×10^{-7} M fluorescein-labelled albumin (fluorescein: albumin ratio 1.4:1) and 4×10^{-6} M

TABLE 1

Determination of albumin in serum samples^a
(All concentrations in mg dl⁻¹)

Sample	ANS-binding f.i.a. method	Energy-transfer immunoassay—f.i.a. method	Electroimmunoassay method
1	3700 ± 180 (100) [10]	3860 ± 200 (100) [8]	3800 ± 140 (150) [5]
2	3600 ± 170 (100) [10]	3320 ± 170 (500) [8]	3680 ± 80 (150) [8]
3	4380 ± 150 (40) [10]	4810 ± 150 (500) [8]	4500 ± 140 (150) [7]
4	3675 ± 200 (75) [8]	3460 ± 220 (100) [4]	3080 ± 80 (150) [5]

^aNumbers in parentheses are the factors by which serum samples were diluted before study; numbers in square brackets are the numbers of measurements used in calculating standard deviations.

rhodamine-labelled antibody (rhodamine:albumin ratio 16.5:1). Previous studies [11] had demonstrated that this combination of lightly-labelled antigen and heavily-labelled antibody, with a large excess of the latter, produced optimum results when the assay was performed without automation. Diluted serum samples were injected at S (Fig. 1.) The flow-rate used was 3.8 ml min⁻¹, giving a merging time of 3.2 s and a residual time of 16 s (continuous flow); the sample and reagent volumes were 36 µl. A stopped-flow incubation time of 6 min was used: during this period, the three-way valve, T, was turned to divert the carrier stream through the bypass, and the recorder chart was switched off. The recorder was restarted as T was turned to restart the flow of the sample.

In the analysis of unlabelled (sample) albumin concentrations, the fluorescence of the fluorescein label was determined (the fluorescence of the rhodamine label was too feeble in practice to provide a sensitive assay [11]). Fluorescence intensities were related to the emission from a 2.4×10^{-7} M labelled albumin solution, arbitrarily assigned a value of 100. The results obtained in this way were satisfactory. Readily-measurable fluorescence peaks were obtained (Fig. 3): the coefficient of variation of the results for diluted standard sera was 2.5% at an albumin concentration of 5×10^{-5} M, and 2.3% at a concentration of 10^{-7} M. The standard curve obtained (Fig. 4) showed that albumin concentrations of 10^{-7} M and below could be determined. The values obtained from four test sera are shown in Table 1, along with the results of the ANS binding and electroimmunoassay techniques: agreement between the three methods was generally good.

DISCUSSION

The results demonstrate clearly the suitability of stopped-flow, merging-zone flow-injection analysis for the automation of homogeneous immunoassays: they also confirm the usefulness and sensitivity of a fluorimeter as a

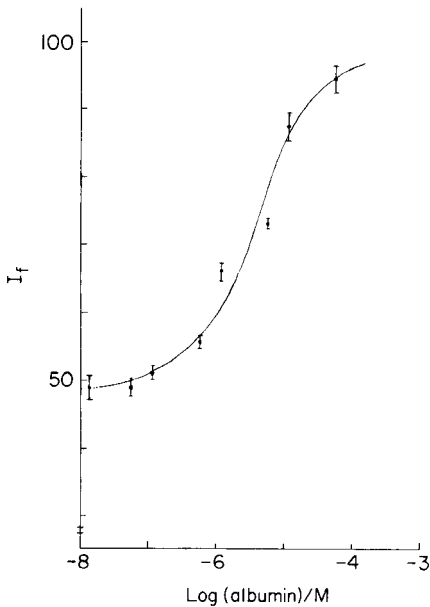


Fig. 4. Standard curve for the energy-transfer immunoassay of serum albumin. Error bars represent standard deviations.

detector for flow-injection methods. In the present assay, the flow-injection approach had several substantial advantages over the static analysis previously described [11]. These included smaller samples, a considerable economy in labelled reagents and a shorter incubation period. The incubation period of 6 min was perfectly adequate in the albumin assay, but there would be no technical objections to the use of longer periods if required in other assays. The use of a flow cell of narrow bore precluded any interference by inner filter effects, and the background fluorescence of the diluted serum was negligible compared with the fluorescein emission. The detection limit of the assay was more than adequate for the determination of albumin in diluted serum samples and in urine (cf. [14]). Improved detection limits could almost certainly have been achieved by the use of a spectrofluorimeter, rather than a filter fluorimeter, as the detector. Detailed studies of the fluorescein rhodamine energy-transfer pair have shown that larger quenching and enhancement effects occur at narrower spectral bandwidths [11].

The relatively low sampling rate available in this stopped-flow assay can be improved by modifications to the manifolds [6], but in any event provides a faster throughput of samples than the manual method. Two further small problems were noted, the first being the need to carry out frequent checks (by injecting air bubbles) to ensure synchronous merging of the sample and reagent: very fine adjustments in the flow rate could be

achieved by means of a screw clip attached to a short length of thin-walled tubing inserted in one of the channels (e.g. in tube a in Fig. 1). The second problem was the tendency of air bubbles to form in the carrier streams: this effect could be avoided by equilibrating the samples and the reagents at 37°C before beginning an analysis.

A wide variety of other homogeneous immunoassays should be suitable for automation by using flow-injection analysis, including fluorescence quenching, enhancement and polarisation assays. The present energy-transfer approach can also be applied in analyses for many other macromolecules and low-molecular-weight species such as drugs and hormones. Flow-injection techniques will thus be increasingly used in this branch of clinical and biochemical analysis.

We are grateful to the Medical Research Council for a Project Grant in support of this research. We also thank A. Stevens and J. Swithenbank for excellent technical assistance.

REFERENCES

- 1 J. Růžička and E. Hansen, *Anal. Chim. Acta*, 78 (1975) 17.
- 2 K. K. Stewart, G. R. Beecher and P. E. Hare, *Fed. Proc.*, 33 (1974) 1439.
- 3 D. Betteridge, *Anal. Chem.*, 50 (1978) 832A.
- 4 E. H. Hansen, J. Růžička and B. Rietz, *Anal. Chim. Acta*, 89 (1977) 241.
- 5 J. Růžička, E. H. Hansen, A. K. Ghose and H. A. Mottola, *Anal. Chem.*, 51 (1979) 199.
- 6 J. Růžička and E. H. Hansen, *Anal. Chim. Acta*, 99 (1978) 37.
- 7 J. Růžička and E. H. Hansen, *Anal. Chim. Acta*, 106 (1979) 207.
- 8 H. Bergamin F^o, E. A. G. Zagatto, F. J. Krug and B. F. Reis, *Anal. Chim. Acta*, 101 (1978) 17.
- 9 E. A. G. Zagatto, F. J. Krug, H. Bergamin F^o, S. S. Jorgensen and B. F. Reis, *Anal. Chim. Acta*, 104 (1979) 279.
- 10 E. F. Ullman, M. Schwarzberg and K. E. Rubenstein, *J. Biol. Chem.*, 251 (1976) 4172.
- 11 C. S. Lim, J. N. Miller and J. W. Bridges, *Anal. Biochem.*, submitted.
- 12 J. I. Braithwaite and J. N. Miller, *Anal. Chim. Acta*, 106 (1979) 395.
- 13 V. J. Bowman, Ph. D. thesis, Loughborough University (1975).
- 14 J. Woo, M. Floyd, D. C. Cannon and B. Kahan, *Clin. Chem.*, 24 (1978) 999.

SIMULTANEOUS DETERMINATION OF NITRATE AND NITRITE BY FLOW INJECTION ANALYSIS

M. F. GINÉ, H. BERGAMIN F^o*, E. A. G. ZAGATTO and B. F. REIS

Centro de Energia Nuclear na Agricultura, CEP. 13.400 Piracicaba, S. Paulo (Brasil)

(Received 27th June 1979)

SUMMARY

An automatic method for the simultaneous determination of nitrate and nitrite by flow injection analysis is described. Nitrate is reduced to nitrite with a copperized cadmium column. Nitrite is diazotized and coupled with *N*-(1-naphthyl)ethylenediammonium dichloride. The merging zones approach is used to minimize reagent consumption. The injector system is arranged so that two peaks are obtained, one corresponding to nitrite and the other to nitrite plus nitrate. A sampling rate of about 90 samples per hour is possible; the precision is better than 0.5% for nitrite in the range 0.1–0.5 mg l⁻¹ and 1.5% for nitrate in the range 1.0–5.0 mg l⁻¹.

Since its inception in 1975 [1], flow injection analysis has undergone fast development. Devices such as special injection valves [1–4], dampeners [5], solvent extraction chambers [3], distillation units [6], etc., have been designed with a view to automation of many different types of analysis. The concept of merging zones in flow injection analysis was introduced in 1978 [7]. The injector port had then the function of introducing simultaneously both sample and reagent into the analytical system. This led to a drastic reduction of the reagent consumed [7, 8], allowed the analysis of acidic samples without pre-neutralization [9], and, in connection with a stopped-flow procedure, was employed in enzymatic assays based on slow reactions [10]. The use of this technique to perform standard addition, and also to improve sensitivity in turbidimetry, is a common practice in this laboratory.

Another function which can be performed by the injector port is the commutation of parts of the manifold during sample and reagent injection. Development of flow injection analysers based on this idea have opened up new possibilities for carrying out simultaneous determinations without splitting, blank corrections, assays of very variable samples, etc.

The main purpose of this paper is to describe a method for the simultaneous determination of nitrate and nitrite in soil and water samples, by using a spectrophotometric method for nitrite and reduction of nitrate to nitrite with a copperized cadmium column [11, 12]. A special injector-commutator which operates in two positions is described. In one position, the sample is injected and the column is placed in the analytical line, the

resulting signal corresponding to nitrate plus nitrite. In the other position, the sample is injected again but the column is bypassed, so that the signal corresponds to nitrite alone. The merging zones approach is used to minimize reagent consumption.

EXPERIMENTAL

Flow system

The flow injection system without sample splitting is outlined in Fig. 1. The sample and reagent are injected into corresponding carrier streams. At point X, the sample zone meets the reagent R_2 , which acts as reduction catalyst, masking agent [16] and buffer. After coil C_1 , the sample zone enters the reduction column, nitrate being reduced to nitrite. At point Y, the sample zone meets the colour-forming reagent, R_1 , starting the diazotization and coupling reactions. After the reaction coil, C_2 , the absorbance corresponding to nitrite (original plus reduced nitrate) is measured at 540 nm. In the alternative mode (dotted lines in the flow diagram), the column is replaced by simple tubing, and only the nitrite originally present in the sample is measured.

The flow rates indicated in Fig. 1 were fixed to permit the analysis of 90 samples per hour with adequate sample dilution by the confluent streams. The optimum pumping rate of the colour reagent R_1 was established by using a 0.2 ppm N (as nitrite) solution in an infinite volume situation [6] and increasing the flow rate from 0.23 to 1.6 ml min⁻¹; maximum absorbance was found for the range 0.9–1.1 ml min⁻¹.

The peristaltic pump, tubing, connectors, flow cell, spectrophotometer and recorder were the same as used in earlier work [6]. The reduction column was made from a glass tube (3 mm i.d.) filled with copperized cadmium filings, held in position by glass wool plugs.

The injector-commutator (Fig. 2) was made from perspex and had charac-

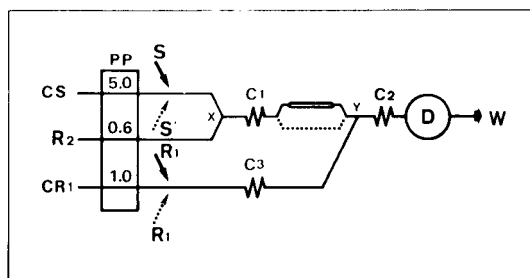


Fig. 1. Flow diagram of the system. C_S (water) and C_{R_1} (8% phosphoric acid) are the carrier streams corresponding to the sample (S) and reagent (R_1). R_2 is the masking, buffering and catalytic reagent, PP is the peristaltic pump; flow rates are given in ml min⁻¹. C_1 , C_2 and C_3 are coils with lengths of 15, 150 and 15 cm, respectively. The column is placed between coils C_1 and C_2 . D is the detection unit and W denotes waste. For details, see text.

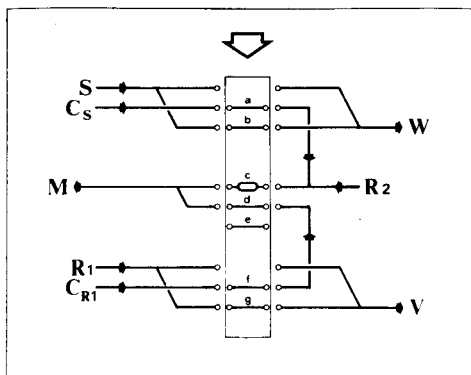


Fig. 2. Schematic diagram of the injector commutator in the position for nitrate plus nitrite analysis. *a* and *b* are the sample loops, *c* is the reduction column, *d* and *e* are connectors, and *f* and *g* are the reagent loops. *M* represents the manifold. The other symbols are explained in the text.

teristics similar to those of the multiple proportional injector [8]. In the position shown in Fig. 2, the sample (*S*) is aspirated to fill the sample loop (*b*), the colour-forming reagent (R_1) is pumped to fill the reagent loop (*g*), and these loops define exactly the sample and reagent volumes. The excess of sample goes to waste (*W*), while the excess of reagent, slightly diluted by the reagent carrier stream, is directed to the reagent recovery vessel (*V*). In this position, the reduction column (*c*) is placed in the analytical line. The previously injected sample and reagent aliquots (*a*, *f*) are transported for analysis by the corresponding carrier streams (C_S and C_{R_1}). In the other position, the sample and reagent are aspirated again and the entire process is similar, except that the reduction column is replaced by tube (*d*).

Reagents

All reagents were of analytical grade and distilled-deionized water was used in all experiments. Copperized cadmium filings were prepared daily by treating cadmium filings (20–40 mesh) as described elsewhere [12].

The colour reagent R_1 was prepared by dissolving 20 g of sulphanilamide and 1 g of *N*-(1-naphthyl)-ethylenediammonium dichloride in 100 ml of 80% phosphoric acid and diluting to 1 l with water. This solution was stored in a refrigerator. Reagent R_2 was prepared by dissolving 100 g of ammonium chloride, 20 g of sodium tetraborate and 1 g of Na_2EDTA in 1 l of water; this solution is stable.

Samples and standards

Water samples from the Piracicaba region were collected in polyethylene vessels and analyzed immediately. Soil extracts were obtained as described by Bremner [13].

The aqueous 1000 ppm NO_3 -N stock solution (6.07 g $NaNO_3$ l^{-1}) and 1000 ppm NO_2 -N stock solution (4.92 g $NaNO_2$ l^{-1}) were treated with a few

drops of chloroform and kept in a refrigerator. The nitrite solution was standardized against a 0.1 N permanganate solution.

Working standards containing both nitrate and nitrite were prepared by appropriate dilutions and covered the ranges 0.0–0.5 ppm NO_2^- -N and 0.0–5.0 ppm NO_3^- -N. For soil analysis, the standards were diluted with the corresponding extractant. Only one standard containing 0.50 ppm NO_2^- -N is necessary for calculation purposes; a 0.50 ppm NO_3^- -N standard is useful for checking the reduction conditions.

Optimization of the flow system

The infinite volume situation [6] was employed to define the optimum reaction coil length. With the system indicated in Fig. 1, the column was bypassed and a 0.2 ppm NO_2^- -N solution replaced the sample carrier stream. Coil lengths of 20, 44, 94, 148, 200 and 250 cm were tested for coil C₂. For each situation, the percentage reaction was determined by stopping the pump after achievement of the plateau, allowing full development of the reaction in the flow cell (Fig. 3). A 150-cm coil permitted 80% of the complete reaction. Longer coils provided better sensitivity but required larger sample volumes [14], causing a significant decrease in the sampling rate.

The optimum length of the reduction column was established similarly by using a 0.2 ppm NO_3^- -N solution, the reaction coil being 150 cm. Reduction column lengths of 2.0, 3.5 and 10.7 cm were tested (Fig. 4). The injector-commutator allowed the columns to be replaced easily without disturbing the system. For each situation, the percentage reduction was determined by comparison of the plateau achieved with that corresponding to a 0.2 ppm NO_2^- -N solution processed in the same way. A column length of 5.2 cm was

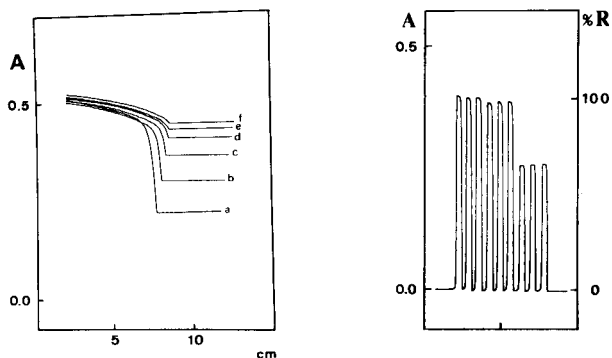


Fig. 3. The influence of the reaction coil length. Curves a–f correspond to coil lengths of 20, 44, 94, 148, 200 and 250 cm, respectively. The parallel lines on the right indicate the steady-state. The break points correspond to pump stoppage, and the lines to the left show the reaction development in a static situation. Paper speed, 0.5 cm min^{-1} .

Fig. 4. The influence of the reduction column length. From left to right, the peaks (in triplicate) correspond to column lengths of 10.7, 3.5 and 2.0 cm, respectively.

chosen, because the reduction was almost complete and reproducibility was good.

With these dimensions of the system, the sample injection volumes were fixed as 75 μ l and 15 μ l in order to give suitable measuring conditions. The synchronization coil C_3 (15 cm) and injected volume of reagent (50 μ l) were adjusted to incorporate the merging zones approach in the proposed method.

The dispersion factors were estimated with a 0.2 ppm NO_2^- -N standard, as described earlier [14].

RESULTS AND DISCUSSION

Some analytical characteristics of the proposed method are apparent from the calibration data given in Fig. 5. As each position of the commutator defines a different system, two baselines are observed. For pure nitrate standards, no signal was recorded when the system was in the nitrite analysis position, but of course when pure nitrite standards were used, signals were obtained in both positions (Fig. 5d). This must be taken into account in calculating nitrate concentrations. The net peak height for nitrate is calculated from the expression: $H(\text{nitrate}) = H(\text{total}) - \alpha H(\text{nitrite})$, where H represents peak height; α is defined as the ratio between the two peak heights corresponding to nitrite alone with and without the reductor column and must be determined before any routine run (Fig. 6). From the calibration runs in Fig. 5, this ratio was calculated as 0.131, with a coefficient of variation of 4.3%.

The difference in the peak heights of the same standard (Fig. 5d) reflects the different dispersion in each analytical position; this is mainly due to the different injected volumes and not to the presence of the column. The

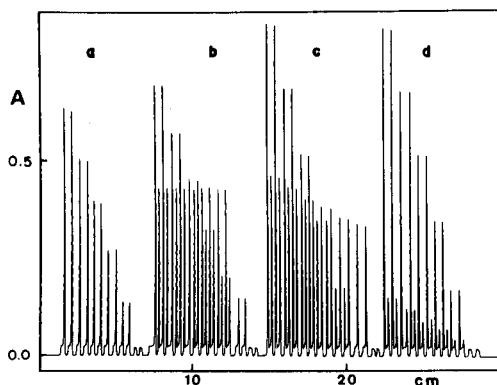


Fig. 5. Characteristics of the proposed system. (a) Nitrate standards (5.0, 4.0, 3.0, 2.0, 1.0, 0.0 ppm NO_3^- -N). (b) Mixed standards containing nitrate (5.0, 4.0, 3.0, 2.0, 1.0 ppm NO_3^- -N) plus 0.5 ppm NO_2^- -N; the four small peaks to the right correspond to a standard containing 1 ppm NO_3^- -N without nitrite and to a blank injection. (c) Mixed standards containing nitrite (1.0, 0.8, 0.6, 0.4, 0.2, 0.0 ppm NO_2^- -N) plus 2.5 ppm NO_3^- -N. (d) Nitrite standards (1.0–0.0 ppm NO_2^- -N). Paper speed, 0.5 cm min^{-1} .

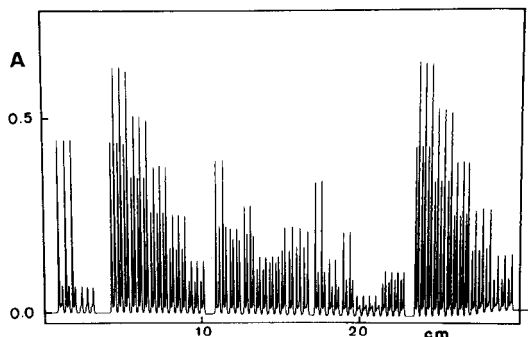


Fig. 6. Routine run of seven water samples with standard addition. From left to right: a 0.5 ppm NO_2^- -N standard followed by a 0.5 ppm NO_3^- -N standard; a calibration run with mixed standards (5.0–1.0 ppm NO_2^- -N plus 0.5–0.1 ppm NO_3^- -N); seven samples with standard addition; seven original samples; and the calibration graph again. Paper speed, 0.5 cm min^{-1} .

column appears to have very little effect on sample dispersion. The measured dispersion factors were 0.35 and 0.05, allowing an increase in sensitivity by injecting larger sample volumes.

On a routine basis, 75 samples per hour were analyzed for both anions (Fig. 6), with a relative standard deviation of 1.5% and 0.5% for nitrate and nitrite, respectively. A sampling rate of about 90 samples per hour is possible with a carryover less than 1%.

The results of the recovery tests made with water samples and soil extracts are shown in Table 1. The sample showing low nitrite recovery was abnormally coloured; the effect is not apparent in the nitrate recovery because of the higher sample dispersion.

TABLE 1

Recovery data related to water and soil samples

Water				Soil extracts ^a	
$[\text{NO}_2^-]\text{-N}$ (ppm)	Recovery ^b (%)	$[\text{NO}_3^-]\text{-N}$ (ppm)	Recovery ^b (%)	$[\text{NO}_3^-]\text{-N}$ (ppm)	Recovery ^c (%)
0.11	102.6	0.84	98.3	4.39	98.8
0.10	101.8	0.88	97.9	3.82	95.2
0.07	99.8	0.17	100.4	1.97	98.0
0.07	88.0	0.17	98.6	3.80	102.1
0.25	99.7	0.55	97.3	2.22	100.4
0.17	100.0	0.46	99.8	4.02	98.9
0.40	100.5	0.57	98.3	5.43	95.1

^aThe NO_2^- -N contents of the soil extracts were below 0.05 ppm. ^bAfter addition of 5 ml of a 10.0 ppm NO_3^- -N plus 1.0 ppm NO_2^- -N solution to 45 ml of sample. ^cAfter addition of 5 ml of a 30.0 ppm NO_3^- -N to 45 ml of sample.

The utilization of the two alternative systems allows the simultaneous determination of two species present in different concentration ranges in the sample with only one detector. There is no loss of reproducibility or reduction in the sampling rate, such as occur when sample splitting is used.

The authors thank Drs. E. H. Hansen and J. Růžička for providing the reagents and Peter B. Vose for assistance in the preparation of the original manuscript. Partial support of this project by FINEP (Financiadora de Estudos e Projetos, Brasil) and by the Secretaria da Indústria, Ciência e Tecnologia do Estado de São Paulo (Brasil) is greatly appreciated.

REFERENCES

- 1 J. Růžička and E. H. Hansen, *Anal. Chim. Acta*, 78 (1975) 145.
- 2 J. W. B. Stewart, J. Růžička, H. Bergamin F^o and E. A. G. Zagatto, *Anal. Chim. Acta*, 81 (1976) 371.
- 3 H. Bergamin F^o, J. X. Medeiros, B. F. Reis and E. A. G. Zagatto, *Anal. Chim. Acta*, 101 (1978) 9.
- 4 J. Růžička, E. H. Hansen, H. Mosbaek and F. J. Krug, *Anal. Chem.*, 49 (1977) 1858.
- 5 H. Bergamin F^o, B. F. Reis and E. A. G. Zagatto, *Anal. Chim. Acta*, 97 (1978) 427.
- 6 E. A. G. Zagatto, B. F. Reis, H. Bergamin F^o and F. J. Krug, *Anal. Chim. Acta*, 109 (1979) 45.
- 7 H. Bergamin F^o, E. A. G. Zagatto, F. J. Krug and B. F. Reis, *Anal. Chim. Acta*, 101 (1978) 17.
- 8 E. A. G. Zagatto, F. J. Krug, H. Bergamin F^o, S. S. Jørgensen and B. F. Reis, *Anal. Chim. Acta*, 104 (1979) 279.
- 9 B. F. Reis, H. Bergamin F^o, E. A. G. Zagatto and F. J. Krug, *Anal. Chim. Acta*, 107 (1979) 47.
- 10 J. Růžička and E. H. Hansen, *Anal. Chim. Acta*, 106 (1979) 207.
- 11 R. S. Lambert and R. J. DuBois, *Anal. Chem.*, 43 (1971) 955.
- 12 A. Henriksen and A. R. Selmer-Olsen, *Analyst*, 95 (1970) 514.
- 13 J. M. Bremner, in C. A. Black (Ed.), *Methods of Soil Analysis*, American Society of Agronomy, Madison, 1965, p. 1215.
- 14 J. Růžička and E. H. Hansen, *Anal. Chim. Acta*, 99 (1978) 37.

DETERMINATION OF WATER BY FLOW-INJECTION ANALYSIS WITH THE KARL FISCHER REAGENT

INGRID KÅGEVALL, OVE ÅSTRÖM and ANDERS CEDERGREN*

Department of Analytical Chemistry, University of Umeå, S-901 87 Umeå (Sweden)

(Received 10th July 1979)

SUMMARY

A method for the determination of water in organic solvents by flow-injection analysis (f.i.a.) is described. The method, which is based on the reaction between water and the Karl Fischer reagent, is capable of 120 determinations per hour. The concentration range 0.01–5% (v/v) of water can be covered by using a single Karl Fischer reagent solution. The results obtained with a specially constructed potentiometric detector showed a relative standard deviation of less than 0.5% (v/v). This value was about 3 times less than that obtained with a spectrophotometric detector. The f.i.a. technique is shown to offer some unique possibilities in minimizing interferences associated with the standard Karl Fischer batch titration method.

Measurement of the water content in a wide variety of materials is a problem of universal interest and the determination of water has consequently become one of the commonest procedures in chemical laboratories. A comprehensive review of chemical and physical methods for the determination of water has recently been published [1]. Among the various techniques used, e.g., gas-chromatographic, gravimetric, spectroscopic (n.m.r., u.v., i.r.), titrimetric (Karl Fischer), the last is probably the most generally used. It has been applied to the determination of water in numerous organic and inorganic matrices including saturated or unsaturated hydrocarbons, alcohols, halides, acids, acid anhydrides, esters, ethers, amines, amides, nitroso- and nitro compounds, sulphides, hydroperoxides and dialkyl peroxides.

However, many interferences are associated with the Karl Fischer method. Active carbonyl compounds, for example, cause the formation of water through reaction with methanol which is the main constituent of the ordinary Karl Fischer reagent. Other interfering substances which cause a different type of error include mercaptans and certain amines which react with the iodine present in the Karl Fischer reagent. Negative errors will thus arise in determinations of water in solvents like peroxy acids, diacyl peroxide, and quinones because of the formation of iodine. In some cases the Karl Fischer reagent has been modified successfully in order to minimize or eliminate these interferences.

There are two additional main drawbacks associated with the standard Karl Fischer method. First, it is time-consuming because of the rather slow rate of reaction between water and the Karl Fischer reagent near the end-point of the titration. Secondly, the analyst has to handle rather large volumes of toxic reagent which is potentially dangerous.

In order to overcome some of these drawbacks, the possibilities of using flow-injection analysis (f.i.a.) were considered. This technique was originally described by Růžička and co-workers [2–11] and involves the introduction of the sample into an unsegmented carrier stream with subsequent transportation to the detector. The degree of dispersion of the sample zone can be controlled by varying parameters such as the coil length and the flow-rate. The f.i.a. technique has been shown to be a very flexible and powerful analytical tool, and has been applied to procedures such as extraction, acid–base titrations, dialysis, dilution and multiple determinations. For the determination of water by the Karl Fischer method, it should be possible to develop a completely closed system by exploiting this technique. It should also be possible to take full advantage of one of the other main properties of the f.i.a. method, namely the rapidity of determination.

It has recently been shown [12, 13] that the reaction rate in the Karl Fischer determination can be speeded up by more than 100 times either by lowering the concentration of iodide in the reaction mixture [12] or by using a reagent based on a formamide–pyridine mixture [13] rather than the conventional mixture of methanol and pyridine. The rapid rate of the main reaction obtained by using such reagents can be used to minimize effects from side reactions in a flow-injection system by keeping the reaction time at a minimum. This constitutes an important advantage of the f.i.a. technique compared with ordinary batch titrations. In addition, the f.i.a. technique may offer other unique possibilities for the elimination of interferences.

This paper describes a f.i.a. system for the determination of water with a methanolic Karl Fischer (K.F.) reagent, and includes the characterization of two different types of detectors, one based on zero-current potentiometry and the other on spectrophotometry.

EXPERIMENTAL

Instrumentation

The reagent was driven by a four-channel peristaltic pump, a Minipuls 2 (Gilson, France). Silicone rubber tubing was chosen in order to withstand the very reactive K.F. reagent. Several other tubings were investigated but none was found to be sufficiently inert.

Spectrophotometric detector. The spectrophotometer, built in this department, consisted of a small grating monochromator, (Model GM 100, Schoeffel Instrument GmbH, Germany), a lens lamp, a u.v.-enhanced photodiode and a flow-through cuvette (Helma Model 178, 31-QS, volume 8 μ l, light path 10 mm).

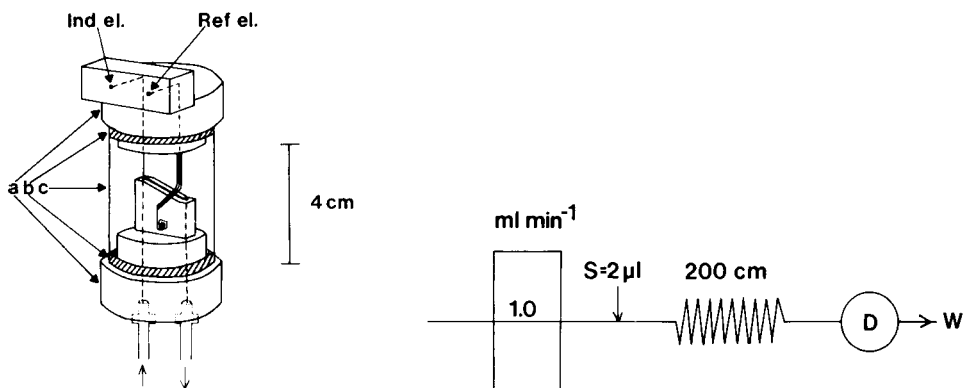


Fig. 1. The potentiometric flow cell. (a) Teflon blocks; (b) O-rings; (c) glass cylinder.

Fig. 2. Flow injection manifold for spectrophotometric or potentiometric determination of water in organic solvents with Karl Fischer reagent. (S) Point of injection (sample loop); (D) detector; (W) waste.

Potentiometric detector. The configuration of the potentiometric detector is shown in Fig. 1. The carrier solution was pumped through a 0.5-mm hole in the lower teflon block, into which a 0.1-mm platinum wire indicator electrode was inserted. The solution then passed down a groove of the declining part of the teflon block to the exit.

The indicator electrode was inserted 3 cm into the hole. If the electrode just reached the exit of the bore there was an increase in the sensitivity but the stability and reproducibility were very poor. These drawbacks arise from the fact that the electrode must be very precisely and reproducibly located in the flowing stream. By inserting to a distance of 3 cm, these disadvantages can be almost eliminated. By filling the cell just to a point at which there was only a small liquid film between the exit solution and the residual cell solution, mixing in the cell was kept to a minimum. The other platinum electrode was insulated except for the terminating spiral; since it is exposed to an almost unchanging environment it can function as a pseudo-reference system. The small change in the reagent in the cell compartment does not significantly affect the measurement. No serious error should result from a systematic drift because the peak height is always related to the base-line.

The platinum pseudo-reference electrode was chosen partly because of the inertness of platinum and partly to achieve an air-tight cell with exclusion of water.

Potentiometer and recorder. The signals from the two detectors were monitored either by a lin-log amplifier or by a follower connected to a HP Moseley 680 recorder. Additionally, an interface was inserted between the amplifiers and the recorder, which allowed the peak maximum to be locked automatically on a meter while the recorder continuously displayed the actual potential output [14].

Reagents and standards

All organic liquids were of analytical grade. Solvents were dried before use with molecular sieves (3 or 4 Å). The mixtures of water and the organic solvents were standardized coulometrically [15]. All solutions were calibrated except for the acetone mixtures. Owing to the formation of water by the ketal reaction, a graphical estimation of the concentration of water in dried acetone was done amperometrically; it was found to be below 0.01%. This was possible by performing the determination at a high concentration of iodine, so that the rate of the main reaction was sufficiently high to permit a differentiation.

The Karl Fischer reagent contained 25.4 g of iodine, 38.4 g of sulphur dioxide and 80 ml of pyridine, diluted to 1 l with methanol [16, 17].

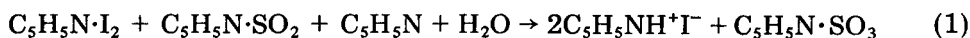
Manifold and measurement technique

The manifold used in the flow-injection system is outlined in Fig. 2. The tubings were made from teflon (0.5 mm i.d.) and the end-connectors were ordinary chromatographic connectors (Altex). Samples (2 μ l) were injected with a standard liquid chromatography inlet slide valve for low pressure (Cheminert) at point S into the carrier and reagent stream of Karl Fischer solution which was pumped at a flow rate of 1 ml min⁻¹. After the injection, a 200-cm reaction coil sufficed to achieve the desired reaction. The change in concentration of the reagent was then measured either spectrophotometrically at 625 nm or potentiometrically with the platinum electrode system.

RESULTS AND DISCUSSION

Kinetics

The main Karl Fischer reaction, according to Mitchell [18], is



which, in the presence of methanol, proceeds further



This reaction scheme has been criticized by several investigators. Verhoeff and Barendrecht [12] proposed the existence of a methyl-sulphite complex instead of the pyridine-sulphur dioxide complex. The kinetics of reaction (1) have been studied in two independent reports and it has been shown that the reaction is first order with respect to the concentration of iodine, sulphur dioxide and water [12, 17]. The value of the rate constant in 0.20 M solution of iodide has been estimated to be about $1 \times 10^3 \text{ l}^2 \text{ mol}^{-2} \text{ s}^{-1}$ [12, 13, 17]. This value increases with decreasing concentration of iodide. For example, the value of the rate constant is enhanced by a factor of two when the concentration of iodide is lowered from 0.20 M to 0.15 M as estimated from the diagram given by Verhoeff [19].

In order to estimate the time needed for a complete reaction to take place under conditions appropriate to flow-injection analysis, the following calculation was performed. The iodine concentration of the Karl Fischer reagent used was assumed to be 0.04 M and the concentration of sulphur dioxide to be 0.54 M. Further it was assumed that 2 μl of a sample containing 3% of water was introduced and mixed instantaneously with 100 μl of the reagent and that no further dilution occurred during transport to the detector. The time required for 99.9% reaction should then be about 2 s. The value of the rate constant used in these calculations, $1 \times 10^3 \text{ l}^2\text{mol}^{-2}\text{s}^{-1}$, should have been somewhat higher because the concentration of iodide in this example never exceeds 0.18 M.

These calculations were complemented by f.i.a. experiments performed under conditions corresponding to the discussed example. In these experiments, which are summarized in Fig. 3, the signal from the spectrophotometric detector was measured as a function of the reaction coil length. It can be seen that the peak height increases with increasing residence time, passes through a maximum, and then decreases again. The rising part of the curve corresponds to a situation where the dispersion is not sufficiently

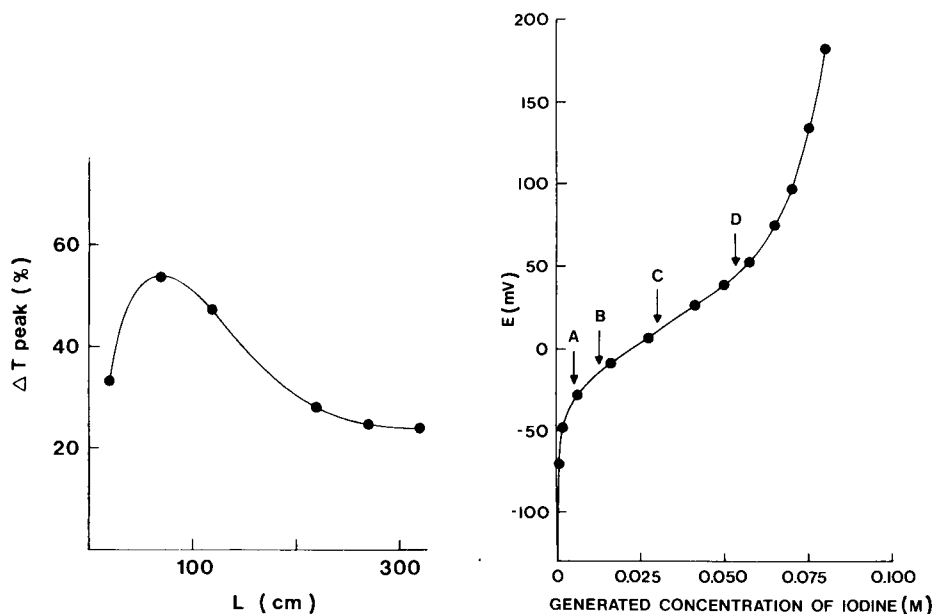


Fig. 3. Dependence of the peak height on the reaction coil length (L). Samples (2 μl) containing 3% water in ethanol were injected into a flow (1 ml min^{-1}) of 0.04 M Karl Fischer reagent.

Fig. 4. The potential of the platinum electrode as a function of iodine concentration generated in a coulometric cell. The starting concentration of iodide was 0.2 M.

large to allow iodine to be in excess of water. Consequently, it is difficult to estimate the shortest time needed for completion of the main reaction. Nevertheless, the shape of the curve to the right of the maximum value in Fig. 3 indicates that the main reaction has been completed. The extent of dispersion will thus determine the shape of the latter part of the curve.

The potentiometric detector

As noted previously [16], stable redox potential values are obtained with a platinum electrode in Karl Fischer titrations. A platinum electrode was used in a recent investigation of redox potentials of the Ce(III)/Ce(IV) couple [20] by the f.i.a. technique. In order to characterize the redox properties of a platinum electrode in the configuration used here, values of the electrode potential were determined as a function of the concentration of iodine, which was generated by constant-current coulometry; the results are shown in Fig. 4. The shape of the potentiometric curve indicates the existence of the strong triiodide complex between iodine and iodide. Thus, for low iodine concentrations the potential-determining factor is probably the logarithm of $[I_3^-]/[I^-]^3$ while for high concentrations of iodine the logarithm of $[I_2]^3/[I_3^-]^2$ will predominate. The points marked A, B, C and D in Fig. 4 denote the various strengths of the Karl Fischer reagent used in the study represented in Fig. 5. This figure shows the response of the potentiometric detector for the various strengths of Karl Fischer reagent as a function of the

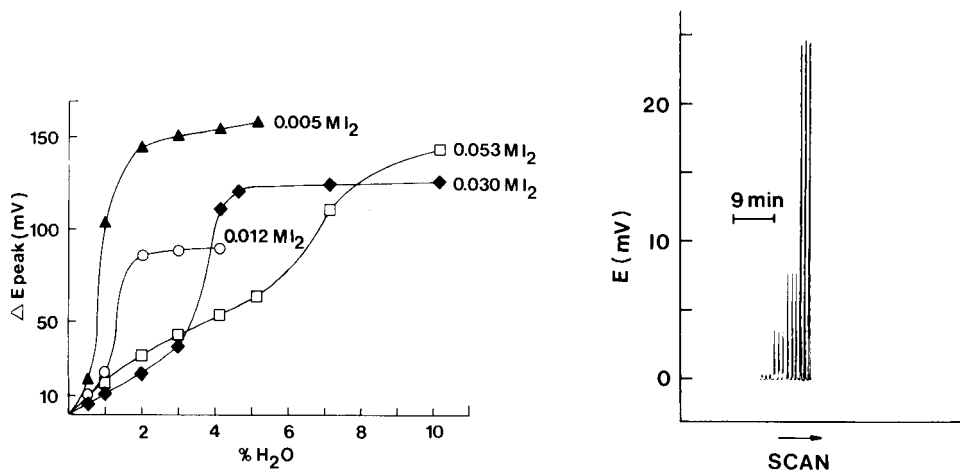


Fig. 5. Peak height values obtained with the potentiometric detector as a function of the percent water in ethanol for various strengths of the Karl Fischer reagent. The total concentration of iodide was 0.2 M in each of the reagents.

Fig. 6. Recorder output from the potentiometric detector for the determination of water in acetonitrile. The signals from left to right correspond to 0.10, 0.49, 0.99 and 2.77% of water, respectively.

concentration of water in the sample. As can be seen, there are large differences in the shapes of the curves. However, comparison of the curves obtained in the flow-injection experiments with the results shown in Fig. 4 indicates that the shapes of approximately the first 3/4 of each curve fit very well. The disagreement between the last quarters of the curves can be explained by either incomplete main reaction or by slow response of the indicator electrode for low iodine concentrations. As indicated in Fig. 4, the working concentration range as well as the sensitivity can be further increased if higher iodine concentrations than 0.05 M are used provided that the total concentration of iodine is the same. In practice, it is difficult to prepare such a strong reagent because of side reactions and moisture in the chemicals used. One simple way, illustrated in Fig. 4, involves electrical preparation of the reagent. The kinetics of the main reaction should be extremely rapid for very high concentrations of iodine mainly because of the low concentration of iodide present in such a reagent.

The precision of the potentiometric measurement is given in Table 1 for a 0.058 M Karl Fischer reagent; the relative standard deviation is less than 0.5% over the whole concentration range. This implies that the stability of the detector is very good; this is also demonstrated in Fig. 6 which shows a recorded scan of some samples in the concentration range 0.1–3% of water.

The spectrophotometric detector

Figure 7 shows the response of the spectrophotometric detector as a function of the concentration of water in the sample for three different strengths of the Karl Fischer reagent. These results were obtained at 625 nm; at this wavelength no significant absorbance is obtained for a spent reagent. It can be seen that the linear range of the calibration curve can be extended but at the expense of decreased sensitivity. The fact that linear curves are obtained over a large concentration range of water indicates that the reaction is almost complete and that Beer's law is followed. Although it is not clearly seen in Fig. 7, there is a slight deviation from linearity in the first part of the curves. This cannot be explained at present but is currently being investigated. The precision of the measurements is given in Table 1 for a 0.033 M Karl Fischer reagent. The percent standard deviation varies between 0.5 and 1.5% which is about three times that obtained with the potentiometric detector. The stability is illustrated in Fig. 8 which shows a recorded scan of some samples in the concentration range 0.1–3% water.

Effects of solvents

Figure 9 shows the influence of various solvents on the potentiometric and spectrophotometric determinations of water, respectively. The shapes of the curves are in good agreement with those shown in Figs. 5 and 7. Owing to the formation of water through the reaction between acetone and methanol, the acetone curve lies above all other curves in both diagrams. The slight deviations between the remaining curves may be due to several factors,

TABLE 1

Determination of water in ethanol with the potentiometric and spectrophotometric detectors. Reagents: ordinary 0.058 M Karl Fischer reagent for the potentiometric method and ordinary 0.033 M Karl Fischer reagent (wavelength 625 nm) for the spectrophotometric method.

Potentiometric detector			Spectrophotometric detector		
H ₂ O (%)	Peak height (mV)	R.s.d. (%)	H ₂ O (%)	Peak height (abs.)	R.s.d. (%)
0.110	3.36	0.47	0.110	0.014	1.0
0.550	13.1	0.54	0.615	0.065	1.5
1.06	21.0	0.41	1.06	0.106	1.2
2.97	46.1	0.19	2.97	0.306	0.23
4.83	63.2	<0.1	4.83	0.497	0.50

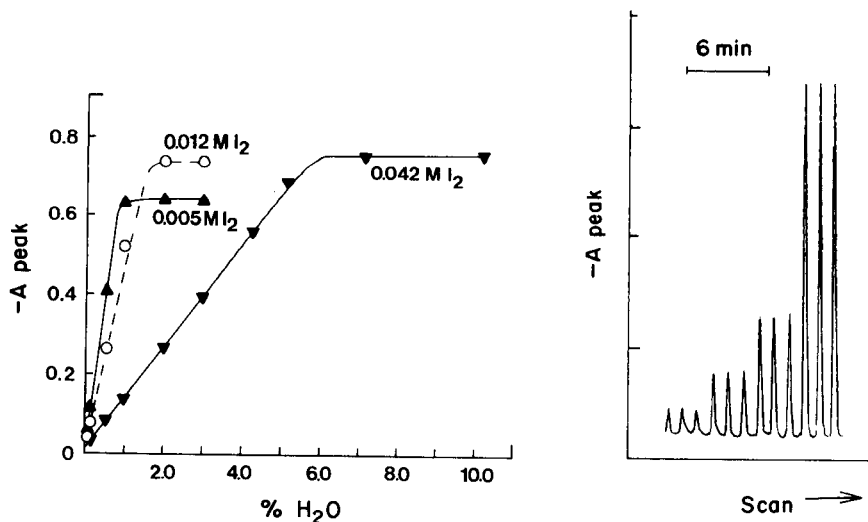


Fig. 7. Peak height values obtained with the spectrophotometric detector as a function of the percent water in ethanol for various strengths of the Karl Fischer reagent. The total concentration of iodide was 0.2 M in each of the reagents.

Fig. 8. Recorder output from the spectrophotometric determination of water in acetonitrile. The signals from left to right correspond to 0.10, 0.49, 0.99 and 2.77% of water, respectively.

but they are surprisingly small in view of the very different properties of the solvents chosen for these experiments. The viscosity, for example, varies between 0.32 and 2.3 centipoise. Further, various contributions from the solvent polarity to the dispersion might be considered as a consequence of the variation in the dielectric constants. The values for acetic acid and acetonitrile

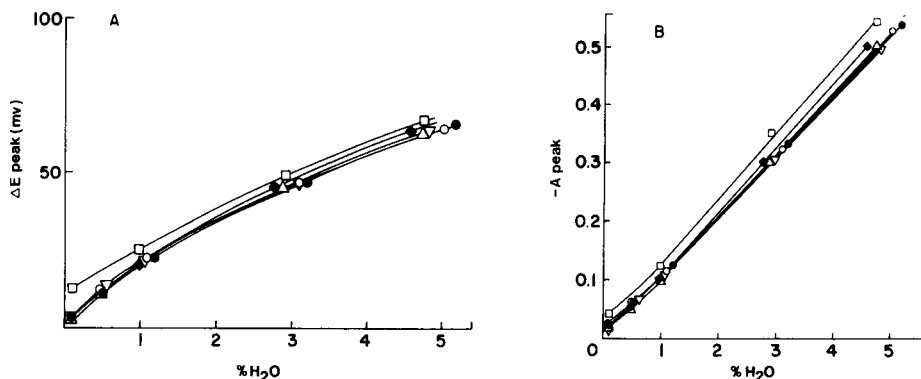


Fig. 9. Potentiometric (A) and spectrophotometric (B) calibration curves for the determination of water in different organic solvents. (♦) acetonitrile; (○) propanol; (◻) acetone; (▽) ethanol; (△) methanol; (●) acetic acid. The strength of the Karl Fischer reagent was 0.06 M for potentiometric measurements and 0.03 M for spectrophotometric measurements (at 625 nm).

are 6 and 37, respectively. In addition, adsorption effects between the solvents and the teflon tube may occur, and this might also influence the extent of dispersion. A closer examination of the shapes of the peaks showed that their form is not exactly the same for different solvents. These effects are under study at present.

As demonstrated in Fig. 9 the determination of water in acetone is easily performed with the f.i.a. technique. Such determinations are troublesome when the conventional Karl Fischer batch titration procedure is used. Similar advantages with the f.i.a. technique were obtained for acetic acid, because there was no noticeable contribution from the water produced in the esterification reaction between this acid and methanol.

CONCLUSIONS

This proposed method yields results which are comparable in precision and accuracy with those obtained by using the conventional Karl Fischer procedure. The advantages and disadvantages, which are concerned with the present state of the method, can be summarized as follows.

One advantage is the rapidity of the determination: the f.i.a. method is at least ten times faster than the conventional Karl Fischer method. Safety is improved, because the closed system prevents the analyst from coming in contact with the toxic reagent except during reagent loading. There is less influence from interfering side-reactions compared with the conventional batch titration. Another great advantage is the low cost per determination; about 2000 determinations can be made per litre of reagent.

Among the disadvantages, the sensitivity is not as good as that obtained with the conventional Karl Fischer method. However, the method described has not been optimized with respect to sensitivity. Simply by increasing the

sample volume, the working range of the method might be extended to 0.001–5% of water. Another disadvantage is the variation in results caused by solvent effects. The origin of this variation is under study and, on the basis of increased knowledge, it should be possible to design an f.i.a. system which can compensate for this.

REFERENCES

- 1 J. Mitchell, Jr. and D. M. Smith, *Aquametry Part 1: A Treatise of Methods for the Determination of Water*, 2nd edn., Wiley, New York, 1977.
- 2 J. Růžicka and E. H. Hansen, *Anal. Chim. Acta*, 78 (1975) 145. Dan. pat. appl. No. 4846/74 (1974), U.S. pat. 4,0022,575.
- 3 J. Růžicka and J. W. B. Stewart, *Anal. Chim. Acta*, 79 (1975) 79.
- 4 J. W. B. Stewart, J. Růžicka, H. Bergamin Filho and E. A. Zagatto, *Anal. Chim. Acta*, 81 (1976) 371.
- 5 J. Růžicka, J. W. B. Stewart and E. A. Zagatto, *Anal. Chim. Acta*, 81 (1976) 387.
- 6 J. W. B. Stewart and J. Růžicka, *Anal. Chim. Acta*, 82 (1976) 137.
- 7 J. Růžicka and E. H. Hansen, *Anal. Chim. Acta*, 87 (1976) 353.
- 8 J. Růžicka, E. H. Hansen and E. A. Zagatto, *Anal. Chim. Acta*, 88 (1977) 1.
- 9 E. H. Hansen, J. Růžicka and B. Rietz, *Anal. Chim. Acta*, 89 (1977) 241.
- 10 J. Růžicka, E. H. Hansen and H. Mosbaek, *Anal. Chim. Acta*, 92 (1977) 235.
- 11 J. Růžicka and E. H. Hansen, *Anal. Chim. Acta*, 99 (1978) 37.
- 12 J. C. Verhoeff and E. Barendrecht, *J. Electroanal. Chem.*, 71 (1976) 305.
- 13 A. Cedergren, *Talanta*, 25 (1978) 229.
- 14 E. Lundberg, *Appl. Spectrosc.*, 32 (1978) 276.
- 15 A. Cedergren, *Talanta*, 21 (1974) 367.
- 16 A. Cedergren, *Talanta*, 21 (1974) 553.
- 17 A. Cedergren, *Talanta*, 21 (1974) 265.
- 18 J. Mitchell, Jr. and D. M. Smith, *Aquametry*, Interscience, New York, 1948.
- 19 J. C. Verhoeff, *Mechanism and Reaction Rate of the Karl-Fischer Titration Reaction*, Dissertation, Amsterdam, 1977, p. 92.
- 20 B. Karlberg and S. Thelander, *Analyst*, 103 (1978) 1154.

FLOW INJECTION ANALYSIS FOR MONITORING CHEMILUMINESCENT REACTIONS

J. L. BURGUERA and ALAN TOWNSHEND*

*Chemistry Department, University of Birmingham, P.O. Box 363, Birmingham
B15 2TT (Gt. Britain)*

S. GREENFIELD

*Albright and Wilson, P.O. Box 80, Oldbury, Warley, W. Midlands B69 4LN
(Gt. Britain)*

(Received 18th August 1979)

SUMMARY

Various coiled flow cells are tested for monitoring the chemiluminescence produced by the cobalt-catalysed oxidation of luminol by hydrogen peroxide and the fluorescein-sensitized oxidation of sulphide by sodium hypochlorite. When a 6-coil cell is used, 10^{-3} –100 ng of Co^{2+} and 1–1000 ng of S^{2-} can be determined in 10- and 100- μl samples, respectively.

Chemiluminescent reactions usually produce transient emissions. Thus, in order to measure such emissions generated in a flow system, the emitting species must be within the path of the detector whilst the emission is occurring. In the first example of flow injection analysis based on chemiluminescent detection, in which copper was used to catalyse the luminol–hydrogen peroxide reaction, this was achieved by passing the solutions through a coil of tubing placed in front of a photomultiplier [1]. Burguera and Townshend [2] investigated the effects of various mixing chamber designs and flow rates for achieving maximum light output whilst the mixed solutions were in view of the detector. They used the chemiluminescence produced by benzoyl peroxide oxidation of amines [3], and showed that a 2-ml cell, with solvent and amine pumped in at 0.08 ml s^{-1} and oxidant at 0.04 ml s^{-1} gave the greatest light intensity. Such a procedure gave improved detection limits, precision and linear ranges for the determination of amines, and of cobalt by its catalysis of the luminol–hydrogen peroxide reaction [2], compared to direct injection into a stationary solution in a cell. Additional advantages are the introduction of the sample into the flow system remote from the mixing chamber, thus avoiding the problems that can occur with stray light when a syringe is introduced directly into the mixing chamber, and the continuous use of the same mixing cell, thus avoiding problems with replacement of cells after each measurement and of discrete dosing of reagents.

This paper reports some further improvements in the use of flow injection analysis for monitoring chemiluminescent reactions, in which the mixing chamber is replaced by various coils placed in front of the detector. The cobalt(II)-catalysed oxidation of luminol [2] by hydrogen peroxide and the oxidation of sulphide by sodium hypochlorite in the presence of fluorescein [4, 5] are studied as typical chemiluminescent reactions of analytical utility.

EXPERIMENTAL

Apparatus

The chemiluminescence measurements were carried out in the flow system shown in Fig. 1. The sample was injected by means of a 10- μ l glass syringe through a self-sealing rubber septum into a premixed reagent stream. The solutions passed through the coiled flow cell shown in Fig. 2, which was positioned in the cell compartment in front of the circular (ca. 1.6-cm diameter) lens focused on the detector of a Cecil CE202 spectrophotometer. The coil tubing was of 2-mm i.d.

Reagents

All reagents were laboratory-reagent grade, unless otherwise stated, and all water was double-distilled.

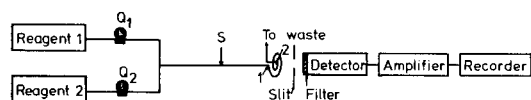


Fig. 1. Flow injection apparatus used for chemiluminescence measurements. $Q_1 = 0.08$, $Q_2 = 0.04$ ml s^{-1} ; 100 mm of teflon tube, 3.5 mm i.d., from sample injection point (s) to cell entrance (1). Point 2 is the cell exit.

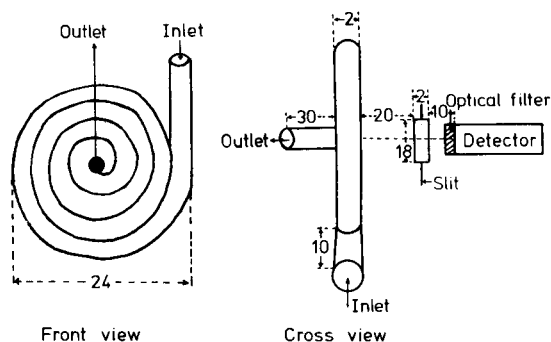


Fig. 2. The 4-coil glass flow cell and its position with respect to the detector (dimensions in mm).

Stock luminol solution (10^{-3} M) was prepared by dissolving 0.0307 g of luminol (B.D.H.) in 250 ml of 0.1 M sodium carbonate buffer, pH 10.0.

Stock cobalt(II) solution ($100 \mu\text{g ml}^{-1}$) was prepared by dissolving 0.0403 g of $\text{CoCl}_2 \cdot 6\text{H}_2\text{O}$ in 100 ml of double-distilled water. Working solutions were prepared daily by appropriate dilution with water.

Stock sulphide solution ($100 \mu\text{g ml}^{-1}$) was prepared by dissolving 0.075 g of $\text{Na}_2\text{S} \cdot 9\text{H}_2\text{O}$ (B.D.H.) in 0.1 M sodium carbonate buffer, pH 11.5, and diluting to 100 ml with this buffer solution. Working solutions were prepared daily by appropriate dilution with the buffer solution.

Sodium hypochlorite (0.1 M) and hydrogen peroxide (0.01 M) were prepared from a sodium hypochlorite solution (12% w/v available chlorine; Hopkin and Williams) and 100-volume hydrogen peroxide solution (Fisons), respectively.

Fluorescein solution (10^{-3} M) was prepared by dissolving 0.0322 g of fluorescein (B.D.H.) in 100 ml of the carbonate buffer solution, pH 11.5.

Basic procedure for chemiluminescence measurements with the coiled cell

The reagent streams (see Fig. 1) were of hydrogen peroxide (Q_1) and luminol (Q_2) or sodium hypochlorite (Q_1) and fluorescein (Q_2) for the determination of cobalt(II) or sulphide, respectively. The reaction was started by rapidly injecting (in < 0.5 s) 10 μl or 100 μl of cobalt(II) or sulphide solution, respectively, into the mixed reagent stream. The emission intensity was recorded as a function of time over 5 s at 425 nm and 520 nm for the cobalt and sulphide systems, respectively. For calibration purposes the experiment was repeated with each standard solution of cobalt(II) or sulphide. Calibration graphs were constructed of maximum emission intensity vs. cobalt(II) or sulphide concentration.

The same procedure was used to determine 'unknown' samples.

The procedures based on the mixing cell and pulse techniques were as described previously [2, 3].

RESULTS

Injection of a cobalt(II) solution into a hydrogen peroxide—luminol stream produced a chemiluminescence emission which reached maximum intensity after 3 s and then decayed rapidly. Similarly, injection of sulphide into the hypochlorite—fluorescein solution produced maximum intensity after 4 s. Typical emission—time responses are shown in Figs. 3 and 4.

The effect of the number of coils in the flow cell is shown in Fig. 5 for the cobalt system. The increase in the number of coils was achieved by adding to the outermost coil, thus the overall diameter of the cell increased with the number of coils. Under the flow conditions used, greatest emission intensity was obtained in the 6-coil cell (0.6-ml capacity). Under these conditions the time taken from injection to entering the cell (point 1 in

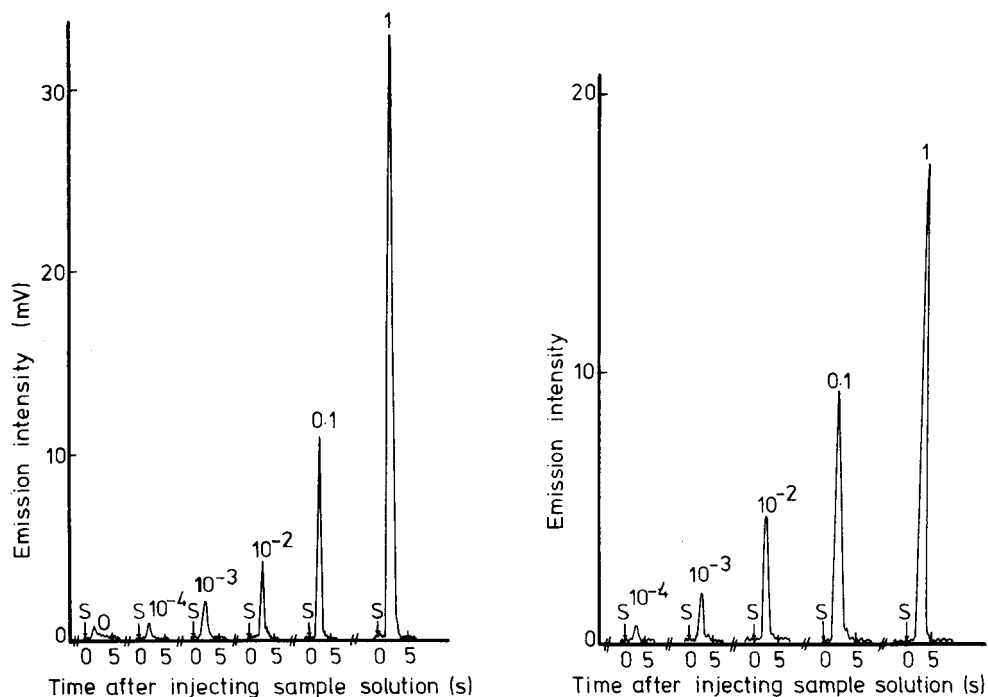


Fig. 3. Responses obtained in a 6-coil cell by injecting $10 \mu\text{l}$ of cobalt(II) solutions; $0.01 \text{ M H}_2\text{O}_2$ (0.08 ml s^{-1}), 10^{-3} M luminol-pH 10.0 carbonate buffer (0.04 ml s^{-1}). Numbers are ng of cobalt in the injected solution.

Fig. 4. Responses obtained in a 6-coil cell by injecting $100 \mu\text{l}$ of sulphide solutions; 0.1 M NaOCl (0.08 ml s^{-1}), 10^{-3} M fluorescein, pH 11.5 (0.04 ml s^{-1}). Numbers are μg of sulphide in the injected solution.

Fig. 1) in all systems was 0.8 s ; the time taken for the solution to flow through the 6-coil cell was 5.0 s . This gave adequate time for maximum emission to occur whilst the emitting solution was within view of the detector. The 2-coil cell, which required only 1.6 s for the solution to flow through it, did not allow maximum intensity to be achieved before the solution left the cell (at point 2 in Fig. 1). The 4-coil cell had an intermediate behaviour, the flow-through time being 2.4 s . Obviously, the times, etc., will change with the flow rates used.

The effect of the sample volume injected was studied for both reactions. Figure 6 shows the effect of volume for the cobalt-catalysed reaction with 4- and 6-coil cells. Greater emission is achieved with a smaller volume in the smaller cell; $10 \mu\text{l}$ was found to give the greatest intensity for cobalt and $100 \mu\text{l}$ for sulphide in a 6-coil cell.

Calibration graphs were obtained for each of the systems investigated. In Figs. 7 and 8, the log-log graphs are compared with those obtained by using the mixing cell flow system [2] and a pulse injection system, in which the sample is injected into a stationary mixture of reagents in front of a

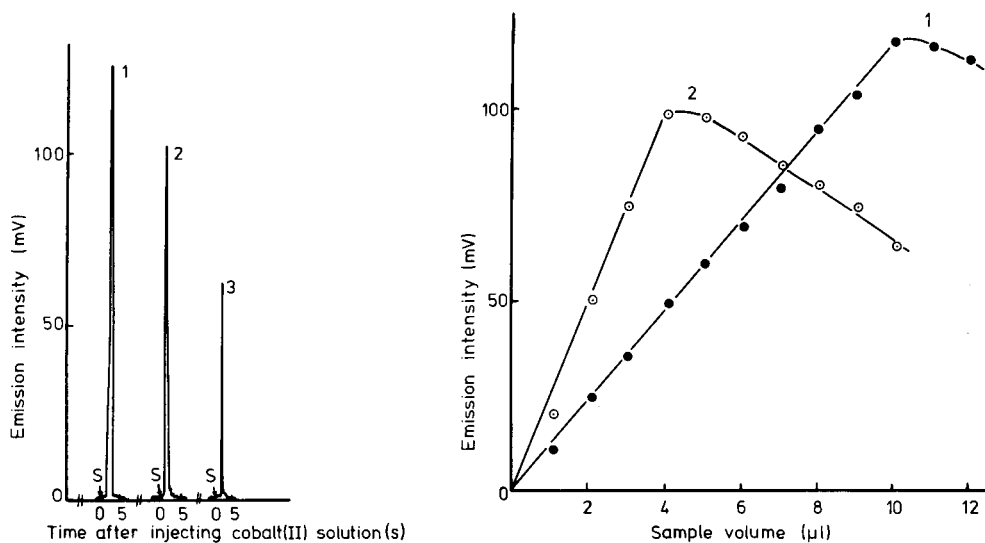


Fig. 5. Responses obtained in cells with (1) 6 coils, (2) 4 coils and (3) 2 coils by injecting $10 \mu\text{l}$ of 1 ppm cobalt(II) solution. Other conditions as in Fig. 3.

Fig. 6. Effect of sample volume for (1) a 6-coil cell, and (2) a 4-coil cell; $0.01 \mu\text{g}$ of cobalt(II); other conditions as in Fig. 3.

detector [3]. The increase in sensitivity over the pulse technique, and the rather lesser increase over the previous flow system, are readily apparent. The detection limits (2σ) obtained by the present technique were 0.1 and $0.6 \mu\text{g}$ of cobalt in sample volumes of 10 and $100 \mu\text{l}$, respectively. The coefficients of variation for 1 ng of cobalt were 1.5, 2.2 and 6.0% (5 measurements each) for the 6-coil cell, mixing cell and pulse techniques, respectively. For sulphide, the detection limit was 0.4 ng in a sample volume of 1 ml. The coefficient of variation was 4.4% for 100 ng of sulphide (6 measurements).

DISCUSSION

The flow system involving the coiled cell provides an extremely sensitive and simple means of monitoring chemiluminescent reactions. The results achieved are precise and can be obtained in a few seconds. The systems used in the present investigation allow determinations of 10^{-3} – 100 ng of cobalt and 1 – 1000 ng of sulphide. The particular sulphide system was chosen for its relative insensitivity; other systems in which hydrogen peroxide catalysed by peroxidase or osmium tetroxide is used are at least 100 times as sensitive [5]. A further advantage of the present system is the very small blank emission. Chemiluminescence stimulated by trace metals or other impurities in the reagents will be generated soon after reagent mixing, and may have decayed before entering the measuring cell. Thus

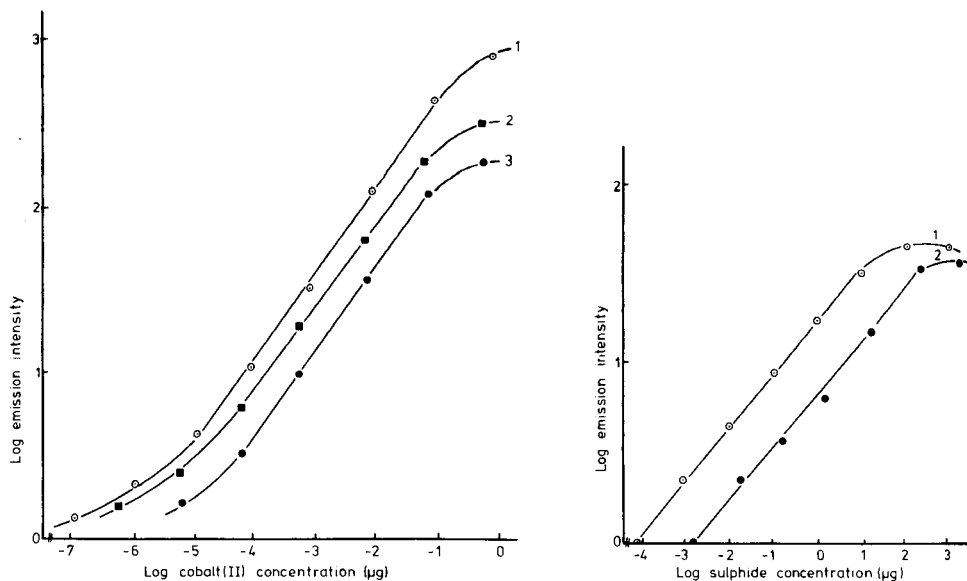


Fig. 7. Calibration graphs for cobalt(II) obtained with three different mixing systems: (1) 6-coil cell, 10- μ l sample, 0.01 M H_2O_2 (0.08 ml s^{-1}), 10^{-3} M luminol—pH 10.0 carbonate buffer (0.04 ml s^{-1}); (2) flow system with a 2.0-ml mixing cell, 300- μ l sample, luminol and H_2O_2 stream (0.04 ml s^{-1}), double-distilled water stream (0.08 ml s^{-1}); (3) pulse technique, 600- μ l sample, other concentrations as in (1).

Fig. 8. Calibration graphs for sulphide obtained with two different mixing systems: (1) 6-coil cell, 100- μ l sample, 0.1 M NaOCl (0.08 ml s^{-1}), 10^{-3} M fluorescein, pH 11.5 (0.04 ml s^{-1}); (2) pulse technique, 1-ml sample, other concentrations as in (1).

only impurities introduced with the sample are likely to contribute to the blank emission.

The system described is an attempt to evaluate some characteristics of a flow system for monitoring chemiluminescent signals. The requirements are somewhat different from those systems in which non-transient signals are measured. In particular, the maximum intensity of the transient signal is very much dependent on the rate of mixing of sample and reagent. Thus devising means of achieving rapid mixing whilst retaining as much as possible of the simplicity of the flow injection technique are likely to be a priority in the continuing investigations on this topic.

J. L. Burguera thanks FONINVES, Venezuela, for financial support.

REFERENCES

- 1 G. Rule and W. R. Seitz, Paper No. 18, 11th Annual Symp. on Advanced Analytical Concepts for the Clinical Laboratory, Oak Ridge, Tenn., April 1979.
- 2 J. L. Burguera and A. Townshend, Proc. Anal. Div. Chem. Soc., 16 (1979) 263.
- 3 H. L. Burguera and A. Townshend, Talanta, 26 (1979) 795.
- 4 D. Klockow and J. Teckentrup, Talanta, 23 (1976) 889.
- 5 J. L. Burguera and A. Townshend, Talanta, in press.

EXTRACTION BASED ON THE FLOW-INJECTION PRINCIPLE Part 4. Determination of Extraction Constants

PER-ARNE JOHANSSON*, BO KARLBERG** and SIDSEL THELANDER

Astra Pharmaceuticals AB, Analytical Control, S-151 85 Södertälje (Sweden)

(Received 29th August 1979)

SUMMARY

A new approach to the determination of extraction constants is described. The aqueous and organic phases, the former containing the counter ion, are pumped continuously as small segments through an extraction coil. The sample ion is introduced into the aqueous phase before it enters the coil, where the ion-pair extraction takes place (during 20 s). After leaving the extraction coil, a certain fraction of the organic phase is pumped through the flow-cell of the spectrophotometer. The extraction constants are calculated by slope analysis from the experimental data (absorbance and counter ion concentration). The constants usually agreed within ± 0.1 (log units) with values obtained from batch experiments.

In Part 2 of this series [1] a flow-injection method for the determination of codeine by ion-pair extraction was described. Suitable extraction conditions were calculated by use of the acid dissociation and distribution constants for codeine and picric acid and the extraction constant for the ion pair between codeine and picrate.

Extraction constants are mostly determined by batch extraction which is a relatively time-consuming procedure. The aqueous and organic phases are usually shaken for at least 20 min. After centrifugation, the organic phase is syphoned off and the equilibrium concentration of the ion pair is measured (usually spectrophotometrically) [2]. Recently, mechanization of the batch extraction procedure has been described, either by use of an AKUFVE apparatus [3] or related spectrophotometric titration equipment [4]. Other rapid methods have also been developed, but these have been based on different principles such as t.l.c. [5] and potentiometric two-phase titration [6, 7].

Continuous extraction systems both with [8–11] and without [1, 12–14] air segmentation have been devised for ion-pair extractions, but so far there has been no report of the use of such a system for the determination of extraction constants. In the present paper, therefore, the design of a flow-injection system for this purpose is discussed. The possibilities and limitations of flow injection for the determination of extraction constants are also considered.

**Present address: Bifok AB, S-194 05 Upplands-Vasby, Sweden.

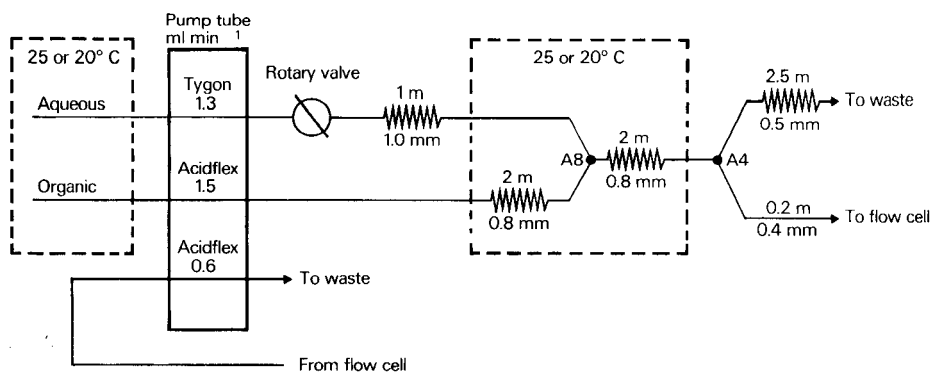


Fig. 1. Manifold for the determination of extraction constants.

EXPERIMENTAL

Apparatus

The flow-injection system is shown in Fig. 1. The aqueous and organic phases were pumped by a four-channel peristaltic pump (Gilson Medical Electronics, France) fitted with Tygon and Acidflex pump tubes (Technicon, Tarrytown, U.S.A.). All other tubing was of teflon, the lengths and inner diameters being given in Fig. 1. The diameters of the coils were 4 cm, except for the coil in the aqueous phase (the mixing coil) which had a diameter of 1.5 cm.

The sample was introduced into the aqueous phase via a rotary valve with a volume of $40 \mu\text{l}$ (Rheodyne, Berkeley, U.S.A.) or $25 \mu\text{l}$ (Bifok AB, Upplands-Väsby, Sweden). Segments of aqueous and organic phase of length 2–3 mm were obtained by the segmentor as described previously [1]. The separator was also the same as used previously [15]. The absorbance of the organic phase was measured at 355 nm in a spectrophotometer with a $10\text{-}\mu\text{l}$ flow cell (Spectromonitor II, LDC, Riviera Beach, U.S.A.) and a recorder (Kontron, Zurich).

The aqueous and organic phases as well as the extraction coil were thermostatted in a water bath at 20°C or 25°C (Fig. 1). The pH of the aqueous phase was measured before equilibration with the organic phase.

Chemicals and reagents

Amantadine hydrochloride (Hässle—Ciba—Geigy AB, Mölndal, Sweden), brompheniramine maleate, codeine phosphate and metoprolol tartrate were of pharmacopoeial grade. Tetraethylammonium bromide, tetrapropylammonium bromide and sodium octyl sulphate (Eastman Kodak, N.Y., U.S.A.) were used as obtained. Chloroform (p.a.) was shaken several times with water to remove ethanol.

Phosphate buffers of pH 6.49 (unless otherwise stated) and ionic strength 0.1 were prepared by dissolving known amounts of sodium dihydrogenphosphate and disodium hydrogenphosphate in water.

Buffered picrate solutions were prepared by neutralizing picric acid with sodium hydroxide and adding hydrogenphosphates and water as above. These solutions were degassed before use. All other chemicals and reagents were of analytical grade.

Procedure

The aqueous and organic phases are pumped through the system before each run during at least 30 min in order to obtain stable flow rates. The sample (amine salt or quaternary ammonium compound) is dissolved in phosphate buffer and this solution is injected into the aqueous stream of the same pH and ionic strength but also contains $(1-10) \times 10^{-3}$ M picrate. The concentration of the sample is chosen so that an absorbance of 0.7–0.9 is obtained at peak maximum when the sample is injected into the 10^{-2} M picrate solution. When changing to a new aqueous phase in a run, this solution is pumped through the system for 2 min before the sample is injected. The injections are carried out at least in duplicate; the absorbances at the peak maxima should agree to within a factor of 0.98–1.02. The flow rates of the aqueous and organic phases are measured immediately before and after each run. Finally the extraction constant is calculated by slope analysis.

RESULTS AND DISCUSSION

The determination of an extraction constant, i.e. the equilibrium constant for the process $\text{HB}^+ + \text{P}^- \rightleftharpoons \text{HBP}_{\text{org}}$, can be carried out by the flow-injection technique in several ways. The symbols used are defined in Table 1. The aqueous and organic phases are pumped continuously through narrow tubes. An aqueous sample is introduced into the aqueous stream and an organic one into the organic stream. After segmentation, equilibrium is attained in a helical coiled tube of sufficient length. Then a fraction of the organic or aqueous phase is pumped through a detector, by which HBP_{org} or, for instance, HB^+ is measured (see Table 2).

In the present paper, a flow-injection system in which the ion pair is measured spectrophotometrically in the organic phase is discussed. The samples are injected into the aqueous phase (Table 2, mode 1).

Dispersion of the sample

The total dispersion, D_{tot} , in the flow-injection system is defined [16] by $D_{\text{tot}} = C_{\text{HB}}^0([\text{HBP}]_{\text{cell}})^{-1}$. For an extraction system it may be convenient to divide the system into two parts and consider the dispersion before and after the extraction coil. The dispersion within the extraction coil is assumed to be negligible [1, 15]. The following relations will then be valid: $D_{\text{pre}} = C_{\text{HB}}^0(C_{\text{HBmix}})^{-1}$; $D_{\text{post}} = [\text{HBP}]_{\text{org}}([\text{HBP}]_{\text{cell}})^{-1}$ and $C_{\text{HBmix}} = C_{\text{HB}} = [\text{HB}^+] + r[\text{HBP}]_{\text{org}}$. Combination of these equations with the extraction constant gives:

$$D_{\text{tot}} = D_{\text{pre}}D_{\text{post}}(r + (K_{\text{ex(HBP)}}[\text{P}^-])^{-1}) \quad (1)$$

TABLE 1

Symbols used

HB^+ = organic ammonium ion; B = unprotonated amine
 P^- = extractable, light-absorbing anion, e.g. picrate
 Y^- = extractable anion (not light-absorbing)
 $[\text{B}]$ and $[\text{B}]_{\text{org}}$ = highest molar concentration of B in the aqueous and organic phase, respectively, in the sample zone at equilibrium (in the extraction coil immediately before the separator)
 a_{H^+} = hydrogen ion activity
 $K_{\text{HB}} = a_{\text{H}^+}[\text{B}][\text{HB}^+]^{-1}$ = acid dissociation constant of HB^+
 $K_{\text{D}(\text{B})} = [\text{B}]_{\text{org}}[\text{B}]^{-1}$ = distribution constant of B
 $K_{\text{ex}(\text{HBP})} = [\text{HBP}]_{\text{org}}([\text{HB}^+][\text{P}^-])^{-1}$ = extraction constant of HBP
 r = volume of organic to aqueous phase (phase ratio), i.e. the ratio between the flow rates of the two liquid phases
 C_{HB}^0 = initial total concentration of HB^+ (the injected sample)
 C_{HBmix} = highest total concentration of HB^+ in the sample zone immediately before segmentation
 C_{HB} = highest total concentration of HB^+ in the sample zone at equilibrium (immediately before separation)
 $[\text{HBP}]_{\text{cell}}$ = highest concentration of the ion pair HBP in the sample zone in the flow-cell of the spectrophotometer
 A = absorbance at peak maximum
 ϵ = molar absorptivity of the ion pair HBP in the organic phase
 l = length of cuvette; D_{tot} = total dispersion of sample
 D_{pre} and D_{post} = dispersion of the sample before and after the extraction coil
 A_{max} and A_{min} = absorbance at peak maximum with the highest (C^0) and lowest ($0.1 C^0$) counter ion concentration

TABLE 2

Different experimental modes for determination of extraction constants by flow injection

Mode	Species injected	Species varied	Species detected	Mode	Species injected	Species varied	Species detected
1	HB^+	P^-	HBP_{org}	5	HBP_{org}	HBP_{org}	HBP_{org}
2			HB^+	6			P^-
3	P^-	HB^+	HBP_{org}	7			HB^+
4			P^-	8	B_{org}	P^-	HBP_{org}
				9			HB^+

which demonstrates that the total dispersion depends not only on D_{pre} and D_{post} , but also on the phase ratio r and $K_{\text{ex}(\text{HBP})}[\text{P}^-]$, i.e. the distribution ratio for the sample HB^+ .

It may be pointed out that eqn. (1) is also applicable to the extraction of non-ionized species. $K_{\text{ex}(\text{HBP})}[\text{P}^-]$ should then be replaced by the distribution ratio for an acid or a base [2], and the technique may thus be used to determine distribution constants (partition coefficients).

The dispersion of the sample before and after the extraction coil was

determined in separate runs. D_{pre} was estimated from the absorbances measured when an aqueous picrate solution was fed into the flow-cell instead of the segmentor and then when the same picrate solution was injected into an identical aqueous phase free from picrate. D_{post} was then calculated from the product $D_{\text{pre}}D_{\text{post}}$ which was obtained in connection with the evaluation of the extraction constant (see below). For the extraction system shown in Fig. 1 D_{pre} was about 13 ($D_{\text{pre}} = 23$ with the 25- μl rotary valve) and D_{post} about 1.3.

Concentration of the counter ion

The introduction of the sample ion, HB^+ , into the aqueous stream of the counter ion, P^- , will decrease C_{P}^0 if the dispersion is small. This can be illustrated by the expression $C_{\text{Pmix}} = C_{\text{P}}^0(D_{\text{pre}} - 1)(D_{\text{pre}})^{-1}$, where C_{Pmix} is the lowest concentration of P^- in the sample zone immediately before segmentation. In systems having $D_{\text{pre}} > 10$ the decrease in counter-ion concentration can be neglected and the above equation can be written $C_{\text{Pmix}} = C_{\text{P}}^0 = [\text{P}^-] + r[\text{HBP}]_{\text{org}}$. If $C_{\text{P}}^0 \gg C_{\text{HB}}$, this equation simplifies to $C_{\text{P}}^0 = [\text{P}^-]$. In the present work the experimental conditions were chosen so that the simplified equation was valid.

Calculation of the extraction constants

By combining Beer's law, i.e. $A = \epsilon l[\text{HBP}]_{\text{cell}}$ with eqn. (1) and the initial definition of D_{tot} , the following equation can be derived:

$$1/A = (rD_{\text{pre}}D_{\text{post}}/\epsilon lC_{\text{HB}}^0) + (D_{\text{pre}}D_{\text{post}}/\epsilon lC_{\text{HB}}^0K_{\text{ex(HBP)}})[\text{P}^-]^{-1} \quad (2)$$

A plot of $1/A$ vs. $1/[\text{P}^-]$ should give a straight line with an intercept, $I = rD_{\text{pre}}D_{\text{post}}(\epsilon lC_{\text{HB}}^0)^{-1}$, and a slope, $S = D_{\text{pre}}D_{\text{post}}(\epsilon lC_{\text{HB}}^0K_{\text{ex(HBP)}})^{-1}$. Plots according to eqn. (2) are shown in Figs. 2 and 3. Straight lines were obtained in all cases and S increased with decreasing $K_{\text{ex(HBP)}}$ (cf. Table 3 and Fig. 2) as predicted. A further test of the validity of this equation is demonstrated in Fig. 3 which shows that both I and S decrease with increasing sample concentration, C_{HB}^0 . The residence time of the sample in the extraction coil was about 20 s.

The extraction constants of the quaternary ammonium ions were calculated by use of the relation $I/S = rK_{\text{ex(HBP)}}$, and are presented in Table 4. The $K_{\text{ex(HBP)}}$ value of the tetrapropylammonium ion agreed rather well with the batch value, while that of the tetraethylammonium ion was much higher. The poor agreement in the latter case can be explained by the method of calculation because the intercept, I , becomes more uncertain when S is high. A better agreement between the $K_{\text{ex(HBP)}}$ values was obtained when the extraction constant of the tetraethylammonium ion was calculated from the equation for the slope (see above). This procedure takes a little more time, however, since $D_{\text{pre}}D_{\text{post}}$ and ϵ must be determined in separate runs.

It should be mentioned that an equation analogous to eqn. (2) has previously been used to calculate extraction constants from batch extraction data [21].

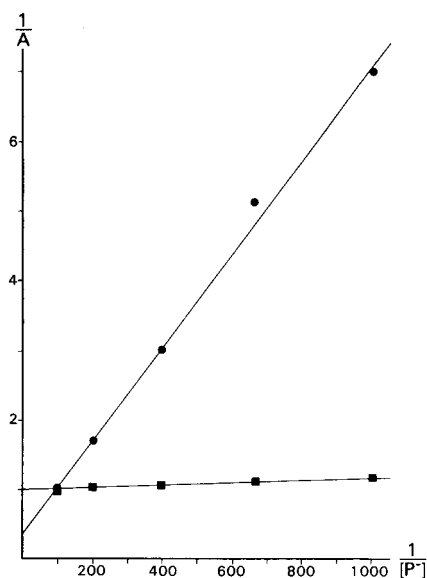


Fig. 2. Extraction of quaternary ammonium ions as ion pairs with picrate: (●) tetraethylammonium ions; (■) tetrapropylammonium ions.

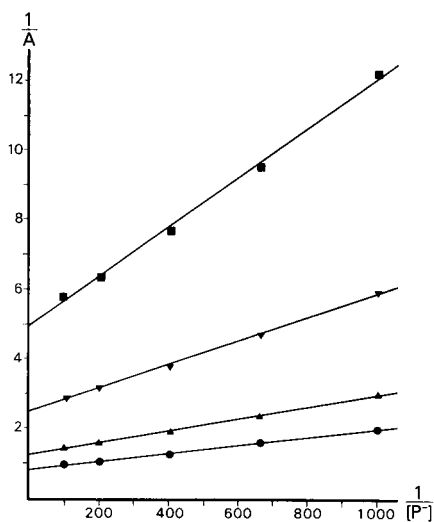


Fig. 3. Extraction of codeine as an ion pair with picrate. Sample concentrations ($\times 10^4$ M): (■) 2.5; (▼) 4.9; (▲) 9.9; (●) 14.8.

TABLE 3

Acid dissociation constants, distribution constants, extraction constants and molar absorptivities of the picrate ion pairs with chloroform as the organic phase (P^- = picrate, Y^- = octyl sulphate)

Compound, HB^+	Temp. ($^{\circ}C$)	pK'_{HB}	$-\log (K'_{HB}K_{D(B)})$	$\epsilon_{355} (\times 10^4)$ ($l \text{ mol}^{-1} \text{ cm}^{-1}$)	$\log K_{ex(HBP)}$	$\log K_{ex}^{\ddagger}(HBY)$
Amantadine	25	—	7.93 ^a	—	1.62 ^a	—
Brompheniramine	25	9.31 [7]	4.58 [7]	—	5.89 [18]	—
Codeine	25	8.21 [17]	5.85 [19]	1.55	3.63 ^b	2.82 ^a
Metoprolol	25	9.68 [6]	6.85 ^a	1.52	3.02 ^b	—
Tetraethylammonium	20	—	—	1.27 ^c	1.32 [20]	—
Tetrapropylammonium	20	—	—	1.27	3.64 [20]	—

^aDetermined by two-phase titration [6, 17]. ^bDetermined by batch extraction [20].

^cEstimated [20].

Magnitude of the extraction constants

It is evident from Fig. 2 and Table 4 that only $K_{ex(HBP)}$ values within a relatively narrow range can be determined. If the concentration of the counter ion is varied within one power of ten, the following expressions will be valid: $S = (A_{max} - A_{min}) C_P^0 (9 A_{max} A_{min})^{-1}$ and $I = (10 A_{min} - A_{max}) (9 A_{max} A_{min})^{-1}$.

Combination of these equations with the equation for I/S gives

TABLE 4

Extraction of quaternary ammonium ions as ion pairs with picrate
(Total dispersion 20–680; sample volume 40 μ l; mixing coil 1 m; extraction coil 2 m;
 $\alpha_{\text{HB}} = 1.00$.)

HB ⁺	$C_{\text{HB}}^0 \times 10^4$	Flow rate ^a (ml min ⁻¹)		$A_{\text{max}}/A_{\text{min}}$	$D_{\text{pre}}D_{\text{post}}$	log $K_{\text{ex}}(\text{HBP})$	
		CHCl ₃	H ₂ O			This work	Other method
Tetraethyl- ammonium	75.9	1.53	1.33	7.04	16.9	1.68 1.41 ^b	1.32
Tetrapropyl- ammonium	15.2	1.53	1.33	1.16	16.9	3.69 3.69 ^b	3.64

^a $r = 1.15$. ^bCalculated from the slope S (see text).

TABLE 5

Range of applicability of the method at different counter ion concentrations and phase ratios

C_{P}^0 ($\times 10^3$)	r	log $K_{\text{ex}}(\text{HBP})$	C_{P}^0 ($\times 10^3$)	r	log $K_{\text{ex}}(\text{HBP})$
1–10	0.5	1.40–4.25	2.5–25	0.5	1.00–3.85
	1.0	1.10–3.95		1.0	0.70–3.55
	2.0	0.80–3.65		2.0	0.40–3.25

$$K_{\text{ex}}(\text{HBP}) = (1/rC_{\text{P}}^0)[(10 - A_{\text{max}}/A_{\text{min}})/(A_{\text{max}}/A_{\text{min}} - 1)] \quad (3)$$

According to eqn. (3), the ratio $A_{\text{max}}/A_{\text{min}}$ should lie within the limits $1 < A_{\text{max}}/A_{\text{min}} < 10$. Equation (3) also shows that the higher the value of r or C_{P}^0 , the smaller the $K_{\text{ex}}(\text{HBP})$ values that can be determined. It may be pointed out that with the present separator it is possible to vary r only to a limited extent [15].

An illustration to the effect of the r and C_{P}^0 values on the magnitude of $K_{\text{ex}}(\text{HBP})$ is given in Table 5, which also gives the range of applicability of the method assuming that $1.1 \leq A_{\text{max}}/A_{\text{min}} \leq 9.0$. For example, by use of $C_{\text{P}}^0 = (1-10) \times 10^{-3}$ M and $r = 1$, it should be possible to determine $K_{\text{ex}}(\text{HBP})$ values within the range 13–8900.

Screening of the extraction constant and experimental conditions

The sample, e.g. an organic ammonium ion, HB⁺, is injected into the aqueous stream which contains the counter ion, P⁻. Two runs are made, the first at C_{P}^0 and the second at 0.1 C_{P}^0 . If the ratio between the corresponding absorbances, A_{max} and A_{min} , lies outside the interval $1.1 \leq A_{\text{max}}/A_{\text{min}} \leq 9.0$, then $K_{\text{ex}}(\text{HBP})$ cannot be determined without changing the

experimental conditions. A higher value of C_p^0 should be tested if $A_{\max}/A_{\min} > 9.0$ and a lower value if $A_{\max}/A_{\min} < 1.1$. In the latter case, which indicates a high extraction constant, it may also be possible to increase A_{\max}/A_{\min} by the addition of an extractable anion or change of pH, as will be discussed below.

High extraction constants

Extraction constants higher than those indicated in Table 5 can be determined if HB^+ takes part in side reactions such as protolysis or extraction with another counter ion [2]. This may be expressed by the conditional extraction constant:

$$K_{\text{ex(HBP)}}^* = K_{\text{ex(HBP)}}(\alpha_{\text{HB}})^{-1} \quad (4)$$

and $K_{\text{ex(HBP)}}$ in eqn. (2) should be replaced by $K_{\text{ex(HBP)}}^*$. Accordingly, there are two ways in which the extraction constant can be determined, viz. from a plot of $1/A$ vs. $1/[P^-]$ at constant α_{HB} or from a plot of $1/A$ vs. α_{HB} at constant $[P^-]$.

If protolysis of HB^+ occurs and an extractable anion, Y^- , is also present, then α_{HB} will assume the form:

$$\alpha_{\text{HB}} = 1 + K'_{\text{HB}}(1 + rK_{\text{D(B)}})(a_{\text{H}^+})^{-1} + rK_{\text{ex(HBY)}}[\text{Y}^-] \quad (5)$$

An illustration of the use of eqns. (2), (4) and (5) for the determination of high extraction constants is given in Figs. 4 and 5. The extraction constants are

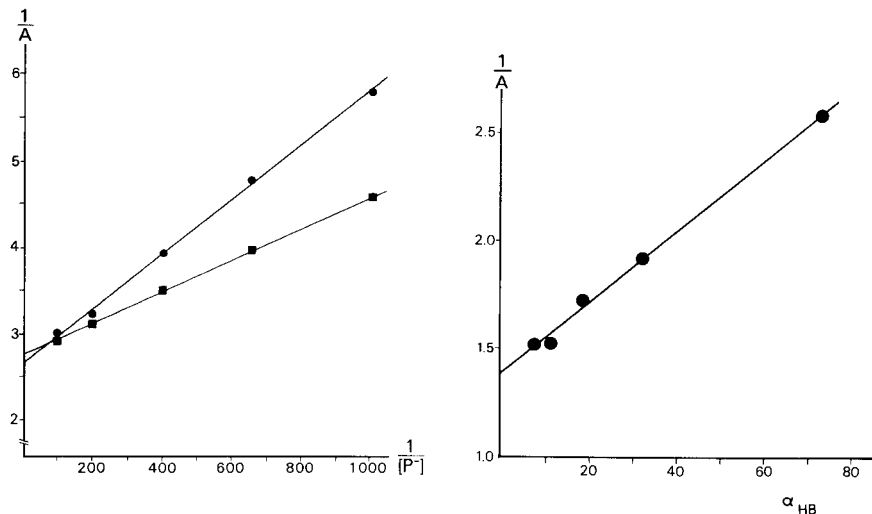


Fig. 4. Determination of high extraction constants. Distribution as base with constant α_{HB} for a 7.55×10^{-4} M brompheniramine sample. (■) $\alpha_{\text{HB}} = 609$, pH 7.29; (●) $\alpha_{\text{HB}} = 1058$, pH 7.53.

Fig. 5. Determination of high extraction constants. Distribution as ion pair with constant $[P^-]$ for a 6.4×10^{-4} M codeine sample. Anion Y^- is octyl sulphate $(5-125) \times 10^{-3}$ M.

presented in Table 6, which also gives the α_{HB} values. The latter were calculated by use of the constants in Table 3.

With the exception of metoprolol, the agreement between the $K_{\text{ex(HBP)}}$ values determined by the flow-injection and other methods was good. It can also be seen that an extraction time of about 5 s (0.5-m coil) only gave a slight change in the $K_{\text{ex(HBP)}}$ values of codeine and metoprolol compared with the values obtained with the 2-m coil.

The extraction constant of metoprolol was 0.1–0.2 (log units) higher than the batch value and decreased with the sample concentration. Since no side reaction was observed in the batch extraction experiments in the same concentration range, it is possible that the extraction time was insufficient.

Side reactions

Concentration-dependent side reactions such as dissociation or dimerization of the ion pair in the organic phase are often encountered in work on the determination of extraction constants [2]. If these kinds of reactions occur, plots of $1/A$ vs. $1/[P^-]$ will not give straight lines since $K_{\text{ex(HBP)}}^*$ changes with A , i.e. the total concentration of the ion pair in the organic phase. The evaluation of $K_{\text{ex(HBP)}}^*$ can then be made in the usual way [2] from plots of, e.g., $K_{\text{ex(HBP)}}^*$ vs. $([\text{HB}^+][\text{P}^-])^{-1/2}$ (dissociation), provided that D_{pre} , D_{post} and ϵ are known.

Stability of flow rates

An illustration of the effects of change in flow rate is given in Fig. 4; if the flow rates had been stable, then the intercepts should have been the same. Usually, the flow rates did not change more than 1%. Only in two runs were larger changes observed and in both cases it was the flow rate of the organic phase that increased by 4% and 6%. Although changes of this magnitude can be accepted for screening purposes, a better flow rate stability is needed for more accurate work.

The reason is that a change of the flow rates will also change r and the extraction constant will consequently either be higher or lower than the true value (eqn. 2). Besides, changes of the flow rates of the aqueous and organic phases through the flow cell will change $D_{\text{pre}}D_{\text{post}}$ and hence also the intercept and slope of eqn. (2). Changes of the flow rate of the organic phase through the extraction coil also influence $D_{\text{pre}}D_{\text{post}}$ (Table 7). This effect, however, seems to be negligible for the changes of flow rate encountered in this work.

Stability constants in unstable systems

In the batch procedure for the determination of extraction constants shaking times ranging from 2 min to 16 h have been reported [20, 22]. In the present work, however, the aqueous and organic phases are in contact with each other for a much shorter time (about 20 s when an extraction coil of 2 m is used). The good agreement between the extraction constants

TABLE 6

Extraction of amines as ion pairs with picrate

HB ^a	$C_{HB} \times 10^4$	Extraction coil (m)	Flow rate (ml min ⁻¹)		α_{HB}	A_{max}/A_{min}	$D_{pre}D_{post}$	log $K_{ex}(HBP)$	
			CHCl ₃	H ₂ O				This work	Other method
A. (Total dispersion 19-46; sample volume 40 μ l; mixing coil 1 m) ^a									
Codeine	14.9	0.5	1.52	1.30	6.11	1.98	18.7	3.61	3.63
	2.46	2	1.48	1.31	5.95	2.09	16.7	3.57	
	4.93	2	1.48	1.31	5.95	2.07	16.8	3.58	
	9.85	2	1.48	1.31	5.95	2.09	16.8	3.57	
	14.8	2	1.48	1.48	5.95	2.10	16.6	3.56	
	6.4	2	1.32 ^b	1.62 ^b	7.74-72.8 ^b	1.69	14.4	3.58 ^b	
Metoprolol	16.8	0.5	1.52	1.30	1.51	1.82	18.8	3.11	3.02
	3.35	4	1.45	1.39	1.45	1.71	16.6	3.21	
	8.38	4	1.45	1.39	1.45	1.76	16.6	3.17	
	13.4	4	1.45	1.39	1.45	1.79	16.8	3.15	
B. (Total dispersion 36-780; sample volume 25 μ l; mixing coil 0.6 m; extraction coil 2 m) ^c									
Amantadine	21.6		1.68	1.40	1.04	6.84	28 ^d	1.59	1.62
Brompheniramine	7.55		1.66	1.40	609 ^e	1.56	28 ^d	5.89	5.89
	7.55		1.66	1.40	1058 ^f	1.92	28 ^d	5.88	
Codeine	4.97		1.68	1.40	6.22	1.84	26.8	3.69	3.63
Metoprolol	5.77		1.68	1.40	1.52	1.60	29.1	3.25	3.02
	11.6		1.53	1.33	1.50	1.66	29.5	3.22	
	23.1		1.53	1.33	1.50	1.69	29.0	3.19	

^a $r = 1.04-1.17$. ^bThe same system as in ref. 1, $r = 0.82$, octyl sulphate = $(5-125) \times 10^{-3}$ M, $C_{\beta} = 2.5 \times 10^{-2}$ M. $r = 1.15-1.20$.

^dEstimated, the same runs as codeine and metoprolol at the flow rates. ^epH 7.29. ^fpH 7.53.

TABLE 7

Influence of the flow rate of the organic phase on the dispersion
 (The extraction system was as used previously [1]; $C_p^0 = 4 \times 10^{-3}$ M, $C_{HB}^0 = 5 \times 10^{-4}$ M)

Flow rate (ml min ⁻¹)		<i>r</i>	$D_{pre}D_{post}^a$	
CHCl ₃	H ₂ O			
0.84	1.76	0.48	9.9	
1.20	1.77	0.68	9.2	
1.69	1.72	0.98	8.6	
2.50	1.75	1.43	8.4	
3.55	1.74	2.05	9.1	

^aCalculated by use of eqns. (2), (4) and (5) and the constants in Table 3.

obtained with the continuous extraction system and batch methods in most cases suggests that equilibrium can be attained rather rapidly in ion-pair extractions. In such cases it might be possible to determine extraction constants in systems where either the ion-pair components or the organic phase deteriorates with time, e.g. by hydrolysis, provided that these reactions are slower than the ion-pair extraction. Distribution studies on unstable drugs by use of the AKUFVE apparatus have already been described [3], but the flow-injection technique would probably be a very useful alternative.

Conclusions

Extraction constants can be determined in a continuous extraction system with the flow-injection technique, using extraction times of about 20 s. The method is rapid and could therefore be particularly attractive for the screening of partition properties. Since extraction, phase separation and measurement can be carried out in a few seconds, the technique might be useful for studying ion-pair equilibria in reactive systems. Peristaltic pumps are less suitable when reproducible and/or very stable flow rates are needed.

REFERENCES

- 1 B. Karlberg, P.-A. Johansson and S. Thelander, *Anal. Chim. Acta*, 104 (1979) 21.
- 2 G. Schill, *Separation Methods for Drugs and Related Compounds*, Apotekarsocieteten, Stockholm, 1978, Ch. 3, and refs. therein.
- 3 S. S. Davis, G. Elson, E. Tomlinson, G. Harrison and J. C. Dearden, *Chem. Ind.*, (1976) 677.
- 4 F. F. Cantwell and H. Y. Mohammed, *Anal. Chem.*, 51 (1979) 218.
- 5 K. Gröningson, H. Westerlind and R. Modin, *Acta Pharm. Suec.*, 12 (1975) 97.
- 6 P.-A. Johansson and K. Gustavii, *Acta Pharm. Suec.*, 14 (1977) 1.
- 7 P.-A. Johansson, *Acta Pharm. Suec.*, 14 (1977) 363.
- 8 O. Eriksson and L. Nyberg, *Automation in analytical chemistry*, Technicon Symposia 1967, Vol. II, Mediad, White Plains, N.Y., 1967, pp. 269-273.
- 9 D. L. Robertson, F. Matsui and W. N. French, *Can. J. Pharm. Sci.*, 7 (1972) 47.

- 10 J. C. Gfeller and G. Frey, *Fresenius Z. Anal. Chem.*, 291 (1978) 332.
- 11 J. C. Gfeller, J. M. Huen and J. P. Thevenin, *J. Chromatogr.*, 166 (1978) 133.
- 12 L. Nyberg, *J. Pharm. Pharmacol.*, 22 (1970) 500.
- 13 K. Kina, K. Shiraishi and N. Ishibashi, *Talanta*, 25 (1978) 295.
- 14 K. Tsuji, *J. Chromatogr.*, 158 (1978) 337.
- 15 B. Karlberg and S. Thelander, *Anal. Chim. Acta*, 98 (1978) 1.
- 16 J. Růžička and E. H. Hansen, *Anal. Chim. Acta*, 99 (1978) 37.
- 17 P.-A. Johansson and K. Gustavii, *Acta Pharm. Suec.*, 13 (1976) 407.
- 18 S. Hugosson, L. Nyberg and L. Nilsson, *Acta Pharm. Suec.*, 9 (1972) 249.
- 19 G. Schill, R. Modin and B.-A. Persson, *Acta Pharm. Suec.*, 2 (1965) 119.
- 20 K. Gustavii and G. Schill, *Acta Pharm. Suec.*, 3 (1966) 241.
- 21 H. K. Biswas and B. M. Mandal, *Anal. Chem.*, 44 (1972) 1636.
- 22 T. D. Doyle and J. B. Proctor, *J. Assoc. Off. Agric. Chem.*, 59 (1976) 1175.

DIFFERENTIAL KINETIC ANALYSIS AND FLOW INJECTION ANALYSIS

Part 3. The (2.2.2) Cryptates of Magnesium, Calcium and Strontium

HENRIK KAGENOW and ARNE JENSEN*

*Department of Chemistry AD, The Royal Danish School of Pharmacy,
2 Universitetsparken, DK-2100 Copenhagen Ø (Denmark)*

(Received 10th July 1979)

SUMMARY

Simultaneous determinations of strontium and magnesium or calcium ions in solution can be done by differential kinetic analysis in continuous flow systems. Two different approaches are described; both are based on the differences between the dissociation rates of the cryptand (2.2.2) complexes of the metal ions, in the presence of potassium ions as scavenger and phthalein complexone as the chromogenic reagent for the released metal ions. Analyses were carried out at 40 h^{-1} , injected sample volumes were 25–150 μl .

In Part 2 [1] of this series, differential kinetic determination of magnesium and calcium was achieved in a flow injection system, based on the dissociation of their complexes with a (2.2.1) cryptand. Cryptand (2.2.2) displays very high $\text{Ca}^{2+}/\text{Sr}^{2+}$ and $\text{Mg}^{2+}/\text{Sr}^{2+}$ selectivity compared to other similar ligands [2]. Thus, substitution reactions can be used for the simultaneous determination of strontium and calcium or magnesium for which the rate-determining step is the characteristic rate of dissociation for each metal complex. Two approaches to the analysis of the alkaline earth ions in question (methods A and B) have been investigated based on this principle.

EXPERIMENTAL

Reagents

All chemicals used were of analytical-reagent grade and redistilled degassed water was used throughout.

The cryptand (2.2.2) was used as received (E. Merck). Standard aqueous solutions of the ligand (10^{-2} M), which were stored in brown glass bottles, were checked by potentiometric titration with 0.1 M hydrochloric acid. The solutions were found to be stable for at least 2 months. The metal salts used were all nitrates and solutions were standardized by titration with EDTA.

Different reagent solutions were used for the two methods (A and B). Reagent A consisted of 1.5 M KNO_3 , $1.05 \times 10^{-1} \text{ M}$ triethanolamine and $1.5 \times 10^{-3} \text{ M}$ phthalein complexone, to which was added 2% (v/v) glycerine, pH

9.40. Reagent B comprised 0.5 M KNO_3 , 1.35×10^{-1} M triethanolamine and 5.0×10^{-3} M phthalein complexone to which was added 2% (v/v) glycerine before adjustment to pH 9.00 with nitric acid. Both reagent solutions were stable for more than 2 months.

The carrier solution was 2% (v/v) glycerine in water for both methods.

Magnesium and strontium standards were 4.00×10^{-4} – 2.00×10^{-3} M, calcium standards were 2.00×10^{-4} – 1.00×10^{-3} M. The various concentrations of mixed solutions are shown in Tables 1–3.

Apparatus

The spectrophotometers, flow-through cuvettes (80 μl), recorders, peristaltic pump, thermostats and injection port (150- μl sample) used for method A were as described earlier [1]. For method B slight changes were made, in that a Hellma flow-through cuvette (OS-178.13), volume 8 μl , and an Ismatec Model MP-13 GJ 4 pump (Ismatec, Switzerland), operated at speed "10",

TABLE 1

Simultaneous determination of magnesium and strontium ions by method A

Sample		Mg(NO ₃) ₂ found ($\times 10^{-4}$ M)	Relative error (%)	Sr(NO ₃) ₂ found ($\times 10^{-4}$ M)	Relative error (%)
Mg(NO ₃) ₂ ($\times 10^{-4}$ M)	Sr(NO ₃) ₂ ($\times 10^{-4}$ M)				
4.00	16.00	4.28	+7.0	16.50	+3.1
8.00	12.00	8.03	+0.4	12.34	+2.8
4.00	12.00	4.22	+5.5	12.21	+1.8
8.00	8.00	8.10	+1.3	8.31	+3.9
4.00	8.00	4.22	+5.5	7.83	-2.1
16.00	4.00	16.54	+3.4	4.16	+4.0
8.00	4.00	8.09	+1.1	4.38	+9.5
4.00	4.00	4.21	+5.3	4.24	+6.0

TABLE 2

Simultaneous determination of magnesium and strontium ions by method B

Sample		Mg(NO ₃) ₂ found ($\times 10^{-4}$ M)	Relative error (%)	Sr(NO ₃) ₂ found ($\times 10^{-4}$ M)	Relative error (%)
Mg(NO ₃) ₂ ($\times 10^{-4}$ M)	Sr(NO ₃) ₂ ($\times 10^{-4}$ M)				
4.00	16.00	4.33	+8.3	15.46	-3.4
8.00	12.00	7.79	-2.6	11.71	-2.4
4.00	12.00	4.08	+2.0	11.80	-1.7
8.00	8.00	8.04	+0.5	7.85	-1.9
4.00	8.00	4.02	+0.5	8.12	+1.5
16.00	4.00	16.08	+0.5	4.06	+1.5
8.00	4.00	7.92	-1.0	4.10	+2.5
4.00	4.00	4.21	+5.3	4.14	+3.5

TABLE 3

Simultaneous determination of calcium and strontium ions by method B

Sample		Ca(NO ₃) ₂ found (× 10 ⁻⁴ M)	Relative error (%)	Sr(NO ₃) ₂ found (× 10 ⁻⁴ M)	Relative error (%)
Ca(NO ₃) ₂ (× 10 ⁻⁴ M)	Sr(NO ₃) ₂ (× 10 ⁻⁴ M)				
2.00	16.00	2.19	+9.5	16.10	+0.6
6.00	12.00	6.27	+4.5	11.92	-0.7
2.00	12.00	2.16	+8.0	11.92	-0.7
8.00	8.00	8.15	+1.9	6.89	-13.9
4.00	8.00	3.86	-3.5	8.96	+12.0
8.00	4.00	7.98	-0.3	3.52	-12.0
6.00	4.00	5.98	-0.3	4.48	+12.0
2.00	4.00	2.04	+2.0	3.94	-1.5

were used. The injection device used in method B was a double injector of the "sandwich" type [3]; in order to obtain a high degree of choice for the optimal sample volumes for injection, changeable loops, instead of bores alone, were used for the introduction of the samples into the flow system [4].

The manifolds used are shown in Fig. 1 (method A) and Fig. 2 (method B), together with the appropriate experimental parameters. A mixture (1 + 1) of metal ion solution and 3.00 × 10⁻³ M cryptand (2.2.2) solution was injected at S_A whereas undiluted metal ion solution was injected at S_{B1} and, simultaneously, a mixture (1 + 1) of metal ion solution and 3.00 × 10⁻³ M cryptand (2.2.2) solution at S_{B2}. In all cases these mixtures were prepared by means of automatic pipettes just prior to injection; cryptand (2.2.2) was always in excess in the resulting mixture.

The manifold building units and connections used were as described previously [5], except for the mixing chamber (Fig. 3), which constitutes part of the manifold for method B.

Measuring procedures

Method A. This was carried out according to the principles described for the Mg—Ca—cryptand (2.2.1) system [1] with strontium as the slower reacting ion. In order to obtain both a high sampling rate and a reasonable fraction of the Sr(cryptand (2.2.2))²⁺ complex dissociated before measurement at D₂, it was necessary to increase the rate of dissociation by thermostating coil 2 at 80°C. The pH in the sample zone is about 1 unit lower at 80°C than at room temperature, mainly because the pK_a of triethanolamine decreases with increasing temperature (dpK_a/dT = -0.020 at 25°C [6]). As the colour intensity of the metal—phthalein complexone complexes decreases with decreasing pH (cf. the acid—base properties of phthalein complexone), acceptable absorbance readings were obtained by cooling the flowing stream in coil 3 before measurement.

Method B. In this method, sample injection took place simultaneously at

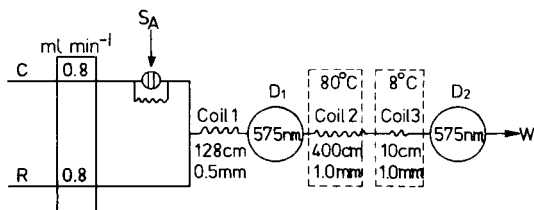


Fig. 1. Manifold for method A for the determination of magnesium (or calcium) and strontium ions. (C) Carrier stream; (R) reagent stream; (S_A) point of injection (150- μ l sample); (D_1) detector 1 (flow cell, volume 80 μ l); (D_2) detector 2 (flow cell, volume 80 μ l); (W) waste.

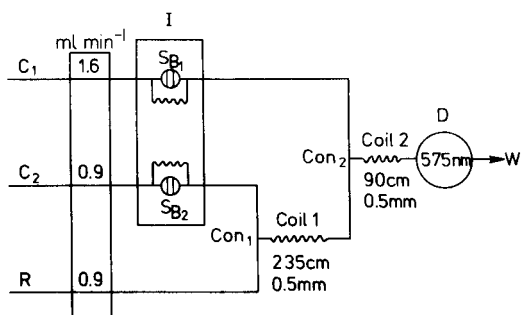


Fig. 2. Manifold for method B for the determination of magnesium (or calcium) and strontium ions. (C_1) Carrier stream; (C_2) carrier stream; (R) reagent stream; (S_{B1}) and (S_{B2}) points of injection (25- μ l and 50- μ l samples, respectively); (I) double injector for simultaneous injection of samples 1 and 2; (Con_1) confluence point 1, T-connector; (Con_2) confluence point 2, mixing chamber, volume 3 μ l; (D) detector (flow cell, volume 8 μ l); W, waste. ($D_{t1} = 7.0$, $T_1 = 9$ s; $D_{t2} = 10.4$, $T_2 = 36$ s.)

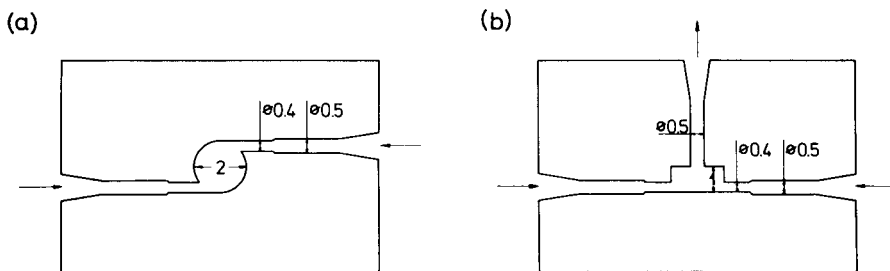


Fig. 3. Perspex mixing chamber. (a) Top view; (b) side view. Dimensions in mm; chamber volume 3 μ l.

S_{B1} and S_{B2} . The zone from S_{B2} met the reagent solution at Con_1 and dissociation of the metal cryptates took place while passing through coils 1 and 2; in coil 2 the sample zone was further diluted with the carrier solution merging at Con_2 . The short time of reaction, i.e. the residence time from

Con₁ to D, allows only a negligible fraction of the strontium cryptate present to be dissociated, and the absorbance obtained at D (peak 2) can be directly related to the concentration of magnesium (or calcium) ions.

While the sample injected at S_{B2} was in coil 1, the sample from S_{B1} travelled from the point of injection to the detector (D). As the metal ions present were not complexed with cryptand (2.2.2), they all reacted with the indicator when mixed with the reagent solution at Con₂ and in the subsequent coil 2 (the reagent solution had previously been diluted at Con₁). The absorbance at D (peak 1), therefore, represents the total concentration of strontium and magnesium (or calcium) ions. Combination of the results obtained for peaks 1 and 2 gives the concentration of strontium ion and magnesium (or calcium) ion, respectively, in the original sample. Coils 1 and 2 were chosen so as to give a short increase in residence time for the sample injected at S_{B2} but no carryover between peaks 1 and 2, i.e. between the two sample zones.

Samples and standards were injected in triplicate. Linear calibration graphs were calculated by the least-squares method from the absorbances. All correlation coefficients were ≥ 0.998 .

RESULTS AND DISCUSSION

Method A

Figure 4 shows the recorded absorbance readings obtained at each detector for a set of magnesium standards. Good base-line stability at both detection points and good reproducibility are observed. The responses obtained for a series of strontium standards were similar to those shown in Fig. 4b, except for lower sensitivity. The attainment of a stable base-line at D₂, however, often proved to be a serious problem because the chemical system was very

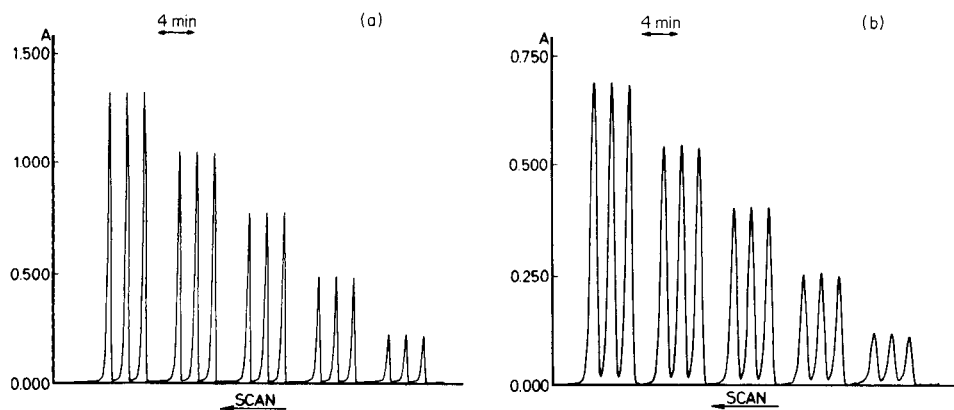


Fig. 4. Responses for magnesium by method A with detection (a) at D₁ for (right to left) 4.00, 8.00, 12.00, 16.00 and 20.00 $\times 10^{-4}$ M magnesium; (b) at D₂, solutions as in (a). Sampling frequency, 40 h⁻¹.

sensitive to small temperature changes, which occurred over a moderate period of time, because of the high reaction temperature and the large temperature gradients necessary for the analytical procedure. Another problem associated with the high reaction temperature was that the polyethylene tubing started to deteriorate when exposed to the reagent solution at 80°C for several hours. As the simultaneous determination of calcium and strontium ions by this method yielded poor results (not presented here), mainly because of a pronounced tailing effect observed for samples containing calcium ions, a different approach was introduced (method B). The fact that the tailing was observed only for calcium-containing samples might be due to the much higher absorptivity of the phthalein complexone complex of calcium ions than those of magnesium and strontium ions in the medium where the detection takes place. Efforts to remove the tailing effect by increasing the time intervals between sample injections improved the results somewhat, but led to a sampling frequency which was unsuitable for practical use.

Results for the determination of magnesium and strontium ions in various mixed solutions are given in Table 1. The general trend towards slightly positive deviations from the correct values is due to the fact that the stability constant of the cryptand (2.2.2) complex of strontium is not as large as was assumed when the analytical procedure was designed.

Method B

Figure 5 shows the absorbance readings obtained for sets of standard solutions of strontium and magnesium ions, respectively, determined by method B. The responses obtained for calcium ions were similar to those shown for magnesium except that the absorbances were about 12% greater. Again, good base-line stability and reproducibility are observed. The dispersions of the samples injected at points S_{B1} and S_{B2} were $D_{t,1} = 7.0$ and $D_{t,2} = 10.4$, respectively, and the associated residence times were $t_1 = 9$ s and $t_2 = 36$ s. When the corresponding dispersion coefficients are measured without regard to the dilution occurring at the confluence points and theoretical dispersion values are calculated from f.i.a. theory [7] and known flow rates, the results obtained are 6.6 and 10.1, respectively, which agree well with the experimental values.

Mixing chamber

In order to obtain a reasonably high sampling frequency, it is important to minimize the dispersion (sample zone width) of the two simultaneously injected samples. Given a set of system parameters (flow rates, volumes of injection etc.), the only means of controlling the dispersion is by varying the coil length. As the minimum length of coil 1 is determined by the requirement that no carryover between samples 1 and 2 should occur, minimization of the overall dispersion can be accomplished by reducing the length of coil 2 only. Depending on the shape of confluence point 2, there is a certain minimum length of coil 2 for sufficient mixing of the confluent streams;

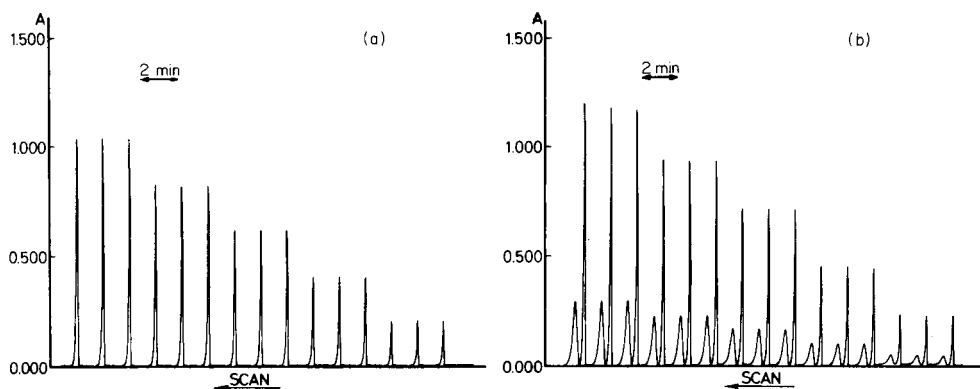


Fig. 5. Responses obtained by method B for (a) strontium standards containing (right to left) 4.00, 8.00, 12.00, 16.00 and 20.00 $\times 10^{-4}$ M; (b) magnesium standards, concentrations as in (a). Sampling frequency, 40 h^{-1} .

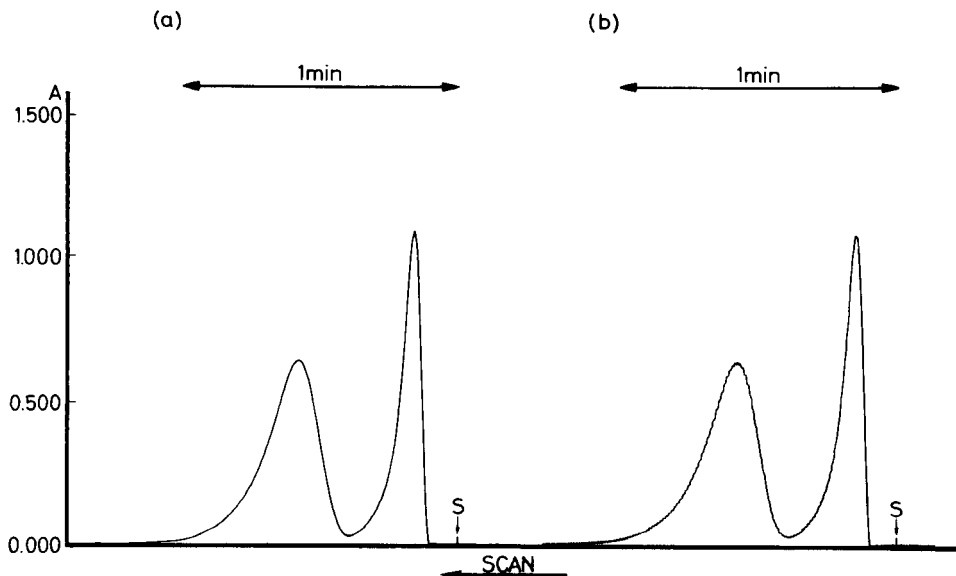


Fig. 6. Effect of mixing chamber. Experimental set-up as in Fig. 2 with (a) mixing chamber at confluence point 2, and (b) T-connector at confluence point 2. S, sample injection. Same metal standard injected in (a) and (b).

shorter coil lengths will result in systematic noise because of inefficient mixing, as shown in Fig. 6(b) where a T-connector is used as confluence point 2. On the introduction of a mixing chamber with the design and dimensions shown in Fig. 3 as the confluence point, more efficient mixing is obtained (Fig. 6a) without any notable increase in dispersion. The necessary minimum length of coil 1 permits efficient mixing of reagent and carrier (C_2) streams with an ordinary T-connector as confluence point 1.

Determinations were done at a sampling rate of 40 h^{-1} ; if a 1% carryover between peak 2 in one determination and peak 1 in the succeeding determination were accepted, a sampling rate of about 55 h^{-1} could be obtained.

Results for the determination of magnesium and strontium ions in various mixed solutions are given in Table 2, and for calcium—strontium mixtures in Table 3. No general trend in deviations from the correct values is observed, but the accuracy, of course, decreases as the ratio between the absorbance signals from each metal ion in a particular mixture becomes more extreme.

From these results it is concluded that the combined use of f.i.a. and the differential kinetic principle can be applied for the simultaneous determination of strontium and magnesium or calcium ions in solutions when cryptand (2.2.2) is used as the complexing agent and method B is employed. Reagent and cryptand consumptions were low for both methods. Reduction of the cryptand consumption can, however, be accomplished if the initial complexing of the metal ions is done within the flow system by applying the merging zones principle [4, 8]; this, combined with the simultaneous determination of magnesium and calcium in environmental samples, will be the subject of the next paper in this series.

The authors express their thanks to Dr. P. Specht of Merck, Denmark, for donating a sample of cryptand (2.2.2).

REFERENCES

- 1 D. Espersen and A. Jensen, *Anal. Chim. Acta*, 108 (1979) 241.
- 2 J. M. Lehn and J. P. Sauvage, *J. Am. Chem. Soc.*, 97 (1975) 6700.
- 3 J. Mindegaard, *Anal. Chim. Acta*, 104 (1979) 185.
- 4 H. Bergamin F², E. A. G. Zagatto, F. J. Krug and B. F. Reis, *Anal. Chim. Acta*, 101 (1978) 17.
- 5 J. H. Dahl, D. Espersen and A. Jensen, *Anal. Chim. Acta*, 105 (1979) 327.
- 6 D. D. Perrin and B. Dempsey, *Buffers for pH and Metal Ion Control*, Chapman and Hall, London, 1974, p. 161.
- 7 J. Růžička and E. H. Hansen, *Anal. Chim. Acta*, 99 (1978) 37.
- 8 J. Růžička and E. H. Hansen, *Anal. Chim. Acta*, 106 (1979) 207.

A MODELLING APPROACH TO ESTABLISH EXPERIMENTAL PARAMETERS OF A FLOW-THROUGH TITRATION

H. F. R. REIJNDERS and J. J. VAN STADEN

National Institute of Public Health, Bilthoven (The Netherlands)

G. H. B. EELDERINK

Control Engineering Laboratory, Delft University of Technology (The Netherlands)

B. GRIEPINK*

Laboratory for Analytical Chemistry, University of Utrecht, Croesestraat 77^a, 3522 AD Utrecht (The Netherlands)

(Received 21st August 1979)

SUMMARY

A flow-through titrimeter with optical detection and the flow-through titration of sulphate have been studied by using control engineering methods. Qualitative chemical descriptions and systems analysis yield a model covering different precipitation rates of barium sulphate. The validity of the model is proved by comparing simulated and real experiments. Possible uses of the model are indicated. The signal of the titrimeter is shown to be independent of dilution and turbidity, because of the special detection arrangement.

Many analytical systems can be described in control engineering terms [1—3]. Computer simulation on a mathematical model of such a system reduces the number of experiments required to develop the optimal analytical system. Moreover, the mathematical model itself is a help in understanding the processes involved in the analysis.

Recently a flow-through titration of sulphate was described [4, 5]. To study this titration system in greater detail, it was decided to establish a mathematical model which in turn could help to find the optimal settings of several parameters involved. The titrimeter has been described elsewhere [6, 7]. Figure 1 presents its main parts; the sample from a turntable is mixed with a setpoint solution [consisting of a barium sulphate suspension, barium ions and dimethylsulphonazo-III (DMSA)] and fed to a titration cell (8 ml). The excess of solution is pumped to waste. The reaction involved is: $\text{Ba}(\text{DMSA}) + \text{SO}_4^{2-} \rightleftharpoons \text{BaSO}_4 + \text{DMSA}^{2-}$. The bulb L emits white light which passes alternately through two interference filters f_1 and f_2 (yielding wavelengths λ_1 and λ_2 , respectively) mounted on a spinning wheel. From the data shown in Fig. 2 one of the wavelengths λ_1 is chosen at the isosbestic point in which the transmittance is not affected by the chemical reaction; the transmittance at the other wavelength λ_2 depends on the concentrations of $\text{Ba}(\text{DMSA})$ and

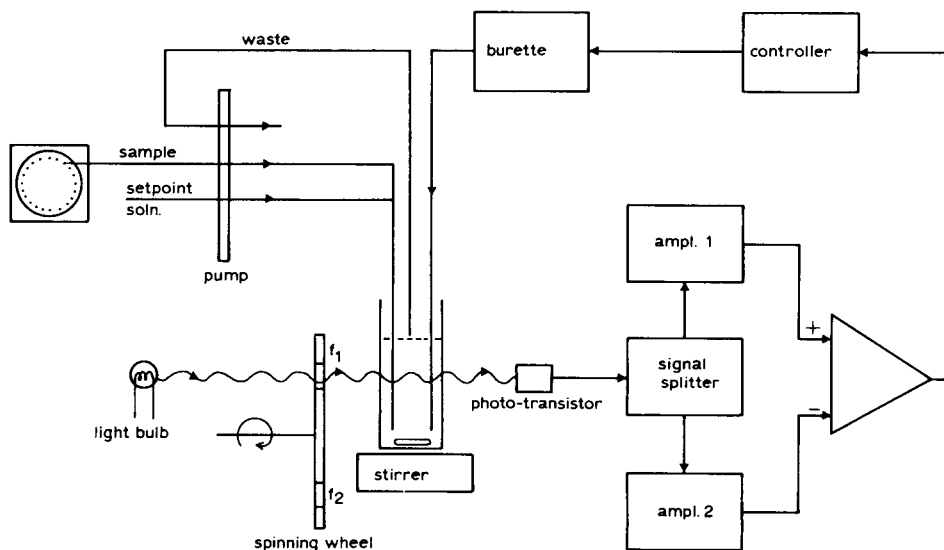


Fig. 1. Scheme of the flow-through titrimeter.

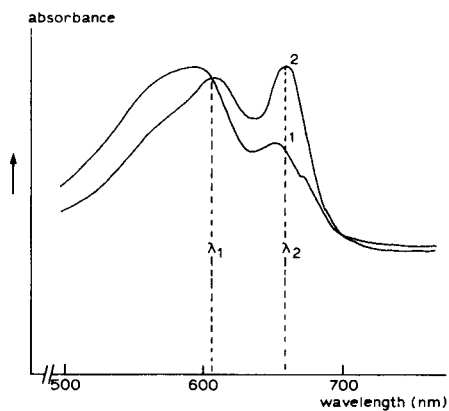


Fig. 2. Absorption spectra of DMSA (1) and Ba(DMSA) (2).

DMSA²⁻. The transmittances at both wavelengths are detected by a single photo-transistor. The resulting signals are subtracted, yielding a signal U after amplification.

In the following paragraphs, it is proved that this procedure makes the signal itself independent of the turbidity in the solution and also of dilution by any other solution. However, dilution of a system in chemical equilibrium may cause a shift in this equilibrium which influences the signal. The influence of this shift on the system may be calculated.

The first part of this paper describes a mathematical treatment of the

system and a calculation of the influence of a shift in the Ba(DMSA)—sulphate ratio. The second part deals with the mathematical model of the complete flow-through titration of sulphate.

MODELLING OF THE TITRIMETER

The model to be defined will describe the way in which a number of factors influences the signal U of the titrimer. A functional block scheme (Fig. 3) of the device is first set up in which those factors are taken into account which relate to the physical and chemical processes involved between the initial radiation I_0 and the final signal U . The value of the signal U depends on several factors: the turbidity, the concentrations of the species involved, the radiation intensity, the sensitivity of the photodetector, etc. By a proper setting of amplifications and a correct selection of wavelengths, the signal U equals zero in the setpoint situation. In this way a number of influences are eliminated.

In a first approach each effect is described separately in terms of the transfer functions of the several blocks. A transfer function is defined here as the mathematical expression of the relation between input and output of a block. Sometimes the transfer function can be measured for each block, but mostly it can be measured only for a larger part of a loop, comprising several individual transfer functions. Therefore transfer functions cannot be established solely by measurement, but also must be derived from chemical and physical reasoning. A list of symbols that will be used is given in Table 1.

The transfer function H_f of the filters is defined as: $H_f = I_f/I_0$. As previously described [7] the turbidity causes a transfer function H_t of the form:

$$H_t = I_t/I_f = \exp(-n\pi r^2 Q_{\lambda,r} l) \quad (1)$$

The transfer function H_c for the transmittance of the coloured species is given by the Lambert—Beer law:

$$H_c = I/I_t = \exp(-\epsilon c l) \quad (2)$$

The transfer functions of the detector and amplifier are, respectively,

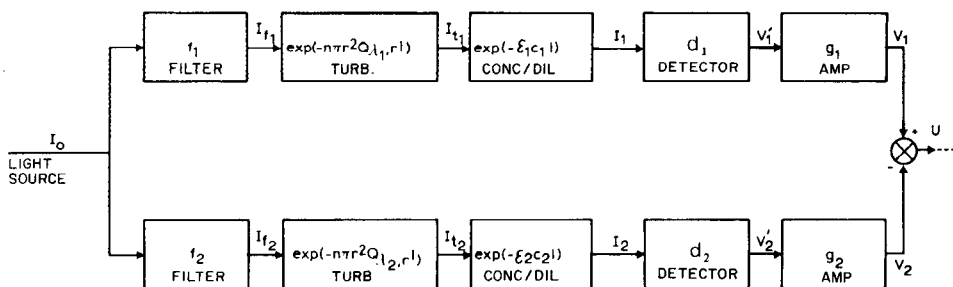


Fig. 3. Functional block scheme of the titrimer with transfer functions for each block. For simplicity the symbol H is omitted from the blocks.

TABLE 1

List of symbols used

Symbol	Meaning	Symbol	Meaning
H	$H(p)$: transfer function in the Laplace domain	I	Intensity of the transmitted light
p	Laplace operator	λ	Wavelength
c	Total concentration of indicator	l	Optical pathlength of the titration cell
c_{SO_4}	Sulphate concentration in the titration cell	m	Amount of indicator
c_{SO_4}	Sulphate concentration in the sample	n	Number of solid particles per volume
ϵ	Molar absorptivity	$Q_{\lambda,r}$	Scattering-efficiency factor
I_0	Intensity of incident light	r	Radius of solid particle
I_f	Intensity of the transmitted light from an interference filter	U	Output signal of the titrimeter
I_t	Intensity of transmitted light from a turbid solution containing light-absorbing species	V	Signal at the end of a pathway of the titrimeter
		V'	Signal from the phototransistor
		v	Volume of solution in the titration cell

$H_d = V'/I = d$ and $H_a = V/V' = g$. The transfer functions for each block are indicated in Fig. 3. The preceding equations yield for the signal V in each of the pathways: $V = I_0 H_{\text{tot}}$, in which $H_{\text{tot}} = H_f H_t H_c H_d H_a$.

The device is set in such a way that in the setpoint situation the resulting signal U equals zero, the signals in each pathway (V_1 and V_2 , respectively) being equal: $H_{\text{tot}1} = H_{\text{tot}2}$.

The influences on the resulting signal U of the subtraction photometric device of this kind [6] caused by small variations in the parameters of the several transfer functions are considered below. Some of the known properties [7] of subtraction photometry are simply mentioned; others are considered in more detail.

Light intensity

Small voltage fluctuations of the bulb, causing small fluctuations in the relative spectral intensities, are of little importance in this system because only one bulb is involved and the wavelengths are selected close to each other. Thus spectral bias in I_0 is negligible and fluctuations are eliminated by subtraction of V_1 and V_2 .

Turbidity

As already shown [7] the number of particles per volume affects the value of V . Thus from the equation $V = I_0 H_{\text{tot}}$:

$$dV/dn = I_0 dH_{\text{tot}}/dn = I_0 (dH_{\text{tot}}/dH_t) = (dH_t/dn) = I_0 H_{\text{tot}} (I/H_t) (dH_t/dn)$$

$$\text{where } dH_t/dn = -\pi r^2 Q_{\lambda,r} l \exp(-n\pi r^2 Q_{\lambda,r} l) = K_t H_t \quad (3)$$

If K_t is a constant defined as $K_t = -\pi r^2 Q_{\lambda,r} l$, then $dV = -K_t I_0 H_{\text{tot}} dn$.

The change dU in the final signal at point U caused by a change of turbidity is expressed as:

$$dU/dn = I_0 H_{\text{tot}} (-K_{t1} + K_{t2}) \quad (4)$$

It can reasonably be assumed that the scattering of light by solid particles in the case of the two close wavelengths 1 and 2 does not differ measurably, thus $K_{t1} = K_{t2}$. Equation (4) shows that under the assumption made above turbidity does not affect the final signal at point U .

Dilution

Dilution, for example, by addition of a volume dv of titrant, causes a change in signal V . Dilution affects not only the concentrations of the coloured species (H_c) but also the number of scattering particles per volume (H_t).

From the equation $V = I_0 H_{\text{tot}}$,

$$\frac{dV}{dv} = I_0 \frac{dH_{\text{tot}}}{dv} = I_0 \frac{dH_{\text{tot}}}{dH_c H_t} \frac{dH_c H_t}{dv} = I_0 H_{\text{tot}} \frac{dH_c H_t}{H_c H_t dv} = I_0 H_{\text{tot}} \left(\frac{dH_t}{H_t dv} + \frac{dH_c}{H_c dv} \right) \quad (5)$$

The effect of the turbidity dH_t/dv can be rewritten by using eqn. (3): $dH_t/dv = (dH_t/dn) \cdot (dn/dv) = -K_t H_t n/v$. This leads to the same conclusion that was reached for turbidity; thus eqn. (5) can be simplified to:

$$dV/dv = I_0 H_{\text{tot}} dH_c/H_c dv \quad (6)$$

If there is no shift in the chemical equilibrium involved, ϵ is independent of the concentration of the species to be detected. Thus

$$dH_c/dv = (dH_c/dc) \cdot (dc/dv) \quad (7)$$

where $c = m/v$. From eqns. (5–7) in conjunction with the setpoint situation $H_{\text{tot}1} = H_{\text{tot}2}$, it is possible to derive the equations:

$$dV/dv = I_0 H_{\text{tot}} \epsilon lc/v \text{ and } dU/dv = I_0 H_{\text{tot}} (K_{c1} - K_{c2}) \text{ in which } K_c = \epsilon lc/v.$$

If the setpoint is properly chosen, $K_{c1} = K_{c2}$ and dU is independent of dilution.

In the system involved, dilution actually causes a shift in the chemical equilibrium and so the absorbance depends on the experimental conditions. It was shown, however, that the effect of dilution is negligible in comparison to the effect of sulphate addition. The experimental data proved that the dilution effect was less than 0.5% of the signal change caused by the corresponding sulphate addition.

On account of the above considerations, the block scheme of Fig. 3 was simplified to that presented in Fig. 4(a), which gives the non-linear function between U and C_{SO_4} shown in Fig. 4(b).

MODEL OF THE FLOW-THROUGH TITRATION SYSTEM

To establish a realistic model of a complete flow-through titration system, several processes must be considered; these are presented as functional blocks in Fig. 5. The first block is self-explanatory. The detection block involves

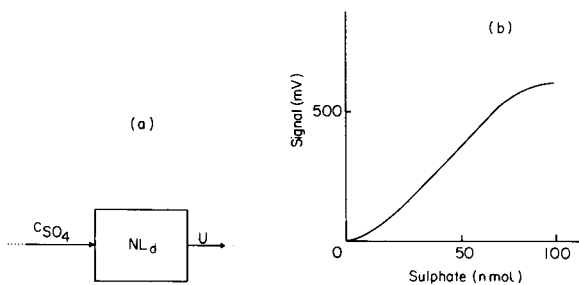


Fig. 4. (a) Simplified block scheme of the titrimeter. (b) Non-linear function representing the detector response on addition of sulphate to 8 ml of setpoint solution in the titration cell.

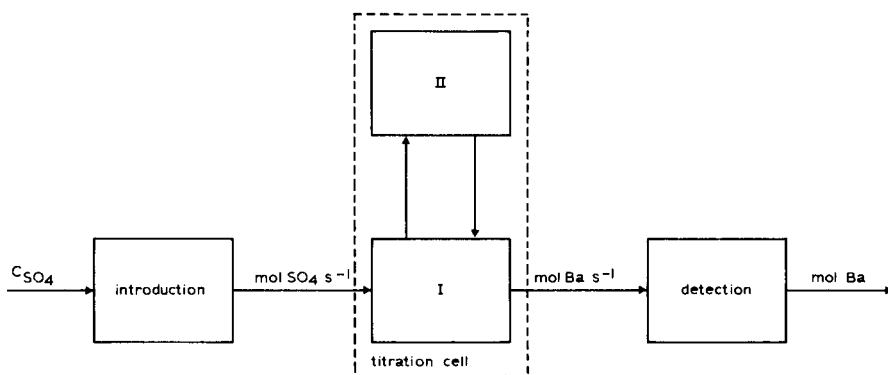


Fig. 5. Functional block scheme of the flow-through titrimeter (for explanation see text).

the non-linear function of Fig. 4(b) representing the extended model of Fig. 3 and the titrant addition. The process in the titration cell, within the dashed lines in the block scheme, is more difficult to describe. The transfer function is affected by the mixing efficiency and the rate of the chemical reaction. Block I accounts for the flow-through behaviour and the precipitation process. Block II accounts for the effects which determine the rate of the precipitation process. These transfer functions cannot be measured independently because the transfer function of the detector is always present. It is assumed that in the transfer functions of detection and electronic amplification, the dynamic part may be neglected because of relatively fast response.

Several factors are involved in the reaction rate of the titration process, e.g. the apparent pH, the water content of the setpoint solution and the active surface of the precipitated barium sulphate which assists further nucleation. In the first attempt at modelling, the influence of the nature and amount of barium sulphate in the titration cell was studied, because the other factors can be kept constant whereas the barium sulphate precipitate varies.

Qualitative description of the precipitation process

From several measurements of the dynamic behaviour of the system on addition of sulphate, it was found that the presence of freshly prepared barium sulphate accelerated the rate of further precipitation of barium sulphate. Relatively large amounts of aged barium sulphate had the same effect. These findings are in agreement with generally accepted theories. Because the set-point solution is saturated with barium sulphate and the excess of barium ions is high, the reaction rate is not primarily dependent on the sulphate concentration. However, as the reaction is not homogeneous, the number of active sites on which the precipitate is formed governs the reaction rate. This number of active sites decreases with time. The use of an average value of the time constant is not permissible in modelling because the number of active sites available during the titration is variable.

A qualitative description of the processes observed is given in Fig. 6. When a sulphate-containing sample enters the cell, the reaction rate is low, depending on the amount of barium sulphate. The period before t_1 describes the aging of the precipitate present. If this precipitate is relatively fresh (some minutes old) the number of active sites is such that upon sulphate addition (at t_1) precipitation starts. As the titration proceeds, with formation of the first precipitate, the number of active sites increases (t_2). Cluster formation retards this process and when the addition of sulphate is stopped, cluster formation causes a drop in the number of active sites (t_3-t_4). Finally the rate of decrease of the number of active sites is about the same as before t_1 . The process is thus essentially non-linear.

Qualitative modelling

The final model tested is presented in Fig. 7. In the introduction model, the sample reaches the cell after a lapse of time which may be calculated from the system dimensions and flow rates. The duration of introduction is given by T_d . Since the introduction time is rather long, the sample introduction can be assumed to be block-shaped; the height of the block at the output of the introduction system depends on the flow of the sample line and the sulphate concentration of the sample. After T_d seconds, this height becomes zero because of the transfer function $H = \exp(-pT_d)$.

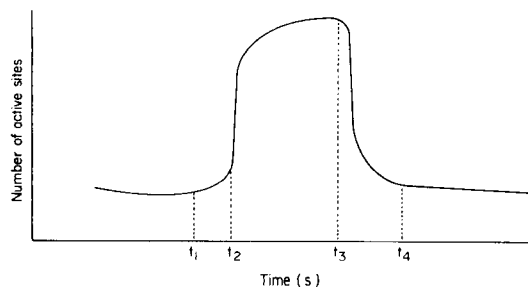


Fig. 6. Visualization of the number of active sites during the titration process.

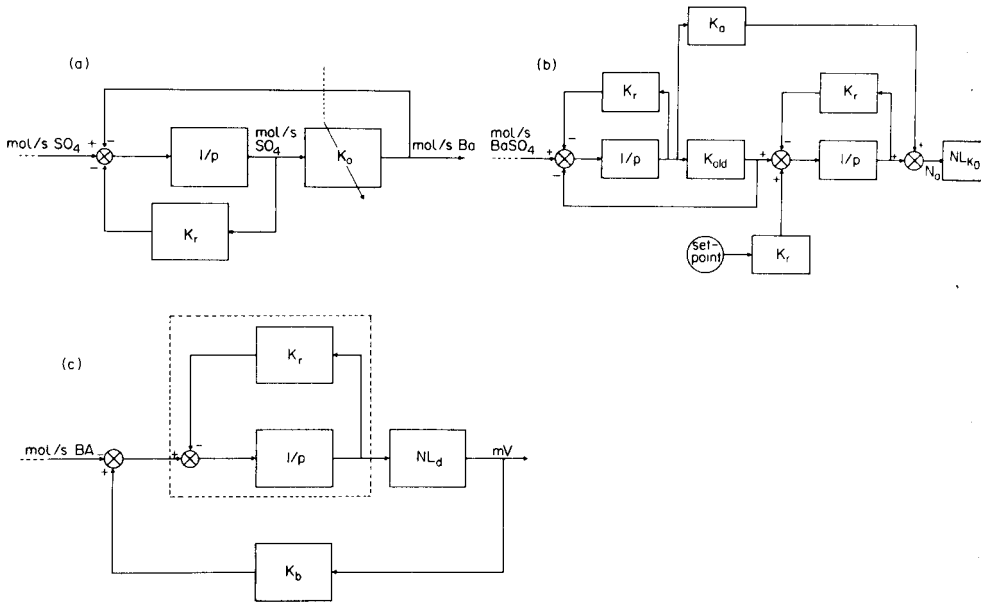


Fig. 7. (a) Block scheme of the model of the titration process. (b) Block scheme of the model of the process of formation of active sites. (c) Block scheme of the model of the detection system.

The process in the titration cell is represented in Fig. 7(a). The titration cell acts as an integrator ($H = 1/p$) on introduction of sulphate. The amount of free sulphate ions inside the cell will decrease because of two effects: (i) the sulphate reacts with the barium ions present or added (K_0) and (ii) the effluent from the cell will contain unreacted sulphate (K_r). The amount of sulphate removed is proportional to the quotient of flow rate through the cell and the cell content. The replacement factor K_r is determined by system dimensions and is independent of the reaction rate process. The replacement may cause a systematic error, which should be low so that the ratio between K_r and the reaction rate K_0 must be low ($K_0 \gg K_r$).

The model in Fig. 7(b) accounts for the formation of active sites which influences the precipitation process of barium sulphate. The output of this model determines the value of K_0 . Based on the chemical reasoning outlined above, this model includes the effects caused by old and fresh barium sulphate. The total amount of barium sulphate determines the number of active sites (N_a). However, the contribution of fresh barium sulphate to the number of active sites is larger than that of old barium sulphate. K_a is the ratio between these contributions. The relation (NL_{K_0}) between K_0 and the number of active sites (N_a) is given by

$$K_0 = 1/(K_M + K_N/N_a) \tag{8}$$

where K_M represents the maximum reaction rate and the factor K_N defines the influence of N_a on K_0 . In Fig. 7(b), K_{old} accounts for the effect of aging. Naturally, the amount of fresh barium sulphate decreases with time. Finally it is assumed that all barium sulphate formed on introduction of sulphate into the titration cell is fresh barium sulphate.

The model of the detection system is given in Fig. 7(c). The non-linear element NL_d has been indicated in Fig. 4(b). As this function was determined under static conditions, the input C_{SO_4} can be replaced by C_{Ba} . The part of Fig. 7(c) boxed in dashed lines accounts for the flow-through aspect by which the cell content, including unreacted barium ions are continuously pumped off. The output signal of the burette is fed back via K_b (K_b = burette constant) to the input of the cell.

Quantitative modelling

The models indicated above were used in establishing the final model in Fig. 8. Most of the constants of the model could be calculated from the system dimensions or the results of static measurements. The values given in the blocks are based on the dimensions used (μl , mV, nmol and s). In order to introduce the dynamic behaviour of the precipitation process in the presence of barium sulphate into the model, K_{old} , K_a and K_N had to be estimated. This was done by fitting simulated [8] responses with two responses of the

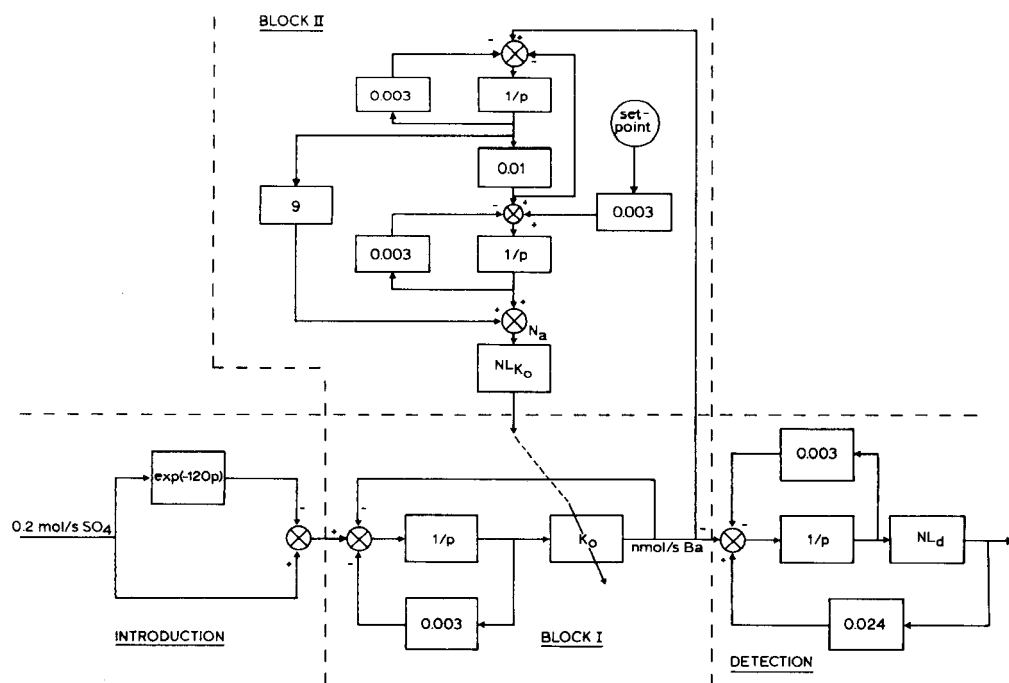


Fig. 8. Block scheme of the model of the flow-through titration.

flow-through titrimeter obtained on continuous addition of $0.2 \text{ nmol SO}_4^{2-} \text{ s}^{-1}$ during 60 s using the model of Fig. 8 and adjusting K_{old} , K_{a} and K_{N} . The setpoint solution contained 20 nmol of barium sulphate. Curve 2 of Fig. 9(a) presents the measured response. Then after 200 s, the sulphate was titrated, the burette disconnected and the same sulphate addition repeated; this gave curve 1. The steeper part at the beginning of curve 1 is explained by the presence of freshly precipitated barium sulphate and an extra amount of old barium sulphate. The fitted responses simulated by the computer are presented as dotted lines.

DISCUSSION AND RESULTS OF SIMULATION

It was found that K_{a} depends on the method of preparation of the setpoint solution. Although the solutions were prepared as reproducibly as possible, variation in K_{a} may be introduced. The values of K_{old} , K_{a} and K_{N} found by curve fitting lead to the following conclusions: (i) the time constant of the aging process is about 100 s; (ii) fresh barium sulphate provides 10 times more active sites than the old precipitate; (iii) the change of reaction rate on the change of the number of active sites is in the region of $4 \times 10^{-4} \text{ mol s}^{-1}$.

The model was first used to predict the response of the flow-through titrimeter upon two successive titrations of 25 nmol of sulphate in the presence of 20 nmol of barium sulphate in the titration cell originating from the setpoint solution. For the second titration, which was carried out 300 s after the first one, the remaining barium sulphate formed during the first titration is added to the 20 nmol of barium sulphate from the setpoint solution. To simulate the second titration the initial amounts of fresh and old barium sulphate are corrected for the remaining amounts of these species formed during the first titration. In Fig. 9(b) the simulated curves are indicated by dotted lines: curve 1 represents the first titration and curve 2 the second one. The

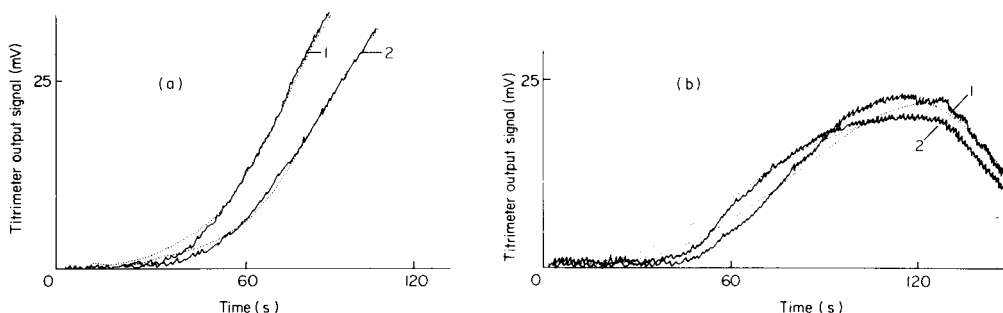


Fig. 9. Comparison of simulated (dotted lines) and experimental responses. (a) For continuous introduction of $0.2 \text{ nmol SO}_4^{2-} \text{ s}^{-1}$ in the presence of 20 nmol of BaSO_4 : (1) 200 s after the first titration was carried out; (2) before any titration. (b) For titration of 25 nmol of sulphate in the presence of 20 nmol of BaSO_4 : (1) the first titration; (2) 300 s after the first titration.

recoveries, defined as the ratio between sulphate found by titration and given sulphate, obtained by simulation of the titrations were 82% and 84.5%, respectively. Real experiments carried out under the same circumstances as used for simulation gave recoveries of 86% and 92%, respectively.

The same model was used to simulate the response on introduction of $0.2 \text{ nmol SO}_4^{2-} \text{ s}^{-1}$ during 70 s in the presence of 100 nmol of barium sulphate. The only adaptation in the model was the adjustment of the value of the setpoint (Fig. 7b). Figure 10(a) shows the simulated (dotted line) and real response. The model was also used to simulate a titration of 25 nmol of sulphate in the presence of 100 nmol of barium sulphate; the simulated and real curves are shown in Fig. 10(b). The recovery found by simulation was 90%; real measurements gave a recovery of 96%.

Although on titration of 25 nmol of sulphate in the presence of 20 nmol of barium sulphate the agreement between real and predicted curves is not complete, the simulated response predicts the relation between the slopes and the maximum values sufficiently. The behaviour of the response obtained with the real system at the beginning may be caused by a slight deviation from the setpoint. The other simulated and real responses show good conformity.

Figure 11 presents the reaction rate curves corresponding to the simulated titration curves of Figs. 9(b) and 10(b). The simulation indicates that the improvement of the recovery is caused mainly by the higher initial value of the reaction rate (K_0). Another way of achieving a higher value of K_0 is to form fresh barium sulphate continuously in the titration cell. This may be accomplished by a continuous inflow of sulphate solution into the cell. The simulation of such a system on continuous introduction of sulphate at a rate of 0.2 nmol s^{-1} to the titration cell indicated a recovery of 98%. This has not yet been verified in practice because the equipment required is not available.

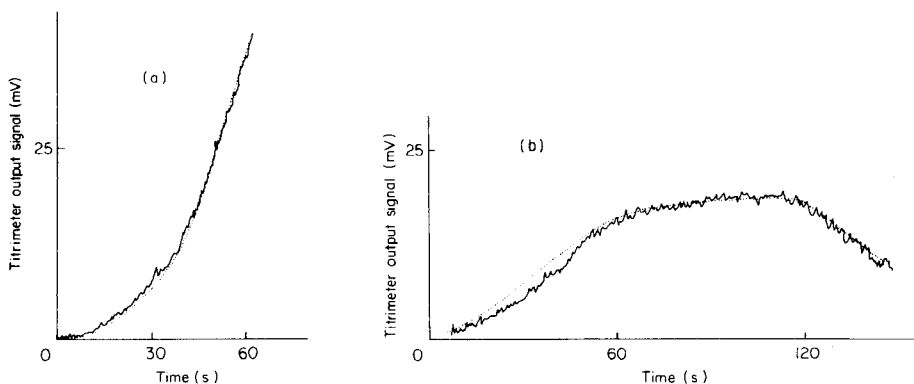


Fig. 10. Comparison of simulated (dotted line) and experimental responses. (a) For continuous introduction of $0.2 \text{ nmol SO}_4^{2-} \text{ s}^{-1}$ in the presence of 100 nmol of BaSO_4 ; (b) for titration of 25 nmol of sulphate in the presence of 100 nmol of BaSO_4 .

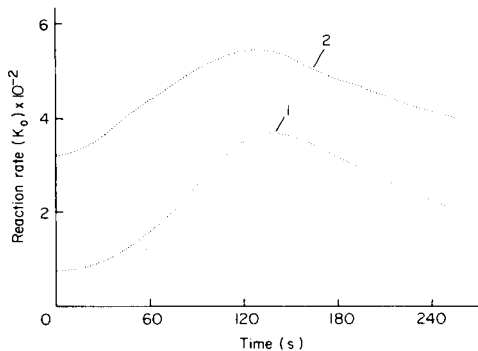


Fig. 11. Reaction rate curves on titration of 25 nmol of sulphate in the presence of (1) 20 nmol of BaSO_4 and (2) 100 nmol of BaSO_4 .

Conclusion

The effects of the various physical parameters on the signal of the titrimeter have been calculated. Dilution effects are negligible compared with the effect of sulphate addition. These calculations were confirmed by experiment.

The model developed predicts the behaviour of the tested system well. The simulations indicate that the reaction rate of the precipitation of barium sulphate is about 5 times higher with fresh barium sulphate than with old precipitate. It is concluded from the simulations that the recovery is improved by increasing the amount of barium sulphate in the setpoint solution. This conclusion was confirmed by experiment.

This paper shows the basic ideas necessary for describing flow-through titrimetric systems, which will ease the modelling of other flow-through systems. The models obtained may be used to optimize flow-through systems with respect to accuracy, recovery and titration rate.

REFERENCES

- 1 G. H. B. Eelderink, H. B. Verbruggen, F. A. Jutte, W. J. van Oort and B. Griepink, *Fresenius Z. Anal. Chem.*, 280 (1976) 273.
- 2 W. Jongkind, G. H. B. Eelderink, H. B. Verbruggen, W. J. van Oort and B. Griepink, *Fresenius Z. Anal. Chem.*, 286 (1977) 76.
- 3 G. Veenendaal, F. A. Jutte, G. H. B. Eelderink, H. B. Verbruggen, W. J. van Oort and B. Griepink, *Fresenius Z. Anal. Chem.*, 285 (1977) 337.
- 4 H. F. R. Reijnders, J. J. van Staden, G. H. B. Eelderink and B. Griepink, *Fresenius Z. Anal. Chem.*, 292 (1978) 290.
- 5 H. F. R. Reijnders, J. J. van Staden and B. Griepink, *Fresenius Z. Anal. Chem.*, 293 (1978) 413.
- 6 W. Jongkind, G. H. B. Eelderink, H. B. Verbruggen, W. J. van Oort and B. Griepink, *Fresenius Z. Anal. Chem.*, 286 (1977) 72.
- 7 W. J. van Oort, P. C. Schalkwijk, R. A. Brandenburg and B. Griepink, *Fresenius Z. Anal. Chem.*, 276 (1975) 181.
- 8 P. P. J. van den Bosch, Proceedings of the IFAC symposium on computer aided design of control systems, Zürich, 1979.

CONTROLLED DYNAMIC TITRATOR

S. M. ABICHT*

Fachrichtung Organische und Instrumentelle Analytik, Universität des Saarlandes, D-6600 Saarbrücken (Federal Republic of Germany)

(Received 20th July 1979)

SUMMARY

The controlled dynamic titrator described operates with constant titrant flow and time-proportional sample flow; sample and titrant are mixed in a microcell and the equivalence point is reached when the products of the normalities and flow rates of the titrant and the sample are equal. Titration times are measured and printed out. The concentration of the sample is inversely proportional to the titration time. The automatic titrator is discontinuous and suitable for on-line and off-line use. The cycle time of the motor-driven programmer is 2 min. Flow-through detectors for potentiometric, photometric or voltammetric indication can be used for a selection of acid–base and redox titrations. With this equipment, titration of large series of liquid samples with similar contents is simple.

With the development of new automatic equipment, titrimetric analysis has become increasingly important, for it is one of the most accurate and most selective wet chemical methods. Most of the commercially available automatic titrators work in a batch mode; sample and titrant are mixed in a single vessel until the end-point is reached. Precise end-points are usually calculated from the titration curve by appropriate mathematical approximation techniques [1–4]. The most important drawback of the automatic batch-mode titrators is the relatively complicated and costly mechanics necessary for sample exchange and for rinsing the indication unit.

During the last 15 years, different types of continuous flow titrators have been described. Their common characteristic is that the equivalence point is reached when the products of the normalities (N) and the flow rates (v , ml min⁻¹) are equal. Thus the conventional equivalence equation is replaced by $N_t v_t = N_s v_s$, where subscripts t and s refer to the titrant and sample, respectively. To establish N_s , one of the four parameters is usually varied, while the other three are kept constant. The end-point signal can be obtained either after a certain time, or at a particular pump speed, or after a defined tube length, etc. In the classical continuous titration mode, introduced by Blaedel and Laessig [5], v_s , N_s and N_t are constant, and the reagent stream

*Present address: Baeretstr. 6, CH-3930 Visp, Switzerland.

v_t is varied until the end-point is reached. A change in the sample concentration is followed by a corresponding change in the titrant flow, so that the titrant flow is directly proportional to the sample concentration. Equipment of this type is used in the control loop of continuous processes in chemical industry. The rate of revolution of the titrant pump can easily be measured in the control loop [6].

Pauschmann [7] developed an automatic continuous titrator, where the sample is pumped at constant speed, together with a colour indicator, through a channel to which the titrant is added through holes bored along the length of this channel. The end-point is indicated by a colour change which occurs in one of the segments and depends only on the sample concentration, when v_s and N_t are constant, and v_t is increased. In this case, the sample concentration is directly related to the length of the channel. This concept formed the basis of an instrument with a choice of detection modes such as potentiometry, amperometry, thermometry, conductivity, etc. [8].

The gradient titration technique of Fleet and Ho [9] is based on the principle of varying the concentration of the titrant, while the other parameters are kept constant. Here, the sample concentration is directly proportional to the titrant concentration. The titrant gradient is produced by premixing titrant and solvent in the manner conventional for liquid chromatography. This device makes it possible to titrate discrete samples in continuous flow systems. Titrant gradients also form the basis of the triangle-programmed titration technique of Nagy et al. [10, 11]. The titrant is generated coulometrically in a triangular manner by a controlled current source; after mixing with the constantly flowing sample two end-points are obtained, whose time difference is directly proportional to the sample concentration.

Růžička et al. [12] combined the new concept of flow injection analysis with titration. The concentration and flow rate of the titrant are constant. After the sample injection the sample is mixed with the constantly flowing titrant in a small mixer and then passes to a flow-through detector. The time of passage of the reacted sample zone through the detector is proportional to the sample concentration. Calcium was titrated with EDTA with potentiometric indication and strong bases with acid and photometric indication. The sampling frequency was between 20 and 60 titrations per hour. Aström [13] demonstrated that even single-point titrations [14] can be performed by flow-injection analysis with good precision and reproducibility. The sampling rate can be increased up to 700 per hour, because the peak value is used to calculate the sample concentration, even when the baseline has not been reached.

Ashworth et al. [15] introduced a new principle for an automatic continuous titrator with conductimetric indication: the concentrations of titrant and sample as well as the titrant flow are kept constant, while the sample flow is increased with time. Based on this principle, the continuous titrator described here is more highly automated and different detection units are used. The system is called a controlled dynamic titrator [16].

PRINCIPLE OF THE CONTROLLED DYNAMIC TITRATOR

Titrant and sample are continuously mixed in a microcell (Fig. 1). The titrant flow is constant, whereas the sample flow follows a straight-line function, $v_s = kt$, for a titration time t (min) with the proportionality constant k (ml min^{-2}). The time-dependent flow makes it possible to start with a new sample at constant intervals, i.e. to work discontinuously. All operational steps, i.e. start of titrant and sample flow, switching of valves, etc., are controlled by a motor-driven programmer with a cycle of 2 min (Fig. 2). The titrations are performed in a continuous flow system. For a sample flow $v_s = kt$, the sample concentration is calculated from $N_s = N_t v_t / kt$, i.e. the concentration of the sample is inversely proportional to the titration time t and all other parameters are constant.

Figure 2 shows all the important parts of the dynamic titrator. Prepared liquid samples are placed in the automatic sampler. Every 2 min the sample burette takes a new sample and gets the order to start the titration by delivering the liquid into the mixing cell. The titrant flow is started at exactly the same time as the sample burette. A second pump delivers a constant solvent flow into the mixing cell, where it is homogenized with the titrant and the sample. After a short reaction tube, the mixture enters a flow-through detector, and then flows to waste. Titration times are measured and printed out together with the sample number.

EXPERIMENTAL

Apparatus

Burette. The sample volume needed is only 2 ml, most of which is necessary to rinse the old sample from the system. The motor generator (Birotax/Brion,

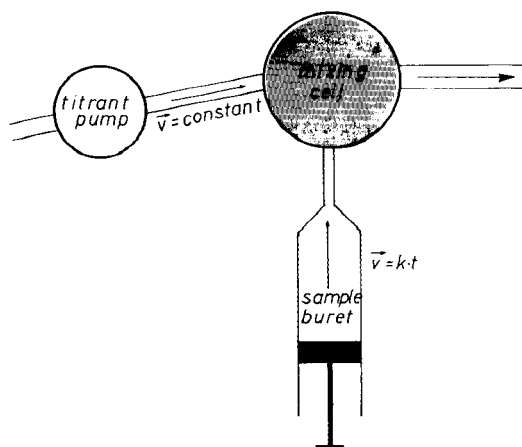


Fig. 1. Basic system of dynamic titration.

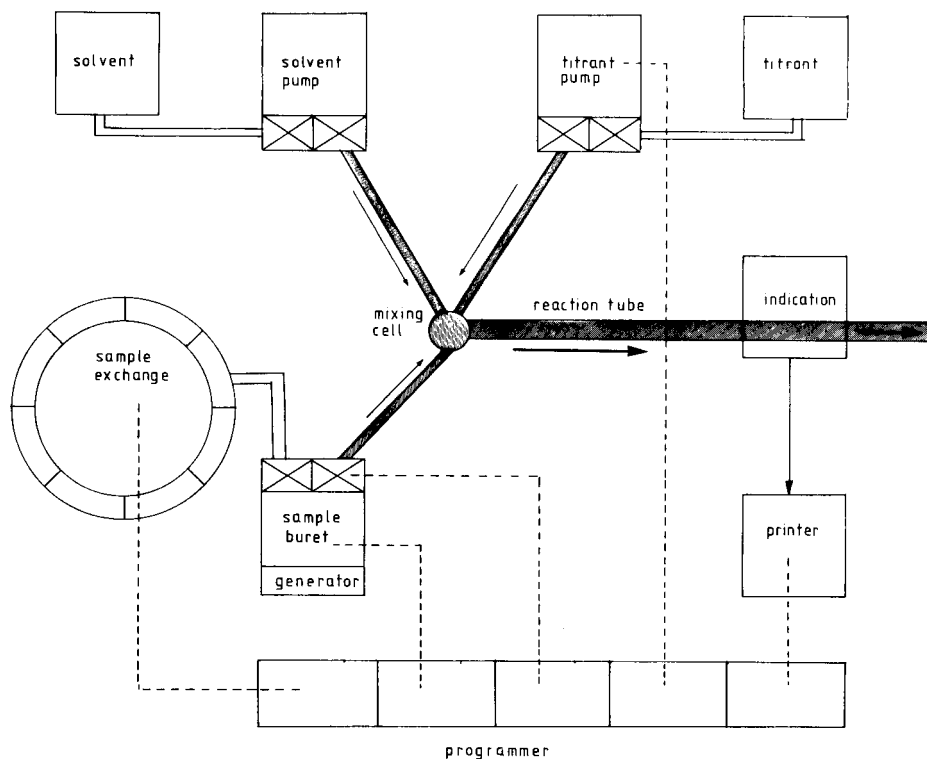


Fig. 2. Schematic diagram of the titrator.

Leroux & Cie, Paris, type I) is driven by a voltage source which produces an exactly linear time-dependent voltage. The motor drives the pointer axis of a Ströhlein measuring mechanism, which itself drives the piston of a 0.6-ml Ströhlein burette. A specially constructed valve with a short switching time connects the burette to the mixing chamber and to the sampler. The total available titration time is limited by the burette volume (V) and the proportionality constant k : $V = \int_0^t kt = 0.5 kt^2$; thus $t = 1.2$ min for $V = 0.6$ ml, $k = 0.85$ ml min⁻².

Sampler. A Technicon Autosampler III model containing 40 glass vessels was used. The autosampler is switched on and off by a pulse from the programmer.

Solvent and titrant pump. Two identical constant-flow pumps (Labotron, Gelting, Germany; model LDP 13 A) were used. The valves were specially constructed. The maximum flow rate of each pump was 5.3 ml min⁻¹.

Mixing cell. Mixing cells with very small diameters were constructed. The liquids are delivered through holes (0.2 mm i.d.) which meet tangentially in the mixing chamber (Fig. 3). The mixing cells have volumes of 10–70 μ l. Connections to the valves and to the detection cell are made from polyethylene tubes (0.03 in. i.d.). Some mixing cells were constructed with an

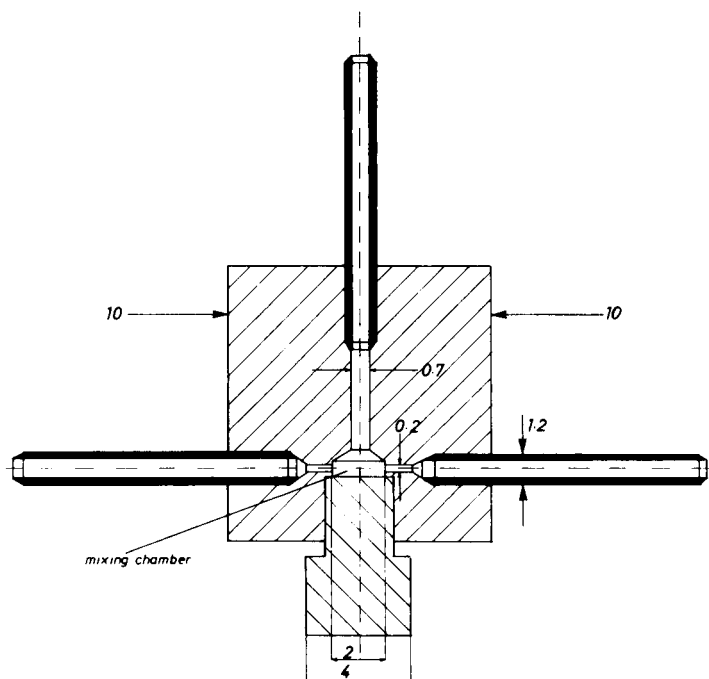


Fig. 3. Mixing cell (longitudinal section) made of plexiglas or Kel-F, with tubules of stainless steel. Dimensions in mm.

internal tube in the mixing chamber, to extend the reaction time without excessive zone broadening. The linear flow velocity is much higher than in conventional batch mixing, being more than 3000 mm s^{-1} .

In a special version, a mixing cell was developed where the titrant is generated coulometrically (Fig. 4). A constant-current source was built for the mA range (5–20 mA). With this combination, iodine or bromine titrants were generated.

Indication systems

To start a dynamic titration, the burette and titrant pump or current source are activated. Almost instantly (dead time is short), the excess of titrant reaches the detector which produces an increase of signal. At the end-point, the signal decreases again and the time difference between them is measured and printed out; Fig. 5 shows such titration curves. For time measuring, a counter was constructed and built into a printer (Practical Automation Inc., model 7). The accuracy of the time printout was $\pm 0.01 \text{ s}$.

Four different flow-through detectors were used: conductimetric [15], photometric and potentiometric at zero current and constant current.

Photometric indication. A flow-through cell (Fig. 6) with a total volume of $100 \mu\text{l}$ was constructed [17] and used for acid–base titrations with acid–

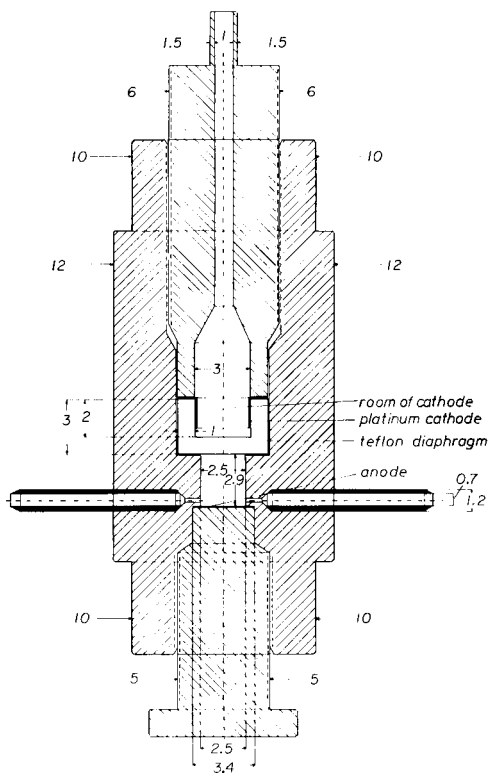


Fig. 4. Coulometric flow-through cell. Titrant and sample are mixed in the anode chamber, where simultaneously the coulometric reagent is generated. The cathode compartment is separated by a teflon diaphragm (0.25-mm diameter holes in a sheet of teflon) from the anode chamber. Part of the mixture leaves the cell at the top, loaded with generated hydrogen; the other part leaves the cell into the titration system through an outlet in the anode chamber (not shown in the figure). The speeds of the 2 flows are controlled by the lengths of attached capillaries. All dimensions in mm.

base indicators and redox titrations with redox indicators. The light source was a micro-lamp (Mikroglühlampengesellschaft, Hamburg, type 1041-1, 12 V, 25 mA). Interchangeable Schott interference filters were used.

Potentiometric indication. A combined pH electrode (Schott; Mikro-pH-Einstabmesskette) was used with a special flow-through cell. The potential was measured by a Knick digital pH meter (type 650).

Voltammetric indication. Different flow-through voltammetric detectors were developed, one of which is shown in Fig. 7. The total volume is less than 5 μl . The two platinum sheets are used as electrodes and the titration mixture is forced between them. The potential is measured and amplified in a special TitraVIT device [18], which also acts as the current source for the polarization current. The 6-V exit of the TitraVIT triggers the counter for the time measurement. The TitraVIT was also used to automate the potentiometric and photometric measurements.

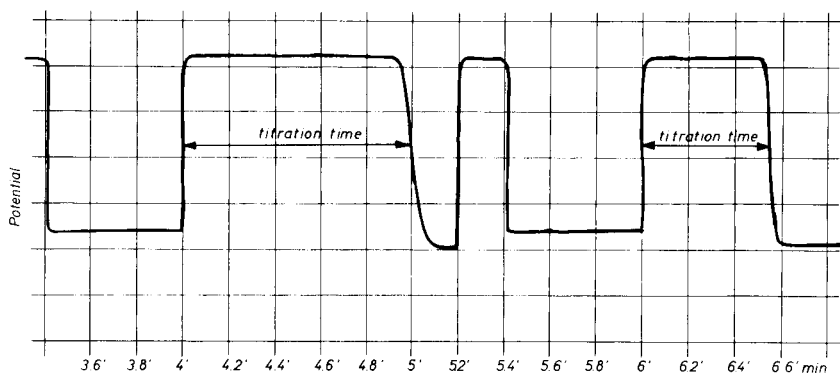


Fig. 5. Typical dynamic recorder chart for potentiometric detection. One titration begins with the arrival of excess of titrant at $t = 4$ min. The titration time is measured and printed out. A second cycle (beginning at $t = 6$ min) with a shorter titration time corresponds to a higher sample concentration. The potential jump between the 2 titrations results from the end of the sample burette, before the titrant pump stops.

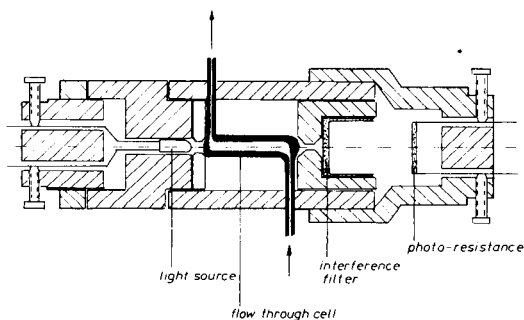


Fig. 6. Flow-through cell for photometric indication (longitudinal section).

Programmer

A motor-driven programmer with a time cycle of 2 min and with eight independent switches was used (Mauell, PS 355). Figure 8 shows the program of one cycle. At zero time, the motor burette starts and reaches its maximum speed at $t = 73$ s (switch 3). Sample change is triggered at $t = 67$ s (switch 8). At $t = 79$ s the sample valve opens (switch 4) and from $t = 81$ s to $t = 95$ s the valve of a special rinsing pump is opened (switch 6), so that the burette can be rinsed with the new sample. After rinsing, the burette refills with new sample (from $t = 98$ s to $t = 118$ s, switch 1) and the burette valve closes at $t = 118$ s. The system is then ready for the next titration. In the cycle between two titrations the valve of the titrant pump changes direction (switch 2) to avoid any disturbing change during titration. From

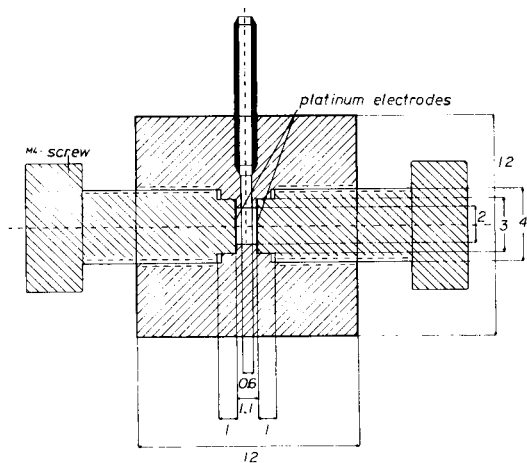


Fig. 7. Flow-through cell for constant-current potentiometric indication (longitudinal section). The entry cannot be seen in the plane of this section.

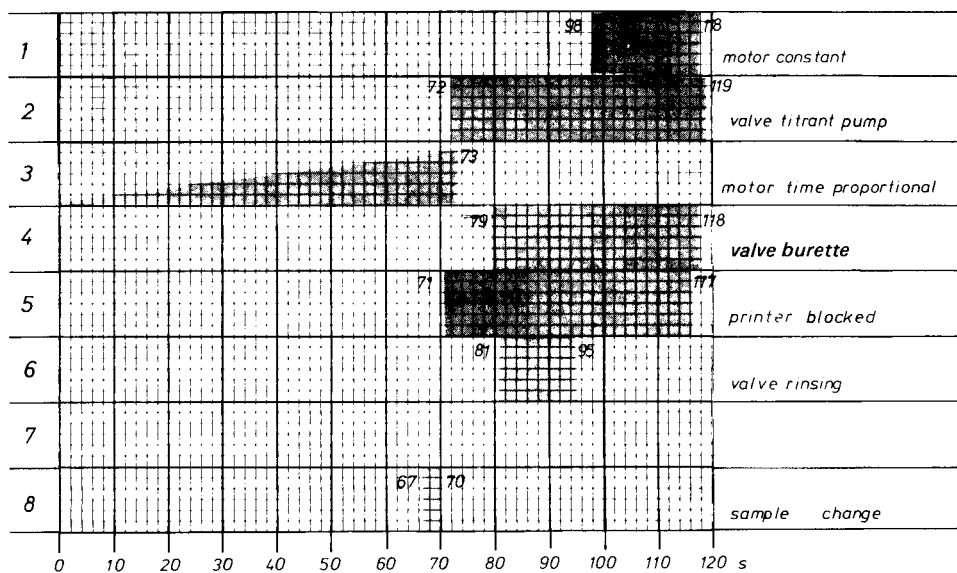


Fig. 8. Completion of a 2-min program in the dynamic titrator. One or more functions can be activated by one switch. The switches are adjusted easily by hand for special titration problems.

$t = 71$ s to $t = 117$ s the printer is blocked to prevent the printout of results which do not correspond to a titration (cf. Fig. 5).

Reagents

All reagents were of commercially available analytical quality. In some

cases Brij (Merck) was added to prevent gas bubbles sticking in the photometric cell.

RESULTS AND DISCUSSION

Titrations of weak and of strong acids with sodium hydroxide were carried out with photometric or with potentiometric detection: hydrochloric acid, potassium hydrogenphthalate, acetic acid, citric acid, oxalic acid, tartaric acid, succinic acid and malic acid were titrated in the concentration range 10^{-2} – 10^{-3} mol l⁻¹. With the photometric detector, both constant-rate pumps delivered sodium hydroxide, an acid–base indicator being added to one flow to produce the initial signal in the detector. With potentiometric detection, the initial signal was generated by switching on the titrant pump with sodium hydroxide, whereas the solvent flow was very dilute acid.

Ascorbic acid and hydroquinone were titrated with cerium(IV); the barium salt of diphenylamine sulphonic acid was used for photometric indication. Other successful titrations were: ascorbic acid with bromine (from bromide and bromate in strong acid) or with coulometrically generated iodine; thiosulphate with iodine; elaidic acid with coulometrically generated bromine in methanol; and primary aromatic amines with sodium nitrite. All these titrations were detected with constant-current potentiometry.

Attempts were also made to use air-segmented reaction tubes, but reasonable results could be obtained only by empirical calibration. The other results obtained corresponded to results obtained by batch-mode titrations, within a relative error of 1%. The repeatability was also better than 1%.

The accuracy of the dynamic titration method was limited mainly by the mechanical part of the sample burette which produces a theoretical, but not in detail a practical, function $v = kt$. The resulting error becomes small for $t > 10$ s. The total available concentration range then corresponds to 1:10, which can be exceeded by switching to another constant titrant flow. Although the sample concentration is inversely proportional to the titration time, so that a shorter titration time corresponds to a higher sample concentration, the precision is not limited seriously over a wide range.

The equipment offers possibilities for other modes of detection such as potentiometry with ion-selective electrodes [19], and thermometry [20], or for further automation. The titration times in seconds could be automatically converted to sample concentrations with an on-line desk calculator or a programmable pocket calculator with printer. The programmer could also be integrated in the calculator.

This system is suitable for on-line or off-line process control as well as for serial titrations. There are few problems in changing the detection unit or in adapting the system for special titration purposes.

REFERENCES

- 1 G. Gran, *Acta Chem. Scand.*, 4 (1950) 559.
- 2 H. J. Keller and W. Richter, *Metrohm Bull.*, 2 (1971) 173.
- 3 K. Waldmeier and W. Rellstab, *Fresenius Z. Anal. Chem.*, 264 (1973) 337.
- 4 S. Ebel and S. Kalb, *Fresenius Z. Anal. Chem.*, 278 (1976) 109.
- 5 W. J. Blaedel and R. H. Laessig, *Anal. Chem.*, 36 (1964) 1617.
- 6 M. Jola, *Chimia*, 33 (1979) 208.
- 7 H. Pauschmann, *Fresenius Z. Anal. Chem.*, 245 (1969) 42.
- 8 Ciba AG, *German Offenlegungsschrift*, 2 001 707 (1970).
- 9 B. Fleet and A. Y. W. Ho, *Anal. Chem.*, 46 (1974) 9.
- 10 G. Nagy, Zs. Feher, K. Tóth and E. Pungor, *Anal. Chim. Acta*, 91 (1977) 87, 97; 100 (1978) 181.
- 11 G. Nagy, Z. Lengyel, Zs. Feher, K. Tóth and E. Pungor, *Anal. Chim. Acta*, 101 (1978) 261.
- 12 J. Růžicka, E. H. Hansen and H. Mosbaek, *Anal. Chim. Acta*, 92 (1977) 235.
- 13 O. Aström, *Anal. Chim. Acta*, 105 (1979) 67.
- 14 W. Leithe, *Chem. Ing. Tech.*, 3 (1964) 112.
- 15 M. R. F. Ashworth, W. Walisch, W. Becker and F. Stutz, *Fresenius Z. Anal. Chem.*, 273 (1975) 275.
- 16 S. M. Abicht, *Dissertation, Saarbrücken*, 1979.
- 17 G. Lazik, *Universität des Saarlandes, personal communication*.
- 18 W. Walisch, *Chim. Anal. (Paris)*, 2 (1957) 63.
- 19 D. C. Cowell, *Med. Lab. Sci.*, 35 (1978) 265.
- 20 W. R. McLean and G. E. Penketh, *Talanta*, 15 (1968) 1185.

THE RESPONSE SURFACE OF AN AMPEROMETRIC FLOW CELL DETECTOR BASED ON A ROTATING DISK ELECTRODE FOR H.P.L.C. AND CONTINUOUS FLOW ANALYSIS

K. BRUNT*, C. H. P. BRUINS, D. A. DOORNBOS and B. OOSTERHUIS

Optimization Research Group, Laboratory for Pharmaceutical and Analytical Chemistry, Antonius Deusinglaan 2, 9713 AW Groningen (The Netherlands)

(Received 13th July 1979)

SUMMARY

The amperometric detector flow cell based on a rotating disk electrode can be used in conjunction with continuous flow analysis as well as with h.p.l.c. The response surface of the detector as a function of flow rate, electrode rotation speed and concentration of electroactive species (hexacyanoferrate(II)) is measured in combination with continuous flow analysis. When the electrode is stationary, the detector behaves as a wall-jet detector. Rotating the electrode results in a completely different hydrodynamic flow pattern in the flow cell. The response becomes independent of the flow rate and is linearly related to the electrode rotation speed. The influence of nozzle height in the flow cell on the detector response in combination with h.p.l.c. is described. With certain combinations of nozzle height and rotation speeds, a favourable flow pattern appears to be created in the cell and the sensitivity is increased considerably.

Several electrochemical techniques have been applied in detectors for high-performance liquid chromatography (h.p.l.c.) [1]. The almost classic cells are the thin-layer cell [2] and the wall-jet cell [3], both of which are commercially available. Recently an entirely new design of amperometric detector flow cell, based on a rotating disk electrode (RDE), was introduced [4]. The response of an amperometric detector depends on the mass transport of the electroactive species from the bulk solution in the flow cell to the electrode surface, assuming that the reaction rate at the electrode surface is infinitely fast compared with the mass transfer rate through the diffusion layer at the electrode. The thickness of this layer depends mainly on the flow cell geometry and on the fluid velocity in the detector flow cell. The effect of rotating the electrode in the flow cell is two-fold. First, rotating the electrode decreases the thickness of the diffusion layer at the electrode surface, so that the concentration gradient from the bulk solution to the electrode surface increases. According to Fick's law, the mass transport of the electroactive species through the diffusion layer also has to be faster. This results in a higher sensitivity than in a flow cell with a stationary electrode. Secondly, the thickness of the diffusion layer at the electrode surface

is almost entirely determined by the rotation speed of the electrode, and the detector response becomes independent of the fluid velocity in the flow cell. The response of other amperometric flow cells is flow-rate dependent [5, 6].

This paper describes the influence of flow rate, rotation speed and sample concentration on the detector response. The response surface as a function of these parameters is measured by using the detector in combination with continuous flow analysis. In combination with h.p.l.c. the influence of the height of the RDE in the flow cell on the detector response is discussed.

EXPERIMENTAL

Flow cell design

The design and operation of the prototype flow cell have been described [4]. The detector flow cell is essentially a wall-jet detector constructed with a RDE. The sample solution, entering through a narrow inlet, impinges normally on the RDE, and streams upwards between the RDE and the cell wall through a connecting channel to a compartment in which the reference and auxiliary electrode are located, and then to waste. In contrast to the prototype [4] the cone at the bottom of the flow cell was replaced by a flat bottom; it was therefore necessary to take care not to damage the surface of the electrode on the bottom of the cell when mounting the RDE. The rotation speeds of the RDE were measured with a stroboscope (Philips RR 9107).

Different electrode materials were used. For the continuous flow analysis experiments the RDE material consisted of home-made carbon paste (35% Dow Corning high-vacuum silicone grease and 65% w/w of graphite powder, UCP-1-M, Ultra Carbon, Bay City, Michigan). In the h.p.l.c. experiments the RDE was a wax-impregnated graphite electrode (PAR 9319).

Other apparatus

In the continuous flow analysis system a LKB Vario Perspex Pump was used with plastic tubing (Technicon). The flow rate of the pump was adjustable between 0.2 and 2.0 ml min⁻¹.

The liquid chromatograph was constructed from a Spectra Physics pump, model 740, a Rheodyne sample injection valve, model 70-10, with a 20- μ l sample loop, and a reversed-phase column (Lichrosorb RP-8, 10 μ m), 30 cm long and 4.6 mm internal diameter.

A Princeton Applied Research polarograph model 174A was used as a potentiostat in the normal d.c. mode. The reference electrode was an SCE; the auxiliary electrode was a platinum wire. In the continuous flow analysis experiments the potential of the working electrode was +550 mV vs. SCE whereas during the h.p.l.c. experiments the potential of the working electrode was +800 mV vs. SCE. The impedance in the detector flow cell was measured with a Radiometer conductivity meter type CDM 2.

Chemicals

The chemicals (analytical-reagent grade) were used as received. The buffer solution for continuous flow analysis consisted of 0.1 M acetic acid adjusted to pH 4.5 with pellets of sodium hydroxide. For h.p.l.c., a solution of 0.1 M acetic acid containing tetramethylammonium bromide (0.15 g l^{-1}), adjusted to pH 5.0 as above, was used as a mobile phase at a flow rate of 1.0 ml min^{-1} . As a test compound, potassium hexacyanoferrate(II) was used as a solution in the pH 4.5 buffer for the continuous flow analysis and in the mobile phase for the h.p.l.c. experiments.

RESULTS AND DISCUSSION

All symbols used are defined in Table 1.

Continuous flow analysis

The limiting current of the oxidation of hexacyanoferrate(II) in the detector was measured at different electrode rotation speeds (0, 17, 21, 26, 29, 31, 41 rps), flow rates (0.42, 0.64, 0.88, 1.08, 1.28, 1.62, 2.01 ml min^{-1}) and hexacyanoferrate(II) concentrations (1.16, 2.35, 4.69, 7.04, 9.38, $14.1 \mu\text{M}$). The response surface obtained is a four dimensional graph in a space defined by the dimensions detector response (in nA), concentration (in μM), flow rate (ml min^{-1}) and electrode rotation speed (in rps). Parts of this response surface are shown in Figs. 1 and 2 in three-dimensional graphs, fixing the fourth dimension at a constant value. Figure 1 shows the response

TABLE 1

Symbols used in the discussion

i	detector response in nA	d	nozzle diameter
k, K	constants	r	radius of the disk electrode
C	concentration of electroactive component	h	nozzle height
V	volume flow rate	z	axial coordinate
$f(V)$	function of V	x	radial coordinate
N	rotation speed of RDE in rps	$Z = z/d$	dimensionless axial coordinate
$g(N)$	function of N	$R = x/d$	dimensionless radial coordinate
i_d	limiting diffusion current	$H = h/d$	dimensionless nozzle height
n	number of electrons involved in the electrode reaction	$\omega = 2\pi N$	angular velocity of RDE
F	Faraday constant	$\phi Re = \omega r_0^2/\nu$	rotational Reynolds number
D	diffusion coefficient	r_0	total disk radius (sum of the working and non-working area).
ν	kinematic viscosity		

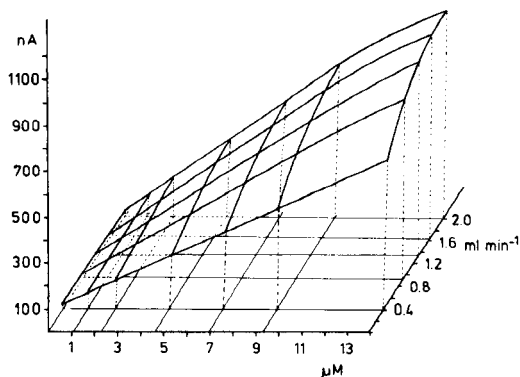


Fig. 1. The response surface of the detector flow cell as a function of the concentration of hexacyanoferrate(II) and the flow rate at the stationary electrode ($N = 0$ rps).

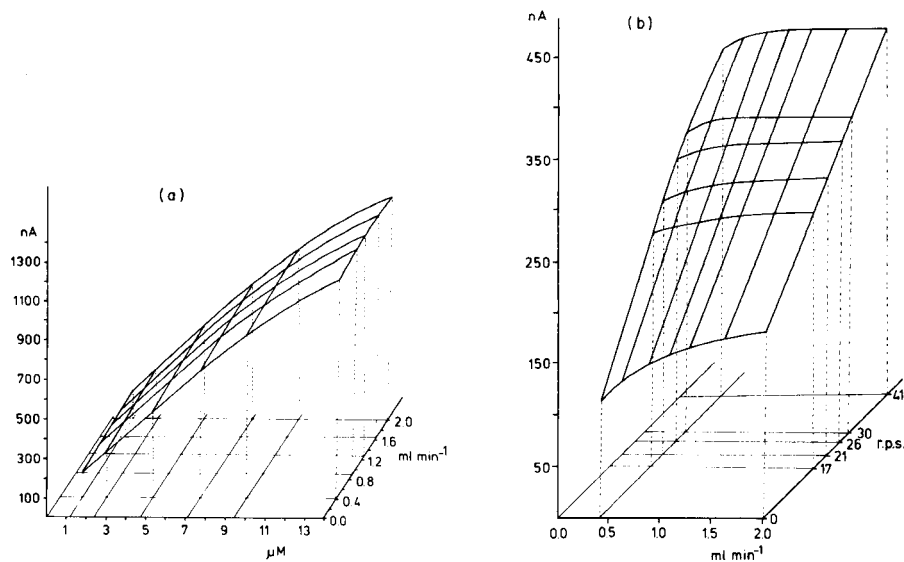


Fig. 2. The response surface of the detector flow cell as a function of (a) the concentration of hexacyanoferrate(II) and the flow rate at a constant electrode rotation speed of 17 rps; (b) the flow rate and the electrode rotation speed at a constant hexacyanoferrate(II) concentration ($2.35 \mu\text{M}$).

surface at the stationary electrode; in this case the detector is used as an ordinary wall-jet detector. Figure 2 represents the response surface of the rotating electrode under different conditions.

As is well known, the response of an amperometric detector depends only on the mass transfer rate of the electroactive species through the diffusion layer to the electrode surface. In the present flow cell the thickness of this diffusion layer is a summation of the effects of the flow rate in the cell and

the electrode rotation speed. Therefore the detector response is also a similar function of the flow rate and rotation speed: $i = k C [f(V) + g(N)]$. Figure 1 represents the simplest response surface, the detector being used as a wall-jet detector. Because there is no rotation, this equation can be simplified to $i = kCf(V)$. The hydrodynamics of fluid flow from a jet of fluid which spreads out radially over a plane surface, the fluid outside the jet being at rest, has been described by Glauert [7]. This pure hydrodynamic flow description was transformed in terms of hydrodynamic voltammetry by Yamada and Matsuda [6]. They derived an expression, eqn. (1), for the limiting diffusion current at a wall-jet electrode in hydrodynamic voltammetric terms, assuming that the cell diameter is large enough to neglect the cell wall effects on the flow boundary layer at the electrode surface.

$$i_d = (1.60 K) n F C D^{2/3} \nu^{-5/12} V^{3/4} d^{-1/2} r^{3/4} \quad (1)$$

Notably, this equation does not contain any function of the distance between the nozzle exit and the electrode surface, the so-called nozzle height.

A later study by Chin and Tsang [8] concerning mass transfer to a circular disk electrode in a wall-jet configuration in an infinitely large solution showed that different flow patterns exist in the cell as well as at the electrode surface. The character of the flow depends, inter alia, on the dimensionless axial position Z and the dimensionless radial position R with respect to the centre of the disk electrode (stagnation point). It also appears that the mass transfer rate is independent of the dimensionless nozzle height if $0.2 < H < 6$. At $H > 6$ the mass transfer rate diminishes.

By means of a curve-fitting program [9], the response surface of the detector flow cell used as a wall-jet detector (Fig. 1) was fitted to the equation $i = k C f(V)$, taking for $f(V)$ a power function analogous to eqn. (1). The high impedance in the flow cell between the electrodes ($\pm 60 \text{ k}\Omega$) caused a large voltage drop which will result in deviations from the linear relationship between the detector response and the concentration [10]. In consequence, only measurements in which the detector response current did not exceed 600 nA were taken into account for the curve-fitting program [9]. The fitting resulted in the relationship:

$$i = 58.5 C V^{0.29} + 15.8 \quad (2)$$

with a squared multiple correlation coefficient of 0.9975. The calculated intercept of 15.8 nA was caused by the background current in the detector flow cell (Table 2). The linear relationship between the detector response and the hexacyanoferrate(II) concentration at constant volume flow rates was very good, as can be seen in Table 3. At high concentrations of hexacyanoferrate(II) and at high flow rates, deviations from eqn. (2) occurred, caused by the above-mentioned voltage drop caused by the ohmic resistance in the flow cell (Fig. 1).

The detector response was increased considerably by rotating the electrode as can be seen in Fig. 2b and by comparing Fig. 1 and Fig. 2a. It is

TABLE 2

Background detector current as a function of the flow rate V (ml min^{-1}) and the rotation speed N (rps) of the RDE

N	Background current (nA)			N	Background current (nA)		
	$V = 0.42$	$V = 1.08$	$V = 2.01$		$V = 0.42$	$V = 1.08$	$V = 2.01$
0	15	15	15	29	22	21	21
17	20	19	19	31	22	21	21
21	21	20	20	41	23	23	22
26	21	20	20				

TABLE 3

Calibration curves and squared correlation coefficients (R^2) obtained with the wall-jet detector at different flow rates V (ml min^{-1}) for potassium hexacyanoferrate(II)

V	Calibration curve $i = aC + b^a$	R^2	V	Calibration curve $i = aC + b^a$	R^2
0.42	$i = 46.6C + 6.2^b$	0.9992	1.28	$i = 62.3C + 17.4^c$	0.9996
0.64	$i = 51.6C + 14.7^b$	0.9998	1.62	$i = 66.2C + 18.4^c$	0.9996
0.88	$i = 57.7C + 13.7^c$	0.9994	2.01	$i = 68.2C + 19.4^c$	0.9993
1.08	$i = 59.5C + 16.9^c$	0.9999			

^aCalculated by linear fitting: a = sensitivity in $\text{nA l } \mu\text{mol}^{-1}$, b = intercept in nA . ^bLinear range 1.1–14.1 $\mu\text{mol l}^{-1}$. ^cLinear range 1.1–9.4 $\mu\text{mol l}^{-1}$.

remarkable that the influence of the flow rate is negligible compared to the influence of the rotation speed (Fig. 2b). Also striking is the linear relationship between the detector response and the rotation speed of the RDE.

In the mass transport equation, eqn. (3) derived by Levich [11] for a reversible electrode reaction at a rotating disk electrode, the limiting current is proportional to the square root of the rotation speed:

$$i_d = 1.95 nFD^{2/3} \nu^{-1/6} \omega^{1/2} r^2 C \quad (3)$$

A boundary condition for the validity of eqn. (3) is that the flow regime has to be laminar. In the Levich theory of turbulent flow at an RDE [11], there are several differences from eqn. (3). Only an approximate equation could be derived. The linear relationship between i_d and C is not affected but the proportionality between i_d and $\omega^{1/2}$ is changed in an almost linear relationship between i_d and ω .

The onset of turbulence with an RDE is quite clearly a critical function of the centering and the smoothness of the disk electrode, shaft wobble, etc. The limits of a laminar flow regime for a very smooth and well centered RDE are up to rotational Reynolds numbers ϕRe of 10^4 – 10^5 . However, with most practical RDE's, the ϕRe limit of the laminar flow regime is lowered

by a factor of 10, because of the non-ideal construction of the electrode [12]. Probably account must also be taken that the RDE in the detector flow cell is situated in a very small volume and not in a so-called infinitely large solution. Therefore even at low rotation speeds the flow pattern in the cell will change from laminar to turbulent. In consequence the flow pattern in the detector flow cell with the RDE differs fundamentally from the flow pattern in the wall-jet detector.

Figure 2b shows that at high rotation speeds and low flow rates the detector response is no longer proportional to ω and that the flow rate has some influence. At high rotation speeds the diffusion layer at the electrode surface is very thin, resulting in a high concentration gradient and fast mass transport to the electrode. At low flow rates the mass transport of the electroactive species through the diffusion layer is faster than the rate of supply of the electroactive species to the detector cell. Depletion occurs at the electrode, the concentration gradient decreases and consequently the mass transport rate to the electrode surface decreases, which results in a lower detector response. At high flow rates there is no question of depletion effects in the detector cell and the detector response is limited by the diffusion current, as predicted by Levich's theory of turbulent flow at an RDE. Figure 3 illustrates clearly the depletion effect. At low flow rates the linear relationship between the rotation speed and the percentage of electroactive species which reacts at the electrode disappears. Although the percentage of oxidized electroactive species at low flow rates is considerably higher than the percentage at high flow rates, the absolute rate of oxidation is less than at high flow rates, which results in the observed decreased detector response.

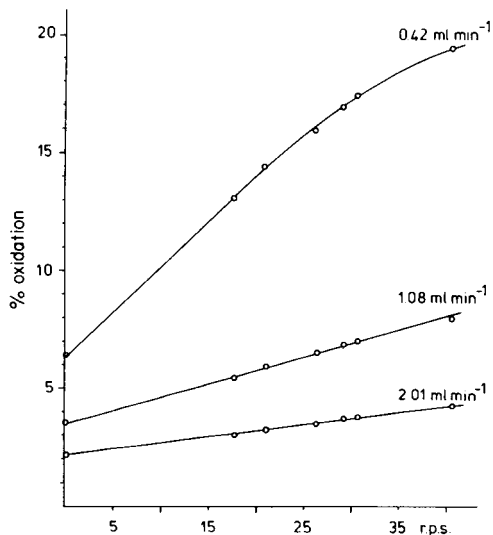


Fig. 3. Percentage of electroactive species oxidized at the electrode in the flow cell as a function of the flow rate and rotation speed. Sample concentration $4.69 \mu\text{M}$.

By means of a curve-fitting program the response surface of the detector flow cell was fitted to the equation $i = k C [f(V) + g(N)]$. The measurements at the stationary electrode were not taken into account because, as argued above the flow in the detector cell with the RDE differs fundamentally from the flow in a wall-jet detector. Only measurements in which the detector response current did not exceed 600 nA were used for the fitting procedure in order to eliminate the voltage drop effect; the measurements at low flow rates (0.42 and 0.64 ml min⁻¹) were also ignored in order to eliminate the influence of the depletion effect in the cell. As an analogy to the theory of the wall-jet electrode and of Levich's theory of an RDE, power functions were chosen for $f(V)$ and $g(N)$. The fitting procedure resulted in

$$i = 15.2 CV^{0.05} + 2.1 CN^{1.00} + 35.5 \quad (4)$$

with a squared multiple correlation coefficient of 0.9987. As in eqn. (2), the intercept of 35.5 nA is mainly caused by the detector background current (Table 2). The calculation shows that the detector response is independent of the flow rate ($V^{0.05} \approx 1$) and is linearly proportional to the rotation speed of the electrode. These results are in good agreement with the theory of turbulent flow at an RDE.

High-performance liquid chromatography

A fundamental difference exists in the use of a detector in combination with h.p.l.c. or in combination with continuous flow analysis. In continuous flow analysis the detector response is measured when the concentration of the compound of interest has reached a constant level in the flow cell, while in combination with h.p.l.c. the detector has to monitor a continuously changing concentration level in the flow cell. Therefore a detector for h.p.l.c. has to fulfil more stringent criteria, as has been discussed in detail by Scott [13].

There is a linear relationship between the amount of electroactive species in the introduced sample and the detector response at different rotation speeds of the RDE (Fig. 4). The detection limit has not been determined exactly, but was less than 1 ng of iron(II) per sample. It was not possible to use an anion-exchange column instead of a reversed-phase column. Because of its high negative charge, the hexacyanoferrate(II) ion was absorbed strongly on the former. However, it was eluted with the solvent front from the reversed-phase column. The samples had been dissolved in the mobile phase before they were introduced onto the column. No signal from the solvent front was observed by injecting blank samples. An advantage of elution of the sample with the solvent front is that it results in a very narrow chromatographic peak. Hence, it is easy to verify to what extent the detector parameters contribute to peak broadening.

According to Yamada and Matsuda [6] and Chin and Tsang [8], the response of a wall-jet electrode is independent of the nozzle height if $0.2 < H < 6$. Transformed to the dimensions of the present flow cell with a nozzle diameter

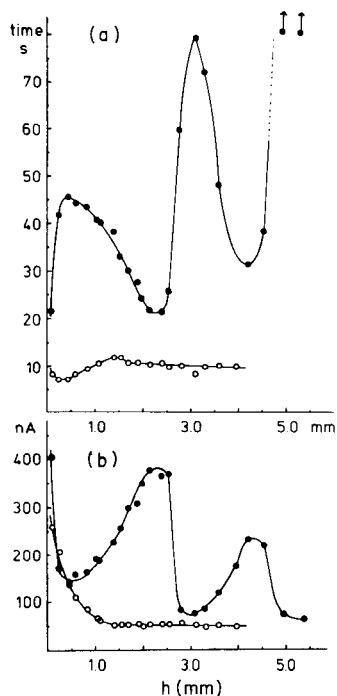
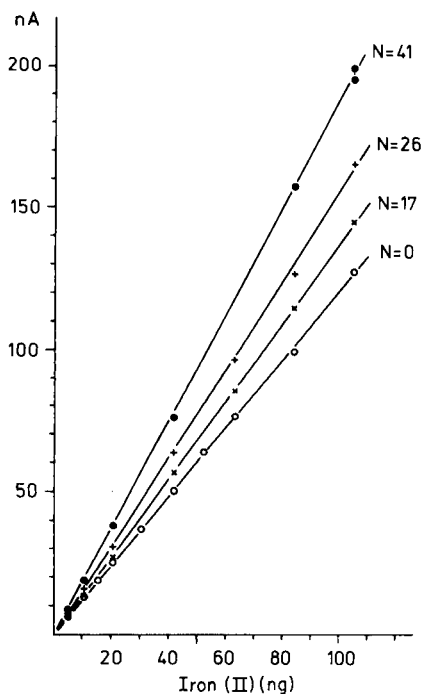


Fig. 4. Graphs of peak height (nA) of the detector response vs. the amount of iron(II) (ng) in 20- μ l samples of potassium hexacyanoferrate(II) at different rotation speeds (rps) of the RDE. Nozzle height 0.3 mm.

Fig. 5. Influence of the nozzle height on the detector performance with a stationary (\circ) and a rotating (\bullet , 21 rps) electrode at a constant sample concentration of 105 ng of iron(II) in 20- μ l samples. (a) Peak width as a function of nozzle height; (b) sensitivity of detector response as a function of nozzle height.

$d \approx 1$ mm, it is obvious that the detector response must be independent of the nozzle height if h is in the range 0.2–6 mm. In the range 1.5–5 mm (detector flow cell volume 95–320 μ l) the response of the wall-jet detector was in fact independent of the nozzle height. Neither the peak height (nA) nor the peak width (in s at 10% of the peak height) changed (Fig. 5, 0 rps). The detector response increased considerably at $h < 1.5$ mm but the peak width remained more or less constant.

Rotating the electrode in the flow cell resulted in a completely different behaviour of the detector response as a function of the nozzle height. It appeared that some favourable and some unfavourable cell configurations existed. With a favourable configuration the sensitivity was increased considerably compared with the wall-jet detector, although the chromatographic peak showed some tailing. The peak width at 50% peak height for a rotating electrode was smaller than for the wall-jet detector, but the peak width at 10% of the peak height was larger in the case of rotation (Fig. 5).

However, in contrast with current opinion concerning the volume of h.p.l.c. detector flow cells, it appears that for the present flow cell, a flow cell volume of 152 μl ($h = 2.4$ mm) provides better sensitivity than a volume of 32 μl ($h = 0.5$ mm) and is comparable with a flow cell volume of 6 μl ($h = 0.1$ mm), under the reported experimental conditions. This unusual behaviour of the detector validates the conclusion that completely different flow patterns exist in the wall-jet detector flow cell and in the cell with an RDE. The explanation of the increased sensitivity of the detector response as a function of the cell configuration has probably much to do with the hydrodynamic flow pattern of the fluid in the flow cell with the RDE and is the subject of current investigations.

The authors thank Mr. J. F. C. Nienhuis for constructing the electrochemical flow cell. We are also indebted to Drs. J. W. Weyland for doing the non-linear model fitting, and for the statistical calculations (TT WESP Program, Computer Centre, State University, Groningen, November 1977).

REFERENCES

- 1 K. Brunt, *Pharm. Weekbl.*, 113 (1978) 689.
- 2 P. T. Kissinger, C. Refshange, R. Dreiling and R. N. Adams, *Anal. Lett.*, 6 (1973) 465.
- 3 B. Fleet and C. J. Little, *J. Chromatogr. Sci.*, 12 (1974) 747.
- 4 B. Oosterhuis, K. Brunt, B. H. C. Westerink and D. A. Doornbos, *Anal. Chem.*, in press.
- 5 K. Brunt and C. H. P. Bruins, *J. Chromatogr.*, 172 (1979) 37.
- 6 J. Yamada and H. Matsuda, *J. Electroanal. Chem.*, 44 (1973) 189.
- 7 M. B. Glauert, *J. Fluid Mech.*, 1 (1956) 625.
- 8 D. T. Chin and C. H. Tsang, *J. Electrochem. Soc.*, 125 (1978) 1461.
- 9 L. Meites, General multiparametric curve-fitting program CFT3, Clarkson College of Technology, Potsdam, N.Y., 1974.
- 10 K. Brunt, C. H. P. Bruins and D. A. Doornbos. *Proc. Int. Conf. on Electroanalysis in Hygiene, Environmental, Clinical and Pharmaceutical Chemistry*, April 1979, London, Elsevier, Amsterdam, in press.
- 11 V. G. Levich, *Physicochemical Hydrodynamics*, Prentice Hall, Englewood Cliffs, 1962, Chaps. 2 and 3.
- 12 R. N. Adams, *Electrochemistry at Solid Electrodes*, M. Dekker, New York, 1969, Chap. 4.
- 13 R. P. W. Scott, *Liquid Chromatography Detectors*, Elsevier, Amsterdam, 1977, Chaps. 2 and 3.

DETERMINATION OF IRON(II) AND IRON(III) BY FLOW INJECTION AND AMPEROMETRIC DETECTION WITH A GLASSY CARBON ELECTRODE

J. W. DIEKER and W. E. VAN DER LINDEN*

Laboratory for Analytical Chemistry, University of Amsterdam, Nieuwe Achtergracht 166, 1018 WV Amsterdam (The Netherlands)

(Received 23rd July 1979)

SUMMARY

Flow injection analysis can be used for the determination of both iron(II) and iron(III) with an amperometric detector. The flow-through cell contains a glassy carbon electrode. Selection of the appropriate voltammetric technique, choice of the indication potentials, sample size, composition of the carrier stream, etc., are discussed. The limit of determination is about 10^{-6} M; the calibration curves are linear in the concentration ranges 10^{-3} – 10^{-5} M for iron(III) and 5×10^{-4} – 10^{-5} M for iron(II). To illustrate the potentialities of the proposed method, standard rocks have been analysed.

For many iron determinations, it is important to know not only the total concentration, but also the relative contribution of its valence states, Fe(II) and Fe(III). Beyer et al. [1] have investigated the determination of iron(II), iron(III) and total iron at a dropping mercury electrode (DME) by means of d.c. and a.c. polarography. Moore [2], used d.c. voltammetry at a platinum electrode for the same purpose. A preliminary study of the continuous analysis of iron(II) and iron(III) in process streams has been published by Parry and Anderson [3], using pulse polarography at a DME.

The purpose of the work described here was to investigate the possibilities of determining iron(II) and iron(III) by means of flow injection. An electrochemical flow-through cell provided with a glassy carbon electrode was used for the amperometric detection by d.c. voltammetry. The two valence states were differentiated by an appropriate choice of the indication potentials. Calibration, reproducibility, interferences and other aspects are discussed below.

EXPERIMENTAL

Equipment and chemicals

The detector used was the same as described before [4]. An SCE with a teflon capillary was used as the reference electrode. In some experiments when the carrier stream contained a fixed concentration of chloride, a silver/silver chloride wire reference electrode was used.

A PAR 174 polarographic analyser in the d.c. mode was employed for all experiments. Current-time relations were recorded with a Servogor RE 541. To determine the appropriate applied potentials for indication, current-potential curves were recorded for injections of equal amounts of samples. The applied potentials selected were +0.8 V for iron(II) and +0.2 V for iron(III). All potentials are referred to the SCE if not stated otherwise.

The peristaltic pump was a Gilson minipuls 2 model. The teflon tubes (0.8 mm i.d.) were connected with zero dead-volume connectors (Pierce Chromatoflo). The samples were injected in the carrier stream by means of a sample loop (sample injections slide valve, Pierce Chromatoflo). A straight tube (37 cm long) was used to connect the sample loop and the electrochemical flow-through cell. The tube of the sample loop (490 μ l) was coiled with a diameter of about 3 cm. The carrier stream was a 0.1 M perchloric acid-0.001 M potassium chloride solution, if not stated otherwise. The temperature of the carrier solution was controlled (25°C) by a thermostated water-bath (Haake NB 22).

All chemicals used were analytical grade. Iron(II) ammonium sulphate and iron(III) nitrate were used for preparation of the standard solutions of iron(II) and iron(III), respectively. In all experiments distilled water was used.

Procedure for the determination of iron(II) and iron(III) in standard rocks

About 250 mg of a dried sample was accurately weighed in a platinum crucible, and 5 ml of (1 + 1) sulphuric acid and 2.5 ml of hydrofluoric acid (40%) were added. The lidded crucible was placed on a sand-bath for 18 min. The sand-bath was maintained at $240 \pm 10^\circ\text{C}$ by means of a contact thermometer and a hot plate (Pyro-mag Stir, Cenco). During the decomposition, nitrogen was passed over the crucible. The crucible content was poured into about 150 ml of a solution containing 0.25 M boric acid and 10^{-3} M potassium chloride. This solution was transferred quantitatively to a 250-ml volumetric flask and diluted to volume with the boric acid-potassium chloride solution. Solutions were measured as soon as possible. In this case, the carrier stream was a 0.25 M boric acid-0.1 M perchloric acid-0.001 M potassium chloride solution.

RESULTS AND DISCUSSION

Selection of the voltammetric procedure

In a previous paper [4] the results of a comparative study on d.c., pulse and differential pulse techniques applied to amperometric detection at a glassy carbon electrode in an electrochemical flow-through cell were presented. It was shown that the d.c. mode is the most favourable, as long as adsorption of the reaction products does not occur; if adsorption occurs, the pulse method is recommended, although the limit of detection is somewhat poorer, because of electrochemical reactions of the electrode material [5].

To establish which mode should be preferred for the detection of iron(II) and iron(III), information about the adsorption is required. Štulík and Hora [6] have studied the influence of adsorption for the reduction of iron(III) at a rotating platinum electrode. To eliminate adsorption these authors applied potential pulses for cleaning the electrode. A constant signal was obtained with this method, whereas a decrease in the signal was observed with d.c. voltammetry. However, these experiments were carried out in a quiescent solution, hence the results are not necessarily relevant to flow conditions.

To obtain information about the adsorption of iron(II) and iron(III) at a glassy carbon electrode under f.i.a. conditions, several large volume injections ($490 \mu\text{l}$) of both 10^{-4} M iron(II) and 10^{-4} M iron(III) solutions were made. The d.c. mode was used and the applied potentials were + 0.8 V and + 0.2 V, respectively. The relative standard deviation of the peak currents obtained within a period of 4 h was 2% ($n = 22$) for iron(II) and 2.9% ($n = 28$) for iron(III). These results indicate that under f.i.a. conditions no noticeable adsorption takes place and therefore the d.c. mode can be used.

Calibration

The linearity of the response of the electrochemical cell was tested by injection of large sample volumes ($490 \mu\text{l}$) of iron(II) and iron(III) solutions. For iron(II), a linear relationship was obtained in the concentration range 10^{-5} – 5×10^{-4} M. For iron(III), the relationship was linear over the range 10^{-5} – 10^{-3} M. At lower concentrations, small deviations were observed for both iron(II) and iron(III). The limit of determination was about 5×10^{-7} – 10^{-6} M. Both the drift in the baseline and the noise were about the same as described previously [4].

Sample size in relation to the reproducibility of the signal

In the following discussion, a stepwise response experiment is considered in which a concentration profile is applied to the electrochemical detector. The transfer function obtained depends on the construction of the electrochemical cell, the mode in which the instrument is used, and the electrode reaction of the compound to be considered. If the electrode reaction is irreversible, like the reaction of iron at glassy carbon, the transfer function will comprise an additional factor because of the kinetics of the electrode reaction. When iron(II) or iron(III) reacted at the electrode, variations in the transfer function were found experimentally. Although this had little influence on the steady-state signal, relatively large variations were observed in the steep part of the response curve. Corresponding variations in the peak heights were found in the flow injection procedure depending on the sample volume. A sample loop of $160 \mu\text{l}$ (yielding a maximum signal corresponding to 40% of the steady-state signal) showed much larger variations than a sample loop of $490 \mu\text{l}$ (maximum signal corresponding to 90% of the steady-state signal). In the latter case, the reproducibility of the peak currents was

found to be satisfactory during a prolonged period of time for both iron(II) and iron(III) and about 40 samples/hour could be analysed at a flow rate of 1 ml min^{-1} .

The peak current was influenced by fluctuations in the temperature of the carrier stream and the sample. A change of 5°C in temperature gave a change of about 10% in the peak height.

Composition of the carrier stream

For many determinations of iron, it is necessary to carry out a dissolution procedure with strong acids, e.g., in the case of standard rocks. Hydrochloric acid, perchloric acid and sulphuric acid were therefore examined as carrier solutions at concentration levels of 0.1 and 0.01 M. In the case of hydrochloric acid, spikes on the peak currents and baseline were observed. The reproducibility of the peak currents was found to be satisfactory at both concentration levels for perchloric acid and sulphuric acid, even when the iron sample also contained 0.1 M hydrochloric acid. Thus it can be concluded that iron can be determined in solutions containing perchloric acid, sulphuric acid and hydrochloric acid. The i_p vs. E curves for the oxidation of iron(II) both in perchloric acid and sulphuric acid in the presence and the absence of 10^{-3} M chloride at pH 1 as well as pH 2 were found to be close together. The same was true for the i_p vs. E curves for the reduction of iron(III). Higher pH values were not studied because of the interaction of iron(III) with hydroxyl ions. Although hydrolysis would be avoided by addition of complexing agents, the reduction wave would then shift to more negative potentials resulting in a less favourable indication potential. At the low pH values used, the conditional constants of most iron complexes are so small that apart from fluoride ions for instance, complexing agents would have little effect on the indication potential.

Interferences

Interferences can be electrochemical or chemical in nature. Compounds that can be reduced at a glass carbon electrode at $+0.2 \text{ V}$ vs. SCE will interfere in the determination of iron(III) whereas compounds which can be oxidized at $+0.8 \text{ V}$ vs. SCE are interferences in the determination of iron(II). Interferences might be expected from copper(II) and mercury(II). The reduction of copper(II) at pyrolytic graphite electrodes occurs at potentials more positive than that predicted by the Nernst equation [7]. This can be attributed [8] to the difference in bonding energy between the atomic copper layer and the electrode surface, and the bonding energy between copper-copper layers. Several investigators [9, 10] have made similar observations for other metals at solid electrodes. Štulíková and Vydra [11] have studied the interaction between copper and glassy carbon. They concluded that copper(II) is not reduced to elemental copper at the more positive potentials, but to copper(I) which tends to adsorb at the electrode surface. This effect is less important in chloride medium. For the present

purpose, it was important to know to what extent this effect occurs at the indication potential used for the determination of iron(III). Therefore, i_p vs. E curves were recorded for solutions containing Fe(II), Fe(III), Cu(II) or Hg(II), in the absence (Fig. 1a) and presence (Fig. 1b) of 10^{-3} M chloride. The following effects in chloride medium are apparent: (i) the reduction of copper(II) or the adsorption of copper(I) is indeed not significant; (ii) the Fe(II)/Fe(III) system becomes more reversible; (iii) the mercury wave is shifted to more negative potentials because of complex formation between mercury(II) and chloride ions. The shape of the f.i.a. peaks of copper(II) in the steep part of the wave is somewhat deformed. The interferences of these and other ions in the determinations of iron(II) and iron(III) at pH 1 are indicated in Table 1. Obviously, strong oxidants, e.g. oxygen and reductants will interfere.

Analysis of standard rocks

It was important to carry out the decomposition at about 240°C at which temperature gentle boiling was obtained. The heating should be stopped when most of the hydrofluoric acid and water has been evaporated. Although the fluoride ion concentration after the dissolution procedure will be low, particularly at low pH values, complex formation of iron(III) with

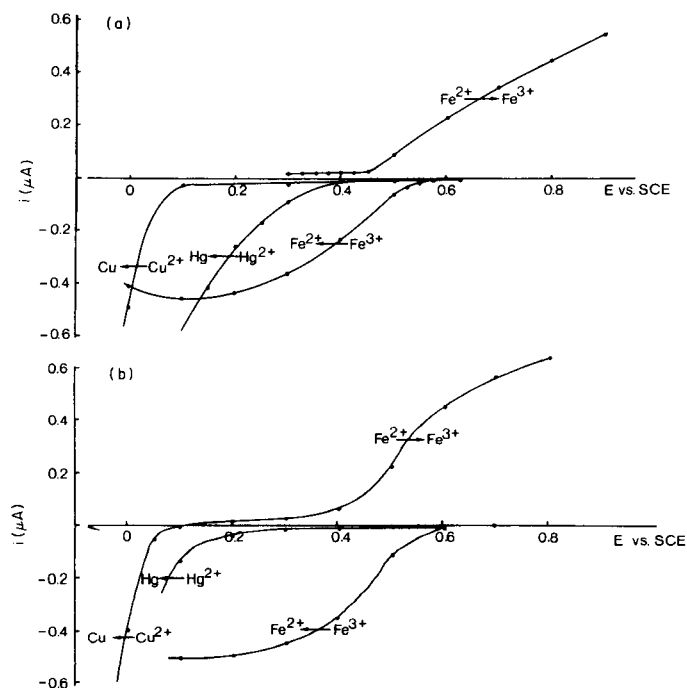


Fig. 1. i_p vs. E curves of solutions containing 10^{-4} M Fe(II), Fe(III), Cu(II) or Hg(II) at pH 1: (a) in the absence and (b) in the presence of 10^{-3} M chloride.

TABLE 1

Interferences on the determination of iron(III) and iron(II) at pH 1 with an applied potential of 0.2 V for iron(III) and 0.8 V for iron(II) for 490- μ l samples

Sample	\bar{i}_p (sample) \bar{i}_p (Fe)	Corr. ^a	S.d. (%) ^b	
Interferences on iron(III)				
10 ⁻⁴ M Fe ³⁺	1			
10 ⁻⁴ M Fe ³⁺ , 10 ⁻⁴ M Cu ²⁺	1.05	1.04	0.6	(4)
10 ⁻⁴ M Cu ²⁺	0.005		17.0	(3)
10 ⁻⁴ M Fe ³⁺ , 10 ⁻³ M Cu ²⁺	0.99	0.98	0.8	(4)
10 ⁻³ M Cu ²⁺	0.012		12.5	(3)
10 ⁻⁴ M Fe ³⁺ , 10 ⁻⁴ M VO ²⁺	0.95	0.95	2.2	(6)
10 ⁻⁴ M VO ²⁺	— ^c			
10 ⁻⁴ M Fe ³⁺ , 10 ⁻⁴ M Hg ²⁺	0.99	0.98	0.3	(4)
10 ⁻⁴ M Hg ²⁺	0.006		15.7	(3)
10 ⁻⁴ M Fe ³⁺ , Hg ²⁺ , Cu ²⁺ , VO ²⁺ , Mn ²⁺	0.93	0.95	1.2	(4)
Same mixture without Fe ³⁺	-0.024		2.9	(3)
10 ⁻⁴ M Fe ³⁺ , MoO ₄ ²⁻ , Mn ²⁺ , WO ₄ ²⁻	1.02	0.99	2.4	(6)
Same mixture without Fe ³⁺	0.035		4.8	(3)
Interferences on iron(II)				
10 ⁻⁴ M Fe ²⁺	1			
10 ⁻⁴ M Fe ²⁺ , 10 ⁻⁴ M Cu ²⁺	1.01	1.01	0.8	(4)
10 ⁻⁴ M Cu ²⁺	—			
10 ⁻⁴ M Fe ²⁺ , 10 ⁻³ M Cu ²⁺	1.06	1.06	2.1	(4)
10 ⁻³ M Cu ²⁺	—			
10 ⁻⁴ M Fe ²⁺ , 10 ⁻⁴ M Hg ²⁺	1.00	0.98	0.2	(4)
10 ⁻⁴ M Hg ²⁺	0.02		12.8	(4)
10 ⁻⁴ M Fe ²⁺ , 10 ⁻⁴ M VO ²⁺	1.01	0.94	2.8	(7)
10 ⁻⁴ M VO ²⁺	0.07		3.2	(4)
10 ⁻⁴ M Fe ²⁺ , VO ²⁺ , Hg ²⁺ , Cu ²⁺ , Mn ²⁺	1.00	1.00	1.8	(4)
Same mixture without Fe ²⁺	—			
10 ⁻⁴ M Fe ²⁺ , MoO ₄ ²⁻ , WO ₄ ²⁻ , Mn ²⁺	1.01	0.99	0.4	(4)
Same mixture without Fe ²⁺	0.015		14.0	(5)

^a \bar{i}_p (Sample)/ \bar{i}_p (Fe) corrected for reference solution. ^bStandard deviation on i_p with number of determinations in parentheses. ^cInjection of the vanadyl solution alone gives a positive peak and a negative peak of the same height.

fluoride can occur. This complex formation will influence the indication potential for the determination of iron(III). According to the literature [12–14], boric acid can be used to minimize the effect of the excess of hydrofluoric acid by the formation of fluoroboric acid. The presence of boric acid will lead to a decrease of the value of the conditional stability constant of the iron(III) fluoride complex resulting in a less negative shift of the reduction wave as can be seen from the i_p vs. E curve of iron(II) and iron(III) shown in Fig. 2. From Fig. 2, suitable indication potentials for iron(II) and iron(III) are +0.7 V and -0.3 V (vs. Ag/AgCl) respectively.

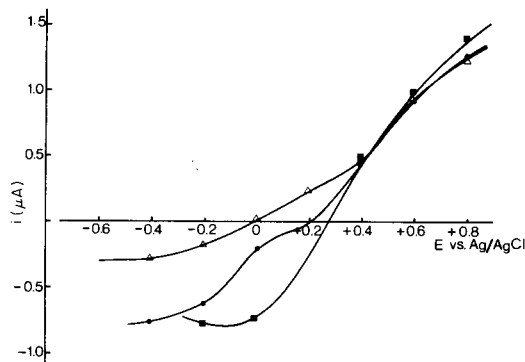


Fig. 2. i_p vs. E curves of a solution containing 10^{-4} M Fe(II) and Fe(III) at pH 1 in 0.05 M hydrofluoric acid: (●) in the presence of 0.25 M boric acid; (▲) in the absence of boric acid; (■) in the absence of both hydrofluoric and boric acids.

TABLE 2

Weight percentages of iron(II) and iron(III) in U.S. Geological Survey Standard Rocks by f.i.a.

U.S.G.S. standard (split/position)	F.i.a. results ^a (%)		Published averages (and ranges) ^b	
	Fe(II)	Fe(III)	Fe(II)	Fe(III)
AGV 1 (97/22)	1.57 ± 5 (4)	3.21 ± 5 (4)	1.59 (1.38–1.96)	3.15 (2.88–3.47)
G 2 (7/24)	1.06 ± 5 (5)	0.83 ± 7 (5)	1.13 (0.91–1.40)	0.76 (0.50–1.05)
BCR 1 (65/20)	6.49 ± 5.5 (6)	2.65 ± 3 (6)	6.84 (6.47–7.35)	2.57 (2.22–3.15)

^aWith relative standard deviation and number of determinations in parentheses.

^bCalculated from reference [1].

For the analysis of rocks, the standard addition method was used. The results obtained (corrected for the blank) for some U.S. Geological Survey Standard Rocks are presented in Table 2. The standard deviation of the results is determined mainly by the decomposition process and not by the flow injection analysis itself.

The authors express their gratitude to Mr. P. J. de Goede and Mr. E. van Zalen for their experimental help and to Prof. Dr. G. den Boef for his advice during the preparation of the manuscript.

REFERENCES

- 1 M. E. Beyer, A. M. Bond and R. J. W. McLaughlin, *Anal. Chem.*, 47 (1975) 479.
- 2 W. M. Moore, *Anal. Chim. Acta*, 105 (1979) 99.
- 3 E. P. Parry and D. P. Anderson, *Anal. Chem.*, 45 (1973) 489.
- 4 J. W. Dieker, W. E. van der Linden and H. Poppe, *Talanta*, 26 (1979) 511.
- 5 J. W. Dieker, W. E. van der Linden and H. Poppe, *Talanta*, 25 (1978) 151.
- 6 K. Štulík and V. Hora, *J. Electroanal. Chem.*, 70 (1976) 253.

- 7 B. H. Vassos and H. B. Mark Jr., *J. Electroanal. Chem.*, 13 (1967) 1.
- 8 *Encyclopedia of Electrochemistry of the Elements*, Vol. II, Ch. 6, U. Bertocci and D. Turner (Eds.), M. Dekker, New York, 1974.
- 9 S. P. Perone, *Anal. Chem.*, 35 (1963) 2091.
- 10 E. Schmidt and R. Gygax, *J. Electroanal. Chem.*, 12 (1966) 300.
- 11 M. Štulíková and F. Vydra, *J. Electroanal. Chem.*, 44 (1973) 117.
- 12 D. D. Perrin, *CRC Crit. Rev. Anal. Chem.*, 5 (1975-76) 85.
- 13 U. Abed, *Anal. Chim. Acta*, 47 (1969) 495.
- 14 H. N. S. Schafer, *Analyst*, 91 (1966) 755.

DETERMINATION OF CYANIDES BY CONTINUOUS DISTILLATION AND FLOW ANALYSIS WITH CYLINDRICAL AMPEROMETRIC ELECTRODES

B. PIHLAR* and L. KOSTA

Department of Chemistry, Edvard Kardelj University, Ljubljana (Yugoslavia)

(Received 2nd August 1979)

SUMMARY

A continuous system for the determination of free and complex cyanides has been developed. Hydrogen cyanide is released in an acidic solution in a counter-current system operated by a peristaltic pump, absorbed in dilute sodium hydroxide and then fed into the amperometric detector with a cylindrical silver flow-through electrode. The parameters affecting the release and absorption of cyanide, as well as the electrode response and sensitivity, are described. Differentiation between total cyanide and strongly bound metal cyanide complexes is achieved by u.v. decomposition of the complexes.

Flow analysis has recently found a wide variety of analytical applications. The renaissance of interest in this methodology is connected with flow injection analysis introduced by Růžička and Hansen [1] who contributed to better understanding of its principles [2] and extended this approach to a number of analytical methods [3]. Progress in this field has been supported by the development of flow-through detectors among which electrochemical sensors have a significant place [3-9].

In monitoring toxic pollutants for environmental control, automated systems are desirable; flow-injection or continuous flow analysis appear promising in this respect. An analytical system based on this principle, with an amperometric flow-through electrode, has been dealt with in another paper [10]. The alkaline sample was injected into the system, either directly or after distillation in Conway cells, depending on its complexity. The presence of certain electroactive interfering compounds and strict requirements regarding pH, however, caused difficulties in the continuous mode of operation. The present investigation concentrates on the development of a continuous distillation unit which could solve the above problems and extend the applicability of the system to a wide range of samples including heavily contaminated waste waters and effluents.

EXPERIMENTAL

Apparatus

The manifold arrangement for continuous determination of cyanide

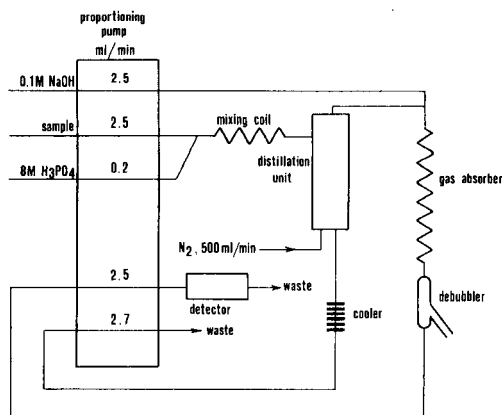


Fig. 1. Manifold for automated determination of cyanide.

is shown in Fig. 1. Its main components are the distillation unit with absorber, the electrode with potentiostat, a peristaltic pump (Technicon Proportioning Pump II) and connecting tubing. The acidified sample is pumped into the distillation unit and the released hydrogen cyanide is carried by a stream of nitrogen into the absorption column containing sodium hydroxide. All connecting tubes are 0.5 mm i.d. except the mixing coil (0.5-m of polyethylene tubing, 0.75 mm i.d.). The amperometric flow-through detector is as described previously [10]. The potential of the silver working electrode is kept at -0.5 V vs. mercury(I) sulphate (Radiometer K 6112) by means of a potentiostat; the anodic current, recorded on a Varian A-25 strip-chart recorder, results from the reaction $\text{Ag} + 2\text{CN}^- \rightarrow \text{Ag}(\text{Cn})_2^- + \text{e}^-$.

The distillation unit and absorber are shown in greater detail in Fig. 2. The former is constructed of borosilicate glass, half-packed with glass helices and wrapped with a heating wire (50 ohms to which 70 V a.c. are applied from a variable transformer); a 100-W heating tape could also be used. The nitrogen stream enters at the bottom of the distillation column and carries hydrogen cyanide through the condenser into the absorption unit. Sodium hydroxide (0.1 M) is pumped to the top of the absorption column. The large contact area between the thin film of base and the gas ensures quantitative absorption of the cyanide. The solution then passes through a gas-liquid separator (with a holdup volume of 1 ml) to the electrode. The reflux from the condenser (1.5 ml) and the solution are cooled and pumped to waste. All components are mounted vertically on a perspex board.

The decomposition of strongly bound metal cyanide complexes is achieved by irradiating samples (10 ml) acidified with 0.1 ml of phosphoric acid (1 + 1) in a 10-ml cylindrical silica cell. A 100-W u.v. source (Applied Photophysics mercury lamp 100 LQ) is used. As shown in Fig. 3 the cell is connected by means of a screw thread to a bent borosilicate glass tube containing 1 ml of 2.5 M sodium hydroxide. The lamp is positioned on the

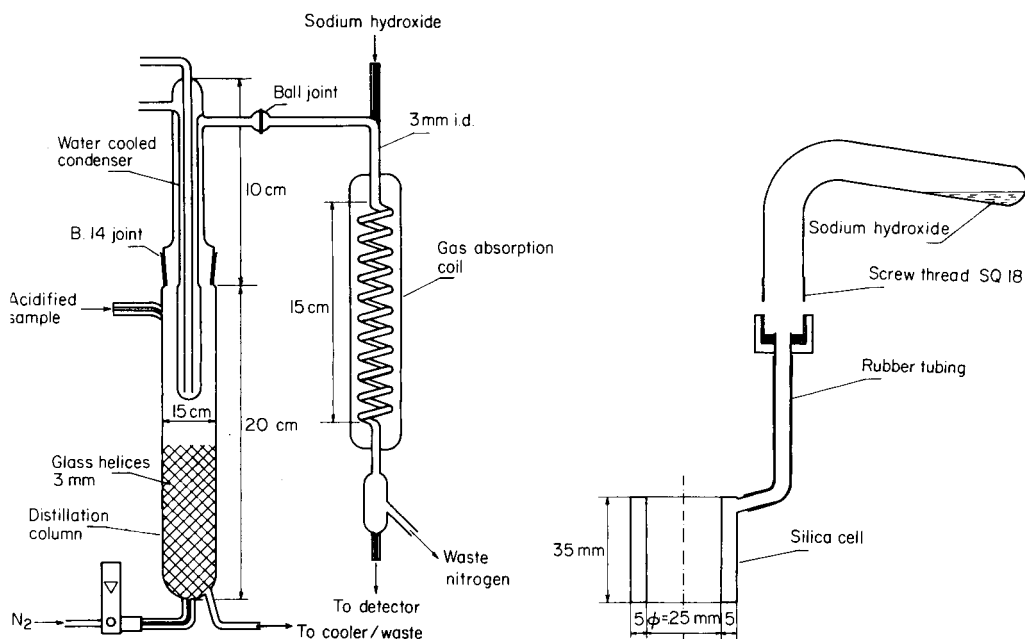


Fig. 2. Distillation unit and HCN absorption coil.

Fig. 3. Apparatus for u.v. decomposition of strongly bound cyanide complexes.

axis of the cylindrical irradiator and the solution is exposed for 3–4 min. Subsequently the sample is neutralized with sodium hydroxide by mixing solutions from the two compartments whereupon total cyanide is determined.

Reagents

Cyanide stock solution containing $1 \text{ mg CN}^- \text{ ml}^{-1}$ in 0.1 M sodium hydroxide was standardized titrimetrically. Standards of lower concentrations were prepared by serial dilution with 0.1 M sodium hydroxide. Samples containing chlorine were treated with sodium arsenite or ascorbic acid using starch-iodide paper as indicator. Sulphide was removed by precipitation with lead carbonate, but according to Goulden et al. [11] it could also be eliminated with sodium hydrogensulphite.

RESULTS AND DISCUSSION

Reported results for cyanide in real samples such as surface and waste waters, effluents from galvanic plants etc. are frequently of poor accuracy because of lack of selectivity and limited sensitivity of the techniques applied. These could be improved to some extent by preliminary separation of gaseous hydrogen cyanide [11–15]. In our earlier work distillation in Conway dishes combined with flow injection proved satisfactory [10]. The cyanide flow-through electrode operated at the stated hydrodynamic conditions

ensured reliable determinations from several g l^{-1} to $<1 \mu\text{g l}^{-1}$ with a linear response over the whole operating range. Its sensitivity increased with the $2/3$ power of the electrode length and the $1/3$ power of volume flow rate. The newly developed distillation unit provides for continuous monitoring as well as for automated analysis of discrete samples and eliminates interferences occurring in complex industrial and municipal wastes. An optimization procedure was used for factors such as the temperature in the distillation column (with determination of the fraction of volatilized sample), carrier gas flow, absorber-to-sample flow ratio, kind and strength of the acid used and the configuration of absorption and distillation units, so that the recoveries of the distillation/the absorption steps could be adjusted to exploit fully the operating range of the electrode. The apparatus shown in Fig. 2 was found to satisfy all the stated requirements.

As shown in Table 1, cyanide is quantitatively recovered except in the highest concentration range where overloading of the distillation and/or absorption units occurs. However, these losses can easily be eliminated by adjusting the ratio of sample to absorber flow. Furthermore, for the lowest range the same modification can be used to improve the sensitivity and detection limit by an order of magnitude. In Fig. 4 typical steady-state calibration responses are reproduced for $0.2\text{--}1 \text{ mg CN}^{-1} \text{ l}^{-1}$ for both direct passage of standards through the electrode and distillation of the same solutions. It can be seen that in this range losses of cyanide are negligible.

Unknown cyanide concentration can be determined either from a calibration graph or by the standard addition technique. The latter is preferred when the viscosity of the sample differs markedly from that of the standards, especially when transient measurements are made.

Figure 5 shows the effect of different sampling times, obtained by introducing a solution containing $100 \mu\text{g CN}^{-1} \text{ l}^{-1}$. Note that a sampling time of 30 s gives 75% of the steady-state reading, whereas in 1 min over 90% of the plateau value is obtained. From the logarithmic dependence of concentration against time it was found that for the selected conditions the lag phase was 1 min and the half-wash time 20 s. These parameters could not be improved by air segmentation because dynamic equilibrium in the distillation column was the main factor determining the response of the whole system. Alternating samples and washing solution every 30 s enabled 60 samples per

TABLE 1

Distillation recoveries of cyanide

CN ⁻ conc. (mg l ⁻¹)	0.001	0.01	0.1	1	10	100	1000
Recovery(%) ^a	100 ± 2	101 ± 1	100 ± 1	99 ± 1	97 ± 0.8	95 ± 0.5	90 ± 0.5

^aBased on three steady-state measurements.

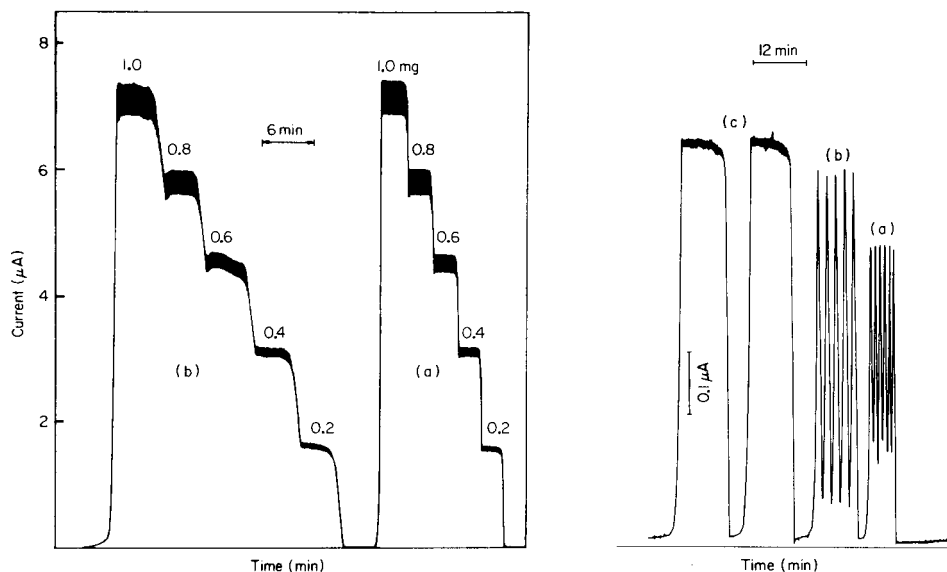


Fig. 4. Steady-state curves obtained by (a) direct introduction of cyanide standards into 0.1 M NaOH, and (b) by distillation of the same solutions. The numbers on the curves refer to $\text{mg CN}^- \text{l}^{-1}$.

Fig. 5. Introduction of $100 \mu\text{g CN}^- \text{l}^{-1}$ solution into distillation apparatus for: (a) 30 s (sampling-to-wash ratio 1:1); (b) 60 s; (c) to obtain steady-state value.

hour to be determined. For samples differing markedly with respect to cyanide concentration the sampling rate must be decreased to ensure better sample discrimination.

Differentiation between free and complex cyanides

The concentration of free cyanide ions in an aqueous medium depends on the pH of the solution [12] and on the content on heavy metal ions forming cyanide complexes of different stabilities. Both ion-selective electrodes [12] and amperometric detectors [10] measure only free cyanide ions; however, for accurate determination of the total amount of cyanide, the kinds of metal ions present as well as the relevant stability constants must be known. The most stable complexes usually found in waste waters are those of iron(II), iron(III) and cobalt(III). According to Royer et al. [14] they can be decomposed by the modified Serfass distillation or by u.v. irradiation [11]. Samples containing a large amount of suspended matter are not completely decomposed by using the silica coil as proposed by Goulden et al. [11]. The u.v. irradiator shown in Fig. 3 proved to be more efficient owing to its favourable geometry which allows full exploitation of the radiation source in addition to flexibility with respect to the duration of exposure. An irradiation time of 3–4 min was found to be sufficient for normal transparent samples. In the presence of organic matter, prolonged

irradiation and additional air cooling were required to avoid boiling of the solution (in the present experimental conditions boiling occurred after 6 min). To prevent oxidation of cyanide in the gas phase the silica cell must be completely filled with the solution. Therefore the side-arm of the cell was shielded with rubber tubing and the absorption vessel was made from borosilicate glass. The required pH of the solution during irradiation (<3) and for final measurement (>11) was obtained by appropriate addition of phosphoric acid or sodium hydroxide. When the above requirements were met, iron complexes corresponding to a total cyanide content of 100 mg l^{-1} were quantitatively decomposed.

Table 2 shows the results for three samples of tap water and for a pond suspected of contaminating the local water supply line. A larger concentration of iron in all samples except sample 1 confirmed the correlation between metal and cyanide content. Even substantial amounts of heavy metals such as zinc, copper and cadmium did not affect the measurement since their complexes readily yield hydrogen cyanide on acidification.

Sample pretreatment with u.v. radiation is not recommended in the presence of compounds capable of releasing cyanide ions, e.g. thiocyanates or nitriles.

Interfering substances and/or strong complexes accumulate and thermally dissociate in the distillation unit, causing oscillation of the plateau of the signal. Volatile oxidizing agents such as chlorine must be destroyed with sodium arsenite. At the trace level, filtration of the alkaline samples on cellulose papers is not recommended because of the possible interference; centrifugation or filtration through synthetic membrane filters must be used instead.

The methodology and apparatus described has been in use for a year and tested on a great number of samples of different types. The results have demonstrated that the distillation technique combined with the amperometric flow-through detector is a reliable approach to the determination of cyanide in complex samples down to the $\mu\text{g l}^{-1}$ level. The system can be applied to automated discrete sample analysis as well as to continuous monitoring and speciation studies.

TABLE 2

Determination of free and total cyanide in drinking waters and in a polluted pond

Sample	Free cyanide ($\mu\text{g l}^{-1}$)	Total cyanide ($\mu\text{g l}^{-1}$)	Total iron ($\mu\text{g l}^{-1}$)
Tap water 1	1.1	4.3	5
Tap water 2	0.3	19.5	12
Tap water 3	0.2	17.0	10
Polluted pond	35.0	105	45

REFERENCES

- 1 J. Růžicka and E. H. Hansen, *Anal. Chim. Acta*, 78 (1975) 145.
- 2 J. Růžicka and E. H. Hansen, *Anal. Chim. Acta*, 99 (1978) 37.
- 3 D. Betteridge, *Anal. Chem.*, 50 (1978) 832A.
- 4 Zs. Fehér, G. Nagy, K. Tóth and E. Pungor, *Analyst*, 99 (1974) 699.
- 5 P. T. Kissinger, *Anal. Chem.*, 49 (1977) 447A.
- 6 P. L. Bailey, *Anal. Chem.*, 50 (1978) 698A.
- 7 W. J. Blaedel and L. N. Klatt, *Anal. Chem.*, 38 (1966) 879.
- 8 J. Růžicka, E. H. Hansen and E. A. Zagatto, *Anal. Chim. Acta*, 88 (1977) 1.
- 9 S. G. Weber and W. C. Purdy, *Anal. Chim. Acta*, 100 (1978) 531.
- 10 B. Pihlar, L. Kosta and B. Hristovski, *Talanta*, 26 (1979) 805.
- 11 P. D. Goulden, B. K. Afghan and P. Brooksbank, *Anal. Chem.*, 44 (1972) 1845.
- 12 R. A. Durst, *Anal. Lett.*, 10 (1977) 961.
- 13 D. B. Easty, W. J. Blaedel and L. Anderson, *Anal. Chem.*, 43 (1971) 509.
- 14 J. L. Royer, J. E. Twichell and S. M. Muir, *Anal. Lett.*, 6 (1973) 619.
- 15 K. Wissner, *Fresenius Z. Anal. Chem.*, 286 (1977) 351.

APPLICATIONS OF A VOLTAMMETRIC FLOW-THROUGH CELL IN ON-LINE ANALYSIS FOR ORGANIC COMPOUNDS

ARI IVASKA*

Department of Analytical Chemistry, Åbo Akademi, 20500 Åbo 50 (Finland)

W. FRANKLIN SMYTH

Department of Chemistry, Chelsea College, Manresa Road, London SW 3 (Gt. Britain)

(Received 30th July 1979)

SUMMARY

A flow-through voltammetric cell is described and the d.c. and pulse working modes are studied in on-line situations. On-line analysis of different compounds has been done by (a) direct oxidation at a glassy carbon electrode, (b) direct reduction or (c) direct oxidation at a mercury-coated solid electrode, and (d) cathodic stripping by first depositing the compound on a mercury film and then employing a cathodic d.c. voltage scan. The linear range and the detection limit of the on-line method are better than those in quiescent solutions.

Different electrochemical flow-through cells based on voltammetric or coulometric principles have frequently been reported [1, 2]. These cells can be used either to monitor electrochemically active species in flowing streams or as detectors in high-performance liquid chromatography (h.p.l.c.). In most studies the indicator electrode is a solid electrode of platinum, carbon paste or glassy carbon principally because solid electrodes have distinct advantages in flowing streams over the dropping mercury electrode (DME). The large positive potential range of solid electrodes allows analyses for compounds which are oxidized at more positive potentials than that corresponding to the dissolution of mercury. High flow rates can also be used to increase either the sampling rate or the sensitivity by increased mass transport to the electrode. With the DME, high flow rates cause problems because drop formation is influenced by the flow and may not be uniform. With time-dependent modes like pulse and differential pulse, the response to a prematurely dislodged drop is rapid with a slow recovery resulting in extra noise. The most serious disadvantage with solid electrodes is the non-renewal of their surface; this has led to some recent designs of flow-through cells with the DME as the working electrode [3, 4].

In the present paper applications of a voltammetric flow-through cell to the determination of selected organic compounds are discussed. Particular attention is given to the utilization of different working principles in the operation of the cell for various depolarizers.

EXPERIMENTAL

Instrumentation

The electrochemical cell used, of the wall-jet type [5], is a slight modification of a previous design [6]. A schematic diagram is given in Fig. 1. The incoming solution impinges on the surface of the working glassy carbon electrode (3-mm Tokai glassy carbon rod) and then passes the tip of the saturated calomel reference electrode (SCE). The platinum auxiliary electrode is placed near the working electrode. All potentials mentioned are referred to the SCE. The cell body is made of plexiglas; the volume is adjustable; about 80 μl was used throughout this study. A PAR 174A polarograph was used for the voltammetric measurements. Solutions were pumped with a three-bar peristaltic pump with variable rotation speed; flow rates of 2–5 ml min^{-1} were used. The currents were recorded with a strip chart recorder. The temperature was maintained at ca. 22°C.

Reagents

All chemicals used were of analytical-reagent grade. An acetate buffer of pH 4 (0.1 M) was used in the oxidation studies of *p*-nitroso-*N,N*-diethylaniline. Solutions contained 10% (v/v) methanol to keep the organic compounds in solution and to aid dissolution of the reactants and products of the electrode reactions. Nitrazepam was studied in 0.1 M sulphuric acid–10% methanol. The oxidation and cathodic stripping of 1,3-dimethyl-5-ethyl-5'(*p*-chlorophenyl)-2-thiobarbituric acid were studied in Britton–Robinson buffer of pH 8.

Procedures

In the direct oxidation and reduction studies, the supporting electrolyte was first pumped through the electrochemical cell. After a steady background current had been obtained, the analyte solution was pumped and the current change recorded. When high current ranges were used in the d.c. working mode, a steady background current was obtained immediately

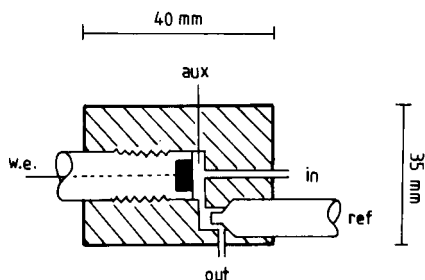


Fig. 1. The flow-through cell with a glassy carbon working electrode (w.e.), a reference electrode (ref) and a platinum wire auxiliary electrode (aux).

whereas for low ranges (e.g. 0.02–0.2 μA) a period of 2–15 min was required to achieve steady values. The pulse mode generally required more time for attainment of a steady background current; at the lowest current range used (1 μA) the time required was 5–10 min. The mercury-coated glassy carbon electrode in the d.c. mode behaved similarly in this respect to the glassy carbon electrode. When a new mercury surface was plated it took 5–15 min before a steady background current was achieved. When the current range was kept constant for a series of different concentrations of the same electroactive compound, the background current reached its steady-state value in the d.c. mode about 20 s after the changeover from analyte to supporting electrolyte when the glassy carbon electrode was used with or without the mercury film; 1–2 min was needed for the pulse mode.

The mercury film on the glassy carbon electrode was plated by electrolyzing mercury at -1.0 V for 4 min from a flow of 10^{-2} M mercury(II) nitrate solution in 0.01 M nitric acid pumped at a rate of ca. 2 ml min^{-1} . After the plating, the electrode was held at $+0.1$ V for 2 min, to remove any co-plated metallic impurities. The film was mechanically removed daily and replated as above on the following morning. Occasional anomalous results were traced to defects in the film; these disappeared when a new film was plated.

In on-line cathodic stripping, plating was effected in 4 min from a slowly flowing stream of the sample at $+0.15$ V. After plating, the electrode potential was switched off and the flow was changed to the buffer. After the cell had filled with buffer, the flow was stopped and a d.c. scan from -0.2 V to -0.8 V was employed.

RESULTS AND DISCUSSION

Direct current (d.c.) voltammetry

The electrochemical cell described was used in on-line analysis for *p*-nitroso-*N,N*-diethylaniline [7] based on oxidation of the compound at the glassy carbon electrode at $+1.0$ V in 0.1 M acetate buffer of pH 4. A linear relationship between current and concentration was found over the range 8×10^{-5} – 10^{-8} M (see below). The detection limit for the hydrodynamic d.c. method was much lower than that for the d.c. mode in quiescent solutions. Even with differential pulse polarography at the DME in a quiescent solution, the detection limit for *p*-nitroso-*N,N*-diethylaniline is 8×10^{-8} M, i.e., almost one order of magnitude poorer than that of the proposed on-line method.

The main reasons for the increased sensitivity of the d.c. voltammetric detector in flowing streams are: (i) the current is increased because of increased mass transport to the electrode, the diffusion layer being thinner in flowing streams; (ii) the background current is decreased because at constant potential no current is needed to charge the double layer and the oxidation states of the functional groups on the carbon electrode surface are in equilibrium.

Pulse voltammetry

In the pulse mode, potential pulses are applied to the electrode for short times; with the PAR 174A used the pulse duration was 56.7 ms and the current was sampled for the final 16.7 ms of the pulse. The potential pulses are stepped up from an initial potential to a pulse potential which, in on-line analysis, is selected so that the compound under study reacts at the electrode. The initial or rest potential is chosen so that the compound does not undergo any significant electrochemical reaction. The current measured in the pulse mode depends on both these potentials because of the electrochemical reactions at the pulse or working potential and because of the different background currents at the two potentials. The dependence of the current on the initial potential was studied under hydrodynamic conditions for the oxidation of an 8×10^{-5} M solution of *p*-nitroso-*N,N*-diethylaniline at +1.0 V. The results (Fig. 2) show that a definite change in the current is obtained at less than +0.8 V when the initial potential becomes less positive than the half-wave potential. The continuous increase in the current with decreasing initial potential is due to the change in the high background current of the glassy carbon electrode [8].

When the potential pulse is applied both the capacitive and the faradaic current start to decrease. With mercury electrodes, the capacitive current decreases to zero within 10–20 ms, whereas with glassy carbon electrodes the decrease may take up to 200 ms [8]. This time also depends on the amplitude of the potential pulse and the initial potential. Solid electrodes generally have a higher double-layer capacitance possibly because of the build-up of point charges on the uneven surface.

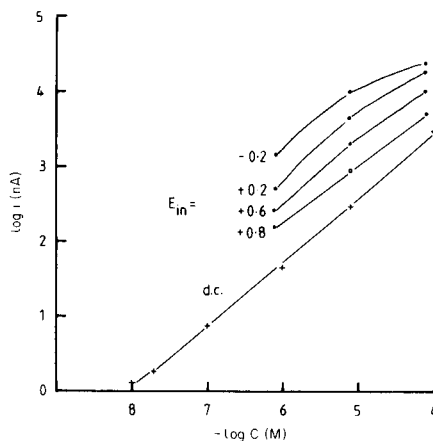
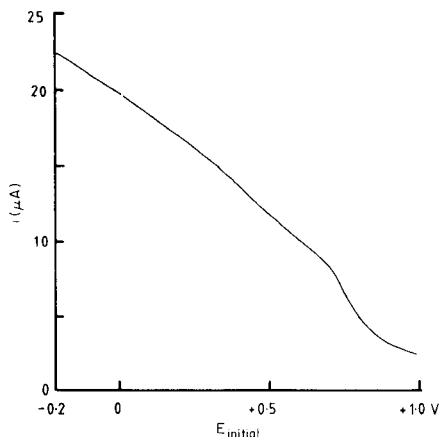


Fig. 2. Dependence of the current on the initial potential (E_{initial}) in the oxidation of *p*-nitroso-*N,N*-diethylaniline at +1.0 V.

Fig. 3. Calibration plots for *p*-nitroso-*N,N*-diethylaniline obtained by the hydrodynamic d.c. method and pulse method with variable initial potential. The working potential, E_w , is +1.0 V.

The high capacitance of the glassy carbon electrode is its main restriction for use with time-dependent techniques like cyclic voltammetry and pulse voltammetry. When low concentrations are determined by the pulse mode, the capacitive current cannot be neglected compared with the faradaic current. The initial potential should not be too far from the working potential so as to allow the capacitive current to decrease to zero during the pulse time. In this study, $1 \mu\text{A}$ was the lowest current range which could be used with the pulse mode; in lower ranges the capacitive current at the end of the pulse was still higher than the current range used, resulting in overloading of the instrument.

The pulse mode was also used in on-line analysis for *p*-nitroso-*N,N*-diethylaniline. The calibration curves over the studied concentration range 8×10^{-7} – 8×10^{-5} M are shown in Fig. 3 with different initial potentials. The detection limit was found to be about 8×10^{-7} M. It can be seen that the calibration curves with the pulse mode begin to curve when the initial potential is less than +0.7 V. Deviation from linearity is greater, the further the initial potential is from the working potential. This is a result of the high capacitive current which has not decreased to zero at the end of the pulse and so adds to the current measured. The detection limit for this nitroso compound is poorer with the pulse mode than with the d.c. mode because the high capacitive current limits the sensitivity of the faradaic current measurement.

The high and variable background current in the pulse mode arises not only from the capacitive current but also from the charge involved in changing the several oxide forms (e.g., hydroxyl, carbonyl, carboxyl, ether and quinoidal structures) on the glassy carbon electrode to a new state of equilibrium when the potential varies. Because these surface reactions are slow, the oxidation states of the groups are not the same in every pulse, giving a variable addition to the measured current.

Effect of the flow rate

The mass transport to the electrode surface, on which the response depends, varies greatly with the hydrodynamic conditions in the cell. The dependence of the current on the flow rate in the cell used here was studied in the d.c. mode with an 8×10^{-7} M solution of *p*-nitroso-*N,N*-diethylaniline and in the pulse mode with an 8×10^{-6} M solution. The working potential was +1.0 V and in the pulse mode the initial potential was +0.7 V. The general relationship between the limiting current i_l , the bulk concentration of the electroactive species c_0 and flow rate v is given [9] by $i_l = knFc_0v^\beta$, where n is the number of electrons involved, F is the Faraday constant, and k is a constant depending on the viscosity of the fluid, the diffusion coefficient of the species and geometrical parameters of the cell and the electrode. Under laminar flow conditions the exponent β should be 0.5.

In the d.c. mode, the current was found to increase with increasing flow rate in the range 2–12 ml min⁻¹. When the logarithm of the current was

plotted against the logarithm of the flow rate a linear plot was obtained with a slope of 0.43. This indicates that the flow conditions are almost laminar in the cell.

In the pulse mode the current was almost independent of the flow rate over the range studied; the relative standard deviation was about 4%. This is in accordance with the results found by others in convective mass transport systems [10, 11]. It has been reported that with a solid electrode the current obtained in the differential pulse mode is rather independent of flow rate [11, 12]. However, when the DME is used, the current has been stated to depend on the flow rate [3]. In the d.c. mode at the DME, after the flow rate had reached a certain level, the signal was independent of the flow rate [4].

Response time

The response time referred to here is the time from the instant when the sample solution enters the cell to the time when the current reaches 99% of its steady-state value. In the d.c. mode the response time was 20 s and was found to be quite independent of the concentration and flow rate. The response time in the pulse mode was also independent of flow rate and concentration, but depended on the difference between the initial and working potentials. When *p*-nitroso-*N,N*-diethylamine was studied at +1.0 V, the response times for initial potentials of +0.7 V and -0.2 V were 1 min and 4 min, respectively.

Comparison between d.c. and pulse modes in on-line analysis

The advantages of the d.c. mode are that it is very sensitive, exhibits a large linear calibration range, and has a short response time and low noise level. In the pulse mode, the noise level is higher, as indicated above, so that the relative standard deviation is greater than in the d.c. mode at every concentration level. When the test compounds or their electrolysis products are strongly adsorbed on the surface, the pulse mode has the advantage over the d.c. mode that at correctly chosen initial potentials the adsorbed species can be stripped off or desorbed from the electrode surface. Because the working potential is applied only for a short time and for most of the experimental time the electrode is at a potential where no electrochemical reactions occur, fouling of the electrode is effectively prevented and long-term stability is achieved [11, 13]. Moreover, when samples with concentration levels of 10^{-3} M and even higher are used, the pulse mode is more advantageous than the d.c. mode because small variations in the background current do not affect the measurement of the relatively high faradaic current and the electrode surface is kept clean electrically. The pulse mode is also independent of flow-rate variations and should be used when a constant flow rate cannot be maintained. The fouling of the electrode surface in the d.c. mode can be diminished by having, e.g., methanol in the sample and by using a washing period between different samples [7].

Applications of the flow-through cell

The cell described has been used in several different applications of on-line methods of analysis. Direct oxidation of the compound at the glassy carbon electrode is described above. Direct reduction of the compound at a thin mercury film plated on the glassy carbon electrode is also possible. The mercury film enlarges the useful negative potential range of the solid carbon electrode and thus its applicability. The 1,4-benzodiazepine drug, nitrazepam, was studied in a 0.1 M sulphuric acid–10% methanol mixture by the d.c. voltammetric on-line method by using the reduction of the nitro group in the molecule. The voltammogram obtained is given in Fig. 4. Because the current fluctuations caused by the pressure pulses from the peristaltic pump become larger the more negative the potential, a highly acidic medium was used to shift the half-wave potential of the reduction of the nitro group to less negative potentials; in the medium used it was around -0.2 V so the working potential was chosen as -0.3 V. The current versus concentration plot was linear over the range 5×10^{-4} – 5×10^{-6} M and the detection limit was 10^{-6} M. At this latter level the background noise became about half the reduction current. The relative standard deviation varied somewhat with the concentration; the average value for the whole concentration studied was 3%. The results are summarized in Table 1.

Some sulphur-containing organic compounds are oxidized at positive potentials on the mercury film electrode and form mercury salts. This

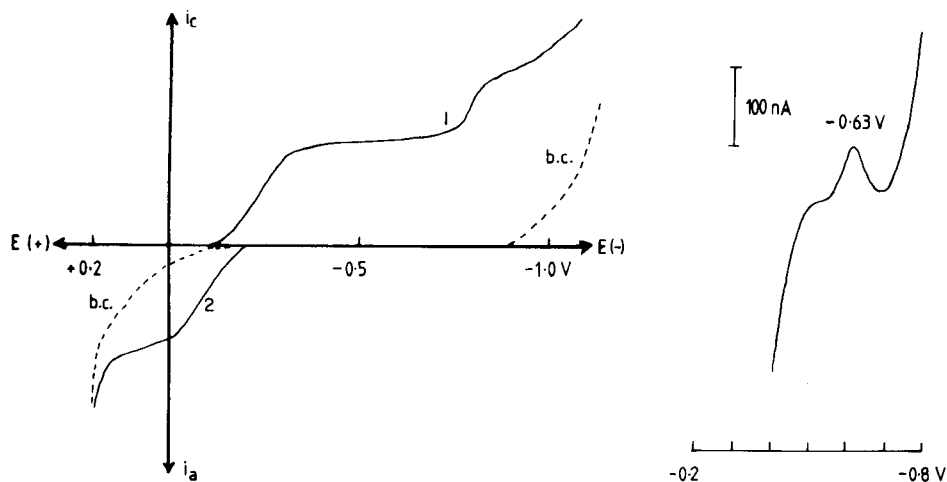


Fig. 4. Hydrodynamic d.c. voltammograms for (1) 5×10^{-4} M nitrazepam in a 0.1 M H_2SO_4 –10% methanol mixture, and 10^{-4} M (2) for a solution of the 2-thiobarbituric acid derivative in Britton–Robinson buffer of pH 8. The background currents (b.c.) in these solutions are also shown. The working electrode is a glassy carbon electrode coated with a thin film of mercury.

Fig. 5. A cathodic voltage scan with the stripping peak after plating of a 10^{-6} M solution of the 2-thiobarbituric acid derivative on a mercury film electrode.

TABLE 1

Applications of the voltammetric flow-through cell

Method of on-line analysis	Compound	Voltammetric mode	Linear range (M)	Detection limit (M)	R (%)
Oxidation on glassy carbon	<i>p</i> -Nitroso- <i>N,N</i> -diethyl-aniline	d.c.	8×10^{-5} — 10^{-8}	10^{-8}	1
		n.p.	8×10^{-5} — 8×10^{-7}	8×10^{-7}	3
Reduction on Hg film	Nitrazepam	d.c.	5×10^{-4} — 5×10^{-6}	10^{-6}	3
Oxidation on Hg film	2-Thiobarbituric acid	d.c.	5×10^{-5} — 5×10^{-6}	2×10^{-6}	6
Cathodic stripping	2-Thiobarbituric acid	d.c.	2×10^{-5} — 5×10^{-7}	10^{-7}	9

reaction can be used in on-line analysis. The hydrodynamic d.c. voltammogram of the 1,3-dimethyl-5-ethyl-5'(*p*-chlorophenyl)-2-thiobarbituric acid is also shown in Fig. 4. This 2-thiobarbituric acid is oxidized at potentials more positive than 0.0 V in pH 8 Britton—Robinson buffer, which is the most suitable pH value based on studies in quiescent solutions with the DME [14]. A working potential of +0.1 V was used in the on-line studies. The linear range was 5×10^{-5} — 5×10^{-6} M and the detection limit 2×10^{-6} M. The standard deviation is around 6% at the higher concentrations and approximately 30% at the detection limit.

Cathodic stripping can also be used. The same 2-thiobarbituric acid derivative as above was also examined by an on-line method involving cathodic stripping. The compound was first deposited on the mercury film at +0.15 V from pH 8 solution. During the deposition period of 4 min, the sulphur in the molecule reacts with mercury to form mercury(II) sulphide [14]. After the plating, a cathodic d.c. voltage scan was employed from -0.2 to -0.8 V. The stripping peak appears at -0.63 V; a typical voltage scan is shown in Fig. 5. The linear range of this method was 2×10^{-5} — 5×10^{-7} M and the detection limit was 10^{-7} M; this is an order of magnitude better than that obtained by using cathodic stripping at the hanging mercury drop electrode with differential pulse polarography in quiescent solution [14]. The relative standard deviation varied from 9% to 20% at concentrations from 10^{-5} M to 5×10^{-7} M (Table 1).

Conclusions

The voltammetric flow-through technique provides a flexible method of analysis and should be applicable to many kinds of compounds. The method is fast and could easily be fully automated as indicated by Pungor et al. [15].

The d.c. voltammetric on-line method exhibits a large linear response range with a low detection limit. These parameters are better than those obtained with ordinary static polarographic techniques.

The noise from the peristaltic pump in the form of pressure pulses is a serious limitation of the method and is especially pronounced at negative potentials. The fluctuating flow changes the diffusion layer resulting in changes in the measured current. The more pronounced effect at negative potentials is due to the presence of small amounts of dissolved oxygen despite purging with nitrogen. More stable flow control would decrease the noise level considerably because the diffusion layer would be less affected. Even with the d.c. mode, the flow-rate fluctuations caused by the peristaltic pump caused additional errors which are reflected in the high relative standard deviations obtained in some cases.

REFERENCES

- 1 P. Kissinger, *Anal. Chem.*, 49 (1977) 447A.
- 2 W. R. Heineman and P. Kissinger, *Anal. Chem.*, 50 (1978) 166R.
- 3 P. W. Alexander and M. H. Shah, *Talanta*, 26 (1979) 97.
- 4 L. Michel and A. Zátka, *Anal. Chim. Acta*, 105 (1979) 109.
- 5 B. Fleet and C. Little, *J. Chromatogr. Sci.*, 12 (1974) 747.
- 6 J. Burmciz, Ph.D. thesis, Chelsea College, University of London, 1979.
- 7 A. Ivaska and W. F. Smyth, in W. F. Smyth (Ed.), *Proceedings of Electroanalysis in Hygiene, Clinical, Environmental and Pharmaceutical Chemistry*, held at Chelsea College, Easter 1979, Elsevier, Amsterdam, 1979.
- 8 J. W. Dieker, W. E. van der Linden and H. Poppe, *Talanta*, 25 (1978) 151.
- 9 V. G. Levich, *Physicochemical hydrodynamics*, Prentice-Hall, 1962, p. 90, 298.
- 10 D. J. Myers, R. A. Osteryoung and J. Osteryoung, *Anal. Chem.*, 46 (1974) 2089.
- 11 J. W. Dieker, W. E. van der Linden and H. Poppe, *Talanta*, 26 (1979) 511.
- 12 D. Swartzfager, *Anal. Chem.*, 48 (1976) 2189.
- 13 A. MacDonald and P. D. Duke, *J. Chromatogr.*, 83 (1973) 331.
- 14 Y. Vaneesorn and W. F. Smyth, *Anal. Chim. Acta*, in press.
- 15 Zs. Fehér, G. Nagy, L. Bezur, J. Szovik, K. Tóth and E. Pungor, *Hung. Sci. Instrum.*, 45 (1979) 1.

CONTINUOUS POTENTIOMETRIC DETERMINATION OF SULPHATE IN A DIFFERENTIAL FLOW SYSTEM

MAREK TROJANOWICZ

Department of Chemistry, University of Warsaw, Warsaw (Poland)

(Received 11th July 1979)

SUMMARY

Continuous monitoring of sulphate in a differential flow system equipped with two lead ion-selective electrodes is described. All solutions contained 75% methanol and were adjusted to pH 4. In the flow cell, a standard solution of lead(II) is pumped past the first sensing electrode and is mixed with the sample stream containing sulphate in a small mixing chamber; the mixture containing excess of lead(II) and lead sulphate precipitate then flows through the second sensing electrode chamber. The potential difference depends on the sulphate content in the sample. The effects of lead electrode passivation and the interferences of calcium and chloride are discussed. The system is useful for routine sulphate determination in the range 30–400 mg l⁻¹ with an accuracy of ±5%.

Although several sulphate-sensitive membrane electrodes have been reported [1–6], potentiometric methods for the determination of sulphate with ion-selective electrodes usually involve precipitation titrations with lead(II) solution and a lead-selective electrode [7]. Such titrations in aqueous organic solvents allow sulphate to be determined in samples containing above 5 mg SO₄ l⁻¹.

A frequently emphasized advantage of ion-selective electrodes is the possibility of their application as sensors in continuous measurements in flow systems. Quite a number of continuous determinations with direct methods based on calibration curves, standard addition methods, gradient titrations and injection techniques have been reported. Although indirect measurements with membrane electrodes are commonly used, there are few examples of differential continuous determinations of components. Such possibilities, in the case of sulphate determinations, were suggested very early [8]. The aim of this work was to examine the possibilities of sulphate determination in a differential flow system with two lead-selective electrodes.

EXPERIMENTAL

Apparatus and procedure

Lead(II) ion activity measurements were done with home-made all-solid-

state lead electrodes, in which the membrane contained a mixture of lead selenide and silver sulphate. The membrane pellets were mounted in epoxy resin. The saturated calomel reference electrode was a Radiometer type K401.

Potential measurements under static or flowing conditions were done with a digital Orion Ionalyzer (model 801A) interfaced to a digital Orion printer (model 751). For continuous measurements, a VEB MLW peristaltic pump (type DP2-2) was used with tygon tubing (Ismatec, Switzerland).

The cell for continuous measurements (Fig. 1) was made of perspex and equipped with a miniature magnetic stirrer. The internal diameter of the channels was 2 mm. The capacity of the mixing chamber up to the outlet level was 0.6 cm³. The working surface area of the electrode in the flow cell was 15 mm². The manifold used is outlined in Fig. 2. The glass parts (mixing coil, debubbler, etc.) were from Technicon.

The electrical circuit (Fig. 3) for the measurement of the potential difference between the two sensing electrodes comprised a controlled voltage source for the base-line correction as well as stabilized voltage sources for the independent polarization of both electrodes. The millivoltmeter enabled the potential of each lead electrode to be controlled against a reference electrode placed in the mixing chamber.

Reagents

The standard lead(II) solutions were 2.0×10^{-4} M and 1×10^{-3} M lead perchlorate solution in 75% (v/v) methanol which was 0.05 M in sodium perchlorate and adjusted to pH 4.0 with acetic acid.

Sodium perchlorate solution (0.066 M) in methanol adjusted as above to pH 4.0 was mixed with distilled water (for slope estimation) or with the sulphate-containing sample.

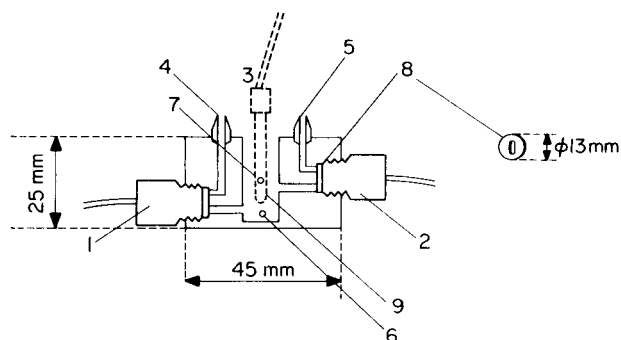


Fig. 1. Flow cell for differential determination of sulphate. (1, 2) Lead electrodes; (3) reference electrode; (4) inlet for standard lead(II) solution to the Pb-1 electrode chamber; (5) outlet for lead(II) solution after Pb-2 electrode; (6) inlet for solution containing sulphate; (7) outlet for excess of solution in mixing chamber; (8) spacer; (9) mixing chamber.

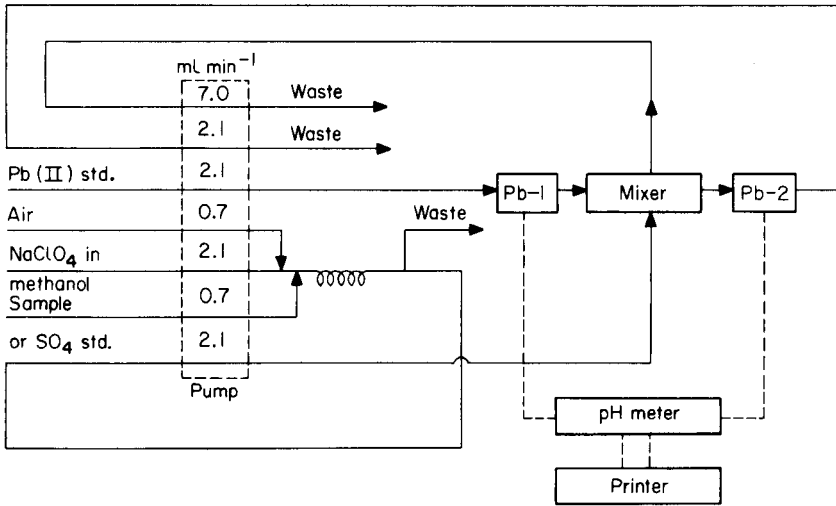


Fig. 2. Flow diagram for differential determination of sulphate.

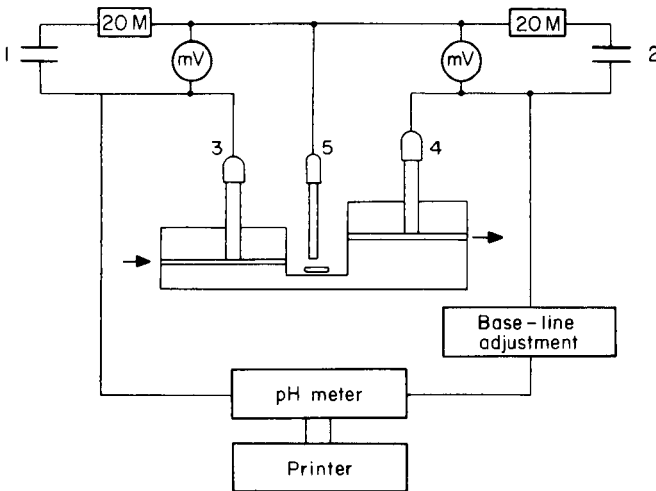


Fig. 3. Measuring arrangement in differential flow system. (1, 2) Stabilized voltage source; (3, 4) lead(II)-sensitive electrodes; (5) reference or Pt electrode.

All solutions were prepared from analytical-grade reagents and triply-distilled water from quartz apparatus.

PRINCIPLE OF MEASUREMENT

In the flow cell (Fig. 1), standard lead(II) solution passes through the contact chamber of the first lead electrode (Pb-1), is mixed with the solution containing sulphate and, after a fraction of the lead ions has precipitated

as the sparingly soluble lead sulphate, flows through the second lead electrode (Pb-2) chamber. The potential of the Pb-1 electrode is given by

$$E^I = E_0^I + S \log c_{Pb} \quad (1)$$

where E_0^I is a constant, S is the potential response slope, and c_{Pb} is the concentration of the standard lead(II) solution. Because of unavoidable differences in the E_0 values of the two electrodes, a small additional potential difference is applied from an external source; in this way, it is possible to make $E_0^I = E_0^{II}$, if the potential response slopes of the two electrodes are in satisfactory agreement. In the flow cell, when the standard lead(II) solution is mixed with an equal volume of aqueous methanolic sodium perchlorate solution containing neither sulphate nor lead(II), the solution flowing through the Pb-2 electrode chamber is diluted by half, so that

$$E_1^{II} = E_0^{II} + S \log(c_{Pb}/2) \quad (2)$$

The potential difference ΔE_1 between the two lead electrodes allows the response slope to be estimated:

$$\Delta E_1 = E_1^{II} - E^I = S \log (c_{Pb}/2c_{Pb}) = -0.3 S \quad (3)$$

When the solution entering the mixing chamber contains sulphate, the potential of the Pb-2 electrode is expressed by

$$E_2^{II} = E_0^{II} + S \log [(c_{Pb} V_{Pb} - c_{SO_4} V_{SO_4}) / (V_{Pb} + V_{SO_4})] \quad (4)$$

where c_{SO_4} is the sulphate concentration, and V_{Pb} and V_{SO_4} are the volumes of the solutions entering the mixing chamber per time unit (i.e., the flow rate). If $\Delta E_2 = E_2^{II} - E_1^{II}$, then from eqns. (2) and (4):

$$10^{\Delta E_2/S} = [2V_{Pb} / (V_{Pb} + V_{SO_4})] - [2c_{SO_4} V_{SO_4} / c_{Pb} (V_{Pb} + V_{SO_4})] \quad (5)$$

Because the flow rates of the standard lead(II) solution and the sulphate-containing solution are equal ($V_{Pb} = V_{SO_4}$), eqn. (5) can be simplified to

$$10^{\Delta E_2/S} - 1 = -c_{SO_4} / c_{Pb} \quad (6)$$

For a set of measurements with the same standard lead(II) solution and constant flow rates, the value $R = -c_{Pb}$ can be expressed by

$$R = c_{SO_4} [10^{\Delta E_2/S} - 1]^{-1} \quad (7)$$

In the above equations, c_{SO_4} indicates the concentration of the sulphate solution entering the mixing chamber. This solution is diluted in comparison to the sulphate-containing solution entering the flow system by a factor b : $c_{SO_4} = c_{SO_4}^0 / b$, where $c_{SO_4}^0$ is the concentration of the initial sample or sulphate standard solution (in this system $b \cong 4$). Equation (7) then becomes

$$R' = R b = c_{SO_4}^0 [10^{\Delta E_2/S} - 1]^{-1} \quad (8)$$

When $V_{SO_4} \neq V_{Pb}$, because of a difference in tubing diameter for example, the factor a can be introduced: $V_{SO_4} = a V_{Pb}$. Then from eqn. (5):

$$10^{\Delta E_2/S} = [2/(1+a)] - [2c_{\text{SO}_4}^0 a/b c_{\text{Pb}}(1+a)] \quad (9)$$

Value a can be found from experimental data by using the equation

$$a = [-10^{\Delta E_2/S} + 2]/[10^{\Delta E_2/S} + 2c_{\text{SO}_4}^0/b c_{\text{Pb}}] \quad (10)$$

From eqn. (9),

$$R'' = c_{\text{SO}_4}^0 [10^{\Delta E_2/S} - 2/(1+a)]^{-1} \quad (11)$$

where $R'' = -0.5 c_{\text{Pb}}(1+a)b/a$.

The system is calibrated by determining the potential response slope from the measured ΔE_1 values and calculating the constants a and R'' from the measured ΔE_2 values for one or more standard sulphate solutions. The sulphate content in unknown samples can be determined by measuring the ΔE_2 values for given samples and calculating from eqn. (11).

RESULTS AND DISCUSSION

Choice of experimental conditions

Because of the relatively high solubility of lead sulphate in water, precipitation titrations of sulphate are usually done in various binary aqueous-organic mixtures containing, for example, dioxane, methanol, isopropanol or acetone. In order to determine their characteristics, the lead-selective electrodes were calibrated under the experimental conditions recommended recently for titrations [9, 10]. Calibration curves (Fig. 4) for the electrodes in the pPb range 2-4.7 were obtained in aqueous solution containing acetate buffer, in isopropanol (as recommended by Scheide and Durst [10]) and in 75% methanolic solution containing 0.05 M sodium perchlorate and pH 4.0 [9]. The best results were obtained in the methanolic solution; good agreement was observed for the potential response slopes of the two lead electrodes used. The calibration curves for the two electrodes were parallel but displaced from each other by a few millivolts. Steady electrode potential values (i.e., changes below 0.1 mV min^{-1} in the pPb range considered) were found for times less than 2 min after changes of solution concentration.

A commonly known inconvenience in the application of lead(II)-sensitive membrane electrodes is the instability of the E_0 value, which is attributed to surface oxidation of the membrane material [11, 12]. This process is accelerated in the presence of oxidants in solution, e.g. peroxides present in dioxane, which eliminated such solvents as suitable titration media. The changes of E_0 value with time were different for the two electrodes used, which made it impossible to obtain satisfactorily precise results. In order to stop this oxidation, formaldehyde and ascorbic acid were introduced with the standard lead(II) solution but this procedure was not successful. The lead-selective electrodes were therefore cathodically polarized against a platinum or saturated calomel electrode as anodes immersed in the solution in the mixing chamber. The use of a saturated calomel electrode was preferred because it allowed simultaneous checks on the stability of the

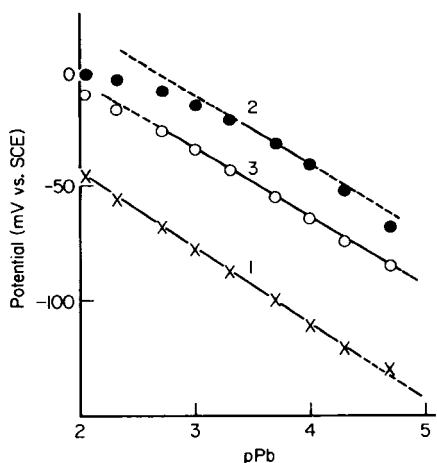


Fig. 4. Calibration curves for lead(II)-sensitive electrode in different media: (1) 0.001 M acetate buffer in water, pH 4.7; (2) 75% isopropanol; (3) 75% methanol—0.05 M NaClO₄, pH 4.

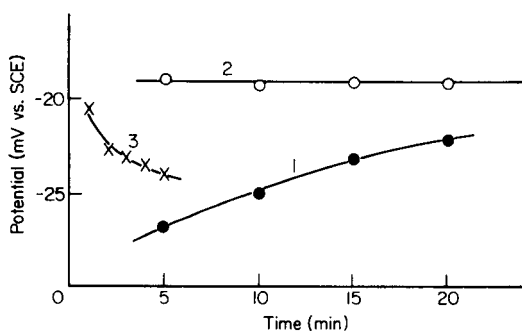


Fig. 5. Effect of cathodic polarization on stability of potential of lead(II)-sensitive electrode at pPb 3.0 in 75% methanol at pH 4: (1) without polarization; (2) polarization with 0.015 μ A; (3) polarization with 0.100 μ A.

potential of the sensing electrode. When a 0.015- μ A polarizing current was applied, the increase of potential at pPb 3.0 was stopped (Fig. 5). If the polarization current was too large, the opposite result was observed, i.e. the potential decreased. It was also found that the optimum intensity of the polarizing current depended, to some extent, on the level of the lead(II) activity in the solution. Changes of the lead electrode potentials during long-term measurements in solutions of pPb 4.00—4.70 are listed in Table 1. These three standard lead(II) solutions (in 75% methanol—0.05 M NaClO₄, pH 4) were changed every 10 min. Obviously, the data obtained when a polarizing current of 0.025 μ A was applied show satisfactory stability.

For proper functioning, it is important to maintain a constant methanol content in the solution in the Pb-1 electrode chamber, as well as in the solution entering the Pb-2 electrode chamber. Kakabadse et al. [13] have indicated a relationship between membrane electrode potentials and the content of methanol in binary solvents. This phenomenon was observed also for lead(II)-sensitive electrodes (Table 2). Accordingly, in the system used here, the aqueous solution containing sulphate was diluted (1 + 3) with 0.066 M sodium perchlorate in methanol; both the standard lead(II) and sulphate-containing solutions thus entered the mixing chamber with the same methanol content and sodium perchlorate concentration.

TABLE 1

Potentials of a lead(II)-sensitive electrode vs. SCE, measured in flow conditions with cathodic electrode polarization at $0.025 \mu\text{A}$. The values listed were measured 10 min after the standard lead(II) solutions had been changed.

Successive sets of measurements	Potentials for lead(II) standards of pPb			Experimental slope mV/pPb
	4.70	4.30	4.00	
1	-39.1	-30.0	-20.5	26.6
2	-39.7	-29.0	-20.7	27.1
3	-40.2	-29.3	-21.5	26.7
4	-40.7	-29.8	-21.0	28.1
5	-40.7	-30.0	-22.0	26.7

TABLE 2

The effect of methanol content on the potential of the lead(II)-sensitive electrode. All solutions were 0.05 M in NaClO_4 at pH 4.0.

Methanol content (% v/v)	Electrode potential (mV)	
	pPb 4.30	pPb 4.00
60	-92.0	-85.4
75	-83.9	-75.9
90	-63.2	-55.6

TABLE 3

Results of calibration of the differential flow system for seven sulphate standards in two ranges (see text)

Lead standard (M)	Mean value a	Mean value R''	Standard deviation of R''
2×10^{-4}	0.907	-8.40×10^{-4}	0.24×10^{-4}
1×10^{-3}	0.904	-4.19×10^{-3}	0.17×10^{-3}

Calibration of the flow system, interference tests and application

The reproducibility of the R'' value for two different concentrations of standard lead(II) solutions is shown in Table 3. When a 2×10^{-4} M lead(II) standard solution is used, sulphate can be determined in the concentration range 30–90 mg l^{-1} ; with a 10^{-3} M lead(II) standard solution, the viable range is 100–400 mg l^{-1} . The standard deviations are satisfactory (Table 3). Determination of sulphate at higher concentrations becomes more difficult because larger amounts of lead(II) sulphate accumulate in the tubes. At

TABLE 4

Results of sulphate determination in the presence of calcium and chloride. Each sample contained sulphate at the 48.0 mg l^{-1} level ($a = 1.02$, $R'' = -8.37 \times 10^{-4}$)

Interfering ion	Concn. taken (mg l^{-1})	Sulphate found (mg l^{-1})	Deviation (%)
—	—	46.4	-3.3
Cl^-	35	48.4	+0.8
	70	48.8	+1.7
	175	51.7	+7.7
Ca^{2+}	20	46.0	-4.2
	40	46.4	-3.3
	80	46.4	-3.3
	400	41.2	-14

TABLE 5

Results of sulphate determination in tap water

Successive sets of measurements	R	a	Sample no.	Sulphate concn. (mg l^{-1})		Error (%)
				Titration	Flow system	
I	-8.30×10^{-4}	0.93	1	80.7	77.6	-3.8
					79.2	-1.9
II	-8.30×10^{-4}	0.93	1	80.7	80.7	0
					80.7	0
			2	71.6	76.9	+7.4
				76.5	+6.8	
III	-8.37×10^{-4}	1.02	1	80.7	78.0	-3.3
			3	76.2	76.0	-0.3
			4	79.3	77.2	-2.6
			5	70.4	75.2	+6.8

sulphate contents below 100 mg l^{-1} , the system works for at least one week without the necessity of cleaning. With the flow rates used, stable ΔE_2 values were noted 3 min after changes of the sample solutions. Despite the electrode polarization during measurements, it is necessary to polish the electrode surface once daily.

In precipitation titrations of sulphate, interfering effects of chloride and calcium ions have been noted [9]. To estimate this effect in the flow system, some measurements were done in samples containing sulphate and an excess of chloride or calcium. The results (Table 4) indicate that 5-fold and higher molar amounts of those ions can cause errors.

The results of sulphate determination in tap water by using the differential

system and the titration method [9] are given in Table 5. The difference between the results of the two methods rarely exceeds $\pm 5\%$ at the 80 mg l^{-1} level.

The most important sources of error in the method developed are: limited reproducibility of the peristaltic pump (ca. $\pm 5\%$), limited precision of reading of ΔE_2 value because of potential oscillations of $\pm 0.3 \text{ mV}$, and changes of temperature in the unthermostated system.

Conclusions

The assembly of the differential continuous flow system with two lead electrodes seemed to be attractive because of the possibility of eliminating drifts of electrode potential with time. However, even for two apparently identical electrodes, the potential drifts were not equal, and simultaneously the potential response slope also decreased. Therefore it was necessary to apply cathodic polarization of the electrodes. In this situation, the potential of the sensing Pb-2 electrode can be measured and checked against a reference electrode of constant potential value under given conditions. Because a methanolic solution of lead(II) perchlorate was used as standard solution, it was suitable to use a lead(II)-sensitive electrode as reference. This eliminated the liquid junction and the electrolyte leakage from classical reference electrodes. A similar role could be played by a sodium-sensitive electrode, as the standard solution also contains a constant sodium concentration.

The author thanks Prof. Adam Hulanicki for stimulating this work and valuable discussions.

REFERENCES

- 1 G. A. Rechnitz, Z. F. Lin and S. B. Zamochnick, *Anal. Lett.*, 1 (1967) 29.
- 2 G. A. Rechnitz, G. M. Fricke and M. S. Mohan, *Anal. Chem.*, 44 (1972) 1098.
- 3 G. A. Rechnitz and M. S. Mohan, *Anal. Chem.*, 45 (1973) 1323.
- 4 E. Pungor and J. Havas, *Acta Chim. Acad. Sci. Hung.*, 50 (1966) 77.
- 5 O. G. Takaishvili, E. P. Motsonelidze, Yu. M. Karachentseva and P. I. Davitaya, *Zh. Anal. Khim.*, 30 (1975) 1629.
- 6 E. W. Baumann, *Anal. Chim. Acta*, 99 (1978) 247.
- 7 M. Trojanowicz and A. Hulanicki, *Chem. Anal. (Warsaw)*, 22 (1977) 615.
- 8 *Orion Res. Newsl.*, 2 (1970) 21.
- 9 A. Hulanicki, R. Lewandowski and A. Lewenstam, *Analyst*, 101 (1976) 939.
- 10 E. P. Scheide and R. A. Durst, *Anal. Lett.*, 10 (1977) 55.
- 11 M. Mascini and A. Liberti, *Anal. Chim. Acta*, 60 (1972) 405.
- 12 G. J. M. Heijne, W. E. van der Linden and G. den Boef, *Anal. Chim. Acta*, 100 (1978) 193.
- 13 G. J. Kakabadse, H. Abdulahed Maleila, M. N. Khayat, G. Tassopoulos and A. Vahdati, *Analyst*, 103 (1978) 1046.

CONTINUOUS MONITORING OF HEAVY METALS IN INDUSTRIAL WASTE WATERS

H. CNOBLOCH*, W. KELLERMANN, D. KÜHL, H. NISCHIK, K. PANTEL and H. POPPA

Siemens AG, Forschungslaboratorien, P.O. Box 3240, D-8520 Erlangen (Federal Republic of Germany)

(Received 11th July 1979)

SUMMARY

A relatively simple instrument is described for the continuous screening of groups of heavy metal ions in sewage and waters. The method is based on coulometric principles after concentration by preelectrolysis. The following metals can be detected: Ag, Hg, Pb, Cu, Co, Fe, Cd, Zn and Ni. An automatic laboratory model of the heavy metal ion detector has been tested successfully for eight months at the inlet of a municipal sewage plant and for nine months at the outlet of a neutralization plant of a galvanic shop.

Heavy metal ions are poisons which in a dissolved form or as hydroxide sludge can cause total breakdown of a sewage plant by inhibiting the biological degradation process. The organisms present in the waters may be severely damaged by such metal ions even at concentrations well below 1 mg l^{-1} . These heavy metals can be transferred to man by the nutritional chain [1]. This has caused many national authorities to fix limiting values for the input of sewage to public sewage plants [2] as well as for purified waste water which is to be added to surface waters [3]. These limiting values are normally monitored only discontinuously by analyzing random samples in the laboratory. The reasons for this are the lack of maintenance-free devices for continuous sampling and the unwieldiness of present laboratory equipments for field work.

The aim of the work discussed here was to develop a simpler method for the continuous detection of heavy metals in sewage and waters. The primary object was to screen for heavy metal groups rather than to determine the individual metals as exactly as possible. The apparatus developed serves mainly as a monitor which sets off an alarm when the given limiting value is exceeded. The operator of sewage plants or galvanic shops should then be in a position to take countermeasures immediately so as to prevent major disturbances. This method is not intended to replace exact methods of water analysis for determining heavy metals but to limit the number of such analyses to cases where critical values have already been reached or exceeded.

Principles of the measuring system

The determination of heavy metal ions is based on the principle of coulometry after the metals have been concentrated by electrolysis [4, 5]. The measuring cell contains two platinum electrodes and a stirrer. The stirrer creates a well defined thin diffusion layer at the electrode surface. This leads to large response signals and consequently to better sensitivity; the reproducibility of readings is also improved. The sequence of events is as follows. First, the measuring cell is filled with the waste-water sample (pH 3.5), the metals are deposited on the cathode at a constant d.c. voltage, and the cell is emptied. Secondly, the cell is filled with pure electrolyte (buffer solution pH 3.5), and the metals are brought into solution by reversing the d.c. voltage; the electrical charge expended is a measure of the metal ion concentration of the waste water. The oxidation process is done in pure solution to prevent false response signals which might otherwise result from the presence of other oxidizable substances, especially organic compounds, in the original sample solution. The polarity of the electrodes is interchanged after each measurement; thorough cleaning of the electrodes is thus assured before every response signal.

The heavy metals Ag, Hg, Pb, Cu, Co, Fe, Cd, Zn and Ni are detected under the following conditions: pH 3.5 (citrate-sulphuric acid solution); specific electrical conductivity $\kappa > 1000 \mu\text{S cm}^{-1}$; reduction voltage E_{red} , -5.5 V ; reduction time t_{red} , 3 min; oxidation voltage E_{ox} , $+0.7 \text{ V}$; integration time t_{ox} , 10 s. The voltage signs refer to the polarity of working electrode versus the counter electrode. The detection limit ranges between 0.1 mg l^{-1} and 10 mg l^{-1} . A response signal is obtained if one or several of the above-mentioned metals are present. The signal for a single metal can be evaluated quantitatively; only semi-quantitative results are possible when several metals are present. The number of detectable heavy metal ions can obviously be varied by the choice of deposition voltage. The detection limit can be altered by varying the deposition time.

EQUIPMENT

The heavy metal ion detector is represented schematically in Fig. 1; Fig. 2 is a block diagram of the electronic circuits. Two variations of the apparatus are available: in one, atmospheric oxygen has free access to the water sample; in the other, access of air is prevented by nitrogen. A nitrogen atmosphere is sufficient and saturation of the solution is unnecessary. The use of nitrogen is necessary only when oxidation reactions with formation of precipitates, or bacterial growth, would occur in the presence of air. This normally happens only with heavily polluted water samples (e.g. in sewage plants); otherwise, the analysis does not require additional protective measures. To prevent accumulation of bacterial growth, it is advantageous to prepare all connections and tanks from opaque materials.

The water samples, previously prepared for measurement (see below), are

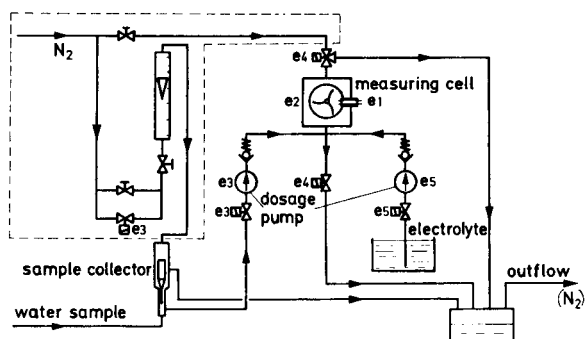


Fig. 1. Schematic diagram of the heavy metal ion detector.

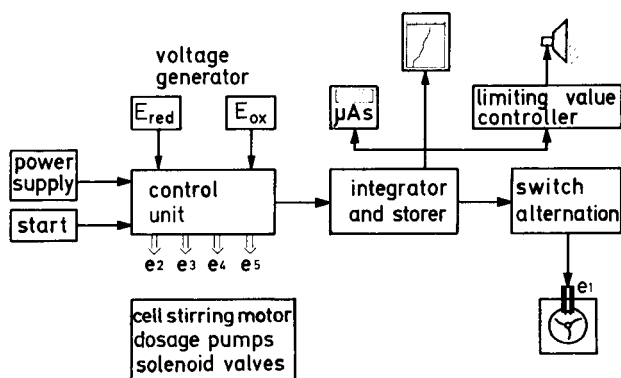


Fig. 2. Block diagram of the electronic circuitry.

passed continuously to the sample collector. The sample is delivered from this collector to the measuring cell by means of pump $e3$. After deposition of heavy metals on the cathode at the voltage preset at $e1$, the measuring cell is emptied by opening the solenoid valves $e4$. The cell is then filled with pure electrolyte via pump $e5$. After the metals have been redissolved at the preset oxidation voltage, the electrolyte is passed to waste and the cell is ready for the next sample.

The 0.05 M sodium citrate–0.025 M sulphuric acid solution which is used for pH adjustment is also applicable as electrolyte. In order to achieve reasonably well defined conditions, the volume of pure electrolyte should always be greater than that of the sample. This helps to clean the cell; when nitrogen is used, the solutions are forced from the cell under pressure.

The complete unit is quite compact and can be placed on a trolley along with two 20-l containers for the necessary reagents.

RESULTS

In a normal municipal sewage plant, the sewage is purified mechanically and biologically, and the sludge accumulating in the plant is also subjected to biological treatment. Thus it is necessary to install detectors for dissolved heavy metal ions at the inlet prior to the sand filter and aeration units (detector 1), and in the sludge tank which contains metals as hydroxides or adsorbed on solid particles (detector 2). Most of the heavy metals in wastes come from galvanic plants; thus a third detector is required in the outflow from the galvanic plant before it joins ordinary domestic and industrial waste waters (detector 3) for passage through a coarse filter bed preceding detector 1. By tracking the responses of the three detectors, the sources of problems are readily identified.

Preparation of samples in a municipal sewage plant

The preparation of samples from municipal sewage was one of the most difficult tasks in testing the heavy metal ion detector. The process adopted for waste waters is shown in Fig. 3. The sample is taken continuously from the waste-water channel by a plate filter (1) and adjusted to pH 3.5 with the buffer solution. During this acidification, a precipitate is again formed in the sample so that water must be filtered for a second time. The sample can be passed to the analyzer after the second filtration (3).

Figure 4 shows the scheme for preparing samples from the sewage sludge. The sludge is heated in a tank (2) with sulphuric acid. The sample is then filtered (3) and adjusted to pH 3.5 with the buffer solution. The analysis can then be carried out.

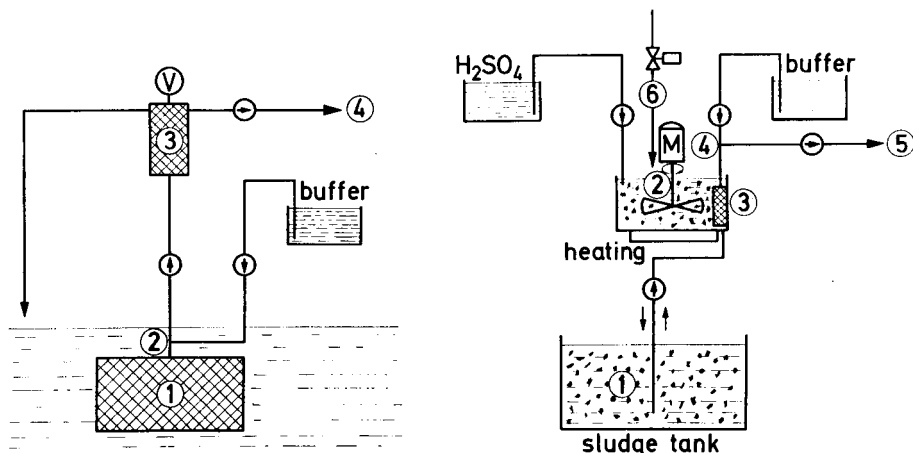


Fig. 3. Preparation of samples from waste-water channel. (1) Plate filter; (2) adjustment to pH 3.5; (3) vibration filter; (4) outlet to analyzer.

Fig. 4. Preparation of samples from sludge tank. (1) Sampling; (2) dissolution; (3) plate filter; (4) adjustment to pH 3.5; (5) outlet to analyzer; (6) purification.

The anaerobic digesters are charged discontinuously. Thus, ample time ranging from 1 to 24 h is always available for preparing the samples. Not all metal hydroxides are brought into solution during this procedure since the process depends very largely on the age of the precipitates. However, the sparingly soluble or insoluble precipitates are not critical in the anaerobic digester because only dissolved metal ions affect the anaerobic treatment of the sludge.

The filters employed are self-purifying. The pore diameter of the filter is smaller than that of the anticipated impurities, which are therefore deposited only on the surface of filter whence they can be removed either by water streaming past or by vibrating the filter. Filter vibration is employed only when small quantities of fluids are available. A copolymer of PVC and acrylonitrile supported on a nylon screen was used as the filter. The filter was 0.1-mm thick and the pore diameter was $0.2 \mu\text{m}$. With such a filter and at a water velocity of 1 m s^{-1} in the channel a sample can be taken from the sewage for a period of 2–4 weeks without maintenance. The same operating periods are also attainable with the vibration filter with 100-Hz oscillation.

Bacterial growth in the tubes and in the storage tanks created great difficulties at the beginning of the experiments. It is known from polarography that gelatine solutions susceptible to bacterial attack can be rendered stable by adding a few drops of toluene per litre of the solution [6]. Experiments showed that during the reduction phase the heavy metal ion determination is affected by coverage of the electrode at toluene concentrations above 50 mg l^{-1} (Fig. 5). The electrode poisoning is reversible, and the initial values

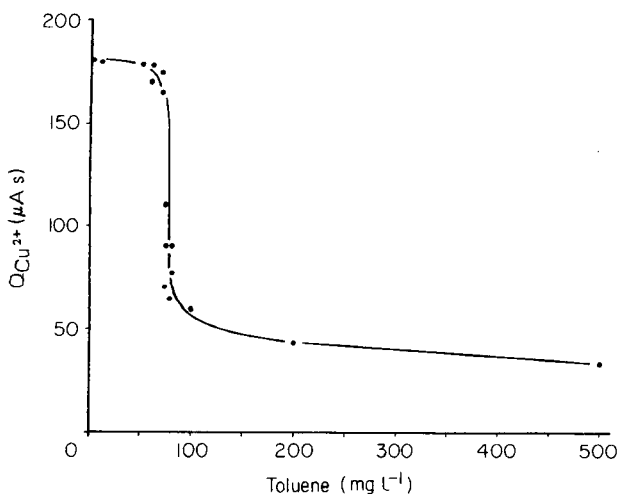


Fig. 5. Charge dependence on the toluene concentration at the detection of $1 \text{ mg Cu}^{2+} \text{ l}^{-1}$. $\text{pH} = 3.5$, $E_{\text{red}} = -3 \text{ V}$, $t_{\text{red}} = 5 \text{ min}$, $E_{\text{ox}} = +0.75 \text{ V}$, $t_{\text{ox}} = 2 \text{ s}$. $Q_{\text{Cu}^{2+}}$ = charge to be applied for the anodic dissolution of copper.

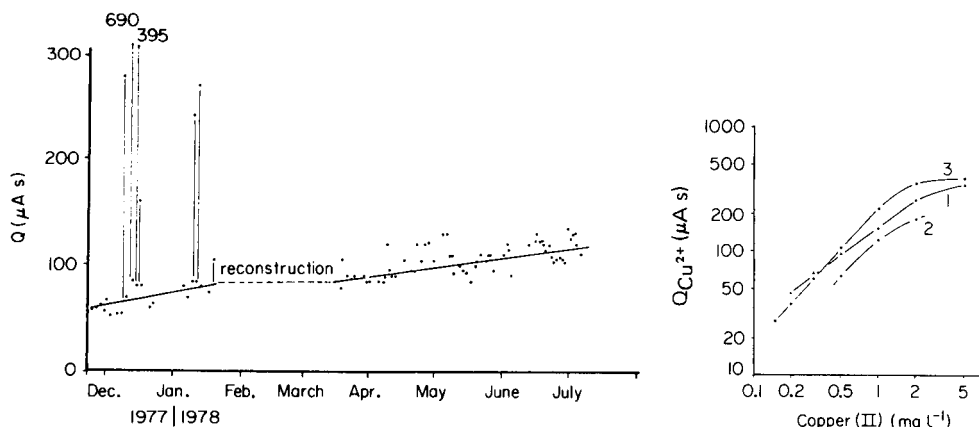


Fig. 6. Long-term test with the heavy metal ion detector in a municipal sewage plant. Conditions: $\text{pH} = 3.5$, $E_{\text{red}} = -3 \text{ V}$, $t_{\text{red}} = 5 \text{ min}$, $E_{\text{ox}} = +0.75 \text{ V}$, $t_{\text{ox}} = 2 \text{ s}$, Q = electrical charge.

Fig. 7. Calibration curves for copper: (1) before long-term test; (2) check points in sewage; (3) after the long-term test. Conditions: $\text{pH} = 3.5$; $E_{\text{red}} = -3 \text{ V}$; $t_{\text{red}} = 10 \text{ min}$; $E_{\text{ox}} = +0.7 \text{ V}$; $t_{\text{ox}} = 6 \text{ s}$.

are obtained again after a few measuring cycles. During the oxidation phase, however, toluene does not interfere even at a concentration of 500 mg l^{-1} in the electrolyte solution. The results of laboratory experiments which were subsequently confirmed in field tests showed that the growth of the anaerobic bacterial strains were largely inhibited by the addition of toluene. The minimum concentration of toluene added was 25 mg l^{-1} , which lies below the electrochemical critical level of 50 mg l^{-1} .

Long-term test in a municipal sewage plant

The charge behaviour during 8 months of continuous testing at the inlet of the sewage plant is shown in Fig. 6. In addition to the uniform rise of the base charge, a few peaks, some very high ones, were observed during the initial testing phase. The detector was coupled with a sampler which ensured a water sample automatically when a preset charge was exceeded. The analysis of the water samples which corresponded to these peaks yielded in no case a concentration of heavy metal ions. An explanation for the peaks could be found only in inadequate removal of waste water from the analyzer before oxidation. As a result, oxidizable substances present in the solution were measured, which simulated a metal ion concentration. Reconstruction of the unit as described under Experimental ensured a better replacement of waste water by the pure electrolyte solution, so that interfering oxidizable substances, especially organic compounds, were no longer present in the solution.

In the second phase of the tests, peaks were no longer observed, but

merely a gradual rise of the base charge; this increase was caused by roughening of the electrode surface. Scanning electron microscope pictures of a platinum electrode before and after this 8-month continuous testing show that the original bright surface has been strongly tarnished and roughened during the long-term operation. Should the increase in the base charge interfere, the electrodes have to be polished at intervals of about 8 weeks.

The stability of the response signal was examined by recording calibration curves at different times. Figure 7 shows three calibration curves for copper ions in the range $0.1\text{--}5\text{ mg l}^{-1}$. Curve (1) was recorded in the laboratory with clean aqueous standard solutions before the long-term operation started. Curve (2) was recorded during the long-term test in the sewage plant by adding copper(II) ions to the sewage. Curve (3) was plotted, like curve (1) with clean solutions in the laboratory after the end of the long-term test.

For a screening technique the agreement of the curves can be described as very good, especially when it is considered that the test set-up was altered during the test. The deviations from the first calibration curve at $1\text{ mg Cu}^{2+}\text{ l}^{-1}$ is approximately $\pm 30\%$.

Test of heavy metal ion detector in a galvanic shop

After the continuous test of the detector in a municipal sewage plant, its applicability for monitoring the galvanic waste waters was also checked. The preparation of samples from galvanic waste waters was much easier than that from sewage. As a rule, water need not be filtered so that only the pH adjustment with the buffer is necessary.

Figure 8 shows the charge behaviour during the monitoring of the galvanic waste waters by the detector. The increase of the base charge in this test was considerably less than it was in the case of the sewage plant operation. The resulting peaks could be clearly assigned to the heavy metal ions by carrying out parallel analyses with atomic absorption spectrometry. The

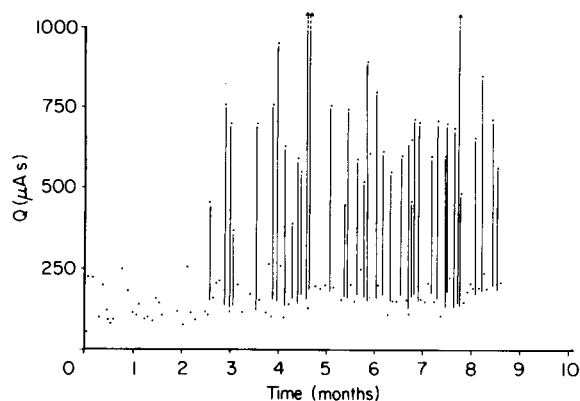


Fig. 8. Long-term test with the heavy metal ion detector in a galvanic shop. Conditions: $\text{pH} = 3.5$; $E_{\text{red}} = -3\text{ V}$; $t_{\text{red}} = 5\text{ min}$; $E_{\text{ox}} = +0.7\text{ V}$; $t_{\text{ox}} = 6\text{ s}$.

metals found were Cu, Ni and Zn at concentrations up to 50 mg l^{-1} . Control analyses without detector signals always yielded metal ion concentrations below 0.1 mg l^{-1} . Typical recorder charts showed peaks corresponding to $700 \mu\text{A s}$, which were caused by a mean heavy metal ion concentration of $2 \text{ mg Cu}^{2+} \text{ l}^{-1}$ and $1 \text{ mg Ni}^{2+} \text{ l}^{-1}$.

During the operation of the detector, chemicals are required only for the preparation of the electrolyte and for the buffer solution. The chemicals cost 0.35 DM/day , when successive measurements were taken at 7-min intervals.

DISCUSSION

The long-term tests described show that the heavy metal ion detector can be employed successfully for monitoring sewage plants and galvanic waste waters. The instrument itself requires little maintenance. The cost of the chemicals for the analysis is low. The preparation of samples when the detector is used in sewage plants requires maintenance. The sampling must be thoroughly checked every 2–4 weeks. The preparation of samples in monitoring galvanic waste waters is without problems and, like the instrument itself, requires little maintenance.

During the operation of the detector, it is of particular importance that the oxidation of the deposited heavy metals takes place in a clean and defined electrolyte solution. If oxidizable substances are present in this solution, their conversion will lead to response signals which simulate those of heavy metals.

REFERENCES

- 1 O. Klee, *Reinigung industrieller Abwässer*, Franckh'sche Verlagshandlung, Stuttgart, 1970, p. 80.
- 2 See, e.g., *Hinweise für das Einleiten von Abwasser aus gewerblichen und industriellen Betrieben in eine öffentliche Abwasseranlage*. ATV-Regelwerk "Abwasser", Arbeitsblatt A115. Gesellschaft zur Förderung der Abwassertechnik e.V, Bonn, 1970, p. 6.
- 3 See, e.g., *Normalwerte für Abwasserreinigungsverfahren*. Sonderdruck der Länderarbeitsgemeinschaft Wasser-LAWA. Verlag Wasser und Boden, Hamburg, 1970.
- 4 H. Cnobloch, W. Kellermann, H. Nischik, K. Pantel and F. v. Sturm, *Siemens Forsch.- u. Entwickl.-Ber.*, 8 (1979) 221.
- 5 H. Cnobloch, E. Ecker and J. Vanhumbeeck, *Chem. Ing. Tech.*, 51 (1979) 641.
- 6 M. v. Stackelberg, *Polarographische Arbeitsmethoden*, Verlag Walter de Gruyter, Berlin, 1950, p. 69.

FAST ANALYSIS RATES IN CONTINUOUS FLOW METHODS BY USING A MODIFIED METHOD OF CURVE REGENERATION

E. B. M. DE JONG* and A. H. WEYDEN

Laboratory of Clinical Chemistry, St. Elisabeth's Hospital, Tilburg (The Netherlands)

(Received 16th August 1979)

SUMMARY

Curve regeneration accelerates sample throughput in continuous flow techniques, but earlier procedures have been limited by the requirement for relatively noise-free instrumental performance. In the proposed instrumental method of curve regeneration, the differential is expressed as a form of the Savitzky—Golay equation. This reduces sensitivity to fast noise, provides excellent performance monitoring, forms plateaux and returns to baseline at analysis speeds in excess of 120 samples/hour even when dialysis is involved.

Continuous flow techniques have dominated automatic chemical analyses for almost two decades. The success of the technique lies in its mechanical simplicity and hence its mechanical reliability and flexibility. Obviously, therefore, investigators have devised various methods for increasing the rate of analysis, which is commonly 40–60 samples/hour, for large workloads. One solution has involved miniaturisation, method-to-method optimisation and electronic assistance for data reading and output. This solution has been employed in the Technicon 20-channel SMAC system operating at 150 samples/hour and in the single-channel instruments described by Neeley et al. [1, 2] operating at similar speeds.

Various workers have described techniques for faster analysis rates by eliminating the air bubble and injecting measured aliquots of sample directly into a high-velocity reagent stream. For example, White and Fitzgerald [3, 4] described methods based on photochemical reactors with spectrophotometric or pH measurements, whereas Růžička et al. [5, 6] have reported numerous methods based on dispersion effects. However, when such analytically complicated steps as dialysis are involved, the analysis rate drops to below that achieved by bubble-segmented continuous flow. For example, in determining phosphate in serum standards, Hansen and Růžička [7] reported analysis rates of 50/hour whereas the standard AutoAnalyzer method operates at 60/hour. Since somewhat less than one-third of all reported continuous flow systems are hydraulically "simple", the mere absence of air-segmentation is of limited value for increased analysis rates.

Walker et al. [8] first provided evidence that the heights of AutoAnalyzer

peaks could be instrumentally predicted from the first few seconds of their rise. Thus waiting for a peak to come to its maximum and then fall wasted considerable time, time which could be used to accelerate the analytical rate. They called this process "curve regeneration". The method of Walker et al. has however restricted this technique to "high quality traces". For the determination of urea, which employs both a 95°C heating bath and dialysis, an analysis rate of 200 samples/hour was reported [8]. Jacklyn and co-workers [9, 10] have outlined a computer programme which uses curve regeneration to determine chloride, carbon dioxide, sodium and potassium at 150 samples/hour, using AutoAnalyzer II technology.

Following the theoretical work of Thiers et al. [11], Walker et al. [12] showed that the exponential portions of an AutoAnalyzer curve obeyed the equation

$$E = y_t + b \, dy/dt \quad (1)$$

where E is the plateau or maximum height of the peak, y_t is the height at peak time t , b is a constant (in seconds), and t is the time (s). Since y_t was continuously measured by the colorimeter and recorder, t was known and a constant b could be experimentally determined for each assay, only the term dy/dt had to be calculated in order to solve for E at any point y_t . As the curve was rising (or falling), Walker et al. employed simple differentiating amplifiers for the circuitry of their curve-regeneration apparatus. Unfortunately, fast noise, however small, can have virtually infinite slope, i.e. dy/dt can approach infinity, hence this technique could be used only on relatively noise-free systems. This is a very difficult condition to maintain in routine use, and has probably prevented the wide acceptance which the technique deserves.

The elegant equation derived by Savitzky and Golay [13], which combines both smoothing and differentiation, can be used to overcome the limitations of the original instrumental designs of Walker and co-workers [8, 9], i.e. the use of differentiating amplifiers to solve their equation. The Savitzky and Golay equation covers a very wide range of curve forms. For the present purpose, it was assumed that any 4.5-s interval of an AutoAnalyzer curve could be expressed accurately enough as a simple quadratic: $y_t = a + bt + ct^2$, where a , b , c are constants, and t is time. Within this 4.5-s interval, it was further assumed that 9 readings of the curve as it was being generated, were sufficient for smoothing, as this interval spanned the oscillating noise interval generated by the peristaltic pump (2-s intervals). These points are designated as $y_{-4}, y_{-3} \dots y_0, y_{+1} \dots y_{+4}$.

According to the Savitzky-Golay equation, therefore,

$$dy_0/dt = -4y_{-4} - 3y_{-3} - 2y_{-2} - y_{-1} + y_{+1} + 2y_{+2} + 3y_{+3} + 4y_{+4} \quad (2)$$

Electronically timed, the curve regenerator used here takes a new set of readings every 0.5 s from the colorimeter, solves eqn. (2) and, having determined dy/dt , solves eqn. (1) and passes the computed value of E to the

recorder. The generation of the peak or plateau is thereby greatly accelerated. Equally important, the return to baseline is also greatly accelerated. Hence, with analytical rates of 120 and more samples per hour, it is possible to achieve, for the first time in AutoAnalyzer technology, a steady-state plateau and a baseline control, both of which are extremely important factors in obtaining higher analytical precision. Baseline drift accounts for a high proportion of the uncertainty of instrumental readings.

EXPERIMENTAL

The electronic circuitry to solve the above equation is simple (Fig. 1). H_{+4} to H_{-4} are analogue shift registers; C are capacitors for storing voltages Y_{+4} to Y_{-4} . Switches S_{+4} to S_{-4} are closed and opened by electrical impulses through D_0 to D_8 from a clock circuit C_p . The outputs of registers H_{+1} to H_{+4} are fed to a summing network SJ_1 , and those of registers H_{-1} to H_{-4} to network SJ_2 . Each network contains resistors R_1 – R_4 in the ratio 1:2:3:4. Output from SJ_2 goes to the inverting input of a differential amplifier while that from SJ_1 goes to the non-inverting input of a differential amplifier.

The output from the differentiating amplifier which is the smoothed differential dy/dt of the Savitzky–Golay formula, passes to a multiplier circuit M into which is dialled from the potentiometer P , the voltage value

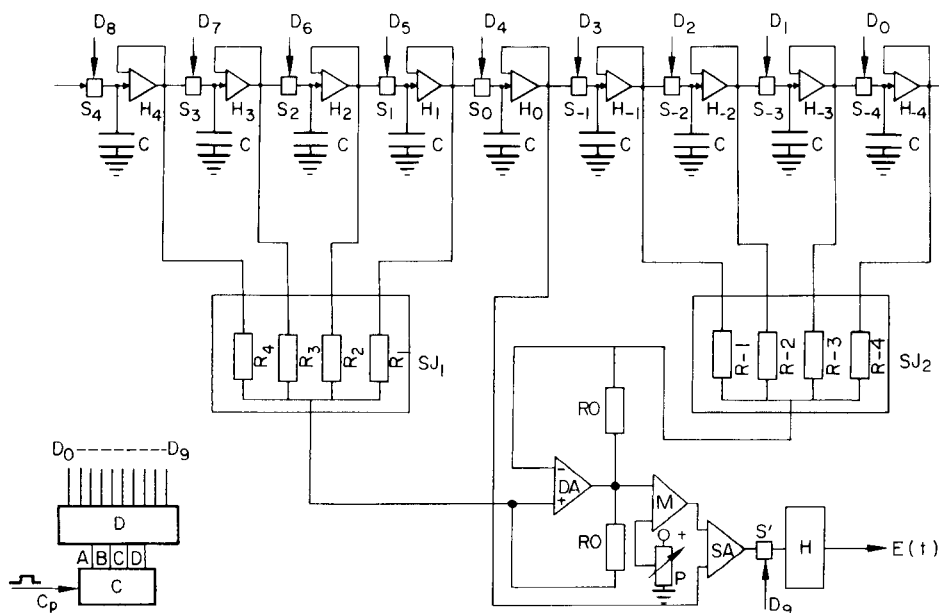


Fig. 1. Electronic circuitry. For explanation, see text.

b. From *M* the output, $b dy/dt$ is then fed to the summing amplifier SA with the voltage Y_0 from the shift register H_0 . At the completion of the cycle from clock C_p , an impulse D_9 closes switch S' and transfers the voltage values $Y + b dy/dt (= E)$ to the holding amplifier H where it is read by a recorder for analogue presentation or by a DVM for computer calculation.

Readings are taken every 0.5 s and as there are 9 points for each calculation, the curve is smoothed over 4.5 s (see above). The sequence of events is as follows: at 0.05... s intervals, switches S_{-4} to S_{+4} are in turn closed and opened by sequential impulses through D_0 to D_8 from the clock circuit C_p . Thus the voltages are shifted from left to right once every 0.5 s. Immediately, on the completion of this shift, switch S' is closed and opened by an impulse D_9 and the calculated E_0 value is passed to H . The cycle then recommences. The interval can obviously be altered at will simply by changing the clock frequency.

In continuous flow technology, however, spurious sharp discontinuities in a curve can occur which would seriously distort any curve fitting. If such a spurious reading persisted for 4.5 s in the region of a peak, it would lead to incorrect values. For this reason, some form of filter circuit must also be built into the electronic system to reject spurious readings. Figure 2 shows the circuit employed here: the entry switch S_4 remains open if the input signal has a sharp discontinuity, i.e., if the differential of the signal with respect to time is very large. The input signal is monitored by the differentiating amplifier 18. The output from 18 is the input of gate circuit 19, which will only pass signals which lie between the upper and lower threshold voltages applied through 23 and 24. The output from 19 activates the NAND gate 20 to pass the impulse D_8 which closes switch S_4 , thus accepting the input signal for the curve-regenerating circuit.

RESULTS AND DISCUSSION

The value and significance of b is exactly as defined by Walker et al. [8] and b is determined experimentally in the same way, i.e. the value of b is set to bring each curve to the baseline. If b is too large (Fig. 3, a and b), the curve drops below the baseline; if it is too small, the curve does not return to

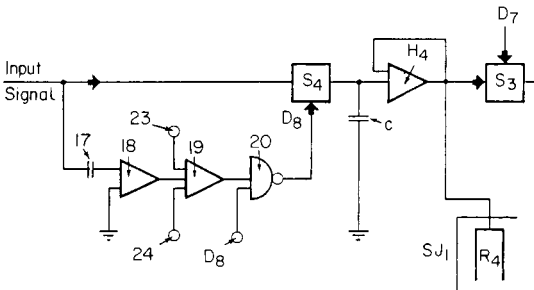


Fig. 2. Filter circuit.

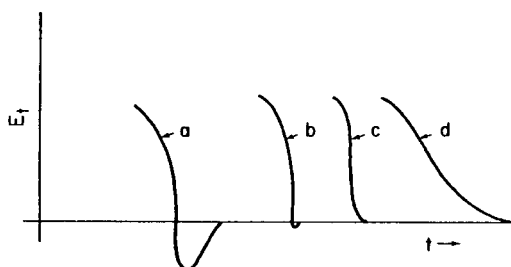


Fig. 3. Peak shapes for different values of b .

the baseline owing to the long wash-out time (Fig. 3, d). However, once determined, a change in the value of the b multiplier generally indicates a deteriorating hydraulic system. The b value itself is therefore a good diagnostic measure of instrument performance or a quantitative function monitor.

In this laboratory, the operators (more than 50) are obliged to maintain a performance log for each instrument. The b value which can be read directly off the instrument must be entered. The stability and use of the b value is obvious from Table 1 which has been taken directly from the laboratory log-books. The ready acceptance of this technique shows it to be totally practicable, i.e., sufficiently simple for routine use.

To demonstrate the effectiveness of curve regeneration in a normally slow hydraulic system run at high speed, Fig. 4 shows typical curves obtained in a conventional determination of creatinine with dialysis [14]. Dialysis is generally assumed to be the major factor restricting analytical speed. The curves obtained showed a good plateau when the recorder chart speed was sufficiently accelerated. Unlike other fast analytical techniques, samples

TABLE 1

Values of b for separate instruments over 1 week

Test	Date and b value					
	11th	12th	13th	14th	15th	17th
Potassium	5.80	5.60	5.98	5.10	5.80	—
Sodium	5.80	5.60	5.98	5.10	5.80	—
Bun	5.65	5.60	5.90	5.80	5.80	5.80
Creatinine	10.2	10.2	10.2	10.2	10.3	10.3
Glucose hexokinase	10.4	10.3	10.3	10.3	10.3	10.3
Total bilirubin	7.25	8.00	8.00	8.00	8.02	8.02
Direct bilirubin	7.50	7.50	7.50	7.32	7.32	6.86
Alk. phos.	9.71	9.71	9.70	10.12	10.12	10.12
Total protein	7.80	7.80	7.80	7.80	7.97	7.80
Albumin	9.40	9.40	9.39	9.40	9.40	9.40
Cholesterol enzymatic	10.5	10.5	10.5	10.5	10.5	10.5
Triglycerides	15.95	15.95	15.95	15.95	15.90	15.95

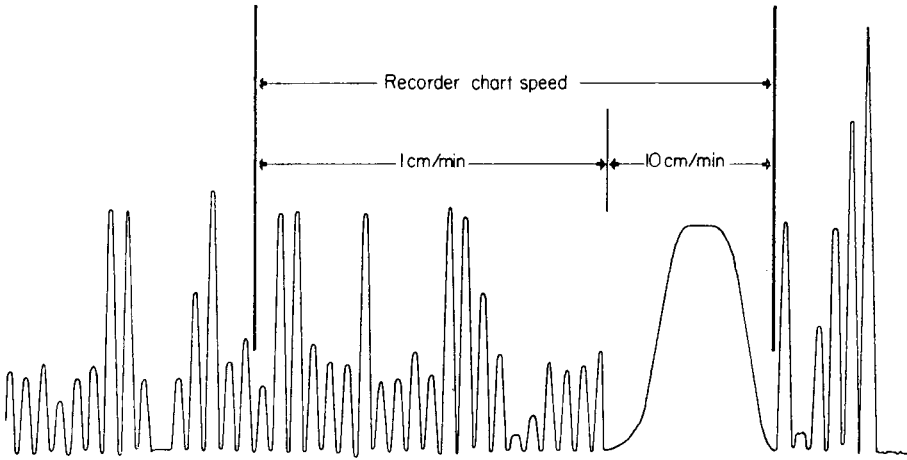


Fig. 4. Recorder output for the determination of creatinine with dialysis (f.s.d. 0.16 absorbance) in various samples.

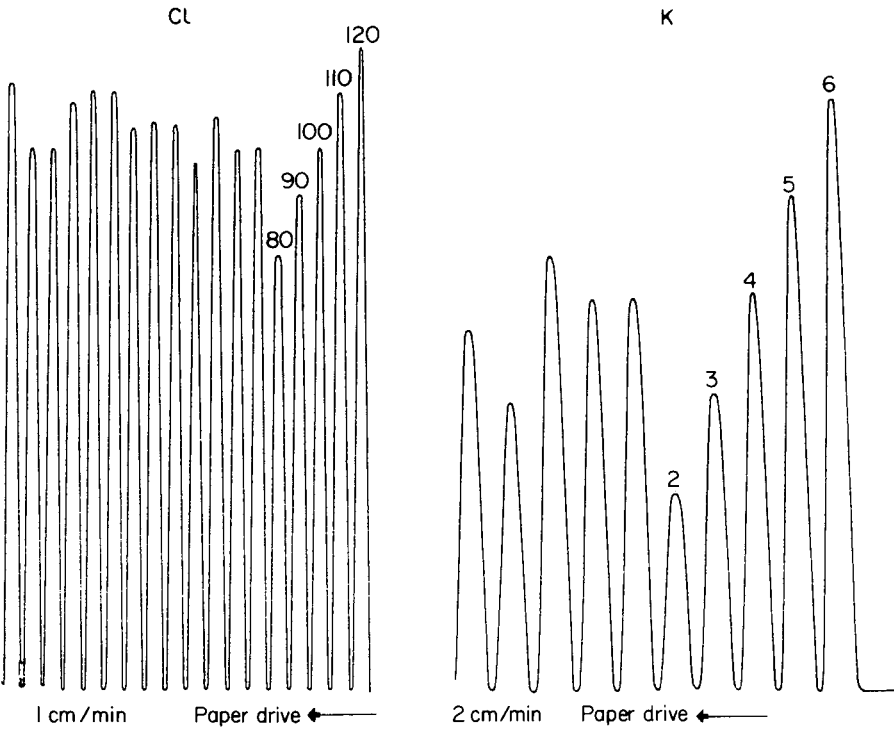


Fig. 5. Recorder outputs for serum chloride and potassium assay [14] at 120 samples/hour. The numbers on the peaks correspond to meq l⁻¹.

are analysed singly. The standard deviation of 22 serum samples run sequentially at a concentration of 2.60 mg% ($234.1 \mu\text{mol l}^{-1}$) was 0.034. Both baseline drift and carryover are negligible.

To emphasize further that curve regeneration can be employed routinely even in complicated systems, some results are given for a double dialysis system developed for the determination of chloride [14]. The double dialysis was needed to dilute the chloride concentration sufficiently for simple application of the sensitive reagent TPTZ. Figure 5 shows the traces obtained for chloride at 120 samples/hour. The coefficient of variation was 0.61% at the $100 \text{ meq Cl}^{-1} \text{ l}^{-1}$ level ($n = 10$).

The applicability of the curve regeneration technique to instruments other than colorimeters was also demonstrated. Figure 5 shows the curves obtained from the flame photometric determination of potassium also at 120 samples/hour [14]. Similar curves were obtained for sodium.

One of the successes of continuous flow analysis for both the operator and the laboratory manager has been the simplicity of monitoring instrumental performance. Poorly shaped or noisy curves mean unreliable results. Any technique which increases speed but decreases performance monitoring is essentially a retrograde step. With curve regeneration, speed is increased, but more important performance monitoring and hence the reliability of results have also been improved. The method developed as described above, has been in routine use on 12 AutoAnalyzer channels for five years.

We thank Dr. H. W. Holy (Technicon International Division S.A., Geneva, Switzerland) for his assistance in the preparation of the manuscript.

REFERENCES

- 1 W. E. Neeley, S. C. Wardlaw, T. Yates, W. G. Hollingsworth and M. E. T. Swinnen, *Clin. Chem.*, 22 (1976) 227.
- 2 W. E. Neeley, S. Wardlaw and M. E. T. Swinnen, *Clin. Chem.*, 20 (1974) 78.
- 3 V. R. White and J. M. Fitzgerald, *Anal. Chem.*, 44 (1972) 1267.
- 4 V. R. White and J. M. Fitzgerald, *Anal. Chem.*, 47 (1975) 903.
- 5 J. W. B. Stewart and J. Růžička, *Anal. Chim. Acta*, 82 (1976) 137.
- 6 J. Růžička and E. H. Hansen, *Anal. Chim. Acta*, 99 (1978) 37.
- 7 E. H. Hansen and J. Růžička, *Anal. Chim. Acta*, 87 (1976) 353.
- 8 W. H. C. Walker, J. Townsend and P. M. Keane, *Clin. Chim. Acta*, 36 (1972) 119.
- 9 M. A. MacAulay, J. M. Mathers, C. L. Jacklyn and C. A. Munro, *Clin. Biochem.*, 9 (1976) 111.
- 10 C. L. Jacklyn, C. D. Kriz and M. A. MacAulay, *Clin. Biochem.*, 11 (1978) 10.
- 11 R. E. Thiers, R. R. Cole and W. J. Kirsch, *Clin. Chem.*, 13 (1967) 451.
- 12 W. H. C. Walker, J. C. Shepherdson and G. K. McGowan, *Clin. Chim. Acta*, 35 (1971) 455.
- 13 A. Savitzky and M. J. E. Golay, *Anal. Chem.*, 36 (1964) 1627.
- 14 E. B. M. De Jong, H. M. J. Goldschmidt, A. C. M. Van Alpen and J. A. Loog, submitted for publication.

Short Communication

THE DETERMINATION OF SULPHATE BY FLOW-INJECTION ANALYSIS WITH EXPLOITATION OF pH GRADIENTS AND EDTA

S. BABAN, D. BEETLESTONE, D. BETTERIDGE* and P. SWEET

Chemistry Department, University College, Swansea SA2 8PP (Gt. Britain)

(Received 18th July 1979)

Summary. A modified method for the turbidimetric determination of sulphate as barium sulphate is proposed. The carrier stream is an alkaline barium–EDTA solution; the sample zone is sufficiently acidic to allow precipitation of barium sulphate. The excess of EDTA in the carrier stream ensures that residual precipitate is redissolved and the system kept clean.

Flow-injection analysis (f.i.a.) is simple, accurate and rapid, typical sampling rates being 120–150 per hour [1]. The method is based on rapid injection of an aqueous sample into a carrier stream of reagent, without air segmentation. In this communication the usefulness of f.i.a. is demonstrated for the turbidimetric determination of sulphate by exploiting the masking properties of EDTA and the pH gradients which develop across the sample–carrier interface.

Krug et al. [2] described a method for the determination of sulphate, using the turbidity of barium sulphate. In some applications there is build-up of precipitate, which leads to low precision and ultimately blocks the tubing. One way of overcoming this is to use alkaline EDTA solution to redissolve the precipitate. Thus the carrier solution contains barium(II) with an excess of EDTA at pH 10, whereas the sample is acidic. During the mixing, precipitation occurs under the acidic conditions of the sample zone, but the precipitate is redissolved outside this zone, by the self-cleansing action of the carrier. The EDTA also serves to reduce interference from metal ions.

Experimental

Carrier solutions. For the method of Krug et al., a barium chloride solution (0.05 M) containing 0.005% polyvinyl alcohol was mixed (1 + 1) with 0.01 M hydrochloric acid. For the modified method, a mixture (1 + 1) of barium chloride solution (0.04 M) and EDTA solution (0.05 M) was adjusted to pH 10 with ammonia solution.

Standards. A solution (1000 ppm sulphate) of sodium sulphate was standardised gravimetrically, and diluted to give solutions of sulphate in the 20–200 ppm range. For the method of Krug et al. [2], the diluent was water; for the modified method it was 0.2 M hydrochloric acid, the final pH being 1.5.

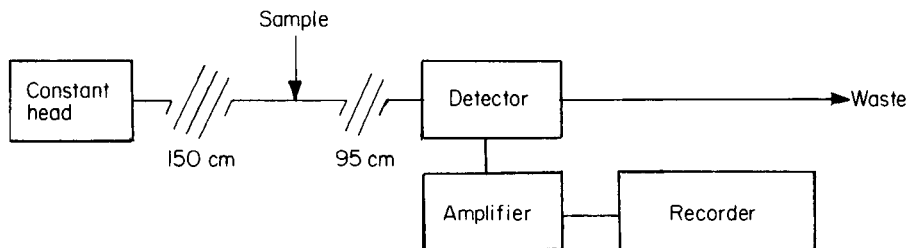


Fig. 1. Block diagram of the f.i.a. system for the determination of sulphate.

pH adjustment. Below pH 2 the pH was controlled by addition of hydrochloric acid. For pH 2–4, standard phthalate buffers [3] were used.

Apparatus: Figure 1 is a block diagram of the apparatus used. The constant head device provided a constant flow rate of 2 ml min^{-1} . Samples were injected from a disposable plastic syringe (1 ml) through a septum valve into the reagent stream. The connecting polyethylene tubing, also used for coils, had an internal diameter of 0.86 mm. The reaction coil was 95 cm long and the pressure-buffer coil was 150 cm long.

The detector used was that developed by Betteridge et al. [4]; the cell has a 2-cm path length and a central bore of 1 mm, which is slightly larger than the internal diameter of the polyethylene tubing. The light source is an LED driven from a constant 15-V source with a current-limiting resistor; the detector is a phototransistor biased at a constant voltage.

Recommended procedure. After adjustment of the carrier flow rate to 2 ml min^{-1} , aliquots ($200 \mu\text{l}$) of sample solution acidified to pH 1.5 were injected, and the resultant turbidity was measured.

Results and discussion

Effect of pH. It is well known that barium sulphate dissolves in an excess of alkaline EDTA. The relative importance of pH and concentrations of EDTA, barium and sulphate ions on the precipitation of barium sulphate may be deduced from plots of the conditional solubility constant of barium sulphate and pSO_4 as a function of pH (Fig. 2). The calculations were made by standard procedures and took into account the protonation of sulphate [5]. Although the analyses are not done under non-equilibrium conditions, these calculations serve as a useful guide. The curves in Fig. 2 indicate that the concentrations of barium and EDTA should be maximal, and the values recommended in the Experimental correspond to the practical limits imposed by the solubilities of barium chloride and EDTA. It is also evident that the minimum pH of the sample plug after reaction with EDTA should be in the region pH 1–4.

Experiments were done with acid–base indicators in the sample solution in order to establish the pH of the sample at the point of detection. These led to the establishment of the optimum conditions given above. Finally, the

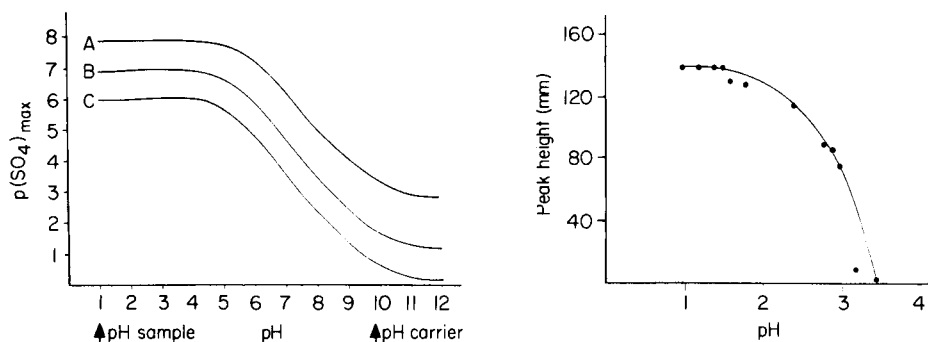


Fig. 2. Theoretical $p(\text{SO}_4)_{\text{max}}$ vs. pH in presence of 1.25×10^{-2} M EDTA and varying amounts of Ba^{2+} : $[\text{Ba}^{2+}] = [\text{SO}_4^{2-}] = 10^{-2}$ M (curve A), 10^{-3} M (curve B), 10^{-4} M (curve C).

Fig. 3. Effect of pH of the solution injected on precipitation of sulphate.

effect of pH of the sample was measured (Fig. 3); the method is, as predicted, quite pH-dependent. The pH also affects the structure of the barium sulphate. A precipitate obtained from a solution with a pH in the range 0–1.5 consists of large well shaped crystals. At pH 1.5–3 uneven crystals of medium particle size are obtained, whereas at pH 3–7, the precipitate is amorphous. EDTA also affects the crystal growth [6]. Hence it is possible that the increased sensitivity obtained here is a consequence of a different crystal size compared with that found in the method of Krug et al. [2].

Sensitivity and precision. Calibration curves for the two methods are shown in Fig. 4; when due allowance is made for the different recorder scales, it can be seen that the modified method is more sensitive than the original. (The sensitivity of the earlier method is improved by using a tube length of 95 cm rather than the 200 cm originally proposed.) The useful working range of the method is extended from 30–80 to 40–160 ppm of sulphate. The precision was generally of the order 1–2%.

Scavenging effect of EDTA. One of the attractive features of f.i.a. is the way in which the carrier can act as a wash solution. This aspect is emphasised in the modified method by having excess of alkaline EDTA in the carrier stream. The practical effect was to reduce greatly the clogging of the system by precipitated barium sulphate. It was virtually impossible to measure reliably the rate of precipitate build-up, but qualitatively the modified system was far superior to the earlier one in this respect.

Interferences. The effects of some interferences are shown in Fig. 5. The interferences were chosen on the basis that they might be masked by EDTA (cations), or they would be worse in alkaline solution (phosphate) or they have proven difficult in this system (dextran, nitrate). The results show that the modified method is marginally better, but that nitrate at high concentration is a serious interference in both methods.

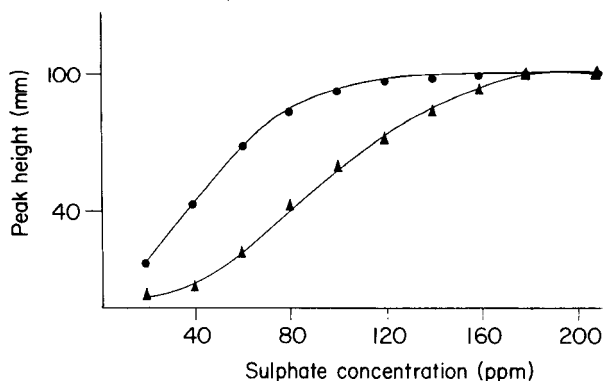


Fig. 4. Calibration graphs for sulphate with (●) BaCl₂ + PVA + HCl carrier (100 mm = 5 V); (▲) BaCl₂ + EDTA carrier at pH 10 (100 mm = 3 V).

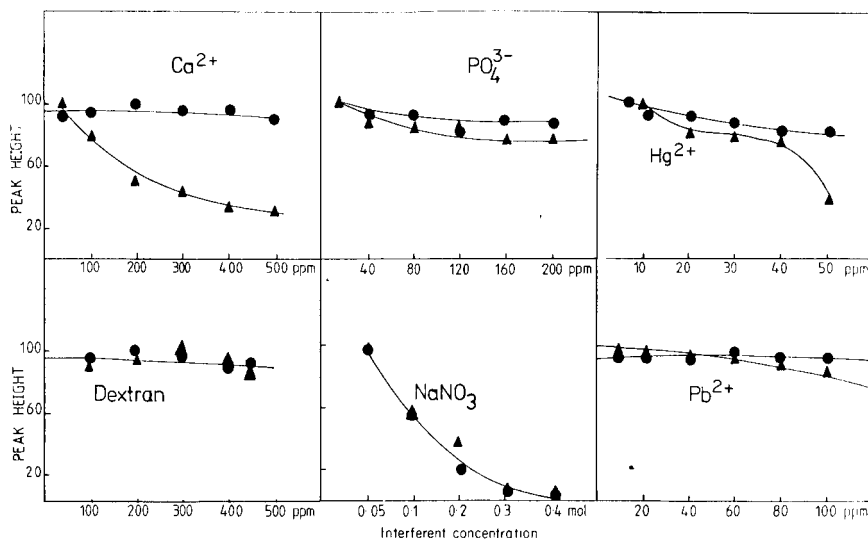


Fig. 5. Effect of interferences on determination of 100 ppm of sulphate: (●) by the recommended method with EDTA; (▲) by the method of Krug et al. without EDTA.

Applications. The recommended procedure was applied to the analysis of river and sea water and compared with a gravimetric procedure. For a river water, the f.i.a. method gave a result of 72 ppm (67 ppm by conventional gravimetry) and a result of 1600 ppm (1643 ppm by gravimetry) for a sea-water sample diluted 10 times. Satisfactory agreement was also obtained with an effluent from a local industry, which had been analysed independently in the industrial laboratory.

Conclusion. This work demonstrates the value of using pH gradients in f.i.a. The use of alkaline EDTA is more effective than polyvinyl alcohol in

minimising build-up of barium sulphate in the determination of sulphate in flowing systems.

We are grateful to the University of Sulimaniya and to the SRC for maintenance grants for S.B. and P.S., respectively, and to NATO Grant No. 1492.

REFERENCES

- 1 J. Růžička and E. H. Hansen, *Anal. Chim. Acta*, 78 (1975) 145.
- 2 F. J. Krug, H. Bergamin F^o, E. A. G. Zagatto and S. S. Jørgensen, *Analyst*, 102 (1977) 503.
- 3 R. C. Weast (Ed.), *Handbook of Chemistry and Physics*, 53rd edn., CRC Press, Cleveland.
- 4 D. Betteridge, E. L. Dagless, B. Fields and N. Grave, *Analyst*, 103 (1978) 897.
- 5 A. Ringbom, *Complexation in Analytical Chemistry*, Wiley, New York, 1963.
- 6 L. Erdey, *Gravimetric Analysis, Part 3*, Pergamon, Oxford, 1965.

Short Communication

SELECTIVE DETERMINATION OF GALLIUM BY FLOW INJECTION FLUORIMETRY

NOBUHIKO ISHIBASHI*, KENYU KINA** and YOSHIHIDE GOTO***

Faculty of Engineering, Kyushu University, Hakozaki, Fukuoka, 812 (Japan)

(Received 6th August 1979)

Summary. Gallium can be determined fluorimetrically, with linear response in the range 2.2×10^{-5} M– 1.08×10^{-4} M, by means of chelate formation with lumogallion; fluorescence is enhanced by mixing with a polyethylene glycol monolauryl ether solution. Up to 10-fold molar amounts of aluminum can be tolerated, because of the slow formation rate of the aluminum–lumogallion chelate.

Lumogallion [4-chloro-6-(2,4-dihydroxyphenylazo)-1-hydroxybenzene-2-sulfonic acid] is a very sensitive ligand for the fluorimetric determination of gallium and aluminum [1, 2]. When it is used for gallium, removal or masking of aluminum is usually necessary to avoid interference. In previous papers [3, 4] it was shown that the aluminum interference can be reduced considerably by selective extraction of the gallium chelates with lumogallion analogs into methyl isobutyl ketone. This communication describes the selective determination of gallium by utilization of the difference in reaction rates for chelation of gallium and aluminum with lumogallion. Aluminum ions are relatively inert in chelate formation or ligand-exchange reactions. Complete chelation of aluminum with lumogallion requires heating [2], whereas chelation of gallium does not. The exchange rate of water molecule between bound water and bulk water is about 10^4 times faster in the hydrated gallium ion than in the aluminum ion [5]. Accordingly, the flow-injection method was expected to be useful for avoiding the aluminum interference, as it should be possible to detect the fluorescence of the gallium–lumogallion chelate before that of the aluminum chelate becomes measurable.

Experimental

Equipment. A schematic diagram of the flow-injection system is shown in Fig. 1. Teflon tubing was used (i.d. 0.5 mm). A 10- μ l sample aliquot was injected manually by means of a syringe through the silicone rubber septum of the sample injector A, through which a carrier stream of lumogallion

*Present address: Dojindo Laboratories, Kengun-machi, Kumamoto, Japan.

***Present address: Shimonoseki-shi Shiyakusho, Kankyo-bu, Shimonoseki, Japan.

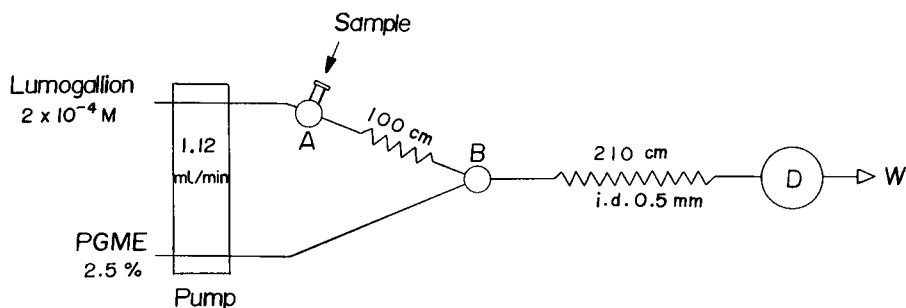


Fig. 1. Flow injection system.

solution (2×10^{-4} M) was pumped at 1.12 ml min^{-1} (9.5 cm s^{-1}). The tube from A to B constituted the reaction tube, in which the gallium–lumogallion chelate was formed. At B, the stream of lumogallion solution was mixed with a stream of the nonionic surfactant polyethylene glycol monolauryl ether (PGME) flowing at the same rate. After passing through the 210-cm mixing coil, the fluorescence intensity was measured by a spectrofluorimeter (Hitachi 204, 150 W Xenon arc lamp) equipped with a $100\text{-}\mu\text{l}$ flow-through cell. The concentration of the gallium–lumogallion chelate was obtained from the fluorescence peak height on a recorder. The excitation and emission wavelengths used were 490 and 553 nm, respectively [6].

Reagents. A gallium stock solution (0.01 M) was prepared by dissolving 1 g of gallium oxide (purity 99.99%) in 1 l of 1 M HCl. The aluminum stock solution (0.1 M) was prepared from aluminum potassium sulfate in 0.01 M HCl. The stock solution of lumogallion (1×10^{-3} M) was diluted with a pH 3.4 acetate buffer. PGME was dissolved in water (see below). All other chemicals were of analytical reagent grade, and water was redistilled.

Results and discussion

The relationship between the tube length and the fluorescence peak height was investigated. With a constant length of mixing tube (117 cm), the peak height remained almost constant for reaction tube lengths between 39 and 100 cm but it tended to become lower with longer reaction tubes (200 cm), perhaps because of axial dispersion of the sample zone. The effect of the mixing tube length on peak height was also examined; the fluorescence was unchanged for variations in length between 117 and 210 cm.

The fluorescence of the gallium–lumogallion chelate is known to be greatly enhanced by the addition of surfactants especially the nonionic PGME [6]. However, preliminary tests showed that injection of a gallium sample into a lumogallion stream containing PGME gave a lower fluorescence signal than that in an absence of PGME. The reason may be that lumogallion molecules are absorbed by PGME micelles before they can react fully with gallium. Accordingly, the manifold system shown in Fig. 1, in which PGME was added after completion of the chelation, was adopted. PGME concentrations of 2.5% and above gave a fluorescence enhancement of about 4-fold (at

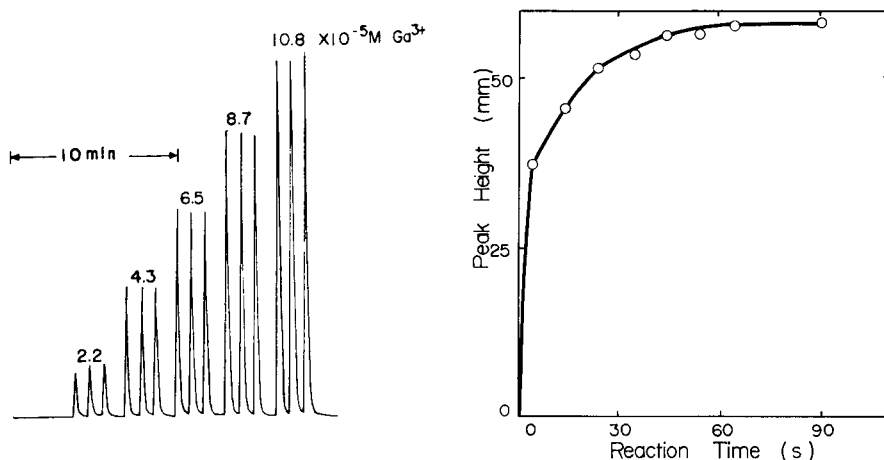


Fig. 2. Fluorescence peak heights for calibration of the gallium determination with the manifold shown in Fig. 1.

Fig. 3. Formation rate of the gallium—lumogallion chelate. Gallium concentration, $1 \times 10^{-5} \text{ M}$; carrier solutions, $1 \times 10^{-5} \text{ M}$ lumogallion and 2.5% PGME; reaction tube, 39 cm; mixing tube, 210 cm.

the excitation and emission wavelengths recommended) compared to the results obtained in the absence of PGME. Figure 2 shows the fluorescence peaks obtained for samples containing 2.2×10^{-5} – $1.08 \times 10^{-4} \text{ M}$ gallium; each sample was injected in triplicate and the mean values of the peak heights were directly proportional to the concentration of gallium. Judging from the investigation of reaction rates (see below), the injected gallium was completely converted to the lumogallion chelate in the 100-cm reaction tube.

Removal of aluminum interference. The formation rates of gallium and aluminum with lumogallion were compared in order to estimate the possibility of selective determination of gallium. The formation rates were measured in the flow injection system with a 39-cm reaction tube and a 210-cm mixing tube. Immediately after $10 \mu\text{l}$ of the gallium solution had been injected into the lumogallion stream, the stream was stopped, so that chelate formation proceeded in the reaction tube. After a predetermined reaction time, the flow was restarted and merged with the PGME stream, and the fluorescence was measured. The sample was apparently diluted at least 10-fold after injection, judging from the width of the fluorescence peak. The variation in peak height with reaction time for 10^{-5} M gallium solution is illustrated in Fig. 3. Similar results were obtained for $2 \times 10^{-6} \text{ M}$ and $5 \times 10^{-6} \text{ M}$ gallium solutions. When aluminum solutions were tested, a reaction was observed only after reaction times exceeding 1 h.

Rate constants were obtained by assuming that the reaction between gallium and lumogallion is first order with respect to gallium in the presence of a large excess of lumogallion, and the following equation was derived:

In $[G]_0/[G] = k [L] t = k' t$, where $[G]$ is the free gallium concentration at time t , $[G]_0$ is its initial concentration, $[L]$ is the lumogallion concentration, and k ($l \text{ mol}^{-1} \text{ s}^{-1}$) and k' (s^{-1}) are apparent rate constants. $[G]$ was calculated from the relation $[G] = [G]_0 - [GL]$, as the gallium—lumogallion chelate concentration, $[GL]$, was obtained from the fluorescence peak height. From the observed values of $[G]$ against t , k was calculated to be about $4 \times 10^3 \text{ l mol s}^{-1}$ for gallium. A similar calculation for the aluminum chelate formation yielded a k value of 1.7 l mol s^{-1} . The formation rate of the aluminum—lumogallion chelate is thus more than 1000 times slower than that of the gallium chelate, which indicates that up to 10-fold amounts of aluminum should not interfere with the determination of gallium, although 100-fold amounts would interfere. In order to verify this prediction, 10^{-4} M gallium solutions containing aluminum in excess were analyzed. The results agreed with the theoretical expectations; aluminum in 100-fold molar excess gave positive errors of about 10%.

Effect of diverse ions. The effects of Mg(II), Fe(II, III), Co(II), Ni(II), Cu(II), Zn(II) were examined by measuring the fluorescence peak heights for mixed solutions of gallium and the diverse ion. The results are listed in Table 1. The presence of 100-fold amounts of iron(III) and copper(II) gave large negative errors.

The authors thank the Ministry of Education of Japan for financial support (Project No. 485191).

TABLE 1

Effects of diverse ions on the determination of $1.0 \times 10^{-4} \text{ M}$ gallium ($10\text{-}\mu\text{l}$ injections)^a

Metal ion added	Ga recovery (%)			Metal ion added	Ga recovery (%)		
	Molar ratio [M]: [Ga]				Molar ratio [M]: [Ga]		
	1	10	100		1	10	100
Mg(II)	104	102	102	Co(II)	98	98	100
Al(III)	100	102	109	Ni(II)	101	99	102
Fe(II)	97	95	83	Cu(II)	95	71	4
Fe(III)	96	87	17	Zn(II)	100	98	98

^aCarrier solutions and tube lengths are the same as those in Fig. 1.

REFERENCES

- 1 E. A. Bozhevol'nov, A. M. Lukin and M. N. Gradinarskaya, *Avtomat. Svarka SSSR*, 1959, No. 116838; *Anal. Abstr.*, 7 (1960) Abs. 3164.
- 2 Y. Nishikawa, K. Hiraki, K. Morishige and T. Shigematsu, *Bunseki Kagaku*, 16 (1967) 692.
- 3 K. Kina, K. Shiraishi and N. Ishibashi, *Bunseki Kagaku*, 25 (1976) 501.
- 4 K. Kina, K. Hirokata and N. Ishibashi, *Bunseki Kagaku*, 26 (1977) 246.
- 5 D. Fiat and R. E. Connick, *J. Am. Chem. Soc.*, 90 (1968) 608.
- 6 K. Kina and N. Ishibashi, *Microchem. J.*, 19 (1974) 26.

Short Communication

POTENTIOMETRIC DETERMINATION OF PROTEINS WITH AN AMMONIA SENSOR

MARCO MASCINI* and RITA GIARDINI

Istituto di Chimica Analitica, Università di Roma (Italy)

(Received 9th July 1979)

Summary. A flow system is described for the cleavage of proteins with immobilized protease enzyme to L-amino acids which are then converted to ammonia with glass-immobilized L-amino acid oxidase. An ammonia gas electrode is used as detector. Immobilization techniques are discussed, as are optimum conditions for L-phenylalanine. Bovine serum albumin was determined in the range 0.1–100 $\mu\text{g ml}^{-1}$. Human blood sera required dilution for analysis.

The impact of selective electrodes in clinical laboratory measurements has been considerable [1]. Proteins have been successfully determined with a silver sulfide membrane electrode [2–4]. In the work reported here the behaviour of an ammonia sensor [5, 6] in the determination of amino acids was studied. A flow-through ammonia sensor was used in combination with immobilized protease and L-amino acid oxidase reactors. The enzymatic reactions were allowed to proceed for a fixed time so that the release of ammonia was not quantitative but amino acid concentrations in the range 0.1–100 $\mu\text{g ml}^{-1}$ could be determined at a rate of 8 samples/hour with good reproducibility.

Experimental

Ammonia sensor. The probe was assembled with an antimony pH electrode [5] in a mode suitable for flow analysis (Fig. 1). The dead volume of the chamber was 40 μl , and the flow rates were regulated to ca. 0.3 ml min^{-1} . Rapid washing of the line was therefore possible.

Manifold. The flow system is shown in Fig. 2. The lines were thermostatted at $25.0 \pm 0.1^\circ\text{C}$. Potentiometric measurements were made with an AMEL Model 331 pH meter in conjunction with an Omniscribe Recorder. In preliminary work, soluble enzyme was used and an additional line with a thermostat coil was included. The enzymatic reaction time was 2–3 min.

Reagents and samples. Bovine serum albumin was obtained from Sigma Fraction V powder. Serum was obtained from the University Hospital. The enzymes used were L-amino acid oxidase from *Adamanteus crotalus* (Sigma, crude, type 1, 0.4 IU mg^{-1}) and protease (Sigma, protease pancreatic crude, type 1, 9 IU mg^{-1}). The controlled-pore glass was Sigma PG-75-120 (70 nm).

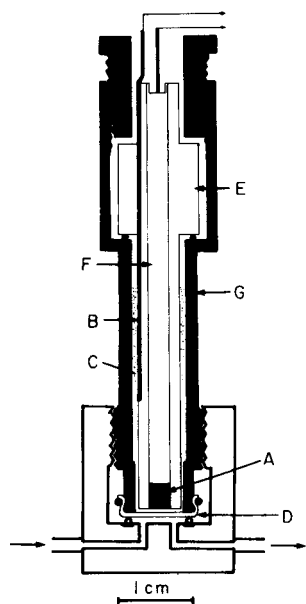


Fig. 1. Ammonia flow-through sensor. (A) Sb pellet; (B) Ag/AgCl reference electrode; (C) internal reference solution; (D) permeable teflon membrane; (E) polyethylene tube; (F) metal contact; (G) external PVC tube.

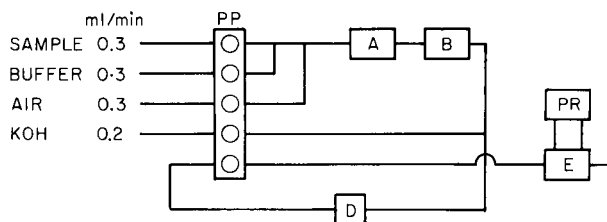


Fig. 2. Flow-through electrode manifold. (PP) Peristaltic pump; (A) reactor with immobilized protease; (B) reactor with immobilized L-amino acid oxidase; (D) debubbler; (E) ammonia sensor; (PR) potentiometer with recorder.

γ -Aminopropyltriethoxysilane (EGA Chemie AG) and glutaraldehyde (25%, Merck) were used. Other reagents were of analytical grade (Merck).

Silanization of porous glass with γ -aminopropyltriethoxysilane. Controlled pore glass (10 g) was washed for 15 min in 100 ml of boiling 5% nitric acid. After decantation, the glass was washed several times with distilled water, dried at 95°C, and then immersed in 50 ml of an aqueous 10% (v/v) solution of γ -aminopropyltriethoxysilane adjusted to pH 5 with glacial acetic acid. The mixture was heated, with stirring, at 80°C for 1 h. After cooling, the solution was decanted, and the glass was washed thoroughly with water and dried for 2 h at 120°C.

Coupling of enzymes to alkylamine glass. For the glutaraldehyde procedure, 2 g of the alkylamine glass was added to 10 ml of a 2.5% (v/v) glutaraldehyde solution in phosphate buffer pH 6.9. The mixture was kept at room temperature for 1 h under moderate vacuum (water pump). The activated glass was then washed several times with water. To 1 g of glass, 5 ml of enzyme solution (1 mg ml⁻¹) was added and the reaction was allowed to proceed for 2 h at 4°C under moderate vacuum. The product was washed with phosphate buffer and stored in a refrigerator. For the diazotization procedure, 1 g of the alkylamine glass was refluxed for 1 h with 10 ml of chloroform containing 0.1 g of *p*-nitrobenzoyl chloride.

After cooling, the glass was decanted, washed several times with chloroform, and dried at 70°C for 30 min. The aryl nitro glass (1 g) was reduced with 10 ml of aqueous 1% (w/v) sodium dithionite ($\text{Na}_2\text{S}_2\text{O}_4$) solution at pH 8.5 by refluxing for 1 h. The arylamine glass obtained was decanted and washed with water; 1 g of this glass was diazotized by mixing with 10 ml of 2 M hydrochloric acid and 0.25 g of sodium nitrate for 30 min in ice water. The glass was then washed with water and cold 1% (w/v) sulfamic acid solution. The diazotized product (1 g) was added to 10 ml of enzyme solution (1 mg ml⁻¹) in hydrogencarbonate buffer (0.05 M); after reaction for 1 h in ice water, the glass was decanted, washed with distilled water and stored in a refrigerator. The glutaraldehyde procedure was used for both L-amino acid oxidase and protease whereas the diazo procedure was used only for the former.

Preparation of reactor with immobilized enzyme. The glass (1 g) with enzyme immobilized was placed in a polyethylene tube (4 mm i.d., 40 cm long) and held in position with glass wool.

Results and discussion

Linear calibration plots with Nernstian slope were obtained for the flow-through ammonia electrode (Fig. 1) in pure ammonium chloride solutions in the range 10^{-2} M– 5×10^{-6} M when the internal solution was 10^{-2} M ammonium ion– 10^{-1} M chloride. The range of linear behaviour was reduced to 10^{-2} – 5×10^{-4} M when the internal solution was 10^{-1} M ammonium ion– 10^{-1} M chloride. The more dilute solution was therefore preferred. Standard solutions of ammonia were prepared by adding 1 M potassium hydroxide to standard solutions of ammonium chloride.

To establish the optimum conditions, L-phenylalanine was selected as model compound for tests with soluble L-amino acid oxidase (0.1 mg ml⁻¹) in phosphate buffer at pH 6.9. The calibration plot was linear for the range 10^{-5} – 10^{-3} M L-phenylalanine but the difference between the ammonia and L-amino acid calibration curves showed that the enzymatic reaction was incomplete. A study of parameters influencing the reaction, i.e., temperature, time, pH and enzyme concentration, essentially confirmed earlier results [7, 8]. Thus the optimum temperature was 37°C, the reaction time giving maximum values of ΔE was 10 min, and the optimum pH of the enzyme reaction was around pH 7. This pH is a compromise between the optimum pH of the enzyme and the optimum for the reaction. The pK_a value of phenylalanine is 5.9, hence the anionic form of the amino acid, which is responsible for the reaction, predominates at the recommended pH. The best concentration of enzyme giving maximum linear range was 0.1 mg ml⁻¹. These conditions were used for guidance in the application of the immobilized enzymes.

Immobilized enzymes. The L-amino acid oxidase was immobilized for convenient use by procedures A and B. The calibration curves obtained (Fig. 3) demonstrate the superiority of the diazo procedure; between 2 and 30

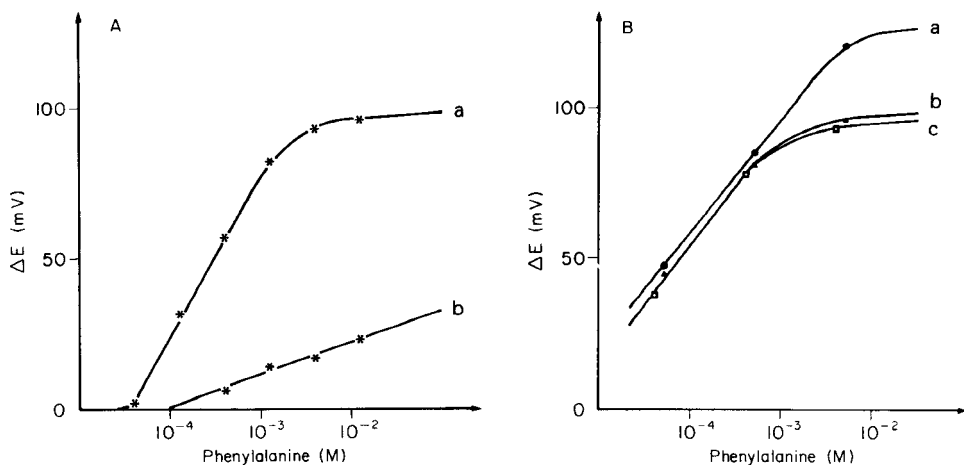


Fig. 3. Calibration curves for L-phenylalanine with immobilized enzyme in phosphate buffer pH 6.9 at 37°C. (A) Glutaraldehyde procedure; (B) diazotization procedure. (a) After immobilization, (b) after 48 h, (c) after 30 days.

days there was only a slight decrease of activity. The calibration curves for several other substrates with the immobilized enzyme are shown in Fig. 4. The phosphate buffer at pH 6.9 is optimal for the enzyme activity but it is evident that lysine ($pK_a = 9.5$) reacts very slowly. This can be ascribed to the predominance of the cationic form of lysine at pH 6.9. However, it is impossible to achieve a single optimum pH for all amino acids, and so all further experiments were carried out at pH 6.9. The output for a set of consecutive samples of phenylalanine used to obtain a calibration curve is shown in Fig. 5. The run shows that around 8 samples per hour can be analyzed.

Analysis of standard sera. Some results of clinical interest obtained with the manifold shown in Fig. 2 are illustrated in Fig. 6. The calibration curve for bovine serum albumin is compared with that for a standard serum obtained from the University Hospital; the serum was diluted to obtain the four concentrations measured. The proteins in the serum are clearly less reactive than bovine serum albumin (Sigma). Calibration curve (b) of Fig. 6

TABLE 1

Analysis of human sera

Sample ^a	1	2	3	4	5	6
Potentiometric result (g/100 ml)	3.4	6.9	6.7	5.9	6.7	6.9
Colorimetric result ^b (g/100 ml)	2.3	6.6	6.7	6.1	6.1	6.7

^aAll samples were prediluted 1:10 with phosphate buffer pH 7.9, except sample 1 which was prediluted 1:30.

^bStandard method used in the University Hospital.

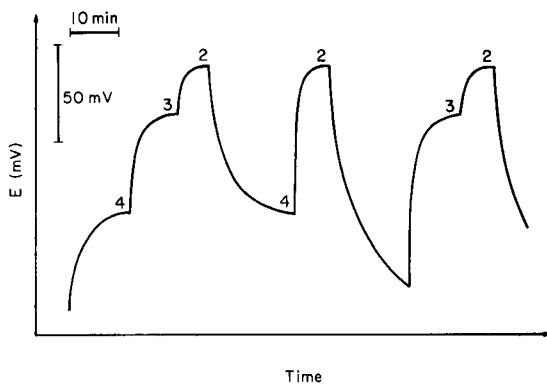
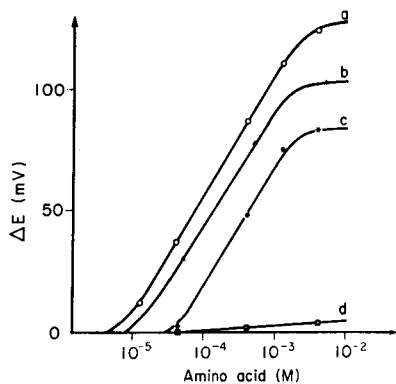


Fig. 4. Calibration curves for some L-amino acids with immobilized enzyme (procedure B) at pH 6.9: (a) leucine, (b) phenylalanine, (c) cysteine, (d) lysine.

Fig. 5. Response times for L-phenylalanine at concentrations of (2) 10⁻² M, (3) 10⁻³ M, (4) 10⁻⁴ M.

was used in analyzing a series of patient sera; the results (Table 1) show good correlation, except perhaps for sample 1.

The protease enzyme was immobilized because it degrades rapidly in solution, hydrolyzing in a few days even at 5°C. At 37°C, hydrolysis is faster and the blank gives a potential value which corresponds to significant autodegradation of enzyme to L-amino acids.

The high nitrogen content of proteins allows this simple technique to be applied to quite low concentrations. The ammonia sensor has advantages over the sulfide-selective electrode [2, 3] in that it is more accurate and easier to standardize. The immobilizing techniques for the enzymes require further development so that greater sensitivity, and so shorter analysis times, can be achieved for an automatic system.

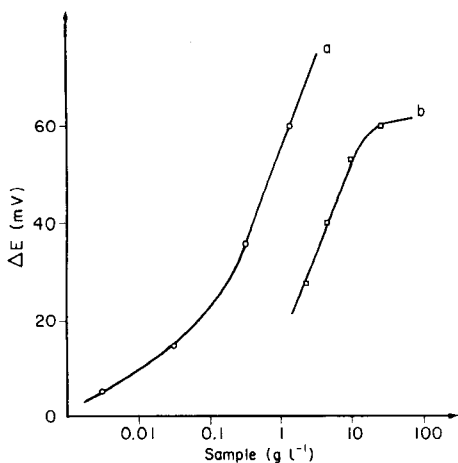


Fig. 6. Calibration curves for (a) bovine serum albumin and (b) human blood serum at pH 6.9. L-amino acid oxidase immobilized by procedure B and protease by procedure A.

REFERENCES

- 1 R. P. Buck, *Anal. Chem.*, 50 (1978) 17 R.
- 2 P. D'Orazio and G. A. Rechnitz, *Anal. Chem.*, 49 (1977) 41.
- 3 P. W. Alexander and G. A. Rechnitz, *Anal. Chem.*, 46 (1974) 250; 46 (1974) 860.
- 4 B. S. Harrap and L. C. Gruen, *Anal. Biochem.*, 42 (1971) 398.
- 5 M. Mascini and C. Cremisini, *Anal. Chim. Acta*, 92 (1977) 277.
- 6 M. Mascini and C. Cremisini, *Anal. Chim. Acta*, 97 (1978) 237.
- 7 G. G. Guilbault and G. J. Lubrano, *Anal. Chim. Acta*, 69 (1974) 183.
- 8 G. Johansson, K. Edstrom and L. Ogren, *Anal. Chim. Acta*, 85 (1976) 55.

AUTHOR INDEX

- Abicht, S. M.
Controlled dynamic titrator 247
- Åström, O., see Kågevall, I. 199
- Baban, S.
—, Beetlestone, D., Betteridge, D. and Sweet, P.
Determination of sulphate by flow-injection analysis with exploitation of pH gradients and EDTA 319
- Beetlestone, D., see Baban, S. 319
- Berg, J. H. M. van den, see van den Berg, J. H. M. 91
- Bergamin F^o, H., see Gine, M. F. 191
- Betteridge, D., see Baban, S. 319
- Bridges, J. W., see Lim, C. S. 183
- Bruins, C. H. P., see Brunt, K. 257
- Brinkman, U. A. Th., see Scholten, A. H. M. T. 137
- Brinkman, U. A. Th., see Werkhoven-Goewie, C. E. 147
- Brown, J. F., see Stewart, K. K. 119
- Brunt, K.
—, Bruins, C. H. P., Doornbos, D. A. and Oosterhuis, B.
The response surface of an amperometric flow cell detector based on a rotating disk electrode for h.p.l.c. and continuous flow analysis 257
- Burguera, J. L.
—, Townshend, A. and Greenfield, S.
Flow injection analysis for monitoring chemiluminescent reactions 209
- Cedergren, A., see Kågevall, I. 199
- Cnobloch, H.
—, Kellermann, W., Kühn, D., Nischik, H., Pantel, K. and Poppa, H.
Continuous monitoring of heavy metals in industrial waste waters 303
- Deelder, R. S., see van den Berg, J. H. M. 91
- de Jong, E. B. M.
— and Weyden, A. H.
Fast analysis rates in continuous flow methods by using a modified method of curve regeneration 311
- Dieker, J. W.
— and van der Linden, W. E.
Determination of iron(II) and iron(III) by flow injection and amperometric detection with a glassy carbon electrode 267
- Doornbos, D. A., see Brunt, K. 257
- Eelderink, G. H. B., see Reijnders, H. F. R. 235
- Egberink, H. G. M., see van den Berg, J. H. M. 91
- Fehér, Z., see Tóth, K. 45
- Franklin Smyth, W., see Ivaska, A. 283
- Frei, R. W., see Scholten, A. H. M. T. 137
- Frei, R. W., see Werkhoven-Goewie, C. E. 147
- Giardini, R., see Mascini, M. 329
- Giné, M. F.
—, Bergamin F^o, H., Zagatto, E. A. G. and Reis, B. F.
Simultaneous determination of nitrate and nitrite by flow injection analysis 191
- Golden B. M., see Stewart, K. K. 119
- Goto, Y., see Ishibashi, N. 325
- Greenfield, S., see Burguera, J. L. 209
- Griepink, B., see Reijnders, H. F. R. 235
- Hansen, E. H., see Ramsing, A. 165
- Hansen, E. H., see Ružička, J. 19
- Horvai, G., see Tóth, K. 45
- Ishibashi, N.
—, Kina, K. and Goto, Y.
Selective determination of gallium by flow injection fluorimetry 325
- Ivaska, A.
— and Franklin Smyth, W.
Applications of a voltammetric flow-through cell in on-line analysis for organic compounds 283
- Jensen, A., see Kagenow, H. 227

- Johansson, P.-A.
—, Karlberg, B. and Thelander, S.
Extraction based on the flow-injection principle. Part 4. Determination of extraction constants 215
- Jong, E. M. B. de, see de Jong, E. B. M. 311
- Kagenow, H.
— and Jensen, A.
Differential kinetic analysis and flow injection analysis. Part 3. The (2.2.2) cryptates of magnesium, calcium and strontium 227
- Kågevall, I.
—, Åström, O. and Cedergren, A.
Determination of water by flow-injection analysis with the Karl Fischer reagent 199
- Karlberg, B.
— and Thelander, S.
Extraction based on the flow-injection principle. Part 3. Fluorimetric determination of vitamin B₁ (thiamine) by the thiochrome method 129
- Karlberg, B., see Johansson, P.-A. 215
- Kellermann, W., see Cnobloch, H. 303
- Kina, K., see Ishibashi, N. 325
- Kosta, L., see Pihlar, B. 275
- Kühl, D., see Cnobloch, H. 303
- Landis, J. B.
Rapid determination of corticosteroids in pharmaceuticals by flow injection analysis 155
- Lim, C. S.
—, Miller, J. N. and Bridges, J. W.
Automation of an energy-transfer immunoassay by using stopped-flow injection analysis with merging zones 183
- Linden, W. E. van der, see Dieker 267
- Linden, W. E. van der, see Reijn, J. M. 105
- Mascini, M.
— and Giardini, R.
Potentiometric determination of proteins with an ammonia sensor 329
- Miller, J. N., see Lim, C. S. 183
- Nagy, G., see Tóth, K. 45
- Nischik, H., see Cnobloch, H. 303
- Oosterhuis, B., see Brunt, K. 257
- Pantel, K., see Cnobloch, H. 303
- Pihlar, B.
— and Kosta, L.
Determination of cyanides by continuous distillation and flow analysis with cylindrical amperometric electrodes 275
- Poppa, H., see Cnobloch, H. 303
- Poppe, H.
Characterization and design of liquid phase flow-through detector systems 59
- Poppe, H., see Reijn, J. M. 105
- Pungor, E., see Tóth, K. 45
- Ramsing, A.
—, Růžicka, J. and Hansen, E. H.
A new approach to enzymatic assay based on flow-injection spectrophotometry with acid-base indicators 165
- Reijn, J. M.
—, van der Linden, W. E. and Poppe, H.
Some theoretical aspects of flow injection analysis 105
- Reijnders, H. F. R.
—, van Staden, J. J., Eelderink, G. H. B. and Griepink, B.
A modelling approach to establish experimental parameters of a flow-through titration 235
- Reis, B. F. see Giné, M. F. 191
- Růžicka, J.
— and Hansen, E. H.
Flow injection analysis. Principles, applications and trends 19
- Růžicka, J., see Ramsing, A. 165
- Scholten, A. H. M. T.
—, Brinkman, U. A. Th. and Frei, R. W.
Photochemical reaction detectors in continuous-flow systems — applications to pharmaceuticals 137
- Snyder, L. R.
Continuous-flow analysis: present and future 3
- Staden, J. J. van, see Reijnders, H. F. R. 235
- Stewart, K. K.
—, Brown, J. F. and Golden, B. M.
A microprocessor control system for automated multiple flow injection analysis 119
- Sweet, P., see Baban, S. 319
- Thelander, S., see Johansson, P.-A. 215
- Thelander, S., see Karlberg, B. 129

- Tijssen, R.
Axial dispersion and flow phenomena in helically coiled tubular reactors for flow analysis and chromatography 71
- Tóth, K.
—, Nagy, G., Fehér, Z., Horvai, G. and Pungor, E.
The application of electroanalytical detectors in continuous flow analysis 45
- Townshend, A., see Burguera, J. L. 209
- Trojanowicz, M.
Continuous potentiometric determination of sulphate in a differential flow system 293
- van den Berg, J. H. M.
—, Deelder, R. S. and Egberink, H. G. M.
Dispersion phenomena in reactors for flow analysis 91
- van der Linden, W. E., see Dieker, J. W. 267
- van der Linden, W. E., see Reijn, J. M. 105
- van Staden, J. J., see Reijnders, H. F. R. 235
- Werkhoven-Goewie, C. E.
—, Brinkman, U. A. Th. and Frei, R. W.
The use of solvent segmentation in continuous-flow systems, and fluorescence labelling by derivatization 147
- Weyden, A. H., see de Jong, E. B. M. 311
- Zagatto, E. A. G., see Giné, M. F. 191

(continued from outside of cover)

Automation of an energy-transfer immunoassay by using stopped-flow injection analysis with merging zones C. S. Lim, J. N. Miller (Loughborough, Gt. Britain) and J. W. Bridges (Guildford, Gt. Britain)	183
Simultaneous determination of nitrate and nitrite by flow injection analysis M. F. Giné, H. Bergamin F ^o , E. A. G. Zagatto and B. F. Reis (Sao Paulo, Brasil)	191
Determination of water by flow-injection analysis with the Karl Fischer reagent I. Kågevall, O. Åström and A. Cedergren (Umeå, Sweden)	199
Flow injection analysis for monitoring chemiluminescent reactions J. L. Burguera, A. Townshend (Birmingham, Gt. Britain) and S. Greenfield (Warley, Gt. Britain)	209
Extraction based on the flow-injection principle. Part 4. Determination of extraction constants P.-A. Johansson, B. Karlberg and S. Thelander (Södertälje, Sweden)	215
Differential kinetic analysis and flow injection analysis. Part 3. The (2.2.2) cryptates of magnesium, calcium and strontium H. Kagenow and A. Jensen (Copenhagen, Denmark)	227
A modelling approach to establish experimental parameters of a flow-through titration H. F. R. Reijnders, J. J. van Staden (Bilthoven, The Netherlands), G. H. B. Eelderink (Delft, The Netherlands) and B. Griepink (Utrecht, The Netherlands)	235
Controlled dynamic titrator S. M. Abicht (Saarbrücken, W. Germany)	247
The response surface of an amperometric flow cell detector based on a rotating disk electrode for h.p.l.c. and continuous flow analysis K. Brunt, C. H. P. Bruins, D. A. Doornbos and B. Oosterhuis (Groningen, The Netherlands)	257
Determination of iron(II) and iron(III) by flow injection and amperometric detection with a glassy carbon electrode J. W. Dieker and W. E. van der Linden (Amsterdam, The Netherlands)	267
Determination of cyanides by continuous distillation and flow analysis with cylindrical amperometric electrodes B. Pihlar and L. Kosta (Ljubljana, Yugoslavia)	275
Applications of a voltammetric flow-through cell in on-line analysis for organic compounds A. Ivaska (Åbo, Finland) and W. Franklin Smyth (London, Gt. Britain)	283
Continuous potentiometric determination of sulphate in a differential flow system M. Trojanowicz (Warsaw, Poland)	293
Continuous monitoring of heavy metals in industrial waste waters H. Cnobloch, W. Kellermann, D. Kühn, H. Nischik, K. Pantel and H. Poppa (Erlangen, W. Germany)	303
Fast analysis rates in continuous flow methods by using a modified method of curve regeneration E. B. M. de Jong and A. H. Weyden (Tilburg, The Netherlands)	311

Short Communications

The determination of sulphate by flow-injection analysis with exploitation of pH gradients and EDTA S. Baban, D. Beetlestone, D. Betteridge and P. Sweet (Swansea, Gt. Britain)	319
Selective determination of gallium by flow injection fluorimetry N. Ishibashi, K. Kina and Y. Goto (Fukuoka, Japan)	325
Potentiometric determination of proteins with an ammonia sensor M. Mascini and R. Giardini (Rome, Italy)	329
Author Index	335

CONTENTS

International Conference on Flow Analysis, September 11–13, 1979

Foreword	1
Continuous-flow analysis: present and future L. R. Snyder (Tarrytown, NY, U.S.A.)	3
Flow injection analysis. Principles, applications and trends J. Růžička and E. H. Hansen (Lyngby, Denmark)	19
The application of electroanalytical detectors in continuous flow analysis K. Tóth, G. Nagy, Z. Fehér, G. Horvai and E. Pungoř (Budapest, Hungary)	45
Characterization and design of liquid phase flow-through detector systems H. Poppe (Amsterdam, The Netherlands)	59
Axial dispersion and flow phenomena in helically coiled tubular reactors for flow analysis and chromatography R. Tijssen (Amsterdam, The Netherlands)	71
Dispersion phenomena in reactors for flow analysis J. H. M. van den Berg, R. S. Deelder and H. G. M. Egberink (Geleen, The Netherlands)	91
Some theoretical aspects of flow injection analysis J. M. Reijnders, W. E. van der Linden and H. Poppe (Amsterdam, The Netherlands)	105
A microprocessor control system for automated multiple flow injection analysis K. K. Stewart, J. F. Brown and B. M. Golden (Beltsville, MD, U.S.A.)	119
Extraction based on the flow-injection principle. Part 3. Fluorimetric determination of vitamin B ₁ (Thiamine) by the thiochrome method B. Karlberg and S. Thelander (Södertälje, Sweden)	129
Photochemical reaction detectors in continuous-flow systems — applications to pharmaceuticals A. H. M. T. Scholten, U. A. Th. Brinkman and R. W. Frei (Amsterdam, The Netherlands)	137
The use of solvent segmentation in continuous-flow systems, and fluorescence labelling by derivatization C. E. Warkhoven-Goewie, U. A. Th. Brinkman and R. W. Frei (Amsterdam, The Netherlands)	147
Rapid determination of corticosteroids in pharmaceuticals by flow injection analysis J. B. Landis (Kalamazoo, MI, U.S.A.)	155
A new approach to enzymatic assay based on flow-injection spectrophotometry with acid–base indicators A. Ramsing, J. Růžička and E. H. Hansen (Lyngby, Denmark)	165

(continued on inside page of cover)

© Elsevier Scientific Publishing Company, 1980.

All rights reserved. No part of this publication may be reproduced, stored in a retrieval system or transmitted in any form or by any means, electronic, mechanical, photocopying, recording or otherwise, without the prior written permission of the publisher, Elsevier Scientific Publishing Company, P.O. Box 330, 1000 AH Amsterdam, The Netherlands.

Submission of an article for publication implies the transfer of the copyright from the author to the publisher and is also understood to imply that the article is not being considered for publication elsewhere.

Submission to this journal of a paper entails the author's irrevocable and exclusive authorization of the publisher to collect any sums or considerations for copying or reproduction payable by third parties (as mentioned in article 17 paragraph 2 of the Dutch Copyright Act of 1912 and in the Royal Decree of June 20, 1974 (S. 351) pursuant to article 16 b of the Dutch Copyright Act of 1912) and/or to act in or out of court in connection therewith.

Printed in The Netherlands.